Aix-Marseille Université

Thèse

pour l'obtention du grade de :

Docteur en Sciences

Mention « Océanographie »

présentée et soutenue par

Mathieu Caffin

Devenir de la fixation d'azote et export de carbone dans l'océan Pacifique tropical sud-ouest.

Pour une soutenance prévue le 21 Décembre 2018 devant le jury composé de :

Pr.	Frank DEHAIRS	Professeur émérite VUB, Brussels	(Rapporteur)
Dr.	Ingrid OBERNOSTERER	Directrice de recherche CNRS LOMIC, Banyuls sur mer	(Rapporteur)
Dr.	Carolin LÖSCHER	Assistant professor SDU, Odense	(Examinateur)
Pr.	Bernard QUEGUINER	Professeur des universités MIO, Marseille	(Examinateur)
Dr.	Sophie BONNET	Directrice de recherche IRD MIO, Marseille	(Directrice de Thèse)
Pr.	Thierry MOUTIN	Professeur des universités MIO, Marseille	(Co-Directeur de Thèse)

Résumé

Ce travail de thèse réalisé dans le cadre du projet OUTPACE porte sur la quantification de la diazotrophie et son influence sur les cycles biogéochimiques dans l'océan de surface Pacifique tropical sud-ouest, une région particulièrement sous-échantillonnée à ce jour. Les objectifs de ce travail étaient (1) de quantifier la fixation de N_2 et identifier les principaux acteurs de la diazotrophie dans cette région, (2) d'évaluer l'influence de la fixation de N_2 sur la production primaire et sur l'export de carbone, (3) d'identifier les voies de transfert de l'azote fixé dans la chaine trophique planctonique.

Il a été mis en évidence que la région du Pacifique tropical sud-ouest était un hot spot de fixation de N_2, avec des taux moyens de 570 μmol N m^{-2} d^{-1}. Dans la région, la diazotrophie pourrait représenter une source de 16 Tg N an^{-1}, contribuant ainsi à environ 15 % des apports d'azote par la diazotrophie à l'échelle globale. Deux sous-régions distinctes ont été identifiées au cours de la campagne OUTPACE (transect allant de la Nouvelle Calédonie à la Polynésie Française). A l'ouest, les eaux oligotrophes des archipels Mélanésiens présentaient des taux de fixation de N_2 élevés ($\sim$600 μmol N m^{-2} d^{-1}) et la communauté diazotrophe était dominée par *Trichodesmium*. A l'est, les eaux ultra-oligotrophes de la gyre du Pacifique sud présentaient des taux de fixation de N_2 plus faibles ($\sim$90 μmol N m^{-2} d^{-1}) et la communauté diazotrophe était dominée par les UCYN-B. Le long du transect OUTPACE, les taux de fixation de N_2 étaient positivement corrélés à la production primaire, à la production bactérienne, aux abondances en picoplancton et en bactéries hétérotrophes.

Des bilans d'azote associés à une stratégie lagrangienne réalisés au niveau de trois stations représentatives de la région montrent que la fixation de N_2 contribuait à plus de 90 % des apports d'azote nouveau dans la couche euphotique, supérieur aux apports de nitrates par diffusion verticale turbulente (1-8 %) et aux apports atmosphériques (< 1,5 %). La fixation de N_2 soutenait donc la quasi intégralité de la production primaire nouvelle, 13-18 % de la production primaire totale dans la région des archipels Mélanésiens et 3 % à l'ouest de la gyre du Pacifique sud. Les e-ratio (export carbone particulaire / production primaire) mesurés dans la région (jusqu'à 9,7 %) sont nettement plus forts que ceux mesurées dans d'autres régions oligotrophes impactées par la diazotrophie, et montrent l'importante capacité d'export de la région. Les organismes diazotrophes présents dans la colonne d'eau n'étaient pas efficacement exportés vers l'océan profond, suggérant que la majeure partie de l'export était indirect, après transfert de l'azote fixé vers les organismes planctoniques non diazotrophes et leur export subséquent.

L'étude des voies de transfert de l'azote fixé montre qu'entre 7 et 15 % de la fixation de N_2 totale était transféré vers les organismes non-diazotrophes. Les principaux bénéficiaires de cet azote étaient le picoplancton autotrophe (*Synechococcus*, *Prochlorococcus*) suivi par les bactéries hétérotrophes. De plus, le transfert d'azote fixé vers le zooplancton qui a été très peu étudié jusqu'à maintenant, représentait 8$\pm$5 % de la fixation de N_2 totale lorsque les *Trichodesmium* dominaient et 28$\pm$7 % lorsque les UCYN-B dominaient.

Ces travaux de thèse démontrent que la diazotrophie soutient la pompe biologique dans l'océan Pacifique tropical sud-ouest, et qu'elle peut jouer un rôle déterminant dans la structure des communautés planctoniques et les cycles biogéochimiques du carbone et de l'azote dans les régions oligotrophes.

Mots clés : Fixation d'azote, relargage, transfert, export particulaire, pompe biologique, cycles biogéochimiques

Abstract

This PhD thesis, achieved within the framework of the OUTPACE project, focuses on the quantification of diazotrophy and its influence on biogeochemical cycles in the western tropical South Pacific Ocean, a critically under-sampled region so far. The aim of this work is to (1) quantify N_2 fixation and identify the main contributors of diazotrophy in this region, (2) assess the influence of N_2 fixation on primary production and carbon export, (3) identify transfer pathways of the fixed nitrogen in the planktonic food web.

We have found that the western tropical South Pacific Ocean was a hotspot of N_2 fixation, with N_2 fixation rates of 570 μmol N m^{-2} d^{-1} on average. In the region, diazotrophy would be a source of 16 Tg N yr^{-1}, contributing to more than 10 % of the nitrogen input by diazotrophy in the global ocean. Two distincts sub-regions were identified during the OUTPACE cruise (transect from New Caledonia to French Polynesia). In the western part, the oligotrophic waters of the Melanesian archipelago presented high N_2 fixation rates ($\sim$600 μmol N m^{-2} d^{-1}) and diazotrophes were dominated by *Trichodesmium*. In the eastern part, the ultra-oligotrophic waters of the South Pacific gyre presented lower N_2 fixation rates ($\sim$90 μmol N m^{-2} d^{-1}), and diazotrophs were dominated by UCYN-B. Along the OUTPACE transect, N_2 fixation rates were positively correlated with the primary production, the bacterial production, picoplankton and heterotrophic bacteria abundances.

The nitrogen budgets, performed using a lagrangian strategy at three representative stations of the region, show that N_2 fixation contributed to more than 90 % of the of new nitrogen input in the photic layer, then nitrate input by vertical diffusion (1-8 %) and atmospheric deposition (< 1.5 %). N_2 fixation sustained almost all of the new production and contributed to 13-18 % of the primary production in the Melanesian archipelago and 3 % in the South Pacific gyre. The e-ratios (particulate carbon export / primary production) measured in the region (up to 9.7 %) are far higher than the one measured in other regions impacted by diazotrophy, revealing the high export efficiency of this region. Diazotrophs in the water column were not effeciently exported, suggesting an indirect export after transfer of fixed nitrogen through non-diazotrophic planktonic organisms, which were subsequently exported.

The study of the transfer pathways of the fixed nitrogen has shown that 7 to 15 % of total N_2 fixation was transferred to non-diazotrophs. The main beneficiaries of this nitrogen were autotrophic picoplancton (*Synechococcus*, *Prochlorococcus*) and heterotrophic bacteria. In addition, the transfer of fixed nitrogen to zooplankton which has been poorly studied, represented 8$\pm$5 % of the total N_2 fixation when *Trichodesmium* was dominant, and 28$\pm$7 % when it was UCYN-B.

This PhD thesis indicates that diazotrophy sustains the biological pump in the western tropical South Pacific Ocean, and can have a critical influence in the planktonic community structure and in biogeochemical cycles of carbon and nitrogen in oligotrophic regions.

Keywords : Dinitrogen fixation, release, transfer, particulate export, biological pump, biogeochemical cycles

Remerciements

Je veux exprimer ici mes remerciements à toutes les personnes qui ont contribué de près ou de loin à la réalisation de cette thèse.

Je tiens à exprimer en premier lieu toute ma gratitude et ma reconnaissance à mes directeurs de thèse Sophie Bonnet et Thierry Moutin. Je les remercie de m'avoir permis de participer à cette passionnante aventure humaine et scientifique qu'a été la campagne océanographique OUTPACE. Ces 45 jours de mission ont été pour moi les prémisses de trois années d'expériences passionnantes et enrichissantes. Je les remercie d'avoir mis en oeuvre les moyens nécessaires qui m'ont permis d'effectuer mes premiers travaux de recherche dans d'excellentes conditions. La patience, la disponibilité et la confiance qu'ils m'ont accordés a permis de mener à bien cette thèse.

Je souhaite remercier Richard Sempéré, directeur du MIO, de m'avoir permis d'effectuer ma thèse au sein de son laboratoire. Je souhaite exprimer ma gratitude à Ingrid Obernosterer, Frank Dehairs, Carolin Löscher et Bernard Quéguiner qui ont accepté d'évaluer mes travaux de recherche. J'en profite pour remercier Bernard de m'avoir ouvert au monde de la biogéochimie de l'azote et des diazotrophes lorsqu'il était mon professeur, il y a maintenant cinq ans. Vielen Dank Carolin, dass Sie akzeptiert haben meine Doktorarbeit zu prüfen, welche ich sieben Jahre nach Ihnen verteidigen werde.

Je remercie très chaleureusement Edouard Hnawia, directeur du centre IRD de Nouvelle-Calédonie, et Fabrice Colin pour l'accueil qu'ils m'ont offert à mon arrivée à Nouméa. Merci pour leur soutien indéfectible au cours de cette belle année passée en Nouvelle Calédonie.

Mes remerciements vont également aux personnes qui m'ont accompagné au MIO, en particulier à l'équipe CYBELE. Merci à Véro, Sandra et Aude pour leur disponibilité au laboratoire. Je les remercie du temps qu'elles ont mis à disposition pour me former. Merci aux physiciens, Pascale, Anne et Andrea de m'avoir permis de continuer à garder un pied dans leur monde et pour leur appuis scientifique. Merci à France pour son indéfectible soutien. Merci à Mar et à Hugo de m'avoir permis de faire mes premières armes expérimentales sur la diazotrophie à leurs cotés. Merci à Thibaut de m'avoir soutenu à sa façon très personnelle. Et merci à Gérald pour ses conseils scientifiques et personnels, particulièrement pour le Carver.

Ces trois années de thèse (et celles de Master) n'auraient pas eu le même goût sans Louise ma soeur de thèse. A défaut d'avoir pu partager mon bureau avec elle, nous avons partagé tout le reste de notre temps au MIO ensemble ! Je la remercie très chaleureusement et amicalement pour tous les moments que nous avons passés ensemble.

Un grand merci à mes collègues et amis de Toulouse, de Marseille et de Nouméa avec qui j'ai passé de bons moments au cours de ces trois années : Guillaume, Anne-Sophie, Audrey, Guillaume, Mika, Isis, Tom, Valentine, Andreas, Julie, Germain, Lucas, Thomas et Valentin. Je reviens infiniment marqué de mon séjour sur le territoire Calédonien, en particulier suite à la rencontre de mon ami Emmrick. Oleti Emmrick.

Enfin, je remercie ma famille pour leur soutien et leur patience. Je remercie mes parents de m'avoir toujours poussé à faire ce qui me plaisait et me passionnait. Je les remercie de m'avoir toujours tiré vers le haut, c'est en parti grâce à eux que je suis arrivé jusqu'ici. Merci à mon frère Edouard et à ma soeur Louise qui sont venu porter leur soutien jusqu'en Nouvelle Calédonie. Je ne pourrais finir cette page sans un immense merci à Anne qui partage avec moi cette aventure depuis le début. Merci d'avoir toujours été à mes côtés, de m'avoir suivi à l'autre bout du monde, de m'avoir soutenu, de m'avoir supporté, d'avoir supporté la lourde présence de mon ordinateur entre nous, et la lourde absence de mon esprit ces dernières semaines. A tous, merci.

Table des matières

Chapitre 1

Introduction générale

Sommaire

1.1 Contexte scientifique

Le changement climatique est aujourd'hui reconnu comme l'un des enjeux environnementaux majeur du XXI^{e} siècle. Ce phénomène d'envergure n'a pas de frontière et affecte la totalité du globe et ses écosystèmes. Depuis le début du XIX^{e} siècle avec la révolution industrielle, la concentration en dioxyde de carbone (CO_2) dans l'atmosphère n'a cessé d'augmenter. Les mesures effectuées depuis 1958 à la SCRIPPS Institution of Oceanography (Californie) et à l'observatoire de Mauna Loa (Hawaii) (Fig. 1.1) témoignent de l'augmentation continuelle de la pression partielle de CO_2 atmosphérique, qui est passée de 280 ppm à plus de 400 ppm entre l'ère préindustrielle et aujourd'hui. Cette augmentation (constatée sur à peine 200 ans) est de l'ordre de grandeur des variations observées entre périodes glaciaires et inter-glaciaires qui sont d'environ 100 000 ans. Elle est majoritairement due aux activités anthropiques telles que l'utilisation de combustibles fossiles, la production de ciment et la déforestation (Hegerl et al., 2007). Ce CO_2 présent en quantité de plus en plus élevée dans l'atmosphère est du CO_2 anthropique. En moins de 200 ans, les activités de l'Homme ont rejeté dans l'atmosphère entre 340 et 420 Pg de carbone sous forme de CO_2 (Sabine et al., 2004), et les émissions annuelles ne cessent d'augmenter, passant de $\sim$5.5 Pg C an^{-1} en 1970 (Raupach et al., 2007) à $\sim$ 10 Pg C an^{-1} aujourd'hui (Le Quéré et al., 2018). Tout comme le méthane, les oxydes nitreux et les chlorofluorocarbones, le CO_2 est un gaz à effet de serre, participant ainsi au réchauffement de la Terre. Alors que les activités anthropiques agissent comme une source de CO_2 pour l'atmosphère, l'océan est quant à lui un puits majeur de CO_2 et a absorbé $\sim$30-40 % des émissions de CO_2 anthropique depuis 1870, empêchant une plus grande accumulation de CO_2 dans l'atmosphère, et donc une plus grande augmentation de la température de surface de la Terre (DeVries, 2014; Sabine et al., 2004; Takahashi et al., 2002). L'océan joue un rôle central dans la régulation de la concentration atmosphérique de CO_2 anthropique. Il est donc aujourd'hui indispensable d'améliorer notre compréhension de son rôle sur le cycle du carbone afin de comprendre et prévoir quelle sera l'évolution du climat dans les décennies à venir.

L'absorption de ce CO_2 anthropique par l'océan est d'une part réalisée par la « pompe de solubilité » correspondant aux échanges de gaz à la surface de l'océan. D'autre part, cette absorption est réalisée par la « pompe biologique » à carbone correspondant au transfert de carbone depuis la surface vers l'océan profond par l'intermédiaire de processus biologiques (Fig. 1.2).
La pompe de solubilité, aussi appelée pompe physique, est le processus physico-chimique par lequel le carbone sous forme de CO_2 est transporté depuis l'océan de surface vers l'océan profond. Ce processus est contrôlé par la thermodynamique du CO_2 à l'interface atmosphère-océan et il est conditionné par la circulation thermohaline mondiale. Sous les hautes latitudes (particulièrement dans l'océan Austral et l'océan Atlantique nord), les eaux de surface se refroidissent et se saturent en CO_2, la solubilité du CO_2 dans l'eau

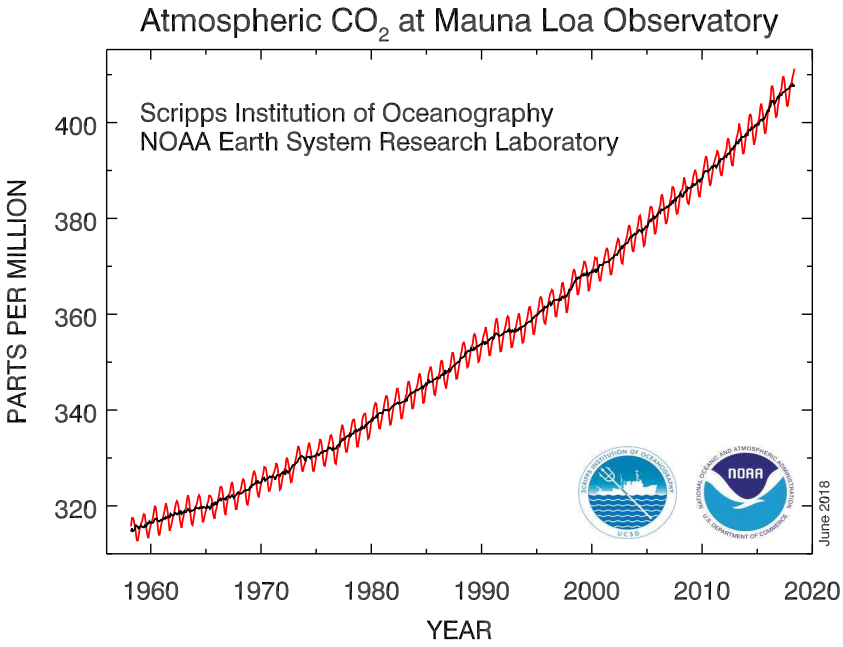

Figure 1.1 Concentrations moyennes en CO_2 atmosphérique (ppm) de 1958 à 2018 mesurés à la Scripps Institution of Oceanography (Californie) et à Mauna Loa (Hawaii) (Dlugokencky and Tans, 2018)

.

de mer augmentant avec la diminution de la température. En se refroidissant, les eaux de surface deviennent plus denses et plongent vers l'océan profond, soustrayant à l'atmosphère le CO_2 dissous en surface, avant de revenir en surface 100 à 1000 ans plus tard (Broecker, 1991).

La pompe biologique est le processus par lequel le carbone minéral est transformé sous sa forme organique via la production primaire, et est exporté de la couche de surface vers l'océan profond via la chute de matière particulaire. Dans la couche éclairée de l'océan (couche euphotique), le phytoplancton convertit le CO_2 en carbone organique par photosynthèse, en utilisant l'énergie lumineuse et les nutriments disponibles. La production primaire (50 Pg C an^{-1}, Field et al., 1998) est principalement assurée par les organismes phytoplanctoniques qui constituent le premier maillon de la chaine trophique marine. D'une part, les organismes phytoplanctoniques sont consommés par les organismes planctoniques hétérotrophes, qui sont eux même consommées par les maillons supérieurs de la chaine trophique, transférant ainsi le carbone organique dans le réseau trophique. D'autre part, le carbone organique dissous produit par le relargage du phytoplancton, et l'activité du zooplancton qui le consomme, est consommé par les bactéries hétérotrophes. Ces bactéries hétérotrophes sont ensuite consommées par les organismes proto-zooplanctoniques et les nano-flégéllés hétérotrophes. Ce concept est appelé boucle microbienne, ou réseau microbien. Une partie du carbone organique est exportée hors

de la couche euphotique par sédimentation de la matière particulaire (détritus, pelotes fécales, cellules, carcasses de zooplancton, agrégats), et par mélange vertical de carbone organique dissous et de matière particulaire entre la couche euphotique et les couches plus profondes de l'océan. Seule une infime proportion du carbone issu de la production primaire de surface ($\sim$0,2 Pg C an^{-1}) atteint le plancher océanique pour être stockée dans les sédiments pendant plusieurs millénaires (Ciais et al., 2014), représentant un puits durable de carbone pour l'atmosphère.

Cette pompe biologique a été considérée jusque dans les années 1990-2000 à l'équilibre (Broecker, 1991; Murnane et al., 1999), mais le changement climatique global engendre des altérations (Sarmiento and Gruber, 2004) qui ont pu être mises en évidence, par exemple, au niveau de la station d'observation à long terme HOT (Hawaii Ocean Time-series) dans la gyre subtropical de l'océan Pacifique Nord. En effet, les observations ont montré une diminution de plus de 50 % du stock de phosphate disponible pour les organismes en 5 ans (entre 1989 et 1994, Karl et al., 1997). Cette diminution engendre un déséquilibre de la quantité de nutriments disponibles dans les eaux de surfaces, induisant un changement de nutriment limitant pour la production primaire. Ainsi, la pompe biologique qui était auparavant limitée principalement par l'azote se trouve également limitée par la disponibilité en phosphate dans cette région, devenant de plus en plus oligotrophe. Des études basées sur l'estimation de la production primaire à partir d'image satellites ont confirmé l'augmentation du degré d'oligotrophie de la gyre (Gregg et al., 2005), ainsi que l'expansion de cette région oligotrophe (McClain et al., 2004; Polovina et al., 2008). Les auteurs en ont conclu que le réchauffement des eaux de surfaces et l'augmentation en conséquence de la stratification ont induit une diminution de la biomasse phytoplanctonique et de la production primaire dans la gyre du Pacifique subtropical nord (Polovina et al., 2008), induisant ainsi une diminution de l'efficacité de la pompe biologique.

1.2 Le rôle clé de l'azote dans l'océan

Comme tout organisme photosynthétique, le phytoplancton a besoin d'énergie lumineuse et d'éléments nutritifs pour transformer la matière minérale en matière organique. La couche euphotique étant par définition non limitée par la lumière, c'est la disponibilité en éléments nutritifs qui limite la production primaire. Les éléments limitant la production primaire sont d'une part les macro-nutriments inorganiques, tels que l'azote (N), le phosphore (P) ou le silicium (Si). D'autre part, il y a les micro-nutriments qui sont nécessaires en plus faibles quantités, tels que le fer (Fe), le Zinc (Zn), le cobalt (Co), ou le nickel (Ni). Dans la couche euphotique de l'océan, les concentrations en éléments nutritifs sont souvent très faibles du fait de la consommation de ces derniers par les organismes phytoplanctoniques. Les concentrations en chacun de ces éléments nutritifs sont très hétérogènes à l'échelle de l'océan mondial. En dehors des régions HNLC (Hight Nutrient Low Chlorophyll) caractérisées par une limitation en Fe, l'azote apparaît comme le

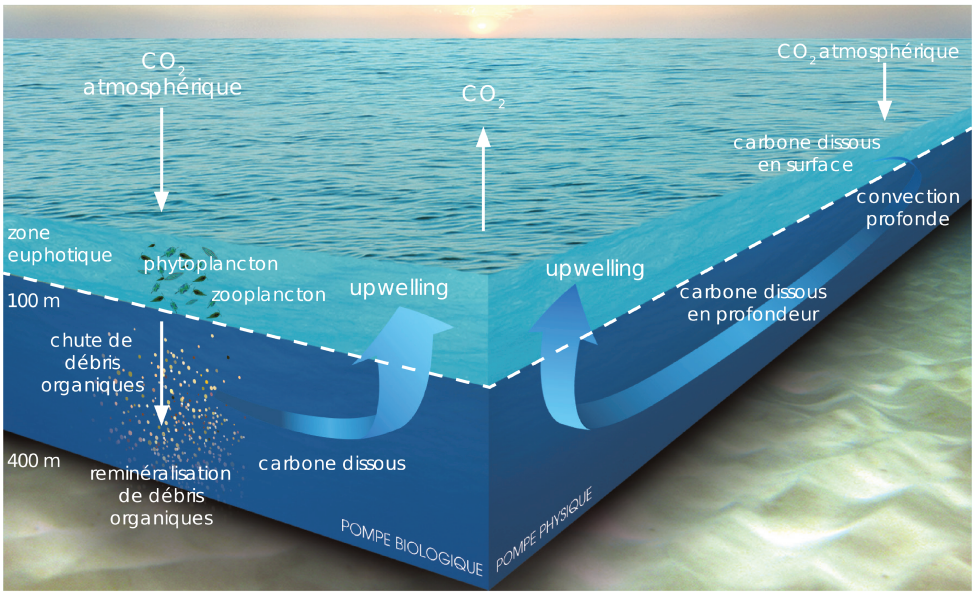

Figure 1.2 Représentation simplifiée des processus impliqués dans la pompe biologique et la pompe de solubilité (Bopp et al., 2002)

.

principal élément limitant la production primaire dans l'océan actuel (Moore et al., 2013), en particulier dans les régions oligotrophes (l'océan tropical et subtropical) stratifiées, qui occupent 80 % de la surface de l'océan global (Longhurst et al., 1995).
L'azote existe sous plusieurs formes dans l'environnement marin et sous 5 états stables d'oxydation à la différence des autres macro-nutiments, excepté le carbone (Table 1.1). L'azote peut passer d'une forme stable à une autre par différents processus qui ont lieu dans l'océan, dont la fixation de N_2 (Fig. 1.3). A l'échelle mondiale, la majeure partie de l'azote biodisponible pour les organismes marins se trouve sous forme minérale (Nitrate (NO_3^-), ~88 % de l'azote biodisponible), et sous forme d'azote organique dissous (ci-après dénommé DON) dans une plus faible proportion (~12 % de l'azote biodisponible, Table : 1.2), dont les concentrations moyennes sont respectivement de 7 et 6 μmol L^{-1} dans la couche euphotique. Cependant ces concentrations sont variables dans le temps et l'espace à l'échelle de l'océan mondial. Les concentrations en NO_3^- peuvent atteindre plusieurs μmol L^{-1} dans les régions eutrophes et sont quasi-indétectables avec les instruments de mesure actuels dans le vaste océan oligotrophe. Le diazote (N_2) est le réservoir majeur d'azote dans l'océan représentant plus de 90 % du stock d'azote océanique, mais il n'est biodisponible que pour certains organismes spécialisés appelés diazotrophes (ou fixateurs de N_2).

Les premières études sur le cycle de l'azote en milieu oligotrophe datent des années 1960 en mer des Sargasses (Menzel and Ryther, 1961). Pendant la même décennie, Dugdale and Goering (1967) définissent les notions de « production nouvelle » et « production régénérée », associées à la source d'azote qui alimente la production primaire. Dans la couche euphotique, la production nouvelle est alimentée par les sources d'azote nouveau. Ces sources sont principalement, en milieu hauturier, le N_2 fixé par les diazotrophes, le

NO_3^- provenant des eaux sous-jacentes (apportées en surface par le mélange vertical et par la diffusion turbulente), et l'azote issu des dépôts atmosphériques. La production régénérée est quant à elle alimentée par les sources autochtones d'azote dans la couche euphotique, principalement l'ammonium (NH_4^+) dérivé de processus biologiques. La fraction de la production primaire provenant des sources d'azote nouveau est définie par le f-ratio (Eppley and Peterson, 1979). Lorsque le système est à l'état d'équilibre, à de grandes échelles de temps et d'espace, la production nouvelle est considérée comme égale à la production primaire exportable (appelée production exportée) (Eppley and Peterson, 1979). Ainsi, les apports d'azote nouveau dans la couche euphotique sont impliqués dans l'efficacité et l'intensité de la production primaire, et par extension dans l'efficacité de la pompe biologique et de l'export.

La majeure partie de l'océan de surface ($\sim$ 80 %) est caractérisée par une faible disponibilité en azote pour les organismes marins, limitant ainsi la production primaire et l'efficacité de la pompe biologique dans l'océan mondial (Falkowski, 1997; Moore et al., 2013; Zehr, 2011). A l'échelle mondiale, la source majeure d'azote nouveau dans l'océan de surface est la fixation de N_2 (Gruber, 2008). Depuis les dernières décennies, des efforts scientifiques considérables ont été effectués pour améliorer notre connaissance de ce processus (e.g. review de Sohm et al., 2011), mais de nombreuses questions subsistent encore aujourd'hui concernant l'impact de la fixation de N_2 sur les cycles biogéochimiques et sur l'export de carbone, en particulier en milieu hauturier.

Nomenclature	Formule chimique	Degré d'oxydation
Nitrate	NO_3^-	+V
Nitrite	NO_2^-	+III
Oxyde nitreux	N_2O	+I
Diazote	N_2	0
Ammonium	NH_4^+	-III
Azote organique dissous	DON	-III
Azote organique particulaire	PON	-III

Tableau 1.1 Les formes stables de l'azote dans l'océan et leur degré d'oxydation

Forme	Concentration moyenne dans la couche euphotique (μmol L^{-1})	Stock océanique mondial (Tg N)	Temps de résidence (ans)
Nitrate	7	$5{,}8 \times 10^5$	370
Nitrite	0,1	160	
Ammonium	0,3	340	0.05
Azote organique dissous	6	$7{,}7 \times 10^4$	20
Diazote	450	1×10^7	54 000

Tableau 1.2 Inventaire océanique et temps de résidence d'azote disponible pour la production primaire, d'après Gruber (2008)

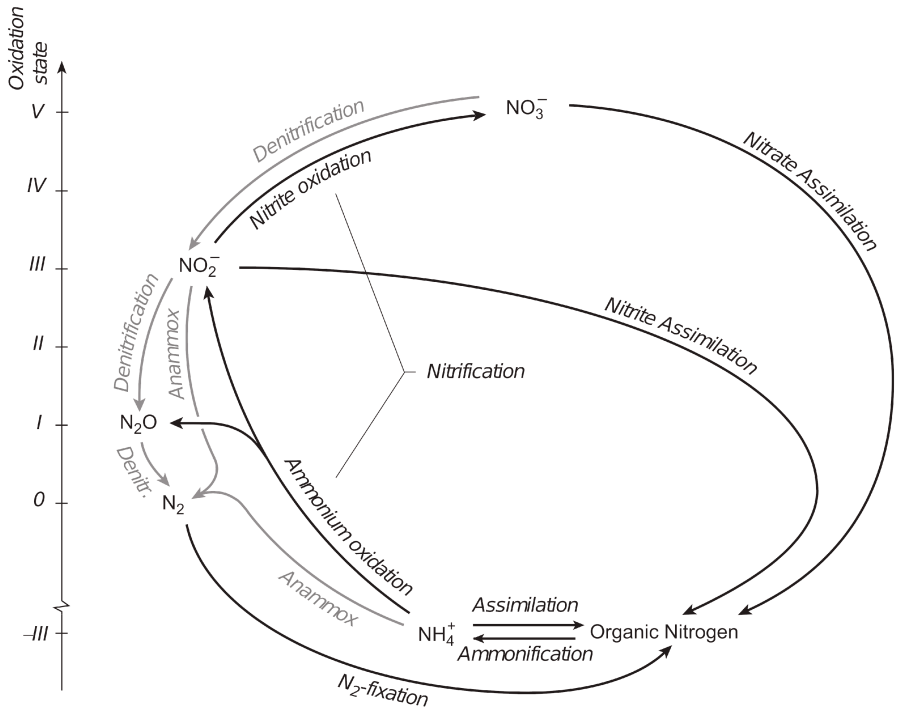

Figure 1.3 Formes chimiques majeures et transformations de l'azote dans l'océan. Les différentes formes chimiques sont associées à leur degré d'oxydation D'après Gruber (2008)

.

1.3 La fixation d'azote

1.3.1 Importance biogéochimique de la fixation d'azote dans l'océan oligotrophe

L'azote est un des éléments majeurs à la base de la vie terrestre et marine. Environ 78 % de l'atmosphère terrestre est composée de N_2, ce qui fait de ce gaz une source d'azote inépuisable. La concentration moyenne élevée du N_2 (450 μmol L^{-1}) dans l'océan de surface, ainsi que son temps de résidence élevé (54 000 ans) témoignent de sa sous-consommation (Table : 1.2), du à son caractère non biodisponible pour le phytoplancton, excepté pour les diazotrophes.

Les bilans d'azote sur l'ensemble de l'océan deviennent de plus en plus complets, et ne cessent de réévaluer à la hausse la part due à la fixation de N_2. Les premières estimations proposaient un flux de N_2 océanique de 10-20 Tg N a^{-1} à l'échelle globale (Capone and Carpenter, 1982). Les estimations actuelles considèrent que les apports d'azote dus à la fixation de N_2 sont de l'ordre de 100 à 200 Tg N a^{-1} (Gruber, 2008; Karl et al., 2002; Voss et al., 2013, Table 1.3). Ces bilans montrent que la fixation de N_2 est la source majeure d'azote nouveau à l'océan. L'azote joue un rôle central dans le contrôle de la production primaire océanique (Falkowski, 1997; Moore et al., 2013; Tyrrell, 1999). Ainsi, l'apport

de cet azote nouveau par la diazotrophie dans l'océan de surface illustre le lien étroit qui existe entre les cycles biogéochimiques du carbone et de l'azote. Il est donc nécessaire de mieux connaître le rôle de la fixation de N_2 sur l'efficacité et l'intensité de la production primaire et de la pompe biologique.

Processus	Codispoti et al.	Galloway et al.	Gruber
Fixation N_2 pélagique (Tg N a^{-1})	117	106	120 ± 50
Fixation N_2 benthique (Tg N a^{-1})	15	15	15 ± 10
Apports fluviaux (DON) (Tg N a^{-1})	34	18	35 ± 10
Apports fluviaux (PON) (Tg N a^{-1})	42	30	45 ± 10
Apports atmosphériques (Tg N a^{-1})	86	33	50 ± 20
Somme des apports (Tg N a^{-1})	294	202	265 ± 55

Tableau 1.3 Bilan global des apports d'azote de Codispoti et al. (2001), Galloway et al. (2004) et Gruber (2004), d'après Gruber (2008)

1.3.2 Distribution biogéographique de la fixation de N_2

Les efforts de quantification de la fixation de N_2 ont permis de mettre en relief la distribution hétérogène du processus de diazotrophie au sein de la colonne d'eau, à faible échelle spatiale (Bombar et al., 2015) ainsi que la forte variation spatiale qui peut exister au sein d'un même bassin océanique (Luo et al., 2012). Bien qu'un effort important ait été réalisé par la communauté scientifique pour quantifier la diazotrophie à l'échelle mondiale, il reste de nombreuses régions de l'océan mondial non explorées (Fig. 1.4, Landolfi et al., 2018; Luo et al., 2012). Alors que les régions du Pacifique tropical nord, de l'Atlantique tropical nord et du Pacifique tropical sud-est ont été fortement échantillonnées (e.g. Benavides and Voss, 2015; Luo et al., 2012) à la fois lors de campagnes océanographiques et grâce à des stations d'observation à long terme (stations HOT et BATS), les régions de l'océan Indien et de l'océan Pacifique tropical sud-ouest restent fortement sous échantillonnées (Fig. 1.4). Cela est du au fait que la majeure partie des mesures de fixation de N_2 a été réalisée d'une part dans les régions où était suspectée la diazotrophie (dans les régions chaudes de l'océan) et d'autre part essentiellement dans les régions proches des grands laboratoires de recherches océanographiques ayant la possibilité de déployer des moyens logistiques pour étudier le processus, couvrant ainsi les grandes gyres du Pacifique nord et de l'Atlantique nord.

Dans l'océan Pacifique sud-est, un important effort de recherche a eu lieu ces dernières année à la suite des travaux de Deutsch et al. (2007). Ces auteurs ont suggéré qu'il existerait un couplage spatial étroit entre les pertes d'azote (par les processus de dénitrification et anammox) et les gains d'azote (par fixation de de N_2) au niveau de la zone de minimum d'oxygène (OMZ) associées aux zones d'upwelling sur le bord est des bassins océaniques. Les processus de dénitrification et d'anammox ayant lieu dans les OMZ (Dalsgaard et al.,

2012; Farías et al., 2009), il était prédit que les pertes dans ces régions étaient rapidement contrebalancées par la fixation de N_2. La région de l'upwelling du Pérou-Chili étant une grande région OMZ, il était alors envisagé qu'elle était aussi une région de forte diazotrophie. Cette hypothèse a motivé de nombreuses campagnes océanographiques dans la région du Pacifique tropical sud-est, qui ont montré des taux de fixation de N_2 assez faibles ((< 50-100 μmol m^2 d^{-1}, 2-36 mmol m^2 y^{-1}, Bonnet et al., 2013; Dekaezemacker et al., 2013; Fernandez et al., 2011, 2015; Knapp et al., 2016; Loescher et al., 2014; Moutin et al., 2008; Raimbault and Garcia, 2008), et très loin d'équilibrer les pertes par dénitrification et anammox comme proposé par Deutsch et al. (2007).

La région ouest du Pacifique tropical sud restait encore très peu explorée. De rares études ont rapporté au large de la Nouvelle Calédonie des taux de fixation d'azote très élevés (150-700 μmol m^2 d^{-1}, Garcia et al., 2007), en relation avec la disponibilité en phosphate dans le milieu (Moutin et al., 2005; Van Den Broeck et al., 2004), ce qui corroborait avec la présence récurrente d'efflorescences phytoplanctoniques identifiées sur les images satellites en période estivale (Dupouy et al., 2000). D'autres études avaient montré la présence de diazotrophes en mer de Corail et dans les eaux Fidjiennes (Moisander et al., 2010), laissant penser que cette région pouvait être propice à la diazotrophie sans pour autant que ce processus soit quantifié à l'échelle du Pacifique sud-ouest.

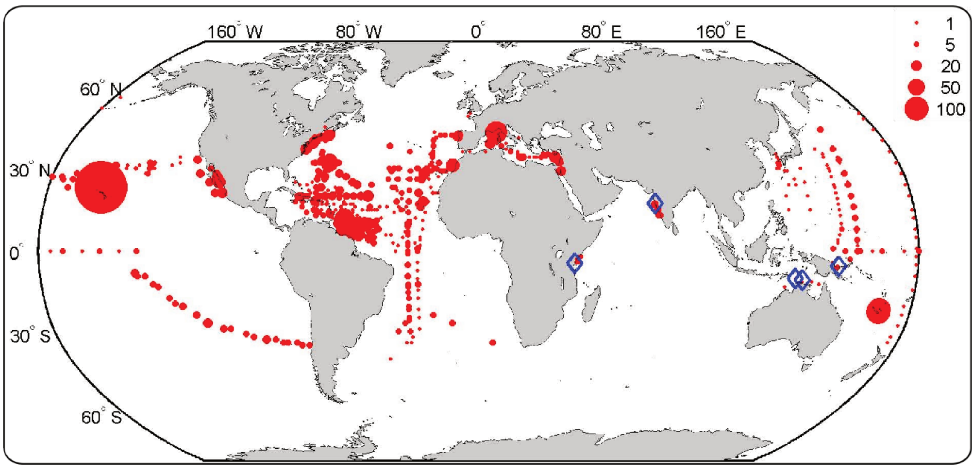

Figure 1.4 Carte de distribution spatiale des flux de fixation de N_2 mesurés dans l'océan global en nombre de points de donnée. D'après Luo et al. (2012).

.

Les diverses études portant sur la diazotrophie ont permis de mettre en relief que ce processus est très variable dans le temps et dans l'espace à l'échelle de l'océan mondial (Luo et al., 2012; Sohm et al., 2011). Les organismes diazotrophes sont, par définition, non limités par la disponibilité en azote, contrairement à la majorité du phytoplancton. Cela implique que d'autres facteurs environnementaux peuvent contrôler la distribution et l'activité des organismes diazotrophes, tels que la lumière, la disponibilité en éléments nutritifs, la température, les forçages physiques, ou la pression partielle de CO_2 (e.g. Breit-

barth et al., 2007; Church et al., 2009; Fong et al., 2008; Fu et al., 2008; Hutchins et al., 2007; Levitan et al., 2007) qui ont fait l'objet de nombreuses études en laboratoire, sur le terrain et de modélisation.

A l'heure actuelle l'influence de ces facteurs sur la distribution biogéographique de la fixation de N_2 à l'échelle de l'océan mondial est encore mal connue. Un effort de la communauté scientifique a été déployé il y a quelques années afin de répertorier et d'unir dans une même base de donnée toutes les mesures de fixation de N_2, et de quantification d'organismes diazotrophes de l'océan mondial (Luo et al., 2012). Ces données ont été ajoutées et stockées dans la base de données globale MAREDAT (MARine Ecosystem DATa) qui inclue les données de 9 groupes planctoniques fonctionnels dont les diazotrophes. En parallèle de chacune des mesures réalisées, les paramètres environnementaux disponibles ont aussi été enregistrés en chaque point. Luo et al. (2014) ont fait une étude statistique des données afin de comprendre les liens existants entre les paramètres environnementaux et la diazotrophie à l'échelle mondiale. Cette étude a permis de montrer que la fixation de N_2 est en premier lieu expliquée par l'irradiance solaire, et par la température de surface qui sont deux paramètres liés entre eux. Ainsi les basses latitudes, fortement soumise aux radiations solaires, et présentant des températures de surfaces élevées sont un environnement propice au développement des organismes fixateurs de N_2 (Fig. 1.5). Ces résultats sont cohérents avec les travaux de Breitbarth et al. (2007), qui montrent que la gamme de températures optimales est typique des températures des eaux de surfaces sous les tropiques (25-28 $^{\circ}$C). Ce lien peut également provenir de la relation étroite entre la température et la disponibilité nutritive comme cela a été montré dans le Pacifique tropical sud-ouest (Moutin et al., 2005; Van Den Broeck et al., 2004) sans qu'un effet direct de la température sur la croissance des diazotrophes soit à considérer. Notons, que certains organismes diazotrophes ont aussi été observés dans des régions froides comme en baie de Chesapeake (Short et al., 2004) ou en mer Baltique (Stal et al., 2003).

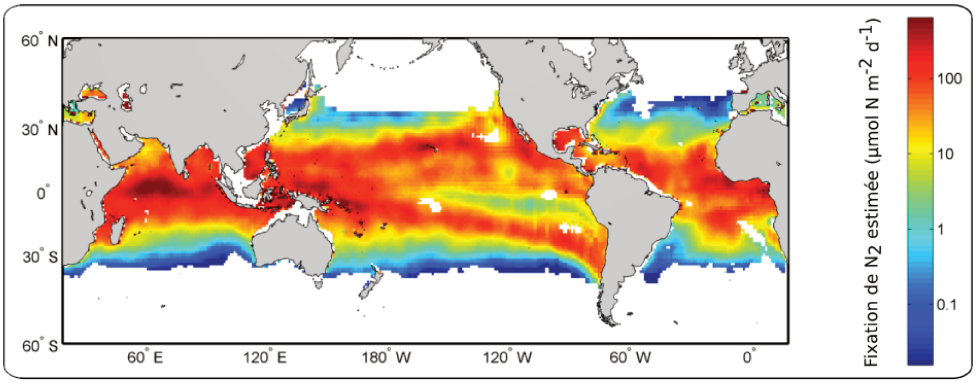

Figure 1.5 Carte des flux intégrés de fixation de N_2 dans l'océan global estimé à partir de l'analyse statistique des données compilées par Luo et al. (2012). D'après Luo et al. (2014).

.

1.3.3 Les fixateurs d'azote

Les organismes diazotrophes peuvent fixer le N_2 atmosphérique dissous dans l'eau de mer grâce à l'enzyme nitrogenase qui leur permet de rompre la triple liaison covalente de la molécule de N_2 pour la réduire en deux molécules d'ammoniac selon la réaction :
$N_2 + 8H^+ + 16ATP + 8e^- = 2NH_3 + H_2 + 16ADP + 16Pi$

L'enzyme nitrogénase est composée de deux métalloenzymes contenant 34 atomes de fer : la dinitrogénase (protéine FeMo) et la dinitrogénase réductase (protéine Fe). Il a ainsi été montré que la disponibilité en fer dans l'océan contrôlait la fixation de N_2 dans certaines régions (e.g. Berman-Frank et al., 2007; Mills et al., 2004). Les différentes protéines nitrogénase sont relativement similaires entre les diazotrophes et sont codées par trois gènes : *nif*H, *nif*D et *nif*K. Le gène *nif*H est le plus souvent utilisé pour les études phylogénétiques (Zehr and Turner, 2001; Zehr et al., 1998, 2008). Les principaux organismes responsables de la fixation de N_2 (Fig. 1.6) dans l'océan sont :

- les cyanobactéries filamenteuses non-hétérocystées, telles que *Trichodesmium* (Capone et al., 1997; Carpenter, 1983) qui sont les plus étudiées (depuis les années 1970). Les efflorescences de ces organismes forment de larges et longs radeaux de colonies à la surface de l'océan, visibles à l'oeil

- les cyanobactéries hétérocystées vivant en symbiose avec les diatomées (nommées DDA : Diatom-Diazotrophic Association, Villareal (1994), telles que *Richelia intracllularis* en symbiose avec les diatomées *Rhizosolenia* et *Hemiaulus*, identifiables par microscopie ;

- les cyanobactéries unicellulaires nommées UCYN et subdivisées en 3 groupes (A, B et C) basés sur la séquence du gène *nif*H (Zehr and Turner, 2001; Zehr et al., 1998, 2008). Les premières UCYN à avoir été découvertes sont celles du groupe B (*Crocosphaera watsonii)* et du groupe C, disponibles en cultures et dont les abondances (en particulier pour les UCYN-B) sont du même ordre de grandeur que celles de *Trichodesmium* dans certaines régions tropicales (Bonnet et al., 2009; Luo et al., 2012; Moisander et al., 2010; Montoya et al., 2004). Les UCYN-C sont principalement retrouvées en zones côtières et sont peu étudiées en milieu hauturier (Bauer et al., 2008; Ohki et al., 2008). Les UCYN-A (*Candidtus atelocyanobacterium thalassa*), dont la découverte est la plus récente (Zehr et al., 2008), n'ont pas encore été isolées et mises en culture, limitant ainsi la compréhension de leur écologie. Elles seraient les organismes diazotrophes les plus abondants de l'océan mondial (Luo et al., 2012) ;

- les diazotrophes non-cyanobactériens, dont la séquence du gêne *nif*H a permis d'attester la présence dans le Pacifique et l'Atlantique jusqu'à des profondeurs pouvant aller entre 200 et 2000 m (e.g. Benavides et al., 2018; Bombar et al., 2016; Loescher et al., 2014; Moisander et al., 2017).

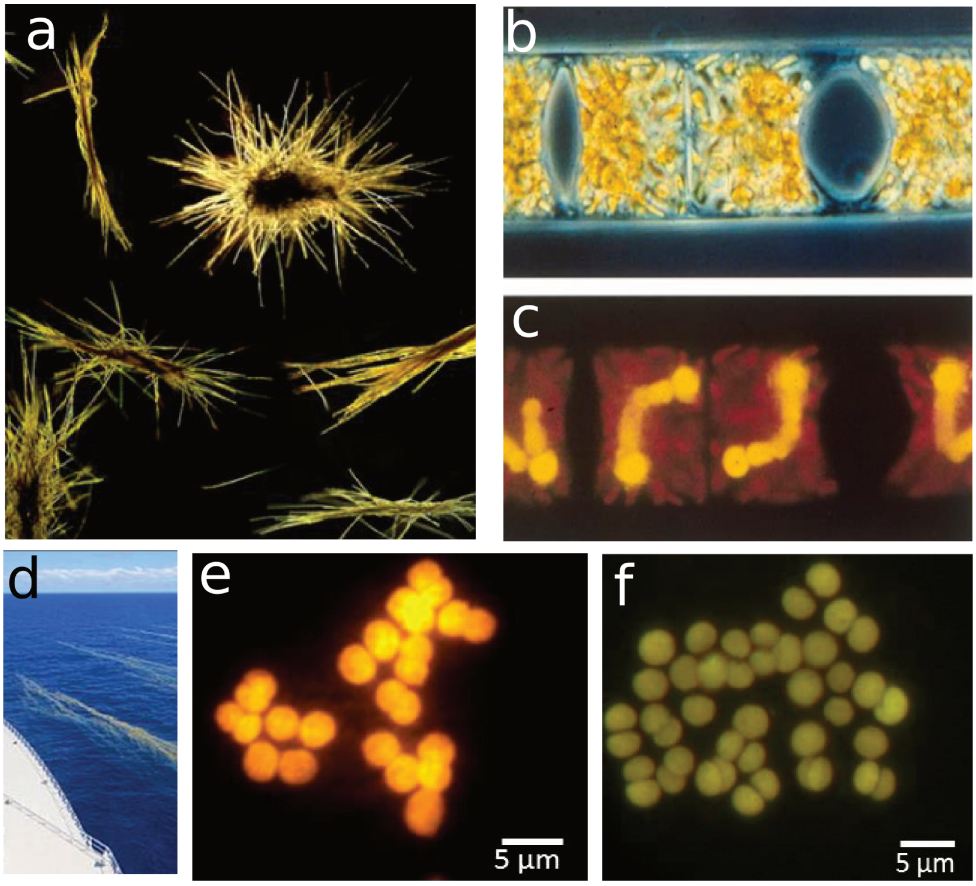

Figure 1.6 Photographies de principaux organismes diazotrophes marins. a) ***Trichodesmium*** vus au microscope, dont les colonies forment des fagots (tufts en anglais) ou des touffes (puffs en anglais ; Photo : B. Bergman, Stockholm University). b) et c) ***Richelia intracellularis*** dans la diatomée ***Hemiaulus sp.*** (Photo : D. Caron, Woods Hole Oceanographic Institution). d) efflorescence de ***Trichodesmium*** visible à l'oeil nu depuis un navire océanographique. e) UCYN-B (Photo : R. Foster, Stockholm University) et f) UCYN-C (Photo : S. Bonnet, MIO) prises en microscopie à épifluorescence.

1.4 Devenir de l'azote fixé : état de l'art

Jusqu'à maintenant, nous avons vu que la fixation de N_2 était la source majeure d'azote nouveau dans la couche productive de l'océan à l'échelle mondiale, et que différents facteurs environnementaux pouvaient contrôler la biogéographie de la diazotrophie dans l'océan mondial. Cependant, le devenir de cet azote dans l'océan a été très peu étudié, principalement à cause de verrous méthodologiques rendant complexes les recherches portant sur cette question. Dans les régions oligotrophes de l'océan, où la fixation de N_2 soutient la majeure partie de la production nouvelle, le devenir du N_2 fixé détermine potentiellement l'intensité de la production primaire et secondaire et par extension l'efficacité de la pompe biologique (Karl et al., 1997, 2012). Dans ces régions oligotrophes, aujourd'hui nous ne savons pas si cet azote dérivé de la diazotrophie, aussi dénommé DDN (Diazotroph-Derived N : Azote dérivé de la diazotrophie), est directement exporté hors de la couche euphotique, s'il est recyclé par la boucle microbienne en surface et/ou s'il est transféré à d'autres organismes planctoniques, favorisant le développement de la chaine trophique marine et l'export indirect de matière. Dans cette section nous faisons une synthèse bibliographique des travaux ayant permis de quantifier le devenir de l'azote fixé dans la couche euphotique et en dehors.

1.4.1 Relargage de l'azote fixé par les diazotrophes

Il y a presque 40 ans, l'idée que les diazotrophes puissent relarguer une part de l'azote qu'ils fixent a été émise (Devassy et al., 1978, 1979). Dans les milieux oligotrophes limités en azote, où les diazotrophes sont les plus abondants, cela peut avoir des répercussions importantes pour les organismes planctoniques environnants, la chaine trophique marine et les cycles biogéochimiques associés.
A la fin des années 1970, dans l'océan Indien, des premières études ont mesuré des concentrations élevées en DON et en NH_4^+ pendant et à la suite d'efflorescences de *Trichodesmium* (Devassy et al., 1978, 1979; Glibert and O'Neil, 1999). Ces premières observations suggéraient ainsi que les *Trichodesmium* relarguaient dans le compartiment dissous une partie du N_2 qu'ils avaient fixé, pouvant potentiellement être consommé par les communautés planctoniques environnantes. Les premières mesures directes de relargage réalisées dans les années 1990 ont montré que des colonies isolées de *Trichodesmium* provenant de l'océan Atlantique tropical relarguaient ~ 50 % du N_2 fixé (Glibert and Bronk, 1994). Des accumulations de DON et de NH_4^+ ont ensuite été observées à proximité d'efflorescences de *Trichodesmium* dans les océans Pacifique (Karl et al., 1997, 1992) et Atlantique (Lenes et al., 2001), bien que cela n'ait pas toujours été les cas (Bonnet et al., 2016a; Hansell and Carlson, 2001). Ce relargage a aussi été observé dans des cultures de *Trichodesmium* sénescentes (Mulholland and Capone, 2000), possiblement à cause du processus de mort programmée des cellules, se traduisant par une interruption brutale et synchronisée de l'activité métabolique (Berman-Frank et al., 2004).

De nombreuses études en cultures (Benavides et al., 2013; Berthelot et al., 2015a; Mulholland et al., 2004a; Mulholland and Bernhardt, 2005) et sur le terrain (Berthelot et al., 2017; Konno et al., 2010; Mulholland et al., 2004b, 2006) ont quantifié les taux de relargage, de *Trichodesmium* principalement, en utilisant comme méthode la différence entre la mesure des taux de fixation de N_2 brutes (méthode de réduction de l'acétylène (ARA), Dilworth, 1966) et les taux de fixation de N_2 nets (méthode du marquage isotopique au $^{15}N_2$, Montoya et al., 1996). Ces études ont montré que le N_2 fixé puis relargué dans le compartiment dissous, représente entre 10 et 80 % ($\sim$ 50 % en moyenne) de la fixation de N_2 totale. La remise en question de la fiabilité de la méthode du marquage isotopique au $^{15}N_2$ remet en question la fiabilité de cette méthode différentielle (Mohr et al., 2010), conduisant à une potentielle surestimation de l'azote fixé puis relargué. Une méthode alternative basée sur la mesure directe de l'enrichissement isotopique en ^{15}N du compartiment dissous après enrichissement en $^{15}N_2$ (Glibert and Bronk, 1994; Slawyk and Raimbault, 1995) permet de palier à ce biais méthodologique. Cette méthode présente l'intérêt de pouvoir obtenir un ratio entre la fixation de N_2 et l'azote fixé relargué en s'affranchissant d'une potentielle sous-estimation du flux relargué. Les études sur le terrain basées sur cette méthode ont montré que l'azote fixé puis relargué représente de 10 à plus de 80 % de la fixation de N_2 totale (Benavides et al., 2013; Berthelot et al., 2017; Glibert and Bronk, 1994; Konno et al., 2010). Au travers de différentes études menées sur cette thématique, il est montré que le relargage de l'azote fixé serait plus grand lorsque les *Trichodesmium* dominent la communauté diazotrophes (Berthelot et al., 2017; Bonnet et al., 2016a; Glibert and Bronk, 1994; Konno et al., 2010), que lorsque ce sont les UCYN (Benavides et al., 2013; Bonnet et al., 2016b). Enfin, les taux de relargage d'azote fixé sont généralement inférieurs dans les cultures monospécifiques (e.g. Benavides et al., 2013; Berthelot et al., 2015a) que sur le terrain (e.g. Berthelot et al., 2017; Bonnet et al., 2016b), et ceci est à mettre en relation avec des processus exogènes tels que la lise virale (Hewson et al., 2004; Ohki, 1999) et/ou le "sloopy feeding" (traduction littérale : broutage bâclé) par les copépodes (O'Neil, 1999) qui ont lieu en milieu naturel et sont réduits en culture.

1.4.2 Transfert d'azote fixé vers la chaine trophique planctonique

L'azote fixé puis relargué dans l'océan de surface est potentiellement disponible pour les communautés planctoniques environnantes. Devassy et al. (1979) dont l'étude a mis en évidence des concentrations élevées en DON et en NH_4^+ autour des efflorescences de *Trichodesmium*, ont aussi observé pour la première fois une augmentation de l'abondance en diatomées à la suite de déclin d'une efflorescence de *Trichodesmium*, suivi d'une augmentation de l'abondance de dinoflagellés, d'algues vertes et finalement de copépodes. Dans l'océan Atlantique tropical, des fortes abondances de phytoplancton non-diazotrophes ont été observées à la suite d'efflorescences de *Trichodesmium* (Mulholland et al., 2004b), et plus récemment Chen et al. (2011) ont montré une corrélation positive entre les

abondances de *Trichodesmium* et de diatomées dans le courant de Kurushio. Ainsi, ces différentes études mettent en avant un lien entre les efflorescences de diazotrophes et les organismes non-diazotrophes.

Une méthode utilisant le fractionnement de taille couplé à la méthode du marquage isotopique au $^{15}N_2$ a permis de montrer le transfert de N_2 fixé vers les organismes non diazotrophes. En présence d'une efflorescence de *Trichodesmium*, Bryceson and Fay (1981) ont montré que $\sim$ 10 % du N_2 fixé par les *Trichodesmium*, récupérés dans la fraction >30 μm, était transféré vers les organismes non-diazotrophes récupéré dans la fraction <30 μm. D'autres études ont montré que lors d'efflorescences de *Trichodesmium* (Garcia et al., 2007; Mulholland et al., 2004b), de *Nodularia* et de *Aphanizomenon* (Ohlendieck et al., 2000), 5 à 10 % de l'azote fixé était transféré vers le pico-phytoplancton.

Cependant, les méthodes utilisant le fractionnement de taille posent problème car elles ne permettent pas de différencier le N_2 transféré vers le pico-plancton non diazotrophe, du N_2 fixé par les diazotrophes picoplanctoniques, en particulier UCYN-A, qui est l'un des diazotrophes les plus abondants de l'océan (Luo et al., 2012). Ainsi, ces méthodes surestiment potentiellement le transfert d'azote fixé, et ne sont pas utilisables pour étudier le transfert du N_2 fixé par les UCYN. De plus, avec les méthodes de fractionnement de taille il n'est pas possible de savoir quels organismes non-diazotrophes (autotrophes ou hétérotrophes, petits ou grands organismes) bénéficient le plus du transfert de l'azote fixé.

Le développement et l'utilisation récente de la spectrométrie de masse des ions secondaires à haute résolution (nanoSIMS) couplée au marquage isotopique au $^{15}N_2$ et au tri cellulaire par cytométrie en flux (Berthelot et al., 2016; Bonnet et al., 2016a,b) a prouvé son efficacité pour quantifier spécifiquement le transfert de l'azote fixé vers les différents groupes phytoplanctoniques et les bactéries marines. En utilisant cette méthode lors d'une efflorescence de *Trichodesmium* dans l'océan Pacifique tropical sud-ouest, Bonnet et al. (2016a) ont montré qu'après 48 h entre 13 $\pm$ 2 et 48 $\pm$ 5 % du N_2 fixé était relargué dans le compartiment dissous et que 6 $\pm$ 1 à 8 $\pm$ 2 % de l'azote fixé était transféré vers les organismes non-diazotrophes, principalement vers les diatomées (45 $\pm$ 4 à 61 $\pm$ 38 %) et les bactéries (22 $\pm$ 27 à 38 $\pm$ 12 %). L'expérience en mésocosme VAHINE réalisée dans le lagon néo-calédonien lors d'une efflorescence d'UCYN-C (Bonnet et al., 2016b) a montré qu'après 48 h 16 $\pm$ 6 % du N_2 fixé était excrété dans le compartiment dissous, et 21 $\pm$ 4 % de l'azote fixé était transféré vers les organismes non-diazotrophes, principalement vers le pico-plancton (18 $\pm$ 4 %) et les diatomées (3 $\pm$ 2 %). Une étude comparative a été réalisée en stimulant des efflorescences de *Trichodesmium* et d'UCYN (Berthelot et al., 2016), et a montré que le transfert de l'azote fixé était deux fois plus important avec *Trichodesmium* qu'avec les UCYN.

Enfin, les différences de taux de transfert d'azote fixé qui peuvent résider entre les différentes expériences menées jusqu'à aujourd'hui laissent à penser que ces processus sont fortement dépendants de l'environnement dans lequel ils ont lieu, et de l'état physiologique des dia-

zotrophes. Cependant, l'étude et la quantification du transfert d'azote fixé de différents organismes diazotrophes vers différents groupes planctoniques n'a jamais été étudié dans l'océan ouvert, où la majorité de la fixation de N_2 mondiale à lieu.

1.4.3 Transfert vers le niveau trophique supérieur : le zooplancton

Concernant les plus hauts niveaux trophiques, les faibles signatures isotopiques naturelles $\delta^{15}N$ du zooplancton démontrent que la fixation de N_2 peut significativement contribuer aux besoins en azote du zooplancton dans les régions à forts taux de fixation de N_2 (Aberle et al., 2010; Hunt et al., 2016; Landrum et al., 2011; Loick-Wilde et al., 2012; Mompeán et al., 2013; Montoya et al., 2002; Sommer et al., 2006; Wannicke et al., 2013). Quelques études mentionnent le broutage actif des *Trichodesmium* par certains copépodes (*Micro-* and *Macrosetella* sp., O'Neil and Roman, 1992; O'Neil et al., 1996). Cependant, la consommation de *Trichodesmium* peut être toxique pour la plupart des brouteurs (Guo and Tester, 1994; Hawser and Codd, 1992; Hawser et al., 1992), et la faible signature isotopique $\delta^{15}N$ mesurée dans le zooplancton en présence de *Trichodesmium* provient probablement du transfert indirect vers les autres organismes planctoniques et par les processus de recyclage (Capone and Montoya, 2001; Capone et al., 1994; Letelier and Karl, 1996) plutôt que du broutage direct. Une étude récente basée sur le marquage isotopique au $^{15}N_2$ dans les eaux lagonaires de Nouvelle-Calédonie (Hunt et al., 2016) a montré que l'azote issu de la diazotrophie était plus efficacement transféré vers le zooplancton lorsque les UCYN dominent la communauté diazotrophes que lorsque ce sont les *Trichodesmium* et les DDA. Cela indiquerait que le transfert d'azote fixé vers le zooplancton est fortement lié à la structure des communautés de diazotrophes. Le zooplancton constitue une voie de transfert de la matière produite par l'activité planctonique, soit vers les plus hauts niveaux trophiques, soit une voie d'export vers les couches plus profondes de l'océan. Les études mentionnées précédemment montrent un possible transfert de l'azote fixé et de la production associé vers le zooplancton. Cependant, ce transfert d'azote fixé n'a jusqu'à aujourd'hui jamais été quantifié. L'étude qui a mis en évidence le transfert d'azote fixé provenant d'UCYN et de *Trichodesmium* a eu lieu en milieu lagonaire, ainsi il n'y a aujourd'hui aucune connaissance sur cette question en milieu hauturier où les assemblages planctoniques et la pression de broutage sont différents.

1.4.4 Export de l'azote fixé hors de la couche euphotique

Les organismes diazotrophes et non-diazotrophes, ainsi que les organismes supérieurs de la chaine marine trophique sont potentiellement exportables vers l'océan profond, transportant avec eux une quantité d'azote et de carbone sous forme organique. Il est aujourd'hui reconnu que l'apport d'azote nouveau par la fixation de N_2 soutient une part importante de la production marine à l'échelle globale, et que ce processus peut aussi

amorcer et soutenir la séquestration de CO_2 (Karl et al., 2003).
La faible signature isotopique $\delta^{15}N$ mesurée sur la matière particulaire recueillie dans les pièges à particules et dans la colonne d'eau des océans Pacifique tropical nord (Karl et al., 1997, 2012; Scharek et al., 1999a,b) et Atlantique (Altabet, 1988; Bourbonnais et al., 2009; Knapp et al., 2005; Mahaffey et al., 2003) indiquent que jusqu'à 60 % de l'azote exporté provient de la fixation de N_2, et montre ainsi qu'une part du N_2 fixé par les diazotrophes est exporté hors de la couche euphotique. Plus récemment, l'étude de Böttjer et al. (2017) a révélé que dans la gyre de l'océan Pacifique tropical nord, la fixation de N_2 supporte entre 26 et 47 % de l'export d'azote particulaire sur une période de 9 ans à la station ALOHA. L'efficacité d'export de l'azote et du carbone associé à la fixation de N_2 semble être dépendant des organismes diazotrophes en présence dans la colonne d'eau.
Les *Trichodesmium* sont rarement retrouvés dans les pièges à particules (Chen et al., 2003; Walsby, 1992) et sont préférentiellement reminéralisés en surface (Scharek et al., 1999a). Le maintien des populations de *Trichodesmium* en surface est probablement du à la présence de vacuoles gazeuses qui leur permettent de contrôler leur flottabilité (Walsby, 1992; White et al., 2006).
Les DDAs ont une efficacité d'export élevée contrairement aux *Trichodesmium*. De forts flux d'export associés à la présence de DDAs ont été observés dans le panache du fleuve Amazone (Subramaniam et al., 2008). Des efflorescences de DDAs sont régulièrement observées durant la période estivale à la station ALOHA, et sont associées à des pics d'export de matière particulaire (Karl et al., 2012). Lorsqu'ils sont exportés vers les couches plus profondes de l'océan, ces organismes séquestrent avec eux de l'azote et du carbone issus de la fixation de N_2 et de la photosynthèse.
Enfin, l'export associé aux UCYN est très peu étudié à ce jour, alors que ces organismes peuvent contribuer à la fixation de N_2 autant que *Trichodesmium* dans certaines régions de l'océan. A la station ALOHA, White et al. (2012) ont montré que l'export de carbone induit par la fixation de N_2 de UCYN peut représenter jusqu'à 18 % de l'export total. Plus récemment, Bonnet et al. (2016b) ont montré que les UCYN peuvent être exportées après un processus d'agrégation qui rend la sédimentation plus efficace. A l'heure actuelle, les études montrent que la fixation de N_2 soutient une part de l'azote exporté, mais elles ne permettent pas de savoir si cet azote fixé a été exporté directement (i.e. par sédimentation des organismes diazotrophes eux même), ou indirectement, (i.e. par sédimentation des organismes s'étant développés à partir d'azote provenant de la diazotrophie). La réponse à cette question représente un challenge méthodologique car elle nécessite de quantifier l'abondance de diazotrophes dans les pièges à particules, et de la comparer à l'abondance de diazotrophes dans la colonne d'eau, en suivant la même masse d'eau pendant plusieurs jours.

Cette synthèse bibliographique met en évidence le rôle central de la fixation de N_2 dans le fonctionnement des écosystèmes marins oligotrophes, où la diazotrophie représente la source majeure d'azote nouveau dans ces régions pauvres en nutriments. Cet azote nouveau issue de la diazotrophie fertilise l'océan de surface et soutient la production nouvelle ainsi que l'export de matière hors de la couche euphotique. Cependant, les voies de transfert et d'export, direct ou indirect sont très peu documentées, et le sont principalement en zones côtières. Ce manque de connaissances s'explique par l'absence de méthodes permettant de suivre le transfert de l'azote fixé dans le réseau trophique jusqu'à très récemment.

1.5 Objectifs de la thèse

Si aujourd'hui il est admis que la fixation de N_2 joue un rôle de fertilisant naturel dans l'océan de surface, le devenir du N_2 dans la colonne d'eau et dans la chaine planctonique marine reste très mal compris, et non quantifié. L'objectif de ce travail de thèse est d'apporter un éclairage sur la compréhension du devenir du N_2 fixé par les diazotrophes en milieu hauturier. Ce travail de thèse s'est déroulé dans le cadre de la campagne océanographique OUTPACE, qui a eu lieu dans l'océan Pacifique tropical sud-ouest. Cette région a jusqu'à maintenant été très peu échantillonnée, et très peu étudiée en ce qui concerne la fixation de N_2. Le travail de thèse présenté ici se concentre sur les objectifs scientifiques suivants :

(1) Quantifier la fixation de N_2 et identifier les principaux acteurs de la diazotrophie ;
(2) Évaluer l'influence de la fixation de N_2 sur la production primaire et sur l'export de carbone ;
(3) Identifier les voies de transfert par lesquelles la fixation de N_2 fertilise naturellement l'océan Pacifique tropical sud-ouest.

Cette thèse a été réalisée dans le cadre du projet OUTPACE (Oligotrophic to UlTra-oligotrophic PACific Experiment), coordonné par Thierry Moutin et Sophie Bonnet, et financée par l'Agence Nationale de la Recherche française (ANR), le programme LEFE-CyBER (CNRS-INSU), l'IRD et le CNES, dont les principaux objectifs de recherche sont décrit à la page suivante.

Le manuscrit s'articule autour de trois chapitres visant à répondre à chacune des trois problématiques énoncées ci-dessus par des stratégies indépendantes et complémentaires, le tout réalisé lors de la campagne océanographique du programme OUTPACE.
- Afin de répondre à la question scientifique **(1)**, nous avons dans un premier temps synthétisé les données de fixation de N_2 des dernières campagnes océanographiques qui ont eu lieu dans le Pacifique tropical sud-ouest, et nous les avons comparées aux résultats de la base de donnée mondiale MAREDAT. Dans un second temps, nous nous sommes concentrés sur la campagne océanographique OUTPACE, et nous avons mesuré la fixation de N_2 spécifique à chacun des groupes dominants de diazotrophes. De plus, nous nous sommes attachés à évaluer le potentiel impact biogéochimique des différents paramètres environnementaux sur les différents groupes de diazotrophes en présence. Les résultats obtenus ont fait l'objet de deux publications, l'une publiée sous forme de Commentaire dans la revue *PNAS*. L'autre a été publié dans le journal *Biogeosciences*. Ces deux publications sont présentées dans le chapitre 2.
- Pour répondre à la problématique scientifique **(2)**, nous avons réalisé des bilans d'azote dans la couche éclairée de l'océan et évalué le rôle de la fixation de N_2 sur la production

primaire et sur l'export de carbone. Le rôle de la fixation de N_2 a été évalué à courte échelle de temps et d'espace lors de la campagne océanographique OUTPACE en utilisant une stratégie lagrangienne. Les résultats obtenus ont fait l'objet d'un article publié dans le journal *Biogeosciences* présenté dans le chapitre 3.
- La stratégie utilisée pour répondre à la question **(3)** a consisté à réaliser des expériences en microcosmes à bord, aux mêmes stations où ont été réalisés les bilans d'azote, en couplant l'utilisation du marquage isotopique, du tri-cellulaire et du nanoSIMS, afin de caractériser et quantifier le transfert de N_2 fixé par les diazotrophes vers les organismes planctoniques non-diazotrophes en milieu hauturier. Cette étude est présentée dans le chapitre 4, et a fait l'objet d'une publication dans le journal *Biogeosciences*.

La figure conceptuelle (Fig. 1.7) représente de manière schématique les questionnements scientifiques de ce travail. La question (1), concernant l'intensité et les acteurs de la fixation d'azote est représentée par le cube jaune, et correspond au chapitre 2. La question (2) concernant les bilans d'azote et l'export est représentée par les cubes jaune et orange, et correspond au chapitre 3. Enfin la question (3), relevant du devenir de l'azote fixé dans la chaine trophique est représentée par les cubes jaune et violet, et correspondent au chapitre 4. La synthèse ainsi que la mise en perspective des résultats dans un contexte plus général est disponible dans le chapitre 5 de ce manuscrit.

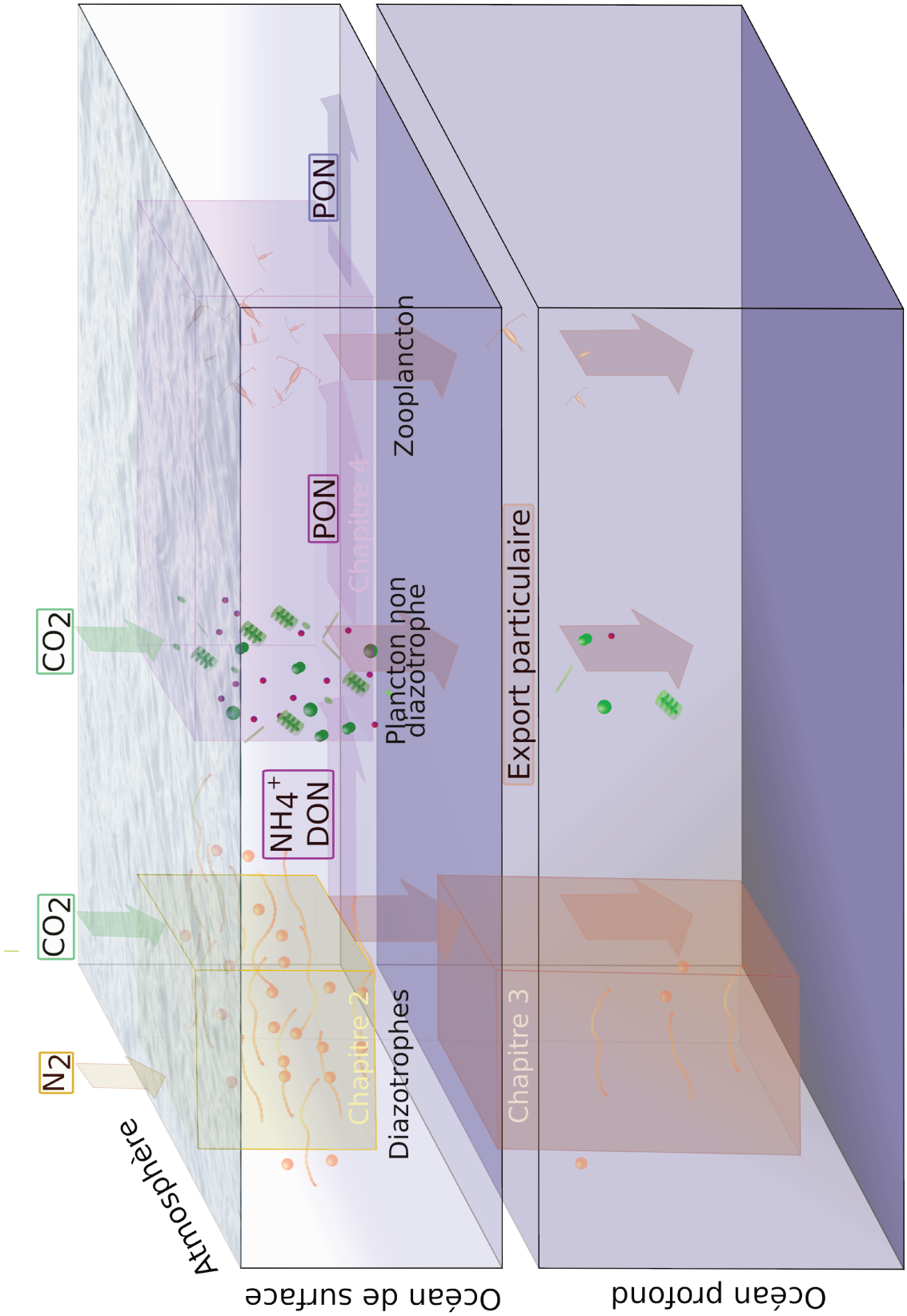

Figure 1.7 Représentation schématique du devenir de l'azote fixé par les diazotrophes dans la chaine trophique marine et de son export hors de la couche de surface. Les boites et les flèches colorées font références aux chapitres dont elles font l'objet d'étude : jaune pour le chapitre 2, orange pour le chapitre 3 et violet pour le chapitre 4.

Le projet OUTPACE

Durée du projet : 2014-2018
Coordination : Thierry Moutin (AMU-MIO) et Sophie Bonnet (IRD-MIO)
Financement (665 k€) : ANR Grands défis sociétaux, INSU-LEFE-CYBER, CNES, IRD, GOPS, MIO-Actions Sud
Nombre de scientifiques impliqués : 60 dont 8 thèses.
Laboratoires français impliqués : MIO, LOV, LEGOS, LOCEAN, LPO, EIO
Laboratoires étrangers impliqués : Columbia University (USA), University of South Pacific (Fidji), University Bar Ilan (Israel), Florida State University (USA), Woods Hole Oceanographic Institution (USA), University of Stockholm (Suède)

Cette thèse s'inscrit intégralement dans le cadre du projet **OUTPACE** (Oligotrophic to UlTra-oligotrophic PACific Experiment) dont les objectifs scientifiques sont :
- Fournir une description du contexte biogéochimique et de la diversité biologique en différentes zones de l'océan Pacifique tropical sud-ouest pendant la période de stratification maximale (i.e. l'été austral) ;
- Étudier la production et le devenir de la matière organique, et en particulier la production soutenue par les organismes diazotrophes, dans trois environnements contrastés ;
- Obtenir une représentation des principaux flux biogéochimiques et de la dynamique de la chaîne trophique planctonique.

Numéro spécial en cours de *Biogeosciences*
Éditeurs : Thierry Moutin, Sophie Bonnet, Kelvin Richards, Douglas G. Capone, Emilio Maranon, Laurent Mémery
`https://www.biogeosciences.net/special_issue894.html`

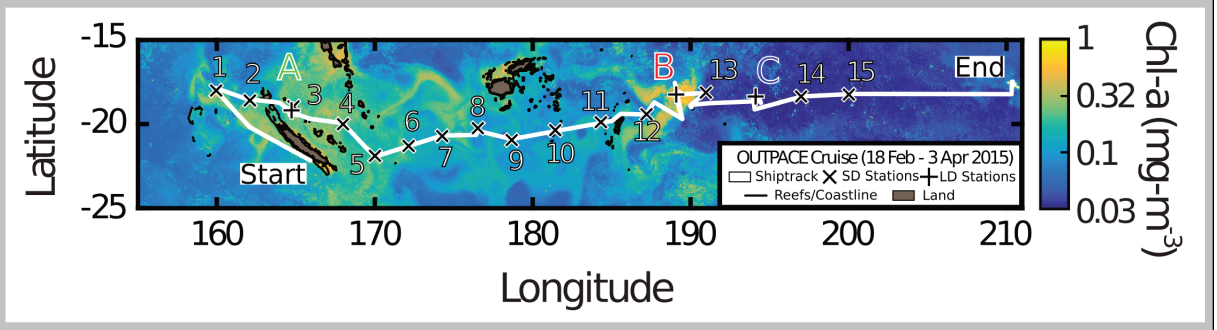

Transect de la campagne OUTPACE de la Nouvelle Calédonie à la Polynésie française avec la localisation des stations courtes (1 à 15) et longues (A, B et C), superposé à la carte de la concentration quasi-lagrangienne en chlorophylle de surface (A. de Verneil).

Chapitre 2

L'océan Pacifique tropical sud-ouest, un 'hot spot' de fixation de N_2 - Quantification et distribution biogéographique de la diazotrophie

Sommaire

2.1 Avant-propos

Durant les deux dernières décennies les recherches sur la fixation de N_2 se sont intensifiées, mais comme nous l'avons vu dans le chapitre introductif, l'effort de recherche est très hétérogène sur l'ensemble de l'océan mondial. La communauté scientifique a intensément étudié la fixation de N_2 dans les océans Atlantique nord (Benavides and Voss, 2015) et Pacifique nord (e.g. Böttjer et al., 2017), où ont été implantées les stations HOT et BATS permettant de suivre à long terme l'évolution des processus biogéochimiques dans ces régions. Durant les dix dernières années, la communauté scientifique a intensément échantillonné le Pacifique tropical sud-est à la suite du questionnement scientifique sur le couplage spatial entre les processus de pertes et gains d'azote pour l'océan (Deutsch et al., 2007). D'autres régions de l'océan mondial sont restées sous échantillonnées comme le Pacifique tropical sud-ouest (Luo et al., 2012). Pourtant, historiquement, la présence d'organismes diazotrophes avait été remarquée puisque James Cook au XVIIIe siècle mentionnait déjà dans ses carnets de bord des observations de colonies de *Trichodesmium* par le botaniste Joseph Banks en mer de Corail, appelées à l'époque 'sciure de mer'. Au siècle suivant, lors de son voyage autour du monde à bord du Beagle, Charles Darwin mentionnait lui aussi la présence de colonie de *Trichodesmium*. Il y a une vingtaine d'année, Dupouy et al. (2000) ont observé des variations annuelles des concentrations en chlorophylle depuis l'espace, attribuant les fortes valeurs estivales à des efflorescences de *Trichodesmium*, par la suite confirmées par des observations aériennes. Les quelques campagnes océanographiques ayant récemment eu lieu dans la région ouest du Pacifique tropical sud-ouest, en mer des Salomon, de Bismarck (Berthelot et al., 2017; Bonnet et al., 2009, 2015) et de Arafura (Messer et al., 2015; Montoya et al., 2004) ont reporté des taux de fixation de N_2 élevés, principalement dus aux températures de surface supérieures à 25 $^\circ$C et aux apports continus de nutriments d'origines terrigènes et volcaniques (Labatut et al., 2014; Radic et al., 2011). La région plus centrale du Pacifique tropical sud-ouest, comprenant les archipels Mélanésiens (Nouvelle Calédonie, Vanuatu, Fiji) et jusqu'à la faille de Tonga, a encore moins été échantillonnée. Dans les eaux de Nouvelle Calédonie, de forts taux de fixation de N_2 (Garcia et al., 2007) et de fortes abondances de *Trichodesmium* (Rodier and Le Borgne, 2008) ont été mesurés, et mis en relation avec la disponibilité en phosphate dans le milieu (Moutin et al., 2005; Van Den Broeck et al., 2004). Une étude longitudinale, traversant les archipels Mélanésiens a mis en évidence de forts taux de fixation de N_2 en lien avec les apports de nutriments par lessivage des sols (Shiozaki et al., 2014). Ces observations semblent indiquer que l'océan Pacifique tropical sud-ouest, et plus particulièrement la région des archipels Mélanésiens, est le siège d'une intense fixation de N_2. Les raisons pour lesquelles cette région serait une niche écologique favorable pour les diazotrophes restent toujours méconnues. Pour répondre à ce type de question il est usuel d'étudier les liens statistiques existant entre la variation spatiale de la fixation de N_2 et celle des paramètres environnementaux communément

admis pour contrôler ce processus : concentrations en Fe, NO_3^- et phosphate inorganique dissous (DIP) de surface, dépôts atmosphériques, température de surface, rayonnement solaire moyen dans la couche de mélange. Le manque de données de fixation de N_2 dans la région et celles concernant la distribution spatiale des paramètres environnementaux pouvant contrôler la fixation de N_2, dans la région sont principalement à l'origine de cette lacune cognitive.

Ce chapitre s'articule autour des campagnes océanographiques réalisées ces dernières années dans l'océan Pacifique tropical sud-ouest, et plus particulièrement lors de la campagne OUTPACE sous forme de deux articles. - Le premier article est une synthèse des données de taux de fixation de N_2 mesurés lors de 5 campagnes océanographiques réalisées dans l'océan Pacifique tropical sud-ouest par l'équipe 'diazotrophie' du MIO. Les taux de fixation de N_2 mesurés dans cette région ont été comparés à ceux mesurés dans le reste de l'océan mondial, compilés dans la base de données globale MAREDAT (Luo et al., 2012). Dans le cadre de ma thèse, j'ai participé à la campagne océanographique OUTPACE et participé à l'échantillonnage des données de fixation de N_2 relatives à cette campagne. Je n'ai cependant pas participé aux autres campagnes (MoorSPICE, PANDORA et BIFURCATION) qui ont eu lieu avant le début de ma thèse.
- Le second article est centré sur les données de la campagne océanographique OUTPACE, et présente de manière détaillée les mesures de fixation de N_2 à la fois de la communauté totale, mais également des taux spécifiques à chaque groupe majeur de diazotrophe. De plus, cet article évalue le potentiel impact biogéochimique des différents paramètres environnementaux sur la biogéographie de la diazotrophie dans la région.

2.2 L'océan Pacifique tropical sud-ouest : un hotspot de diazotrophie

2.2.1 Résumé

Ce travail synthétise les données de fixation de N_2 des campagnes océanographiques OUTPACE, MoorSPICE, PANDORA, BIFURCATION et EUC-Fe ayant eu lieu dans l'océan Pacifique tropical sud-ouest. Ces données sont comparées aux données de fixation de N_2 de la base de données globale MAREDAT. Les résultats montrent que l'océan Pacifique tropical sud-ouest est un hot spot de diazotrophie, présentant des taux de fixation de N_2 de 570 μmol N m^{-2} d^{-1} en moyenne. Ces taux sont 3 à 4 fois plus forts que les taux prédits par les modèles dans cette région ($\sim$ 150-200 μmol N m^{-2} d^{-1}, Gruber, 2016) et dans la gamme haute ($\sim$ 100-1000 Luo et al., 2012) des taux recensés dans la base de données mondiale MAREDAT.

2.2.2 Article # 1 : Un hot spot de fixation de N_2 dans l'océan Pacifique tropical sud-ouest plaide pour un découplage spatial entre la fixation de N_2 et la dénitrification. *Bonnet et al., 2017.*

Hot spot of N_2 fixation in the western tropical South Pacific pleads for a spatial decoupling between N_2 fixation and denitrification

Sophie Bonnet[1], Mathieu Caffin[1], Hugo Berthelot[1] and Thierry Moutin[1]

[1]Aix Marseille Université, CNRS/INSU, Université de Toulon, IRD, Mediterranean Institute of Oceanography (MIO) UM110, 13288, Marseille, France

Publié dans *PNAS* en Mars 2017

LETTER

Hot spot of N_2 fixation in the western tropical South Pacific pleads for a spatial decoupling between N_2 fixation and denitrification

Sophie Bonnet[a,b,1], Mathieu Caffin[b], Hugo Berthelot[b], and Thierry Moutin[b]

Nitrogen (N) is the building block of life. Quantifying the sources and sinks of N to the ocean is essential for predicting its productivity and potential carbon sequestration. In his paper, Gruber (1) seeks for "elusive marine nitrogen fixation" following results from Knapp et al. (2), who measured unexpectedly low N input through N_2 fixation in the eastern tropical South Pacific (ETSP), seriously bringing into question the proposed close spatial coupling between N input (through N_2 fixation) and loss (through denitrification) (3). Here, we compile data from recently published and unpublished studies revealing a hot spot of N_2 fixation in the western tropical South Pacific (WTSP) arguing for a spatial decoupling between N sources and sinks in the South Pacific.

Based on four cruises performed between 2012 and 2015 during austral winter and summer conditions, with a total of more than 600 $^{15}N_2$ incubations-based measurements, and particularly a 4,000-km zonal transect at ~20°S in 2015 (OUTPACE cruise: dx.doi.org/10.17600/15000900), we report N_2 fixation rates of 570 μmol $N{\cdot}m^{-2}{\cdot}d^{-1}$ on average over the WTSP (Fig. 1). They are far higher than model predictions for the area (~150–200 μmol $N{\cdot}m^{-2}{\cdot}d^{-1}$) (1) and in the upper range (100–1,000 μmol $N{\cdot}m^{-2}{\cdot}d^{-1}$) of rates gathered in the global N_2 fixation Marine Ecosytem Data (MAREDAT) database (4).

The close spatial coupling between N sources and sinks in the Pacific was hypothesized because denitrification in the oxygen minimum zones (OMZs) creates excess phosphorus (P) surface waters (nitrate-poor but phosphate-rich), that is, potential ideal niches for N_2 fixation. Downstream of the OMZs, surface waters were supposed to gradually lose this excess P through N_2 fixation, restoring the system to a "Redfieldian" balance (3). However, predicted and actual measurements of N_2 fixation in the South Pacific are not in agreement (1): unexpected low N_2 fixation rates are measured in the ETSP (2) and in the South Pacific Gyre (2, 5), and we report here high N_2 fixation rates in the WTSP (Fig. 1). Such a hot spot of N_2 fixation in the WTSP is likely due to the alleviation of iron limitation, a major component of the nitrogenase enzyme that catalyzes N_2 fixation (6), when waters originating from the east reach the WTSP through the South Equatorial Current (SEC) (Fig. 1). Surface iron concentrations are indeed higher in the WTSP [average, 0.57 nM (7)] than in the central and ETSP [~0.10–0.30 nM (8)], where it limits N_2 fixation (9). The WTSP appears to provide optimal environmental conditions for diazotrophs to bloom extensively, but this region deserves special attention to better identify the reasons for such an ecological success.

Such a hot spot in the WTSP sheds light on the elusive marine nitrogen fixation in the Pacific (1) and indicates that this region may play an obvious role in replenishing the Pacific Ocean in N, which could partly counterbalance the N losses in the ETSP.

Acknowledgments

This research is a contribution of the OUTPACE project (dx.doi.org/10.17600/15000900) managed by the MIO funded by the Agence Nationale de la Recherche (Grant ANR-14-CE01-0007-01), the Les enveloppes fluides de l'Environnement (LEFE)-CyBER program [CNRS-Institut National des Sciences de l'Univers (INSU)], the IRD, the Grand Observatoire du Pacifique Sud (GOPS) program (IRD), and the Centre National d'Etudes Spatiales (CNES) (BC T23, ZBC 4500048836), MoorSPICE (DOI: 10.7284/903044), PANDORA (dx.doi.org/10.17600/12010050), and BIFURCATION (dx.doi.org/10.17600/12100100) projects managed by Laboratoire d'Etudes en Géophysique et Océanographie Spatiales (LEGOS) and SCRIPPS Institution of Oceanography, part of the Climate and Ocean: Variability, Predictability and Change (CLIVAR)/Southwest Pacific Ocean Circulation and Climate Experiment (SPICE) International Program, and funded by NSF Grant OCE1029487, Agence Nationale de la Recherche Grant ANR-09-BLAN-0233-01, and INSU/LEFE projects Solwara and SPICEMoor.

[a]Aix Marseille Université, Toulon Université, CNRS, Institut de Recherche pour le Développement (IRD), Observatoire des Sciences de l'Univers Pythéas, Mediterranean Institute of Oceanography (MIO), Unité Mixte 110, 98848 Noumea, New Caledonia; and [b]Aix Marseille Université, Toulon Université, CNRS, IRD, Observatoire des Sciences de l'Univers Pythéas, MIO, Unité Mixte 110, 13288 Marseille, France

Author contributions: S.B. and T.M. designed research; S.B., M.C., and H.B. performed research; S.B. and M.C. contributed new reagents/analytic tools; S.B. and M.C. analyzed data; H.B. and T.M. added suggestions on the paper; and S.B. wrote the paper.

The authors declare no conflict of interest.

[1]To whom correspondence should be addressed. Email: sophie.bonnet@univ-amu.fr.

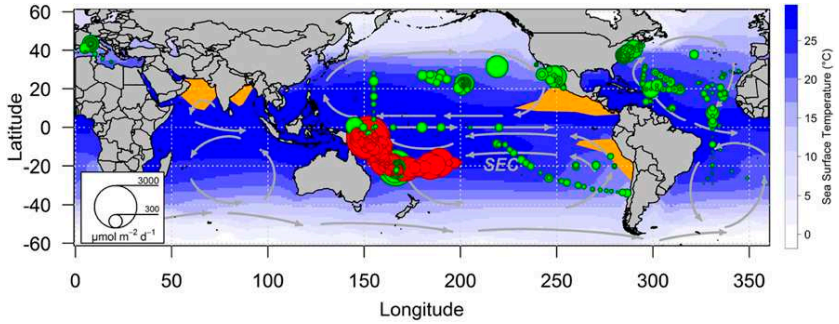

Fig. 1. N_2 fixation in the world's oceans quantified using $^{15}N_2$ incubation-based measurements. Green dots: integrated N_2 fixation rates (in micromoles of nitrogen per square meter per day) from the MAREDAT database (4) and Knapp et al. (2). Red dots: N_2 fixation rates quantified at 57 stations (WTSP) including data from Bonnet et al. (2015), DOI 10.1002/2015GB005117, using either the $^{15}N_2$ bubble addition method or the enriched seawater method (10). To ensure accurate rate calculations, the $^{15}N/^{14}N$ ratio of the N_2 pool in the incubation bottles was systematically measured. Discrete rate measurements were depth integrated over the photic layer using trapezoidal integration. Gray arrows: main surface currents. SEC: South Equatorial Current. Orange shaded areas: main OMZs.

1 Gruber N (2016) Elusive marine nitrogen fixation. *Proc Natl Acad Sci USA* 113(16):4246–4248.
2 Knapp AN, Casciotti KL, Berelson WM, Prokopenko MG, Capone DG (2016) Low rates of nitrogen fixation in eastern tropical South Pacific surface waters. *Proc Natl Acad Sci USA* 113(16):4398–4403.
3 Deutsch C, Sarmiento JL, Sigman DM, Gruber N, Dunne JP (2007) Spatial coupling of nitrogen inputs and losses in the ocean. *Nature* 445(7124):163–167.
4 Luo YW, et al. (2012) Database of diazotrophs in global ocean: Abundances, biomass and nitrogen fixation rates. *Earth Syst Sci Data* 5(1):47–106.
5 Moutin T, et al. (2008) Phosphate availability and the ultimate control of new nitrogen input by nitrogen fixation in the tropical Pacific Ocean. *Biogeosciences* 5(1): 95–109.
6 Raven JA (1988) The iron and molybdenum use efficiencies of plant growth with different energy, carbon and nitrogen source. *New Phytol* 109:279–287.
7 Campbell L, Carpenter EJ, Montoya JP, Kustka AB, Capone DG (2005) Picoplankton community structure within and outside a *Trichodesmium* bloom in the southwestern Pacific Ocean. *Vie Milieu* 55:185–195.
8 Blain S, Bonnet S, Guieu C (2008) Dissolved iron distribution in the tropical and subtropical South Eastern Pacific. *Biogeosciences* 5:269–280.
9 Dekaezemacker J, et al. (2013) Evidence of active dinitrogen fixation in surface waters of the eastern tropical South Pacific during El Nino and La Nina events and evaluation of its potential nutrient controls. *Global Biogeochem Cycles* 27:1–12.
10 Mohr W, Grosskopf T, Wallace DW, LaRoche J (2010) Methodological underestimation of oceanic nitrogen fixation rates. *PLoS One* 5(9):e12583.

2.3 Acteurs et biogéographie de la diazotrophie dans l'océan Pacifique tropical sud-ouest

2.3.1 Résumé

Dans cette étude, nous présentons les taux de fixation de N_2 le long d'un transect de $\sim$ 4000 km dans l'océan Pacifique tropical sud-ouest, une région particulièrement sous échantillonnée de l'océan mondial. Les échantillons d'eau ont été collectés dans la couche euphotique le long d'un transect ouest-est de 160 $^\circ$ E à 160 $^\circ$ O, couvrant ainsi des régimes trophiques contrastés, allant des eaux oligotrophes des archipels Mélanésiens aux eaux ultra-oligotrophes de la gyre du Pacifique sud. La fixation de N_2 a été détectée aux 17 stations échantillonnées, présentant des taux intégrés moyens de 631 $\pm$ 286 μmol N m^{-2} d^{-1} dans les eaux des archipels Mélanésiens (de 196 à 1153 μmol N m^{-2} d^{-1}) et de 85 $\pm$ 79 μmol N m^{-2} d^{-1} dans les eaux de la gyre du Pacifique sud (de 18 à 172 μmol N m^{-2} d^{-1}). Deux cyanobactéries, les longues filamenteuses *Trichodesmium* et les plus petites UCYN-B, dominaient la communauté diazotrophe énumérée ($>$ 80 %) et les comptages de gène *nif*H (cDNA $>$ 105 copies *nif*H L^{-1}) dans la région MA. Les analyses isotopiques à l'échelle cellulaire réalisées à certaines stations, par spectrométrie de masse des ions secondaires à l'échelle nanométrique (nanoSIMS), ont révélé que *Trichodesmium* était tout le temps le principal contributeur de la fixation de N_2 dans la région des archipels Mélanésiens, comptant pour 47,1–83,8 % de la fixation de N_2 totale particulaire. Les facteurs environnementaux pouvant expliquer le plus plausiblement les taux de fixation de N_2 exceptionnellement hauts dans la région des archipels Mélanésiens sont discutés en détail, en soulignant le rôle de la disponibilité en micro et macro nutriments (e.g. Fe), de la température de surface et de la courantologie.

2.3.2 Article # 2 : Caractérisation en profondeur de l'activité diazotrophique à travers l'océan Pacifique tropical sud-ouest, un hot spot de fixation de N_2. *Bonnet et al., 2018.*

In-depth characterization of diazotroph activity across the western tropical South Pacific hotspot of N_2 fixation (OUTPACE cruise)

Sophie Bonnet[1 2], Mathieu Caffin[2], Hugo Berthelot[2 3], Olivier Grosso[2], Mar Benavides[4], Sandra Helias-Nunige[2], Cécile Guieu[5 6], Marcus Stenegren[7], and Rachel Ann Foster[7].

[1]Aix Marseille Université, CNRS/INSU, Université de Toulon, IRD, Mediterranean Institute of Oceanography (MIO) UM110, 98800, Nouméa, New Caledonia

[2]Aix Marseille Université, CNRS/INSU, Université de Toulon, IRD, Mediterranean Institute of Oceanography (MIO) UM110, 13288, Marseille, France

[3]Laboratoire des sciences de l'environnement marin, IUEM, Université de Brest-UMR 6539 CNRS/UBO/IRD/Ifremer, Plouzané, France

[4]Marine Biology Section, Department of Biology, University of Copenhagen, 3000 Helsingor, Denmark

[5]Sorbonne Universités, UPMC Université Paris 06, CNRS, Laboratoire d'Océanographie de Villefranche (LOV), 06230 Villefranche-sur-Mer, France

[6]Center for Prototype Climate Modeling, New York University Abu Dhabi, P.O. Box 129188, Abu Dhabi, United Arab Emirates

[7]Department of Ecology, Environment, and Plant Sciences, Stockholm University, Stockholm, 10690, Sweden

Publié dans *Biogeosciences* en Juillet 2018

Biogeosciences, 15, 4215–4232, 2018
https://doi.org/10.5194/bg-15-4215-2018

Biogeosciences Open Access EGU

In-depth characterization of diazotroph activity across the western tropical South Pacific hotspot of N_2 fixation (OUTPACE cruise)

Sophie Bonnet[1,2], Mathieu Caffin[2], Hugo Berthelot[2,3], Olivier Grosso[2], Mar Benavides[4], Sandra Helias-Nunige[2], Cécile Guieu[5,6], Marcus Stenegren[7], and Rachel Ann Foster[7]

[1]Aix Marseille Univ., Université de Toulon, CNRS, IRD, MIO UM 110, 13288, Noumea, New Caledonia
[2]Aix Marseille Univ., Université de Toulon, CNRS, IRD, MIO UM 110, 13288, Marseille, France
[3]Laboratoire des sciences de l'énvironnement marin, IUEM, Université de Brest-UMR 6539 CNRS/UBO/IRD/Ifremer, Plouzané, France
[4]Marine Biology Section, Department of Biology, University of Copenhagen, 3000 Helsingør, Denmark
[5]Sorbonne Universités, UPMC Université Paris 06, CNRS, Laboratoire d'Océanographie de Villefranche (LOV), 06230 Villefranche-sur-Mer, France
[6]Center for Prototype Climate Modeling, New York University Abu Dhabi, P.O. Box 129188, Abu Dhabi, United Arab Emirates
[7]Department of Ecology, Environment, and Plant Sciences, Stockholm University, Stockholm, 10690, Sweden

Correspondence: Sophie Bonnet (sophie.bonnet@univ-amu.fr)

Received: 29 December 2017 – Discussion started: 11 January 2018
Revised: 15 May 2018 – Accepted: 4 June 2018 – Published: 12 July 2018

Abstract. Here we report N_2 fixation rates from a $\sim$ 4000 km transect in the western and central tropical South Pacific, a particularly undersampled region in the world ocean. Water samples were collected in the euphotic layer along a west to east transect from 160° E to 160° W that covered contrasting trophic regimes, from oligotrophy in the Melanesian archipelago (MA) waters to ultra-oligotrophy in the South Pacific Gyre (GY) waters. N_2 fixation was detected at all 17 sampled stations with an average depth-integrated rate of $631 \pm 286\,\mu mol\,N\,m^{-2}\,d^{-1}$ (range 196–1153 $\mu mol\,N\,m^{-2}\,d^{-1}$) in MA waters and of $85 \pm 79\,\mu mol\,N\,m^{-2}\,d^{-1}$ (range 18–172 $\mu mol\,N\,m^{-2}\,d^{-1}$) in GY waters. Two cyanobacteria, the larger colonial filamentous *Trichodesmium* and the smaller UCYN-B, dominated the enumerated diazotroph community (> 80 %) and gene expression of the *nifH* gene (cDNA > 10^5 *nifH* copies L^{-1}) in MA waters. Single-cell isotopic analyses performed by nanoscale secondary ion mass spectrometry (nanoSIMS) at selected stations revealed that *Trichodesmium* was always the major contributor to N_2 fixation in MA waters, accounting for 47.1–83.8 % of bulk N_2 fixation. The most plausible environmental factors explaining such exceptionally high rates of N_2 fixation in MA waters are discussed in detail, emphasizing the role of macro- and micro-nutrient (e.g., iron) availability, seawater temperature and currents.

1 Introduction

In the ocean, nitrogen (N) availability in surface waters controls primary production and the export of organic matter (Dugdale and Goering, 1967; Eppley and Peterson, 1979; Moore et al., 2013). The major external source of new N to the surface ocean is biological di-nitrogen (N_2) fixation (100–150 $Tg\,N\,yr^{-1}$, Gruber, 2008), the reduction of atmospheric gas (N_2) dissolved in seawater into ammonia (NH_3^+). The process of N_2 fixation is mediated by diazotrophic organisms that possess the nitrogenase enzyme, which is encoded by a suite of nif genes. These organisms provide new N to the surface ocean and act as natural fertilizers, contributing to sustaining ocean productivity and eventually carbon (C) sequestration through the N_2-primed prokaryotic C pump (Caffin et al., 2018a; Karl et al., 2003, 2012). This N source is continuously counteracted by N losses, mainly driven by denitrification and anammox, which convert reduced forms of N (nitrate, NO_3^-, nitrite NO_2^-, NH_4^+) into N_2. Despite the

Published by Copernicus Publications on behalf of the European Geosciences Union.

critical importance of the N inventory in regulating primary production and export, the spatial distribution of N gains and losses in the ocean is still poorly resolved.

A global-scale modeling study predicted that the highest rates of N_2 fixation would be located in the South Pacific Ocean (Deutsch et al., 2007; Gruber, 2016). These authors also concluded that processes leading to N gains and losses are spatially coupled to oxygen-deficient zones such as in the eastern tropical South Pacific (ETSP), which harbors NO_3^--poor but phosphate-rich surface waters, i.e., potentially ideal niches for N_2 fixation (Zehr and Turner, 2001). However, recent field studies based on several cruises and independent approaches, including $^{15}N_2$ incubation-based measurements and geochemical $\delta^{15}N$ budgets, have consistently measured low N_2 fixation rates (average range $\sim$0–60 µmol N m^{-2} d^{-1}) in the surface ETSP waters (Dekaezemacker et al., 2013; Fernández et al., 2011, 2015; Knapp et al., 2016; Loescher et al., 2014). Low activity in the ETSP has been largely attributed to iron (Fe) limitation (Bonnet et al., 2017; Dekaezemacker et al., 2013), as Fe is a major component of the nitrogenase enzyme complex required for N_2 fixation (Raven, 1988). However, the western tropical South Pacific (WTSP) was recently identified as having high N_2 fixation activity (Bonnet et al., 2017), and collectively these studies plead for a basin-wide spatial decoupling between N_2 fixation and denitrification in the South Pacific Ocean.

The WTSP is a vast oceanic region extending from Australia in the west to the western boundary of the South Pacific Gyre in the east (hereafter referred to as GY waters) (Fig. 1). It has been chronically undersampled (Luo et al., 2012) as compared to the tropical North Atlantic (Benavides and Voss, 2015) and North Pacific (e.g., Böttjer et al., 2017) oceans; however, recent oceanographic surveys performed in the western part of the WTSP, in the Solomon, Bismarck (Berthelot et al., 2017; Bonnet et al., 2009, 2015) and Arafura (Messer et al., 2015; Montoya et al., 2004) seas, report extremely high N_2 fixation rates (> 600 µmol N m^{-2} d^{-1}, i.e., an order of magnitude higher than in the ETSP) throughout the year. In these regions, high N_2 fixation has been attributed to sea surface temperatures > 25 °C and continuous nutrient inputs of terrigenous and volcanic origin (Labatut et al., 2014; Radic et al., 2011). The central and eastern parts of the WTSP, a vast oceanic region bordering Melanesian archipelagoes (New Caledonia, Vanuatu, Fiji) up to the Tonga trench (hereafter referred to as MA waters) have been far less investigated. One study (Shiozaki et al., 2014) reported high surface N_2 fixation rates close to the Melanesian islands in relation to nutrients supplied by land runoff. However, the lack of direct N_2 fixation measurements over the full photic layer impedes accurate N budget estimates in this region. In addition, the reasons for such an ecological success of diazotrophs in the WTSP are still under debate (Bonnet et al., 2017) as the horizontal and vertical distribution of environmental parameters potentially controlling N_2 fixation, in particular measured Fe concentrations, are still scarce in this region.

Recurrent blooms of the filamentous cyanobacterium *Trichodesmium*, one of the most abundant diazotrophs in our oceans (Luo et al., 2012), have been consistently reported in the WTSP since the James Cook (Cook, 1842) and Charles Darwin expeditions, and later confirmed by satellite observations (Dupouy et al., 2011, 2000) and microscopic enumerations (Shiozaki et al., 2014; Tenório et al., 2018). However, molecular studies based on the *nifH* gene abundances have shown high densities of unicellular diazotrophic cyanobacteria (UCYN) in the WTSP (Moisander et al., 2010). Three main groups of UCYN (A, B and C) can be distinguished based on *nifH* gene sequences. In the warm (> 25 °C) waters of the Solomon Sea, UCYN from group B (UCYN-B) cooccur with *Trichodesmium* at the surface, and together dominate the diazotrophic community (Bonnet et al., 2015), while UCYN-C are also occasionally abundant (Berthelot et al., 2017). Further south in the Coral and Tasman seas, UCYN-A dominates the diazotroph community (Bonnet et al., 2015; Moisander et al., 2010). Both studies reported a transition zone from UCYN-B-dominated communities in warm (> 25 °C) surface waters to UCYN-A-dominated communities in colder (< 25 °C) waters of the western part of the WTSP. Further east in the MA waters, *Trichodesmium* and UCYN-B co-occur and account for the majority of total *nifH* genes detected (Stenegren et al., 2018). Although molecular methods greatly enhanced our understanding of the biogeographical distribution of diazotrophs in the WTSP, DNA-based *nifH* counts do not equate to metabolic activity. Thus, the contribution of each dominant group to bulk N_2 fixation is still lacking in the WTSP. Previous studies showed that different diazotrophs have different fates in the ocean: some are directly exported, and others release and transfer part of the recently fixed N to the planktonic food web and indirectly fuel export of organic matter (Bonnet et al., 2016a, b; Karl et al., 2012). Consequently assessing the relative contribution of each dominating group of diazotrophs to overall N_2 fixation is critical to assess the biogeochemical impact of N_2 fixation in the WTSP.

In the present study, we report new bulk and group-specific N_2 fixation rate measurements from a $\sim$4000 km transect in the western and central tropical South Pacific. The goals of the study were (i) to quantify both horizontal and vertical distribution of N_2 fixation rates in the photic layer in relation to environmental parameters, (ii) to quantify the relative contribution of the dominant diazotrophs (*Trichodesmium* and UCYN-B) to N_2 fixation based on cell-specific measurements, and (iii) to assess the potential biogeochemical impact of N_2 fixation in this region.

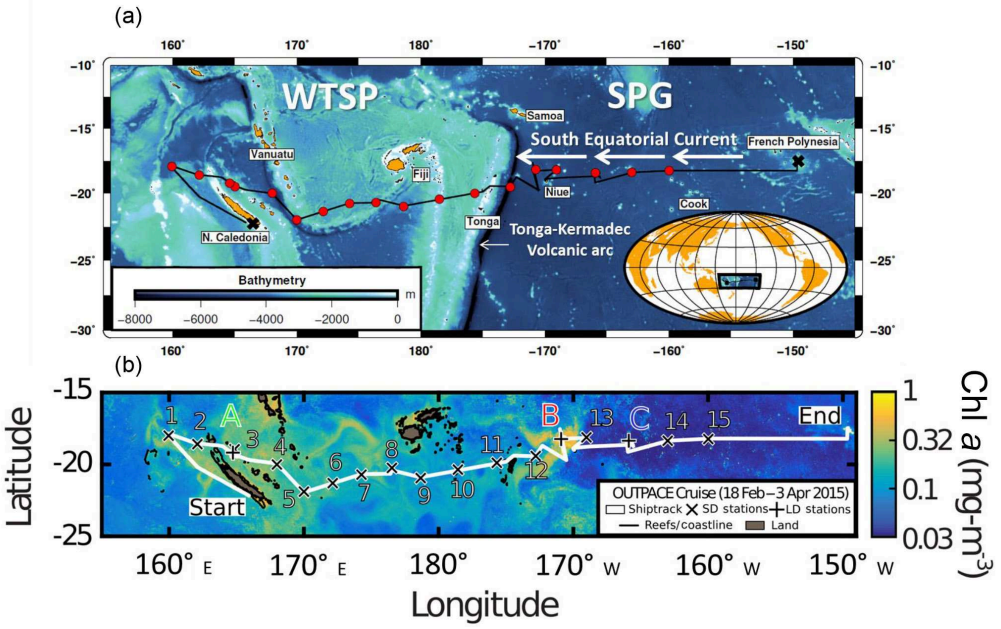

Figure 1. (a) Map of the western and central Pacific and associated seas (courtesy T. Wagener and A. De Verneil). **(b)** Sampling locations superimposed on composite sea surface Chl *a* concentrations during the OUTPACE cruise (19 February–3 April, quasi-Lagrangian weighted mean Chl *a*). Short-duration (X) and long-duration (+) stations are indicated. The satellite data are weighted in time by each pixel's distance from the ship's average daily position for the entire cruise. The white line shows the vessel route (data from the hull-mounted ADCP positioning system; courtesy A. De Verneil).

2 Methods

Samples were collected during the 45-day OUTPACE (Oliotrophic to UlTra oligotrophic PACific Experiment) cruise (DOI: https://doi.org/10.17600/15000900) onboard the R/V *L'Atalante* in February–March 2015 (austral summer). The west to east zonal transect along ∼ 19° S started in Noumea (New Caledonia) and ended in Papeete (French Polynesia) (Fig. 1). It covered a trophic gradient from oligotrophy (deep chlorophyll maximum (DCM) located at ∼ 100 m) in MA waters around New Caledonia, Vanuatu, Fiji and Tonga, to ultra-oligotrophy (DCM located at 115–150 m) in GY waters located at the western boundary of the South Pacific Gyre (Moutin et al., 2017, for details on this cruise). Data were collected at 17 stations including 14 short-duration (SD; 8 h) stations (SD1 to SD15; note that SD13 was not sampled) and 3 long-duration (LD; 7 days) stations (LDA, LDB and LDC). Vertical (0–200 m) profiles of temperature, salinity, and chlorophyll fluorescence were obtained at all 17 stations using a Seabird 911 plus CTD (conductivity, temperature, depth) equipped with a Wetlabs ECO-AFL/FL fluorometer. Seawater samples were collected by 12 L Niskin bottles mounted on the CTD rosette.

2.1 Macro-nutrient and dissolved Fe concentration analyses

Samples for the quantification of nitrate (NO_3^-) and dissolved inorganic phosphorus (DIP) concentrations were collected at 12 depths between 0 and 200 m in acid-washed polyethylene bottles, poisoned with mercuric chloride ($HgCl_2$, final concentration 20 mg L^{-1}) and stored at 4 °C until analysis. Concentrations were determined using standard colorimetric techniques (Aminot and Kérouel, 2007) on a Bran Luebbe AA3 autoanalyzer. Detection limits for the procedures were 0.05 µmol L^{-1} for NO_3^- and DIP.

Samples for determining dissolved Fe concentrations were collected and analyzed as described in Guieu et al. (2018). Briefly, samples were collected using a Titane rosette mounted with 24 Teflon-coated 12 L GoFlos deployed with a Kevlar cable. Dissolved Fe concentrations were measured by flow injection with online preconcentration and chemiluminescence detection according to Bonnet and Guieu (2006). The reliability of the method was monitored by analyzing the D1 SAFe seawater standard (Johnson et al., 2007), and an internal acidified seawater standard was measured daily to monitor the stability of the analysis.

The sampling and analytical methods used to analyze the other parameters reported in the correlation table (Table 2) are described in detail in the methods sections for related pa-

Table 1. ^{15}N / ^{14}N ratio of suspended particulate nitrogen (PN) (average over the photic layer) across the OUTPACE transect.

Station no.	^{15}N / ^{14}N ratio – PN_{susp} (‰)
MA waters	
1	2.00
2	0.78
3	0.57
A	–
4	2.71
5	1.57
6	1.91
7	0.50
8	−2.45
9	−2.21
10	−2.70
11	−7.05
12	1.89
B	−2.88
Average MA waters	−0.41
GY waters	
C	7.91
14	8.72
15	7.55
Average GY waters	8.06

pers in this issue (Bock et al., 2018; Fumenia et al., 2018; Stenegren et al., 2018; Van Wambeke et al., 2018).

2.2 Bulk N_2 fixation rate measurements

Whole water (bulk) N_2 fixation rates were measured in triplicate at all 17 stations using the $^{15}N_2$ isotopic tracer technique (adapted from Montoya et al., 1996). The $^{15}N_2$ bubble technique was intentionally chosen due to the time limitation on making enriched $^{15}N_2$ seawater inoculates (e.g., 6–9 depths = 6–9 inoculates) and the larger sample bottles required for making proper estimates of activity in oligotrophic environments. In addition, we aimed to avoid any potential overestimation due to trace metal and dissolved organic matter (DOM) contaminations often associated with the preparation of the $^{15}N_2$-enriched seawater (Klawonn et al., 2015; Wilson et al., 2012) in our incubation bottles as Fe and DOM have been found to control N_2 fixation or *nifH* gene expression in this region (Benavides et al., 2017; Moisander et al., 2011). However, the ^{15}N / ^{14}N ratio of the N_2 pool available for N_2 fixation (the term AN_2 used in Montoya et al., 1996) was measured in all incubation bottles by membrane inlet mass spectrometry (MIMS) to ensure accurate rate calculations (see below).

Seawater samples were collected from Niskin bottles into 10 % HCl-washed, sample-rinsed (three times) light-transparent polycarbonate (2.3 L) bottles from six depths (75, 50, 20, 10, 1, and 0.1 % surface irradiance levels) at all short-duration stations SD1 to SD15 and nine depths (75, 50, 35, 20, 10, 3, 1, 0.3, and 0.1 % surface irradiance levels) at LD A, LDB and LD C, corresponding to the sub-surface (5 m) down to 80 to 180 m, depending on the station. Bottles were sealed with caps fitted with silicon septa and amended with 2 mL of 98.9 at. % $^{15}N_2$ (Cambridge isotopes). The purity of the $^{15}N_2$ Cambridge isotope stocks was previously checked by Dabundo et al. (2014) and more recently by Benavides et al. (2015) and Bonnet et al. (2016a). They were found to be lower than 2×10^{-8} mol : mol of $^{15}N_2$, leading to a potential N_2 fixation rate overestimation of < 1 %. Each bottle was shaken 20 times to break the $^{15}N_2$ bubble and facilitate its dissolution, and was incubated for 24 h. At SD stations, bottles were incubated in on-deck incubators connected to surface circulating seawater at the specified irradiances using blue screening as the duration of the station (8 h) was too short to deploy in situ mooring lines. At LD stations (7 days), one profile was incubated following the same methodology in on-deck incubators and another replicate profile was incubated in situ for comparison on a drifting mooring line located at the same depth from which the samples were collected. Incubations were stopped by filtering the entire incubation bottle onto pre-combusted (450 °C, 4 h) 25 mm diameter glass fiber filters (GF/F, Whatman, 0.7 µm nominal pore size). Filters were subsequently dried at 60 °C for 24 h before analysis of ^{15}N / ^{14}N ratios and particulate N (PN) determinations using an elemental analyzer coupled to a mass spectrometer (EA-IRMS, Integra CN, SerCon Ltd) as described in Bonnet et al. (2011).

To ensure accurate rate calculations, the ^{15}N / ^{14}N ratio of the N_2 pool in the incubation bottles was measured on each profile from triplicate surface incubation bottles from SD1 to SD14 and at all depths at SD15 and LD stations. Briefly, 12 mL was subsampled after incubation into Exetainers fixed with $HgCl_2$ (final concentration 20 mg L^{-1}) that were preserved upside down in the dark at 4 °C until analyzed using a MIMS according to Kana et al. (1994). Lastly, we collected time zero samples at each station to determine the natural N isotopic signature of ambient particulate N (PN). The minimum quantifiable rates (quantification limit, QL) calculated using standard propagation of errors via the observed variability between replicate samples measured according to Gradoville et al. (2017) were 0.035 nmol N L^{-1} d^{-1}.

Discrete N_2 fixation rate measurements were depth integrated over the photic layer using trapezoidal integration procedures. Briefly, the N_2 fixation at each pair of depths is averaged, and then multiplied by the difference between the two depths to get a total N_2 fixation in that depth interval. These depth interval values are then summed over the entire depth range to get the integrated N_2 fixation rate. The rate nearest

Table 2. Summary of relationships between measured N_2 fixation rates and various physical and biogeochemical parameters. Also shown are correlations between measured rates and the several diazotrophic or non-diazotrophic planktonic groups enumerated at the respective stations. The corresponding unit is given for each parameter, and Spearman's rank correlation ($n = 102$, $\alpha = 0.05$) is provided; significant correlations ($p < 0.05$) are indicated by an asterisk (*).

	Variable	Unit	N_2 fixation Spearman's correlation coefficient
Physical and biogeochemical parameters	Pressure	dbar	−0.705*
	Temperature	°C	0.658*
	Salinity	psu	−0.701*
	Oxygen	$\mu mol\,kg^{-1}$	0.151
	PAR	$\mu mol\ photons\ m^{-2}\ s^{-1}$	0.319*
	NO_3^-	$\mu mol\,L^{-1}$	−0.544*
	NH_4^+	$\mu mol\,L^{-1}$	−0.024
	DIP	$\mu mol\,L^{-1}$	−0.770*
	$Si(OH)_4$	$\mu mol\,L^{-1}$	−0.724*
	Dissolved Fe	$nmol\,L^{-1}$	0.398*
	DON	$\mu mol\,L^{-1}$	0.517*
	DOP	$\mu mol\,L^{-1}$	0.418*
	DOC	$\mu mol\,L^{-1}$	0.573*
	PON	$\mu mol\,L^{-1}$	0.721*
	POC	$\mu mol\,L^{-1}$	0.723*
	Biogenic silica	$\mu mol\,L^{-1}$	0.274*
	Chl *a*	$\mu g\,L^{-1}$	0.266*
	Primary production	$\mu g\,C\,L^{-1}\,h^{-1}$	0.657*
	Bacterial production	$\mu mol\,C\,L^{-1}\,h^{-1}$	0.692*
	T_{DIP}	days	−0.721*
Planktonic groups	*Trichodesmium* sp.	*nifH* copies L^{-1}	0.729*
	UCYN-A1	*nifH* copies L^{-1}	−0.051
	UCYN-A2	*nifH* copies L^{-1}	−0.147
	UCYN-B	*nifH* copies L^{-1}	0.511*
	het-1	*nifH* copies L^{-1}	0.538*
	het-2	*nifH* copies L^{-1}	0.576*
	het-3	*nifH* copies L^{-1}	0.276*
	Prochlorococcus sp.	cell mL^{-1}	0.697*
	Synechococcus sp.	cell mL^{-1}	0.720*
	Pico-eukaryotes	cell mL^{-1}	−0.450*
	Bacteria	cell mL^{-1}	0.780*
	Protists	cell mL^{-1}	0.680*

the surface is assumed to be constant up to 0 m (Knap et al., 1996).

2.3 Statistical analyses

Spearman's rank correlation was used to examine the potential relationships between N_2 fixation rates and hydrological, biogeochemical, and biological parameters across the longitudinal transect ($n = 102$, $\alpha = 0.05$). A non-parametric Mann–Whitney test ($\alpha = 0.05$) was used to compare the MIMS data obtained following on-deck versus in situ incubations, and to compare nutrient and Chl *a* distributions between the western part and the eastern part of the transect.

2.4 Group-specific N_2 fixation rate measurements

2.4.1 Experimental procedures

At three stations along the transect (SD2, SD6, LDB), where *Trichodesmium* and UCYN-B accounted for > 90 % of the total diazotrophic community (see below and Stenegren et al., 2018), eight additional polycarbonate (2.3 L) bottles were collected from the surface (50 % light irradiance) to determine *Trichodesmium* and UCYN-B-specific N_2 fixation rates by nanoSIMS and quantify their contribution to bulk N_2 fixation. Two of these bottles were amended with $^{15}N_2$ as described above for further nanoSIMS analyses on individual cells (the six remaining bottles were used for DNA and RNA

analyses; see below) and were incubated for 24 h with the incubation bottles dedicated to bulk N_2 fixation measurements in on-deck incubators as described above. To recover large-size diazotrophs (*Trichodesmium*) after incubation, 1.5 L was filtered on 10 µm pore size 25 mm diameter polycarbonate filters. The cells were fixed with paraformaldehyde (PFA) (2 % final concentration) for 1 h at ambient temperature (∼ 25 °C) and the filters were then stored at −20 °C until nanoSIMS analyses. To recover small-size diazotrophs (UCYN-B), samples were collected for further cell sorting by flow cytometry prior to nanoSIMS; 1 L of the remaining $^{15}N_2$ labelled bottle was filtered onto 0.2 µm pore size 47 mm polycarbonate filters. Filters were quickly placed in a 5 mL cryotube filled with 0.2 µm filtered seawater with PFA (2 % final concentration) for 1 h at room temperature in the dark. The cryovials were vortexed for 10 s to detach the cells from the filter (Thompson et al., 2012) and stored at −80 °C until cell sorting. Cell sorting of UCYN-B was performed on a Becton Dickinson Influx Mariner (BD Biosciences, Franklin Lakes, NJ) high-speed cell sorter of the Regional Flow Cytometry Platform for Microbiology (PRECYM), hosted by the Mediterranean Institute of Oceanography, as described in Bonnet et al. (2016a) and Berthelot et al. (2016). After sorting, the cells were dropped onto a 0.2 µm pore size polycarbonate 13 mm diameter polycarbonate filter connected to a low-pressure vacuum pump, and then stored at −80 °C until nanoSIMS analyses. Special care was taken to drop the cells on a surface as small as possible (∼ 5 mm in diameter) to ensure the highest cell density possible to facilitate subsequent nanoSIMS analyses.

2.4.2 Abundance of diazotrophs by microscopy and qPCR methods

The abundance of *Trichodesmium* filaments and the average number of cells per filament were determined microscopically: 1 to 2.2 L was filtered on 2 µm polycarbonate filters. The cells were fixed with PFA prepared with filtered seawater (2 % final concentration) for 1 h at 4 °C and stored at −20 °C until counting using an epifluorescence microscope (Zeiss Axioplan, Jena, Germany) fitted with a green (510–560 nm) excitation filter. The whole filter was counted and the number of cells per trichome were counted on at least 10 filaments per station.

Four other diazotrophic phylotypes were quantified using quantitative PCR (qPCR) as they were not easily quantifiable by standard epifluorescence microscopy: UCYN-A1, UCYN-B and two heterocystous symbionts of diatom–diazotroph associations (DDAs): *Richelia intracellularis* associated with *Rhizosolenia* spp. (het-1) and *R. intracellularis* associated with *Hemiaulus* spp. (het-2). Triplicate 2.3 L bottles were filtered onto 25 mm diameter 0.2 µm Supor filters with a 0.2 µm pore size at each station using a peristaltic pump. The DNA extraction and TaqMAN qPCR assays are fully described in Stenegren et al. (2018). To quantify *nifH* gene expression, additional triplicate 2.3 L bottles were filtered as described above. The filters were placed into pre-sterilized bead-beater tubes (Biospec Products Inc., Bartlesville, OK, USA) containing a 250 µL Lysis buffer (Qiagen RNeasy) amended with 1 % β-mercaptoethanol and 30 µL of 0.1 mm glass beads (Biospec Products Inc.). The time of filtering for RNA varied between stations (17:00–21:00). Filters were flash frozen in liquid nitrogen and stored at −80 °C until RNA extraction. The RNA extraction and reverse transcription (RT) were performed as previously described using a Super-Script III first-strand cDNA synthesis kit (Invitrogen Corp., Carlsbad, CA, USA) including the appropriate negative controls (water and No-RT) (Foster et al., 2010). The *nifH* gene expression for het-1, het-2, *Trichodesmium*, UCYN-A1, and UCYN-B was as described previously (Foster et al., 2010).

2.4.3 nanoSIMS analyses, data processing and group-specific rate calculations

NanoSIMS analyses were performed using an N50 nanoSIMS instrument (Cameca, Gennevilliers, France) at the French National Ion MicroProbe Facility according to Bonnet et al. (2016a, b) and Berthelot et al. (2016). Briefly, a ∼ 1.3 pA cesium (16 KeV) primary beam focused onto a ∼ 100 nm spot diameter was scanned across a 256 × 256 or 512 × 512 pixel raster (depending on the image size) with a counting time of 1 ms per pixel. Samples were pre-sputtered prior to analyses with a current of ∼ 10 pA for at least 2 min to achieve sputtering equilibrium and ensure a consistent implantation and analysis of the cell interior by removing the cell surface. Negative secondary ions ($^{12}C^{14}N^-$, $^{12}C^{15}N^-$) were collected by electron multiplier detectors, and secondary electrons were also imaged simultaneously. A total of 10–50 serial quantitative secondary ion images were generated that were combined to create the final image. Mass resolving power was ∼ 8000 in order to resolve isobaric interferences; 20 to 100 planes were generated for each cell analyzed. NanoSIMS runs are time-intensive and not designed for routine analysis, but a minimum of 250 cells of UCYN-B per station and 30 *Trichodesmium* filament portions were analyzed to take into account the variability of activity among the population.

Data were processed using the LIMAGE software. Briefly, all scans were corrected for any drift of the beam and sample stage during acquisition. Isotope ratio images were created by adding the secondary ion counts for each recorded secondary ion for each pixel over all recorded planes and dividing the total counts by the total counts of a selected reference mass. Individual *Trichodesmium* filaments and UCYN-B cells were easily identified on nanoSIMS images that were used to define regions of interest (ROIs). For each ROI, the ^{15}N / ^{14}N ratio was calculated.

Trichodesmium and UCYN-B cellular biovolume was calculated from cell-diameter measurements performed on ∼ 50

cells or trichomes per station using an epifluorescence microscope (Zeiss Axioplan, Jena, Germany) fitted with a green (510–560 nm) excitation filter. UCYN-B had a spherical shape and *Trichodesmium* cells were assumed to have a cylindrical shape. The carbon content per cell was estimated from the biovolume according to Verity et al. (1992) and the N content was calculated based on C : N ratios of 6 for *Trichodesmium* (Carpenter et al., 2004) and 5 for UCYN-B (Dekaezemacker and Bonnet, 2011; Knapp et al., 2012). ^{15}N assimilation rates were expressed "per cell" and calculated as follows (Foster et al., 2011, 2013): assimilation (mol N cell^{-1} d^{-1}) = ($^{15}N_{ex} \times N_{con}$)/ N_{sr}, where $^{15}N_{ex}$ is the excess ^{15}N enrichment of the individual cells measured by nanoSIMS after 24 h of incubation relative to the time zero value, N_{con} is the N content of each cell determined as described above, and N_{sr} is the excess ^{15}N enrichment of the source pool (N_2) in the experimental bottles determined by MIMS (see above). Standard deviations were calculated using the variability of N isotopic signatures measured by nanoSIMS on replicate cells. The relative contribution of *Trichodesmium* and UCYN-B to bulk N_2 fixation was calculated by multiplying cell-specific N assimilation by the cell abundance of each group, relative to bulk N_2 fixation determined at the same time.

3 Results

3.1 Environmental conditions

Seawater temperature ranged from 21.4 to 30.0 °C in the sampled photic layer (0 to ∼ 80–180 m) over the cruise transect (Fig. 2a). The mixed layer depth (MLD) calculated according to the de Boyer Montégut et al. (2004) method was located around 20–40 m throughout the zonal transect: maximum temperatures were measured in the surface mixed layer (∼ 0–20/40 m) and remained almost constant along the longitudinal transect with 29.1 ± 0.3 °C in MA waters and 29.5 ± 0.4 °C in GY waters.

Based on other hydrographic measurements (dissolved nutrients, dissolved Fe and Chl *a* concentrations), the longitudinal transect was divided into two sub-regions: (1) the MA region from station SD1 (160° E) to LDB (165° W), and (2) the GY sub-region from station LDB (165 ° W) to SD15 (160° W). Chl *a* concentration in the upper 50 m was significantly ($p < 0.05$) higher in MA waters (0.17 µg L^{-1} on average) than in GY waters (0.06 µg L^{-1} on average) (Figs. 1 and 2b). The DCM was located around 80–100 m in MA waters and deepened to ∼ 150 m in GY waters, indicating higher oligotrophy in the GY region. Surface NO_3^- concentrations (Fig. 2c) were consistently close to or below the detection limit (0.05 µmol L^{-1}) in the upper water column (0–50 m) throughout the transect and the depth of the nitracline gradually deepened from ∼ 75–100 m in MA waters to ∼ 115 m in GY waters. DIP concentrations were slightly higher than or close to detection limits (0.05 µmol L^{-1}) in MA surface waters (0–50 m), and the phosphacline was shallower (20–45 m) than the nitracline and DIP concentrations increased significantly ($p < 0.05$) in GY waters and ranged from 0.13 to 0.17 µmol L^{-1} (Fig. 2d).

3.2 N isotopic signature of the N_2 pool after incubation

The ^{15}N enrichment of the N_2 pool after 24 h of incubation with the $^{15}N_2$ tracer was on average 6.145 ± 0.798 at. % ($n = 54$) in bottles incubated in on-deck incubators and significantly higher ($p < 0.05$) in bottles incubated on the mooring line (7.548 ± 0.557 at. % ($n = 44$), Fig. 3a). However, the depth of incubation on the mooring line (between 5 and 180 m) did not have any significant effect ($p > 0.05$) on the isotopic signature of the N_2 pool at LDB and LDC, which remained constant over the water column (Fig. 3b).

3.3 Natural isotopic signature of suspended particles and N_2 fixation rates

The natural N isotopic signature of suspended particles measured over the photic layer was on average −0.41 ‰ in MA waters and 8.06 ‰ in GY waters (Table 1). Those isotopic values were used as time zero samples to calculate N_2 fixation rates.

N_2 fixation was detected at all 17 sampled stations and the average measured N_2 fixation rates in the two previously defined sub-regions were (1) 8.9 ± 10 nmol N L^{-1} d^{-1} (range QL-48 nmol N L^{-1} d^{-1}) over the photic layer in MA waters, and 2) 0.5 ± 0.6 nmol N L^{-1} d^{-1} (range QL-4.0 nmol N L^{-1} d^{-1}) in GY waters (Fig. 2e). In MA waters, N_2 fixation was largely restricted to the mixed layer, where average rates were 15 nmol N L^{-1} d^{-1}, with local maxima (> 20 nmol N L^{-1} d^{-1}) at stations SD1, SD6 and LDB and local minima (< 5 nmol N L^{-1} d^{-1}) at SD8 and SD10. In GY waters, maximum rates reached 1–2 nmol N L^{-1} d^{-1} and were located deeper in the water column (∼ 50 m). When integrated over the photic layer, N_2 fixation represented an average net N addition of 631 ± 286 µmol N m^{-2} d^{-1} (range 196–1153 µmol N m^{-2} d^{-1}) in MA waters and of 85 ± 79 µmol N m^{-2} d^{-1} (range 18–172 µmol N m^{-2} d^{-1}) in GY waters.

N_2 fixation rates were significantly positively correlated with seawater temperature and photosynthetically active radiation (PAR) ($p < 0.05$), significantly negatively correlated with depth and salinity ($p < 0.05$) and not significantly correlated with dissolved oxygen concentrations ($p > 0.05$) (Table 2). N_2 fixation rates were significantly positively correlated with dissolved Fe, dissolved organic N (DON), phosphorus (DOP), carbon (DOC), particulate organic N (PON), particulate organic carbon (POC), biogenic silica (BSi), Chl *a* concentrations, and primary and bacterial production ($p < 0.05$), and significantly negatively correlated with concentration of dissolved nutrients: NO_3^-, NH_4^+, DIP and sil-

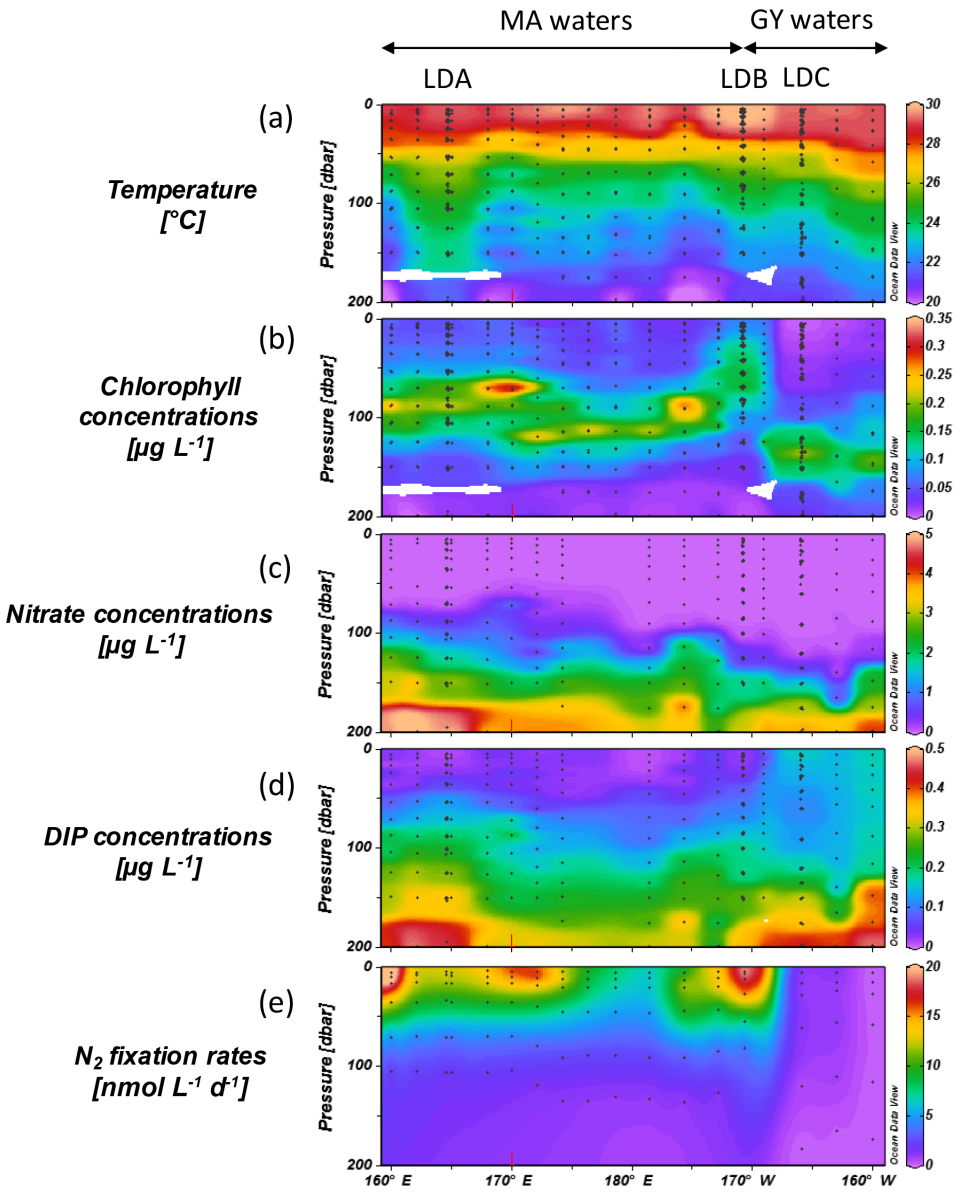

Figure 2. Horizontal and vertical distributions of **(a)** seawater temperature (°C), **(b)** chlorophyll fluorescence (µg L^{-1}), **(c)** NO_3^- (µmol L^{-1}), **(d)** DIP (µmol L^{-1}) and **(e)** N_2 fixation rates (nmol N L^{-1} d^{-1}) across the OUTPACE transect. LD stations are noted and the extent of the two defined sub-regions: MA: Melanesian archipelago waters, GY: South Pacific Gyre waters. *Y* axis: pressure (dbar), *X* axis: longitude; black dots correspond to sampling depths at the various SD and LD stations.

icate ($p < 0.05$). N_2 fixation rates were significantly positively correlated with *nifH* abundances for *Trichodesmium* spp., UCYN-B and the symbionts of DDAs (het-1, het-2) ($p < 0.05$) and not significantly correlated with UCYN-A1 and UCYN-A2 abundances ($p > 0.05$) (Table 2). Regarding non-diazotrophic plankton, N_2 fixation rates were significantly positively correlated with *Prochlorococcus* spp., *Synechococcus* spp., heterotrophic bacteria and protist abundances ($p < 0.05$) and significantly negatively correlated with picoeukaryotes ($p < 0.05$).

3.4 Contribution of *Trichodesmium* and UCYN-B to N_2 fixation and nitrogenase gene expression

At the three stations where cell-specific N_2 fixation rates were estimated by nanoSIMS (SD2, SD6 and LDB), the most abundant diazotroph phylotype was *Trichodesmium* with 1.3×10^5, 3.3×10^5 and 1.2×10^5 cells L^{-1}, respectively, followed by UCYN-B, whose abundances were 2.0×10^4, 1.5×10^5 and 3.8×10^2 *nifH* copies L^{-1}, respectively. Het-1 and het-2 combined were 1 to 2 orders of magnitude lower, ranging from 1.0 to 9.9×10^3 *nifH* copies L^{-1}, and UCYN-

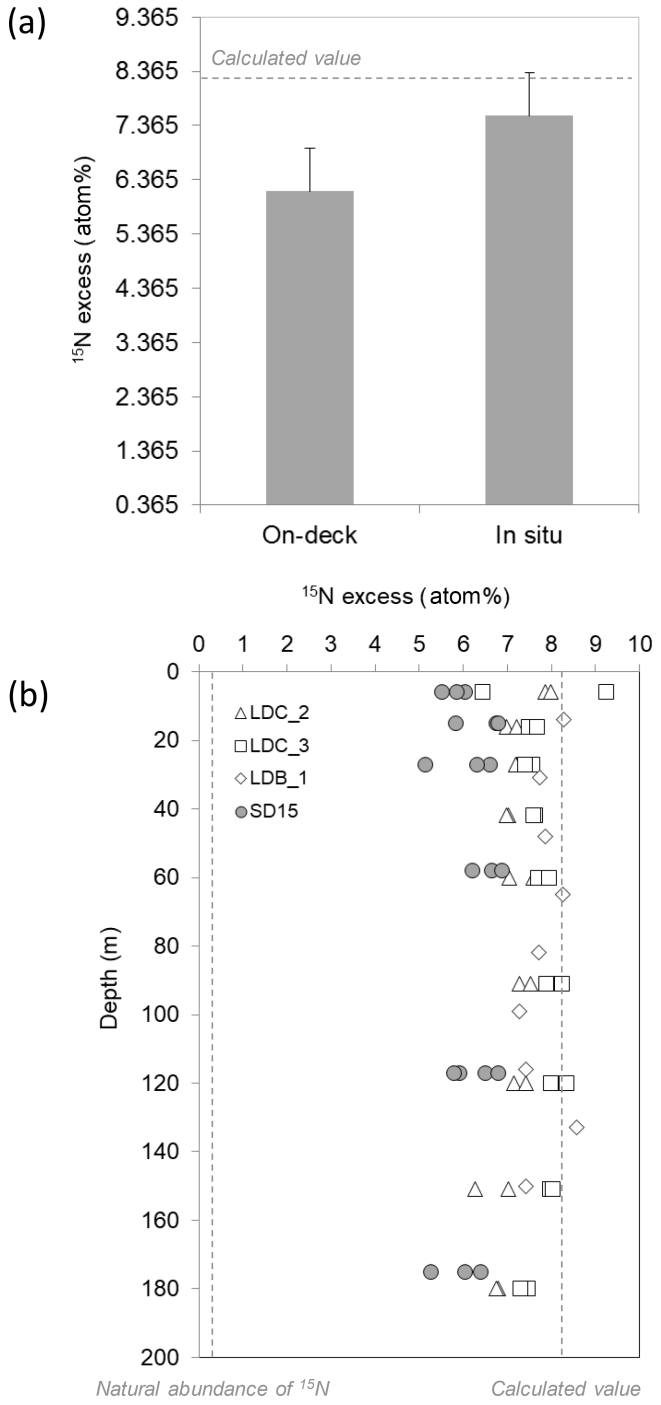

Figure 3. (a) The average measured ^{15}N / ^{14}N ratio of the N_2 pool in the incubation bottles incubated either in on-deck incubators ($n = 54$) or in situ (mooring line) ($n = 44$). The dashed lines represent the theoretical value (~ 8.2 at. %) calculated assuming complete isotopic equilibration between the gas bubble and the seawater based on gas constants. Error bars represent the standard deviation **(b)** depth profiles of the ^{15}N / ^{14}N ratio of the N_2 pool in the incubation bottles incubated either in on-deck incubators (filled symbols) or on an in situ mooring line (open symbols).

A1 were below detection at the three stations. In summary, *Trichodesmium* and UCYN-B accounted for 98.2, 99.8 and 92.1 % of the total diazotroph community (based on the phylotypes targeted here) at SD2, SD6 and LDB, respectively (Table 3).

The ^{15}N / ^{14}N ratios of individual cells/trichomes of UCYN-B and *Trichodesmium* were measured via nanoSIMS analyses and used to estimate single-cell N_2 fixation rates. A summary of the enrichment values and cell-specific N_2 fixation is provided in Table 3. Individual trichomes exhibited significant ^{15}N enrichments (0.610 ± 0.269, 0.637 ± 0.355 and 0.981 ± 0.466 at. % at stations SD2, SD6 and LDB, respectively) compared with time zero samples (0.369 ± 0.002 at. %). UCYN-B were also significantly ^{15}N-enriched, with 1.163 ± 0.531 and 0.517 ± 0.237 at. % at SD2 and SD6, respectively (note that no UCYN-B could be sorted and analyzed by nanoSIMS at LDB as they accounted for only 0.3 % of the diazotroph community). Cell-specific N_2 fixation rates of *Trichodesmium* were 38.9 ± 8.1, 29.3 ± 5.4 and 123.8 ± 24.8 fmol N cell^{-1} d^{-1} at SD2, SD6 and LDB. Cell-specific N_2 fixation of UCYN-B was 30.0 ± 6.4 and 6.1 ± 1.2 fmol N cell^{-1} d^{-1} at SD1 and SD6. The contribution of *Trichodesmium* to bulk N_2 fixation was 83.8, 47.1 and 52.9 % at stations SD2, SD6 and LDB, respectively. The contribution of UCYN-B was 10.1 and 6.1 % at SD2 and SD6, respectively (Table 3).

The in situ *nifH* expression for all diazotroph groups targeted by qPCR was estimated using a TaqMAN quantitative reverse transcription PCR (RT-qPCR) (Table 4). The sampling and filtering time (17:00–21:00 h) was not optimal for quantifying the *nifH* gene expression for all diazotrophs; however, it provides useful information about which diazotrophs were potentially active during the experiment and complements the nanoSIMS analysis which measures the in situ activity. Both *Trichodesmium* and UCYN-B dominated the biomass (Stenegren et al., 2018), as did their *nifH* gene expression at all three stations, especially SD2 and SD6. Of the two DDAs, het-1 had a higher *nifH* gene expression, which was consistent with its higher *nifH* abundance by DNA qPCR (Stenegren et al., 2018). UCYN-A1 was consistently below detection for the *nifH* gene expression and was also the least detected diazotroph by *nifH* qPCR (Stenegren et al., 2018).

4 Discussion

4.1 Methodological considerations: the importance of measuring the ^{15}N / ^{14}N ratio of the N_2 pool

Our understanding of the marine N cycle relies on accurate estimates of N fluxes to and from the ocean. Here we decided to use the "bubble addition method" to minimize potential trace metal and organic matter contaminations, which may have resulted in overestimating rates (Klawonn et al.,

Table 3. Summary of diazotroph abundances and nanoSIMS analyses at SD2, SD6 and LDB.

Station no.	*Trichodesmium* abundance (cells L^{-1})	Contribution to diazotroph community (%)	at. % (mean ± SD)	N_2 fixation rates (fmol cell^{-1} d^{-1})	Contribution to bulk N_2 fixation (%)
SD2	1.3×10^5	84.9	0.610 ± 0.269	38.9 ± 8.1	83.8
SD6	3.3×10^5	68.0	0.637 ± 0.355	29.3 ± 5.4	47.1
LDB	1.2×10^5	91.8	0.981 ± 0.466	123.8 ± 24.7	52.9
Station no.	UCYN-B abundance (cells L^{-1})	Contribution to diazotroph community (%)	at. % (mean ± SD)	N_2 fixation rates (fmol cell^{-1} d^{-1})	Contribution to bulk N_2 fixation (%)
SD2	2.0×10^4	13.2	1.163 ± 0.531	30.0 ± 6.4	10.1
SD6	1.5×10^5	31.7	0.517 ± 0.237	6.1 ± 1.2	6.1
LDB	3.8×10^2	0.3	n.d.	n.d.	n.d.

Table 4. Summary of *nifH* gene expression data determined by qRT-PCR at selected stations (SD2, SD6, LDB), where the cell-specific N_2 fixation rates were measured.

Diazotroph	Station SD2 cDNA*nifH* (gene copies L^{-1})	Station SD6 cDNA*nifH* (gene copies L^{-1})	Station LDB cDNA*nifH* (gene copies L^{-1})
Trichodesmium	1.1×10^5	5.1×10^5	5.78×10^4
UCYN-B	1.9×10^5	1.5×10^5	1.03×10^2
het-1	6.83×10^2	1.56×10^3	2.04×10^2
het-2	5.44×10^2	2.14×10^2	bd
UCYN-A1	bd	bd	bd

2015). Moreover, a recent extensive meta-analysis (13 studies, 368 observations) between bubble and enriched amendment experiments to measure $^{15}N_2$ rates reported that underestimation of N_2 fixation is negligible in experiments that last 12–24 h (e.g., error is −0.2 %); hence our 24 h based experiments should be within a small amount of error (Wannicke et al., 2018). However, we paid careful attention to accurately measure the term AN_2 to avoid any potential underestimation and reveal that the way bottles are incubated (on-deck versus in situ) has a great influence on the AN_2 value, and thus on N_2 fixation rates.

Our MIMS results measured a significantly ($p < 0.05$) lower ^{15}N enrichment of the N_2 pool (6.145 ± 0.798 at. %) when bottles were incubated in on-deck incubators compared to when bottles were incubated on the mooring line (7.548 ± 0.557 at. %). This suggests that the $^{15}N_2$ dissolution is much more efficient when bottles are incubated in situ, probably due to the higher pressure in seawater at the depth of incubation (1.5 to 19 bars between 5 and 180 m) compared to the pressure in the on-deck incubators (1 bar). The seawater temperature checked regularly in the on-deck incubators was equivalent to ambient surface temperature and likely did not explain the differences observed. This result highlights the need to perform routine MIMS measurements to use the most accurate AN_2 value for rate calculations, independently of the $^{15}N_2$ approach used (gas or dissolved). In our study, the theoretical AN_2 value based on gas constant calculations (Weiss, 1970) was ∼ 8.2 at. %, so the deviation from this value is more important when bottles are incubated in on-deck incubators as compared to when they are incubated in situ. This suggests that the use of the bubble addition method without MIMS measurement potentially leads to higher underestimations when bottles are incubated in on-deck incubators, which is the case in the great majority of marine N_2 fixation studies published so far (Luo et al., 2012). We are aware that the dissolution kinetics of $^{15}N_2$ in the incubation bottles may have been progressive along the 24 h of incubation (Mohr et al., 2010); therefore, the N_2 fixation rates provided here represent conservative values.

Despite the AN_2 value being different according to the incubation mode, it did not change with the depth of incubation on the mooring line, indicating that a slightly higher pressure than atmospheric pressure (1.5 bar at 5 m depth) is enough to promote the $^{15}N_2$ dissolution. It also indicates that the slightly lower seawater temperature (22–24 °C) recorded at ∼ 100–180 m where the deepest samples were incubated likely did not affect the solubilization of the $^{15}N_2$ gas. In our study, the vertical profiles performed at LD stations and incubated either on-deck in triplicate or in situ in triplicate reveal identical ($p > 0.05$) N_2 fixation rates regardless of the incubation method used (Caffin et al., 2018b). This indicates that in situ incubations and on-deck incubations that simulate appropriate light levels are a valid methodology for $^{15}N_2$ fixation rate measurements on cruises during which mooring

lines cannot be deployed, as long as routine measurements of the isotopic ratio of the N_2 pool are performed in incubation bottles.

4.2 Drivers of high N_2 fixation rates in the WTSP?

N_2 fixation rates measured in MA waters (average $631 \pm 286\,\mu mol\,N\,m^{-2}\,d^{-1}$) are 3 to 4 times higher than model predictions for this area (150–200 $\mu mol\,N\,m^{-2}\,d^{-1}$, Gruber, 2016). They are in the upper range of the higher category (100–1000 $\mu mol\,N\,m^{-2}\,d^{-1}$) of rates defined by Luo et al. (2012) in the N_2 fixation MAREDAT database for the global ocean and thus identify the WTSP as an area for high N_2 fixation in the global ocean. Recent studies performed in the western part of the WTSP, i.e., in the Solomon, Bismarck (Berthelot et al., 2017; Bonnet et al., 2009, 2015) and Arafura (Messer et al., 2015; Montoya et al., 2004) seas, also reveal extremely high rates ($> 600\,\mu mol\,N\,m^{-2}\,d^{-1}$), indicating that this high N_2 fixation activity area extends geographically west–east from Australia to Tonga and north–south from the Equator to 25–30° S, covering a vast ocean area of $\sim 13 \times 106\,km^2$ (i.e., $\sim 20\,\%$ of the South Pacific Ocean area). However, the driver(s) for diazotrophy in this region is(are) still poorly resolved and raise(s) the question of which factors influence the distribution and activity of N_2 fixation in the ocean. In a global-scale study conducted by Luo et al. (2014), which investigated the correlations between N_2 fixation and a variety of environmental parameters commonly accepted to control this process, they concluded that SST (or surface solar radiation) was the best predictor to explain the spatial distribution of N_2 fixation in the surface ocean. Below we highlight the most plausible factors explaining such high N_2 fixation rates in our study area.

Seawater temperature. Seawater temperature was unlikely to be the factor explaining the differences in N_2 fixation rates observed between MA and GY waters, as it was consistently high ($> 28\,°C$ in the surface mixed layer) and optimal for the growth and nitrogenase activity of most diazotrophs (Breitbarth et al., 2007; Nübel et al., 1997) all along the cruise transect. This indicates that other factors such as nutrient availability may explain the distribution of N_2 fixation.

DIP availability. The ~ 4000 km transect was divided into two main sub-regions: (1) the MA waters, harboring typical oligotrophic conditions with surface NO_3^- and DIP concentrations close to detection limits ($0.05\,\mu mol\,L^{-1}$), a nitracline located at 75–100 m, moderate surface Chl *a* concentrations ($\sim 0.17\,\mu g\,L^{-1}$), a DCM located at ~ 80–100 m and very high N_2 fixation rates ($631 \pm 286\,\mu mol\,N\,m^{-2}\,d^{-1}$ on average), and (2) the GY waters harboring ultra-oligotrophic conditions with undetectable NO_3^-, a deeper nitracline (115 m), and comparatively high DIP concentrations ($0.15\,\mu mol\,L^{-1}$), very low Chl *a* concentrations ($0.06\,\mu g\,L^{-1}$, DCM ~ 150 m) and low N_2 fixation rates ($85 \pm 79\,\mu mol\,N\,m^{-2}\,d^{-1}$).

In the NO_3^--depleted MA waters, low DIP concentrations are indicative of the consumption of DIP by the planktonic community, including diazotrophs. This is consistent with the negative correlation found between N_2 fixation and DIP turnover time (the ratio between DIP concentrations and DIP uptake rates) (Table 2) and suggests a higher DIP limitation when N_2 fixation is high and consumes DIP. The high DIP concentrations ($> 0.1\,\mu mol\,L^{-1}$) in GY surface waters compared to MA waters are consistent with former studies that consider the South Pacific Gyre as a high phosphate, low chlorophyll ecosystem (Moutin et al., 2008), in which DIP accumulates in the absence of NO_3^- and low N_2 fixation activity. In the high phosphate, low chlorophyll scenario, the community is limited by temperature and/or Fe availability (Moutin et al., 2008; Bonnet et al., 2008). During the OUTPACE cruise, the DIP turnover time was variable but close to or below 2 days in MA waters (Moutin et al., 2018), indicating a potential limitation by DIP at some stations. *Trichodesmium*, the most abundant and major contributor to N_2 fixation during the cruise, is known to synthesize hydrolytic enzymes in order to acquire P from the dissolved organic phosphorus pool (DOP) (Sohm and Capone, 2006). Moreover, *Trichodesmium* spp. differs from the other major diazotroph UCYN-B enumerated on the cruise in the forms of organic P it can synthesize. It is thus likely that DOP species that favored *Trichodesmium* over UCYN-B played a role in maintaining high *Trichodesmium* biomass in MA waters. It has to be noted that average DIP turnover times in MA waters were always much higher than those typically measured in severely DIP-limited environments such as the Mediterranean and Sargasso seas (e.g., Moutin et al., 2008), suggesting that DIP concentrations are generally favorable for the development of certain diazotrophs in the WTSP, and do not alone explain why N_2 fixation is high in MA waters and low in GY waters. However, it is likely that the depletion of DIP stocks at the end of the austral summer season forces the decline of diazotrophic blooms in the WTSP (Moutin et al., 2005), concomitantly with the decline of SST.

Fe availability. Before OUTPACE, our knowledge on Fe sources and concentrations in the WTSP was limited, especially in MA waters. During OUTPACE, Guieu et al. (2018) reported high dissolved Fe concentrations in MA waters (range 0.2–66.2 $nmol\,L^{-1}$, 1.7 $nmol\,L^{-1}$ on average over the photic layer), i.e., significantly ($p < 0.05$) higher than those reported in GY waters (range 0.2–0.6 $nmol\,L^{-1}$, 0.3 nM on average over the photic layer). The low dissolved Fe concentrations measured in the GY waters agree well with previous reports for the same region (Blain et al., 2008; Fitzsimmons et al., 2014). However, the high dissolved Fe concentrations measured in MA waters were previously undocumented and reveal several maxima ($> 50\,nmol\,L^{-1}$) between stations SD7 and SD11, indicative of intense fertilization processes taking place in this region. Guieu et al. (2018) found that atmospheric deposition measured during the cruise in this region was too low to explain the observed dissolved Fe concentrations in the surface water column. The seafloor of the WTSP hosts the Tonga–Kermadec subduc-

tion zone which stretches 2500 km from New Zealand to the Tonga archipelago (Fig. 1). It has among the highest densities of submarine volcanoes associated with hydrothermal vents recorded in the ocean (2.6 vents / 100 km, Massoth et al., 2007), which discharge large quantities of material into the water column, including biogeochemically relevant elements such as Fe and Mn. Guieu et al. (2018) used hydrological data recorded by Argo float in situ measurements, atlas data and simulations from a general ocean circulation model to argue that the high dissolved Fe concentrations may be sustained by a submarine source. They show that such Fe inputs could spread throughout the WTSP through mesoscale activity mainly westward through the South Equatorial Current, SEC (Fig. 1). Guieu et al. (2018) hypothesize that the high dissolved Fe concentrations in MA waters compared to the GY ones is due to shallow inputs of hydrothermal origin together with potential Fe input from islands themselves (Shiozaki et al., 2014). In our study, dissolved Fe concentrations were significantly positively correlated with N_2 fixation and help to explain the distribution of N_2 fixation rates measured across the OUTPACE transect.

In summary, our hypothesis to explain the spatial distribution of N_2 fixation in MA waters is the following: when high DIP waters flow westward from the ETSP through the SEC and cross the South Pacific Gyre, N_2-fixing organisms do not develop despite optimal SST ($> 25\,°C$), likely because GY waters are Fe-depleted (Moutin et al., 2008; Bonnet et al., 2008). When the high DIP, low DIN (dissolved inorganic N) waters from the gyre are advected west of the Tonga trench in Fe-rich and warm ($> 25\,°C$) waters, all environmental conditions are fulfilled for diazotrophs to bloom extensively. According to Moutin et al. (2018), the strong depth difference between the nitracline and the phosphacline in MA waters associated with winter mixing allows a seasonal replenishment of DIP, which creates an excess of P relative to N and thus also favors N_2 fixation in this region. Further investigations are required to better quantify Fe input from both islands and shallow volcanoes and associated hydrothermal activity along the Tonga volcanic arc for the upper mixed layer, study the fate of hydrothermal plumes in the water column at the local and regional scales, and investigate the potential impact of such hydrothermal inputs on diazotrophic communities at the scale of the whole WTSP.

N_2 fixation rates were significantly negatively correlated with NO_3^- concentrations, consistent with the high energetic cost of N_2 fixation compared to NO_3^- assimilation (Falkowski, 1983). They were also negatively correlated with depth and logically positively correlated with PAR and seawater temperature, two parameters which are depth dependent. Most N_2 fixation took place in the surface mixed layer and rates were $\sim 15\,\mathrm{nmol\,N\,L^{-1}\,d^{-1}}$ in MA waters with local maxima at stations SD1, SD6 and LDB and local minima at SD8 and SD10. *Trichodesmium*, the most abundant diazotroph enumerated at those stations (Stenegren et al., 2018), is buoyant, and horizontal advection is well known to result in patchy distributions of *Trichodesmium* in the surface ocean (Dandonneau et al., 2003), with huge surface accumulations named slicks, as observed during OUTPACE (Stenegren et al., 2018), surrounded by areas with lower accumulations. These physical processes may explain the differences between stations rather than local enrichments of nutrients due to islands as those three stations where the highest rates were measured are not located close to islands. However, the huge surface bloom observed at LDB (Fig. 1) and extensively studied by de Verneil et al. (2017) was mainly sustained by N_2 fixation (secondary fueling picoplankton and diatoms, Caffin et al., 2018a), rather than deep nutrient inputs (de Verneil et al., 2017). This bloom had been drifting eastwards for several months and initially originated from Fiji and Tonga archipelagoes (https://outpace.mio.univ-amu.fr/spip.php?article160, last access: February 2016), which may have provided sufficient Fe to alleviate limitation and trigger this exceptional diazotroph bloom.

4.3 *Trichodesmium*: the major contributor to N_2 fixation in the WTSP

In MA waters, the dominant diazotroph phylotypes quantified using *nifH* quantitative PCR assays were *Trichodesmium* spp. and UCYN-B (Stenegren et al., 2018), which commonly peaked at $> 10^6$ *nifH* copies $\mathrm{L^{-1}}$ in surface (0–50 m) waters. DDAs (mainly het-1, but het-2 and het-3 were also detected) were the next most abundant diazotrophs (Stenegren et al., 2018). This result is consistent with the fact that abundances of those phylotypes co-varied and were significantly positively correlated with N_2 fixation rates (Table 2). The two UCYN-A lineages (UCYN-A1 and UCYN-A2) were less abundant (< 1.0–$1.5\,\%$ of total *nifH* copies, Stenegren et al., 2018) and not significantly correlated with N_2 fixation rates (Table 2).

The relative contribution of different diazotroph phylotypes to bulk N_2 fixation has been largely investigated through bulk and size fractionation measurements (usually comparing $>$ and $< 10\,\mu m$ size fraction N_2 fixation rates), which may be misleading since some small-size diazotrophs are attached to large-size particles (Benavides et al., 2016; Bonnet et al., 2009) or form colonies or symbioses with diatoms (e.g., UCYN-B, Foster et al., 2011, 2013) and some diazotrophic-derived N released by diazotrophs is assimilated by small and large non-diazotrophic plankton (e.g., Bonnet et al., 2016a). Here we directly measured the in situ cell-specific N_2 fixation activity of the two dominating diazotroph groups in MA waters: *Trichodesmium* and UCYN-B.

At all three studied stations, *Trichodesmium* dominated, accounting for 68.0–91.8 % of the diazotroph community, followed by UCYN-B, accounting for 0.3–31.7 %. In addition, *Trichodesmium* and UCYN-B had the highest measured gene expression (10^2–10^5 cDNA *nifH* copies $\mathrm{L^{-1}}$). It was not surprising that UCYN-B had a high gene expression given that the sampling time occurred later in the day (17:00–

21:00); however, both *Trichodesmium* and het-1 (which typically reduce N_2 and express *nifH* highest during the day, Church et al., 2005) had a detectable and often equally as high expression as UCYN-B. Cell-specific N_2 fixation rates reported here are on the same order of magnitude as those reported for field populations of *Trichodesmium* (Berthelot et al., 2016; Stenegren et al., 2018) and UCYN-B (Foster et al., 2013). *Trichodesmium* was always the major contributor to N_2 fixation, accounting for 47.1–83.8 % of bulk N_2 fixation, while UCYN-B never exceeded 6.1–10.1 %, despite accounting for > 30 % of the diazotroph community at SD6. This may be linked with the lower ^{15}N enrichment at SD6 (0.517 ± 0.237 at. %), which is due to a high proportion of inactive cells (at. % close to natural abundance) compared to SD2, where the majority of cells were active and highly ^{15}N-enriched (1.163 ± 0.531 at. %). Such heterogeneity in N_2 fixation rates among UCYN-B-like cells has already been reported by Foster et al. (2013). Overall, these results show that the most abundant phylotype (*Trichodesmium*) accounts for the majority of N_2 fixation, but not in the same proportion, further indicating that the abundance of micro-organisms in seawater cannot be equated to activity, which has already been reported for other functional groups such as bacteria (Boutrif et al., 2011). In the North Pacific Gyre (station ALOHA), Foster et al. (2013) report a higher contribution of UCYN-B to daily bulk N_2 fixation (24–63 %) during the summer season, indicating that this group likely contributes more to the N budget at station ALOHA than in the WTSP, where *Trichodesmium* seems to be the major player.

5 Ecological relevance of N_2 fixation in the WTSP and conclusions

N_2 fixation was significantly positively correlated with Chl *a*, PON, POC and BSi concentrations, as well as with primary production, suggesting a tight coupling between N_2 fixation, primary production and biomass accumulation in the water column. Based on our measured C : N ratios at each depth, the computation of the N demand derived from primary production measured during OUTPACE (Johnson et al., 2007) indicates that N_2 fixation fueled on average 8.2 ± 1.9 % (range 5.9 to 11.5 %) of total primary production in the WTSP. This contribution is higher than in other oligotrophic regions such as the northwestern Pacific (Shiozaki et al., 2013), ETSP (Raimbault and Garcia, 2008), northeastern Atlantic (Benavides et al., 2013), or the Mediterranean Sea (Bonnet et al., 2011; Ridame et al., 2014), where it is generally < 5 %. However, it is comparable to results found further north in the Solomon Sea (N_2 fixation fueled 9.4 % of primary production, Berthelot et al., 2017), which is part of the WTSP "hotspot" for N_2 fixation (Bonnet et al., 2017). Caffin et al. (2018b, a) show that N_2 fixation represents the major source (> 90 %) of new N to the upper photic (productive) layer during the OUTPACE cruise, before atmospheric inputs and nitrate diffusion across the thermocline, indicating that N_2 fixation supported nearly all new production in this region during austral summer conditions.

The large amount of N provided by N_2 fixation likely stimulated the growth of non-diazotrophic plankton as suggested by significant positive correlations between N_2 fixation rates and the abundance of *Prochlorococcus* spp., *Synechococcus* spp., heterotrophic bacteria and protists. $^{15}N_2$-based transfer experiments coupled with nanoSIMS experiments designed to trace the transfer of ^{15}N in the planktonic food web demonstrated that ∼ 10 % of diazotroph-derived N is rapidly (24–48 h) transferred to non-diazotrophic phytoplankton (mainly diatoms and bacteria) in coastal waters of the WTSP (Bonnet et al., 2016a, b; Berthelot et al., 2016). The same experiments performed in offshore waters during the present cruise confirm that ∼ 10 % of recently fixed N_2 is also transferred to picophytoplankton and bacteria after 48 h (Caffin et al., 2018a). This is in accordance with Van Wambeke et al. (2018), who report that N_2 fixation fuels 40 to 70 % of the bacteria N demand in MA waters. This further demonstrates that N_2 fixation acts as an efficient natural N fertilization in the WTSP, potentially fueling subsequent export of organic material below the photic layer. Caffin et al. (2018a, b) estimated that the e-ratio, which quantifies the efficiency of a system in exporting particulate carbon relative to primary production (e-ratio = POC export/PP), was 3 times higher ($p < 0.05$) in MA waters compared to GY waters. Moreover, e-ratio values were as high as 9.7 % in MA waters, i.e., higher than the e-ratios in most studied oligotrophic regions (Karl et al., 2012; Raimbault and Garcia, 2008), where they rarely exceed 1 %, indicating that production sustained by N_2 fixation is efficiently exported in the WTSP. Diazotrophs were recovered in sediment traps during the cruise (Caffin et al., 2018a, b), but their biomass only accounted for ∼ 5 % (locally 30 % at LDA) of the N biomass in the traps, indicating that most of the export was indirect, i.e., after transfer of diazotroph-derived N to the surrounding planktonic communities that were subsequently exported. A $\delta^{15}N$ budget performed during the OUTPACE cruise reveals that N_2 fixation supports exceptionally high (> 50 % and locally > 80 % of) export production in MA waters (Knapp et al., 2018). Together these results suggest that N_2 fixation plays a critical role in export in this globally important region for elevated N_2 fixation.

The magnitude and geographic distribution of N_2 fixation control the rate of primary productivity and vertical export of carbon in the oligotrophic ocean; thus, accurate estimates of N_2 fixation are of primary importance for oceanographers to constrain and predict the evolution of marine biogeochemical carbon and N cycles. The number of N_2 fixation estimates have increased dramatically at the global scale over the past 3 decades (Luo et al., 2012). The results reported here show that some poorly sampled areas such as the WTSP provide unique conditions for diazotrophs to fix at high rates and contribute to the need to update current N_2 fixation estimates for

the Pacific Ocean. Further studies would be required to assess the seasonal variability of N_2 fixation in this region and perform accurate N budgets. Nonetheless, such high N_2 fixation rates question whether or not these high N inputs can balance the N losses in the ETSP. A recent study based on the N* (the excess of N relative to P) at the whole South Pacific scale Fumenia et al. (2018) reveals a strong positive N* anomaly (indicative of N_2 fixation) in the surface and thermocline waters of the WTSP, which potentially influences the geochemical signature of the thermocline waters further east in the South Pacific through the regional circulation. However, the WTSP is chronically undersampled, and a better description of the mesoscale and general circulation would be necessary to assess how N sources and sinks are coupled at the South Pacific scale.

Data availability. All data and metadata are available at the following web address: http://www.obs-vlfr.fr/proof/php/outpace/outpace.php, last access: June 2018.

Author contributions. SB designed the experiments; SB, MC, HB and MB carried them out at sea. MC, HB, RAF, SHN, CG and OG analyzed the samples; MC and SB analyzed the data. SB prepared the manuscript with contributions from all co-authors.

Competing interests. The authors declare that they have no conflict of interest.

Special issue statement. This article is part of the special issue "Interactions between planktonic organisms and biogeochemical cycles across trophic and N2 fixation gradients in the western tropical South Pacific Ocean: a multidisciplinary approach (OUTPACE experiment)". It is not associated with a conference.

Acknowledgements. This research is a contribution of the OUTPACE (Oligotrophy from Ultra-oligoTrophy PACific Experiment) project (https://outpace.mio.univ-amu.fr/, last access: June 2018) funded by the Agence Nationale de la Recherche (grant ANR-14-CE01-0007-01), the LEFE-CyBER program (CNRS-INSU), the Institut de Recherche pour le Développement (IRD), the GOPS program (IRD) and the CNES (BC T23, ZBC 4500048836). The OUTPACE cruise (http://dx.doi.org/10.17600/15000900, last access: June 2018) was managed by the MIO (OSU Institut Pytheas, AMU) from Marseilles (France). The authors thank the crew of the R/V *L'Atalante* for outstanding shipboard operations. Gilles Rougier and Marc Picheral are warmly thanked for their efficient help in CTD rosette management and data processing, as well as Catherine Schmechtig for the LEFE-CyBER database management and Thibaut Wagener for providing the map of bathymetry. Aurelia Lozingot is acknowledged for the administrative work. Mar Benavides was funded by the People Programme (Marie Skłodowska-Curie Actions) of the European Union's Seventh Framework Programme (FP7/2007-2013) under REA grant agreement number 625185. The participation, nucleic acid sampling and analysis were provided to Rachel A. Foster by the Knut and Alice Wallenberg Foundation. Rachel A. Foster also acknowledges the assistance by Lotta Berntzon, Marcus Stenegren and Andrea Caputo. The satellite products are provided by CLS with the support of CNES.

Edited by: Douglas G. Capone
Reviewed by: Carolin Löscher and three anonymous referees

References

Aminot, A. and Kérouel, R.: Dosage automatique des nutriments dans les eaux marines: méthodes en flux continu, Editions Quae, 2007.

Benavides, M. and Voss, M.: Five decades of N_2 fixation research in the North Atlantic Ocean, Frontiers in Marine Science, 2, 1–20, https://doi.org/10.3389/fmars.2015.00040, 2015.

Benavides, M., Bronk, D. A., Agawin, N. S., Pérez-Hernández, M. D., Hernández-Guerra, A., and Arístegui, J.: Longitudinal variability of size-fractionated N_2 fixation and DON release rates along 24.5° N in the subtropical North Atlantic, J. Geophys. Res.-Oceans, 118, 3406–3415, 2013.

Benavides, M., Moisander, P. H., Berthelot, H., Dittmar, T., and Grosso, O.: Mesopelagic N_2 fixation related to organic matter composition in the Solomon and Bismarck Seas (Southwest Pacific), PLoS One, 10, 12, https://doi.org/10.1371/journal.pone.0143775, 2015.

Benavides, M., Moisander, P. H., Daley, M. C., Bode, A., and Arístegui, J.: Longitudinal variability of diazotroph abundances in the subtropical North Atlantic Ocean, J. Plankton Res., 38, 662–672, 2016.

Benavides, M., Berthelot, H., Duhamel, S., Raimbault, P., and Bonnet, S.: Dissolved organic matter uptake by Trichodesmium in the Southwest Pacific, Sci. Rep.-UK, 7, 41315, https://doi.org/10.1038/srep41315, 2017.

Berthelot, H., Bonnet, S., Grosso, O., Cornet, V., and Barani, A.: Transfer of diazotroph-derived nitrogen towards non-diazotrophic planktonic communities: a comparative study between *Trichodesmium erythraeum*, *Crocosphaera watsonii* and *Cyanothece* sp., Biogeosciences, 13, 4005–4021, https://doi.org/10.5194/bg-13-4005-2016, 2016.

Berthelot, H., Benavides, M., Moisander, P. H., Grosso, O., and Bonnet, S.: High-nitrogen fixation rates in the particulate and dissolved pools in the Western Tropical Pacific (Solomon and Bismarck Seas), Geophys. Res. Lett., 2, 1–10, https://doi.org/10.1002/2017GL073856, 2017.

Blain, S., Bonnet, S., and Guieu, C.: Dissolved iron distribution in the tropical and sub tropical South Eastern Pacific, Biogeosciences, 5, 269–280, https://doi.org/10.5194/bg-5-269-2008, 2008.

Bock, N., Van Wambeke, F., Dion, M., and Duhamel, S.: Microbial community structure in the Western Tropical South Pacific, Biogeosciences Discuss., https://doi.org/10.5194/bg-2017-562, in review, 2018.

Bonnet, S. and Guieu, C.: Atmospheric forcing on the annual iron cycle in the Mediterranean Sea. A one-year survey, J. Geophys. Res., 111, C9, https://doi.org/10.1029/2005JC003213, 2006.

Bonnet, S., Guieu, C., Bruyant, F., Prášil, O., Van Wambeke, F., Raimbault, P., Moutin, T., Grob, C., Gorbunov, M. Y., Zehr, J. P., Masquelier, S. M., Garczarek, L., and Claustre, H.: Nutrient limitation of primary productivity in the Southeast Pacific (BIOSOPE cruise), Biogeosciences, 5, 215–225, https://doi.org/10.5194/bg-5-215-2008, 2008.

Bonnet, S., Biegala, I. C., Dutrieux, P., Slemons, L. O., and Capone, D. G.: Nitrogen fixation in the western equatorial Pacific: Rates, diazotrophic cyanobacterial size class distribution, and biogeochemical significance, Global Biogeochem. Cy., 23, 1–13, https://doi.org/10.1029/2008gb003439, 2009.

Bonnet, S., Grosso, O., and Moutin, T.: Planktonic dinitrogen fixation along a longitudinal gradient across the Mediterranean Sea during the stratified period (BOUM cruise), Biogeosciences, 8, 2257–2267, https://doi.org/10.5194/bg-8-2257-2011, 2011.

Bonnet, S., Rodier, M., Turk-Kubo, K., Germineaud, C., Menkes, C., Ganachaud, A., Cravatte, S., Raimbault, P., Campbell, E., Quéroué, F., Sarthou, G., Desnues, A., Maes, C., and Eldin, G.: Contrasted geographical distribution of N_2 fixation rates and *nifH* phylotypes in the Coral and Solomon Seas (South-Western Pacific) during austral winter conditions, Global Biogeochem. Cy., 29, 11, https://doi.org/10.1002/2015GB005117, 2015.

Bonnet, S., Berthelot, H., Turk-Kubo, K. A., Cornet-Barthaux, V., Fawcett, S., Berman-Frank, I., Barani, A., Grégori, G., Dekaezemacker, J., Benavides, M., and Capone, D. G.: Diazotroph derived nitrogen supports diatom growth in the South West Pacific: A quantitative study using nanoSIMS, Limnol. Oceanogr., 61, 1549–1562, https://doi.org/10.1002/lno.10300, 2016a.

Bonnet, S., Berthelot, H., Turk-Kubo, K., Fawcett, S., Rahav, E., L'Helguen, S., and Berman-Frank, I.: Dynamics of N_2 fixation and fate of diazotroph-derived nitrogen in a low-nutrient, low-chlorophyll ecosystem: results from the VAHINE mesocosm experiment (New Caledonia), Biogeosciences, 13, 2653–2673, https://doi.org/10.5194/bg-13-2653-2016, 2016b.

Bonnet, S., Caffin, M., Berthelot, H., and Moutin, T.: Hot spot of N_2 fixation in the western tropical South Pacific pleads for a spatial decoupling between N_2 fixation and denitrification, P. Natl. Acad. Sci. USA, 114, E2800–E2801, https://doi.org/10.1073/pnas.1619514114, 2017.

Böttjer, D., Dore, J. E., Karl, D. M., Letelier, R. M., Mahaffey, C., Wilson, S. T., Zehr, J. P., and Church, M. J.: Temporal variability of nitrogen fixation and particulate nitrogen export at Station ALOHA, Limnol. Oceanogr., 62, 200–216, https://doi.org/10.1002/lno.10386, 2017.

Breitbarth, E., Oschlies, A., and LaRoche, J.: Physiological constraints on the global distribution of *Trichodesmium* – effect of temperature on diazotrophy, Biogeosciences, 4, 53–61, https://doi.org/10.5194/bg-4-53-2007, 2007.

Boutrif, M., Garel, M., Cottrell, M. T., and Tamburini, C.: Assimilation of marine extracellular polymeric substances by deep-sea prokaryotes in the NW Mediterranean Sea, Environmental microbiology reports, 3, 705–709, https://doi.org/10.1111/j.1758-2229.2011.00285.x, 2011.

Caffin, M., Berthelot, H., Cornet-Barthaux, V., Barani, A., and Bonnet, S.: Transfer of diazotroph-derived nitrogen to the planktonic food web across gradients of N_2 fixation activity and diversity in the western tropical South Pacific Ocean, Biogeosciences, 15, 3795–3810, https://doi.org/10.5194/bg-15-3795-2018, 2018a.

Caffin, M., Moutin, T., Foster, R. A., Bouruet-Aubertot, P., Doglioli, A. M., Berthelot, H., Guieu, C., Grosso, O., Helias-Nunige, S., Leblond, N., Gimenez, A., Petrenko, A. A., de Verneil, A., and Bonnet, S.: N_2 fixation as a dominant new N source in the western tropical South Pacific Ocean (OUTPACE cruise), Biogeosciences, 15, 2565–2585, https://doi.org/10.5194/bg-15-2565-2018, 2018b.

Carpenter, E. J., Subramaniam, A., and Capone, D. G.: Biomass and primary productivity of the cyanobacterium *Trichodesmium* spp. in the tropical N Atlantic ocean, Deep-Sea Res. Pt. I, 51, 173–203, 2004.

Church, M. J., Short, C. M., Jenkins, B. D., Karl, D. M., and Zehr, J. P.: Temporal patterns of nitrogenase gene (*nifH*) expression in the oligotrophic North Pacific Ocean, Appl. Environ. Microb., 71, 5362–5370, https://doi.org/10.1128/aem.71.9.5362-5370.2005, 2005.

Cook, J.: The Voyages of Captain James Cook, vol. 2, William Smith, 1842.

Dabundo, R., Lehmann, M. F., Treibergs, L., Tobias, C. R., Altabet, M. A., Moisander, A. M., and Granger, J.: The contamination of commercial $^{15}N_2$ gas stocks with ^{15}N labeled nitrate and ammonium and consequences for nitrogen fixation measurements, PLoS One, 9, e110335, https://doi.org/10.1371/journal.pone.0110335, 2014.

Dandonneau, Y., Vega, A., Loisel, H., du Penhoat, Y., and Menkes, C.: Oceanic Rossby waves acting as a "hay rake" for ecosystem floating by-products, Science, 302, 1548–1551, https://doi.org/10.1126/science.1090729, 2003.

de Boyer Montégut, C., Madec, G., Fischer, A. S., Lazar, A., and Iudicone, D.: Mixed layer depth over the global ocean: An examination of profile data and a profile-based climatology, J. Geophys. Res.-Oceans, 109, C12, https://doi.org/10.1029/2004JC002378, 2004.

Dekaezemacker, J. and Bonnet, S.: Sensitivity of N_2 fixation to combined nitrogen forms (NO_3^- and NH_4^+) in two strains of the marine diazotroph *Crocosphaera watsonii* (Cyanobacteria), Mar. Ecol. Prog. Ser., 438, 33–46, https://doi.org/10.3354/meps09297, 2011.

Dekaezemacker, J., Bonnet, S., Grosso, O., Moutin, T., Bressac, M., and Capone, D. G.: Evidence of active dinitrogen fixation in surface waters of the Eastern Tropical South Pacific during El Nino and La Nina events and evaluation of its potential nutrient controls, Global Biogeochem. Cy., 27, 1–12, https://doi.org/10.1002/gbc.20063, 2013.

Deutsch, C. A., Sarmiento, J. L., Sigman, D. M., Gruber, N., and Dunne, J. P.: Spatial coupling of nitrogen inputs and losses in the ocean, Nature, 445, 163–167, https://doi.org/10.1038/nature05392, 2007.

de Verneil, A., Rousselet, L., Doglioli, A. M., Petrenko, A. A., and Moutin, T.: The fate of a southwest Pacific bloom: gauging the impact of submesoscale vs. mesoscale circulation on biological gradients in the subtropics, Biogeosciences, 14, 3471–3486, https://doi.org/10.5194/bg-14-3471-2017, 2017.

Dugdale, R. C. and Goering, J. J.: Uptake of new and regenerated forms of nitrogen in primary productivity, Limnol. Oceanogr., 12, 196–206, https://doi.org/10.4319/lo.1967.12.2.0196, 1967.

Dupouy, C., Neveux, J., Subramaniam, A., Mulholland, M. R., Montoya, J. P., Campbell, L., Carpenter, E. J., and Capone, D. G.: Satellite captures Trichodesmium blooms in the southwestern tropical Pacific, EOS Transactions American Geophysical Union, 81, 13–16, 2000.

Dupouy, C., Benielli-Gary, D., Neveux, J., Dandonneau, Y., and Westberry, T. K.: An algorithm for detecting *Trichodesmium* surface blooms in the South Western Tropical Pacific, Biogeosciences, 8, 3631–3647, https://doi.org/10.5194/bg-8-3631-2011, 2011.

Dutheil, C., Aumont, O., Gorguès, T., Lorrain, A., Bonnet, S., Rodier, M., Dupouy, C., Shiozaki, T., and Menkes, C.: Modelling the processes driving *Trichodesmium* sp. spatial distribution and biogeochemical impact in the tropical Pacific Ocean, Biogeosciences Discuss., https://doi.org/10.5194/bg-2017-559, in review, 2018.

Eppley, R. W. and Peterson, B. J.: Particulate organic matter flux and planktonic new production in the deep ocean, Nature, 282, 677–680, https://doi.org/10.1038/282677a0, 1979.

Falkowski, P. G.: Light-shade adaptation and vertical mixing of marine phytoplankton: a comparative field study, J. Mar. Res., 41, 215–237, 1983.

Fernández, C., Farías, L., and Ulloa, O.: Nitrogen Fixation in Denitrified Marine Waters, PLoS One, 6, e20539, https://doi.org/10.1371/journal.pone.0020539, 2011.

Fernández, C., González, M. L., Muñoz, C., Molina, V., and Farias, L.: Temporal and spatial variability of biological nitrogen fixation off the upwelling system of central Chile (35–38.5° S), J. Geophys. Res.-Oceans, 120, 3330–3349, 2015.

Fitzsimmons, J. N., Boyle, E. A., and Jenkins, W. J.: Distal transport of dissolved hydrothermal iron in the deep South Pacific Ocean, P. Natl. Acad. Sci. USA, 111, 16654–16661, 2014.

Foster, R. A., Goebel, N. L., and Zehr, J. P.: Isolation of Calothrix rhizosoleniae (cyanobacteria) strain SC01 from Chaetoceros (Bacillariophyta) spp. diatoms of the Subtropical North Pacific Ocean, J. Phycol., 45, 1028–1037, 2010.

Foster, R. A., Kuypers, M. M. M., Vagner, T., Paerl, R. W., Musat, N., and Zehr, J. P.: Nitrogen fixation and transfer in open ocean diatom-cyanobacterial symbioses, ISME J., 5, 1484–1493, 2011.

Foster, R. A., Sztejrenszus, S., and Kuypers, M. M. M.: Measuring carbon and N_2 fixation in field populations of colonial and free living cyanobacteria using nanometer scale secondary ion mass spectrometry, J. Phycol., 49, 502–516, 2013.

Fumenia, A., Moutin, T., Bonnet, S., Benavides, M., Petrenko, A., Helias Nunige, S., and Maes, C.: Excess nitrogen as a marker of intense dinitrogen fixation in the Western Tropical South Pacific Ocean: impact on the thermocline waters of the South Pacific, Biogeosciences Discuss., https://doi.org/10.5194/bg-2017-557, in review, 2018.

Gradoville, M. R., Bombar, D., Crump, B. C., Letelier, R. M., Zehr, J. P., and White, A. E.: Diversity and activity of nitrogen-fixing communities across ocean basins, Limnol. Oceanogr., 62, 1895–1909, 2017.

Gruber, N.: The marine nitrogen cycle: Overview and challenges. Nitrogen in the Marine Environment, edited by: Capone, D. G., Bronk, D. A., Mulholland, M. R., and Carpenter, E. J., Academic, San Diego, 1–50, 2008.

Gruber, N.: Elusive marine nitrogen fixation, P. Natl. Acade. Sci. USA, 113, 4246–4248, 2016.

Guieu, C., Bonnet, S., Petrenko, A., Menkes, C., Chavagnac, V., Desboeufs, C., Maes, C., and Moutin, T.: Iron from a submarine source impacts the productive layer of the Western Tropical South Pacific (WTSP), Sci. Rep.-UK, 8, 9075, https://doi.org/10.1038/s41598-018-27407-z, 2018.

Johnson, K. S., Elrod, V., Fitzwater, S., Plant, J., Boyle, E., Bergquist, B., Bruland, K., Aguilar-Islas, A., Buck, K., Lohan, M., Smith, G. J., Sohst, B., Coale, K., Gordon, M., Tanner, S., Measures, C., Moffett, J., Barbeau, K., King, A., Bowie, A., Chase, Z., Cullen, J., Laan, P., Landing, W., Mendez, J., Milne, A., Obata, H., Doi, T., Ossiander, L., Sarthou, G., Sedwick, P., Van den Berg, S., Laglera-Baquer, L., Wu, J.-F., and Cai, Y.: Developing standards for dissolved iron in seawater, Eos, Transactions American Geophysical Union, 88, 131–132, 2007.

Kana, T. M., Darkangelo, C., Hunt, M. D., Oldham, J. B., Bennett, G. E., and Cornwell, J. C.: A membrane inlet mass spectrometer for rapid high precision determination of N_2, O_2, and Ar in environmental water samples, Anal. Chem., 66, 4166–4170, 1994.

Karl, D. M., Bates, N. R., Emerson, S., Harrison, P. J., del Octavio Llinâs, C. J., Liu, K.-K., Marty, J.-C., Michaels, A. F., Miquel, J. C., Neuer, S., Nojiri, Y., and Wong, C. S.: Temporal studies of biogeochemical processes determined from ocean time-series observations during the JGOFS era, in: Ocean Biogeochemistry, Springer, Berlin, Heidelberg, 239–267, 2003.

Karl, D. M., Church, M. J., Dore, J. E., Letelier, R. M., and Mahaffey, C.: Predictable and efficient carbon sequestration in the North Pacific Ocean supported by symbiotic nitrogen fixation, P. Natl. Acad. Sci. USA, 109, 1842–1849, https://doi.org/10.1073/pnas.1120312109, 2012.

Klawonn, I., Lavik, G., Böning, P., Marchant, H., Dekaezemacker, J., Mohr, W., and Ploug, H.: Simple approach for the preparation of ^{15}-$^{15}N_2$-enriched water for nitrogen fixation assessments: evaluation, application and recommendations, Front. Microbiol., 6, https://doi.org/10.3389/fmicb.2015.00769, 2015.

Knap, A. H., Michaels, A., Close, H., Ducklow, H. W., and Dickson, A. G. (Eds.): Protocols for the Joint Global Ocean Flux Study (JGOFS) core measurements, JGOFS Rep. 19, 170 p., Carbon Dioxide Inf. Anal. Cent., Oak Ridge Natl. Lab., Oak Ridge, Tenn., 1994.

Knapp, A. N., Dekaezemacker, J., Bonnet, S., Sohm, J. A., and Capone, D. G.: Sensitivity of *Trichodesmium erythraeum* and *Crocosphaera watsonii* abundance and N_2 fixation rates to varying NO_3^- and PO_4^{3-} concentrations in batch cultures, Aquat. Microb. Ecol., 66, 223–236, 2012.

Knapp, A. N., Casciotti, K. L., Berelson, W. M., Prokopenko, M. G., and Capone, D. G.: Low rates of nitrogen fixation in eastern tropical South Pacific surface waters, P. Natl. Acad. Sci. USA, 113, 4398–4403, 2016.

Knapp, A. N., McCabe, K. M., Grosso, O., Leblond, N., Moutin, T., and Bonnet, S.: Distribution and rates of nitrogen fixation in the western tropical South Pacific Ocean constrained by nitrogen isotope budgets, Biogeosciences, 15, 2619–2628, https://doi.org/10.5194/bg-15-2619-2018, 2018.

Labatut, M., Lacan, F., Pradoux, C., Chmeleff, J., Radic, A., Murray, J. W., Poitrasson, F., Johansen, A. M., and Thil, F.: Iron sources and dissolved-particulate interactions in the seawater of the Western Equatorial Pacific, iron isotope perspectives, Global Biogeochem. Cy., 28, 1044–1065, https://doi.org/10.1002/2014GB004928, 2014.

Loescher, C. R., Großkopf, T., Desai, F. D., Gill, D., Schunck, H., Croot, P. L., and Kuypers, M. M.: Facets of diazotrophy in the oxygen minimum zone waters off Peru, The ISME journal, 8, 2180, https://doi.org/10.1038/ismej.2014.71, 2014.

Luo, Y.-W., Doney, S. C., Anderson, L. A., Benavides, M., Berman-Frank, I., Bode, A., Bonnet, S., Boström, K. H., Böttjer, D., Capone, D. G., Carpenter, E. J., Chen, Y. L., Church, M. J., Dore, J. E., Falcón, L. I., Fernández, A., Foster, R. A., Furuya, K., Gómez, F., Gundersen, K., Hynes, A. M., Karl, D. M., Kitajima, S., Langlois, R. J., LaRoche, J., Letelier, R. M., Marañón, E., McGillicuddy Jr., D. J., Moisander, P. H., Moore, C. M., Mouriño-Carballido, B., Mulholland, M. R., Needoba, J. A., Orcutt, K. M., Poulton, A. J., Rahav, E., Raimbault, P., Rees, A. P., Riemann, L., Shiozaki, T., Subramaniam, A., Tyrrell, T., Turk-Kubo, K. A., Varela, M., Villareal, T. A., Webb, E. A., White, A. E., Wu, J., and Zehr, J. P.: Database of diazotrophs in global ocean: abundance, biomass and nitrogen fixation rates, Earth Syst. Sci. Data, 4, 47–73, https://doi.org/10.5194/essd-4-47-2012, 2012.

Luo, Y.-W., Lima, I. D., Karl, D. M., Deutsch, C. A., and Doney, S. C.: Data-based assessment of environmental controls on global marine nitrogen fixation, Biogeosciences, 11, 691–708, https://doi.org/10.5194/bg-11-691-2014, 2014.

Massoth, G., Baker, E., Worthington, T., Lupton, J., de Ronde, C., Arculus, R., Walker, S., Nakamura, K. I., Ishibashi, J. I., and Stoffers, P.: Multiple hydrothermal sources along the south Tonga arc and Valu Fa Ridge, Geochem. Geophys. Geosyst., 8, https://doi.org/10.1029/2007GC001675, 2007.

Messer, L. F., Mahaffey, C., M Robinson, C., Jeffries, T. C., Baker, K. G., Bibiloni Isaksson, J., Ostrowski, M., Doblin, M. A., Brown, M. V., and Seymour, J. R.: High levels of heterogeneity in diazotroph diversity and activity within a putative hotspot for marine nitrogen fixation, ISME J., 10, 1499, https://doi.org/10.1038/ismej.2015.205, 2015.

Mohr, W., Großkopf, T., Wallace, D. W. R., and LaRoche, J.: Methodological underestimation of oceanic nitrogen fixation rates, PLoS ONE, 5, 1–7, https://doi.org/10.1371/journal.pone.0012583, 2010.

Moisander, P. H., Beinart, R. A., Hewson, I., White, A. E., Johnson, K. S., Carlson, C. A., Montoya, J. P., and Zehr, J. P.: Unicellular Cyanobacterial Distributions Broaden the Oceanic N_2 Fixation Domain, Science, 327, 1512–1514, https://doi.org/10.1126/science.1185468, 2010.

Moisander, P. H., Zhang, R. F., Boyle, E. A., Hewson, I., Montoya, J. P., and Zehr, J. P.: Analogous nutrient limitations in unicellular diazotrophs and *Prochlorococcus* in the South Pacific Ocean, ISME J., 6, 733–744, https://doi.org/10.1038/ismej.2011.152, 2011.

Montoya, J. P., Voss, M., Kahler, P., and Capone, D. G.: A simple, high-precision, high-sensitivity tracer assay for N_2 fixation, Appl. Environ. Microb., 62, 986–993, 1996.

Montoya, J. P., Holl, C. M., Zehr, J. P., Hansen, A., Villareal, T. A., and Capone, D. G.: High rates of N_2 fixation by unicellular diazotrophs in the oligotrophic Pacific Ocean, Nature, 430, 1027–1031, https://doi.org/10.1038/nature02824, 2004.

Moore, C. M., Mills, M. M., Arrigo, K. R., Berman-Frank, I., Bopp, L., Boyd, P. W., Galbraith, E. D., Geider, R. J., Guieu, C., Jaccard, S. L., Jickells, T. D., La Roche, J., Lenton, T. M., Mahowald, N. M., Marañón, E., Marinov, I., Moore, J. K., Nakatsuka, T., Oschlies, A., Saito, M. A., Thingstad, T. F., Tsuda, A., and Ulloa, O.: Processes and patterns of oceanic nutrient limitation, Nat. Geosci., 6, 701–710, https://doi.org/10.1038/ngeo1765, 2013.

Moutin, T., Van Den Broeck, N., Beker, B., Dupouy, C., Rimmelin, P., and Le Bouteiller, A.: Phosphate availability controls *Trichodesmium* spp. biomass in the SW Pacific Ocean, Mar. Ecol. Prog. Ser., 297, 15–21, https://doi.org/10.3354/meps297015, 2005.

Moutin, T., Karl, D. M., Duhamel, S., Rimmelin, P., Raimbault, P., Van Mooy, B. A. S., and Claustre, H.: Phosphate availability and the ultimate control of new nitrogen input by nitrogen fixation in the tropical Pacific Ocean, Biogeosciences, 5, 95–109, https://doi.org/10.5194/bg-5-95-2008, 2008.

Moutin, T., Doglioli, A. M., de Verneil, A., and Bonnet, S.: Preface: The Oligotrophy to the UlTra-oligotrophy PACific Experiment (OUTPACE cruise, 18 February to 3 April 2015), Biogeosciences, 14, 3207–3220, https://doi.org/10.5194/bg-14-3207-2017, 2017.

Moutin, T., Wagener, T., Caffin, M., Fumenia, A., Gimenez, A., Baklouti, M., Bouruet-Aubertot, P., Pujo-Pay, M., Leblanc, K., Lefevre, D., Helias Nunige, S., Leblond, N., Grosso, O., and de Verneil, A.: Nutrient availability and the ultimate control of the biological carbon pump in the western tropical South Pacific Ocean, Biogeosciences, 15, 2961–2989, https://doi.org/10.5194/bg-15-2961-2018, 2018.

Nübel, U., Garcia-Pichel, F., and Muyzer, G.: PCR primers to amplify 16S rRNA genes from cyanobacteria, Appl. Environ. Microb., 63, 3327–3332, 1997.

Radic, A., Lacan, F., and Murray, J. W.: Iron isotopes in the seawater of the equatorial Pacific Ocean: New constraints for the oceanic iron cycle, Earth Planet. Sc. Lett., 306, 1–10, 2011.

Raimbault, P. and Garcia, N.: Evidence for efficient regenerated production and dinitrogen fixation in nitrogen-deficient waters of the South Pacific Ocean: impact on new and export production estimates, Biogeosciences, 5, 323–338, https://doi.org/10.5194/bg-5-323-2008, 2008.

Raven, J. A.: The iron and molybdenum use efficiencies of plant growth with different energy, carbon and nitrogen source, New Phytol., 109, 279–287, 1988.

Ridame, C., Dekaezemacker, J., Guieu, C., Bonnet, S., L'Helguen, S., and Malien, F.: Contrasted Saharan dust events in LNLC environments: impact on nutrient dynamics and primary production, Biogeosciences, 11, 4783–4800, https://doi.org/10.5194/bg-11-4783-2014, 2014.

Shiozaki, T., Kodama, T., Kitajima, S., Sato, M., and Furuya, K.: Advective transport of diazotrophs and importance of their nitrogen fixation on new and primary production in the western Pacific warm pool, Limnol. Oceanogr., 58, 49–60, https://doi.org/10.4319/lo.2013.58.1.0049, 2013.

Shiozaki, T., Kodama, T., and Furuya, K.: Large-scale impact of the island mass effect through nitrogen fixation in the western South Pacific Ocean, Geophys. Res. Lett., 41, 2907–2913, 2014.

Sohm, J. A. and Capone, D. G.: Phosphorus dynamics of the tropical and subtropical north Atlantic: *Trichodesmium* spp. versus bulk plankton, Mar. Ecol. Prog. Ser., 317, 21–28, 2006.

Stenegren, M., Caputo, A., Berg, C., Bonnet, S., and Foster, R. A.: Distribution and drivers of symbiotic and free-living diazotrophic cyanobacteria in the western tropical South Pacific,

Biogeosciences, 15, 1559–1578, https://doi.org/10.5194/bg-15-1559-2018, 2018.

Tenório, M. M. B., Dupouy, C., Rodier, M., and Neveux, J.: Trichodesmium and other planktonic cyanobacteria in New Caledonian waters (SW tropical Pacific) during an El Niño episode, Aquat. Microb. Ecol., 81, 219–241, 2018.

Thompson, A. W., Foster, R. A., Krupke, A., Carter, B. J., Musat, N., Vaulot, D., Kuypers, M. M. M., and Zehr, J. P.: Unicellular cyanobacterium symbiotic with a single-celled eukaryotic alga, Science, 337, 1546–1550, https://doi.org/10.1126/science.1222700, 2012.

Van Wambeke, F., Gimenez, A., Duhamel, S., Dupouy, C., Lefevre, D., Pujo-Pay, M., and Moutin, T.: Dynamics and controls of heterotrophic prokaryotic production in the western tropical South Pacific Ocean: links with diazotrophic and photosynthetic activity, Biogeosciences, 15, 2669–2689, https://doi.org/10.5194/bg-15-2669-2018, 2018.

Verity, P. G., Robertson, C. Y., Tronzo, C. R., Andrews, M. G., Nelson, J. R., and Sieracki, M. E.: Relationships between cell volume and the carbon and nitrogen content of marine photosynthetic nanoplankton, Limnol. Oceanogr., 37, 1434–1446, https://doi.org/10.4319/lo.1992.37.7.1434, 1992, 1992.

Wannicke, N., Benavides, M., Dalsgaard, T., Dippner, J. W., Montoya, J. P., and Voss, M.: New Perspectives on Nitrogen Fixation Measurements Using $^{15}N_2$ Gas, Frontiers in Marine Science, 5, 120, 2018.

Weiss, R. F.: The solubility of nitrogen, oxygen and argon in water and seawater, Deep-Sea Res., 17, 721–735, 1970.

Wilson, S. T., Böttjer, D., Church, M. J., and Karl, D. M.: Comparative assessment of nitrogen fixation methodologies conducted in the oligotrophic Noth Pacific Ocean, Appl. Environ. Microb., 78, 6516–6523, https://doi.org/10.1128/aem.01146-12, 2012.

Zehr, J. P. and Turner, P. J.: Nitrogen fixation: Nitrogenase genes and gene expression, in: Methods in Marine Microbiology, Academic Press, New York, 2001.

2.4 Conclusion et perspectives

Le travail de synthèse des données de fixation de N_2, dans l'océan Pacifique tropical sud-ouest révèle que cette région de l'océan mondial est un hot spot de diazotrophie. Ce hot spot présente des taux plus forts que les taux prédits par les modèles dans cette région et dans la gamme haute des taux recensés dans la base de données mondiale MAREDAT. Les données montrent que ce hot spot s'étend sur une vaste région allant de la Mer de Bismarck à la Mer des Salomon (i.e. de l'équateur à 12 $^\circ$ S), plus au sud de la Mer des Salomon jusqu'à la Mer de Corail (i.e. de 12 $^\circ$ S à 25 $^\circ$ S) et s'étend d'ouest en est de l'Australie/Papouasie Nouvelle Guinée à l'ensemble des archipels mélanésiens (Nouvelle Calédonie, Vanuatu, Fidji) et couvre une zone allant jusqu'à l'archipel de Tonga à l'est.
La région du Pacifique tropical sud-ouest, qui est le siège d'une intense diazotrophie couvre une vaste surface s'étendant sur $\sim$ 5,4 x 10^6 km^2. L'ensemble des données de fixation de N_2 récoltées dans cette région permet de pouvoir estimer la source d'azote que représente la diazotrophie à l'échelle annuelle. Pour effectuer ce travail, il est nécessaire de prendre en compte la variabilité saisonnière. Sur les campagnes dont nous avons utilisé les données dans cette étude, trois ont eu lieu durant été austral (MoorSPICE, OUTPACE, EUC-Fe) et deux durant l'hiver austral (PANDORA, BIFURCATION). Cela permet de réaliser un premier bilan prenant en compte la saisonnalité, bien qu'une grande partie des données utilisées soit issues de la campagne OUTPACE réalisée durant l'été austral, pouvant ainsi sur-estimer le bilan. En appliquant la moyenne de 570 μmol N m^{-2} d^{-1} à la surface de la région, nous estimons que le diazotrophie représenterait une source de 16 Tg N an^{-1} dans le Pacifique tropical sud-ouest. Cette source d'azote de 16 Tg N an^{-1} représente $\sim$13 % des apports d'azote par la diazotrophie à l'échelle mondiale (i.e. $\sim$ 6 % des apports totaux d'azote) selon le bilan de Gruber (2008) (Table 1.2) et $\sim$17 % des apports par la fixation de N_2 à l'échelle de l'océan Pacifique selon le bilan de Deutsch et al. (2007), alors que cette région ne représente que 1,7 % de la surface de l'océan mondial. Dans leur étude Deutsch et al. (2007) avaient estimé de très forts taux de fixation de N_2 dans la région du Pacifique tropical sud-est, qui devaient contre-balancer les pertes par dénitrification. Il s'est avéré que dans le Pacifique tropical sud-est, les flux de fixation de N_2 étaient faibles et que la diazotrophie n'apportait à l'océan que $\sim$1,2 Tg N an^{-1}, ce qui est bien inférieur à ce qui avait été prédit, et d'un ordre de grandeur plus faible que l'apport d'azote estimé dans le Pacifique tropical sud-ouest. Les pertes d'azote dans le Pacifique sud-est sont estimées à $\sim$18 Tg N an^{-1} (Hamersley et al., 2007), ce qui est de l'ordre de grandeur des gains que nous avons estimés dans le Pacifique sud-ouest. Les pertes et les gains pourraient alors s'équilibrer à l'échelle du bassin du Pacifique sud, et notre étude plaide ainsi pour un découplage spatial entre celles-ci, contrairement à ce qui avait été suggéré par Deutsch et al. (2007).
Notons que lors des campagnes réalisées dans le Pacifique tropical sud-ouest, deux types de méthode de marquage isotopique au $^{15}N_2$ ont été utilisées : la méthode de la bulle

(Montoya et al., 1996) et celle de l'eau enrichie (Mohr et al., 2010). Dans le cadre de la campagne OUTPACE entre autres, nous avons utilisé la méthode de la bulle conscient des avantages et des inconvénients qu'elle peut représenter, comme indiqué dans l'article de (Bonnet et al., 2018). L'utilisation de cette méthode fait débat au sein de la communauté scientifique car elle sous-estimerait potentiellement les flux de fixation de N_2 (Großkopf et al., 2012; Klawonn et al., 2015; Mohr et al., 2010; Wilson et al., 2012). Si il s'avérait que nous ayons sous-estimé les flux de fixation de N_2 en utilisant la méthode de la bulle, ceci renforcerait le fait que le Pacifique tropical sud-ouest soit un hot spot de fixation de N_2.

La question de savoir « pourquoi cette région est un hot spot de diazotrophie ? », soulève la question de savoir « qu'est ce qui contrôle la diazotrophie dans cette région, et plus généralement dans l'océan ? ». Pour répondre à ce type de question il est usuel d'étudier les liens statistiques existant entre la variation spatiale de fixation d'azote et celle des paramètres environnementaux communément admis pour contrôler ce processus. Dans les eaux des archipels Mélanésiens, les taux de fixation de N_2 sont beaucoup plus forts que dans les eaux de la gyre du Pacifique sud, cependant les températures de surface sont optimales pour le développement des diazotrophes (> 28 °C dans la couche de surface, Rousselet et al., 2018) dans les deux régions. Cela indique que la température de surface ne peut pas expliquer les différences significatives de fixation de N_2 observées entre les deux régions. Les taux de fixation de N_2 sont significativement et positivement corrélés avec les concentrations en chlorophylle *a*, en azote et carbone organique dissous et en silice biogénique, mais aussi avec les taux de production primaire. Ces résultats suggèrent un lien étroit entre diazotrophie, production primaire et accumulation de biomasse dans la colonne d'eau. Notre hypothèse pour expliquer la présence d'un hot spot et la distribution spatiale de la fixation de N_2 dans les archipels Mélanésiens est la suivante : Les eaux chargées en DIP du Pacifique tropical sud-est sont advectées d'est en ouest par le courant sud-équatorial (SEC). Ces eaux traversent la gyre du Pacifique sud où les diazotrophes ne se développent pas, alors que les températures de surface sont optimales (> 25 °C Breitbarth et al., 2007), car les eaux de la gyre sont dépourvues en Fe (Blain et al., 2008; Bonnet et al., 2008; Moutin et al., 2008). Lorsque les eaux de la gyre, chargées en DIP et pauvres en NO_3^-, sont advectées plus à l'ouest dans les eaux chaudes et riches en Fe de la faille de Tonga, toutes les conditions environnementales sont réunies pour que les efflorescences de diazotrophes aient lieu.

L'étude de la diversité des diazotrophes durant OUTPACE (Stenegren et al., 2018) a permis de montrer que dans les eaux des archipels Mélanésiens, *Trichodesmium* domine la communauté diazotrophe, suivi des UCYN-B. De plus, en observant les données de fixation de N_2 spécifique par spectrométrie de masse à ionisation secondaire à l'échelle nanométrique (nanoSIMS) il apparaît que *Trichodesmium* contribue pour 47.1 à 83.8 % de la fixation de N_2 totale particulaire, suivi des UCYN-B qui comptent pour 6.1 à 10.1 % alors qu'elles représentent jusqu'à 30 % de la communauté diazotrophe. Lorsque nous ad-

ditionnons les flux de fixation de N_2 spécifique de chaque groupe, la somme est inférieure au flux de fixation de N_2 total. Cette observation laisse à penser que d'une part, une partie du flux de fixation de N_2 total n'est pas associé aux diazotrophes, mais correspond probablement à une quantité d'azote fixée puis transférée vers d'autres organismes. D'autre part, il est possible qu'une partie du flux de fixation de N_2 total soit associé à des diazotrophes que nous n'avons pas identifiés en qPCR et pas observé par microscopie, tels que les diazotrophes hétérotrophes. Globalement, les résultats montrent que dans la région des archipels Mélanésiens, *Trichodesmium* est le principal acteur de la diazotrophie. Plus à l'est, dans la gyre du Pacifique sud où les flux de fixation de N_2 sont plus faibles, les *Trichodesmium* ne sont plus retrouvés et ce sont les UCYN-B qui sont les principaux acteurs de la diazotrophie.

Cette répartition ouest-est des organismes diazotrophes et les taux de fixation de N_2 contrastés entre la région des archipels Mélanésiens et celle de la gyre du Pacifique sud semblent cohérents avec les provinces biogéochimiques décrites par Longhurst et al. (1995). Dans leur étude basée sur les estimations de production primaire par les images satellites, Longhurst et al. (1995) avaient découpé l'océan mondial en 57 provinces biogéochimiques. Dans la région du Pacifique tropical sud-ouest, ils en avaient identifié deux nommées Western Pacific Archipelagic Deep Basins et South Pacific Subtropical Gyre. Ces deux provinces sont en accord avec celles que nous avons identifiées comme archipels Mélanésiens et ouest de la gyre du Pacifique sud, excepté la limite entre ces deux provinces. Longhurst et al. (1995) estimaient cette limite vers 175 °E, alors que nous l'estimons plus à l'est vers 170 °O, au niveau de l'arc de Tonga.

Nous avons vu que l'océan Pacifique tropical sud-ouest, qui était jusqu'à maintenant largement sous échantillonné, est un hot spot de diazotrophie. Dans cette région de l'océan c'est la disponibilité en éléments nutritifs (Fe et DIP) qui contrôle la fixation de N_2, induisant une séparation nette entre deux provinces distinctes. A l'ouest, dans les eaux des archipels Mélanésiens, la fixation de N_2 est intense et principalement réalisée par *Trichodesmium*. A l'est, dans la région de l'ouest de la gyre du Pacifique sud, la diazotrophie est plus faible et réalisée par les UCYN-B.

L'objectif suivant est de comprendre quel est l'impact biogéochimique de la diazotrophie sur la production primaire et sur l'export de carbone dans cette région, et quelles sont les différences qu'il peut y avoir entre les eaux des archipels Mélanésiens et celles de la gyre du Pacifique sud.

Chapitre 3

La fixation de N_2 : source importante d'azote nouveau et acteur majeur de la pompe biologique dans l'océan Pacifique tropical sud-ouest

Sommaire

3.1 Avant propos

Dans le chapitre précédent, nous avons vu que la région oligotrophe du Pacifique tropical sud-ouest est un hot spot de fixation de N_2. Dans ce chapitre ci, nous allons nous intéresser à l'impact biogéochimique de ce hot spot sur l'écosystème.

La majeure partie de l'océan mondial (80 %) est caractérisée par les écosystèmes oligotrophes dit "low nutrient low chlorophyll" (LNLC, Longhurst et al., 1995), au niveau desquels la faible disponibilité en azote limite le développement des organismes phytoplanctoniques (e.g. Moore et al., 2013). La fixation de N_2 soutient une part importante de la production primaire nouvelle (∼50 %) dans ces régions (Berthelot et al., 2015b; Capone et al., 2005a,b; Garcia et al., 2006; Karl et al., 1997; Moutin et al., 2008) et peut soutenir l'export de carbone et la séquestration de CO_2 (Karl et al., 2003, 2012). En effet, dans ces environnements dépourvus d'azote, la pompe biologique est amorcée par la fixation de N_2 et a été ainsi dénommée « N_2-primed prokaryotic carbon pump » (Karl et al., 2003). La faible signature isotopique $\delta^{15}N$ mesurée sur la matière particulaire recueillie dans les pièges à particules et dans la colonne d'eau dans l'océan Pacifique tropical nord (Böttjer et al., 2017; Karl et al., 1997, 2012; Scharek et al., 1999a,b) et Atlantique (Altabet, 1988; Bourbonnais et al., 2009; Knapp et al., 2005; Mahaffey et al., 2003) montrent qu'une part du N_2 fixé par les diazotrophes est exportée hors de la couche euphotique. *Trichodesmium* est rarement retrouvée dans les pièges à particules (Chen et al., 2003; Walsby, 1992) car ces organismes se maintiennent en surface à l'aide de vacuoles gazeuses qui leur permettent de contrôler leur flottabilité (Walsby, 1992; White et al., 2006). Les DDAs ont une efficacité d'export élevée contrairement à *Trichodesmium*, et de forts flux d'export associés à la présence de DDAs ont été observés dans le panache du fleuve Amazone (Subramaniam et al., 2008) et dans le Pacifique nord (Karl et al., 2012). A la station ALOHA, la part de carbone exportée associée aux UCYN peut représenter jusqu'à 18 % de l'export total (White et al., 2012), mais l'export associé aux UCYN reste très peu étudié à ce jour.
L'impact de la fixation de N_2 sur l'export de carbone et d'azote ainsi que la détermination de l'export direct de diazotrophes ou de l'export indirect (après transfert dans la chaine trophique) est très peu étudié et représente un challenge scientifique et technique. En effet, cela nécessite d'échantillonner dans l'océan une efflorescence de diazotrophes, de déployer des pièges à particules sur le lieu de l'efflorescence, et d'assurer un suivi des caractéristiques biogéochimiques de la masse d'eau influencée par l'efflorescence de diazotrophes pendant plusieurs jours. De plus, la distribution hétérogène des diazotrophes dans l'océan de surface (Bombar et al., 2015) associée au découplage possible entre production en surface et export sous la couche euphotique (Buesseler et al., 2007) rendent ces études extrêmement complexes. Par ailleurs, l'océan étant le siège d'intenses processus de mélanges physiques, il est difficile de suivre une même masse d'eau sur le moyen terme (quelques jours à quelques semaines), et de relier les données récoltées par les pièges à particules et la production observée en surface (Buesseler et al., 2007), à moins de se trou-

ver dans une zone caractérisée par une faible advection. Enfin, il est compliqué de savoir si l'azote fixé (et le carbone associé) a été exporté directement (i.e. par sédimentation des organismes diazotrophes eux mêmes) ou indirectement (i.e. par sédimentation des organismes s'étant développés à partir de l'azote provenant de la diazotrophie).

Dans le chapitre précédent nous avons vu que l'océan Pacifique tropical sud-ouest était un hot spot de fixation de N_2, présentant néanmoins des environnements contrastés en terme de statut trophique, d'intensité de la fixation d'azote et de diversité des diazotrophes. Ces caractéristiques font de cette région, un environnement idéal pour étudier l'impact de la fixation de N_2 sur la production primaire et l'export de carbone et d'azote.

Lors de la campagne océanographique OUTPACE, nous avons étudié ces processus au niveau de trois stations dites de longue durée. A chacune de ces stations, la stratégie lagrangienne mise en oeuvre a permis de suivre une même masse d'eau pendant 5 jours dans deux régions biogéochimiquement contrastées de l'océan Pacifique tropical sud-ouest (les archipels Mélanésiens et le bord ouest de la gyre du Pacifique sud). Le travail présenté dans ce chapitre a pour objectif :

1/ de quantifier la part d'azote nouveau que représente la fixation de N_2 dans la couche euphotique dans ces environnements contrastés, et

2/ d'évaluer le rôle de la fixation de N_2 sur l'export de carbone et d'azote, et quantifier la part que représente l'export direct des organismes diazotrophes.

3.2 Résumé

Dans cette étude, nous avons réalisé des bilans d'azote dans la couche euphotique à trois stations contrastés représentatives des différents régimes trophiques de l'océan Pacifique tropical sud-ouest. Cette étude a été menée au cours de la campagne océanographique OUTPACE pendant l'été austral (Février-Mars 2015). En utilisant une stratégie lagrangienne, nous avons échantillonné une même masse d'eau durant le temps d'occupation de chaque station (5 jours), nous permettant de considérer uniquement les échanges verticaux lors de la réalisation des bilans. Nous avons quantifié les principaux flux d'azote, à la fois entrants (fixation de N_2, diffusion turbulente de nitrate, dépôts atmosphériques) et sortants (export d'azote particulaire) de la couche euphotique. Les trois stations étaient caractérisées par une forte nitracline et des maxima profonds de chlorophylle contrastés, qui étaient moins profonds dans les eaux oligotrophes des archipels Mélanésiens (correspondant aux stations LD A et LD B) que dans les eaux ultra-oligotrophes du gyre de l'océan Pacifique sud (correspondant à la station LD C). Les flux de fixation de N_2 étaient extrêmement élevés, à la fois à la station LD A (593 ± 51 μmol N m^{-2} d^{-1}) et à la station LD B (706 ± 302 μmol N m^{-2} d^{-1}), où la communauté diazotrophe était dominée par *Trichodesmium*. Les taux de fixation de N_2 étaient plus faibles à la station LD C, où les diazotrophes dominants étaient des UCYN. A chacune des stations, la fixation de N_2 était la source principale d'azote nouveau ($> 90\%$) dans la couche euphotique, bien supérieure aux apports de nitrate par diffusion turbulente et aux apports atmosphériques. La fixation de N_2 contribuait à 13-18 % de la production primaire dans la région des archipels Mélanésiens et à 3 % dans les eaux de la gyre du Pacifique sud, soutenant la quasi-totalité de la production nouvelle à chacune des trois stations. Le *e*-ratio (carbone particulaire exporté / production primaire) était maximum à la station LD A (9,7 %), ce qui est plus élevé que les *e*-ratio calculés dans la majorité des régions oligotrophes (< 5 %). Ce résultat reflète l'efficacité élevée de l'océan Pacifique tropical sud-ouest à exporter du carbone par rapport à la production primaire. L'export direct de diazotrophes quantifié par qPCR sur le gène *nif*H dans les pièges à particules pouvait représenter jusqu'à 30,6 % de l'export de carbone particulaire à la station LD A, alors qu'il était inférieur à 5% aux autres stations. Aux trois stations, la somme des apports d'azote dans la couche euphotique était supérieure à la quantité d'azote exportée sous forme de matière organique particulaire. Ce déséquilibre engendrant une accumulation d'azote dans la couche euphotique semble être une caractéristique biogéochimique principale de l'océan Pacifique tropical sud-ouest pendant la saison estivale.

3.3 Article # 3 : La fixation de N_2 comme source majeure d'azote nouveau dans le Pacifique tropical sud-ouest. *Caffin et al., 2018*

N_2 fixation as the dominant new N source in the western tropical South Pacific Ocean

Mathieu Caffin[1], Thierry Moutin[1], Rachel A. Foster[2], Pascale Bouruet-Aubertot[3], Andrea M. Doglioli[1], Hugo Berthelot[1 4], Cécile Guieu[5 7], Olivier Grosso[1], Sandra Helias-Nunige[1], Nathalie Leblond[7], Audrey Gimenez[1], Anne A. Petrenko[1], Alain de Verneil[1 a] and Sophie Bonnet[8]

[1]Aix Marseille Université, CNRS/INSU, Université de Toulon, IRD, Mediterranean Institute of Oceanography (MIO) UM110, 13288, Marseille, France
[2]Stockholm University, Department of Ecology, Environment and Plant Sciences, Stockholm, Sweden
[3]Sorbonne Universités, UPMC Univ. Paris 06, LOCEAN, Paris, France
[4]Laboratoire des sciences de l'environnement marin, IUEM, Université de Brest-UMR 6539 CNRS/UBO/IRD/Ifremer, Plouzané, France
[5]Sorbonne Universités, UPMC Univ Paris 06, CNRS, Laboratoire d'Océanographie de Villefranche (LOV), 06230 Villefranche-sur-Mer, France
[6]The Center for Prototype Climate Modeling, New York University in Abu Dhabi, Abu Dhabi, UAE
[7]Observatoire Océanologique de Villefranche, Laboratoire d'Océanographie de Villefranche, UMR 7093, Villefranche-sur-mer, France
[8]Aix Marseille Université, CNRS, Université de Toulon, IRD, OSU Pythéas, Mediterranean Institute of Oceanography (MIO), UM 110, 98848, Nouméa, New Caledonia
[a]now at : The Center for Prototype Climate Modeling, New York University in Abu Dhabi, Abu Dhabi, UAE

Publié dans *Biogeosciences* en Mai 2018

Biogeosciences, 15, 2565–2585, 2018
https://doi.org/10.5194/bg-15-2565-2018

Biogeosciences Open Access EGU

N_2 fixation as a dominant new N source in the western tropical South Pacific Ocean (OUTPACE cruise)

Mathieu Caffin[1], Thierry Moutin[1], Rachel Ann Foster[2], Pascale Bouruet-Aubertot[3], Andrea Michelangelo Doglioli[1], Hugo Berthelot[1,4], Cécile Guieu[5,6], Olivier Grosso[1], Sandra Helias-Nunige[1], Nathalie Leblond[7], Audrey Gimenez[1], Anne Alexandra Petrenko[1], Alain de Verneil[1,a], and Sophie Bonnet[8]

[1]Aix Marseille Univ., Université de Toulon, CNRS, IRD, MIO UM 110, 13288, Marseille, France
[2]Stockholm University, Department of Ecology, Environment and Plant Sciences, Stockholm, Sweden
[3]Sorbonne Universités, UPMC Univ. Paris 06, LOCEAN, Paris, France
[4]Laboratoire des sciences de l'environnement marin, IUEM, Université de Brest-UMR 6539 CNRS/UBO/IRD/Ifremer, Plouzané, France
[5]Sorbonne Universités, UPMC Univ Paris 06, CNRS, Laboratoire d'Océanographie de Villefranche (LOV), 06230 Villefranche-sur-Mer, France
[6]The Center for Prototype Climate Modeling, New York University in Abu Dhabi, Abu Dhabi, UAE
[7]Observatoire Océanologique de Villefranche, Laboratoire d'Océanographie de Villefranche, UMR 7093, Villefranche-sur-mer, France
[8]Aix Marseille Université, CNRS, Université de Toulon, IRD, OSU Pythéas, Mediterranean Institute of Oceanography (MIO), UM 110, 98848, Nouméa, New Caledonia
[a]now at: The Center for Prototype Climate Modeling, New York University in Abu Dhabi, Abu Dhabi, UAE

Correspondence: Mathieu Caffin (mathieu.caffin@mio.osupytheas.fr)

Received: 2 November 2017 – Discussion started: 6 November 2017
Revised: 10 April 2018 – Accepted: 11 April 2018 – Published: 2 May 2018

Abstract. We performed nitrogen (N) budgets in the photic layer of three contrasting stations representing different trophic conditions in the western tropical South Pacific (WTSP) Ocean during austral summer conditions (February–March 2015). Using a Lagrangian strategy, we sampled the same water mass for the entire duration of each long-duration (5 days) station, allowing us to consider only vertical exchanges for the budgets. We quantified all major vertical N fluxes both entering (N_2 fixation, nitrate turbulent diffusion, atmospheric deposition) and leaving the photic layer (particulate N export). The three stations were characterized by a strong nitracline and contrasted deep chlorophyll maximum depths, which were lower in the oligotrophic Melanesian archipelago (MA, stations LD A and LD B) than in the ultra-oligotrophic waters of the South Pacific Gyre (SPG, station LD C). N_2 fixation rates were extremely high at both LD A ($593 \pm 51\,\mu mol\,N\,m^{-2}\,d^{-1}$) and LD B ($706 \pm 302\,\mu mol\,N\,m^{-2}\,d^{-1}$), and the diazotroph community was dominated by *Trichodesmium*. N_2 fixation rates were lower ($59 \pm 16\,\mu mol\,N\,m^{-2}\,d^{-1}$) at LD C, and the diazotroph community was dominated by unicellular N_2-fixing cyanobacteria (UCYN). At all stations, N_2 fixation was the major source of new N (> 90 %) before atmospheric deposition and upward nitrate fluxes induced by turbulence. N_2 fixation contributed circa 13–18 % of primary production in the MA region and 3 % in the SPG water and sustained nearly all new primary production at all stations. The *e* ratio (*e* ratio = particulate carbon export / primary production) was maximum at LD A (9.7 %) and was higher than the *e* ratio in most studied oligotrophic regions (< 5 %), indicating a high efficiency of the WTSP to export carbon relative to primary production. The direct export of diazotrophs assessed by qPCR of the *nifH* gene in sediment traps represented up to 30.6 % of the PC export at LD A, while their contribution was 5 and < 0.1 % at LD B and LD C, respectively. At the three studied stations, the sum of all N input to the photic layer exceeded the N output through organic matter export. This disequilibrium leading to N accumulation in the upper

Published by Copernicus Publications on behalf of the European Geosciences Union.

layer appears as a characteristic of the WTSP during the summer season.

1 Introduction

Biological nitrogen fixation, the reduction of atmospheric dinitrogen (N_2) to ammonia, is performed by a diverse group of prokaryotic organisms, commonly called diazotrophs. It provides the major external source of bio-available nitrogen (N) to the ocean, before riverine and atmospheric inputs (Deutsch et al., 2007; Gruber, 2008; Gruber and Sarmiento, 1997). In the oligotrophic ocean, N availability often limits phytoplankton growth (e.g. Moore et al., 2013) and N_2 fixation sustains a significant part of new primary production (PP, i.e. the production unrelated to internal recycling of organic matter in the photic layer) such as in the North (Karl et al., 1997) and South Pacific Ocean (Moutin et al., 2008), the western Mediterranean Sea (Garcia et al., 2006), or the tropical North Atlantic (Capone et al., 2005). New N input by N_2 fixation has thus been recognized as a significant process influencing global oceanic productivity, and can eventually fuel CO_2 sequestration through the N_2-primed prokaryotic carbon (C) pump (Karl et al., 2003).

Low $\delta^{15}N$ signatures of particles from sediment traps in the tropical North Pacific (Karl et al., 1997, 2012; Scharek et al., 1999a, b) and Atlantic (Altabet, 1988; Bourbonnais et al., 2009; Knapp et al., 2005; Mahaffey et al., 2003) suggest that at least part of the recently fixed N is ultimately exported out of the photic zone. Knapp et al. (2008) and Bourbonnais et al. (2009) also observed a low $\delta^{15}N$ of NO_3^- (relative to $\delta^{18}O\text{-}NO_3^-$) in surface waters in the western and eastern subtropical Atlantic Ocean, supporting the role of N_2 fixers in these regions. Böttjer et al. (2017) revealed that N_2 fixation supports 26–47 % of particulate N (PN) export over a 9-year time series (2005–2013) period at station ALOHA (North Pacific Subtropical Gyre). Export efficiency may depend on the diazotroph community composition present in surface waters. Blooms of diatom–diazotroph associations (DDAs) systematically observed in late summer at station ALOHA are thought to be directly responsible for the concomitant pulses of particulate export (Karl et al., 2012). High export associated with DDAs has also been observed in the Amazon River plume (Subramaniam et al., 2008), suggesting a high direct export efficiency associated with DDAs. *Trichodesmium* is one of the main contributors to global N_2 fixation (Mahaffey et al., 2005) but is rarely recovered in sediment traps (Chen et al., 2003; Walsby, 1992), suggesting a low direct export efficiency. However, the N_2 fixed by *Trichodesmium* is efficiently transferred to large, non-diazotrophic phytoplankton, such as diatoms (Berthelot et al., 2016; Bonnet et al., 2016a), which can be subsequently exported (Nelson et al., 1995), suggesting a potential indirect export pathway. A recent mesocosm study performed in New Caledonia unexpectedly revealed that the production sustained by unicellular diazotrophic cyanobacteria (hereafter referred to as UCYN) was much more efficient at promoting particle export than the production sustained by DDAs (Berthelot et al., 2015). However, the export efficiency of UCYN has been poorly studied (White et al., 2012) in the open ocean, despite the fact that they contribute as much as *Trichodesmium* to N_2 fixation rates in many parts of the ocean (Bonnet et al., 2009; Martínez-Pérez et al., 2016; Moisander et al., 2010; Montoya et al., 2004). More studies are thus needed to further investigate the ability of different diazotroph communities to fuel direct or indirect particle export in the oligotrophic ocean.

Studying the impact of N_2 fixation on PN export in the ocean and the relative role of each diazotroph group in this process is technically challenging. It requires the measurement of all major N fluxes both entering the photic layer (N_2 fixation, nitrate (NO_3^-) eddy diffusion, atmospheric deposition) and leaving the photic layer (PN export) with an adequate time frame (i.e. linking production and export). In addition, the sampling has to be performed under contrasting situations, for example when either *Trichodesmium* or UCYN dominate the diazotroph community, hence allowing assessment of the potential role of each diazotroph group. Most importantly, such N budgets must be performed in the same water mass to ensure that the particulate matter recovered in the sediment traps corresponds to the production that occurred just above in the photic layer. This is what we did during the OUTPACE (Oligotrophy to UlTra-oligotrophy PACific Experiment) cruise in the western tropical South Pacific (WTSP) in summer 2015, during which we used a Lagrangian strategy.

The WTSP has recently been identified as a hotspot of N_2 fixation, including N_2 fixation rates $> 500\,\mu mol\,N\,m^{-2}\,d^{-1}$ (Bonnet et al., 2017). The region covered by the OUTPACE cruise is characterized by trophic and N_2 fixation gradients (Moutin et al., 2017). The region covered by the OUTPACE cruise encompasses contrasting trophic regimes characterized by strong differences in top nitracline depths, from 46 to 141 m (Moutin et al., 2018), and representing a large part of the oligotrophic gradient at the scale of the world ocean (Moutin and Prieur, 2012; their Fig. 9). The westward oligotrophic waters are characterized by high N_2 fixation rates ($631 \pm 286\,\mu mol\,N\,m^{-2}\,d^{-1}$) mainly associated with *Trichodesmium* (i.e. within the hot spot around Melanesian archipelago waters, hereafter named MA), and the eastward ultra-oligotrophic waters (in the eastern border of the South Pacific Gyre, hereafter named SPG waters) are characterized by low N_2 fixation rates ($85 \pm 79\,\mu mol\,N\,m^{-2}\,d^{-1}$), mainly associated with UCYN (Bonnet et al., 2018; Stenegren et al., 2018). This west to east N_2 fixation gradient has been mainly attributed to a decrease in iron availability in SPG waters as compared to MA waters (Guieu et al., 2018). This region therefore provides ideal conditions to study the potential role of N_2 fixation on particulate export under contrasting situations.

In the present study, we focus on (i) the contribution of N_2 fixation to new N inputs in the WTSP during the summer season, (ii) the coupling between N_2 fixation and export, and (iii) the equilibrium versus disequilibrium between N_2 fixation and particulate N export in the WTSP.

2 Material and methods

2.1 Station sampling strategy

The OUTPACE cruise was carried out during austral summer conditions (18 February–3 April 2015) along a west–east 4000 km transect from New Caledonia (22° S–166° E) to French Polynesia (17°30′ S–149°30′ W). We performed a N budget at three stations, hereafter named long duration (LD), that were chosen according to three criteria: (1) local minima of surface current intensity, (2) different trophic regimes, i.e. oligotrophic vs. ultra-oligotrophic, and (3) different diazotroph communities, i.e. *Trichodesmium* vs. UCYN.

To locate these three stations, we used a Lagrangian strategy developed during previous cruises such as LATEX (Doglioli et al., 2013; Petrenko et al., 2017) and KEOPS2 (d'Ovidio et al., 2015). Briefly, the regions of interest along the vessel route were first characterized at large scale through the analysis of satellite data. The altimetry-derived currents were processed by SPASSO (Software Package for an Adaptive Satellite-based Sampling for Ocean campaigns; http://www.mio.univ-amu.fr/SPASSO/, last access: November 2017) to derive Eulerian and Lagrangian diagnostics of ocean circulation: Okubo–Weiss parameter, particle retention time and advection, Lagrangian coherent structures (d'Ovidio et al., 2015), together with maps of the sea surface temperature and chlorophyll *a* (Chl *a*) concentrations. The satellite data were processed on land in near-real time and transmitted to the ship together with a daily bulletin proposing LD station positions (the complete series of 43 bulletins is available on the OUTPACE website at https://outpace.mio.univ-amu.fr/OUT_Figures/Bulletins/, last access: November 2017). We also performed onboard quantitative polymerase chain reaction (qPCR) analyses on the *nifH* gene to measure the abundance of six groups of diazotrophs (Stenengren et al., 2018). Thus, we located the stations in regions where either *Trichodesmium* or UCYN dominated the diazotroph community. Then, the exact locations of the three LD stations were determined on board in real time from a rapid survey using a moving vessel profiler (MVP), equipped with conductivity–temperature–depth (CTD) and fluorimeter sensors, accompanied by the hull-mounted thermosalinograph and acoustic Doppler current profiler (Moutin et al., 2017). Finally, Surface Velocity Program (SVP) drifters were deployed in order to study the relative dispersion at the surface (de Verneil et al., 2018) during the station occupation.

By using this strategy, LD A station (19°12.8′ S–164°41.3′ E, 25 February–2 March) was positioned in MA waters in the western part of the transect (Fig. 1) offshore from New Caledonia. LD B station (18°14.4′ S–170°51.5′ W, 15–20 March) was positioned in MA waters near the island of Niue and LD C station (18°25.2′ S–165°56.4′ W, 23–28 March) was positioned in the eastern part of the transect, in the SPG near the Cook Islands.

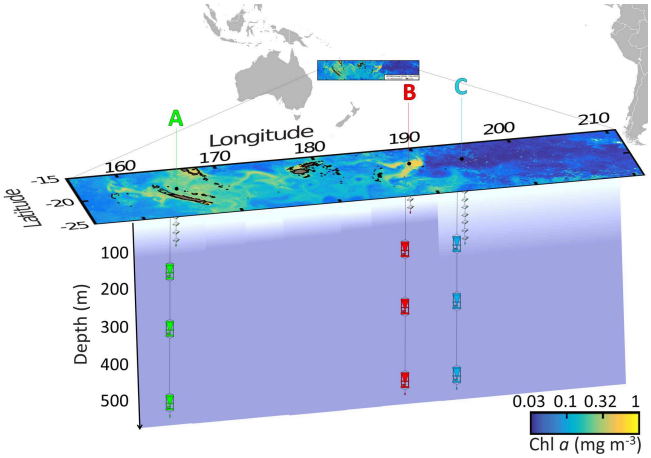

Figure 1. Position of the long-duration stations sampled in this study (OUTPACE cruise): LD A in green, LD B in red and LD C in blue on a quasi-Lagrangian surface Chl *a* concentrations map. The in situ production lines were deployed in the photic layer (from 5 to 105, 80 and 180 m for LD A, LD B and LD C, respectively) and the PPS5 sediment traps were deployed at 150, 330 and 520 m.

Each LD station was investigated for 5 days. The sequence of operations was the following: a drifting array equipped with three PPS5 sediment traps, current meters, oxygen sensors and high-frequency temperature sensors (see https://outpace.mio.univ-amu.fr/spip.php?article75fordetails, last access: November 2017) was deployed at each station on the first day. Then, a series of CTD (SBE 911+ Sea-Bird) casts (0–500 m) were performed every 3–4 h near the actual position of the drifting array to study the high-frequency evolution of temperature, salinity, photosynthetically available radiation (PAR) and chlorophyll *a* fluorescence during the station occupation. Small-scale turbulence was characterized in the first 800 m from microstructure measurements using a vertical microstructure profiler (VMP1000) that was typically deployed prior to or following each CTD cast (Bouruet-Aubertot et al., 2018). Nutrient concentration measurements (0–200 m) were performed every day on the midday CTD casts (hereafter named "nut. CTD"). In addition to the 0–500 m casts every 3–4 h, production casts (0–150 m) (hereafter named "prod. CTD") were performed three times at each LD station (on day 1, 3 and 5) to quantify N_2 fixation and primary production rates. Incubations with tracers (^{14}C and $^{15}N_2$; see below) to quantify N_2 fixation and primary production were performed on an in situ drifting production line deployed for 24 h from dawn to dawn. The drifting array with the traps was recovered at the end of each LD station.

Aerosol sampling was performed throughout the cruise transect. The inputs of new N to the photic layer were induced by three different sources: atmospheric deposition at the air–sea interface, N_2 fixation as an interior source and NO_3^- input by vertical diffusion. The N output was driven by PN sedimentation. The methods for the determination of each parameter are given below.

2.2 Experimental procedures

2.2.1 Physical and chemical parameters, nutrient concentrations and C : N ratios

In situ Chl *a* concentrations were derived from fluorescence measurements performed with a AquaTraka III (Chelsea Technologies Group Ltd) sensor mounted on the CTD. The chlorophyll fluorescence sensor was calibrated prior to the cruise and post-calibration was conducted using all HPLC measurements undertaken during the cruise. PAR was measured on each CTD profile. Phosphate (PO_4^{3-}) and NO_3^- concentrations were measured daily at 12 depths from the surface to 200 m on each nutrient CTD cast using standard colorimetric procedures (Aminot and Kérouel, 2007) on an AA3 AutoAnalyzer (Seal Analytical). After filtration, one sample was directly analysed on board and the other poisoned with 50 µL of $HgCl_2$ (20 g L^{-1}) and stored for analysis after the cruise in the laboratory. The quantification limits were 0.05 µmol L^{-1} for PO_4^{3-} and NO_3^-.

2.2.2 Primary production and associated N uptake

PP was measured in triplicate using the ^{14}C tracer method (Moutin and Raimbault, 2002). Samples were incubated in 320 mL polycarbonate bottles on the in situ drifting production line (Aquamout: https://outpace.mio.univ-amu.fr/spip.php?article75, last access: November 2017) for 24 h from dusk to dusk at 9 depths (75, 54, 36, 19, 10, 3, 1, 0.3 and 0.1 % of surface irradiance levels), corresponding to the subsurface (5 m) down to 105, 80 and 180 m for stations LD A, LD B and LD C, respectively. A N-derived PP (N-PP) was obtained at each depth by dividing PP by the classical C : N Redfield ratio (6.625). Integrated N-PP (iN-PP) over the studied layer (surface to 125, 100 and 200 m for LD A, LD B and LD C, respectively) was calculated by using the trapezoidal method, assuming that surface N-PP was identical to N-PP measured in subsurface (5 m) and considering that N-PP 20 m below the deepest sampled depth was zero (JGOFS, 1988).

2.2.3 Atmospheric deposition

N atmospheric deposition (NO_3^- and NO_2^- (nitrite), hereafter called NO_x) was quantified along the transect after dissolution of aerosols collected continuously during the transect, as described in Guieu et al. (2018). Briefly, the sampling device, designed to avoid ship contamination, was installed at the look-out post in the front of the ship and collected aerosols at $\sim$ 20 L min^{-1} onto polycarbonate filters (47 mm diameter, 0.45 µm porosity, previously acid-cleaned with a 2 % solution of HCl (Merck, Ultrapur, Germany) and thoroughly rinsed with ultra-pure water and dried under a laminar flow bench and stored in acid-cleaned Petri dishes). Dissolution experiments to determine NO_x released in surface seawater after deposition were performed on board using acid-cleaned Sartorius filtration units (volume 0.250 L) and filtered surface (5 m) seawater. Each sample was subjected to two contact times: the first contact was at 1 min, and the second contact was at 24 h. NO_x was analysed using a 1 m long liquid waveguide capillary cell (LWCC) made of quartz capillary tubing, following the protocol described in Louis et al. (2015). An extrapolated NO_x release from dry deposition was estimated on the basis of a deposition velocity of submicron particles (0.4 m s^{-1}; Vong et al., 2010).

2.2.4 Nitrogen fixation rates

N_2 fixation rates were measured using the $^{15}N_2$ tracer method (Montoya et al., 1996, modified; see below), on days 1, 3 and 5 at each LD station (hereafter named in situ_1, in situ_2 and in situ_3, respectively). Seawater was collected from the Niskin bottles in duplicate 4.5 L polycarbonate bottles at nine depths (same depths as for PP). A total of 5 mL of $^{15}N_2$ gas (99 atom% ^{15}N, Eurisotop) was injected into each bottle through the septum cap using a gas-tight syringe. The purity of the $^{15}N_2$ Cambridge isotopes stocks was previously checked by Dabundo et al. (2014) and more recently by Benavides et al. (2015) and Bonnet et al. (2016a). They were found to be lower than 2×10^{-8} mol : mol of $^{15}N_2$, leading to a potential N_2 fixation rates overestimation of < 1 %. All bottles were shaken 20 times to facilitate the $^{15}N_2$ dissolution and incubated in situ on the production line at the same depth of sampling for 24 h from dawn to dawn (hereafter called the "in situ incubation method"). It has been previously shown that the bubble method potentially underestimated N_2 fixation rates (Großkopf et al., 2012; Mohr et al., 2010) compared to methods consisting in adding the $^{15}N_2$ as dissolved in a subset of seawater previously N_2 degassed (Mohr et al., 2010). This underestimation is due to incomplete equilibration of the $^{15}N_2$ gas with surrounding seawater. However, other studies did not find any significant difference between the two methods (Bonnet et al., 2016b; Shiozaki et al., 2015). In the present study, we intentionally decided to use the bubble method due to the high risk of both organic matter and trace metal contamination during the $^{15}N_2$-enriched seawater preparation (Klawonn et al., 2015), which has been seen to enhance N_2 fixation in this area (Benavides et al., 2017; Moisander et al., 2010). However, to minimize possible rate underestimations due to incomplete equilibration of the $^{15}N_2$ gas with surrounding seawater, the final ^{15}N enrichment of the N_2 pool was quantified in the incubation bottles on each profile in triplicate at 5 m and at the deep chlorophyll max-

imum (DCM). After incubation, 12 mL of each 4.5 L bottle was subsampled in Exetainers, fixed with $HgCl_2$ (final concentration 20 µg mL^{-1}), and stored upside down at 4 °C in the dark until analysed onshore within 6 months after the cruise, according to Kana et al. (1994), using a membrane inlet mass spectrometer (MIMS).

For each LD station, in parallel with the last N_2 fixation profile (the in situ_3 profile), we performed a replicate N_2 fixation profile in which bottles were incubated in on-deck incubators (see details on https://outpace.mio.univ-amu.fr/spip.php?article135, last access: November 2017) equipped with circulating seawater at the specified irradiances using blue screening (hereafter called the "deck incubation method"). For these profiles, samples were collected in triplicate at six of the nine depths reported above (75, 54, 36, 10, 1 and 0.1 % surface irradiance level) in 2.3 L polycarbonate bottles amended with 2.5 mL of $^{15}N_2$ gas (99 atom% ^{15}N, Eurisotop) for 24 h.

In both cases, incubations were stopped by gentle filtration (< 0.2 bar) of the samples onto pre-combusted (450 °C, 4 h) Whatman GF/F filters (25 mm diameter, 0.7 µm nominal porosity). Filters were stored in pre-combusted glass tubes at −20 °C during the cruise, then dried at 60 °C for 24 h before analysis onshore. ^{15}N enrichments of PN collected on filters were determined using an elemental analyser coupled to an isotope ratio mass spectrometer (EA-IRMS, Integra2 Sercon Ltd). The accuracy of the EA-IRMS system was systematically checked using International Atomic Energy Agency (IAEA) reference materials, AIEA-N-1 and IAEA-310A. In addition, the ^{15}N enrichment of the ambient (unlabelled) PN was measured in one replicate at each station at the DCM and the subsurface and was used as the "initial" ^{15}N enrichment, as termed in Montoya et al. (1996). The minimum quantifiable rate calculated using standard propagation of errors via the observed variability between replicate samples measured according to Gradoville et al. (2017) was 0.035 nmol N L^{-1} d^{-1}. Integrated N_2 fixation rates over the studied layer were calculated by using the same method as for the iN-PP.

2.2.5 Nitrate turbulent diffusion

NO_3^- inputs from deep waters by turbulent mixing were estimated at the top of the nitracline. The top of the nitracline was found to fall along an isopycnal surface ($\rho = \rho_{NO_3}$), the density of which was determined at each station. The NO_3^- turbulent diffusive flux along the isopycnal surface $\rho = \rho_{NO_3}$ was defined as

$$\mathrm{Flux}_{\rho_{NO_3}}(t) = -K_z(z_{\rho_{NO_3}}t) \times \frac{\mathrm{d}[NO_3]}{\mathrm{d}\rho}(\rho_{NO_3}t) \times \frac{\mathrm{d}\rho}{\mathrm{d}z}(z_{\rho_{NO_3}}t), \quad (1)$$

where K_z is the turbulent diffusion coefficient along the isopycnal $\rho = \rho_{NO_3}$ inferred from VMP1000 measurements performed every 3–4 h during the LD station occupation, as described in Bouruet-Aubertot et al. (2018), $\frac{\mathrm{d}[NO_3]}{\mathrm{d}\rho}$ is the constant slope of the nitracline, calculated for each station, and $\frac{\mathrm{d}\rho}{\mathrm{d}z}$ is the vertical density gradient measured by the VMP1000 at the ρ_{NO_3} isopycnal depth $z_{\rho_{NO_3}}$. The time series of the NO_3^- turbulent diffusive flux was calculated using an hourly temporal interpolation of K_z over the entire duration of each LD station. In addition, daily averages and 5-day averages were computed.

2.2.6 Particulate matter export

Particulate matter export was quantified with three PPS5 sediment traps (1 m^2 surface collection, Technicap, France) deployed for 5 days at 150, 330 and 520 m at each LD station (Fig. 1). We decided to use the same configuration at the three LD stations. The first trap was deployed at 150 m as it is always below the base of the photic layer and therefore below the productivity layer. The depth of 520 m was used because most of the diel zooplankton vertical migrations stopped above this depth, and 330 m was chosen as an intermediary depth. Particle export was recovered in polyethylene flasks screwed on a rotary disk, which allowed the flask to be automatically changed every 24 h to obtain a daily material recovery rate. The flasks were previously filled with a buffered solution (sodium borate) of formaldehyde (final concentration 2 % and pH = 8) and were stored at 4 °C after collection until analysis to prevent degradation of the collected material. The flask corresponding to the fifth day of sampling on the rotary disk was not filled with formaldehyde in order to collect "fresh particulate matter" for further diazotroph quantification, as described below. Thus, this last flask was not used in the particulate export computations reported in Table 1. Onshore, swimmers were handpicked from each sample, quantified and genera-identified. Exported particulate matter and swimmers were both weighed and analysed separately on EA-IRMS (Integra2, Sercon Ltd) to quantify exported PC and PN.

2.2.7 Diazotroph abundance in the traps

Triplicate aliquots of 2 to 4 mL from the flask dedicated to diazotroph quantification were filtered onto 0.2 µm Supor filters, flash-frozen in liquid nitrogen and stored at −80 °C until analysis. Nucleic acids were extracted from the filters as described in Moisander et al. (2008) with a 30 s reduction in the agitation step in a Fast Prep cell disruptor (Thermo, Model FP120; Qbiogene, Inc. Cedex, Frame) and an elution volume of 70 µL. Diazotrophs abundance for *Trichodesmium* spp., UCYN-B (*Crocosphaera watsonii*), UCYN-A1 (*Candidatus Atelocyanobacterium thalassa*), het-1 (*Richelia intracellularis* in symbiosis with *Rhizosolenia*), and het-2 (*Richelia intracellularis* in symbiosis with *Hemiaulus*) were quantified by qPCR analyses on the *nifH* gene using previously described oligonucleotides and assays (Fos-

Table 1. Sediment trap data at the three LD stations. Depth of collection, mean mass flux of dry weight (DW) matter, particulate C and N flux, and mean C : N molar ratio. No data were collected at LD C at 520 m.

Station	Depth m	Mass flux mg DW m^{-2} d^{-1}	PC flux mg C m^{-2} d^{-1}	PN flux mg N m^{-2} d^{-1}	C : N ratio 106 : x
LD A	150	87.2 ± 41.1	27.1 ± 12.1	3.9 ± 1.8	106 : 13
	330	23.9 ± 15.2	5.8 ± 4.0	0.9 ± 0.8	106 : 14
	520	22.3 ± 4.6	4.7 ± 1.0	0.6 ± 0.2	106 : 12
LD B	150	14.1 ± 6.5	3.5 ± 1.3	0.4 ± 0.2	106 : 10
	330	16.8 ± 9.0	3.2 ± 2.0	0.4 ± 0.2	106 : 11
	520	17.9 ± 10.5	3.7 ± 1.4	0.5 ± 0.2	106 : 12
LD C	150	19.6 ± 6.9	3.8 ± 0.8	0.7 ± 0.2	106 : 17
	330	13.6 ± 6.4	2.6 ± 0.9	0.5 ± 0.2	106 : 17
	520	–	–	–	–

ter et al., 2007; Church et al., 2005). The qPCR was conducted in a StepOnePlus system (applied Biosystems, Life Technologies, Stockholm Sweden) with the following parameters: 50 °C for 2 min and 95 °C for 10 min, and 45 cycles of 95 °C for 15 s followed by 60 °C for 1 min. Gene copy numbers were calculated from the mean cycle threshold (C_t) value of three replicates and the standard curve for the appropriate primer and probe set. For each primer and probe set, duplicate standard curves were made from 10-fold dilution series ranging from 10^8 to 1 gene copies per reaction. The standard curves were made from linearized plasmids of the target *nifH* or from synthesized gBLocks gene fragments (IDT technologies, Cralville, Iowa, USA). Regression analyses of the results (number of cycles $= C_t$) of the standard curves were analysed in Excel. Two microlitres of 5 KDa filtered nuclease-free water was used for the no-template controls (NTCs). No *nifH* copies were detected for any target in the NTC. In some samples, only one or two of the three replicates produced an amplification signal; these were noted as detectable but not quantifiable ($<$ QL). A fourth replicate was used to estimate the reaction efficiency for the *Trichodesmium* and UCYN-B targets, as previously described in Short et al. (2004). Seven and two samples were below 95 % in reaction efficiency for *Trichodesmium* and UCYN-B, respectively. The samples with qPCR reaction efficiency below 95 % were excluded. The detection limit for the qPCR assays is 1–10 copies.

To determine directly the biovolume and C content of diazotrophs, cell sizes of *Trichodesmium* and UCYN-B were determined in samples from the photic layer of each LD station. Briefly, 2.3 L of surface (5 m) seawater was gently filtered (< 0.2 bar) onto 2 µm nominal porosity (25 mm diameter) polycarbonate filters, fixed with paraformaldehyde (final concentration 2 %) and stored at −80 °C. Cell length and width measurements were performed on 25 to 50 cells per station at 400 × magnification with a Zeiss Axio Observer epifluorescence microscope. The biovolume (BV) of *Trichodesmium* and UCYN was estimated using the equation for a cylinder and a sphere, respectively (Sun and Liu, 2003). The cellular C contents were determined by using the relation between BV and C content according to Verity et al. (1992). Given that our work was performed in the field on wild populations, we preferred to use the biovolume estimate for C content rather than previously measured values based on published culture data. The C contents estimated here are within the range of those previously reported (Dekaezemacker and Bonnet, 2011; Dron et al., 2013; Hynes et al., 2012; Knapp, 2012; Luo et al., 2012). As DDAs were not easily identified on the filters, the C content was indirectly estimated. We used a C content of 1400 pg C $cell^{-1}$ for *Rhizosolenia* spp. (determined for the OUTPACE cruise; Karine Leblanc, personal communication, 2017) and assumed six cells per trichome of *Richelia intracellularis* (Foster and Zehr, 2006; Villareal, 1989), and one *Richelia* per diatom *Rhizosolenia (*both *Rhizosolenia* spp. and *R. intracellularis* are rarely reported as asymbiotic).

2.2.8 Statistical analyses

Spearman correlation coefficients were used to examine the relationships between DCM and nitracline depths during the station occupation ($\alpha = 0.05$).

A non-parametric Mann–Whitney test ($\alpha = 0.05$) was used to compare N_2 fixation rates obtained using in situ and on-deck incubation methods.

3 Results

3.1 Hydrological background

NO_3^- concentrations in the photic layer were below the quantification limit (0.05 µmol L^{-1}) during the station occupation at the three LD stations. They became quantifiable below 70, 100 and 120 m depth at LD A, B and C, respectively (Fig. 2) and at depths corresponding to a density anomaly of 23.59, 24.34 and 24.66 kg m^{-3}, respectively. The latter

Table 2. Mean daily N budget at the three stations LD A, LD B and LD C.

Characteristics	Units	LD A	LD B	LD C
ρ_{NO_3}	kg m^{-3}	23.59	24.34	24.66
$\frac{d[NO_3]}{d\rho}$	µmol kg^{-1}	3573	5949	8888
Atmospheric deposition (NO_x)	µmol N m^{-2} d^{-1}	0.90	0.51	0.52
N_2 fixation (in situ)	µmol N m^{-2} d^{-1}	593	706	59
NO_3^- diffusion	µmol N m^{-2} d^{-1}	24	7	5
$\sum$N inputs	µmol N m^{-2} d^{-1}	618	714	65
Integrated N-PP	µmol N m^{-2} d^{-1}	3358	5497	1962
Export N – 150 m	µmol N m^{-2} d^{-1}	279	31	47
Export N – 330 m	µmol N m^{-2} d^{-1}	64	29	36
Export N – 520 m	µmol N m^{-2} d^{-1}	44	37	–
e ratio – 150 m	%	9.7	0.7	2.8
e ratio – 330 m	%	2.2	0.6	2.1
e ratio – 520 m	%	1.5	0.8	–

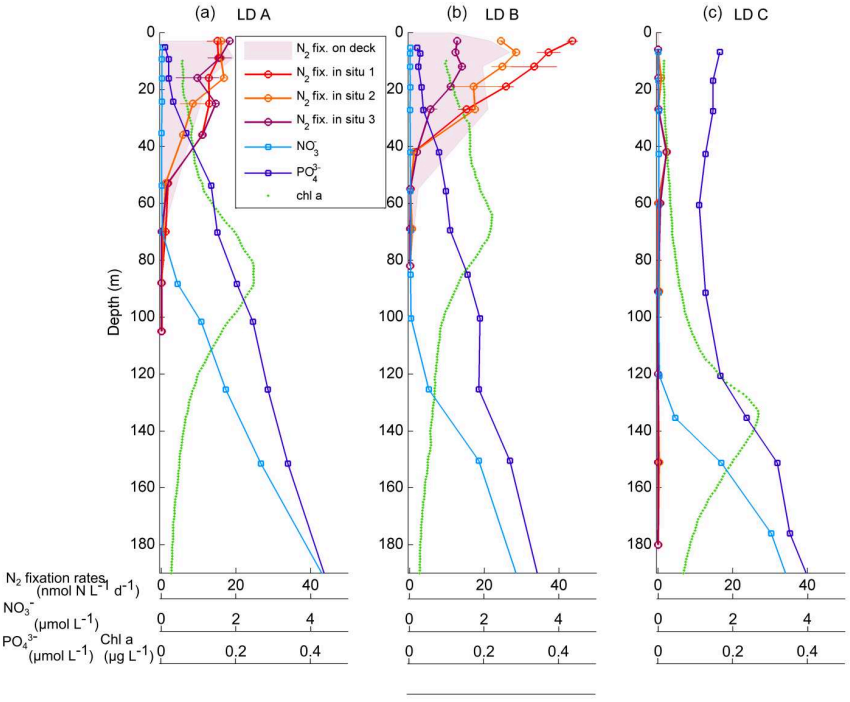

Figure 2. Vertical profiles of net N_2 fixation rates (nmol N L^{-1} d^{-1}) estimated using in situ incubations at day 1 (in situ 1: red circles), day 3 (in situ 2: orange circles) and day 5 (in situ 3: purple) and using on-deck incubations (purple filled area) at stations LD A **(a)**, LD B **(b)** and LD C **(c)**. The NO_3^- concentrations averaged over the 5 days of station occupation are also reported (light blue squares: µmol L^{-1}), as well as PO_4^{3-} concentrations (dark blue squares: µmol L^{-1}), and fluorescence/chlorophyll (green dots: µg L^{-1}).

values correspond to the top of the nitracline; the isopycnal $\rho = \rho_{NO_3}$ (Fig. 3; Table 2). The corresponding $\frac{d[NO_3]}{d\rho}$ values were 3573, 5949 and 8888 µmol kg^{-1} for stations LD A, LD B and LD C, respectively.

Averaged PO_4^{3-} concentrations were close to or below the quantification limit (0.05 µmol L^{-1}) from the surface to 20 m at LD A and LD B, and then increased with depth to reach 0.46 and 0.36 µmol L^{-1} at 200 m at LD A and LD B, respectively (Fig. 2). At LD C, PO_4^{3-} concentrations were always above the quantification limit and varied from 0.11 to 0.17 µmol L^{-1} in the 0–120 m layer. Below 120 m, PO_4^{3-}

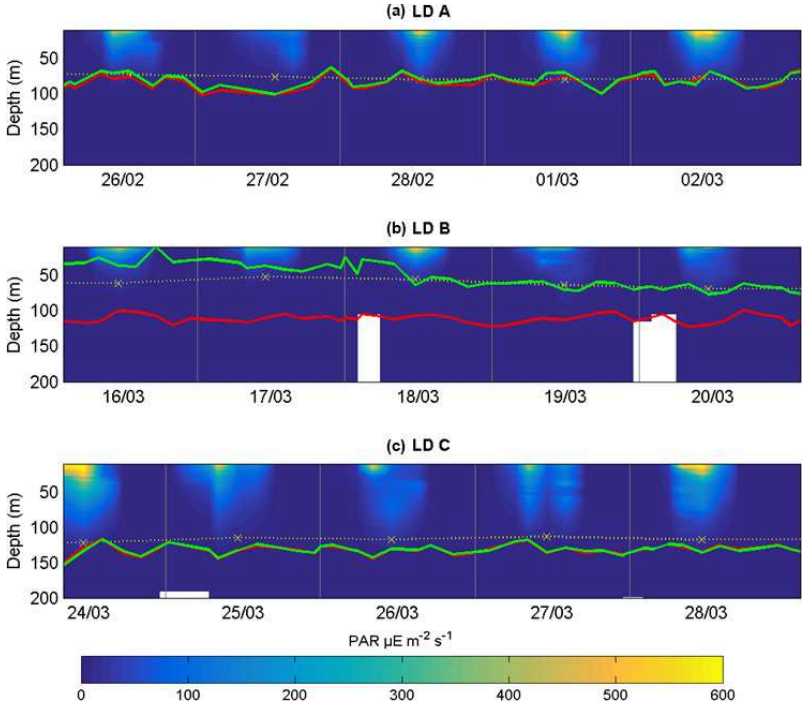

Figure 3. Temporal evolution of PAR, DCM (green line), ρ_{NO_3} (red line), and 1 % of surface PAR (yellow dots and crosses) during the three stations' occupation period (LD A: **a**; LD B: **b**; LD C: **c**).

concentrations increased with depth to reach 0.43 µmol L^{-1} at 200 m.

At LD A, the DCM and the ρ_{NO_3} depths were located between 60 and 100 m (Fig. 3). At LD B, the ρ_{NO_3} was located between 100 and 120 m, while the depth of the DCM increased from 25 to 70 m during the five days that the station was occupied. At LD C, the DCM and the ρ_{NO_3} were below the bottom of the photic layer (110–120 m), varying concurrently between 115 and 155 m. The DCM and ρ_{NO_3} depths were significantly correlated ($p < 0.05$) at LD A and LD C and not correlated ($p > 0.05$) at LD B. The depths of the photic layers, corresponding to 1 % of the surface PAR at midday, were 80–90 m at LD A, 60–70 m at LD B and 110–120 m at LD C.

3.2 Atmospheric deposition

Nitrate dissolution from aerosols occurred rapidly, releasing in seawater on average 1.8 nmol m^{-3} (26 ng m^{-3}) dissolved inorganic nitrogen. Nitrate appeared to be nitrate aerosol since no correlation was observed between nitrate and Fe, Si, Na and Cl (Karine Desboeufs, personal communication, 2017), precluding a mixing with ash or sea salt. Extrapolated dry deposition flux (Table 2) was on average 630 ± 329 nmol m^{-2} d^{-1} (3.22 ± 1.7 mg m^{-2} yr^{-1}).

3.3 N_2 fixation rates

N_2 fixation rates measured using the in situ incubation method ranging from < QL to 19.3 nmol N L^{-1} d^{-1} at LD A, 0.1 to 45.0 nmol N L^{-1} d^{-1} at LD B and < QL to 2.6 nmol N L^{-1} d^{-1} at LD C (Fig. 2). At LD A and LD B, maximum rates were measured near the surface (5 m) where they reached 19.3 and 45.0 nmol N L^{-1} d^{-1}, and decreased with depth down to 0.5 nmol L^{-1} d^{-1} at 70 and 55 m, respectively at LD A and LD B. At LD C, N_2 fixation rates were 2 to 20 times lower than at LD B and LD A, with a maximum of 2.6 nmol N L^{-1} d^{-1} located around 40 m. Close to the surface (5 m), rates were below the quantification limit. At LD A and LD C, the three profiles measured on days 1, 3 and 5 at each station were similar to each other, while at LD B rates measured in the 0–40 m layer were different over the three sampling dates (Fig. 2), with rates decreasing over time.

N_2 fixation rates measured using the deck incubation method were not statistically different (Mann–Whitney paired test, $p < 0.05$) from those measured using the in situ mooring line method (Fig. 2). They ranged 0.1 to 21.0 nmol N L^{-1} d^{-1} at LD A and 0.1 to 30.3 nmol N L^{-1} d^{-1} at LD B, and were below 1.2 nmol N L^{-1} d^{-1} at LD C. Overall, the profiles were similar between the two methods, except the maximum at 40 m at LD C, which was not sampled with the on-deck incubation method. In addition, N_2 fixation rates from days 1–3 were

not statistically different each other (Mann–Whitney paired test, $p < 0.05$).

Integrated N_2 fixation rates were 593 ± 51, 706 ± 302 and $59 \pm 16\,\mu mol\,N\,m^{-2}\,d^{-1}$ at LD A, LD B and LD C, respectively using data from the in situ incubation method (Fig. 2; Table 2) and 628 ± 156, 942 ± 253 and $56 \pm 31\,\mu mol\,N\,m^{-2}\,d^{-1}$ at LD A, LD B, and LD C, respectively, using data from the deck incubation method (Fig. 2). At LD A, 80 % of the integrated N_2 fixation rate was reached at 36 m, at LD B 82 % was reached at 27 m, and at LD C 78 % was reached at 60 m.

3.4 Vertical turbulent diffusive fluxes of nitrate

The averaged NO_3^- input through vertical turbulent diffusion showed strong time variability, with a typical standard deviation of the same order as the mean value (Table 3) and a strong contrast between the western station LD A and the two other stations, with mean values equal to $24.4 \pm 24.4\,\mu mol\,N\,m^{-2}\,d^{-1}$ at LD A and 6.7 ± 5.3 and $4.8 \pm 2.2\,\mu mol\,N\,m^{-2}\,d^{-1}$ at LD B and LD C, respectively (Fig. 4). At LD A, a NO_3^- peak input of $50\,\mu mol\,N\,m^{-2}\,d^{-1}$ was observed on day 1 (26 February), while during days 2 and 3 (27 and 28 February) the daily average input was lower than the average value for the station, between 5 and $10\,\mu mol\,N\,m^{-2}\,d^{-1}$, without any peak input. At the end of LD A (days 4 and 5 – 1 and 2 March), the strongest NO_3^- input variability was observed with instantaneous peaks reaching 46 to $89\,\mu mol\,N\,m^{-2}\,d^{-1}$. When averaged per day, daily input was minimum on day 2 (27 February) with $5\,\mu mol\,N\,m^{-2}\,d^{-1}$ and maximum on day 5 (2 March) with $65\,\mu mol\,N\,m^{-2}\,d^{-1}$ (red lines in Fig. 4a). At LD B, the mean daily NO_3^- input varied within a factor of ~ 5, from $2\,\mu mol\,N\,m^{-2}\,d^{-1}$ on day 5 (20 March) to $11\,\mu mol\,N\,m^{-2}\,d^{-1}$ on day 2 (17 March). The highest daily averages obtained on days 2 and 3 were explained by the occurrence of NO_3^- input peaks. At LD C, NO_3^- input heterogeneously varied between 2 and $10\,\mu mol\,N\,m^{-2}\,d^{-1}$ with minimum daily average on day 4 (27 March; $3\,\mu mol\,N\,m^{-2}\,d^{-1}$) and maximum daily average on day 1 (24 March; $8\,\mu mol\,N\,m^{-2}\,d^{-1}$). Similarly as for the other stations, NO_3^- input peaks were observed during the days of higher mean daily NO_3^- input.

This time variability in NO_3^- input was strongly influenced by the vertical turbulent diffusion coefficient. The K_z time series showed strong variability (Table 3), with peak values occurring intermittently during periods of enhanced turbulence, thus leading to peaks in NO_3^- turbulent diffusive flux.

3.5 Particulate matter export

Mass fluxes recovered in the sediment traps at the three stations over the three sampling depths (150, 330 and 520 m) ranged from 13.6 to 87.2 mg of dry weight (DW) $m^{-2}\,d^{-1}$ (Table 1). At LD A and LD C, fluxes decreased with depth, which was not observed at LD B. Maximum mass fluxes were measured at LD A, with 87.2 mg DW $m^{-2}\,d^{-1}$ at 150 m, 23.9 mg DW $m^{-2}\,d^{-1}$ at 330 m and 22.3 mg DW $m^{-2}\,d^{-1}$ at 520 m. LD B presented the lowest export rate at 150 m (14.1 mg DW $m^{-2}\,d^{-1}$) over the three stations. At LD C, 19.6 mg DW $m^{-2}\,d^{-1}$ of particulate matter was exported at 150 m and the lowest export rate was recorded at 330 m.

Particulate C (PC) and PN recovered in the sediment traps followed the same patterns as the mass fluxes (Table 1), with a maximum export rate at 150 m at LD A and a minimum export rate at LD B and LD C. However, as PN and PC were not always in the same proportion in the exported matter, variations in C : N ratios at the three stations were reduced, with averaged C : N ratios of 8.2 at LD A, 9.1 at LD B and 6.2 at LD C.

The mass of swimmers (zooplankton) recovered in the traps ranged from 10.5 to 376.1 mg DW $m^{-2}\,d^{-1}$ (Table 4) and accounted for 36 to 94 % of total DW. The maximum was found at 330 m at LD A, and 150 m at LD B and LD C. As for particulate matter, zooplankton C (Zoo-C) and N (Zoo-N) mass measured at each depth of each station followed the same pattern as the mass of swimmers recovered. Zoo-C ranged from 4.9 to 129.2 mg C $m^{-2}\,d^{-1}$ and Zoo-N ranged from 1.1 to 19.5 mg N $m^{-2}\,d^{-1}$.

3.6 Direct export of diazotrophs

Trichodesmium abundance measured in the sediment traps at the three stations ranged from below quantification limit ($<$ QL) to 2.67×10^4 *nifH* gene copies mL^{-1} of sediment material ($<$ QL at LD C 330 m and not available at LD A 150 m), and represented less than 0.1 % of *Trichodesmium* abundance integrated over the water column at the three stations based on data of Stenegren et al. (2018). UCYN-B abundance measured in the traps ranged from $<$ QL to 4.27×10^3 *nifH* gene copies mL^{-1}. It accounted for 0.1 to 10.5 % of UCYN-B abundance integrated over the water column at LD A, and < 0.5 % at LD B and LD C. DDAs abundance, restricted to het-1 (*Richelia* associated with *Rhizosolenia* diatoms), ranged from $<$ QL to 1.99×10^4 *nifH* gene copies mL^{-1} ($<$ QL at LD A 150 and 520 m, LD B 150 m and LD C 330 m) and accounted up to 72.6, 2.9 and 0.1 % of DDAs abundance integrated over the water column at LD A, LD B and LD C, respectively. While het-2 (*Richelia* associated with *Hemiaulus* diatoms) were observed in the water column (Stenegren et al., 2018), they were only detected in one sediment trap sample (LD B, 330 m) and $<$ QL in 330 m from LD A and 500 m from LD B. When converted to C, diazotrophs represented between 5.4 and 30.6 % (Fig. 5) of the total PC measured in the traps (Table 1) at LD A, from < 0.1 to 5.0 % at LD B, and < 0.1 % at LD C. *Trichodesmium*, and het-1 were the major contributors to diazotroph export at LD A and LD B (note that *Trichodesmium* data were not available for LD A, 150 m) and UCYN-B and het-1 were the major contributors at LD C.

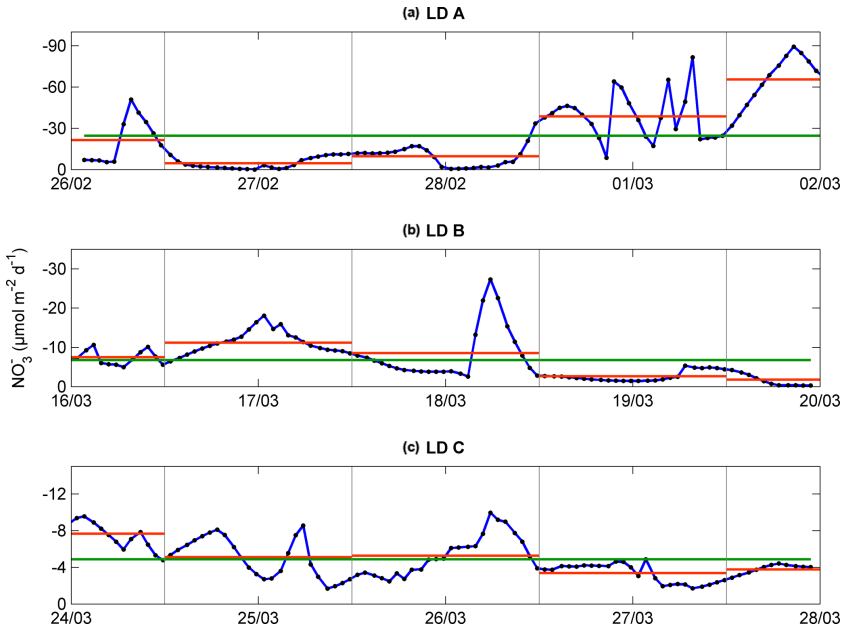

Figure 4. Temporal evolution of upward vertical NO_3^- flux (µmol N m^{-2} d^{-1}) calculated at the top of the nitracline for each station, LD A **(a)**, LD B **(b)**, and LD C **(c)**, after temporal interpolation (blue). Daily mean from noon to noon in dashed orange line and occupation period mean in green line.

Table 3. Mean turbulent diffusion coefficient (K_z), mean nitracline gradient, mean NO_3^- flux and associated standard deviations ($n = 3$) over the station occupation at LD A, LD B and LD C at the top nitracline and at the maximum gradient.

Station	K_z m^2 s^{-1}	Nitracline gradient µmol N m^{-4}	NO_3^- flux µmol N m^{-2} d^{-1}
Top nitracline			
LD A	$1.11 \times 10^{-5} \pm 1.00 \times 10^{-5}$	23 ± 13	24.4 ± 24.4
LD B	$3.59 \times 10^{-6} \pm 3.11 \times 10^{-6}$	21 ± 12	6.7 ± 5.3
LD C	$2.04 \times 10^{-6} \pm 1.11 \times 10^{-6}$	27 ± 13	4.8 ± 2.2
Maximum gradient			
LD A	$1.69 \times 10^{-5} \pm 1.15 \times 10^{-5}$	53 ± 10	79 ± 56
LD B	$4.52 \times 10^{-6} \pm 3.22 \times 10^{-6}$	48 ± 6	19 ± 14
LD C	$2.96 \times 10^{-6} \pm 1.84 \times 10^{-6}$	48 ± 14	21 ± 11

4 Discussion

4.1 Towards a daily N budget

The analysis of hydrographic tracers and velocity structures present during our study at the three stations reveals that horizontal variability due to advection was important at spatial scales larger than the ones sampled at each station (de Verneil et al., 2018). Thus, we consider that we sampled the same water mass at each station and only vertical exchanges controlled input and output of N in the upper water column, which allow us to perform a daily N budget at the three stations, as summarized in Table 2.

4.2 Contribution of N_2 fixation to new N input in the WTSP

The daily N budget (Table 2) indicates that N_2 fixation was the major external source of N to the WTSP, regardless of the degree of oligotrophy, and represents more than 90 % of new N to the surface ocean at every station. This contribution is higher than in previous studies performed in other oligotrophic regions impacted by N_2 fixation (Table 5) such as the tropical North Atlantic (50 %, Capone et al., 2005) and Pacific (30–50 %, Dore et al., 2002; Karl et al., 2002) and higher than the average contribution at the global scale (Gruber, 2008). This previously unreported high contribution of N_2 fixation may have several origins.

Table 4. Zooplankton sediment traps data at the three LD stations. Depth of sampling, mean dry weight (DW) zooplankton recovered in the traps, and C and N associated with zooplankton.

Station	Depth m	Zooplankton DW (swimmers) mg m^{-2} d^{-1}	Zoo-C mg C m^{-2} d^{-1}	Zoo-N mg N m^{-2} d^{-1}	C : N ratio 106 : x
LD A	150	82.1 ± 18.0	42.3 ± 7.6	8.2 ± 1.2	106 : 18
	330	376.1 ± 26.1	129.2 ± 15.5	19.5 ± 4.0	106 : 14
	520	14.1 ± 8.0	5.3 ± 2.2	1.3 ± 0.4	106 : 22
LD B	150	112.9 ± 38.1	57.1 ± 21.7	11.3 ± 4.7	106 : 18
	330	62.3 ± 31.6	27.3 ± 15.5	4.9 ± 2.8	106 : 16
	520	10.5 ± 3.0	4.9 ± 1.2	1.1 ± 0.3	106 : 20
LD C	150	121.3 ± 37.5	41.7 ± 14.8	10.3 ± 5.0	106 : 22
	330	31.0 ± 5.1	14.3 ± 5.0	2.9 ± 1.3	106 : 18
	520	–	–	–	

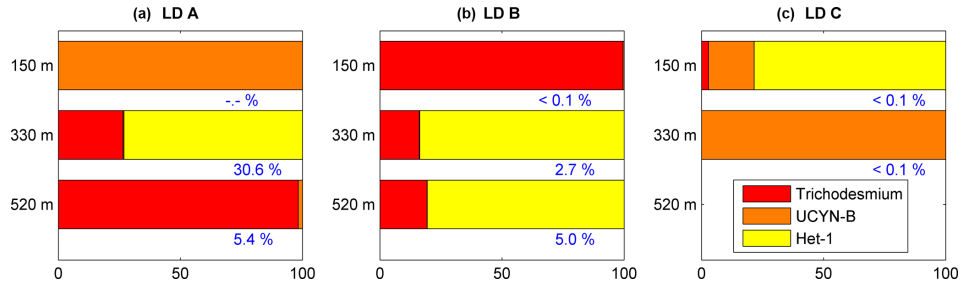

Figure 5. Relative contribution of each diazotroph (*Trichodesmium* in red, UCYN-B in orange and het-1 in yellow) to the total PC associated with diazotrophs (diazotroph-PC) in the sediment traps at 150 m (top), 330 m (middle) and 520 m (bottom), at the three stations LD A **(a)**, LD B **(b)** and LD C **(c)**. Values in blue correspond to the contribution of diazotroph-PC to total PC measured in the traps. No *Trichodesmium* valid data available at LD A 150 m.

Extrapolated NO_x deposition from the atmosphere during OUTPACE (range: 0.34–1.05 µmol m^{-2} d^{-1}) were one order of magnitude lower than predicted with major uncertainties by global models that include wet and gas deposition for that region (Kanakidou et al., 2012). Our flux could be an underestimation as it represents only dry deposition and as gas and organic forms were not measured. At the global scale and depending on the location, organic nitrogen could represent up to 90 % of N atmospheric deposition (Kanakidou et al., 2012), and NH_4^+ could account for ∼ 40 % (Dentener et al., 2006). Even if we double our estimated deposition flux, atmospheric deposition still remained low (< 1.5 %) and consequently represented a minor contribution of the new N input (Table 2). This negligible contribution of atmospheric input to the overall N budget (less than 1.5 %) therefore implies an important contribution of other terms, such as N_2 fixation.

Then, NO_3^- input by vertical turbulent diffusion appeared as the second source (1 to 8 %) of new N at the three stations. This contribution was lower than in previous studies in other oligotrophic regions (Table 5), where NO_3^- input by vertical turbulent diffusion contributes ∼ 18 % of new N in the Indian South Subtropical Gyre (Fernández-Castro et al., 2015), and ∼ 50 % in the tropical North Atlantic (Capone et al., 2005). In most studies (Fernández-Castro et al., 2015; Moutin and Prieur, 2012; Painter et al., 2013), an average K_z value is used (i.e. averaged over the cruise, over a station or over depth) to determine NO_3^- input by turbulence in the photic layer. In this study we performed high-frequency direct measurements of K_z and highlighted the importance of turbulent event pulses on diffusive NO_3^- input. Using a constant K_z of 10^{-5} m^2 s^{-1} at the three stations decreases the NO_3^- input down to 22.9 µmol N m^{-2} d^{-1} at LD A and increases NO_3^- input up to 19.9 and 25.5 µmol N m^{-2} d^{-1} at LD B and LD C, which is 2.7 and 4.8 times higher than using a high-frequency K_z for the latter two stations. The contrasted NO_3^- input observed at the three stations results from the high variability in turbulence along the west–east transects (Bouruet-Aubertot et al., 2018). Thus, using a constant K_z removes the contrasted NO_3^- input between the three stations (∼ 4 times higher at LD A than at LD B and LD C). Consequently, using average K_z values for the turbulent diffusive flux computation can lead to significant bias. In our study, NO_3^- input was calculated at the top of the nitracline. Painter et al. (2013) have demonstrated the variability that may be introduced into the estimated NO_3^- input by the depth of the defined nitracline. With a constant K_z in the 2 cases,

Table 5. Contribution of N_2 fixation and NO_3^- vertical diffusion to new N inputs in oligotrophic region.

Location	Contribution to new N		Source
	N_2 fixation	NO_3^- diffusion	
Tropical North Atlantic	50 %	50 %	Capone et al. (2005)
Subtropical North Atlantic	2 %	–	Mourino-Carballido et al. (2011)
Subtropical South Atlantic	44 %	–	Mourino-Carballido et al. (2011)
South Atlantic Gyre	21 %	24 %	Fernández-Castro et al. (2015)
Indian South Subtropical Gyre	12 %	18 %	Fernández-Castro et al. (2015)
Mediterranean Sea	0–32 %	21–53 %	Moutin and Prieur (2012), Bonnet et al. (2011)
North Pacific Subtropical Gyre	30–50 %	–	Karl et al. (2003)
North Pacific Subtropical Gyre	48 %	52 %	Dore et al. (2002)
Western tropical South Pacific	92–99 %	1–8 %	This study

they estimated that NO_3^- input was 5 times lower at the top of nitracline depth than at the maximum gradient depth. In our study, the NO_3^- input would also be $\sim$ 3–4 times higher if calculated at the maximum gradient depth rather than at the top nitracline, mainly due to the increase in the nitracline gradient up to 48 µmol N m^{-4} (Table 3). However, in all cases, the NO_3^- input by turbulence always represented a minor contribution to the N budget.

Finally, the high contribution of N_2 fixation to new N input in the photic layer results from the intrinsically high N_2 fixation rates we measured in the WTSP (especially in MA waters), which are part of the hotspot of N_2 fixation reported by Bonnet et al. (2017), with rates being in the upper range of rates reported in the global N_2 fixation Marine Ecosystem Data (MAREDAT) database (Luo et al., 2012). Those high N_2 fixation rates are as high as they are westward in the Solomon Sea (Berthelot et al., 2017; Bonnet et al., 2015), extending the hotspot of N_2 fixation to the whole of the WTSP (Bonnet et al., 2017).

The contribution of N_2 fixation to PP was around 13–18 % in MA waters and 3 % in SPG waters. The high contribution measured in the MA region is an order of magnitude higher than that reported in previous studies performed in the Pacific Ocean (Moutin et al., 2008; Raimbault and Garcia, 2008; Shiozaki et al., 2014), the Atlantic Ocean (Fonseca-Batista et al., 2017; Rijkenberg et al., 2011) and the Mediterranean Sea (Moutin and Prieur, 2012), where it never exceeds 5 %, and also slightly higher than the contribution reported from a mesocosm experiment in the New Caledonia lagoon during a UCYN bloom (10.8 $\pm$ 5.0 %; Berthelot et al., 2015). As there was low supply of NO_3^- through vertical diffusion (< 8 %) and atmospheric deposition (< 1.5 %), N_2 fixation sustains nearly all new production during the austral summer in the WTSP.

4.3 Coupling between N_2 fixation and export in the WTSP

Previous studies have used different methods for coupled measurements of N_2 fixation and export (Berthelot et al., 2015; Dore et al., 2008; Karl et al., 2012; Scharek et al., 1999a; Subramaniam et al., 2008; White et al., 2012). The Lagrangian strategy used here was designed to sample the same water mass during the experiment and therefore minimize the methodological issues associated with particulate export flux measurements using sediment traps in the open ocean (Monroy et al., 2017). The severe meteorological conditions due to the development of tropical cyclone Pam (a category 5 storm) that hit the Vanuatu islands on March 2015 required us to establish the LD B station at a more easterly location than initially planned (Moutin et al., 2017). LD B was therefore sampled in a surface bloom with a DCM close to the surface (Fig. 3), in contrast to LD A and LD C, which were sampled in a zone with a DCM near the bottom of the photic layer (Fig. 3). Thus, data from LD B, although presented together with LD A and LD C, will be discussed apart.

Stations LD A and LD C were considered as oligotrophic and ultra-oligotrophic, respectively. PP was twice higher and the DCM shallower at station LD A, compared to LD C. Furthermore, the diazotroph community composition was contrasted between the two stations, with a clear dominance of *Trichodesmium* at LD A (6.6×10^4 *nifH* gene copies L^{-1} at 5 m) and lower abundance of diazotrophs, and a clear domination of UCYN-B (3.6×10^3 *nifH* gene copies L^{-1} at 5 m) and het-1 (3.0×10^3 *nifH* copies L^{-1} at 5 m) (Stenegren et al., 2018) at LD C. The *e* ratio (*e* ratio = PC export / PP) calculated at LD A (9.7 %) was higher than the *e* ratio in most studied oligotrophic regions (Karl et al., 2012; Moutin and Prieur, 2012; Raimbault and Garcia, 2008), where it rarely exceeds 1 %, indicating a high efficiency of the WTSP to export C relative to PP. Moreover, the *e* ratio was higher at LD A (characterized by high N_2 fixation rates, 593 µmol N m^{-2} d^{-1}) than at LD C (characterized by low

N_2 fixation (59 µmol N m^{-2} d^{-1})). This is in agreement with previous studies reporting typical *e* ratios of 1 % in ultra-oligotrophic regions characterized by low N_2 fixation rates (like LD C), such as the eastern SPG (Moutin et al., 2008; Raimbault and Garcia, 2008) or the Mediterranean Sea (Bonnet et al., 2011), and typical *e* ratios of 5 % in regions characterized by high N_2 fixation rates such as station ALOHA (Karl et al., 2012). Taken together, these results suggest that N_2 fixation would enhance particle export. This is supported by Knapp et al. (2018), who showed that nearly all exported production was supported by N_2 fixation in MA waters during the OUTPACE cruise.

At station ALOHA, the *e* ratio varies between 2 and 15 % and is maximum during summer export fluxes of PN, which are attributed to the direct export of DDAs (Karl et al., 2012). In the present study, we investigated the potential direct export of diazotrophs by measuring the abundance of each diazotroph group in the traps. We reveal that the export efficiency of *Trichodesmium*, i.e. the percentage of organisms present in the water column recovered in the traps (< 0.1 %), was lower than that of other diazotrophs, which is in agreement with Walsby (1992) and Chen et al. (2003), who revealed that *Trichodesmium* are rarely recovered in the sediment traps. The export efficiency of UCYN-B (2.3 % on average) and het-1 (4.0 % on average) was higher than that of *Trichodesmium*, which is consistent with Bonnet et al. (2016b) and Karl et al. (2012). In a mesocosm experiment performed in the coastal waters of New Caledonia, Bonnet et al. (2016b) revealed that UCYN-C were efficiently exported thanks to aggregation processes. In this study, the contribution of diazotrophs to PC export was up to 30.6 % at LD A, and was mainly driven by het-1 as the estimated het-1 C content was higher than that of UCYN-B and *Trichodesmium*. This suggests that DDAs were efficiently exported, which is in agreement with previous studies (Karl et al., 2012; Subramaniam et al., 2008). At LD C, less than 0.1 % of the total PC measured in the traps was associated with diazotrophs, which is probably due to lower abundances of het-1 in the traps (< DL) than at LD A and the dominance of UCYN-B (at 330 m) having low cellular C content. The contribution of diazotrophs to PC export at LD A (up to 30.6 % at 330 m) was high compared to what has been measured in a much smaller water column (15 m high mesocosms) in New Caledonia (ca. 20 %; Bonnet et al., 2016a), and suggests that the direct export of diazotrophs should be further investigated in oligotrophic open ocean. To date, few qPCR data on *nifH* from sediment traps are available (Karl et al., 2012) to compare with our study. However, it has to be noted that we measured the highest export and *e* ratio at LD A, where *Trichodesmium* dominated the diazotroph community. This suggests that most of the export was likely indirect, i.e. after the transfer of diazotroph-derived N (DDN) to the surrounding bacterial, phytoplankton and zooplankton communities, as revealed by Caffin et al. (2018) during the same cruise.

Station LD B was studied during a surface *Trichodesmium* bloom; however observations of poor cell integrity were reported (Stenegren et al., 2018) and other evidence indicated the senescence of the bloom (de Verneil et al., 2018). Higher N_2 fixation and integrated PP rates than those measured at LD A and C together, with lower PN export, resulted in an *e* ratio less than 0.8 % (Table 2) at LD B. This very low export efficiency is probably related to the fact that we sampled station LD B during a collapsing *Trichodesmium* bloom (Stenegren et al., 2018) triggered by PO_4^{3-} starvation (de Verneil et al., 2017), as already reported in the WTSP (Moutin et al., 2005). The collapse of *Trichodesmium* blooms can possibly result from viral lysis (Hewson et al., 2004), mainly leading to the release of dissolved N in surrounding waters, or programmed cell death, mainly leading to rapid sinking of biomass, and may influence C export (Bar-Zeev et al., 2013). Programmed cell death (PCD) was detected at LD B (Spungin et al., 2018), indicating that this process cannot be excluded, while *Trichodesmium* was not recovered in the traps (they dominated the export of diazotrophs at 150 m, but altogether the direct export of diazotrophs never exceeded 1.1 % of total export). It is thus likely that most of the N accumulated in the phytoplankton pool (including *Trichodesmium*) was released to the dissolved pool due to grazing and viral lysis, then quickly remineralized due to high microbial activity at LD B (Van Wambeke et al., 2018) and thus would explain the low export rate measured at this station. This result is supported by the efficient transfer of DDN to the surface planktonic food web at this station, as described in Caffin et al. (2018), and previously by Bonnet et al. (2016b) and Berthelot et al. (2016) in the WTSP. Thus, elevated Chl *a* patches such as those we sampled at LD B may be more productive areas than the ambient oligotrophic waters, but less efficient in terms of export, corresponding to the concept of "high-biomass, low-export" (HBLE) environments initially reported for the Southern Ocean (Lam and Bishop, 2007), where surface waters with high biomass were associated with low particle export at depth.

4.4 Disequilibrium of new vs. exported production

The daily N budget computed here reveals that N input into the photic layer through atmospheric deposition, N_2 fixation and vertical NO_3^- diffusion exceeded N output through organic matter export at the three studied stations. This imbalance between new and exported production is also observed in different oligotrophic regions of the ocean, such as the SPG (Raimbault and Garcia, 2008), the Barents Sea (Olli et al., 2002; Reigstad et al., 2008; Wexels Riser et al., 2008), the North and South Atlantic gyres (Thomalla et al., 2006), and the equatorial Pacific (Bacon et al., 1996). It should be noted that our budget was performed at the daily scale, but at the annual or longer timescales, the PN export from the photic layer is supposed to balance new N input (Dore et al., 2002; Eppley and Peterson, 1979).

Table 6. Contribution of N export by active zooplankton migration to total PN export.

Location	% of PN export	Source
Subtropical and tropical Atlantic	7.6	Longhurst et al. (1989, 1990)
North Atlantic BATS	37.3	Dam et al. (1995)
Equatorial Pacific	4.9	Le Borgne and Rodier (1997)
Equatorial Pacific	19.8	Le Borgne and Rodier (1997)
North Atlantic BATS	19.9	Al-Mutairi and Landry (2001)
North Pacific Subtropical Gyre	38	Hannides et al. (2009)
California Current Ecosystem	20	Stukel et al. (2013)
Costa Rica Dome	38	Stukel et al. (2015)

This imbalance between new and exported N frequently reported in the oligotrophic ocean may result from (1) a spatial decoupling between production and export, (2) a temporal decoupling between production and export and/or (3) processes other than particle export such as DON and/or zooplankton export. As we used the Lagrangian strategy described above and confirmed that we sampled the same water at all LD stations during our surveys (de Verneil et al., 2018), the first option (spatial decoupling) can be excluded. The second option would mean that we performed our budget during a period corresponding to production of organic matter that was dissociated from the export that would have occurred later. Such a temporal lag has already been reported in the Southern Ocean (Nodder and Waite, 2001), accompanied by biomass accumulation in the photic layer; therefore, we cannot exclude this hypothesis here. Regarding the third possible explanation, the primary process by which organic matter is exported out of the photic layer is the gravitational sinking of particles to the deep ocean (Karl et al., 1996; Knauer et al., 1990). However, two other main processes can contribute to export: physical mixing resulting in export of dissolved organic matter (Carlson et al., 1994; Carlson and Ducklow, 1995; Copin-Montégut and Avril, 1993; Toggweiler, 1989) and zooplankton diel migrations that actively transport organic matter out of the photic layer (Longhurst et al., 1989, 1990; Longhurst and Glen Harrison, 1988; Vinogradov, 1970). In the present study, the DON export flux was limited to eddy diffusion as we performed our survey during the stratification period, and the low downward flux of DON estimated by Moutin et al. (2018) was unable to explain the observed imbalance. However, zooplankton might play a significant role, although it is hard to quantify. Zooplankton living below the photic layer migrate to the surface at night, and when going down, can increase the export of dissolved and particulate organic and inorganic N through defecation, excretion or mortality (Atkinson et al., 1996; Le Borgne and Rodier, 1997; Dam et al., 1993, 1995; Longhurst et al., 1989, 1990; Longhurst and Williams, 1992; Zhang and Dam, 1998) if it occurs below a barrier to vertical mixing (i.e. nitracline or pycnocline; Longhurst et al., 1989, 1990). Zooplankton has been reported to represent between 4.9 and 38 % of the total export flux (Table 6) in several ecosystems and therefore should be considered in export calculations. Here, we estimated the maximum contribution of zooplankton using the higher value reported in Table 6 (38 %). It reached a maximum of 106 µmol N m^{-2} d^{-1} at LD A, 12 µmol N m^{-2} d^{-1} at LD B and 18 µmol N m^{-2} d^{-1} at LD C at 150 m. By applying this correction to our export values, it cannot explain the observed disequilibrium between new and exported N.

Finally, the zooplankton themselves are sampled by the traps but dead zooplankton were not distinguishable from live swimmers. In the present study, the zooplankton contribution to PN export (Table 4) was high (68 % on average), and above what has ever been measured in other oligotrophic areas such as the Mediterranean Sea (Moutin and Prieur, 2012). Here, all zooplankton recovered in traps were considered as live swimmers and were therefore discarded, which may have lead to an underestimation of the PN export and could also partly explain the observed disequilibrium between new and export production. Further studies should be undertaken to assess the contribution of living versus dead zooplankton to PN.

In summary, we suggest that zooplankton plays a key role on the export in the WTSP and its contribution would increase the particulate export. Moreover, zooplankton activity can transfer N accumulated in the phytoplankton pool to the dissolved pool following grazing and related trophic processes. N from the dissolved pool is then remineralized by microbial activity and accumulates in the photic layer; thus, N is not recovered in sediment traps.

4.5 Methodological underestimation leads to a possible higher contribution of N_2 fixation

In this study we intentionally used the "bubble method" to measure N_2 fixation rates, considering the small differences observed between this method and the method consisting in adding the $^{15}N_2$ as dissolved in a subset of seawater previously N_2 degassed (Mohr et al., 2010) in Pacific waters (Bonnet et al., 2016b; Shiozaki et al., 2015) and the high risk of sample contamination involved when manipulating sample seawater to prepare dissolved $^{15}N_2$ (Klawonn et al., 2015). In addition to the contamination issues, preparing dissolved

$^{15}N_2$ on board represents additional time with samples sitting on the bench or rosette before incubation, which is especially critical in tropical environments. To reduce any potential underestimation, we measured the ^{15}N enrichment of the N_2 pool at the end of the incubation (7.548 ± 0.557 atom%, Bonnet et al., 2018), which was lower than the theoretical value of ~ 8.2 atom% based on gas constants calculations (Weiss, 1970). It should be noted that the sampling procedure used for the ^{15}N enrichment measurement of the N_2 pool can induce gas exchange between the atmosphere and the sample, and a possible N_2 contamination that can lead to a decrease in the ^{15}N enrichment of the sample. Moreover, we are aware that the dissolution kinetics of $^{15}N_2$ in the incubation bottles is progressive along the 24 h of incubation (Mohr et al., 2010). Therefore, the ^{15}N enrichment of the N_2 pool measured with the MIMS at the end of the incubation likely represents maximum values, and the N_2 fixation rates provided in this study represent minimum values. This reinforces the conclusions of this study regarding the prominent role of N_2 fixation in this region. Großkopf et al. (2012) found that the discrepancy between both methods was more important when UCYN dominates the diazotroph community as compared to when *Trichodesmium* dominates. Consequently, N_2 fixation rates in this study are potentially more underestimated in SPG waters than in MA waters. By applying the maximum factor of underestimation found by Großkopf et al. (2012; i.e. 1.7), N_2 fixation in SPG waters would have been higher ($100\,\mu mol\,N\,m^{-1}\,d^{-1}$ instead of 59), which is still far lower than in MA waters and does not change the conclusions of this study.

5 Conclusion

In this study, we successfully used a Lagrangian strategy in the WTSP to follow the same water mass during 5 days in order to perform N budgets during the stratification period (February–March 2015) at three stations. N_2 fixation appeared as a substantial biogeochemical process providing the major external source of N in the photic layer. *Trichodesmium* was the major diazotroph in the oligotrophic MA waters (LD A and LD B), while UCYN dominated the diazotroph community in the ultra-oligotrophic waters of the gyre (LD C). N_2 fixation contributed ~ 13–$18\,\%$ of the estimated PP in the MA region where N_2 fixation rates were high, and $\sim 3\,\%$ in the SPG water where N_2 fixation rates were low. As there was limited supply of NO_3^- through vertical turbulent diffusion ($< 8\,\%$) and dry atmospheric deposition ($< 1\,\%$), N_2 fixation accounted for nearly all new production (more than 90 % of new N). The current coupling between typical high N_2 fixation rates of the WTSP, with the high PN and PC export measured in this region associated with high *e* ratios (up to $\sim 10\,\%$), suggests that N_2 fixation plays an important role in export during austral summer conditions in the WTSP, either directly or indirectly. The export efficiency measured here in the WTSP (LD A) is comparable to that measured in the Southern Ocean (Rembauville et al., 2015), considered as an efficient ecosystem for C export. The oligotrophic ocean represents 60 % of the global ocean surface and therefore may play a more significant role in C export than initially considered (Baines et al., 1994; Wassmann, 1990). Even if the link between N_2 fixation rates and export is obvious, the possible temporal decoupling between these processes and the potential role of zooplankton need to be further investigated. Finally, as Bonnet et al. (2017) have recently shown that the WTSP is a hotspot of N_2 fixation, and as we have shown the importance of this process with regard to the N input and N and C export, we suggest that this region of the world ocean should be further investigated by means of oceanographic cruises and the establishment of time series. This would give us a "big picture" of the role of N_2 fixation on the export in the oligotrophic ocean.

Data availability. All data and metadata are available at the French INSU/CNRS LEFE CYBER database (scientific coordinator: Hervé Claustre; data manager and webmaster: Catherine Schmechtig) at the following web address: http://www.obs-vlfr.fr/proof/php/outpace/outpace.php (INSU/CNRS LEFE CYBER, 2017).

Competing interests. The authors declare that they have no conflict of interest.

Special issue statement. This article is part of the special issue "Interactions between planktonic organisms and biogeochemical cycles across trophic and N_2 fixation gradients in the western tropical South Pacific Ocean: a multidisciplinary approach (OUTPACE experiment)". It is not associated with a conference.

Acknowledgements. This is a contribution of the OUTPACE (Oligotrophy from Ultra-oligoTrophy PACific Experiment) project (https://outpace.mio.univ-amu.fr/, last access: November 2017), funded by the French research national agency (ANR-14-CE01-0007-01), the LEFE-CyBER programme (CNRS-INSU), the GOPS programme (IRD) and the CNES (BC T23, ZBC 4500048836). The project leading to this publication received funding from European FEDER Fund under project 1166-39417. The OUTPACE cruise (https://doi.org/10.17600/15000900, Moutin and Bonnet, 2015) was managed by MIO (OSU Institut Pytheas, AMU) from Marseilles (France). The authors thank the crew of the RV *L'Atalante* for outstanding shipboard operations. Gilles Rougier and Marc Picheral are warmly thanked for their efficient help in CTD rosette management and data processing, as well as Catherine Schmechtig for the LEFE-CyBER database management. Justine Louis is warmly thanked for the analyses of atmospheric DIN on board. The satellite-derived data of sea surface temperature, Chl *a* concentrations and currents have been provided by CLS in the framework of the CNES funding; we warmly thank

Marie Isabelle Pujol and Guillaume Taburet for their support in providing these data. We acknowledge NOAA, and in particular Rick Lumpkin, for providing the SVP drifters.

Edited by: Helge Niemann
Reviewed by: Carolin Löscher, Annie Bourbonnais, and two anonymous referees

References

Al-Mutairi, H. and Landry, M. R.: Active export of carbon and nitrogen at station ALOHA by diel migrant zooplankton, Deep-Sea Res. Pt. II, 48, 2083–2103, https://doi.org/10.1016/S0967-0645(00)00174-0, 2001.

Altabet, M. A.: Variations in nitrogen isotopic composition between sinking and suspended particles: implications for nitrogen cycling and particle transformation in the open ocean, Deep-Sea Res. Pt. A, 35, 535–554, https://doi.org/10.1016/0198-0149(88)90130-6, 1988.

Aminot, A. and Kérouel, R.: Dosage automatique des nutriments dans les eaux marines?: méthodes en flux continu, Ifremer, Plouzané, 2007.

Atkinson, A., Shreeve, R. S., Pakhomov, E. A., Priddle, J., Blight, S. P., and Ward, P.: Zooplankton response to a phytoplankton bloom near South Georgia, Antarctica, Mar. Ecol.-Prog. Ser., 144, 195–210, https://doi.org/10.3354/meps144195, 1996.

Bacon, M. P., Cochran, J. K., Hirschberg, D., Hammar, T. R., and Fleer, A. P.: Export flux of carbon at the equator during the EqPac time-series cruises estimated from ^{234}Th measurements, Deep.-Sea Res. Pt. II, 43, 1133–1153, https://doi.org/10.1016/0967-0645(96)00016-1, 1996.

Baines, S. R., Pace, M. L., and Karl, D. M.: Why does the relationship between sinking flux and planktonic primary production differ between lakes and oceans?, Limnol. Oceanogr., 39, 213–226, 1994.

Bar-Zeev, E., Avishay, I., Bidle, K. D., and Berman-Frank, I.: Programmed cell death in the marine cyanobacterium Trichodesmium mediates carbon and nitrogen export, ISME J., 7, 2340–2348, https://doi.org/10.1038/ismej.2013.121, 2013.

Benavides, M., Berthelot, H., Duhamel, S., Raimbault, P., and Bonnet, S.: Dissolved organic matter uptake by Trichodesmium in the Southwest Pacific, Sci. Rep., 7, 41315, https://doi.org/10.1038/srep41315, 2017.

Berthelot, H., Moutin, T., L'Helguen, S., Leblanc, K., Hélias, S., Grosso, O., Leblond, N., Charrière, B., and Bonnet, S.: Dinitrogen fixation and dissolved organic nitrogen fueled primary production and particulate export during the VAHINE mesocosm experiment (New Caledonia lagoon), Biogeosciences, 12, 4099–4112, https://doi.org/10.5194/bg-12-4099-2015, 2015.

Berthelot, H., Bonnet, S., Grosso, O., Cornet, V., and Barani, A.: Transfer of diazotroph-derived nitrogen towards non-diazotrophic planktonic communities: a comparative study between Trichodesmium erythraeum, Crocosphaera watsonii and Cyanothece sp., Biogeosciences, 13, 4005–4021, https://doi.org/10.5194/bg-13-4005-2016, 2016.

Berthelot, H., Benavides, M., Moisander, P. H., Grosso, O., and Bonnet, S.: High-nitrogen fixation rates in the particulate and dissolved pools in the Western Tropical Pacific (Solomon and Bismarck Seas), Geophys. Res. Lett., 2, 1–10, https://doi.org/10.1002/2017GL073856, 2017.

Bonnet, S., Biegala, I. C., Dutrieux, P., Slemons, L. O., and Capone, D. G.: Nitrogen fixation in the western equatorial Pacific: Rates, diazotrophic cyanobacterial size class distribution, and biogeochemical significance, Global Biogeochem. Cy., 23, 1–13, https://doi.org/10.1029/2008GB003439, 2009.

Bonnet, S., Grosso, O., and Moutin, T.: Planktonic dinitrogen fixation along a longitudinal gradient across the Mediterranean Sea during the stratified period (BOUM cruise), Biogeosciences, 8, 2257–2267, https://doi.org/10.5194/bg-8-2257-2011, 2011.

Bonnet, S., Rodier, M., Turk-Kubo, K. A., Germineaud, C., Menkes, C., Ganachaud, A., Cravatte, S., Raimbault, P., Campbell, E., Quéroué, F., Sarthou, G., Desnues, A., Maes, C., and Eldin, G.: Contrasted geographical distribution of N_2 fixation rates and nifH phylotypes in the Coral and Solomon Seas (southwestern Pacific) during austral winter conditions, Global Biogeochem. Cy., 29, 1874–1892, https://doi.org/10.1002/2015GB005117, 2015.

Bonnet, S., Berthelot, H., Turk-Kubo, K. A., Cornet-Barthaux, V., Fawcett, S., Berman-Frank, I., Barani, A., Grégori, G., Dekaezemacker, J., Benavides, M., and Capone, D. G.: Diazotroph derived nitrogen supports diatom growth in the South West Pacific: A quantitative study using nanoSIMS, Limnol. Oceanogr., 61, 1549–1562, https://doi.org/10.1002/lno.10300, 2016a.

Bonnet, S., Berthelot, H., Turk-Kubo, K., Fawcett, S., Rahav, E., L'Helguen, S., and Berman-Frank, I.: Dynamics of N_2 fixation and fate of diazotroph-derived nitrogen in a low-nutrient, low-chlorophyll ecosystem: results from the VAHINE mesocosm experiment (New Caledonia), Biogeosciences, 13, 2653–2673, https://doi.org/10.5194/bg-13-2653-2016, 2016b.

Bonnet, S., Caffin, M., Berthelot, H., and Moutin, T.: Hot spot of N^2 fixation in the western tropical South Pacific pleads for a spatial decoupling between N_2 fixation and denitrification, P. Natl. Acad. Sci. USA, 114, E2800–E2801, https://doi.org/10.1073/pnas.1619514114, 2017.

onnet, S., Caffin, M., Berthelot, H., Grosso, O., Benavides, M., Helias-Nunige, S., Guieu, C., Stenegren, M., and Foster, R. A.: In depth characterization of diazotroph activity across the Western Tropical South Pacific hot spot of N_2 fixation, Biogeosciences Discuss., https://doi.org/10.5194/bg-2017-567, in review, 2018.

Böttjer, D., Dore, J. E., Karl, D. M., Letelier, R. M., Mahaffey, C., Wilson, S. T., Zehr, J. P., and Church, M. J.: Temporal variability of nitrogen fixation and particulate nitrogen export at Station ALOHA, Limnol. Oceanogr., 62, 200–216, https://doi.org/10.1002/lno.10386, 2017.

Bourbonnais, A., Lehmann, M. F., Waniek, J. J., and Schulz-Bull, D. E.: Nitrate isotope anomalies reflect N_2 fixation in the Azores Front region (subtropical NE Atlantic), J. Geophys. Res.-Ocean., 114, 1–16, https://doi.org/10.1029/2007JC004617, 2009.

Bouruet-Aubertot, P., Cuypers, Y., Le Goff, H., Rougier, G., de Verneuil, A., Doglioli, A., Picheral, M., Yohia, C., Caffin, M., Lefèvre, D., Petrenko, A., and Moutin, T.: Longitudinal contrast in small scale turbulence along 20° S in the Pacific Ocean: origin and impact on biogeochemical fluxes, Biogeosciences Discuss., in preparation, 2018.

Caffin, M., Foster, R., Berthelot, H., and Bonnet, S.: Fate of N_2 fixation in the Western Tropical South Pacific Ocean: Transfer

of diazotroph-derived nitrogen to non-diazotrophic communities and export of diazotrophs, Biogeosciences Discuss., in preparation, 2018.

Capone, D. G., Burns, J. A., Montoya, J. P., Subramaniam, A., Mahaffey, C., Gunderson, T., Michaels, A. F., and Carpenter, E. J.: Nitrogen fixation by Trichodesmium spp.: An important source of new nitrogen to the tropical and subtropical North Atlantic Ocean, Global Biogeochem. Cy., 19, 1–17, https://doi.org/10.1029/2004GB002331, 2005.

Carlson, C. A. and Ducklow, H. W.: Dissolved organic carbon in the upper ocean of the central equatorial Pacific Ocean, 1992: Daily and finescale vertical variations, Deep-Sea Res. Pt. II, 42, 639–656, https://doi.org/10.1016/0967-0645(95)00023-J, 1995.

Carlson, C. A., Ducklow, H. W., and Michaels, A. F.: Annual flux of dissolved organic carbon from the euphotic zone in the northwestern Sargasso Sea, Nature, 371, 405–408, https://doi.org/10.1038/371405a0, 1994.

Chen, Y. L. L., Chen, H. Y., and Lin, Y. H.: Distribution and downward flux of Trichodesmium in the South China Sea as influenced by the transport from the Kuroshio Current, Mar. Ecol.-Prog. Ser., 259, 47–57, https://doi.org/10.3354/meps259047, 2003.

Church, M. J., Short, C. M., Jenkins, B. D., Karl, D. M., and Zehr, J. P.: Temporpl Patterns of nitrogenase gene (nifH) expression in the oligotrophic North Pacific Ocean, Appl. Environ. Microb., 71, 5362–5370, https://doi.org/10.1128/AEM.71.9.5362-5370.2005, 2005.

Copin-Montégut, G. and Avril, B.: Vertical distribution and temporal variation of dissolved organic carbon in the North-Western Mediterranean Sea, Deep-Sea Res. Pt. I, 40, 1963–1972, https://doi.org/10.1016/0967-0637(93)90041-Z, 1993.

Dabundo, R., Lehmann, M. F., Treibergs, L., Tobias, C. R., Altabet, M. A., Moisander, P. H., and Granger, J.: The contamination of commercial $^{15}N_2$ gas stocks with ^{15}N labeled nitrate and ammonium and consequences for nitrogen fixation measurements, PLoS ONE, 9, e110335, https://doi.org/10.1371/journal.pone.0110335, 2014.

Dam, H. G., Miller, C. A., and Jonasdottir, S. H.: The Trophic Role of Mesozooplankton at 47-Degrees-N, 20-Degrees-W during the North-Atlantic Bloom Experiment, Deep-Sea Res. Pt. II, 40, 197–212, https://doi.org/10.1016/0967-0645(93)90013-D, 1993.

Dam, H. G., Roman, M. R., and Youngbluth, M. J.: Downward export of respiratory carbon and dissolved inorganic nitrogen by diel-migrant mesozooplankton at the JGOFS Bermuda time-series station, Deep-Sea Res. Pt. I, 42, 1187–1197, https://doi.org/10.1016/0967-0637(95)00048-B, 1995.

Dekaezemacker, J. and Bonnet, S.: Sensitivity of N_2 fixation to combined nitrogen forms (NO_3^- and NH_4^+) in two strains of the marine diazotroph Crocosphaera watsonii (Cyanobacteria), Mar. Ecol.-Prog. Ser., 438, 33–46, https://doi.org/10.3354/meps09297, 2011.

Dentener, F., Drevet, J., Lamarque, J. F., Bey, I., Eickhout, B., Fiore, A. M., Hauglustaine, D., Horowitz, L. W., Krol, M., Kulshrestha, U. C., Lawrence, M., Galy-Lacaux, C., Rast, S., Shindell, D., Stevenson, D., Van Noije, T., Atherton, C., Bell, N., Bergman, D., Butler, T., Cofala, J., Collins, B., Doherty, R., Ellingsen, K., Galloway, J., Gauss, M., Montanaro, V., Muller, J. F., Pitari, G., Rodriguez, J., Sanderson, M., Solmon, F., Strahan, S., Schultz, M., Sudo, K., Szopa, S., and Wild, O.: Nitrogen and sulfur deposition on regional and global scales: a multimodel evaluation, Global Biogeochem. Cy., 20, GB4003, https://doi.org/10.1029/2005GB002672, 2006.

Deutsch, C. A., Sarmiento, J. L., Sigman, D. M., Gruber, N., and Dunne, J. P.: Spatial coupling of nitrogen inputs and losses in the ocean, Nature, 445, 163–167, https://doi.org/10.1038/nature05392, 2007.

de Verneil, A., Rousselet, L., Doglioli, A. M., Petrenko, A. A., and Moutin, T.: The fate of a southwest Pacific bloom: gauging the impact of submesoscale vs. mesoscale circulation on biological gradients in the subtropics, Biogeosciences, 14, 3471–3486, https://doi.org/10.5194/bg-14-3471-2017, 2017.

de Verneil, A., Rousselet, L., Doglioli, A. M., Petrenko, A. A., Maes, C., Bouruet-Aubertot, P., and Moutin, T.: OUTPACE long duration stations: physical variability, context of biogeochemical sampling, and evaluation of sampling strategy, Biogeosciences, 15, 2125–2147, https://doi.org/10.5194/bg-15-2125-2018, 2018.

Doglioli, A. M., Nencioli, F., Petrenko, A. A., Rougier, G., Fuda, J.-L., and Grima, N.: A software package and hardware tools for in situ experiments in a Lagrangian reference frame, J. Atmos. Ocean. Tech., 30, 1940–1950, 2013.

Dore, J. E., Brum, J. R., Tupas, L. M., and Karl, D. M.: Seasonal and interannual variability in sources of nitrogen supporting export in the oligotrophic subtropical North Pacific Ocean, Limnol. Oceanogr., 47, 1595–1607, 2002.

Dore, J. E., Letelier, R. M., Church, M. J., Lukas, R., and Karl, D. M.: Summer phytoplankton blooms in the oligotrophic North Pacific Subtropical Gyre: Historical perspective and recent observations, Prog. Oceanogr., 76, 2–38, https://doi.org/10.1016/j.pocean.2007.10.002, 2008.

d'Ovidio, F., Della Penna, A., Trull, T. W., Nencioli, F., Pujol, M.-I., Rio, M.-H., Park, Y.-H., Cotté, C., Zhou, M., and Blain, S.: The biogeochemical structuring role of horizontal stirring: Lagrangian perspectives on iron delivery downstream of the Kerguelen Plateau, Biogeosciences, 12, 5567–5581, https://doi.org/10.5194/bg-12-5567-2015, 2015.

Dron, A., Rabouille, S., Claquin, P., Talec, A., Raimbault, V., and Sciandra, A.: Photoperiod length paces the temporal orchestration of cell cycle and carbon-nitrogen metabolism in Crocosphaera watsonii, Environ. Microbiol., 15, 3292–3304, https://doi.org/10.1111/1462-2920.12163, 2013.

Eppley, R. W. and Peterson, B. J.: Particulate organic matter flux and planktonic new production in the deep ocean, Nature, 282, 677–680, https://doi.org/10.1038/282677a0, 1979.

Fernández-Castro, B., Mouriño-Carballido, B., Marañón, E., Chouciño, P., Gago, J., Ramírez, T., Vidal, M., Bode, A., Blasco, D., Royer, S.-J., Estrada, M., and Simó, R.: Importance of salt fingering for new nitrogen supply in the oligotrophic ocean, Nat. Commun., 6, 8002, https://doi.org/10.1038/ncomms9002, 2015.

Fonseca-Batista, D., Dehairs, F., Riou, V., Fripiat, F., Elskens, M., Deman, F., Brion, N., Quéroue, F., Bode, M., and Auel, H.: Nitrogen fixation in the eastern Atlantic reaches similar levels in the Southern and Northern Hemisphere, J. Geophys. Res.-Ocean., 122, 587–601, 2017.

Foster, R. A. and Zehr, J. P.: Characterization of diatom-South Pacific gyrecyanobacteria symbioses on the basis of nifH, hetR and 16S rRNA sequences, Environ. Microbiol., 8, 1913–1925, https://doi.org/10.1111/j.1462-2920.2006.01068.x, 2006.

Foster, R. A., Subramaniam, A., Mahaffey, C., Carpenter, E. J., Capone, D. G., and Zehr, J. P.: Influence of the Amazon River plume on distributions of free-living and symbiotic cyanobacteria in the western tropical north Atlantic Ocean, Limnol. Oceanogr., 52, 517–532, https://doi.org/10.4319/lo.2007.52.2.0517, 2007.

Garcia, N., Raimbault, P., Gouze, E., and Sandroni, V.: Fixation de diazote et production primaire en Méditerranée occidentale, C. R. Biol., 329, 742–750, https://doi.org/10.1016/j.crvi.2006.06.006, 2006.

Gradoville , M. R., Bombar, D., Crump, B. C., Letelier, R. M., Zehr, J. P., and White, A. E.: Diversity and activity of nitrogen-fixing communities across ocean basins, Limnol. Oceanogr., 62, 1895–1909, 2017.

Großkopf, T., Mohr, W., Baustian, T., Schunck, H., Gill, D., Kuypers, M. M. M., Lavik, G., Schmitz, R. A., Wallace, D. W. R., and LaRoche, J.: Doubling of marine dinitrogen-fixation rates based on direct measurements, Nature, 488, 361–364, https://doi.org/10.1038/nature11338, 2012.

Gruber, N.: The Marine Nitrogen Cycle: Overview and Challenges, Nitrogen Mar. Environ., 1–50, https://doi.org/10.1016/B978-0-12-372522-6.00001-3, 2008.

Gruber, N. and Sarmiento, J. L.: Global patterns of marine nitrogen fixation and denitrification, Global Biogeochem. Cy., 11, 235–266, https://doi.org/10.1029/97GB00077, 1997.

Guieu, C., Bonnet, S., Petrenko, A., Menkes, C., Chavagnac, V., Desboeufs, C., Maes, C., and Moutin, T.: Iron from a submarine source impacts the productive layer of the Western Tropical South Pacific (WTSP), Scientific Reports, in review, 2018.

Hannides, C. C. S., Landry, M. R., Benitez-Nelson, C. R., Styles, R. M., Montoya, J. P., and Karl, D. M.: Export stoichiometry and migrant-mediated flux of phosphorus in the North Pacific Subtropical Gyre, Deep-Sea Res. Pt. I, 56, 73–88, https://doi.org/10.1016/j.dsr.2008.08.003, 2009.

Hewson, I., Govil, S. R., Capone, D. G., Carpenter, E. J., and Fuhrman, J. A.: Evidence of Trichodesmium viral lysis and potential significance for biogeochemical cycling in the oligotrophic ocean, Aquat. Microb. Ecol., 36, 1–8, https://doi.org/10.3354/ame036001, 2004.

Hynes, A. M., Webb, E. A., Doney, S. C., and Waterbury, J. B.: Comparison of cultured trichodesmium (cyanophyceae) with species characterized from the field, J. Phycol., 48, 196–210, https://doi.org/10.1111/j.1529-8817.2011.01096.x, 2012.

INSU/CNRS LEFE CYBER: available at: http://www.obs-vlfr.fr/proof/php/outpace/outpace.php (last access: 27 April 2018), 2017.

JGOFS: Core measurements protocols?: report of the core measurement working group, Jt. Glob. Ocean Flux Study, JGOFS repo, SCOR 1-40, 1988.

Kana, T. M., Darkangelo, C., Hunt, M. D., Oldham, J. B., Bennett, G. E., and Cornwell, J. C.: Membrane Inlet Mass Spectrometer for Rapid High-Precision Determination of N_2, O_2, and Ar in Environmental Water Samples, Anal. Chem., 66, 4166–4170, https://doi.org/10.1021/ac00095a009, 1994.

Kanakidou, M., Duce, R. A., Prospero, J. M., Baker, A. R., BenitezNelson, C., Dentener, F. J., Hunter, K. A., Liss, P. S., Mahowald, N., Okin, G. S., Sarin, M., Tsigaridis, K., Uematsu, M., Zamora, L. M., and Zhu, T.: Atmospheric fluxes of organic N and P to the global ocean, Global Biogeochem. Cy., 26, GB3026, https://doi.org/10.1029/2011GB004277, 2012.

Karl, D. M., Christian, J. R., Dore, J. E., Hebel, D. V., Letelier, R. M., Tupas, L. M., and Winn, C. D.: Seasonal and interannual variability in primary production and particle flux at Station ALOHA, Deep-Sea Res. Pt. II, 43, 539–568, https://doi.org/10.1016/0967-0645(96)00002-1, 1996.

Karl, D. M., Letelier, R. M., Tupas, L. M., Dore, J. E., Christian, J. R., and Hebel, D. V.: The role of nitrogen fixation in biogeochemical cycling in the subtropical North Pacific Ocean, Nature, 388, 533–538, https://doi.org/10.1038/41474, 1997.

Karl, D. M., Michaels, A. F., Bergman, B., Capone, D. G., Carpenter, E. J., Letelier, R., Lipschultz, F., Paerl, H., Sigman, D., and Stal, L.: Dinitrogen fixation in the world's oceans, Biogeochemistry, 57–58, 47–98, https://doi.org/10.1023/A:1015798105851, 2002.

Karl, D. M., Bates, N., Emerson, S., Harrisson, P. J., Jeandel, C., Liu, K. K., Marty, J. C., Michaels, A. F., Miquel, J. C., Neuer, S., Nojiri, Y., and Wong, C. S.: Temporal studies of biogeochemical processes determined from ocean time-series observations during the JGOFS era, in: Ocean Biogeochemistry: The role of the ocean carbon cycle in global change, edited by: Fasham, M. J. R., International Geosphere-Biosphere Programme Book Series, Springer-Verlag, New York, 239–267, 2003.

Karl, D. M., Church, M. J., Dore, J. E., Letelier, R. M., and Mahaffey, C.: Predictable and efficient carbon sequestration in the North Pacific Ocean supported by symbiotic nitrogen fixation, P. Natl. Acad. Sci. USA, 109, 1842–1849, https://doi.org/10.1073/pnas.1120312109, 2012.

Klawonn, I., Lavik, G., Böning, P., Marchant, H. K., Dekaezemacker, J., Mohr, W., and Ploug, H.: Simple approach for the preparation of $^{15-15}N_2$-enriched water for nitrogen fixation assessments: Evaluation, application and recommendations, Front. Microbiol., 6, 769, https://doi.org/10.3389/fmicb.2015.00769, 2015.

Knapp, A. N.: The sensitivity of marine N_2 fixation to dissolved inorganic nitrogen, Front. Microbiol., 3, 1–14, https://doi.org/10.3389/fmicb.2012.00374, 2012.

Knapp, A. N., Sigman, D. M., and Lipschultz, F.: N isotopic composition of dissolved organic nitrogen and nitrate at the Bermuda Atlantic Time-series study site, Global Biogeochem. Cy., 19, 1–15, https://doi.org/10.1029/2004GB002320, 2005.

Knapp, A. N., Difiore, P. J., Deutsch, C., Sigman, D. M., and Lipschultz, F.: Nitrate isotopic composition between Bermuda and Puerto Rico: implications for N_2 fixation in the Atlantic Ocean, Global Biogeochem. Cy., 22, GB3014, https://doi.org/10.1029/2007GB003107, 2008.

Knapp, A. N., McCabe, K. M., Grosso, O., Leblond, N., Moutin, T., and Bonnet, S.: Distribution and rates of nitrogen fixation in the western tropical South Pacific Ocean constrained by nitrogen isotope budgets, Biogeosciences Discuss., https://doi.org/10.5194/bg-2017-564, in review, 2018.

Knauer, G. A., Redalje, D. G., Harrison, W. G. and Karl, D. M.: New production at the VERTEX time-series site, Deep-Sea Res. Pt. A, 37, 1121–1134, https://doi.org/10.1016/0198-0149(90)90054-Y, 1990.

Lam, P. J. and Bishop, J. K. B.: High biomass, low export regimes in the Southern Ocean, Deep-Sea Res. Pt. II, 54, 601–638, https://doi.org/10.1016/j.dsr2.2007.01.013, 2007.

Le Borgne, R. and Rodier, M.: Net zooplankton and the biological pump: A comparison between the oligotrophic and mesotrophic equatorial Pacific, Deep-Sea Res. Pt. II, 44, 2003–2023, https://doi.org/10.1016/S0967-0645(97)00034-9, 1997.

Longhurst, A. R. and Glen Harrison, W.: Vertical nitrogen flux from the oceanic photic zone by diel migrant zooplankton and nekton, Deep-Sea Res. Pt. A, 35, 881–889, https://doi.org/10.1016/0198-0149(88)90065-9, 1988.

Longhurst, A. R. and Williams, R. G.: Carbon flux by seasonal vertical migrant cpoepods is a small number, J. Plankton Res., 14, 1495–1509, 1992.

Longhurst, A. R., Bedo, A. W., Harrison, W. G., Head, E. J. H., Horne, E. P., Irwin, B., and Morales, C. E.: NFLUX: a test of vertical nitrogen flux by diel migrant biota, Deep-Sea Res. Pt. A, 36, 1705–1719, https://doi.org/10.1016/0198-0149(89)90067-8, 1989.

Longhurst, A. R., Bedo, A. W., Harrison, W. G., Head, E. J. H., and Sameoto, D. D.: Vertical flux of respiratory carbon by oceanic diel migrant biota, Deep-Sea Res. Pt. A, 37, 685–694, https://doi.org/10.1016/0198-0149(90)90098-G, 1990.

Louis, J., Bressac, M., Pedrotti, M. L., and Guieu, C. Dissolved inorganic nitrogen and phosphorus dynamics in seawater following an artificial Saharan dust deposition event, Frontiers in Marine Science, 2, 27, https://doi.org/10.3389/fmars.2015.00027, 2015.

Luo, Y.-W., Doney, S. C., Anderson, L. A., Benavides, M., Berman-Frank, I., Bode, A., Bonnet, S., Boström, K. H., Böttjer, D., Capone, D. G., Carpenter, E. J., Chen, Y. L., Church, M. J., Dore, J. E., Falcón, L. I., Fernández, A., Foster, R. A., Furuya, K., Gómez, F., Gundersen, K., Hynes, A. M., Karl, D. M., Kitajima, S., Langlois, R. J., LaRoche, J., Letelier, R. M., Marañón, E., McGillicuddy Jr., D. J., Moisander, P. H., Moore, C. M., Mouriño-Carballido, B., Mulholland, M. R., Needoba, J. A., Orcutt, K. M., Poulton, A. J., Rahav, E., Raimbault, P., Rees, A. P., Riemann, L., Shiozaki, T., Subramaniam, A., Tyrrell, T., Turk-Kubo, K. A., Varela, M., Villareal, T. A., Webb, E. A., White, A. E., Wu, J., and Zehr, J. P.: Database of diazotrophs in global ocean: abundance, biomass and nitrogen fixation rates, Earth Syst. Sci. Data, 4, 47–73, https://doi.org/10.5194/essd-4-47-2012, 2012.

Mahaffey, C., Williams, R. G., Wolff, G. A., Mahowald, N. M., Anderson, W., and Woodward, M.: Biogeochemical signatures of nitrogen fixation in the eastern North Atlantic, Geophys. Res. Lett., 30, 33–36, https://doi.org/10.1029/2002GL016542, 2003.

Mahaffey, C., Michaels, A. F., and Capone, D. G.: The conundrum of marine N_2 fixation, Am. J. Sci., 305, 546–595, https://doi.org/10.2475/ajs.305.6-8.546, 2005.

Martínez-Pérez, C., Mohr, W., Löscher, C. R., Dekaezemacker, J., Littmann, S., Yilmaz, P., Lehnen, N., Fuchs, B. M., Lavik, G., Schmitz, R. A., LaRoche, J., and Kuypers, M. M. M.: The small unicellular diazotrophic symbiont, UCYN-A, is a key player in the marine nitrogen cycle, Nat. Microbiol., 1, 16163, https://doi.org/10.1038/nmicrobiol.2016.163, 2016.

Mohr, W., Großkopf, T., Wallace, D. W. R., and LaRoche, J.: Methodological underestimation of oceanic nitrogen fixation rates, PLoS One, 5, 1–7, https://doi.org/10.1371/journal.pone.0012583, 2010.

Moisander, P. H., Beinart, R. A., Voss, M., and Zehr, J. P.: Diversity and abundance of diazotrophic microorganisms in the South China Sea during intermonsoon, ISME J., 2, 954–967, https://doi.org/10.1038/ismej.2008.51, 2008.

Moisander, P. H., Beinart, R. A., Hewson, I., White, A. E., Johnson, K. S., Carlson, C. A., Montoya, J. P., and Zehr, J. P.: Unicellular Cyanobacterial Distributions Broaden the Oceanic N_2 Fixation Domain, Science, 327, 1512–1514, https://doi.org/10.1126/science.1185468, 2010.

Montoya, J. P., Voss, M., Kahler, P., and Capone, D. G.: A Simple , High-Precision , High-Sensitivity Tracer Assay for N_2 Fixation, Appl. Environ. Microbiol., 62, 986–993, 1996.

Montoya, J. P., Holl, C. M., Zehr, J. P., Hansen, A., Villareal, T. A., and Capone, D. G.: High rates of N_2 fixation by unicellular diazotrophs in the oligotrophic Pacific Ocean, Nature, 430, 1027–1031, https://doi.org/10.1038/nature02824, 2004.

Monroy, P., Hernández-García, E., Rossi, V., and López, C.: Modeling the dynamical sinking of biogenic particles in oceanic flow, Nonlin. Processes Geophys., 24, 293–305, https://doi.org/10.5194/npg-24-293-2017, 2017.

Moore, C. M., Mills, M. M., Arrigo, K. R., Berman-Frank, I., Bopp, L., Boyd, P. W., Galbraith, E. D., Geider, R. J., Guieu, C., Jaccard, S. L., Jickells, T. D., La Roche, J., Lenton, T. M., Mahowald, N. M., Marañón, E., Marinov, I., Moore, J. K., Nakatsuka, T., Oschlies, A., Saito, M. A., Thingstad, T. F., Tsuda, A., and Ulloa, O.: Processes and patterns of oceanic nutrient limitation, Nat. Geosci., 6, 701–710, https://doi.org/10.1038/ngeo1765, 2013.

Mourino-Carballido, B., Graña, R., Fernández, A., Bode, A., Varela, M., Domínguez, J., Escànez, J., de Armas, D., and Marañón, E.: Importance of N_2 fixation vs. nitrate eddy diffusion along a latitudinal transect in the Atlantic Ocean, Limnol. Oceanogr., 56, 999–1007, https://doi.org/10.4319/lo.2011.56.3.0999, 2011.

Moutin, T. and Bonnet, S.: OUTPACE, https://doi.org/10.17600/15000900, 2015.

Moutin, T. and Prieur, L.: Influence of anticyclonic eddies on the Biogeochemistry from the Oligotrophic to the Ultraoligotrophic Mediterranean (BOUM cruise), Biogeosciences, 9, 3827–3855, https://doi.org/10.5194/bg-9-3827-2012, 2012.

Moutin, T. and Raimbault, P.: Primary production, carbon export and nutrients availability in western and eastern Mediterranean Sea in early summer 1996 (MINOS cruise), J. Marine Syst., 33–34, 273–288, https://doi.org/10.1016/S0924-7963(02)00062-3, 2002.

Moutin, T., Van Den Broeck, N., Beker, B., Dupouy, C., Rimmelin, P., and Le Bouteiller, A.: Phosphate availability controls Trichodesmium spp. biomass in the SW Pacific Ocean, Mar. Ecol.-Prog. Ser., 297, 15–21, https://doi.org/10.3354/meps297015, 2005.

Moutin, T., Karl, D. M., Duhamel, S., Rimmelin, P., Raimbault, P., Van Mooy, B. A. S., and Claustre, H.: Phosphate availability and the ultimate control of new nitrogen input by nitrogen fixation in the tropical Pacific Ocean, Biogeosciences, 5, 95–109, https://doi.org/10.5194/bg-5-95-2008, 2008.

Moutin, T., Doglioli, A. M., de Verneil, A., and Bonnet, S.: Preface: The Oligotrophy to the UlTra-oligotrophy PACific Experiment (OUTPACE cruise, 18 February to 3 April 2015), Biogeosciences, 14, 3207–3220, https://doi.org/10.5194/bg-14-3207-2017, 2017.

Moutin, T., Wagener, T., Caffin, M., Fumenia, A., Gimenez, A., Baklouti, M., Bouruet-Aubertot, P., Pujo-Pay, M., Leblanc, K., Lefevre, D., Helias Nunige, S., Leblond, N., Grosso, O., and de Verneil, A.: Nutrient availability and the ultimate control of the biological carbon pump in the Western Tropical South Pacific Ocean, Biogeosciences Discuss., https://doi.org/10.5194/bg-2017-565, in review, 2018.

Nelson, D. M., Tréguer, P., Brzezinski, M. A., Leynaert, A., and Quéguiner, B.: Production and dissolution of biogenic silica in the ocean: Revised global estimates, comparison with regional data and relationship to biogenic sedimentation, Global Biogeochem. Cy., 9, 359–372, https://doi.org/10.1029/95GB01070, 1995.

Nodder, S. D. and Waite, A. M.: Is Southern Ocean organic carbon and biogenic silica export enhanced by iron-stimulated increases in biological production? Sediment trap results from SOIREE, Deep-Sea Res. Pt. II, 48, 2681–2701, https://doi.org/10.1016/S0967-0645(01)00014-5, 2001.

Olli, K., Wexels Riser, C., Wassmann, P., Ratkova, T., Arashkevich, E., and Pasternak, A.: Seasonal variation in vertical flux of biogenic matter in the marginal ice zone and the central Barents Sea, J. Marine Syst., 38, 189–204, https://doi.org/10.1016/S0924-7963(02)00177-X, 2002.

Painter, S. C., Patey, M. D., Forryan, A., and Torres-Valdés, S.: Evaluating the balance between vertical diffusive nitrate supply and nitrogen fixation with reference to nitrate uptake in the eastern subtropical North Atlantic Ocean, J. Geophys. Res.-Ocean., 118, 5732–5749, https://doi.org/10.1002/jgrc.20416, 2013.

Petrenko, A. A., Doglioli, A. M, Nencioli, F., Kersalé, M., Hu, Z., and d'Ovidio, F.: A review of the LATEX project: mesoscale to submesoscale processes in a coastal environment, Ocean Dynam., 67, 513–533, 2017.

Raimbault, P. and Garcia, N.: Evidence for efficient regenerated production and dinitrogen fixation in nitrogen-deficient waters of the South Pacific Ocean: impact on new and export production estimates, Biogeosciences, 5, 323–338, https://doi.org/10.5194/bg-5-323-2008, 2008

Reigstad, M., Wexels Riser, C., Wassmann, P., and Ratkova, T.: Vertical export of particulate organic carbon: Attenuation, composition and loss rates in the northern Barents Sea, Deep-Sea Res. Pt. II, 55, 2308–2319, https://doi.org/10.1016/j.dsr2.2008.05.007, 2008.

Rembauville, M., Blain, S., Armand, L., Quéguiner, B., and Salter, I.: Export fluxes in a naturally iron-fertilized area of the Southern Ocean – Part 2: Importance of diatom resting spores and faecal pellets for export, Biogeosciences, 12, 3171–3195, https://doi.org/10.5194/bg-12-3171-2015, 2015.

Rijkenberg, M. J. A., Langlois, R. J., Mills, M. M., Patey, M. D., Hill, P. G., Nielsdóttir, M. C., Compton, T. J., LaRoche, J., and Achterberg E. P.: Environmental forcing of nitrogen fixation in the Eastern Tropical and Sub-Tropical North Atlantic Ocean, PLoS ONE, 6, e28989, https://doi.org/10.1371/journal.pone.0028989, 2011.

Scharek, R., Tupas, L. M., and Karl, D. M.: Diatom fluxes to the deep sea in the oligotrophic North Pacific gyre at Station ALOHA, Mar. Ecol.-Prog. Ser., 182, 55–67, https://doi.org/10.3354/meps182055, 1999a.

Scharek, R., Latasa, M., Karl, D. M., and Bidigare, R. R.: Temporal variations in diatom abundance and downward vertical flux in the oligotrophic North Pacific gyre, Deep-Sea Res. Pt. I, 46, 1051–1075, https://doi.org/10.1016/S0967-0637(98)00102-2, 1999b.

Shiozaki, T., Kodama, T., and Furuya, K.: Large-scale impact of the island mass effect through nitrogen fixation in the western South Pacific Ocean, Geophys. Res. Lett., 41, 2907–2913, https://doi.org/10.1002/2014GL059835, 2014.

Shiozaki, T., Nagata, T., Ijichi, M., and Furuya, K.: Nitrogen fixation and the diazotroph community in the temperate coastal region of the northwestern North Pacific, Biogeosciences, 12, 4751–4764, https://doi.org/10.5194/bg-12-4751-2015, 2015.

Short, S. M., Jenkins, B. D., and Zehr, J. P.: The spatial and temporal distribution of two diazotrophic bacteria in the Chesapeake Bay, Appl. Environ. Microb., 70, 2186–2192, https://doi.org/10.1128/AEM.70.4.2186-2192.2004, 2004.

Spungin, D., Belkin, N., Foster, R., Stenegren, M., Caputo, A., Pujo-Pay, M., Leblond, N., Dupouy, C., Bonnet, S., and Berman-Frank, I.: Programmed cell death in diazotrophs and the fate of organic matter in the Western Tropical South Pacific Ocean during the OUTPACE cruise, Biogeosciences Discuss., https://doi.org/10.5194/bg-2018-3, in review, 2018.

Stenegren, M., Caputo, A., Berg, C., Bonnet, S., and Foster, R. A.: Distribution and drivers of symbiotic and free-living diazotrophic cyanobacteria in the western tropical South Pacific, Biogeosciences, 15, 1559–1578, https://doi.org/10.5194/bg-15-1559-2018, 2018.

Stukel, M. R., Ohman, M. D., Benitez-Nelson, C. R., and Landry, M. R.: Contributions of mesozooplankton to vertical carbon export in a coastal upwelling system, Mar. Ecol.-Prog. Ser., 491, 47–65, https://doi.org/10.3354/meps10453, 2013.

Stukel, M. R., Benitez-Nelson, C. R., Decima, M., Taylor, A. G., Buchwald, C., and Landry, M. R.: The biological pump in the Costa Rica Dome: An open-ocean upwelling system with high new production and low export, J. Plankton Res., 38, 348–365, https://doi.org/10.1093/plankt/fbv097, 2015.

Subramaniam, A., Yager, P. L., Carpenter, E. J., Mahaffey, C., Björkman, K. M., Cooley, S., Kustka, A. B., Montoya, J. P., Sanudo-Wilhelmy, S. A., Shipe, R., and Capone, D. G.: Amazon River enhances diazotrophy and carbon sequestration in the tropical North Atlantic Ocean, P. Natl. Acad. Sci. USA, 105, 10460–10465, https://doi.org/10.1073/pnas.0710279105, 2008.

Sun, J. and Liu, D.: Geometric models for calculating cell biovolume and surface area for phytoplankton, J. Plankton Res., 25, 1331–1346, https://doi.org/10.1093/plankt/fbg096, 2003.

Thomalla, S., Turnewitsch, R., Lucas, M., and Poulton, A.: Particulate organic carbon export from the North and South Atlantic gyres: The $^{234}Th/^{238}U$ disequilibrium approach, Deep-Sea Res. Pt. II, 53, 1629–1648, https://doi.org/10.1016/j.dsr2.2006.05.018, 2006.

Toggweiler, J. R.: Is the downward dissolved organic matter (DOM) flux important in carbon transport?, Productivity in the Ocean: Present and Past, edited by: Berger, W. H., Smetacek, V. S., and Wefer, G., Wiley, New York, 65–83, 1989.

Van Wambeke, F., Gimenez, A., Duhamel, S., Dupouy, C., Lefevre, D., Pujo-Pay, M., and Moutin, T.: Dynamics of phytoplankton and heterotrophic bacterioplankton in the western tropical South Pacific Ocean along a gradient of diversity and activity of diazotrophs, Biogeosciences Discuss., https://doi.org/10.5194/bg-2017-556, in review, 2018.

Verity, P. G., Robertson, C. Y., Tronzo, C. R., Andrews, M. G., Nelson, J. R., and Sieracki, M. E.: Relationships between cell volume and the carbon and nitrogen content of marine photosynthetic nanoplankton, Limnol. Oceanogr., 37, 1434–1446, https://doi.org/10.4319/lo.1992.37.7.1434, 1992.

Villareal, T. A.: Division cycles in the nitrogen-fixing rhizosolenia (Baciliariophyceae)-richelia (nostocaceae) symbiosis, Br. Phycol. J., 24, 357–365, https://doi.org/10.1080/00071618900650371, 1989.

Vinogradov, M. E.: Vertical distribution of the oceanic zooplankton, Moscow: Nauka, 318 pp., 1968 (in Russian), Engl. transl. by Israel Progr. Scient. Transl., Jerusalem, 339 pp., 1970.

Vong, R. J., Vong, I. J., Vickers, D., and Covert, D. S.: Size-dependent aerosol deposition velocities during BEARPEX'07, Atmos. Chem. Phys., 10, 5749–5758, https://doi.org/10.5194/acp-10-5749-2010, 2010.

Walsby, A. E.: The gas vesicles and buoyancy of Trichodesmium, in: Marine pelagic cyanobacteria: Trichodesmium and other diazotrophs, Springer, the Netherlands, 141–161, 1992.

Wassman, F.: Relationships between primary and export production in the boreal coastal zone of the North Atlantic, Limnol. Oceanogr., 35, 464–471, 1990.

Weiss, R. F.: The solubility of nitrogen, oxygen and argon in water and seawater, Deep-Sea Res., 17, 721–735, 1970.

Wexels Riser, C., Wassmann, P., Reigstad, M. and Seuthe, L.: Vertical flux regulation by zooplankton in the northern Barents Sea during Arctic spring, Deep-Sea Res. Pt. II, 55, 2320–2329, https://doi.org/10.1016/j.dsr2.2008.05.006, 2008.

White, A. E., Foster, R. A., Benitez-Nelson, C. R., Masqué, P., Verdeny, E., Popp, B. N., Arthur, K. E., and Prahl, F. G.: Nitrogen fixation in the Gulf of California and the Eastern Tropical North Pacific, Prog. Oceanogr., 109, 1–17, https://doi.org/10.1016/j.pocean.2012.09.002, 2012.

Zhang, X. and Dam, H. G.: Downward export of carbon by die1 migrant mesozooplankton in the central equatorial Pacific, 44, 2191–2202, 1998.

3.4 Conclusion et perspectives

Cette étude, réalisée grâce à la mise en œuvre d'une stratégie lagrangienne nous a permis de réaliser des bilans d'azote au sein de trois masses d'eau représentatives de l'océan Pacifique tropical sud-ouest en période estivale. Ainsi, nous avons montré que la fixation de N_2 est la source majeur d'azote nouveau dans la couche euphotique et qu'elle contribue à une part importante de la production primaire, présentant cependant des nuances d'intensités entre les eaux oligotrophes des archipels Mélanésiens (∼13-18 % de la production primaire) et les eaux ultra-oligotrophes de la gyre du Pacifique sud (∼3 % de la production primaire). A chacune des trois stations, la fixation de N_2 compte pour la quasi intégralité de la production nouvelle puisqu'elle représente plus de 90 % de l'apport d'azote nouveau.

Le couplage qui réside entre les forts taux de fixation de N_2 et les valeurs élevées d'export brut de carbone et d'azote, ainsi que les forts *e*-ratio mesurés dans la région étudiée, suggèrent que la fixation de N_2 joue un rôle important sur l'export de matière particulaire pendant la saison estivale. L'export brut de carbone observé à la station LD A (∼ 0,5-2,5 mmol C m^2 d^{-1}) est de l'ordre de grandeur de l'export qui peut être mesuré dans certaines régions de l'océan Austral (∼ 0,1-1,6 mmol C m^2 d^{-1}, Rembauville et al., 2015), considéré comme un écosystème à fort potentiel d'export de carbone. Cependant, l'océan Austral peut présenter des flux d'export un ordre de grandeur supérieur aux flux que nous avons mesurés (e.g. Jouandet et al., 2011; Savoye et al., 2008). Nos observations suggèrent que les régions oligotrophes, représentant une part importante de l'océan, pourraient avoir une capacité d'export de carbone plus importante qu'initialement considérée, notamment dans les régions fortement impactées par la diazotrophie. Cependant, cette étude donne une image instantanée de ce qui se passe durant la campagne de 45 jours effectuée en été austral, et l'extrapolation quantitative de ces résultats à l'échelle saisonnière ou annuelle reste délicate.

Afin de s'inscrire dans la continuité de ce travail pour étudier le couplage entre la fixation de N_2 et l'export dans le Pacifique tropical sud-ouest, il serait intéressant et nécessaire d'avoir une série temporelle annuelle. Il serait ainsi nécessaire d'installer une ligne de mouillage munie de piège à particules pendant un cycle annuel pour appréhender la variabilité saisonnière des processus, comme c'est la cas à la station HOT où l'influence de la diazotrophie sur l'export a été étudiée sur une série temporelle de 9 ans (Böttjer et al., 2017). Il serait intéressant de coupler ces mesures d'export avec des mesures *in-situ* régulières de fixation de N_2 et d'abondances de diazotrophes pouvant être réalisées par des automates (Bombar et al., 2015; Robidart et al., 2014) ainsi que des observations par satellites. Les données de pièges montrent leurs limites dans cette étude, limite essentiellement liée à la prise en compte du zooplancton. Les protocoles JGOFS, qui ont cadré les recherches océanographiques dans les années 1990-2000, prônent de retirer le zooplancton des pièges. En effet, le zooplancton est depuis longtemps considéré comme une nuisance

pour quantifier le flux particulaire, car celui-ci entre activement dans les pièges pour se nourrir de la matière particulaire qui y est récoltée. En rentrant dans les godets de collecte qui sont empoisonnés, les organismes zooplanctoniques meurent et y restent piégés. Cependant, les organismes zooplanctoniques morts chutent par gravité (sédimentation des carcasses), et contribuent de cette manière à l'export de carbone et d'azote (Steinberg and Landry, 2017). Ils peuvent ainsi représenter une fraction du flux particulaire que l'on cherche à mesurer avec les pièges. Dans notre étude il n'est pas possible de distinguer les organismes qui sont arrivés dans les godets des pièges pour se nourrir de ceux qui ont sédimenté après leur mort. Une alternative à ce problème serait de coupler deux pièges à particules, l'un empoisonné et l'autre non. Dans le piège empoisonné nous récupèrerions tous les organismes zooplanctoniques, et dans celui non empoisonné (ne permettant pas de quantifier correctement l'export de matière particulaire) nous récupèrerions les organismes zooplanctoniques morts par sédimentation des carcasses.

Globalement dans cette étude, le lien entre la fixation de N_2 et l'export, qu'il soit direct ou indirect, semble être évident. Les *e*-ratio mesurés (montant jusqu'à 9,8 %) sont au-dessus des valeurs communément trouvées dans les régions oligotrophes de l'océan, suggérant une forte capacité d'export dans de ce hot spot de diazotrophie. L'étude de Knapp et al. (2018) basée sur les bilans $\delta^{15}N$, réalisés en parallèle dans les pièges à particules, montrent que 50 % à 80 % de l'export de matière particulaire était soutenue par la diazotrophie dans les archipels Mélanésiens, confirmant ainsi que la production exportée dans cette région est soutenue par la diazotrophie. Cependant, les bilans $\delta^{15}N$ ne permettent pas de déconvoluer l'export direct de l'export indirect. La quantification des diazotrophes en qPCR réalisée dans les pièges à particules nous ont permis d'observer que globalement peu de diazotrophes sont retrouvés dans les pièges comparativement aux fortes abondances mesurées dans la colonne d'eau. Ces résultats suggèrent ainsi un faible export direct, probablement due à la dominance des *Trichodesmium* qui sont connus pour être des particules flottantes grâce à leurs vacuoles et sont rarement retrouvés dans les pièges.

Dans ce chapitre, nous avons vu que dans le Pacifique tropical sud-ouest, la fixation de N_2 représente la source majeure d'azote nouveau dans la couche euphotique, aussi bien dans les archipels Mélanésiens qu'à l'ouest de la gyre du Pacifique sud. La fixation de N_2 contribue à une part importante de la production primaire, soutient la quasi intégralité de la production nouvelle et soutient l'export de matière particulaire. Dans cette région dépourvue d'azote disponible, la pompe biologique est amorcée par la fixation de N_2, appelée « N_2-primed prokaryotic carbon pump » (Karl et al., 2003). Cependant, l'export direct de diazotrophes représente une faible proportion de l'export total. Ainsi l'azote (et le carbone associé) issu de la diazotrophie est indirectement exporté, après relargage et transfert vers les maillons supérieurs de la chaine trophique. L'étude du transfert du N_2 fixé par les diazotrophes vers les organismes non-diazotrophes est le sujet du chapitre suivant.

Chapitre 4

Devenir de l'azote fixé et transfert dans la chaine trophique marine

Sommaire

4.1 Avant propos

Dans le chapitre précédent, nous avons vu que le N_2 fixé par les organismes diazotrophes pouvait être directement exporté vers les couches plus profondes de l'océan par sédimentation. Nous nous intéressons ici au devenir de ce N_2 fixé avant son potentiel export, c'est à dire son transfert vers les communautés planctoniques non-diazotrophes (bactériennes, phytoplanctoniques et zooplanctoniques).

L'idée que les diazotrophes puissent relarguer une part de l'azote qu'ils fixent date des années 1970. Dans les milieux oligotrophes limités en azote où les diazotrophes sont présents, ce processus peut avoir des répercussions sur les organismes planctoniques environnants, sur la chaine trophique marine et sur les cycles biogeochimiques associés. Des études menées à la fois en cultures (Benavides et al., 2013; Berthelot et al., 2015a; Mulholland et al., 2004a; Mulholland and Bernhardt, 2005) et sur le terrain (Berthelot et al., 2017; Konno et al., 2010; Mulholland et al., 2004b, 2006) ont montré que ces organismes relarguent dans le compartiment dissous entre 10 et 80 % ($\sim$ 50 % en moyenne) de la fixation de N_2 totale.
Cependant, le transfert de cet azote relargué vers les organismes non-diazotrophes a jusqu'à aujourd'hui été très peu étudié. Les premières observations faites dans l'océan Indien (Devassy et al., 1979) ont montré une augmentation de l'abondance en diatomées à la suite de déclin de l'efflorescence de *Trichodesmium*, suivi d'une augmentation de l'abondance de dinoflagellés, d'algues vertes et finalement de copépodes. Plus récemment, d'autres études dont celle présentée dans la chapitre précédent (Caffin et al., 2018), ont montré que l'azote fixé par les diazotrophes pouvait soutenir la production primaire et d'autres ont mis en évidence des efflorescences d'organismes non-diazotrophes suite à des efflorescences de diazorophes (Chen et al., 2011; Devassy et al., 1978, 1979; Mulholland et al., 2004b). Par exemple à la suite d'une efflorescence de *Trichodesmium*, Devassy et al. (1979) ont observé une efflorescence de diatomée dans l'océan Indien. De manière analogue, des efflorescences de dinoflagellés *Karenia brevis* sont régulièrement observées à la suite des efflorescences de diazotrophes dans le golf du Mexique (Lenes and Heil, 2010; Mulholland et al., 2006). Cependant, les voies de transfert de l'azote dérivé de la diazotrophie vers les organismes non-diazotrophes restent peu connues. Qui des communautés autotrophes ou hétérotrophes, des cellules de grande taille ou de petite taille bénéficie le plus de cet azote nouveau ? Grâce au développement de nouvelles méthodes permettant de tracer et de quantifier spécifiquement le transfert de l'azote fixé par les diazotrophes vers les différents groupes planctoniques (Bonnet et al., 2016a), Berthelot et al. (2016); Bonnet et al. (2016b) ont montré que le transfert d'azote fixé par les diazotrophes vers les organismes non-diazotrophes était de l'ordre de 10 % et que les principaux bénéficiaires étaient les diatomées puis les bactéries hétérotrophes plutôt que le picophytoplancton. Dans certains cas de leurs études, ces auteurs ont montré que les *Trichodesmium* étaient en phase de mort programmée (Spungin et al., 2016), pouvant conduire à un relargage très impor-

tant de NH_4^+ dans le milieu (4 μmol L^{-1}, Bonnet et al., 2016a). Les diatomées étant plus compétitives que le picoplancton dans le milieu riche en nutriments (Falkowski and Knoll, 2011), cela explique probablement leur succès dans ces expériences. Aujourd'hui, les voies de transfert du N_2 fixé par les diazotrophes n'ont jamais été caractérisées en milieu hauturier, qui représente pourtant la majeure partie de l'océan mondial. Les différences qui existent entre les régions côtières et hauturières en termes de concentrations en azote disponible, de niveau d'oligotrophie et de structure des communautés planctoniques laissent à penser que cela peut induire des différences sur le transfert de l'azote fixé, notamment sur les principaux bénéficiaires cet azote fixé.

Concernant le zooplancton, nous avons vu dans le chapitre introductif que les faibles signatures isotopiques naturelles $\delta^{15}N$ mesurées dans le zooplancton (Aberle et al., 2010; Hunt et al., 2016; Landrum et al., 2011; Loick-Wilde et al., 2012; Mompeán et al., 2013; Montoya et al., 2002; Sommer et al., 2006; Wannicke et al., 2013) témoignent d'un transfert de l'azote issu de la diazotrophie vers le zooplancton dans les régions à forts taux de fixation de N_2. De plus, la récente étude de Hunt et al. (2016) basée sur le marquage isotopique au $^{15}N_2$ a montré que la fixation d'azote pouvait soutenir de façon significative la production zooplanctonique ($\sim$ 30-35 %). De plus, ces auteurs ont montré que l'azote fixé était plus efficacement transféré vers le zooplancton lorsque les UCYN dominent la communauté diazotrophe que lorsque ce sont les *Trichodesmium* et les DDA qui dominent, indiquant que le transfert vers le zooplancton est fortement lié à la structure des communautés de diazotrophes. Aujourd'hui d'autres études sont nécessaires pour confirmer l'étude de Hunt et al. (2016) et pour quantifier le transfert d'azote fixé vers le zooplancton en milieu hauturier.

En utilisant un couplage innovant, entre la nanoSIMS, le tri cellulaire et le marquage isotopique au $^{15}N_2$, nous présentons dans ce chapitre les voies de transfert de l'azote fixé vers les communautés planctoniques non-diazotrophes environnantes en milieu hauturier. Nous avons aussi quantifié le transfert de l'azote fixé vers le zooplancton à l'aide d'une méthode basée sur le marquage isotopique au $^{15}N_2$ d'assemblages planctoniques naturels consommés par des copépodes. Cette étude a été menée aux trois stations processus de la campagne océanographique OUTPACE déjà présentée dans le chapitre précédent, dans des régions biogéochimiquement contrastées de l'océan Pacifique tropical sud-ouest, en particulier en termes de diversité et d'activité des organismes diazotrophes.

4.2 Résumé

La fixation de N_2 représente la source majoritaire d'azote nouveau à l'océan, avant les apports fluviaux et atmosphériques. Cependant, le devenir de l'azote fixé dans la chaine trophique marine est aujourd'hui peu compris. Dans cette étude nous avons utilisé la nanoSIMS couplée au marquage isotopique $^{15}N_2$ et au tri cellulaire par cytométrie en flux afin de suivre le transfert de l'azote fixé vers les organismes planctoniques, lorsque la communauté des diazotrophes était dominée soit par *Trichodesmium*, soit par les UCYN-B. Après 48 h, ∼20-40 % du N_2 fixé pendant l'expérience a été relargué dans la fraction dissoute lorsque *Trichodesmium* dominait, alors que le relargage d'azote fixé dans la fraction dissoute n'était pas quantifiable lorsque UCYN-B dominait. Environ 7-15 % de l'azote total fixé (fixation de N_2 nette + relargage) a été transféré vers le plancton non-diazotrophe après 48 h, avec une efficacité de transfert plus élevée (15±3 %) lorsque les UCYN-B dominaient que lorsque *Trichodesmium* dominait (9±3 %). Les pico-cyanobactéries *Synechococcus* et *Prochlorococcus* étaient les principales bénéficiaires du transfert d'azote fixé (∼65-70 %), suivies des bactéries hétérotrophes (∼23-34 %). Le transfert d'azote fixé dans les bactéries était plus élevé (∼34±7 %) lors des expériences dans lesquelles les UCYN-B dominaient que lors des expériences dans lesquelles *Trichodesmium* dominait (∼24±5 %). Concernant les niveaux trophiques supérieurs, le transfert d'azote fixé vers l'espèce de zooplancton dominante était moins efficace (∼5-9 % du transfert) lorsque la communauté diazotrophe était dominée par *Trichodesmium* que lorsqu'elle était dominée par les UCYN-B (∼28±13 % du transfert). A notre connaissance, cette étude fournit pour la première fois une quantification du relargage et du transfert d'azote fixé vers les communautés phytoplanctoniques, bactériennes et zooplanctoniques en milieu hauturier. Bien que les UCYN-B fixent le N_2 à des taux plus faibles que les *Trichodesmium*, l'azote fixé par les UCYN-B semble être plus disponible et transféré plus efficacement dans la chaine trophique marine que l'azote fixé provenant de *Trichodesmium*.

4.3 Article # 4 : Transfert de l'azote fixé vers la chaine trophique planctonique dans des environnements contrastés en terme de diversité et d'activité des organismes diazotrophes dans le Pacifique tropical sud-ouest. *Caffin et al., 2018*

Transfer of diazotroph-derived nitrogen to the planktonic food web across gradients of N_2 fixation activity and diversity in the Western Tropical South Pacific

Mathieu Caffin[1], Hugo Berthelot[1 2], Veronique Cornet-Bartaux[1], Aude Barani[1] and Sophie Bonnet[3]

[1]Aix Marseille Université, CNRS/INSU, Université de Toulon, IRD, Mediterranean Institute of Oceanography (MIO) UM110, 13288, Marseille, France
[2]Laboratoire des sciences de l'environnement marin, IUEM, Université de Brest-UMR 6539 CNRS/UBO/IRD/Ifremer, Plouzané, France
[3]Aix Marseille Université, CNRS/INSU, Université de Toulon, IRD, OSU Pythéas, Mediterranean Institute of Oceanography (MIO), UM 110, 98848, Nouméa, New Caledonia

Publié dans *Biogeosciences* en Juin 2018

Biogeosciences, 15, 3795–3810, 2018
https://doi.org/10.5194/bg-15-3795-2018

Biogeosciences Open Access EGU

Transfer of diazotroph-derived nitrogen to the planktonic food web across gradients of N_2 fixation activity and diversity in the western tropical South Pacific Ocean

Mathieu Caffin[1], **Hugo Berthelot**[1,2], **Véronique Cornet-Barthaux**[1], **Aude Barani**[1], **and Sophie Bonnet**[1,3]

[1]Aix Marseille Univ., Université de Toulon, CNRS, IRD, MIO UM110, 13288, Marseille, France
[2]Laboratoire des sciences de l'environnement marin, IUEM, Université de Brest-UMR6539 CNRS/UBO/IRD/Ifremer, Plouzané, France
[3]Aix Marseille Univ., Université de Toulon, CNRS, IRD, MIO UM110, 98800, Nouméa, New Caledonia

Correspondence: Mathieu Caffin (mathieu.caffin@mio.osupytheas.fr)

Received: 31 December 2017 – Discussion started: 5 January 2018
Revised: 17 May 2018 – Accepted: 29 May 2018 – Published: 21 June 2018

Abstract. Biological dinitrogen (N_2) fixation provides the major source of new nitrogen (N) to the open ocean, contributing more than atmospheric deposition and riverine inputs to the N supply. Yet the fate of the diazotroph-derived N (DDN) in the planktonic food web is poorly understood. The main goals of this study were (i) to quantify how much of DDN is released to the dissolved pool during N_2 fixation and how much is transferred to bacteria, phytoplankton and zooplankton, and (ii) to compare the DDN release and transfer efficiencies under contrasting N_2 fixation activity and diversity in the oligotrophic waters of the western tropical South Pacific (WTSP) Ocean. We used nanometre-scale secondary ion mass spectrometry (nanoSIMS) coupled with $^{15}N_2$ isotopic labelling and flow cytometry cell sorting to track the DDN transfer to plankton, in regions where the diazotroph community was dominated by either *Trichodesmium* or by UCYN-B. After 48 h, ∼ 20–40 % of the N_2 fixed during the experiment was released to the dissolved pool when *Trichodesmium* dominated, while the DDN release was not quantifiable when UCYN-B dominated; ∼ 7–15 % of the total fixed N (net N_2 fixation + release) was transferred to non-diazotrophic plankton within 48 h, with higher transfer efficiencies (15 ± 3 %) when UCYN-B dominated as compared to when *Trichodesmium* dominated (9 ± 3 %). The pico-cyanobacteria *Synechococcus* and *Prochlorococcus* were the primary beneficiaries of the DDN transferred (∼ 65–70 %), followed by heterotrophic bacteria (∼ 23–34 %). The DDN transfer in bacteria was higher (34 ± 7 %) in the UCYN-B-dominating experiment compared to the *Trichodesmium*-dominating experiments (24 ± 5 %). Regarding higher trophic levels, the DDN transfer to the dominant zooplankton species was less efficient when the diazotroph community was dominated by *Trichodesmium* (∼ 5–9 % of the DDN transfer) than when it was dominated by UCYN-B (∼ 28 ± 13 % of the DDN transfer). To our knowledge, this study provides the first quantification of DDN release and transfer to phytoplankton, bacteria and zooplankton communities in open ocean waters. It reveals that despite UCYN-B fix N_2 at lower rates compared to *Trichodesmium* in the WTSP, the DDN from UCYN-B is much more available and efficiently transferred to the planktonic food web than the DDN originating from *Trichodesmium*.

1 Introduction

Nitrogen (N) is one of the basic building blocks of life, though much of the global ocean surface (∼ 70 %) is oligotrophic and characterized by low N availability, which limits primary productivity and phytoplankton growth (Falkowski, 1997; Moore et al., 2013). In these N-depleted areas of the tropical and subtropical ocean, biological dinitrogen (N_2) fixation (the reduction of atmospheric N_2 into bioavailable ammonia) sustains the major part of new production and organic matter export (Bonnet et al., 2009; Caffin et al., 2018; Capone et al., 2005; Karl et al., 2012). At the global scale, N_2 fixation is the major source of new N

Published by Copernicus Publications on behalf of the European Geosciences Union.

to the ocean, before atmospheric deposition and riverine inputs (100–150 Tg N yr^{-1}: Duce et al., 2008; Gruber, 2008). N_2 fixation is performed by prokaryotic organisms termed diazotrophs, which include the non-heterocystous filamentous cyanobacterium *Trichodesmium* (Capone et al., 1997; Carpenter, 1983), heterocystous cyanobacteria living in symbiosis with diatoms (or diatom–diazotroph associations, termed DDAs; Villareal, 1994), unicellular cyanobacteria termed UCYN (subdivided into groups A, B and C based on the nifH gene sequence, (Zehr et al., 1998, 2008; Zehr and Turner, 2001), diverse non-cyanobacterial bacteria (Bombar et al., 2015; Moisander et al., 2014; Riemann et al., 2010), and archaea (Loescher et al., 2014). Although considerable efforts have been made over the past decades to quantify N_2 fixation, identify the major players, and assess their biogeographical distribution in relation to environmental drivers, the fate of new N provided by N_2 fixation in the ocean and its role in the planktonic food web structure and large-scale biogeochemical fluxes are still poorly understood.

Early studies have reported high dissolved organic N (DON) and ammonia (NH_4^+) concentrations during and following *Trichodesmium* blooms in the Indian Ocean (Devassy et al., 1978, 1979; Glibert and O'Neil, 1999), suggesting that *Trichodesmium* release part of the recently fixed N_2 (hereafter referred to as diazotroph-derived N, DDN) to the dissolved pool, which could subsequently be consumed by the surrounding plankton communities. The first direct release measurements were performed in the early 1990s and showed that *Trichodesmium* colonies isolated from the tropical Atlantic Ocean release $\sim 50\,\%$ of the recently fixed N_2 (Glibert and Bronk, 1994). Accumulations of DON and NH_4^+ have subsequently been confirmed near *Trichodesmium* blooms in the Pacific (Karl et al., 1992, 1997) and Atlantic (Lenes et al., 2001) oceans, although not systematically (Bonnet et al., 2016a; Hansell and Carlson, 2001), and in senescent *Trichodesmium* cultures (Mulholland and Capone, 2000), possibly related to the *Trichodesmium* programmed cell death (PCD, Berman-Frank et al., 2004). This DDN release has been attributed (i) to endogenous processes such as the dissipation of excess electrons linked to an excess of light (Wannicke et al., 2009) or to a means for the filamentous diazotrophs to transfer fixed N from N_2-fixing cells to vegetative cells (Mulholland and Capone, 2000) and (ii) to exogenous processes such as viral lysis (Hewson et al., 2004; Ohki, 1999) or "sloppy feeding" by copepods (O'Neil, 1999).

Numerous studies performed in culture (Karl et al., 1992, 1997; Hutchins et al., 2007) and in the field (Benavides et al., 2013b; Konno et al., 2010; Mulholland and Bernhardt, 2005) focused on quantifying this release, and most of them were performed on *Trichodesmium* and were based on the difference between the measurement of gross N_2 fixation (through the acetylene reduction method, Capone, 1993) and net N_2 fixation rates (through the $^{15}N_2$ isotope labelling method, Montoya et al., 1996) (Mulholland et al., 2004a). It was thus shown that the DDN released to the dissolved pool averages $\sim 50\,\%$ (10 to 80 %) of the total N_2 fixation. The estimates based on this approach were then questioned since the discovery of the methodological underestimation of net $^{15}N_2$ rates when the $^{15}N_2$ tracer is injected as a bubble in the incubation bottles (Mohr et al., 2010), leading to a potential overestimation of the DDN release. An alternative approach based on the direct measurement of the ^{15}N enrichment of both the particulate and dissolved pools (Glibert and Bronk, 1994; Slawyk and Raimbault, 1995) after incubation with $^{15}N_2$ presents the advantage of providing a ratio of particulate N_2 fixation vs. DDN release, without being affected by potential underestimation issues. The studies based on this approach reveal that the proportion of DDN released to the dissolved pool ranges from 10 to $> 80\,\%$ of total N_2 fixation measured in the field (Benavides et al., 2013b; Berthelot et al., 2017; Glibert and Bronk, 1994; Konno et al., 2010). The release appears to be higher when *Trichodesmium* dominates the diazotroph community (Berthelot et al., 2017; Bonnet et al., 2016a; Glibert and Bronk, 1994) than when UCYN dominate (Benavides et al., 2013b; Bonnet et al., 2016b). The DDN release is generally much lower ($< 5\,\%$) in monospecific cultures (Benavides et al., 2013a; Berthelot et al., 2015) than in field experiments, suggesting that external factors such as sloppy feeding and viral lysis have a strong influence on the DDN release by diazotrophs in the field.

The DDN released in the surface ocean is potentially available for surrounding planktonic communities, but its fate in the planktonic food web has been poorly quantified, mainly due to methodological locks. Devassy et al. (1979), who reported high DON and NH_4^+ concentrations near *Trichodesmium* blooms, were also the first to observe that during the decline of the *Trichodesmium* blooms, diatom abundances increased, followed by a succession of cladocerans, dinoflagellates, green algae and finally copepods. In the tropical Atlantic Ocean, high abundances of non-diazotrophic phytoplankton have also been observed following *Trichodesmium* blooms (Mulholland et al., 2004b), and more recently, Chen et al. (2011) showed a positive correlation between abundances of *Trichodesmium* and diatoms in the Kuroshio. These studies suggest a link between diazotroph blooms and non-diazotrophic organisms. Studies based on size fractionation carried out during a *Trichodesmium* bloom incubated in the presence of $^{15}N_2$ report that $\sim 10\,\%$ of the fixed N_2 by *Trichodesmium* (recovered in the size fraction $> 30\,\mu m$) was rapidly transferred to non-diazotrophic organisms (recovered in the $< 30\,\mu m$ fraction; Bryceson and Fay, 1981). Using similar methods, other studies suggested that during *Trichodesmium* blooms (Mulholland et al., 2004b; Garcia et al., 2007) and *Nodularia* and *Aphanizomenon* blooms (Ohlendieck et al., 2000), 5 to 10 % of the DDN is transferred to the picoplankton compartment. However, the methods based on size fractionation do not discriminate the DDN transfer towards the non-diazotroph picoplankton to the potentially active N_2 fixation within pi-

coplankton, in particular the UCYN-A, one of the most abundant diazotrophs in our ocean (Luo et al., 2012). This method therefore potentially overestimates the DDN transfer and is not applicable to study the DDN transfer associated with UCYN. Moreover, it is not possible with size fractionation methods to determine which populations (e.g. autotrophic vs. heterotrophic plankton, small vs. large plankton) have benefited the most from this source of new N. The recent use of high-resolution nanometre-scale secondary ion mass spectrometry (nanoSIMS) coupled with $^{15}N_2$ isotopic labelling and flow cytometry cell sorting (Bonnet et al., 2016a, b; Berthelot et al., 2016) has proven its efficiency in the quantification of the DDN transfer to specific groups of phytoplankton and bacteria. Applying this method during *Trichodesmium* blooms in the coastal western tropical South Pacific (WTSP), Bonnet et al. (2016a) revealed that after 48 h 13 ± 2 to 48 ± 5 % of the fixed N_2 was released to the dissolved pool and 6 ± 1 to 8 ± 2 % of this DDN was transferred to non-diazotrophic plankton, mainly diatoms (45 ± 4 to 61 ± 38 %) and bacteria (22 ± 27 to 38 ± 12 %). A mesocosm experiment performed in the New Caledonian lagoon during a UCYN-C bloom (Bonnet et al., 2016b) revealed that after 48 h 16 ± 6 % of the fixed N_2 was released to the dissolved pool and 21 ± 4 % of this DDN was transferred to non-diazotrophic plankton, mainly picoplankton (18 ± 4 %) and diatoms (3 ± 2 %). Finally, a comparative study between *Trichodesmium* vs. UCYN blooms simulated thanks to culture isolates (Berthelot et al., 2016) revealed that the DDN transfer to non-diazotrophic plankton is twice as high with *Trichodesmium* as with UCYN. The differences of DDN release and transfer rates observed between the different field experiments and the different diazotrophs suggest that these processes strongly depend on the physiological state of diazotrophs and the environment. However, the transfer of DDN to different groups of plankton from different diazotrophs (*Trichodesmium* vs. UCYN) in the open ocean, where most global marine N_2 fixation takes place, has never been investigated.

Regarding higher trophic levels, the low ^{15}N isotopic signature ($\delta^{15}N$) of zooplankton reveals that N_2 fixation can significantly contribute to zooplankton N requirements in high N_2 fixation areas (Aberle et al., 2010; Landrum et al., 2011; Loick-Wilde et al., 2012; Mompeán et al., 2013; Montoya et al., 2002; Sommer et al., 2006; Wannicke et al., 2013; Hunt et al., 2016). Few studies report active grazing of *Trichodesmium* by some specific copepods (*Micro-* and *Macrosetella* sp., O'Neil et al., 1996; O'Neil and Roman, 1992). However, *Trichodesmium* has been shown to be toxic for most of the grazers (Guo and Tester, 1994; Hawser et al., 1992; Hawser and Codd, 1992), and the low $\delta^{15}N$ signature found in zooplankton (indicative of DDN consumption) where *Trichodesmium* thrive most likely originates from indirect transfer mediated by recycling processes (Capone et al., 1994; Capone and Montoya, 2001; Letelier and Karl, 1996) rather than from direct grazing. A recent study based on $^{15}N_2$ labelling in the coastal WTSP (Hunt et al., 2016) reveals that the DDN is less efficiently transferred to zooplankton when *Trichodesmium* and DDA dominate the diazotroph community than when UCYN-C dominate, suggesting that the DDN transfer efficiency to zooplankton strongly depends on the diazotroph involved in the N_2 fixation. To our knowledge, this has never been investigated so far in the open ocean.

The WTSP Ocean has recently been identified as a hotspot of N_2 fixation (Bonnet et al., 2017) and is characterized by trophic and N_2 fixation gradients (Moutin et al., 2017), with oligotrophic waters characterized by high N_2 fixation rates (631 ± 286 µmol N m^{-2} d^{-1}) mainly associated with *Trichodesmium* in the western part, and ultra-oligotrophic waters characterized by low N_2 fixation rates (85 ± 79 µmol N m^{-2} d^{-1}) mainly associated with UCYN in the eastern part (Bonnet et al., 2018; Stenegren et al., 2018). We performed a series of experiments under contrasting situations (when either *Trichodesmium* or UCYN was dominating the diazotroph community) to study the fate of DDN in the planktonic food web, with the following specific goals: (1) quantify the proportion of DDN released to the dissolved pool relative to total N_2 fixation, (2) quantify the DDN transfer to the non-diazotrophic phytoplankton and bacteria, and (3) quantify the DDN transfer to zooplankton.

2 Material and methods

2.1 Experimental set-up for DDN transfer experiments in phytoplankton and heterotrophic bacteria

This study was carried out during the OUTPACE (Oligotrophic to UlTra oligotrophic PACific Experiment) cruise (https://doi.org/10.17600/15000900), which took place in February–March 2015 (austral summer) onboard R/V *L'Atalante*. Samples were collected along a ~4000 km west-to-east zonal transect along ~19° S starting in New Caledonia and ending in French Polynesia, crossing Melanesian archipelago waters (hereafter referred to as MA waters) around New Caledonia, Vanuatu, and Fiji up to Tonga and South Pacific Gyre waters located at the western boundary of the South Pacific Gyre (hereafter referred to as GY waters) (see Moutin et al., 2017, for details). Three experiments are reported here (hereafter named E1, E2 and E3). Two were performed at stations located in MA waters: station LD A, 19°12.8′ S–164°41.3′ E, and station LD B, 18°14.4′ S–170°51.5′ W, where *Trichodesmium* accounted for 95 and 100 % of the total diazotroph community quantified by quantitative PCR (Stenegren et al., 2018). The third experiment was performed in GY waters: station LD C, 18°25.2′ S–165°56.4′ W, where UCYN accounted for 82 % of the total diazotroph community (Stenegren et al., 2018).

The experiments were designed according to Bonnet et al. (2016a, b) and Berthelot et al. (2016). For experiments E1 and E2, seawater was collected by the surface underway pumping system at 6 m in depth. For E3, seawater was collected at 55 m in depth using Niskin bottles mounted on a CTD rosette. For all experiments, seawater was collected into eight HCl-washed-sample rinsed (three times) 4.5 L polycarbonate bottles equipped with septum caps; 5 mL of $^{15}N_2$ gas (98.9 at. % $^{15}N_2$, Cambridge isotopes) were injected into all bottles using a gas-tight syringe. The purity of the $^{15}N_2$ Cambridge isotope stocks was previously checked by Dabundo et al. (2014) and more recently by Benavides et al. (2015) and Bonnet et al. (2016b), who concluded that the purity is satisfying (2×10^{-8} mol : mol N of $^{15}N_2$) and therefore does not alter the results presented below. The bottles were shaken 30 times to facilitate the $^{15}N_2$ dissolution and, except for the T0 set of bottles (see below), were incubated for 48 h in on-deck incubators covered with blue screening (50 % surface irradiance for E1 and E2 and 15 % surface irradiance for E3) and cooled with circulating surface seawater. At T0 and after incubation, a set of four bottles was collected and subsampled for the following measurements (see below for methods): N_2 fixation rates, DDN release, quantification of diazotrophs, heterotrophic bacteria and pico-, nano- and micro-phytoplankton enumeration, organic and inorganic nutrient concentrations, and ^{15}N enrichment on diazotrophic and non-diazotrophic plankton. Unless otherwise stated, each parameter reported below was measured in triplicate.

2.2 Net N_2 fixation rates and DDN released to the dissolved pool

N_2 fixation rates were measured using the $^{15}N_2$ isotopic tracer technique (adapted from Montoya et al., 1996), as described in Bonnet et al. (2018).

The DDN released to the dissolved pool in the form of NH_4^+ and DON during the N_2 fixation process was quantified using the three-step diffusion method extensively described in Berthelot et al. (2015) and derived from Slawyk and Raimbault (1995). As the NO_3^- pool was negligible, the total dissolved N (TDN) pool was defined as the sum of DON and NH_4^+ pools ($TDN = DON + NH_4^+$). After incubation with the $^{15}N_2$ tracer, 300 mL of the filtrate passed through pre-combusted Whatman GF/F filters was collected in 500 mL Duran Schott borosilicate flasks, poisoned with $HgCl_2$ (300 µL, final concentration 20 mg L^{-1}) and stored at 4 °C in the dark until analysis. At the end of each step, NH_4^+ and DON fraction were recovered on acidified pre-combusted Whatman GF/F filters, dried 24 h at 60 °C and stored in pre-combusted glass tubes until analysis on an elemental analyser coupled to an isotope ratio mass spectrometer (EA-IRMS, Integra2 Sercon Ltd) as described in Berthelot et al. (2015).

2.3 Inorganic and organic nutrient analyses

NH_4^+ concentrations were measured fluorimetrically according to Holmes et al. (1999) on a FP-2020 fluorimeter (Jasco, detection limit = 3 nM). NO_3^- and nitrite (NO_2^-) concentrations were measured using standard colorimetric procedures (Aminot and Kérouel, 2007) on a AA3 AutoAnalyzer (Seal Analytical). DON concentrations were measured by the wet oxidation method according to Pujo-Pay and Raimbault (1994).

2.4 Plankton abundance determination

The abundance of *Trichodesmium* and UCYN-B was determined microscopically: 2.2 L of each triplicate $^{15}N_2$-amended 4.5 L bottle was gently filtered onto 2 µm pore size, 25 mm diameter Millipore polycarbonate filters and fixed with paraformaldehyde (2 % final concentration) for 1 h. *Trichodesmium* were enumerated on the entire surface of the filter at a ×100 magnification with a Zeiss Axio Observer epifluorescence microscope fitted with a green (510–560 nm) excitation filter. The number of cells per trichome was counted on 20 trichomes for each experiment; we counted an average of 85 and 115 cells trichome^{-1} for E1 and E2, respectively. UCYN-B were counted on 40 fields (1.3 mm^2 fields; 0-2800 UCYN-B per field) scanned and analysed with the ImageJ1 software.

Samples for micro-phytoplankton identification and enumeration were collected in each of the triplicate 4.5 L incubated bottles (except for E1, where only one replicate was available) in five 50 mL sterile polypropylene tubes and preserved in an acidic Lugol solution (0.5 % final concentration). Diatoms were enumerated from a 250 mL subsample following the Utermöhl method (Hasle, 1978), using a Nikon TE2000 inverted microscope equipped with phase contrast and a long-distance condenser. Diatoms were identified to the lowest possible taxonomic level in one of the three replicates.

Pico-phytoplankton, nano-phytoplankton and heterotrophic bacteria abundances were determined by flow cytometry. After incubation, 1.8 mL was subsampled from triplicate 4.5 L bottles into cryotubes, fixed with paraformaldehyde (200 µL, 4 % final concentration) for 5 min at room temperature, flash-frozen in liquid N_2, and stored at −80 °C until analysis on a FACSCalibur (BD Biosciences, San Jose, CA) according to Marie et al. (1999), at the PRECYM flow cytometry platform (https://precym.mio.univ-amu.fr/, last access: 31 December 2017). Phytoplankton communities were clustered as *Prochlorococcus* spp. cell like, *Synechococcus* spp. cell like, nano-eukaryotes cell like, pico-eukaryotes cell like, and UCYN-B cell like. Trucount TM (BD Biosciences) beads were used to determine the volume analysed.

2.5 Cell sorting and sampling for nanoSIMS analyses

For flow cytometry cell sorting and subsequent analysis using nanoSIMS, 1 L of one of the 4.5 L bottles was filtered onto 0.2 µm pore size 47 mm polycarbonate filters to preconcentrate the cells and facilitate cell sorting. Filters were placed in a 5 mL cryotube filled with 0.2 µm filtered seawater and PFA (2 % final concentration), and incubated for 1 h at room temperature in the dark. The cryovials were vortexed for ∼ 20 s to detach the cells from the filter and were stored at −80 °C until analysis. Cell sorting was performed using a BD InfluxTM Mariner (BD Biosciences) high-speed cell sorter at the PRECYM platform, as described in Bonnet et al. (2016a, Supplement). Planktonic groups (picophytoplankton, nano-phytoplankton, bacteria and UCYN-B (for E3 only)) were separated using the same clusters as for the phytoplankton abundance determination. At the issue of the cell sorter, the cells were directly dropped onto a 0.2 µm pore size, 13 mm diameter polycarbonate filter (Millipore) connected to a low-pressure pump in order to concentrate them on a surface as tightly as possible. The filters were stored at −80 °C until nanoSIMS analyses.

To recover large phytoplanktonic cells (*Trichodesmium* and diatoms), 1 L of the same 4.5 L bottle was filtered on 10 µm pore size 25 mm polycarbonate filters. The cells were fixed with PFA (2 % final concentration), incubated 1 h at ambient temperature and stored at −20 °C until nanoSIMS analyses.

2.6 NanoSIMS analyses

Just before nanoSIMS analyses, filters were thawed at ambient temperature and sputtered with gold and palladium to ensure conductivity. Analyses were performed on a NanoSIMS N50 (Cameca, Gennevilliers, France) at the French National Ion MicroProbe Facility as previously described in Bonnet et al. (2016a, b) and Berthelot et al. (2016). Briefly, high-density cell areas were retrieved using the nanoSIMS optical camera (Fig. 1f). Samples were pre-sputtered prior to analyses for at least 2 min to remove surface contaminants and increase conductivity with a ∼ 22 pA caesium primary beam. For the analysis, a ∼ 1.2 pA caesium (16 KeV) primary beam focused onto a ∼ 100 nm spot diameter was scanned across a 256 × 256 or 512 × 512 pixel raster (depending on the image size, which ranged from 20 µm × 20 µm to 40 µm × 40 µm) with a counting time of 1 ms per pixel. Negative secondary ions ($^{12}C^-$, $^{13}C^-$, $^{12}C^{14}N^-$, $^{12}C^{15}N^-$ and $^{28}Si^-$) were collected by electron multiplier detectors, and secondary electrons were imaged simultaneously. A total of 20 serial quantitative secondary ion images were generated to create the final image. Individual cells were easily identified in nanoSIMS secondary electron, $^{12}C^-$, $^{12}C^{14}N^-$ and $^{28}Si^-$ images that were used to define regions of interest (ROIs) around individual cells. A total of ∼ 1500 ROIs were analysed. For each ROI, the ^{15}N enrichment was calculated; ∼ 80 cells on average were analysed for each plankton group and for each experiment (see Table S1 in the Supplement).

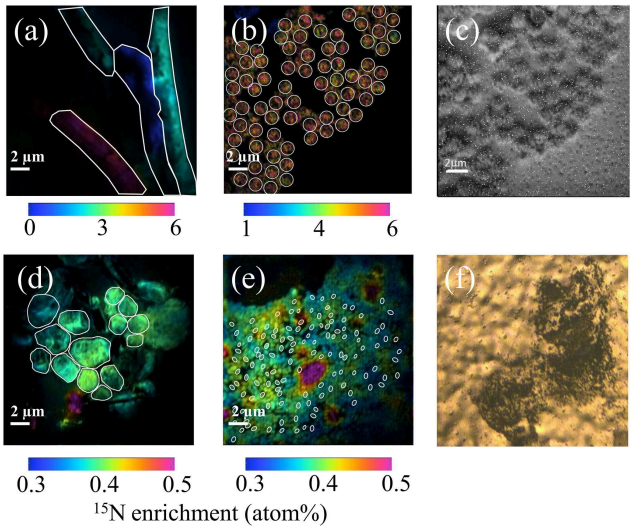

Figure 1. NanoSIMS images showing the ^{15}N enrichment **(a, b, d, e)** after 48 h of incubation in the presence of $^{15}N_2$ for *Trichodesmium* **(a)**, UCYN-B **(b)**, nano-eukaryotes **(d)** and *Synechococcus* **(e)**. The ROIs are represented with white lines. NanoSIMS images showing the secondary electron channel of UCYN **(c)** and optical camera image of *Prochlorococcus* spotted on the filter before NanoSIMS analyses **(f)**.

2.7 Cell-specific N content and DDN transfer calculations

To determine cell-specific N contents, cell sizes of *Trichodesmium* and dominant diatoms were directly measured on each sample collected for microscopy (see Sect. 2.4). For *Trichodesmium*, cell length and width were measured on 25 to 50 cells per sample at ×400 magnification with a Zeiss Axio Observer epifluorescence microscope. For diatoms, the cell cross section and apical and transapical dimensions were measured on at least 20 cells using a Nikon TE2000 inverted microscope equipped with phase contrast and a long-distance condenser. For UCYN-B, cell diameters were directly measured on the nanoSIMS images and further confirmed on microscopic images. The biovolumes (BVs) of *Trichodesmium*, UCYN-B and diatoms were estimated following the geometric model of each cell type (Sun and Liu, 2003). The cellular carbon (C) contents were determined by using the relation between BV and C content according to Verity et al. (1992) for *Trichodesmium* and UCYN-B, and according to Eppley et al. (1970) and Smayda (1978) for diatoms. The N content was calculated based on C : N ratios of 6 for *Trichodesmium* (Carpenter et al., 2004) and 5 for UCYN-B (Dekaezemacker and Bonnet, 2011; Knapp et al., 2012), and a typical Redfield ratio of 6.6 for diatoms.

For *Synechococcus* and *Prochlorococcus* we used the C content reported in Buitenhuis et al. (2012) (255 and 36 fg C cell^{-1}, respectively). For nano-eukaryotes we used the C content reported in Grégori et al. (2001), and converted it into N content according to the C : N Redfield ratio of 6.6 (leading to 3.2, 0.45 and 219 fmol N cell^{-1} for *Synechococcus*, *Prochlorococcus* and nano-eukaryotes). For bacteria, an average N content of 2.1 fg N cell^{-1} (Fukuda et al., 1998) was used. For the pico-eukaryotes, the cellular N content of 9.2 ± 2.9 fmol N cell^{-1} was used as reported in Grégori et al. (2001).

The cell-specific N_2 fixation rates and DDN transfer rates (in nmol N L^{-1} 48 h^{-1}) to non-diazotrophic phytoplankton were calculated for each plankton group analysed as follows:

$$DD^{15}N = \frac{^{15}N_{ex}}{N_{sr}} \times N_{con} \times A,$$

where $^{15}N_{ex}$ (atom %) is the excess ^{15}N enrichment of the individual cells measured by nanoSIMS after 48 h of incubation relative to the time zero value, N_{sr} (atom %) is the excess ^{15}N enrichment of the source pool (N_2) in the experimental bottles determined by MIMS, N_{con} is the cellular N content (in nmol N cell^{-1}) of each cell and A is the abundance of the specific plankton group (in cell L^{-1}). Incertitude was estimated on each variable and the final incertitude was estimated using the propagation error rule.

2.8 Experimental set-up for DDN transfer experiments in zooplankton

The DDN transfer to zooplankton was measured in four experiments performed at the same stations where the E1, E2 and E3 experiments were performed (hereafter named Zoo-1, Zoo-3 and Zoo-4) plus an additional station (Zoo-2) located between LDA and LDB (SD9, 20°57′ S–178°39′ E). *Trichodesmium* dominated the diazotroph community in the Zoo-1, Zoo-2, and Zoo-3 experiments, and UCYN-B dominated the Zoo-4 experiment. The experiments consisted in incubations of freshly collected zooplankton in the presence of the natural planktonic assemblage pre-labelled with $^{15}N_2$ as a food source. In parallel to the experiments described above, six additional HCl-washed-sample rinsed (three times) 1 L polycarbonate bottles equipped with septum caps were collected by the underway pumping system at 6 m in depth for Zoo-1, Zoo-2 and Zoo-3 and with Niskin bottles at 55 m in depth for Zoo-4. All bottles were amended with 1 mL of $^{15}N_2$ (98.9 at. % ^{15}N, Cambridge isotopes). The bottles were shaken 30 times to facilitate the $^{15}N_2$ dissolution and incubated in on-deck incubators for 24–36 h as described above.

The incubation was stopped by filtering the bottles on 0.2 µm pore size 47 mm membrane filters in such a way that the ^{15}N enrichment of the food source provided to zooplankton (hereafter referred to as ^{15}N pre-labelled plankton) does not increase during the course of the experiment. For each experiment, the initial ^{15}N enrichment of the ^{15}N pre-labelled plankton was analysed in triplicate by EA-IRMS. Plankton was then re-suspended in six 1 L bottles filled with 0.2 µm filtered surface seawater collected at the same station. Meanwhile, zooplankton was collected using repeated net tows (120 mesh size) before dawn. Animals were recovered on a 120 µm sieve and placed into 4.5 L polycarbonate bottles filled with 0.2 µm filtered surface seawater in the dark for at least 6 h in order to allow them to empty their guts. Living animals were visually identified and the individuals belonging to the genus *Clausocalanus*, which largely dominated the zooplankton community at all stations (Carlotti et al., 2018), were handpicked and 12 animals were dispatched into each of the three 1 L bottles containing the ^{15}N pre-labelled plankton before being incubated in on-deck incubators for 24 h as described above. The three other bottles were immediately filtered after the introduction of animals, firstly through a 120 µm mesh in order to recover the animals and secondly through precombusted (4 h, 450 °C) GF/F filters, which were used to quantify the isotopic signature of the ^{15}N pre-labelled plankton at the beginning of the experiment, together with the initial NH_4^+ concentrations in the incubation bottles. After 24 h, the triplicate bottles containing the mixture of ^{15}N pre-labelled plankton and zooplankton were filtered in the same way. In addition, the filtrate was recovered as described in Sect. 2.2 in order the measure the NH_4^+ concentration and the ^{15}N enrichment in the dissolved pool by using the two-step diffusion method. The recovered animals were placed on GF/F filters, which were analysed by EA-IRMS as described above in Sect. 2.2.

3 Results

3.1 Description of the biogeochemical context at the studied stations

Regarding the chlorophyll *a* and nutrient concentrations, the four studied stations were divided into two main sub-regions (Table 1): (i) stations of E1/Zoo-1, Zoo-2 and E2/Zoo3 were located in the oligotrophic MA waters characterized by surface chlorophyll *a* concentrations of 0.159–0.377 µg L^{-1} and NO_3^- and PO_4^- concentrations below 50 nmol L^{-1}, (ii) station E3/Zoo-4 located in the ultra-oligotrophic GY waters presenting lower chlorophyll *a* concentrations than in MA waters (0.053 µg L^{-1}), NO_3^- concentration below 50 nmol L^{-1}, and PO_4^- concentration $\sim$ 110 nmol L^{-1}.

Trichodesmium dominated the diazotroph community (95–100 % of total nifH gene copies detected by qPCR, Stenegren et al., 2018) at 6 m in depth in the MA waters (E1/Zoo-1, Zoo-2 and E2/Zoo3), while UCYN-B dominated (82 % of nifH gene copies) at 55 m in depth in the GY waters (E3/Zoo-4 experiment). MA waters were characterized by a higher abundance of pico-phytoplankton (*Synechococcus* and *Prochlorococcus*) and bacteria abundances (125–200 and 271–424 $\times 10^{11}$ cells m^{-2}, respectively) than GY waters

Table 1. Environmental conditions at stations where experiments were performed. Station position, depth of sampling, concentrations of Chl *a*, NO_3^-, NH_4^+, DON, PO_4^-, DOP, dominant phytoplankton communities and dominant diazotrophs.

Experiment		E1/Zoo-1	Zoo-2	E2/Zoo-3	E3/Zoo-4	References
Position	Latitude	19°12.8′ S	20°57′ S	18°14.4′ S	18°25.2′ S	
	Longitude	164°41.3′ E	178°39′ E	170°51.5′ W	165°56.4′ W	
Depth	m	6	6	6	55	
Chl *a*	$\mu g\,L^{-1}$	0.197	0.159	0.377	0.053	Dupouy et al. (2018)
NO_3^-	$nmol\,L^{-1}$	30	< 10	20	20	
NH_4^+	$nmol\,L^{-1}$	5	2	8	1	
DON	$\mu mol\,L^{-1}$	6.20	5.20	6.00	5.15	
PO_4^-	$\mu mol\,L^{-1}$	10	10	20	110	
DOP	$\mu mol\,L^{-1}$	0.15	0.17	0.17	0.15	
Prochlorococcus	10^{11} cells m^{-2}*	122 ± 31		183 ± 27	110 ± 9	Bock et al. (2018)
Synechococcus		3 ± 2		16 ± 9	0.5 ± 0.2	
Bacteria		271 ± 73		424 ± 108	290 ± 32	
Dominant diazotroph	*%nif*H gene copies	*Trichodesmium* 95 %	*Trichodesmium* 99 %	*Trichodesmium* 100 %	UCYN-B 82 %	Stenegren et al. (2018)

* Integrated in the upper photic layer.

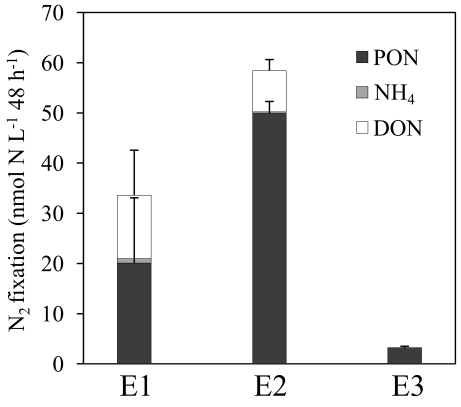

Figure 2. N_2 fixation rates (black, $nmol\,N\,L^{-1}\ 48\,h^{-1}$), DDN release $nmol\,N\,L^{-1}$ ($48\,h^{-1}$) as NH_4^+ (light grey) and DON (white) for each experiment (E1, E2 and E3). Error bars represent the standard deviations of triplicate incubations.

(~ 110 and $\sim 290 \times 10^{11}$ cells m^{-2}, respectively; Bock et al., 2018).

3.2 N_2 fixation and DDN released to the dissolved pool

Net N_2 fixation rates were 20.1 ± 13.4, 49.9 ± 2.4 and $3.2 \pm 0.3\,nmol\,N\,L^{-1}\ 48\,h^{-1}$ for the E1, E2 and E3 experiments, respectively (Fig. 2). The DDN released to the dissolved pool (the sum of DON and NH_4^+) was 14 ± 9 and $8 \pm 2\,nmol\,N\,L^{-1}\ 48\,h^{-1}$ in E1 and E2, and was below quantification limits in E3. Considering gross N_2 fixation as the sum of net N_2 fixation and DDN release rates (Mulholland et al., 2004a), the DDN released to the dissolved pool accounted for 40 ± 27 and 14 ± 4 % of gross N_2 fixation in E1 and E2, respectively (Fig. 4). DON accounted for the major part of the ^{15}N released and accounted for ~ 93 and ~ 96 % of the total N release in E1 and E2, respectively.

3.3 Cell-specific ^{15}N enrichment and DDN transfer to non-diazotrophic plankton

NanoSIMS analyses performed on individual trichomes (E1 and E2) and UCYN-B cells (E3) revealed significant ($p < 0.05$) ^{15}N enrichment after 48 h of incubation (Fig. 1a, b) compared to T0 samples (0.371 ± 0.005 at. %, $n = 5$), indicating active N_2 fixation during the experiments: 1.946 ± 0.837 at. % ($n = 32$) in E1, 1.523 ± 0.477 at. % ($n = 25$) in E2 and 4.707 ± 0.210 at. % ($n = 192$) in E3 (Fig. 3). Cell-specific N_2 fixation rates of *Trichodesmium* were $252.7 \pm 50.5\,fmol\,N\,cell^{-1}\ 48\,h^{-1}$ in E1 and $341.5 \pm 68.3\,fmol\,N\,cell^{-1}\ 48\,h^{-1}$ in E2, and cell-specific rates of UCYN-B were $18.6 \pm 3.8\,fmol\,N\,cell$-1 $48\,h^{-1}$ in E3.

NanoSIMS analyses performed on non-diazotrophic plankton (diatoms and cell-sorted *Synechococcus* (Fig. 1d), *Prochlorococcus*, bacteria, and pico- and nano-eukaryotes (Fig. 1e)) also revealed significant ^{15}N enrichment as compared to T0 values ($p < 0.05$) (Fig. 3). The ^{15}N enrichment of the non-diazotrophic plankton (all groups pooled together) was not statistically different ($p > 0.05$) between E1 and E2. However, it was significantly lower ($p < 0.05$) in E3 compared to E1 and E2.

Over the 48 h of the experiment, 10 ± 2 % of the total DDN was transferred to non-diazotrophic plankton in E1, 7 ± 1 % in E2, and 15 ± 3 % in E3 (Fig. 4). DDN was mainly transferred to pico-cyanobacteria (*Synechococcus* and *Prochlorococcus*), accounting for 73 ± 15, 68 ± 14 and 65 ± 13 % of the total transfer into non-diazotrophs in E1, E2 and E3, respectively (Fig. 4). The transfer into heterotrophic bacteria accounted for 25 ± 5, 23 ± 5 and 34 ± 7 % of the total transfer, in E1, E2 and E3, respectively. Lastly, 50 ± 40, 79 ± 4 and 85 ± 9 % of the newly fixed $^{15}N_2$ remained in the pool of diazotrophs, for E1, E2 and E3, respectively. This pool takes into account the major group of diazotrophs detected and analysed by nanoSIMS at each station (*Trichodesmium*

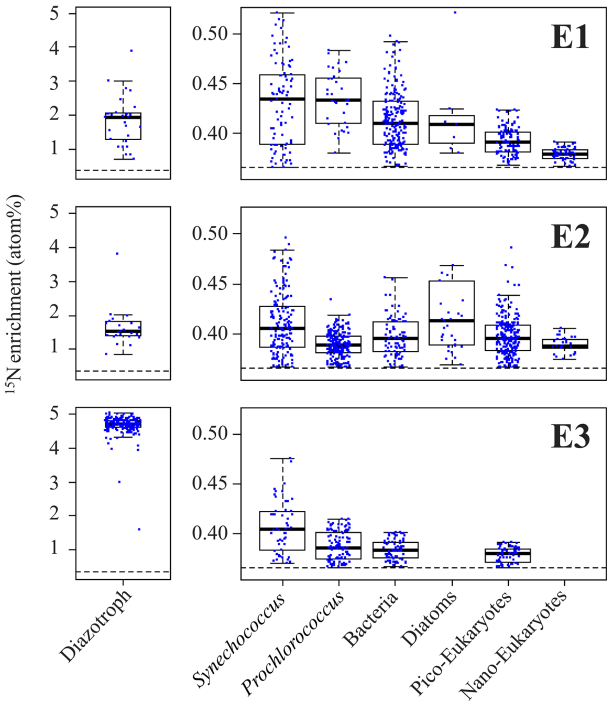

Figure 3. Left panels: boxplot of the ^{15}N enrichment measured in diazotrophs (*Trichodesmium* for E1 and E2, and UCYN-B for E3). Right panels: ^{15}N enrichment measured in non-diazotrophic plankton: *Synechococcus*, *Prochlorococcus*, bacteria, diatoms, pico-eukaryotes and nano-eukaryotes for each experiment. The black dotted line indicates the natural isotopic enrichment.

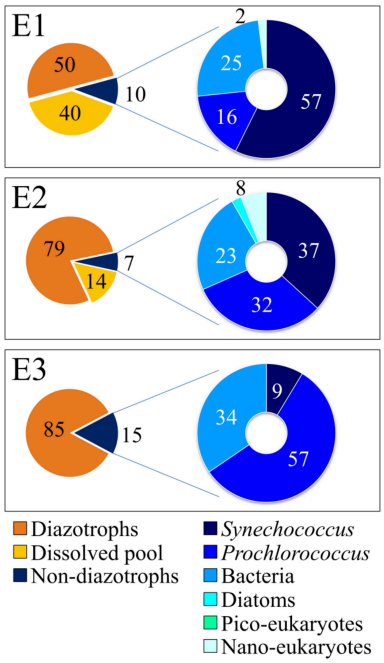

Figure 4. DDN fate after 48 h for each experiment. Left pie charts: orange: DDN remained in diazotrophs (orange); yellow: DDN released to the dissolved pool; dark blue: DDN transferred to non-diazotrophic plankton. Right pie charts, from dark blue to light blue: relative DDN transferred to *Synechococcus*, *Prochlorococcus*, bacteria, diatoms, pico-eukaryotes and nano-eukaryotes in E1 (top), E2 (middle) and E3 (bottom pie chart).

or UCYN-B), other potential diazotrophs that have not been targeted by qPCR (such as non-cyanobacterial diazotrophs), and other groups of non-diazotrophic plankton to which $^{15}N_2$ was transferred but that were not analysed by nanoSIMS (due to their very low abundance).

3.4 DDN transfer to zooplankton

Before incubation with zooplankton, the isotopic enrichment of the ^{15}N pre-labelled plankton was not significantly different in experiments Zoo-1, Zoo-2 and Zoo-3 (dominated by *Trichodesmium*) averaging 1.035 ± 0.091 at. % ($n = 9$). The isotopic enrichment was lower in the Zoo-4 experiment (dominated by UCYN-B), averaging 0.385 ± 0.005 at. % ($n = 3$). After 24 h of incubation with zooplankton, the ^{15}N enrichment of the ^{15}N pre-labelled plankton decreased to 0.431 ± 0.014 at. % on average in Zoo-1, Zoo-2 and Zoo-3, and to 0.372 ± 0.010 at. % in Zoo-4. Meanwhile, the ^{15}N enrichment of zooplankton increased as compared to T0 values (0.383 at. % on average) and reached 0.482, 0.376, 0.513 and 0.368 at. % on average in Zoo-1, Zoo-2, Zoo-3 and Zoo-4, respectively. As the ^{15}N enrichment of the initial source food (^{15}N pre-labelled plankton) was different between the four stations/experiments, and in order to compare the results obtained among experiments, we normalized the values as the percentage of initial amount of ^{15}N atoms in excess in the ^{15}N pre-labelled plankton transferred to the different compartments (i.e. conserved in the ^{15}N pre-labelled plankton pool, transferred to the zooplankton pool and to the NH_4^+ pool) at the end of the incubation. In the experiments where *Trichodesmium* dominated the diazotroph community (Zoo-1, Zoo-2, and Zoo-3), 19 ± 7 to 48 ± 21 % of the initial DD15N remained in the phytoplankton pool, 5 ± 5 to 9 ± 13 % was transferred to the zooplankton and 0.4 ± 0.3 to 7 ± 3 % was transferred to the NH_4^+ pool (Fig. 5). In Zoo-4 (where UCYN dominated the diazotroph community, Table 1), a greater proportion of DD^{15}N was conserved in the phytoplankton (76 ± 34 %), but a greater transfer to the zooplankton was also observed (28 ± 8 %, Fig. 5). The recovery of the initial DD^{15}N was comprised between 29 % and 100 %, suggesting that the remaining fraction was released to the DON pool. Interestingly, the recovery of the DD^{15}N was in surplus in the Zoo-4 experiment (112.5 ± 8.5 %), suggesting that the DD^{15}N transfer in the DON pool is close to zero.

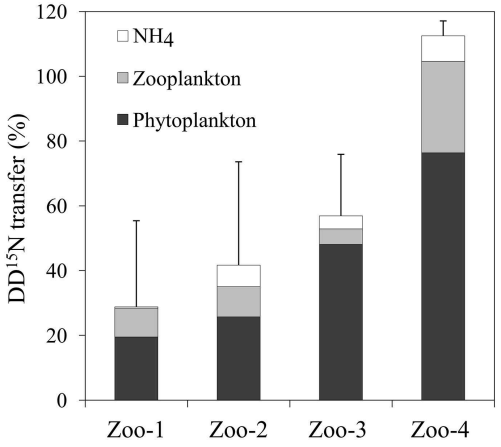

Figure 5. $DD^{15}N$ transferred (%) in the NH_4^+ pool (white), zooplankton (light grey), and what remained in the phytoplankton pool (black) after 24 h of incubation. Error bars represent the standard deviations of triplicate incubations and the propagated analytical errors.

4 Discussion

4.1 DDN release to the dissolved pool

The quantity and quality of N released by diazotrophs to the dissolved pool during N_2 fixation potentially play a key role in shaping the planktonic and microbial food webs. In this study, *Trichodesmium* released 14 ± 4 to 40 ± 57 % of the newly fixed N into the dissolved pool, which is in agreement with values reported in the literature for field studies (Mulholland, 2007; Bonnet et al., 2016a). DON accounted for ~ 95 % of the DDN released by *Trichodesmium* (Fig. 2), according with contributions measured in culture (80–90 %; Berthelot et al., 2015) and in the field (Berthelot et al., 2016). The low contribution of NH_4^+ to the DDN release does not mean that it was not released, but is likely the result of immediate consumption by surrounding plankton, which shows a great affinity for NH_4^+. Similarly, part of the DON released by *Trichodesmium* was probably taken up by heterotrophic and mixotrophic plankton (Bronk et al., 2007), but a significant fraction was likely refractory (not easily available for organisms), leading to the observed accumulation in the dissolved pool. If not refractory, the DON would likely have been immediately assimilated as the regions where these experiments were performed are strongly limited by N availability (Van Wambeke et al., 2008, 2018; Bonnet et al., 2008).

In the E1 experiment, we noticed a large variability of N_2 fixation and DDN release rates among the three replicates, which explains the high standard deviations (Fig. 2): two replicates exhibited net N_2 fixation rates ~ 25–$30\,\mathrm{nmol\,N\,L^{-1}\ 48\,h^{-1}}$ and DDN release rates ~ 7–$10\,\mathrm{nmol\,N\,L^{-1}\ 48\,h^{-1}}$, whereas in the third replicate, the DDN release ($\sim 24\,\mathrm{nmol\,N\,L^{-1}\ 48\,h^{-1}}$) exceeded net N_2 fixation rates ($5\,\mathrm{nmol\,N\,L^{-1}\ 48\,h^{-1}}$). This can be attributed to the decline of *Trichodesmium* in this replicate as we counted much more degraded trichomes in the third replicate. This suggests that decaying *Trichodesmium* release DDN more efficiently than healthy *Trichodesmium*, which has already been observed by Bonnet et al. (2016a). This may also explain why the DDN transfer to non-diazotrophic plankton was slightly higher in E1 (10 ± 2 %) than in E2 (7 ± 1 %), despite both stations being dominated by *Trichodesmium*.

Conversely to E1 and E2, the DDN released by UCYN-B (E3) was not quantifiable in our study. However, significant DDN transfer into non-diazotrophic plankton was detected (15 ± 3 % of the total fixed N, Fig. 4), suggesting that the DDN released to the dissolved pool is likely immediately transferred to surrounding communities. To our knowledge, this is the first report of DDN release in the field in the presence of a diazotroph community dominated by UCYN-B. Bonnet et al. (2016b) report low release from UCYN-C in coastal waters of the WTSP (16 ± 6 % of total N_2 fixation) compared to *Trichodesmium* (13 ± 2 to 48 ± 5 %; Bonnet et al., 2016b). This seems to indicate that the DDN from UCYN is generally lower than the DDN from *Trichodesmium*. Several hypotheses may explain the differences observed between *Trichodesmium* and UCYN. DDN compounds released by UCYN may be more bio-available than the DDN released by *Trichodesmium*, limiting its accumulation. The lack of accumulation in E3 could also be due to the more severe N limitation of planktonic communities in the ultra-oligotrophic waters as compared to MA waters (Van Wambeke et al., 2018), and to the nature of the resident community. *Prochlorococcus* was dominating the planktonic community at LD C (E3) and is known to have a high affinity with its small surface to volume ratio (Partensky et al., 1999). PCD causing *Trichodesmium* bloom demise can also be involved in the relatively high DDN release and accumulation during *Trichodesmium*-dominated experiments (Bar-Zeev et al., 2013). Exogenous factors, such as viral lyses (Fuhrman, 1999) and sloppy feeding (O'Neil and Roman, 1992; Vincent et al., 2007), are also suspected to enhance the DDN release. These factors were found to exert a higher pressure in the MA waters where *Trichodesmium* dominated compared to ultra-oligotrophic waters (Bock et al., 2018), where UCYN-B dominated. Finally, part of the discrepancy might be due to a methodological artefact: different sampling procedures between E1 and E2 (pump) and E3 (Niskin bottles) as the pump is suspected to induce mechanical stress to the cells which may have potentially affected the DDN release.

The DDN release plays a key role in the transfer of N from diazotrophs to the surrounding non-diazotrophs, only it is not a good indicator of the DDN transfer efficiency as we observed that DDN transfer to non-diazotrophs was higher when the release was low (E3) than when it was high (E1 and E2). This has already been observed in coastal waters of the WTSP by Berthelot et al. (2016).

4.2 DDN transfer efficiency and pathways in the WTSP

Here we report for the first time data on the transfer of DDN to the planktonic food web under contrasting diazotroph community composition in the open ocean. We reveal that 7 ± 1 to 15 ± 3 % of the DDN is transferred to the non-diazotrophic plankton (Fig. 4) at short timescales (48 h), which is of the same order of magnitude as the transfer (~ 10 %) reported in coastal waters of the WTSP (Bonnet et al., 2016a; Berthelot et al., 2016). In terms of efficiency, despite UCYN-B fix at lower rates compared to *Trichodesmium*, the DDN originating from UCYN-B is more efficiently transferred to non-diazotrophic plankton (15 ± 3 % of total fixed N in the E3 experiment, Fig. 4) compared to the DDN originating from *Trichodesmium* (10 ± 2 and 7 ± 1 % in the E1 and E2 experiments, respectively). This results is in accordance with the fact that we did not detect any accumulation of ^{15}N-labelled N forms in the dissolved pool (see section above).

Several studies have proven that a fraction of the DDN release is transferred to surrounding non-diazotrophic plankton, and one of them (Bonnet et al., 2016a) concludes that diatoms are the major beneficiaries of the DDN originating from *Trichodesmium* and develop extensively during/after *Trichodesmium* blooms in the coastal WTSP ocean. Despite *Trichodesmium* being rarely recovered in sediment traps (Chen et al., 2003; Walsby, 1992), these authors hypothesize a tight coupling between *Trichodesmium* blooms and export of organic matter as diatoms are efficient exporters of organic carbon to depth (Nelson et al., 1995). In contrast, in the present study, > 90 % of the DDN was transferred to picoplankton (*Synechococcus*, *Prochlorococcus* and bacteria), whatever the station studied (Fig. 4). The cyanobacteria *Synechococcus* and *Prochlorococcus* were the primary beneficiaries (73 ± 15, 68 ± 14 and 65 ± 13 % of the DDN transfer, Fig. 4), which is consistent with Bonnet et al. (2018), who observed a positive correlation between N_2 fixation rates and the abundance of *Synechococcus* and *Prochlorococcus* in the WTSP. We attributed this difference between the present study and the Bonnet et al. (2016a) study to the phytoplanktonic populations present in ambient waters at the time of the experiments. In the Bonnet et al. (2016a) study, diatoms were accounting for ~ 30 % of the non-diazotrophic phytoplankton biomass at T0, whereas diatoms were scarce (1 % of the non-diazotrophic phytoplankton biomass) in our offshore experiments, i.e. too low to show a significant increase in 48 h, even if they benefited from the DDN. However, in E2 (LD B), the diatom abundances were the highest of the three experiments (Leblanc et al., 2018) and the bloom at this station was mainly composed of diatoms and *Trichodesmium*, suggesting that *Trichodesmium* contributed to sustain this bloom.

In the E1 and E2 experiments, where *Trichodesmium* was the dominant diazotroph (Stenegren et al., 2018), the DDN was preferentially transferred to *Synechococcus*, while it was preferentially transferred to *Prochlorococcus* in E3 where UCYN-B was the dominant diazotroph (Stenegren et al., 2018). This suggests a possible coupling between *Synechococcus* and *Trichodesmium* as ever mentioned by Campbell et al. (2005), who report higher *Synechococcus* abundances inside *Trichodesmium* blooms compared to surrounding waters, while it is not the case for other plankton groups. This difference may also be linked with the communities present at the time of the experiments: *Prochlorococcus* accounted for ~ 65 % of pico-phytoplankton in E1 and E2, while it accounted for ~ 80 % in GY in E3. While the transfer of DDN to *Prochlorococcus* and *Synechococcus* together was roughly equivalent for E1 and E2 (~ 70 %, Fig. 4), *Synechococcus* abundances increased by 150 % in E1, and *Prochlorococcus* increased by 12 % during the time course of the experiment, while none of the populations increased in abundance in E2 (Fig. S1 in the Supplement). This result is in agreement with Bock et al. (2018), who report an increase of the grazing pressure with the decrease of the oligotrophic degree as E1 was performed in more oligotrophic waters than E2.

Besides *Prochlorococcus* and *Synechococcus*, heterotrophic bacteria were the second beneficiaries of the DDN, especially when the diazotroph community was dominated by UCYN-B (34 ± 7 % of the DDN transfer, Fig. 4). In this experiment, bacteria abundances increased by 70 % on average (Fig. S1), which is in agreement with Bonnet et al. (2016a, b) and Berthelot et al. (2016), who reported similar bacterial increases in the coastal WTSP. When *Trichodesmium* was the dominant diazotroph, 23–25 % was transferred to bacteria, whose abundance increased by 135 and 15 % in E1 and E2, consistent with Sheridan et al. (2002), who reported higher bacterial abundances in *Trichodesmium* blooms than in surrounding waters. The significant DDN transfer from *Trichodesmium* to bacteria concurs with *Trichodesmium* and bacteria association that has been largely highlighted in the last decades (Hmelo et al., 2012; Paerl et al., 1989; Sheridan et al., 2002). That is in accordance with Van Wambeke et al. (2018), who report that N_2 fixation fuels 3–35 % of bacterial production in MA waters. Then, we could not discriminate the DDN transfer to pico- and nano-eukaryotes, but for diatoms, the DDN transfer represented a low contribution to the overall transfer into non-diazotrophs in this region of the open ocean.

4.3 Transfer of DDN to zooplankton

Regarding higher trophic levels, the experiments performed here show that the DDN transfer to the major group of zooplankton present in this ecosystem (the copepod *Clausocalanus*) was less efficient (Fig. 5) when the diazotroph community was dominated by *Trichodesmium* (~ 5–9 %) than when it was dominated by UCYN-B (~ 28 %). This result is consistent with a previous study based on analogous $^{15}N_2$ labelling method in coastal waters of the WTSP (Hunt et al., 2016), which also report a higher DDN trans-

fer efficiency in the presence of UCYN. Regarding the DDN transfer from UCYN-B, although the transfer experiments to phytoplankton and bacteria (E3) and zooplankton (Zoo-4) were not performed in the same incubation bottles, they consistently report lower ^{15}N enrichments in all the studied pools as compared to the experiments performed when *Trichodesmium* dominated, but in fine, the DDN transfer efficiency was more important in the presence of UCYN. We observed that a larger fraction of DDN was conserved in the UCYN-B pool than in the *Trichodesmium* pool, and a larger part of the DDN was missing (likely associated with the DON pool) with *Trichodesmium* than with UCYN-B (Fig. 5). These observations are consistent with the transfer experiments E1, E2, and E3 which show that *Trichodesmium* released more DDN in the dissolve pool ($DON + NH_4^+$) than UCYN-B. The DDN released in the NH_4^+ pool did not presented significant differences between *Trichodesmium* (Zoo-1, Zoo-2 and Zoo-3) and UCYN-B (Zoo-4), and in all experiments, the DDN contribution was low in the NH_4^+ pool, as it was immediately assimilated by surrounding organisms as explained in Sect. 4.1. We suggest that the DDN transfer was higher with UCYN than with *Trichodesmium* since the UCYN-B can be directly grazed due to their small size (2–3 µm) as mentioned in Hunt et al. (2016), who revealed high UCYN abundances in the copepod guts based on qPCR data, while less *Trichodesmium* was measured. This pleads for a direct transfer of DDN from UCYN-B to zooplankton and an indirect transfer from *Trichodesmium* through non-diazotrophs. At the ecosystem level, even if the DDN transfer efficiency ($\sim 15\,\%$) to zooplankton from UCYN-B is higher than the one of *Trichodesmium*, the ultimate quantity of DDN transferred to secondary producers is higher when *Trichodesmium* dominates, as cell-specific N_2 fixation rates of *Trichodesmium* ($\sim$ 250–340 fmol N cell^{-1} 48 h^{-1}) are far higher than those of UCYN-B (~ 19 fmol N cell^{-1} 48 h^{-1}). This result is in agreement with Carlotti et al. (2018) results based on ^{15}N isotopic data showing that $\sim$ 50–95 and $\sim$ 10–40 % of the zooplankton N content originates from N_2 fixation in MA and GY waters, respectively. Finally, the DDN transferred to zooplankton, either directly or indirectly, may be released in the dissolved pool as NH_4^+, providing additional NH_4^+ from DDN in the environment that is likely assimilated by organisms in N-depleted waters. Thus, zooplankton N release appears as another DDN transfer pathway to the microbial communities in the WTSP. Zooplankton can contribute to organic matter export by production of sinking fecal pellets, active transport to depth and carcass export. These processes are increasingly recognized as important vectors of organic matter export, and the magnitudes of their contributions to organic matter export are highly dependent on regionally variable plankton community structure (Steinberg and Landry, 2017). In the WTSP, where N_2 fixation sustains most of the new primary production (Caffin et al., 2018) and an important fraction of the DDN is transferred to zooplankton, it might play a key role in the export production and hence the CO_2 sink which is the WTSP.

5 Conclusion and ecological impact of N_2 fixation in the WTSP

N_2 fixation acts as a natural N fertilizer in the ocean, releasing DDN in the dissolved pool, which is available for surrounding marine organisms. To our knowledge, this study provides the first quantification of DDN transfer to phytoplankton, bacteria and zooplankton communities in open ocean waters. The main interest of this study was to compare DDN transfer and release under contrasting N_2 fixation activity and diversity.

Here, we reveal that *Trichodesmium* released more DDN than UCYN-B, but a significant part of the DDN released by *Trichodesmium* accumulated in the dissolved pool, while the DDN released by UCYN-B immediately assimilated by the surrounding plankton communities. The DDN transfer efficiency to non-diazotrophic plankton was higher when UCYN-B dominated the diazotroph community than when *Trichodesmium* dominated. In the open ocean, most N_2 fixation is performed by *Trichodesmium* (Capone et al., 1997; Luo et al., 2012); thus, on a global scale most of the DDN transfer can be attributed to *Trichodesmium*. The regions where UCYN are the dominant diazotrophs generally present lower N_2 fixation rates than the ones where *Trichodesmium* dominates, but UCYN provide a continuous source of DDN to surrounding plankton communities. The DDN was transferred to pico-plankton, which dominated the WTSP, suggesting that N_2 fixation fuelled the growth of biomass in the N-depleted environment. This is consistent with Caffin et al. (2018), who revealed that N_2 fixation provides $> 90\,\%$ of the new N to the photic layer of the WTSP. On a larger-scale view, the simulation performed by Dutheil et al. (2018) predicts that diazotrophs will support a large part of primary production ($\sim 15\,\%$) in low nutrient low chlorophyll regions of the Pacific Ocean, comprising the WTSP.

Overall, this study indicates that N_2 fixation plays a key role in the marine biomass production, the structure of the planktonic food web, and finally the export of organic matter towards the deep ocean. The DDN can be exported to the deep ocean by different pathways: (i) the direct of export of diazotrophs, (ii) the export of non-diazotrophs which benefited from the DDN, and (iii) the export of zooplankton which benefited from the DDN. The direct export of diazotrophs accounted for $\sim 30\,\%$ of total C export at LD A (E1), 5 % at LD B (E2) and $< 0.1\,\%$ at LD C (E3) (Caffin et al., 2018). Using a $\delta^{15}N$ budget, Knapp et al. (2018) found that 50–80 % of exported material was sustained by N_2 fixation (this includes both direct and indirect export of DDN). Thus, N_2 fixation has ineluctably a key role in the biological carbon pump, as mentioned in Moutin et al. (2018), who reveal a significant biological "soft tissue" carbon pump in the

MA waters almost exclusively sustained by N_2 fixation, and acting as a net sink for of atmospheric CO_2 in the WTSP.

Data availability. All data and metadata are available at the French INSU/CNRS LEFE CYBER database (scientific coordinator: Hervé Claustre; data manager and webmaster: Catherine Schmechtig) at the following web address: http://www.obs-vlfr.fr/proof/php/outpace/outpace.php (INSU/CNRS LEFE CYBER, 2017).

The Supplement related to this article is available online at https://doi.org/10.5194/bg-15-3795-2018-supplement.

Competing interests. The authors declare that they have no conflict of interest.

Special issue statement. This article is part of the special issue "Interactions between planktonic organisms and biogeochemical cycles across trophic and N_2 fixation gradients in the western tropical South Pacific Ocean: a multidisciplinary approach (OUTPACE experiment)". It is not associated with a conference.

Acknowledgements. This is a contribution of the OUTPACE (Oligotrophy from Ultra-oligoTrophy PACific Experiment) project (https://outpace.mio.univ-amu.fr/, last access: 31 December 2017) funded by the French research national agency (ANR-14-CE01-0007-01), the LEFE-CyBER program (CNRS-INSU), IRD, the GOPS program and the CNES (BC T23, ZBC 4500048836). The OUTPACE cruise (https://doi.org/10.17600/15000900) was managed by the MIO (OSU Institut Pytheas, AMU) from Marseille (France) and received funding from European FEDER Fund under project 1166-39417. The authors thank the crew of the R/V *L'Atalante* for outstanding shipboard operation. Gilles Rougier and Marc Picheral are warmly thanked for their efficient help in CTD rosette management and data processing, as is Catherine Schmechtig for the LEFE CYBER database management. The satellite-derived data of sea surface temperature, chl *a* concentration and current have been provided by CLS in the framework of the CNES funding; we warmly thank Marie Isabelle Pujol and Gillaume Taburet for their support in providing these data. We acknowledge NOAA, and in particular Rick Lumpkin, for providing the SVP drifter.

Edited by: Douglas G. Capone
Reviewed by: Carolin Löscher and one anonymous referee

References

Aberle, N., Hansen, T., Boettger-Schnack, R., Burmeister, A., Post, A. F., and Sommer, U.: Differential routing of "new" nitrogen toward higher trophic levels within the marine food web of the Gulf of Aqaba, Northern Red Sea, Mar. Biol., 157, 157–169, https://doi.org/10.1007/s00227-009-1306-y, 2010.

Aminot, A. and Kérouel, R.: Dosage automatique des nutriments dans les eaux marines: méthodes en flux continu, Editions Quae, 2007.

Bar-Zeev, E., Avishay, I., Bidle, K. D., and Berman-Frank, I.: Programmed cell death in the marine cyanobacterium *Trichodesmium* mediates carbon and nitrogen export, ISME J., 7, 2340–2348, https://doi.org/10.1038/ismej.2013.121, 2013.

Benavides, M., Agawin, N., Arístegui, J., Peene, J., and Stal, L.: Dissolved organic nitrogen and carbon release by a marine unicellular diazotrophic cyanobacterium, Aquat. Microb. Ecol., 69, 69–80, https://doi.org/10.3354/ame01621, 2013a.

Benavides, M., Bronk, D. A., Agawin, N. S. R., Pérez-Hernández, M. D., Hernández-Guerra, A., and Arístegui, J.: Longitudinal variability of size-fractionated N_2 fixation and DON release rates along 24.5°N in the subtropical North Atlantic, J. Geophys. Res., 118, 3406–3415, 2013b.

Benavides, M., Moisander, P. H., Berthelot, H., Dittmar, T., and Grosso, O.: Mesopelagic N_2 fixation related to organic matter composition in the Solomon and Bismarck Seas (Southwest Pacific), PLoS One, 10, e0143775, https://doi.org/10.1371/journal.pone.0143775, 2015.

Berman-Frank, I., Bidle, K. D., Haramaty, L., and Falkowski, P. G.: The demise of the marine cyanobacterium, *Trichodemsium* spp., via an autocatalyzed cell death pathway, Limnol. Oceanogr., 49, 997–1005, 2004.

Berthelot, H., Bonnet, S., Camps, M., Grosso, O., and Moutin, T.: Assessment of the dinitrogen released as ammonium and dissolved organic nitrogen by unicellular and filamentous marine diazotrophic cyanobacteria grown in culture, Front. Mar. Sci., 2, 1–14, https://doi.org/10.3389/fmars.2015.00080, 2015.

Berthelot, H., Bonnet, S., Grosso, O., Cornet, V., and Barani, A.: Transfer of diazotroph-derived nitrogen towards non-diazotrophic planktonic communities: a comparative study between *Trichodesmium erythraeum*, *Crocosphaera watsonii* and *Cyanothece* sp., Biogeosciences, 13, 4005–4021, https://doi.org/10.5194/bg-13-4005-2016, 2016.

Berthelot, H., Benavides, M., Moisander, P. H., Grosso, O., and Bonnet, S.: High-nitrogen fixation rates in the particulate and dissolved pools in the Western Tropical Pacific (Solomon and Bismarck Seas), Geophys. Res. Lett., 2, 1–10, https://doi.org/10.1002/2017GL073856, 2017.

Bock, N., Van Wambeke, F., Dion, M., and Duhamel, S.: Microbial community structure in the Western Tropical South Pacific, Biogeosciences Discuss., https://doi.org/10.5194/bg-2017-562, in review, 2018.

Bombar, D., Taylor, C. D., Wilson, S. T., Robidart, J. C., Rabines, A., Turk-Kubo, K. A., Kemp, J. N., Karl, D. M., and Zehr, J. P.: Measurements of nitrogen fixation in the oligotrophic North Pacific Subtropical Gyre using a free-drifting submersible incubation device, J. Plankton Res., 37, 727–739, https://doi.org/10.1093/plankt/fbv049, 2015.

Bonnet, S., Guieu, C., Bruyant, F., Prášil, O., Van Wambeke, F., Raimbault, P., Moutin, T., Grob, C., Gorbunov, M. Y., Zehr, J. P., Masquelier, S. M., Garczarek, L., and Claustre, H.: Nutrient limitation of primary productivity in the Southeast Pacific (BIOSOPE

cruise), Biogeosciences, 5, 215–225, https://doi.org/10.5194/bg-5-215-2008, 2008.

Bonnet, S., Biegala, I. C., Dutrieux, P., Slemons, L. O., and Capone, D. G.: Nitrogen fixation in the western equatorial Pacific: Rates, diazotrophic cyanobacterial size class distribution, and biogeochemical significance, Global Biogeochem. Cy., 23, 1–13, https://doi.org/10.1029/2008gb003439, 2009.

Bonnet, S., Berthelot, H., Turk-Kubo, K. A., Cornet-Barthaux, V., Fawcett, S., Berman-Frank, I., Barani, A., Grégori, G., Dekaezemacker, J., Benavides, M., and Capone, D. G.: Diazotroph derived nitrogen supports diatom growth in the South West Pacific: A quantitative study using nanoSIMS, Limnol. Oceanogr., 61, 1549–1562, https://doi.org/10.1002/lno.10300, 2016a.

Bonnet, S., Berthelot, H., Turk-Kubo, K. A., Fawcett, S., Rahav, E., L'Helguen, S., and Berman-Frank, I.: Dynamics of N_2 fixation and fate of diazotroph-derived nitrogen in a low-nutrient, low-chlorophyll ecosystem: Results from the VAHINE mesocosm experiment (New Caledonia), Biogeosciences, 13, 2653–2673, https://doi.org/10.5194/bg-13-2653-2016, 2016b.

Bonnet, S., Caffin, M., Berthelot, H., and Moutin, T.: Hot spot of N_2 fixation in the western tropical South Pacific pleads for a spatial decoupling between N_2 fixation and denitrification, P. Natl. Acad. Sci. USA, 114, E2800–E2801, https://doi.org/10.1073/pnas.1619514114, 2017.

Bonnet, S., Caffin, M., Berthelot, H., Grosso, O., Benavides, M., Helias-Nunige, S., Guieu, C., Stenegren, M., and Foster, R. A.: In depth characterization of diazotroph activity across the Western Tropical South Pacific hot spot of N_2 fixation, Biogeosciences Discuss., https://doi.org/10.5194/bg-2017-567, in review, 2018.

Bronk, D. A., See, J. H., Bradley, P., and Killberg, L.: DON as a source of bioavailable nitrogen for phytoplankton, Biogeosciences, 4, 283–296, https://doi.org/10.5194/bg-4-283-2007, 2007.

Bryceson, I. and Fay, P.: Nitrogen fixation in *Oscillatoria (Trichodesmium) erythraea* in relation to bundle formation and trichome differentiation, Mar. Biol., 61, 159–166, 1981.

Buitenhuis, E. T., Li, W. K. W., Vaulot, D., Lomas, M. W., Landry, M. R., Partensky, F., Karl, D. M., Ulloa, O., Campbell, L., Jacquet, S., Lantoine, F., Chavez, F., Macias, D., Gosselin, M., and McManus, G. B.: Picophytoplankton biomass distribution in the global ocean, Earth Syst. Sci. Data, 4, 37–46, https://doi.org/10.5194/essd-4-37-2012, 2012.

Caffin, M., Moutin, T., Foster, R. A., Bouruet-Aubertot, P., Doglioli, A. M., Berthelot, H., Guieu, C., Grosso, O., Helias-Nunige, S., Leblond, N., Gimenez, A., Petrenko, A. A., de Verneil, A., and Bonnet, S.: N_2 fixation as a dominant new N source in the western tropical South Pacific Ocean (OUTPACE cruise), Biogeosciences, 15, 2565–2585, https://doi.org/10.5194/bg-15-2565-2018, 2018.

Campbell, L., Carpenter, E. J., Montoya, J. P., Kustka, A. B., and Capone, D. G.: Picoplankton community structure within and outside a Trichodesmium bloom in the southwestern Pacific Ocean, Vie Milieu, 55, 185–195, 2005.

Capone, D. G.: Determination of nitrogenase activity in aquatic samples using the acetylene reduction procedure, in: Handbook of Methods in Aquat. Microb. Ecol., edited by: Cole, J. J., Lewis Press, Boca Raton, 621–31, 1993.

Capone, D. G. and Montoya, J. P.: Nitrogen fixation and denitrification, Method. Microbiol., 30, 501–515, 2001.

Capone, D. G., Ferrier, M. D., and Carpenter, E. J.: Amino acid cycling in colonies of the planktonic marine cyanobacterium *Trichodesmium thiebautii*, Appl. Environ. Microb., 60, 3989–3995, 1994.

Capone, D. G., Zehr, J. P., Paerl, H. W., Bergman, B., and Carpenter, E. J.: *Trichodesmium*, a globally significant marine cyanobacterium, Science, 276, 1221–1229, 1997.

Capone, D. G., Burns, J. A., Montoya, J. P., Michaels, A. F., Subramaniam, A., and Carpenter, E. J.: New nitrogen input to the tropical North Atlantic Ocean by nitrogen fixation by the cyanobacterium, Trichodesmium spp, Global Biogeochem. Cy., 19, 1–17, https://doi.org/10.1029/2004GB002331, 2005.

Carlotti, F., Pagano, M., Guilloux, L., Donoso, K., Valdés, V., and Hunt, B. P. V.: Mesozooplankton structure and functioning in the western tropical South Pacific along the 20° parallel south during the OUTPACE survey (February–April 2015), Biogeosciences Discuss., https://doi.org/10.5194/bg-2017-573, in review, 2018.

Carpenter, E. J.: Physiology and ecology of marine planktonic *Oscillatoria (Trichodesmium)*, Mar. Biol. Lett., 4, 69–85, 1983.

Carpenter, E. J., Subramaniam, A., and Capone, D. G.: Biomass and primary productivity of the cyanobacterium Trichodesmium spp. in the tropical N Atlantic ocean, Deep-Sea Res. Pt. I, 51, 173–203, 2004.

Chen, Y. L., Tuo, S., and Chen, H. Y.: Co-occurrence and transfer of fixed nitrogen from *Trichodesmium* spp. to diatoms in the low-latitude Kuroshio Current in the North West Pacific, Mar. Ecol.-Prog. Ser., 421, 25–38, 2011.

Chen, Y. L. L., Chen, H. Y., and Lin, Y. H.: Distribution and downward flux of Trichodesmium in the South China Sea as influenced by the transport from the Kuroshio Current, Mar. Ecol.-Prog. Ser., 259, 47–57, https://doi.org/10.3354/meps259047, 2003.

Dabundo, R., Lehmann, M. F., Treibergs, L., Tobias, C. R., Altabet, M. A., Moisander, A. M., and Granger, J.: The contamination of commercial $^{15}N_2$ gas stocks with ^{15}N-labeled nitrate and ammonium and consequences for nitrogen fixation measurements, PLoS One, 9, e110335, https://doi.org/10.1371/journal.pone.0110335, 2014.

Dekaezemacker, J. and Bonnet, S.: Sensitivity of N_2 fixation to combined nitrogen forms (NO_3^- and NH_4^+) in two strains of the marine diazotroph *Crocosphaera watsonii* (Cyanobacteria), Mar. Ecol.-Prog. Ser., 438, 33–46, https://doi.org/10.3354/meps09297, 2011.

Devassy, V. P., Bhattathiri, P. M. A., and Qasim, S. Z.: *Trichodesmium* phenomenon, Indian J. Mar. Sci., 7, 168–186, 1978.

Devassy, V. P., Bhattathiri, P. M. A., and Qasim, S. Z.: Succession of organisms following *Trichodesmium* phenomenon, Indian J. Mar. Sci., 8, 89–93, 1979.

Duce, R., LaRoche, J., Altieri, K., Arrigo, K., Baker, A., Capone, D., Cornell, S., Dentener, F., Galloway, J., Ganeshram, R., Geider, R. J., Jickells, T., Kuypers, M. M., Langlois, R., Liss, P. S., Liu, S. M., Middelburg, J. J., Moore, C. M., Nickovic, S., Oschlies, A., Pedersen, T., Prospero, J., Schlitzer, R., Seitzinger, S., Sorensen, L. L., Uematsu, M., Ulloa, O., Voss, M., Ward, B., and Zamora, L.: Impacts of atmospheric anthropogenic nitrogen on the open ocean, Science, 320, 893–897, 2008.

Dupouy, C., Frouin, R., Tedetti, M., Maillard, M., Rodier, M., Lombard, F., Guidi, L., Picheral, M., Duhamel, S., Charrière, B., and

Sempéré, R.: Diazotrophic Trichodesmium influence on ocean color and pigment composition in the South West tropical Pacific, Biogeosciences Discuss., https://doi.org/10.5194/bg-2017-570, in review, 2018.

Dutheil, C., Aumont, O., Gorguès, T., Lorrain, A., Bonnet, S., Rodier, M., Dupouy, C., Shiozaki, T., and Menkes, C.: Modelling the processes driving Trichodesmium sp. spatial distribution and biogeochemical impact in the tropical Pacific Ocean, Biogeosciences Discuss., https://doi.org/10.5194/bg-2017-559, in review, 2018.

Eppley, R. W., Reid, F. M. H., and Strickland, J. D. H.: Estimates of phytoplankton crop size, growth rate, and primary production, Bull. Scripps Inst. Oceanogr., 17, 33–42, 1970.

Falkowski, P. G.: Evolution of the nitrogen cycle and its influence on the biological sequestration of CO_2 in the ocean, Nature, 387, 272–275, https://doi.org/10.1038/387272a0, 1997.

Fuhrman, J. A.: Marine viruses: biogeochemical and ecological effects, Nature, 399, 541–548, 1999.

Fukuda, R., Ogawa, H., Nagata, T., and Koike, I.: Direct determination of carbon and nitrogen contents of natural bacterial assemblages in marine environments nitrogen contents of natural bacterial assemblages in marine environments, Appl. Environ. Microb., 64, 3352–3358, 1998.

Garcia, N., Raimbault, P., and Sandroni, V.: Seasonal nitrogen fixation and primary production in the Southwest Pacific: nanoplankton diazotrophy and transfer of nitrogen to picoplankton organisms, Mar. Ecol.-Prog. Ser., 343, 25–33, https://doi.org/10.3354/Meps06882, 2007.

Glibert, P. M. and Bronk, D.: Release of dissolved organic nitrogen by marine diazotrophic cyanobacteria, *Trichodesmium* spp., Appl. Environ. Microb., 60, 3996–4000, 1994.

Glibert, P. M. and O'Neil, J. M.: Dissolved organic nitrogen release and amino-acid oxidase activity by *Trichodesmium*, in: Marine cyanobacteria, edited by: ORSTOM, Bulletin de l'Institut Océanographoque, edited by: Charpy, L. and Larkum, T., Paris, 265–271, 1999.

Grégori, G., Colosimo, A., and Denis, M.: Phytoplankton group dynamics in the Bay of Marseilles during a 2-year survey based on analytical flow cytometry, Cytometry, 44, 247–256, 2001.

Gruber, N.: The Marine Nitrogen Cycle: Overview and Challenges, Nitrogen in the Marine Environment, 1–50, https://doi.org/10.1016/B978-0-12-372522-6.00001-3, 2008.

Guo, C. and Tester, P. A.: Toxic effect of the bloom-forming *Trichodesmium* sp. (cyanophyta) to the copepod *Acartia tonsa*, Nat. Toxins, 2, 222–227, https://doi.org/10.1002/nt.2620020411, 1994.

Hansell, D. A. and Carlson, C. A.: Biogeochemistry of total organic carbon and nitrogen in the Sargasso Sea: control by convective overturn, Deep-Sea Res. Pt. II, 48, 1649–1667, 2001.

Hasle, G. R.: The inverted microscope, in: Phytoplankton Manual, edited by Sournia, A., vol. 6, UNESCO Monographs on oceanographic methodology, Paris, 1978.

Hawser, S. P. and Codd, G. A.: The toxicity of *Trichodesmium* blooms from Caribbean waters, in: Marine Pelagic Cyanobacteria: Trichodesmium and other Diazotrophs, edited by: Carpenter, E. J., Capone, D. G., and Rueter, J. G., Springer Netherlands, Dordrecht, 319–329, 1992.

Hawser, S. P., O'Neil, J. M., Roman, M. R., and Codd, G. A.: Toxicity of blooms of the cyanobacterium *Trichodesmium* to zooplankton, J. Appl. Phycol., 4, 79–86, https://doi.org/10.1007/BF00003963, 1992.

Hewson, I., Govil, S. R., Capone, D. G., Carpenter, E. J., and Fuhrman, J. A.: Evidence of *Trichodesmium* viral lysis and potential significance for biogeochemical cycling in the oligotrophic ocean, Aquat. Microb. Ecol., 36, 1–8, https://doi.org/10.3354/ame036001, 2004.

Hmelo, L. R., Van Mooy, B. A. S., and Mincer, T. J.: Characterization of bacterial epibionts on the cyanobacterium *Trichodesmium*, Aquat. Microb. Ecol., 67, 1–14, 2012.

Holmes, R. M., Aminot, A., Kerouel, R., Hooker, B. A., and Peterson, B. J.: A simple and precise method for measuring ammonium in marine and freshwater ecosystems, Can. J. Fish. Aquat. Sci., 56, 1801–1808, 1999.

Hunt, B. P. V., Bonnet, S., Berthelot, H., Conroy, B. J., Foster, R. A., and Pagano, M.: Contribution and pathways of diazotroph-derived nitrogen to zooplankton during the VAHINE mesocosm experiment in the oligotrophic New Caledonia lagoon, Biogeosciences, 13, 3131–3145, https://doi.org/10.5194/bg-13-3131-2016, 2016.

Hutchins, D. A., Fu, F. X., Zhang, Y., Warner, M. E., Feng, Y., Portune, K., Bernhardt, P. W., and Mulholland, M. R.: CO_2 control of *Trichodesmium* N_2 fixation, photosynthesis, growth rates, and elemental ratios: Implications for past, present, and future ocean biogeochemistry, Limnol. Oceanogr., 52, 1293–1304, 2007.

Karl, D. M., Letelier, R., Hebel, D. V., Bird, D. F., and Winn, C. D.: Trichodesmium blooms and new nitrogen in the North Pacific gyre, Springer, 1992.

Karl, D. M., Letelier, R. M., Tupas, L. M., Dore, J. E., Christian, J., and Hebel, D. V.: The role of nitrogen fixation in biogeochemical cycling in the subtropical North Pacific Ocean, Nature, 388, 533–538, https://doi.org/10.1038/41474, 1997.

Karl, D. M., Church, M. J., Dore, J. E., Letelier, R. M., and Mahaffey, C.: Predictable and efficient carbon sequestration in the North Pacific Ocean supported by symbiotic nitrogen fixation, P. Natl. Acad. Sci. USA, 109, 1842–1849, https://doi.org/10.1073/pnas.1120312109, 2012.

Knapp, A. N., Dekaezemacker, J., Bonnet, S., Sohm, J. A., and Capone, D. G.: Sensitivity of *Trichodesmium erythraeum* and *Crocosphaera watsonii* abundance and N_2 fixation rates to varying NO_3^- and PO_4^{3-} concentrations in batch cultures, Aquat. Microb. Ecol., 66, 223–236, 2012.

Knapp, A. N., McCabe, K. M., Grosso, O., Leblond, N., Moutin, T., and Bonnet, S.: Distribution and rates of nitrogen fixation in the western tropical South Pacific Ocean constrained by nitrogen isotope budgets, Biogeosciences, 15, 2619–2628, https://doi.org/10.5194/bg-15-2619-2018, 2018.

Konno, U., Tsunogai, U., Komatsu, D. D., Daita, S., Nakagawa, F., Tsuda, A., Matsui, T., Eum, Y. J., and Suzuki, K.: Determination of total N_2 fixation rates in the ocean taking into account both the particulate and filtrate fractions, Biogeosciences, 7, 2369–2377, https://doi.org/10.5194/bg-7-2369-2010, 2010.

Landrum, J. P., Altabet, M. A., and Montoya, J. P.: Basin-scale distributions of stable nitrogen isotopes in the subtropical North Atlantic Ocean: Contribution of diazotroph nitrogen to particulate organic matter and mesozooplankton, Deep-Sea Res. Pt. I, 58, 615–625, 2011.

Leblanc, K., Cornet, V., Rimmelin-Maury, P., Grosso, O., Hélias-Nunige, S., Brunet, C., Claustre, H., Ras, J., Leblond, N., and

Quéguiner, B.: Silicon cycle in the Tropical South Pacific: evidence for an active pico-sized siliceous plankton, Biogeosciences Discuss., https://doi.org/10.5194/bg-2018-149, in review, 2018.

Lenes, J. M., Darrow, B. P., Catrall, C., Heil, C. A., Callahan, L., Vargo, G. A., Byrne, R. H., Prospero, J. M., Bates, D. E., Fanning, K. A., and Walsh, J. J.: Iron fertilization and the *Trichodesmium* response on the West Florida shelf, Limnol. Oceanogr., 46, 1261–1277, 2001.

Letelier, R. M. and Karl, D. M.: Role of *Trichodesmium* spp. in the productivity of the subtropical north Pacific Ocean, Mar. Ecol.-Prog. Ser., 133, 263–273, 1996.

Loescher, C. R., Großkopf, T., Desai, F. D., Gill, D., Schunck, H., Croot, P. L., Schlosser, C., Neulinger, S. C., Pinnow, N., Lavik, G., Kuypers, M. M., LaRoche, J., and Schmitz, R. A.: Facets of diazotrophy in the oxygen minimum zone waters off Peru, ISME J., 8, 2180–2192, https://doi.org/10.1038/ismej.2014.71, 2014.

Loick-Wilde, N., Dutz, J., Miltner, A., Gehre, M., Montoya, J. P., and Voss, M.: Incorporation of nitrogen from N_2 fixation into amino acids of zooplankton, Limnol. Oceanogr., 57, 199–210, https://doi.org/10.4319/lo.2012.57.1.0199, 2012.

Luo, Y. W., Doney, S. C., Anderson, L. A., Benavides, M., Bode, A., Bonnet, S., Boström, K. H., Böttjer, D., Capone, D. G., Carpenter, E. J., Chen, Y. L., Church, M. J., Dore, J. E., Falcón, L. I., Fernández, A., Foster, R. A., Furuya, K., Gómez, F., Gundersen, K., Hynes, A. M., Karl, D. M., Kitajima, S., Langlois, R. J., LaRoche, J., Letelier, R. M., Maranón, E., McGillicuddy Jr., D. J., Moisander, P. H., Moore, C. M., Mourino-Carballido, B., Mulholland, M. R., Needoba, J. A., Orcutt, K. M., Poulton, A. J., Raimbault, P., Rees, A. P., Riemann, L., Shiozaki, T., Subramaniam, A., Tyrrell, T., Turk-Kubo, K. A., Varela, M., Villareal, T. A., Webb, E. A., White, A. E., Wu, J., and Zehr, J. P.: Database of diazotrophs in global ocean: abundance, biomass and nitrogen fixation rates, Earth Syst. Sci. Data, 4, 47–73, https://doi.org/10.5194/essd-4-47-2012, 2012.

Marie, D., Partensky, F., Vaulot, D., and Brussaard, C.: Enumeration of phytoplankton, bacteria and viruses in marine samples, in: Current Protocols in Cytometry, edited by: Robinson, J. P., John Wiley & Sons, Inc., New York, 11–15, 1999.

Mohr, W., Großkopf, T., Wallace, D. W. R., and LaRoche, J.: Methodological underestimation of oceanic nitrogen fixation rates, PLoS ONE, 5, 1–7, https://doi.org/10.1371/journal.pone.0012583, 2010.

Moisander, A. M., Serros, T., Pearl, R. W., Beinart, A., and Zehr, J. P.: Gammaproteobacterial diazotrophs and *nifH* gene expression in surface waters of the South Pacific Ocean, ISME J., 1–12, https://doi.org/10.1038/ismej.2014.49, 2014.

Mompeán, C., Bode, A., Benítez-Barrios, V. M., Domínguez-Yanes, J. F., Escánez, J., and Fraile-Nuez, E.: Spatial patterns of plankton biomass and stable isotopes reflect the influence of the nitrogen-fixer *Trichodesmium* along the subtropical North Atlantic, J. Plankton Res., 35, 513–525, https://doi.org/10.1093/plankt/fbt011, 2013.

Montoya, J. P., Voss, M., Kahler, P., and Capone, D. G.: A simple, high-precision, high-sensitivity tracer assay for N_2 fixation, Appl. Environ. Microb., 62, 986–993, 1996.

Montoya, J. P., Carpenter, E. J., and Capone, D. G.: Nitrogen fixation and nitrogen isotope abundances in zooplankton of the oligotrophic North Atlantic Ocean, Limnol. Oceanogr., 47, 1617–1628, 2002.

Moore, C. M., Mills, M. M., Arrigo, K. R., Berman-Frank, I., Bopp, L., Boyd, P. W., Galbraith, E. D., Geider, R. J., Guieu, C., Jaccard, S. L., Jickells, T. D., La Roche, J., Lenton, T. M., Mahowald, N. M., Marañón, E., Marinov, I., Moore, J. K., Nakatsuka, T., Oschlies, A., Saito, M. A., Thingstad, T. F., Tsuda, A., and Ulloa, O.: Processes and patterns of oceanic nutrient limitation, Nat. Geosci., 6, 701–710, https://doi.org/10.1038/ngeo1765, 2013.

Moutin, T., Doglioli, A. M., de Verneil, A., and Bonnet, S.: Preface: The Oligotrophy to the UlTra-oligotrophy PACific Experiment (OUTPACE cruise, 18 February to 3 April 2015), Biogeosciences, 14, 3207–3220, https://doi.org/10.5194/bg-14-3207-2017, 2017.

Moutin, T., Wagener, T., Caffin, M., Fumenia, A., Gimenez, A., Baklouti, M., Bouruet-Aubertot, P., Pujo-Pay, M., Leblanc, K., Lefevre, D., Helias Nunige, S., Leblond, N., Grosso, O., and de Verneil, A.: Nutrient availability and the ultimate control of the biological carbon pump in the western tropical South Pacific Ocean, Biogeosciences, 15, 2961–2989, https://doi.org/10.5194/bg-15-2961-2018, 2018.

Mulholland, M. R.: The fate of nitrogen fixed by diazotrophs in the ocean, Biogeosciences, 4, 37–51, https://doi.org/10.5194/bg-4-37-2007, 2007.

Mulholland, M. R. and Bernhardt, P. W.: The effect of growth rate, phosphorus concentration, and temperature on N_2 fixation, carbon fixation, and nitrogen release in continuous cultures of *Trichodesmium* IMS101, Limnol. Oceanogr., 50, 839–849, 2005.

Mulholland, M. R. and Capone, D. G.: The nitrogen physiology of the marine N_2-fixing cyanobacteria *Trichodesmium* spp., Trends Plant Sci., 5, 148–153, 2000.

Mulholland, M. R., Bronk, D. A., and Capone, D. G.: Dinitrogen fixation and release of ammonium and dissolved organic nitrogen by *Trichodesmium* IMS101, Aquat. Microb. Ecol., 37, 85–94, 2004a.

Mulholland, M. R., Heil, C. A., Bronk, D. A., O'Neil, J. M., and Bernhardt, P. W.: Does nitrogen regeneration from the N_2 fixing cyanobacteria, *Trichodesmium* spp. fuel Karenia brevis blooms in the Gulf of Mexico?, Harmful Algae 2002, 47–49, 2004b.

Nelson, D. M., Tréguer, P., Brzezinski, M. A., Leynaert, A., and Quéguiner, B.: Production and dissolution of biogenic silica in the ocean: Revised global estimates, comparison with regional data and relationship to biogenic sedimentation, Global Biogeochem. Cy., 9, 359–372, https://doi.org/10.1029/95GB01070, 1995.

Ohki, K.: A possible role of temperate phage in the regulation of *Trichodesmium*, Bull. Inst. Oceanogr. Monaco, 19, 235–256, 1999.

Ohlendieck, U., Stuhr, A., and Siegmund, H.: Nitrogen fixation by diazotrophic cyanobacteria in the Baltic Sea and transfer of the newly fixed nitrogen to picoplankton organisms, J. Marine Syst., 25, 213–219, 2000.

O'Neil, J. and Roman, M. R.: Grazers and Associated Organisms of Trichodesmium, in: Marine Pelagic Cyanobacteria: Trichodesmium and other Diazotrophs, edited by: Carpenter, E. J., Capone, D. G., and Rueter, J. G., NATO ASI Series, Springer Netherlands, 1992.

O'Neil, J. M.: Grazer interactions with nitrogen-fixing marine Cyanobacteria: adaptation for N-acquisition?, Bull. Inst. Oceanogr. Monaco, 19, 293–317, 1999.

O'Neil, J. M., Metzler, P., and Glibert, P. M.: Ingestion of 15N2-labelled Trichodesmium, and ammonium regeneration by the pelagic harpacticoid copepod Macrosetella gracilis, Mar. Biol., 125, 89–96, 1996.

Paerl, H. W., Priscu, J. C., and Brawner, D. L.: Immunochemical localization of nitrogenase in marine Trichodesmium aggregates: Relationship to N_2 fixation potential, Appl. Environ. Microb., 55, 2965–2975, 1989.

Partensky, F., Hess, W. R., and Vaulot, D.: Prochlorococcus, a marine photosynthetic prokaryote of global significance, Microbiol. Mol. Biol. R., 63, 106–127, 1999.

Pujo-Pay, M. and Raimbault, P.: Improvement of the wet-oxidation procedure for simultaneous determination of particulate organic nitrogen and phosphorus collected on filters, Mar. Ecol.-Prog. Ser., 105, 203–207, https://doi.org/10.3354/meps105203, 1994.

Riemann, L., Farnelid, H., and Steward, G. F.: Nitrogenase genes in non-cyanobacterial plankton: prevalence, diversity and regulation in marine waters, Aquat. Microb. Ecol., 61, 235–247, https://doi.org/10.3354/ame01431, 2010.

Sheridan, C. C., Steinberg, D. K., and Kling, G. W.: The microbial and metazoan community associated with colonies of Trichodesmium spp.: a quantitative survey, J. Plankton Res., 24, 913–922, https://doi.org/10.1093/plankt/24.9.913, 2002.

Slawyk, G. and Raimbault, P.: Simple procedure for simultaneous recovery of dissolved inorganic and organic nitrogen in 15N-tracer experiments and improving the isotopic mass balance, Mar. Ecol.-Prog. Ser., 124, 289–299, https://doi.org/10.3354/meps124289, 1995.

Smayda, T.: What to count, Phytoplankton manual, UNESCO, Paris, 165–166, 1978.

Sommer, F., Hansen, T., and Sommer, U.: Transfer of diazotrophic nitrogen to mesozooplankton in Kiel Fjord, Western Baltic Sea: a mesocosm study, Mar. Ecol.-Prog. Ser., 324, 105–112, 2006.

Steinberg, D. K. and Landry, M. R.: Zooplankton and the ocean carbon cycle, Annu. Rev. Mar. Sci., 9, 413–444, 2017.

Stenegren, M., Caputo, A., Berg, C., Bonnet, S., and Foster, R. A.: Distribution and drivers of symbiotic and free-living diazotrophic cyanobacteria in the western tropical South Pacific, Biogeosciences, 15, 1559–1578, https://doi.org/10.5194/bg-15-1559-2018, 2018.

Sun, J. and Liu, D.: Geometric models for calculating cell biovolume and surface area for phytoplankton, J. Plankton Res., 25, 1331–1346, https://doi.org/10.1093/plankt/fbg096, 2003.

Van Wambeke, F., Bonnet, S., Moutin, T., Raimbault, P., Alarcón, G., and Guieu, C.: Factors limiting heterotrophic bacterial production in the southern Pacific Ocean, Biogeosciences, 5, 833–845, https://doi.org/10.5194/bg-5-833-2008, 2008.

Van Wambeke, F., Gimenez, A., Duhamel, S., Dupouy, C., Lefevre, D., Pujo-Pay, M., and Moutin, T.: Dynamics and controls of heterotrophic prokaryotic production in the western tropical South Pacific Ocean: links with diazotrophic and photosynthetic activity, Biogeosciences, 15, 2669–2689, https://doi.org/10.5194/bg-15-2669-2018, 2018.

Verity, P. G., Robertson, C. Y., Tronzo, C. R., Andrews, M. G., Nelson, J. R., and Sieracki, M. E.: Relationships between cell volume and the carbon and nitrogen content of marine photosynthetic nanoplankton, Limnol. Oceanogr., 37, 1434–1446, https://doi.org/10.4319/lo.1992.37.7.1434, 1992.

Villareal, T. A.: Widespread occurrence of the *Hemiaulus*-cyanobacteria symbiosis in the southwest North Atlantic Ocean, B. Mar. Sci., 54, 1–7, 1994.

Vincent, D., Slawyk, G., L'Helguen, S., Sarthou, G., Gallinari, M., Seuront, L., Sautour, B., and Ragueneau, O.: Net and gross incorporation of nitrogen by marine copepods fed on ^{15}N-labelled diatoms: Methodology and trophic studies, J. Exp. Mar. Biol. Ecol., 352, 295–305, 2007.

Walsby, A. E.: The gas vesicles and buoyancy of *Trichodesmium*, in: Marine pelagic cyanobacteria: Trichodesmium and other diazotrophs, Springer Netherlands, 141–161, 1992.

Wannicke, N., Koch, B. P., and Voss, M.: Release of fixed N_2 and C as dissolved compounds by *Trichodesmium erythreum* and *Nodularia spumigena* under the influence of high light and high nutrient (P), Aquat. Microb. Ecol., 57, 175–189, 2009.

Wannicke, N., Korth, F., Liskow, I., and Voss, M.: Incorporation of diazotrophic fixed N_2 by mesozooplankton – Case studies in the southern Baltic Sea, J. Marine Syst., 117–118, 1–13, 2013.

Zehr, J. P. and Turner, P. J.: Nitrogen fixation: Nitrogenase genes and gene expression, in: Methods in Marine Microbiology, Academic Press, New York, 2001.

Zehr, J. P., Mellon, M. T., and Zani, S.: New nitrogen-fixing microorganisms detected in oligotrophic oceans by amplification of nitrogenase (nifH) genes, Appl. Environ. Microb., 64, 3444–3450, 1998.

Zehr, J. P., Bench, S. R., Carter, B. J., Hewson, I., Niazi, F., Shi, T., Tripp, H. J., and Affourtit, J. P.: Globally Distributed Uncultivated Oceanic N_2-Fixing Cyanobacteria Lack Oxygenic Photosystem II, Science, 322, 1110–1112, https://doi.org/10.1126/science.1165340, 2008.

4.4 Conclusion et perspectives

L'étude menée à l'aide de l'utilisation couplée de la nanoSIMS, du marquage isotopique au $^{15}N_2$ et du tri cellulaire a permis de caractériser et de quantifier pour la première fois le transfert du N_2 fixé par différents organismes diazotrophes, *Trichodesmium* et UCYN-B, en milieu hauturier. Cette étude a permis de montrer que*Trichodesmium* relargue plus d'azote fixé que les UCYN-B. La majorité de la fixation de N_2 est réalisée par *Trichodesmium* dans le Pacifique tropical sud-ouest (chapitre 2), ainsi le fait que *Trichodesmium* fournisse la majorité de l'azote qui alimente la chaine trophique marine de la région, fait de *Trichodesmium* un organisme clé en tant que vecteur de la production biologique et de l'export indirect de carbone associé dans cette région oligotrophe.

Alors que l'azote fixé puis relargué par les UCYN-B est assimilé immédiatement, une part importante de l'azote relargué par *Trichodesmium* s'accumule dans la fraction dissoute. La majorité de cet azote relargué par *Trichodesmium* est sous forme de DON ($\sim$ 95 %), ce qui concorde avec les études précédentes réalisées en culture (Berthelot et al., 2016) et sur le terrain (Bonnet et al., 2016b).
Dans le cadre de notre étude en minicosmes, il n'est pas possible de savoir si le DON relargué par les diazotrophes et accumulé dans le compartiment dissous sera à terme utilisé comme source d'azote par les organismes planctonique, ou s'il fera partie de la fraction du DON, dit réfractaire, inaccessible pour les organismes. Le DON provenant de la fixation de N_2 peut être accumulé à l'échelle d'une année et consommé par le plancton l'année suivante (Dore et al., 2008). Afin de savoir si le DON relargué est potentiellement consommable par les organismes, il serait intéressant de le caractériser précisément par spectrométrie de masse à transformée de Fourier (FT-ICR-MS). Appliquée pour la première fois il y a 15 ans à la matière organique dissoute, elle a permis d'en déterminer de nombreuses molécules qui la compose (Koch et al., 2005; Kujawinski et al., 2002). Plus récemment, cette technique a été utilisée pour caractériser le DON relargué par *Trichodesmium* soutenant les efflorescence de dinoflagellés dans le golfe du Mexique (Sipler et al., 2013). Cette étude a permis de mettre en exergue le relargage de 391 composés de DON pouvant potentiellement servir de source d'azote aux dinoflagellés. De manière analogue, il serait intéressant d'utiliser la FT-ICR-MS pour caractériser les composés du DON excrété par les diazotrophes du Pacifique tropical sud-ouest en milieu naturel et en culture après isolation des souches de diazotrophes rencontrés. Cette étude permettrait de mieux caractériser la potentielle accessibilité des composés relargués sous forme de DON pour la communauté planctonique.

Les résultats de notre étude ont permis de montrer que le N_2 fixé par les diazotrophes peut être rapidement transféré vers les organismes planctoniques non diazotrophes dans le Pacifique tropical sud-ouest. De plus, le transfert est plus efficace lorsque le N_2 est fixé par les UCYN-B (15 ± 3 %) dans les eaux de la gyre du Pacifique sud que lorsqu'il est fixé par les *Trichodesmium* (9 ± 3 %) dans les eaux des archipels Mélanésiens. Globalement,

ces taux de transfert sont du même ordre de grandeur que ceux mesurés dans les régions côtières et lagonaires du Pacifique tropical sud-ouest (Berthelot et al., 2016; Bonnet et al., 2016a,b) alors que la disponibilité en azote est plus faible dans les milieux hauturiers. Nous pourrions nous attendre à voir des taux de transfert plus élevés en milieu hauturier où la demande en azote est plus élevée. Au sein de cette étude, le transfert était plus élevé dans les eaux ultra-oligotrophes de la gyre du Pacifique sud que dans les eaux oligotrophes des archipels Mélanésiens. Cependant les communautés diazotrophes en présence n'étaient pas les mêmes, il est donc impossible de déconvoluer l'effet du degré d'oligotrophie ou des communautés diazotrophes sur l'efficacité de transfert. Il serait envisageable de stimuler artificiellement des efflorescences de diazotrophes en culture, avec un assemblage planctonique identique dans des conditions de disponibilité en azote différentes, et de quantifier les taux de transfert dans chacune des conditions. Cela permettrait de mieux évaluer l'influence du degré d'oligotrophie sur l'efficacité du transfert d'azote vers les communautés planctoniques.

Dans cette étude, nous avons comparé le transfert d'azote vers les différentes catégories planctoniques. Les principaux bénéficiaires de cet azote provenant de la diazotrophie étaient à la fois du plancton autotrophe et hétérotrophe de petite taille. Dans les cas où *Trichodesmium* dominait la communauté diazotrophe, le transfert était principalement réalisé vers les *Synechococcus*. Ce résultat montre un couplage possible entre *Trichodesmium* et *Synechococcus*, ce qui corrobore les analyses statistiques réalisées le long du transect OUTPACE (chapitre 2) indiquant des corrélations positives entre les taux de fixation de N_2 et les abondances en *Trichodesmium* et en *Synechococcus*. Ces observations sont aussi cohérentes avec l'étude de Campbell et al. (2005) qui a reportée des abondances en *Synechococcus* plus élevées dans une efflorescence de *Trichodesmium* que dans les eaux environnantes. Dans les eaux de la gyre du Pacifique sud, où les UCYN-B dominaient la communauté diazotrophe, le transfert était préférentiellement réalisé vers *Prochlorococcus*. Cette différence de principaux bénéficiaires peut être expliquée par la structure des communautés planctoniques au moment de l'expérience. Globalement, l'azote fixé est transféré vers les organismes pico-planctoniques qui dominent la communauté planctonique de l'océan Pacifique tropical sud-ouest, montrant à nouveau que la fixation de N_2 joue un rôle central dans la production primaire de cette région de l'océan oligotrophe. Ces observations sont en accord avec les résultats présentés dans le chapitre 2, montrant que la fixation de N_2 est positivement corrélée à la production primaire, aux abondances de *Synechococcus*, *Prochlorococcus* et bactéries hétérotrophes et à la production bactérienne le long du transect OUTPACE. Les bactéries hétérotrophes bénéficient de 25-35 % du transfert d'azote fixé vers les organismes non-diazotrophes, ce qui corrobore avec l'étude de Van Wambeke et al. (2018) montrant que 3-35 % de la production bactérienne et alimentée par la diazotrophie dans les eaux des archipels Mélanésiens.
La différence majeure entre notre étude en milieu hauturier et les études en milieu côtiers dans les eaux néo-calédoniennes et en mer des Salomon (Berthelot et al., 2016; Bonnet

et al., 2016a,b) réside dans le fait que lors des études côtières le transfert était majoritairement effectué vers le diatomées, ce qui n'est pas le cas ici. Les diatomées ont la caractéristique de participer efficacement à l'export de matière organique (Nelson et al., 1995), ainsi elles participeraient plus efficacement à l'export d'azote fixé (et de carbone associé) hors de la couche euphotique en milieu côtier qu'en milieu hauturier.

Concernant le transfert d'azote fixé vers le zooplancton, cette étude montre qu'il est moins efficace dans les archipels Mélanésiens en présence de *Trichodesmium* (5-9 %) que sur le bord ouest de la gyre du Pacifique sud en présence d'UCYN-B (28 ± 9 %), ce qui est en accord avec les résultats de l'étude de Hunt et al. (2016) menée en milieu côtier. En parallèle de notre étude, en se basant sur la mesure de la signature isotopique naturelle ^{15}N du zooplancton, Carlotti et al. (2018) ont montré que dans les archipels Mélanésiens et dans la région de la gyre du Pacifique sud, respectivement ∼ 50-95 % et ∼ 10-40 % du contenu en azote du zooplancton provenait de la diazotrophie. Bien que l'efficacité de transfert de l'azote fixé par *Trichodesmium* soit plus faible que celle de l'azote fixé par les UCYN-B, *Trichodesmium* fixe ∼ 15 fois plus d'azote que les UCYN-B. Ainsi la quantité ultime d'azote transféré par *Trichodesmium* dans les archipels Mélanésiens est supérieure à celle transféré par les UCYN-B dans la gyre du Pacifique sud, ce qui corrobore avec l'étude de Carlotti et al. (2018).

L'efficacité de transfert plus élevée avec les UCYN-B est probablement due à la petite taille de ces organismes qui peuvent directement être broutés par les copépodes et à la potentielle toxicité des *Trichodesmium* (Guo and Tester, 1994; Hawser and Codd, 1992; Hawser et al., 1992) pouvant influencer significativement leur taux de broutage. Ces observations laissent à penser que dans le cas de *Trichodesmium* le transfert de l'azote fixé serait majoritairement indirecte via les organismes non-diazotrophes consommés par le zooplancton.

Bien que cette étude ait permis de quantifier le transfert d'azote fixé par les diazotrophes vers le zooplancton et complète les études basées sur la signature isotopique naturelle ^{15}N du zooplancton, elle ne permet pas de savoir si le transfert de l'azote fixé se fait préférentiellement par le broutage direct des diazotrophes (transfert direct) ou par le broutage des non-diazotrophes qui ont bénéficié de l'azote issu de la diazotrophie (transfert indirect).

Chapitre 5

Synthèse et perspectives

Ce chapitre présente une synthèse de ce travail de thèse ainsi que quelques perspectives de recherche. Les différentes études menées au cours de cette thèse dans le Pacifique sud-ouest ont permis de répondre aux questions scientifiques suivantes :
(1) Quantifier la fixation de N_2 et identifier les principaux acteurs de la diazotrophie ;
(2) Évaluer l'influence de la fixation de N_2 sur la production primaire et sur l'export de carbone ;
(3) Identifier les voies de transfert par lesquelles la fixation de N_2 fertilise naturellement l'océan Pacifique tropical sud-ouest.

5.1 L'océan Pacifique tropical sud-ouest : un hot spot de diazotrophie

Nous avons vu au travers de la synthèse des données de fixation de N_2, que cette région est un hot spot de fixation de N_2 qui s'étend sur une zone d'environ 5,4 x 10^6 km^2, allant de la mer de Bismarck à la mer des Salomon (i.e. de l'équateur à 12 $^\circ$S), plus au sud de la mer des Salomon jusqu'à la mer de Corail (12 $^\circ$S à et jusqu'à 25-30 $^\circ$S) et s'étend d'ouest en est de l'Australie-Papouasie Nouvelle Guinée à l'ensemble des archipels Mélanésiens (Nouvelle Calédonie, Vanuatu, Fidji) et couvre une zone allant jusqu'à l'arc volcanique de Tonga à l'est. Cette région présente des taux de fixation de N_2 de 570 μmol N m^{-2} d^{-1} en moyenne, qui sont 3 à 4 fois plus forts que les taux prédits dans cette région par les modèles (Gruber, 2016) et dans la gamme la plus haute des taux recensés dans la base de données mondiale de fixation de N_2 MAREDAT (Luo et al., 2012). Nous avons établi un bilan primaire afin d'estimer la source d'azote annuelle que représente la diazotrophie dans la région. Nous estimons que la diazotrophie apporte 16 Tg N an^{-1} dans le Pacifique sud-ouest, ce qui représente un peu plus de 10 % de la contribution de la diazotrophie comme source d'azote à l'échelle globale (Gruber, 2004).
Cependant, ce bilan surestime potentiellement l'apport d'azote car il s'appuie sur une majorité de données issues d'échantillonnages réalisés pendant la période estivale où la diazotrophie est plus intense, et dans des efflorescences de diazotrophes ce qui n'est pas

représentatifs de l'intégralité de la région. Afin d'affiner ce bilan il serait intéressant d'établir une série temporelle de mesure de fixation de N_2 pour évaluer les variations saisonnières de l'intensité de la fixation de N_2 et contraindre le bilan à prendre en compte les valeurs de fixation de N_2 hivernales. Toutefois, les séries temporelles permettent de prendre en considération les variations saisonnières mais elles ne permettent pas d'avoir une couverture spatiale étendue sur l'ensemble d'un bassin.
Par ailleurs, comme nous l'avons évoqué dans le chapitre 2, la méthode de mesure de la fixation de N_2 que nous avons utilisé (la méthode de la bulle, Montoya et al., 1996) est controversée au sein de la communauté scientifique car elle sous-estimerait potentiellement les flux de fixation de N_2 (Großkopf et al., 2012; Klawonn et al., 2015; Mohr et al., 2010; Wilson et al., 2012). Il est donc possible que la valeur 16 Tg N an^{-1} correspondant aux apports d'azote par la diazotrophie dans la région soit sous estimée.

La découverte d'un hot spot de diazotrophie dans le Pacifique tropical sud-ouest permet d'alimenter le débat sur les bilans d'azote à l'échelle globale, et plus particulièrement sur les sources d'azotes issues de la diazotrophie, récemment qualifiées « d'insaisissables » par Gruber (2016). Ces sources d'azote ont été qualifiées ainsi au regard des faibles taux de fixation de N_2 mesurés dans la gyre (Moutin et al., 2008) et le bord sud-est de l'océan Pacifique tropical à proximité de l'Amérique du Sud (Pérou-Chili) (Bonnet et al., 2013; Dekaezemacker et al., 2013; Fernandez et al., 2011, 2015; Knapp et al., 2016; Loescher et al., 2014; Moutin et al., 2008; Raimbault and Garcia, 2008). Cette dernière région est reconnue comme un puits d'azote en raison des processus de dénitrification (Codispoti et al., 2001) et d'anammox (Hamersley et al., 2007) qui y sont actifs. La communauté scientifique s'attendait à mesurer de forts taux de fixation de N_2 pouvant compenser les pertes suite à l'hypothèse d'un couplage spatial étroit entre pertes et gains d'azote à l'est comme proposée par Deutsch et al. (2007). Le hot spot que nous avons identifié dans la région du Pacifique tropical sud-ouest plaide au contraire pour un découplage spatial à l'échelle du bassin du Pacifique sud entre les pertes d'azote à l'est et les gains essentiellement à l'ouest.

Le N^* (Gruber and Sarmiento, 1997) est un traceur qui permet d'expliquer en partie les variations de concentrations en azote dans l'océan liées essentiellement à la dénitrification d'une part et à la fixation de N_2 d'autre part (Deutsch et al., 2007). Le N^* correspond à la différence entre la concentration en nitrate et celle en phosphate multipliée par le rapport de Redfield. Les processus de diazotrophie qui consomme du phosphate et la reminéralisation de la matière organique issue de la diazotrophie participent à augmenter la valeur du N^*. A l'inverse, le processus de dénitrification qui consomme de l'azote diminue la valeur du N^*. Mais l'utilisation de ce traceur n'est pas simple car localement la valeur du N^* peut largement dépendre de la circulation des masses d'eau à une échelle plus globale. L'utilisation de ce traceur permet de donner une image des processus qui régissent les concentrations en azote à grande échelle spatiale. La distribution du N^* à l'échelle du bassin du Pacifique sud (Fumenia et al., 2018) appuie notre hypothèse d'un découplage

spatial entre les pertes et les gains d'azote. Les eaux du haut de la thermocline présentent des valeurs de N^* élevées dans la région du Pacifique tropical sud-ouest ($N^* > 0$), alors que les plus faibles valeurs de N^* sont retrouvées dans la région est du Pacifique sud dans la zone de minimum d'oxygène (OMZ) du Perou-Chili ($N^* < -4$). L'équilibre entre les pertes et les gains d'azote par dénitrification et diazotrophie semblerait se faire à l'échelle du bassin du Pacifique sud.

La dynamique océanique en surface advecte vers le nord-ouest les eaux de l'OMZ du Perou-Chili qui sont le siège d'une intense dénitrification ($N^* < -4$). Ces eaux sont transportées vers l'ouest par le courant sud-équatorial (SEC) pour arriver dans la région du Pacifique tropical sud-ouest (Webb, 2000), hot spot de fixation de N_2 ($N^* > 0$). Une partie de ces eaux se détachent vers le sud et repartent vers l'est dans le courant du Pacifique sud (SPC, Stramma et al., 1995) pour rejoindre le courant du Perou-Chili (Tomczak and Godfrey, 2013) et la région de dénitrification. Dans le chapitre 2, nous avions émis l'hypothèse que le transport des eaux chargées en DIP par le SEC vers les eaux pauvres en DIP du Pacifique tropical sud-ouest (Bonnet et al., 2018), associé aux apports de Fe par hydrothermalisme (Guieu et al., 2018) permettait aux diazotrophes de se développer dans le Pacifique tropical sud-ouest. Nous rappelons que l'hypothèse est la suivante : les eaux chargées en DIP du Pacifique tropical sud est sont advectées d'est en ouest par le SEC. Ces eaux traversent la gyre du Pacifique sud où les diazotrophes ne se développent pas, alors que les températures de surface sont optimales (> 25 °C Breitbarth et al., 2007), car les eaux de la gyre sont dépourvues en Fe (Blain et al., 2008). Lorsque les eaux de la gyre, chargées en DIP et pauvres en NO_3^- (Moutin et al., 2008; Raimbault and Garcia, 2008), sont advectées plus à l'ouest dans les eaux chaudes et riches en Fe de la faille de Tonga (Guieu et al., 2018), toutes les conditions environnementales sont réunies pour que les efflorescences de diazotrophes aient lieu (Fig. 5.1).

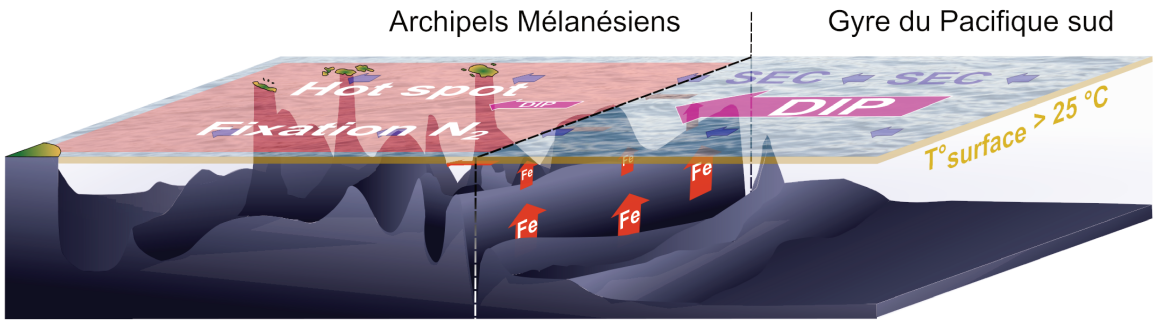

Figure 5.1 Représentation schématique des apports en Fe et en DIP contrôlant la biogéographie de la diazotrophie dans le Pacifique tropical sud-ouest.

.

Dans le Pacifique tropical sud-ouest la fixation d'azote semble être principalement contrôlée par la disponibilité DIP et en Fe (Bonnet et al., 2017, 2018; Guieu et al., 2018; Moutin et al., 2008, 2018). Les concentrations en Fe étaient très peu documentées jusqu'à

présent dans cette région. Il a été montré dans cadre d'OUTPACE que la zone des archipels Mélanésiens était fertilisée en fer, et cela a été mis en relation avec des apports de fer issus de l'activité hydrothermale localisée à faible profondeur (env. 500 m) au niveau de l'arc volcanique de Tonga (Guieu et al., 2018). Shiozaki et al. (2014) ont également évoqué des possibles apports terrigènes au niveau des îles. Les résultats de Guieu et al. (2018) montrent que les concentrations en fer sont relativement fortes (3.9 nmol L^{-1}) sur l'ensemble de la région des archipels Mélanésiens (i.e. 10-30 fois plus fortes que sur le bord ouest de la gyre du Pacifique sud), ce qui suggère des processus de fertilisation sur l'ensemble de la région, ou que les processus de fertilisation par le volcanisme sous marins au niveau de l'arc de Tonga puissent s'étendre régionalement à l'ensemble du Pacifique tropical sud-ouest via la circulation à méso-échelle et le SEC qui transporte les masses d'eau d'est en ouest (Fig. 5.1). Il serait intéressant à l'avenir de quantifier les flux hydrothermaux et leur devenir dans la colonne d'eau tant en termes de dispersion physique, de spéciation chimique, que d'impact (positif ou négatif) sur les cycles biogéochimiques. Cela fera l'objet du projet TONGA (coordination S. Bonnet, C. Guieu) pour lequel une campagne océanographique est prévue en 2019.

Dans l'introduction de ce manuscrit nous avions exprimé le possible contrôle de la fixation de N_2 par des facteurs physique (Church et al., 2009; Fong et al., 2008; Guidi et al., 2012). Dans leurs récents travaux, Rousselet et al. (2018) ont étudié l'influence d'une structure frontale à sub-mésoéchelle sur la structure des communautés planctoniques durant la campagne OUTPACE. Pour ce faire, les abondances en picophytoplancton et bactéries hétérotrophes ont été échantillonnées (à une profondeur de $\sim$5 m) à haute fréquence ($\sim$ 5 km) lors du franchissement d'une structure frontale. Les résultats montrent que la structure frontale affecte la structure des communautés planctoniques en séparant ou concentrant certains organismes d'un côté ou de l'autre du front. Nous avons vu que le Pacifique tropical sud-ouest est une région de diazotrophie très intense et que la fixation de N_2 dans cette région est principalement réalisée par deux organismes, *Trichodesmium* et UCYN-B. Ces deux organismes diazotrophes présentent des caractéristiques de taille et physiologiques différentes pouvant potentiellement être affectées différemment par la dynamique de l'océan. Cette réflexion amène donc à se poser la question suivante « Comment la dynamique océanique à sub-mésoéchelle peut-elle contrôler et influencer la répartition des organismes diazotrophes et l'intensité du processus ? ». Il est fort probable qu'une répartition fractionnée des organismes diazotrophes puisse engendrer des répercussions sur l'intensité de la fixation de N_2, les bilans d'azote qui en découlent dans la couche euphotique et la fertilisation de l'océan par la diazotrophie. Cependant, il est aujourd'hui difficile de résoudre les questions sur la variabilité spatiale et temporelle à haute fréquence de la fixation de N_2 avec les méthodes actuelles qui reposent sur un échantillonnage discret. Le développement de la nouvelle méthode de mesures à haute fréquence utilisant la méthode de la réduction à l'acétylène (ARA) par des incubations continues (FARACAS, Cassar et al., 2018) devrait permettre de répondre à ces nouvelles questions scientifiques

qui couplent la physique à fine échelle et la biogéochimie.

5.2 La fixation de N_2 : une source majeure d'azote dans l'océan Pacifique tropical sud-ouest

Les bilans d'azote réalisés dans l'océan Pacifique tropical sud-ouest au cours de la campagne OUTPACE et présentés dans le chapitre 3, ont permis de mettre en évidence que la diazotrophie était la source majeure d'azote nouveau dans la couche euphotique, aussi bien dans la zone des archipels Mélanésiens qu'à l'ouest de la gyre du Pacifique sud. Ce processus a permis d'apporter à l'océan de surface plus de 90 % de l'azote nouveau, devant les apports de NO_3^- par diffusion turbulente verticale, et les dépôts atmosphériques. Cette contribution est bien plus élevée que dans d'autres régions oligotrophes de l'océan affectées par la fixation de N_2, où elle ne dépasse pas 50 % dans les océans Atlantique nord (Capone et al., 2005a; Mouriño-Carballido et al., 2011), sud (Fernández-Castro et al., 2015; Mouriño-Carballido et al., 2011), Pacifique nord (Dore et al., 2002; Karl et al., 2003), et en mer Méditerranée (Moutin and Prieur, 2012).

Plusieurs raisons peuvent permettre d'expliquer une si haute contribution de la fixation de N_2 aux apports d'azote nouveau.

Premièrement, les apports d'azote via les dépôts atmosphériques mesurés pour la première fois dans cette région au cours de la campagne OUTPACE (Guieu et al., 2018) étaient extrêmement faibles (< 1 %), et en accord avec les dépôts prédits par les modèles globaux (Jickells et al., 2017; Kanakidou et al., 2012), ce qui implique de fait une contribution plus élevée des autres apports.

Deuxièmement, les apports de NO_3^- par diffusion turbulente verticale, que nous avons mesurés avec précision lors des bilans, sont eux aussi faibles. La méthode de quantification des flux de NO_3^- par diffusion turbulente verticale consiste à faire le produit du gradient à la base de la nitracline par le coefficient de diffusion turbulente (Kz). Lors de bilans d'azote analogues réalisés en mer Méditerranée par notre équipe (Moutin and Prieur, 2012), les apports de NO_3^- avaient été estimés en utilisant un Kz moyen pour toute la campagne (10^{-5} m^2 s^{-1}, Cuypers et al., 2012), ce qui rendait les apports uniquement sensibles au gradient de NO_3^-. Dans cette étude nous avons mesuré le Kz à haute fréquence (3-4 h) à chaque station, nous permettant d'estimer avec plus de précision les apports de NO_3^-.
D'une part, ce travail nous a permis de mettre en évidence des évènements courts et intensifs d'apports de NO_3^- à la station la plus à l'ouest (LD A), directement lié aux variations importantes de Kz. Ces variations de Kz, et les évènements courts et intensifs d'apports de NO_3^- qui en résultent, expliquent la raison pour laquelle l'écart-type des apports de NO_3^- est égal à la valeur moyenne. L'origine de ces importantes variations de Kz est due aux ondes internes qui résident dans cette région et qui ont été identifiées par Bouruet-Aubertot et al. (2018) dans un article annexe à ce travail de thèse.
D'autre part, la mesure précise de Kz à chaque station a permis de mettre en évidence

les variations d'apports de NO_3^- qu'il y a entre chacune des stations échantillonnées. La pente de la nitracline étant peu variable d'une station à l'autre, si nous avions pris un Kz moyen alors nous aurions quantifié des apports de NO_3^- identiques pour toutes les stations. Dans notre étude nous avons mesuré des apports de NO_3^- plus faibles aux stations les plus à l'est, ce qui est le reflet d'une diminution du Kz en allant vers l'est. Dans l'article annexe Bouruet-Aubertot et al. (2018), nous avons mesuré et intégré le Kz sous la couche euphotique à chaque station du transect OUTPACE afin d'obtenir une vision de la turbulence dans la région. Les résultats montrent des niveaux de turbulence plus élevés dans la région à l'ouest de 175 $^\circ$O qu'à l'est de cette longitude. Ce contraste se retrouve aussi sur les vitesses de courant de surface mesurés par satellite (données altimétriques AVISO) et sur les vitesses de courants mesurés dans la colonne d'eau par SADCP, qui sont plus élevées à l'ouest qu'à l'est. Dans la partie ouest, la bathymétrie évolue entre quelques centaines de mètres et 4000 m avec des variations topographiques importantes, ce qui pourrait expliquer les vitesses plus élevées. Par comparaison, à l'est la bathymétrie plate, autour de $\sim$ 5000 m, induit moins de turbulence. Notons que les deux régions correspondent aux régions des archipels Mélanésiens et de la gyre du Pacifique sud que nous avons défini en fonction de leur degré d'oligotrophie et qui présentent des différences remarquables concernant la fixation de N_2. La limite de 175 $^\circ$O correspondant à l'arc de Tonga évoqué précédemment. Ainsi, cette analyse de la turbulence le long du transect nous permet de conclure que si la pente du gradient de la nitracline ne varie pas le long du transect (Moutin et al., 2018, en annexe), alors les apports de NO_3^- par diffusion turbulente seraient plus important dans les archipels Mélanésiens que dans la gyre du Pacifique sud.

Troisièmement, la principale raison pouvant expliquer une contribution de plus de 90 % de la fixation de N_2 aux apports d'azote nouveau provient directement des taux élevés de fixation de N_2 que nous avons mesurés, qui font de cette région un hot spot de diazotrophie. Le fait que la fixation de N_2 représente la source majeure d'azote nouveau dans la couche euphotique implique un rôle important de ce processus sur la production marine en surface. Comme nous l'avons montré dans le chapitre 3, la fixation de N_2 compte pour la quasi intégralité de la production nouvelle puisqu'elle représente plus de 90 % de l'apport d'azote nouveau dans la couche euphotique. Sur l'intégralité du transect OUTPACE la fixation de N_2 soutient en moyenne $\sim$8 % de la production primaire totale, ce qui est de l'ordre de grandeur de celle mesurée en mer des Salomon (9,4 % Berthelot et al., 2017) qui se situe au nord-ouest du hot spot de diazotrophie que nous avons identifié. Ces observations renforcent à nouveau l'importance de la diazotrophie dans cette région de l'océan mondial, et le rôle fertilisant qu'a la fixation de N_2 pendant la période estivale.

5.3 La fixation de N_2 fertilise l'océan Pacifique tropical sud-ouest

Le transfert d'azote fixé dans la chaine trophique planctonique a été étudié à trois stations représentatives des différents régimes trophiques pouvant être présents dans l'océan Pacifique tropical sud-ouest (chapitre 4). Le relargage de l'azote fixé dans le compartiment dissous, qui est la voie de transfert vers les autres communautés planctoniques, a été quantifié puis le transfert vers les communautés non-diazotrophes a été étudié à l'aide de la méthode couplée du marquage isotopique au $^{15}N_2$, tri cellulaire et nanoSIMS. De plus, le transfert de l'azote fixé vers le zooplancton a été étudié en conditions hauturières à l'aide d'une méthode basée sur le marquage isotopique au $^{15}N_2$ d'assemblages planctoniques naturels, consommés par des copépodes.

5.3.1 Relargage de l'azote fixé

Notre étude présentée dans le chapitre 4 a montré que la quantité d'azote fixé puis relargué dans le compartiment dissous représentait entre 14 ± 4 et 40 ± 57 % de la fixation de N_2 totale lorsque *Trichodesmium* dominait la communauté diazotrophe, alors qu'elle n'était pas quantifiable lorsque les UCYN-B dominaient Fig. 5.2). La part d'azote fixé puis relargué dans le compartiment dissous par rapport à la fixation d'azote totale en présence de *Trichodesmium* est en accord avec les études précédentes (Bonnet et al., 2016b; Mulholland, 2007) réalisées en milieu naturel.

Dans l'introduction nous avons expliqué que le processus de fixation de N_2 est coûteux en énergie et en Fe. Ainsi, il paraît contre intuitif que l'azote fixé puisse être relargué sous forme de DON et de NH_4^+ pour être soit ré-assimilé, soit définitivement perdu. En milieu naturel, des facteurs exogènes tels que la lyse virale (Hewson et al., 2004) ou le « sloppy feeding » (O'Neil, 1999) participent au relargage de l'azote fixé par les diazotrophes. Cependant, lors d'expériences en culture où ces facteurs n'interviennent pas, du relargage d'azote fixé est néanmoins mesuré (Berthelot et al., 2017; Konno et al., 2010; Mulholland et al., 2004b, 2006), indiquant que c'est potentiellement un processus propre aux diazotrophes. Plusieurs hypothèses ont été avancées pour expliquer ce phénomène.
Premièrement, chez *Trichodesmium* il a été mis en évidence une ségrégation spatiale de la fixation de N_2 et de la photosynthèse au sein des filaments (Finzi-Hart et al., 2009). La ségrégation spatiale se fait par l'intermédiaire de cellules qui se spécialiseraient dans l'un des processus de manière réversible (Bergman et al., 2013; Sandh et al., 2012). Les cellules fixant activement le N_2 assureraient le transfert en azote vers les cellules qui ne fixent pas de N_2 par le processus de relargage (Mulholland, 2007). Chez les UCYN, il a été montré que le processus de fixation de N_2 qui a lieu pendant la nuit est temporellement découplé de la photosynthèse qui a lieu le jour (Fay, 1992; Griffiths et al., 1987) et qu'un processus de spéciation fixation de N_2 / photosynthèse analogue aux *Trichodesmium* serait possible

(Foster et al., 2013). Ainsi, les diazotrophes excréteraient une part de l'azote fixé pour pouvoir subvenir aux besoins des cellules qui ne fixent pas, et subvenir aux besoins de la photosynthèse lors de la phase où la fixation de N_2 est inactive.
Deuxièmement, lors du processus de diazotrophie, la cinétique de production du NH_4^+ produit par la fixation de N_2 est supérieure à la cinétique de métabolisation du NH_4^+ par les cellules (Flores and Herrero, 2005). Cela engendre une accumulation à l'intérieur des cellules dont la concentration serait supérieure à celle du milieu extra-cellulaire. Ce gradient de concentration entre les milieux intra- et extra-cellulaire engendrerait une diffusion du NH_4^+ aux travers de la paroi cellulaire capable de laisser passer les composés azotés (Bjørrisen, 1988; Kleiner, 1985; Van Dommelen et al., 1998). Ainsi, l'azote relargué peut être bénéfique pour les organismes autotrophes, hétérotrophes ou mixotrophes environnants pouvant assimiler le NH_4^+ et/ou le DON. Lorsque les taux de fixation sont élevés comme cela était le cas dans les archipels Mélanésiens, la proportion d'azote relargué (au minimum 14 % de la fixation de N_2 totale) représente une source d'azote largement supérieure à l'apport de NO_3^- par diffusion verticale (1 à 4 % de l'apport d'azote total dans les archipels Mélanésiens).

Notons qu'à l'heure actuelle, peu de données existent sur les taux de relargage en milieu hauturier, ainsi ces données sont d'intérêt majeur pour les modèles biogéochimiques prenant en compte le processus de fixation de N_2, et permettant ainsi de contraindre le processus de relargage et les quantités d'azote disponible pour les organismes environnants.

5.3.2 Transfert vers les communautés planctoniques environnantes

Le transfert de l'azote fixé vers les communautés planctoniques a été quantifié pour la première fois en milieu hauturier au travers de ces travaux de thèse. Entre 7 ± 1 % et 15 ± 3 % de la fixation de N_2 totale a été transféré vers les organismes non planctoniques non diazotrophes durant une période de 48 h Fig. 5.2). Les contributions de l'azote transféré par rapport à la fixation de N_2 totale sont du même ordre de grandeur (∼10 %) que celles qui avait été mesurées précédemment dans les eaux côtières de l'océan Pacifique tropical sud-ouest (Berthelot et al., 2016; Bonnet et al., 2016a,b). Nous aurions pu nous attendre à des taux de transfert plus élevés puisque l'océan ouvert est plus oligotrophe. Dans le chapitre 4, nous avons expliqué ne pas pouvoir déconvoluer l'impact du degré d'oligotrophie de l'impact des différences entre communautés diazotrophes sur les taux de transfert mesurés dans les deux régions du Pacifique tropical sud-ouest.

Notre étude indique une mise à disposition rapide d'une quantité importante d'azote disponible pour les organismes planctoniques environnants. Dans le Pacifique tropical sud-ouest, les principaux bénéficiaires de cet azote provenant de la diazotrophie étaient à la fois du picoplancton autotrophe (*Synechococcus*, *Prochlorococcus*) et hétérotrophe (bactéries hétérotrophes). Ces résultats corroborent les liens statistiques que nous avons

mis en évidence entre la fixation de N_2, les proxies de biomasse (concentrations en azote et carbone organique particulaire), les abondances de *Synechococcus*, de *Prochlorococcus*, de bactérie hétérotrophes et la production bactérienne. De plus, il a été montré que lors de la campagne OUTPACE, la fixation de N_2 alimentait entre 3 et 35 % de la production bactérienne dans les eaux des archipels Mélanésiens (Van Wambeke et al., 2018), là où *Trichodesmium* dominait la communauté diazotrophe. L'étude menée au cours de cette thèse, sur les voies de transfert de l'azote fixé, montre le rôle crucial de la fixation de N_2 comme fertilisant naturel dans cette région de l'océan oligotrophe, permettant le développement des communautés planctoniques dans les eaux dépourvues en azote disponible.

Notons que les principaux bénéficiaires du transfert d'azote fixé ne sont pas les mêmes dans cette étude réalisée en région hauturière que les bénéficiaires des études réalisées en régions plus côtières (Bonnet et al., 2016a,b). Dans les régions côtières les diatomées étaient les principales bénéficiaires du transfert, qui efficacement exportables représentaient une voie potentiellement importante d'export de l'azote fixé. De plus, nos observations confirment l'hypothèse proposée dans l'étude de Bonnet et al. (2016b), plaidant pour une meilleure efficacité du picophytoplancton a assimiler l'azote fixé dans des conditions pauvres en DIP, car ces petits organismes ont un rapport surface/volume qui leur permet d'assimiler plus efficacement le DIP (Moutin et al., 2002), par rapport aux grosses cellules. L'hypothèse posée en introduction, selon laquelle la différence de structure des communautés planctonique entre les régions côtières et hauturières induirait des différences en terme de transfert semble se confirmer.

5.3.3 Transfert de l'azote fixé vers le zooplancton

En réalisant des expériences de broutage d'assemblages planctoniques (marqués au $^{15}N_2$) par des copépodes, nous avons quantifié le transfert de N_2 fixé par les diazotrophes vers le zooplancton en milieu hauturier (entre 5 et 28 % en moyenne, Fig. 5.2). Une efficacité de transfert plus élevée a été observée lorsque les UCYN-B dominaient la communauté diazotrophe que lorsque les *Trichodesmium* dominaient. Ce résultat est cohérent avec l'étude utilisant le modèle 'two-source N isotope mixing model' de Hunt et al. (2016) qui a observé que l'azote fixé était transféré plus efficacement en présence d'UCYN que de *Trichodesmium* ou de DDAs. Les travaux présentés dans cette thèse (basés sur le marquage isotopique au $^{15}N_2$) et ceux de Carlotti et al. (2018) (basés sur la mesure de la signature isotopique naturelle ^{15}N du zooplancton) ont permis de montrer par deux approches différentes que la fixation de N_2 soutenait de façon significative la production zooplanctonique dans le Pacifique tropical sud-ouest. Néanmoins, comme nous l'avons exposé dans le chapitre 4, ces méthodes ne permettent pas de montrer si le transfert d'azote vers le zooplancton est direct ou indirect.

A cours de ce travail, nous avons vu que l'azote issue de la diazotrophie pouvait être exporté directement par sédimentation des organismes fixateurs de N_2 (chapitre 3), ou exporté indirectement via le transfert vers les organismes phytoplanctoniques non dia-

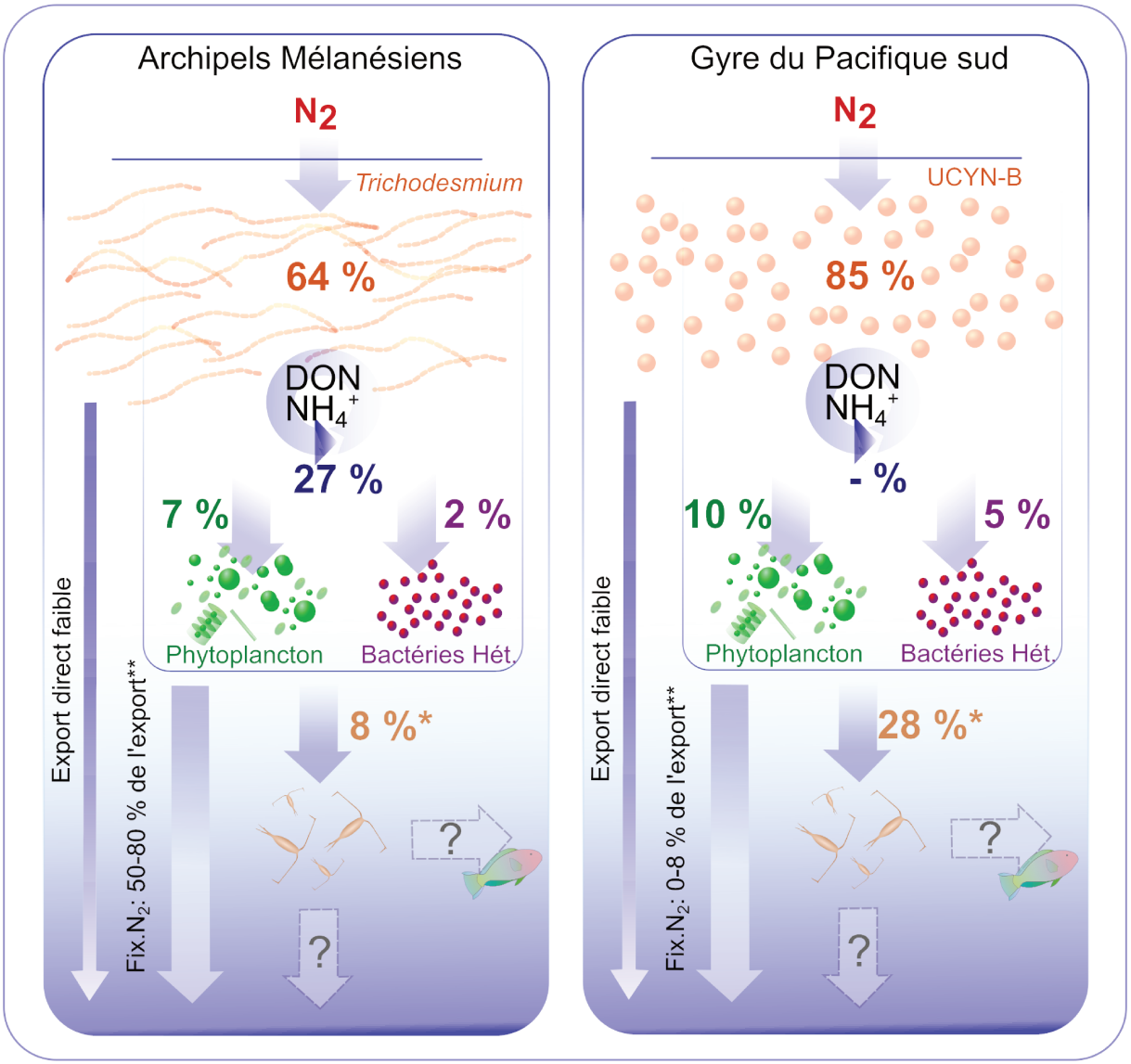

Figure 5.2 Résumé simplifié des voies d'export et de transfert de l'azote fixé par *Trichodesmium* et UCYN-B dans les premiers maillons de la chaine trophique, durant la campagne OUTPACE dans les archipels Mélanésiens et la gyre du Pacifique sud. * : les données de transfert de l'azote fixé vers le zooplancton correspondent à une expérience différente des données de transfert vers le phytoplancton et les bactéries. ** : données issues de Knapp et al. (2018)

.

zotrophes et le zooplancton (chapitre 4), emportant avec eux une quantité de carbone issue de la production primaire. Lorsque nous avons réalisé les bilans d'azote, nous avons observé un fort déséquilibre entre production primaire et production exportée (chapitre 3). Les résultats montrent que la totalité de l'azote et du carbone produit en surface n'est pas exportée dans les couches profondes de l'océan. Ces observations nous ont amené à porter une attention plus poussée sur le potentiel rôle du zooplancton sur l'export. Le zooplancton peut avoir des actions positives ou négatives sur l'export de matière particulaire, soit par des processus qui augmentent la quantité de matière exportée (pelotes

fécales, sédimentation de carcasses), soit qui la diminuent tels que le sloopy feeding ou la prédation (Steinberg and Landry, 2017). En effet, la prédation et donc le contrôle top down qui s'applique sur les premiers maillons de la chaine trophique participe à diminuer les taux d'export car le carbone et l'azote produits par l'activité planctonique sont transférés vers les maillons supérieurs de la chaine trophique (i.e. meso-zooplancton, micro-necton jusqu'aux top prédateurs et mammifères marins). Ces maillons supérieurs participent finalement eux aussi à la pompe biologique mais leur influence n'est pas prise en compte avec les méthodes de mesures traditionnelles car ils ne sont pas retrouvés dans les pièges à particules.
Ces organismes (meso-zooplancton, micro-necton, necton, top prédateurs, mammifères marins) évoluent dans la zones méso et bathy-pélagique de l'océan (200 m - 2500 m) qui est l'un des plus grand habitat sur Terre (Robison, 2004). Cependant le fonctionnement et la structure de ces organismes dans cet environnement n'est pas complètement connu. De plus, le lien qui réside entre les premiers maillons de la chaine trophique en zone euphotique et les maillons supérieurs en zone méso/bathy-pélagique est peu connu.
Il est important de comprendre le fonctionnement de la connexion entre ces deux « mondes » (qui sont aussi deux disciplines de l'océanographie contemporaine), car cette connexion a une influence importante sur la séquestration de carbone et sur le reste de la chaine trophique (jusqu'au top prédateurs). Nous avons vu que le Pacifique sud-ouest était un hot spot de diazotrophie, et que ce processus fertilise l'océan de surface et soutient le développement des premiers maillons de la chaine trophique marine. Ainsi, il est fort probable que dans cette région de l'océan oligotrophe, la diazotrophie soutienne aussi le développement des maillons supérieurs de la chaine trophique, jusqu'aux thons qui sont une ressource importante, un moyen de subsistance, de nourriture et de sécurité économique dans les iles du Pacifique tropical (Bell et al., 2015).

Les méthodes de mesures basées sur le marquage isotopique au $^{15}N_2$, utilisées dans cette thèse limitent l'étude du transfert aux premiers maillons de la chaine trophique. L'utilisation d'outils isotopiques spécialisés sur certains composés azotés, en particulier sur les acides aminés (AA-CSIA), pourrait permettre de suivre le transfert de composés azotés spécifiques aux diazotrophes dans la chaine trophique marine. Ce traceur géochimique permet d'étudier la position des organismes dans la chaine trophique, la longueur de la chaine trophique et les interactions à l'intérieur de celle-ci (Olson et al., 2010). L'utilisation des isotopes stables pour identifier les interactions au sein de la chaine trophique a été largement améliorée par le développement de nouveaux modèles (Jackson et al., 2011) permettant de donner des informations sur l'intégralité de la chaine trophique (Kadoya et al., 2012). De plus, la signature isotopique du carbone sur des acides aminés spécifiques permet de tracer les sources d'origine biologiques du carbone dans les plus hauts niveaux trophiques (Arthur et al., 2014; Larsen et al., 2009).
La signature isotopique des acides gras (SFA) est un autre traceur permettant de suivre et de comprendre les interactions au sein de la chaine trophique. Cette technique est

basée sur le fait que certains organismes à la base de la chaine trophique présentent des profils d'acides gras typiques qui ne sont pas modifiés lors de leur assimilation le long de la chaine trophique (Parrish, 2013). Il serait intéressant d'appliquer cette méthode aux diazotrophes en identifiant la signature isotopique d'un acide gras que serait spécifique aux diazotrophes et de suivre son évolution dans la chaine trophique dans des régions où les taux de fixation de N_2 sont forts.

5.4 La fixation de N_2 et l'export de carbone : la diazotrophie stimule la pompe biologique

L'étude couplée de la fixation de N_2 et de l'export de matière en utilisant une stratégie lagrangienne a permis de confirmer que la diazotrophie peut avoir un rôle clé sur l'export, comme cela avait déjà été signalé dans plusieurs études antérieures dans différentes régions de l'océan (Altabet, 1988; Bourbonnais et al., 2009; Karl et al., 1997, 2012; Knapp et al., 2005; Mahaffey et al., 2003; Scharek et al., 1999a,b) . Notre étude dans l'océan Pacifique tropical sud-ouest montre que dans cette région la fixation de N_2 élevée soutient une part importante de la production primaire. Les *e*-ratio mesurés étaient élevés, montant jusqu'à 9,8 %, ce qui est au-dessus des valeurs communément trouvées dans les régions oligotrophes de l'océan (Karl et al., 2012; Moutin and Prieur, 2012; Raimbault and Garcia, 2008). Ce résultat suggère une forte capacité d'export dans ce hot spot de diazotrophie. Cela est en accord avec l'étude de Knapp et al. (2018) basée sur les budget $\delta^{15}N$ dans les pièges à particules, révélant que 50 % à 80 % de l'export de matière particulaire était soutenue par la diazotrophie dans les archipels Mélanésiens durant la campagne OUTPACE, et confirmant clairement que la fixation de N_2 joue un rôle significatif sur l'export.

Globalement, que ce soit par voie d'export direct ou indirect, ces travaux de thèse ont permis de montrer que la diazotrophie influence la pompe biologique dans l'océan Pacifique tropical sud-ouest durant la période estivale. L'importance de la pompe biologique dans le Pacifique tropical sud-ouest a été étudiée à l'échelle annuelle dans l'article annexe de Moutin et al. (2018) en estimant les variation saisonnières des stocks de carbone/azote/phosphore, organique et inorganique, dissous et particulaire. Globalement, les grandes variations des stocks de DIC dans les eaux de surface des archipels Mélanésiens ne peuvent pas être expliquer par la pompe de solubilité, mais par une importante pompe biologique, soutenue par la fixation de N_2 et contrôlée par la disponibilité du DIP.

Ce travail de thèse a permis de mettre en exergue le hotspot de diazotrophie qui existe dans l'océan Pacifique tropical sud-ouest, et d'évaluer l'influence de la fixation de N_2 sur la production primaire et sur l'export de carbone dans cette région. Nous avons identifié les voies de transfert de l'azote fixé dans les premiers maillons de la chaine trophique marine, et mis en évidence le rôle fertilisant de la diazotrophie dans la couche euphotique, qui est d'un intérêt crucial pour la compréhension des processus qui régissent la pompe biologique dans cette région de l'océan oligotrophe.

Bibliographie

Aberle, N., Hansen, T., Boettger-Schnack, R., Burmeister, A., Post, A. F., and Sommer, U. : Differential routing of 'new' nitrogen toward higher trophic levels within the marine food web of the Gulf of Aqaba, Northern Red Sea, Marine Biology, 157, 157–169, https ://doi.org/10.1007/s00227-009-1306-y, 2010.

Altabet, M. A. : Variations in nitrogen isotopic composition between sinking and suspended particles : implications for nitrogen cycling and particle transformation in the open ocean, Deep Sea Research Part A, Oceanographic Research Papers, 35, 535–554, https ://doi.org/10.1016/0198-0149(88)90130-6, 1988.

Arthur, K. E., Kelez, S., Larsen, T., Choy, C. A., and Popp, B. N. : Tracing the biosynthetic source of essential amino acids in marine turtles using δ13C fingerprints, Ecology, 95, 1285–1293, 2014.

Bauer, K., Díez, B., Lugomela, C., Seppälä, S., Borg, A. J., and Bergman, B. : Variability in benthic diazotrophy and cyanobacterial diversity in a tropical intertidal lagoon, FEMS microbiology ecology, 63, 205–221, 2008.

Bell, J. D., Allain, V., Allison, E. H., Andréfouët, S., Andrew, N. L., Batty, M. J., Blanc, M., Dambacher, J. M., Hampton, J., Hanich, Q., et al. : Diversifying the use of tuna to improve food security and public health in Pacific Island countries and territories, Marine Policy, 51, 584–591, 2015.

Benavides, M. and Voss, M. : Five decades of N2 fixation research in the North Atlantic Ocean, Frontiers in Marine Science, 2, 1–20, https ://doi.org/10.3389/fmars.2015.00040, 2015.

Benavides, M., Agawin, N., Arístegui, J., Peene, J., and Stal, L. : Dissolved organic nitrogen and carbon release by a marine unicellular diazotrophic cyanobacterium, Aquatic Microbial Ecology, 69, 69–80, https ://doi.org/doi:10.3354/ame01621, 2013.

Benavides, M., Bonnet, S., Berman-Frank, I., and Riemann, L. : Deep Into Oceanic N2 Fixation, Frontiers in Marine Science, 5, 108, 2018.

Bergman, B., Sandh, G., Lin, S., Larsson, J., and Carpenter, E. J. : Trichodesmium–a widespread marine cyanobacterium with unusual nitrogen fixation properties, 37, 286–302, https ://doi.org/10.1111/j.1574-6976.2012.00352.x, 2013.

Berman-Frank, I., Bidle, K. D., Haramaty, L., and Falkowski, P. G. : The demise of the marine cyanobacterium, *Trichodemsium* spp., via an autocatalyzed cell death pathway, Limnology and Oceanography, 49, 997–1005, 2004.

Berman-Frank, I., Quigg, A., Finkel, Z. V., Irwin, A. J., and Haramaty, L. : Nitrogen-fixation strategies and Fe requirements in cyanobacteria, Limnology and Oceanography, 52, 2260–2269, https ://doi.org/10.4319/lo.2007.52.5.2260, 2007.

Berthelot, H., Bonnet, S., Camps, M., Grosso, O., and Moutin, T. : Assessment of the dinitrogen released as ammonium and dissolved organic nitrogen by unicellular and filamentous marine diazotrophic cyanobacteria grown in culture, Frontiers in Marine Science, 2, 1–14, https ://doi.org/10.3389/fmars.2015.00080, 2015a.

Berthelot, H., Moutin, T., L'Helguen, S., Leblanc, K., Hélias, S., Grosso, O., Leblond, N., Charrière, B., and Bonnet, S. : Dinitrogen fixation and dissolved organic nitrogen fueled primary production and particulate export during the VAHINE mesocosm experiment (New Caledonia lagoon), Biogeosciences, 12, 4099–4112, 2015b.

Berthelot, H., Bonnet, S., Grosso, O., Cornet, V., and Barani, A. : Transfer of diazotroph-derived nitrogen towards non-diazotrophic planktonic communities : a comparative study between *Trichodesmium erythraeum*, *Crocosphaera watsonii* and *Cyanothece* sp., Biogeosciences, 13, 4005–4021, https ://doi.org/10.5194/bg-13-4005-2016, 2016.

Berthelot, H., Benavides, M., Moisander, P. H., Grosso, O., and Bonnet, S. : High-nitrogen fixation rates in the particulate and dissolved pools in the Western Tropical Pacific (Solomon and Bismarck Seas), Geophysical Research Letters, 2, 1–10, https ://doi.org/10.1002/2017GL073856, 2017.

Bjørrisen, P. K. : Phytoplankton exudation of organic matter : Why do healthy cells do it ? 1, Limnology and oceanography, 33, 151–154, 1988.

Blain, S., Bonnet, S., and Guieu, C. : Dissolved iron distribution in the tropical and sub tropical South Eastern Pacific, Biogeosciences, 5, 269–280, 2008.

Bombar, D., Taylor, C. D., Wilson, S. T., Robidart, J. C., Rabines, A., Turk-Kubo, K. A., Kemp, J. N., Karl, D. M., and Zehr, J. P. : Measurements of nitrogen fixation in the oligotrophic North Pacific Subtropical Gyre using a free-drifting submersible incubation device, Journal of Plankton Research, 37, 727–739, 2015.

Bombar, D., Paerl, R. W., and Riemann, L. : Marine non-cyanobacterial diazotrophs : moving beyond molecular detection, Trends in microbiology, 24, 916–927, 2016.

Bonnet, S., Guieu, C., Bruyant, F., Prasil, O., Van Wambeke, F., Raimbault, P., Moutin, T., Grob, C., Gorbunov, M. Y., Zehr, J. P., Masquelier, S. M., Garczarek, L., and Claustre, H. : Nutrient limitation of primary productivity in the Southeast Pacific (BIOSOPE cruise), Biogeosciences, 5, 215–225, 2008.

Bonnet, S., Biegala, I. C., Dutrieux, P., Slemons, L. O., and Capone, D. G. : Nitrogen fixation in the western equatorial Pacific : Rates, diazotrophic cyanobacterial size class distribution, and biogeochemical significance, Global Biogeochemical Cycles, 23, 2009.

Bonnet, S., Dekaezemacker, J., Turk-Kubo, K. A., Moutin, T., Hamersley, R. M., Grosso, O., Zehr, J. P., and Capone, D. G. : Aphotic N2 fixation in the eastern tropical South Pacific Ocean, PloS one, 8, e81 265, 2013.

Bonnet, S., Rodier, M., Turk-Kubo, K. A., Germineaud, C., Menkes, C., Ganachaud, A., Cravatte, S., Raimbault, P., Campbell, E., Quéroué, F., et al. : Contrasted geographical distribution of N2 fixation rates and nifH phylotypes in the Coral and Solomon Seas (southwestern Pacific) during austral winter conditions, Global Biogeochemical Cycles, 29, 1874–1892, 2015.

Bonnet, S., Berthelot, H., Turk-Kubo, K. A., Cornet-Barthaux, V., Fawcett, S., Berman-Frank, I., Barani, A., Grégori, G., Dekaezemacker, J., Benavides, M., and Capone, D. G. : Diazotroph derived nitrogen supports diatom growth in the South West Pacific : A quantitative study using nanoSIMS, Limnology and Oceanography, 61, 1549–1562, https ://doi.org/10.1002/lno.10300, 2016a.

Bonnet, S., Berthelot, H., Turk-Kubo, K. A., Fawcett, S., Rahav, E., L'Helguen, S., and Berman-Frank, I. : Dynamics of N_2 fixation and fate of diazotroph-derived nitrogen in a low-nutrient, low-chlorophyll ecosystem : Results from the VAHINE mesocosm experiment (New Caledonia), Biogeosciences, 13, 2653–2673, https ://doi.org/10.5194/bg-13-2653-2016, 2016b.

Bonnet, S., Caffin, M., Berthelot, H., and Moutin, T. : Hot spot of N_2 fixation in the western tropical South Pacific pleads for a spatial decoupling between N_2 fixation and denitrification, Proc Natl Acad Sci U S A, 114, E2800–E2801, https ://doi.org/10.1073/pnas.1619514114, 2017.

Bonnet, S., Caffin, M., Berthelot, H., Grosso, O., Benavides, M., Helias-Nunige, S., Guieu, C., Stenegren, M., and Foster, R. A. : In-depth characterization of diazotroph activity across the western tropical South Pacific hotspot of N2 fixation (OUTPACE cruise), Biogeosciences, 15, 4215–4232, 2018.

Bopp, L., Legendre, L., and Monfray, P. : La pompe à carbone va-t-elle se gripper ?, La Recherche, pp. 48–51, 2002.

Böttjer, D., Dore, J. E., Karl, D. M., Letelier, R. M., Mahaffey, C., Wilson, S. T., Zehr, J. P., and Church, M. J. : Temporal variability of nitrogen fixation and particulate nitrogen export at Station ALOHA, Limnology and Oceanography, 62, 200–216, 2017.

Bourbonnais, A., Lehmann, M. F., Waniek, J. J., and Schulz-Bull, D. E. : Nitrate isotope anomalies reflect N2 fixation in the Azores Front region (subtropical NE

Atlantic), Journal of Geophysical Research : Oceans, 114, 1–16, https ://doi.org/10.1029/2007JC004617, 2009.

Bouruet-Aubertot, P., Cuypers, Y., Doglioli, A., Caffin, M., Yohia, C., de Verneil, A., Petrenko, A., Lefèvre, D., Le Goff, H., Rougier, G., Picheral, M., and Moutin, T. : Longitudinal contrast in Turbulence along a ∼19S section in the Pacific and its consequences on biogeochemical fluxes, Biogeosciences Discussions, 2018, 1–29, https ://doi.org/10.5194/bg-2018-170, 2018.

Breitbarth, E., Oschlies, A., and LaRoche, J. : Physiological constraints on the global distribution of Trichodesmium ? effect of temperature on diazotrophy, Biogeosciences, 4, 53–61, 2007.

Broecker, W. S. : The great ocean conveyor, Oceanography, 4, 79–89, 1991.

Bryceson, I. and Fay, P. : Nitrogen fixation in *Oscillatoria (Trichodesmium) erythraea* in relation to bundle formation and trichome differentiation, Marine Biology, 61, 159–166, 1981.

Buesseler, K. O., Antia, A. N., Chen, M., Fowler, S. W., Gardner, W. D., Gustafsson, Ö., Harada, K., Michaels, A. F., V.D., R., Loeff, M., Sarin, M., Steinberg, D. K., and Trull, T. : An assessment of the use of sediment traps for estimating upper ocean particle fluxes, Journal of Marine Research, 65, 345–416, 2007.

Caffin, M., Moutin, T., Foster, R. A., Bouruet-Aubertot, P., Doglioli, A. M., Berthelot, H., Guieu, C., Grosso, O., Helias-Nunige, S., Leblond, N., Gimenez, A., Petrenko, A. A., de Verneil, A., and Bonnet, S. : N_2 fixation as a dominant new N source in the western tropical South Pacific Ocean (OUTPACE cruise), Biogeosciences, 15, 2565–2585, https ://doi.org/10.5194/bg-15-2565-2018, 2018.

Campbell, L., Carpenter, E. J., Montoya, J. P., Kustka, A. B., and Capone, D. G. : Picoplankton community structure within and outside a Trichodesmium bloom in the southwestern Pacific Ocean, Vie et Milieu-Life and Environment, 55, 185–195, 2005.

Capone, D. G. and Montoya, J. P. : Nitrogen fixation and denitrification, Methods in microbiology, 30, 501–515, 2001.

Capone, D. G., Ferrier, M. D., and Carpenter, E. J. : Amino acid cycling in colonies of the planktonic marine cyanobacterium *Trichodesmium thiebautii*, Applied and Environmental Microbiology, 60, 3989–3995, 1994.

Capone, D. G., Zehr, J. P., Paerl, H. W., Bergman, B., and Carpenter, E. J. : Trichodesmium, a globally significant marine cyanobacterium, Science, 276, 1221–1229, 1997.

Capone, D. G., Burns, J. A., Montoya, J. P., Michaels, A. F., Subramaniam, A., and Carpenter, E. J. : New nitrogen input to the tropical North Atlantic Ocean by nitrogen

fixation by the cyanobacterium, Trichodesmium spp, Global Biogeochemical Cycles, 19, 1–17, https ://doi.org/doi:10.1029/2004GB002331, 2005a.

Capone, D. G., Burns, J. A., Montoya, J. P., Subramaniam, A., Mahaffey, C., Gunderson, T., Michaels, A. F., and Carpenter, E. J. : Nitrogen fixation by Trichodesmium spp. : An important source of new nitrogen to the tropical and subtropical North Atlantic Ocean, Global Biogeochemical Cycles, 19, 2005b.

Carlotti, F., Pagano, M., Guilloux, L., Donoso, K., Valdés, V., and Hunt, B. P. V. : Mesozooplankton structure and functioning in the western tropical South Pacific along the 20 ° parallel south during the OUTPACE survey (February–April 2015), Biogeosciences Discussions, 2018, 1–51, https ://doi.org/10.5194/bg-2017-573, 2018.

Carpenter, E. : Physiology and ecology of marine planktonic Oscillatoria (Trichodesmium), Mar Biol Lett, 4, 69–85, 1983.

Cassar, N., Tang, W., Gabathuler, H., and Huang, K. : Method for High Frequency Underway N2 Fixation Measurements : Flow-Through Incubation Acetylene Reduction Assays by Cavity Ring Down Laser Absorption Spectroscopy (FARACAS), Analytical chemistry, 90, 2839–2851, 2018.

Chen, Y. L., Tuo, S., and Chen, H. Y. : Co-occurrence and transfer of fixed nitrogen from *Trichodesmium* spp. to diatoms in the low-latitude Kuroshio Current in the North West Pacific., Marine Ecology Progress Series, 421, 25–38, 2011.

Chen, Y. L. L., Chen, H. Y., and Lin, Y. H. : Distribution and downward flux of Trichodesmium in the South China Sea as influenced by the transport from the Kuroshio Current, Marine Ecology Progress Series, 259, 47–57, https ://doi.org/10.3354/meps259047, 2003.

Church, M. J., Mahaffey, C., Letelier, R. M., Lukas, R., Zehr, J. P., and Karl, D. M. : Physical forcing of nitrogen fixation and diazotroph community structure in the North Pacific subtropical gyre, Global Biogeochemical Cycles, 23, 2009.

Ciais, P., Sabine, C., Bala, G., Bopp, L., Brovkin, V., Canadell, J., Chhabra, A., DeFries, R., Galloway, J., Heimann, M., et al. : Carbon and other biogeochemical cycles, in : Climate change 2013 : the physical science basis. Contribution of Working Group I to the Fifth Assessment Report of the Intergovernmental Panel on Climate Change, pp. 465–570, Cambridge University Press, 2014.

Codispoti, L., Brandes, J. A., Christensen, J., Devol, A., Naqvi, S., Paerl, H. W., and Yoshinari, T. : The oceanic fixed nitrogen and nitrous oxide budgets : moving targets as we enter the anthropocene ?, Scientia Marina, 65, 85–105, 2001.

Cuypers, Y., Bouruet-Aubertot, P., Marec, C., and Fuda, J.-L. : Characterization of turbulence from a fine-scale parameterization and microstructure measurements in the Mediterranean Sea during the BOUM experiment, Biogeosciences, 9, 3131–3149, 2012.

Dalsgaard, T., Thamdrup, B., Farías, L., and Revsbech, N. P. : Anammox and denitrification in the oxygen minimum zone of the eastern South Pacific, Limnology and Oceanography, 57, 1331–1346, 2012.

Dekaezemacker, J., Bonnet, S., Grosso, O., Moutin, T., Bressac, M., and Capone, D. : Evidence of active dinitrogen fixation in surface waters of the eastern tropical South Pacific during El Niño and La Niña events and evaluation of its potential nutrient controls, Global Biogeochemical Cycles, 27, 768–779, 2013.

Deutsch, C., Sarmiento, J. L., Sigman, D. M., Gruber, N., and Dunne, J. P. : Spatial coupling of nitrogen inputs and losses in the ocean, Nature, 445, 163, 2007.

Devassy, V. P., Bhattathiri, P. M. A., and Qasim, S. Z. : *Trichodesmium* phenomenon, Indian Journal of Marine Sciences, 7, 168–186, 1978.

Devassy, V. P., Bhattathiri, P. M. A., and Qasim, S. Z. : Succession of organisms following *Trichodesmium* phenomenon, Indian Journal of Marine Sciences, 8, 89–93, 1979.

DeVries, T. : The oceanic anthropogenic CO_2 sink : Storage, air-sea fluxes, and transports over the industrial era, Global Biogeochemical Cycles, 28, 631–647, 2014.

Dilworth, M. : Acetylene reduction by nitrogen-fixing preparations from Clostridium pasteurianum, Biochimica et Biophysica Acta (BBA)-General Subjects, 127, 285–294, 1966.

Dlugokencky, E. and Tans, P. : Recent Global CO_2 - NOAA/ESR, 2018.

Dore, J., Brium, J. R., Tupas, L. M., and Karl, D. M. : Seasonal and interannual variability in sources of nitrogen supporting export in the oligotrophic subtropical North Pacific Ocean, Limnology and Oceanography, 47, 1595–1607, 2002.

Dore, J. E., Letelier, R. M., Church, M. J., Lukas, R., and Karl, D. M. : Summer phytoplankton blooms in the oligotrophic North Pacific Subtropical Gyre : Historical perspective and recent observations, Progress in Oceanography, 76, 2–38, https ://doi.org/doi:10.1016/j.pocean.2007.10.002,2008, 2008.

Dugdale, R. and Goering, J. : Uptake of new and regenerated forms of nitrogen in primary productivity, Limnology and oceanography, 12, 196–206, 1967.

Dupouy, C., Neveux, J., Subramaniam, A., Mulholland, M. R., Montoya, J. P., Campbell, L., Carpenter, E. J., and Capone, D. G. : Satellite captures Trichodesmium blooms in the southwestern tropical Pacific, EOS, Transactions American Geophysical Union, 81, 13–16, 2000.

Dupouy, C., Benielli-Gary, D., Neveux, J., Dandonneau, Y., and Westberry, T. : An algorithm for detecting Trichodesmium surface blooms in the South Western Tropical Pacific, Biogeosciences, 8, 3631–3647, 2011.

Eppley, R. W. and Peterson, B. J. : Particulate organic matter flux and planktonic new production in the deep ocean, Nature, 282, 677, 1979.

Falkowski, P. and Knoll, A. H. : Evolution of primary producers in the sea, Academic Press, 2011.

Falkowski, P. G. : Evolution of the nitrogen cycle and its influence on the biological sequestration of CO2 in the ocean, Nature, 387, 272, 1997.

Farías, L., Castro-González, M., Cornejo, M., Charpentier, J., Faúndez, J., Boontanon, N., and Yoshida, N. : Denitrification and nitrous oxide cycling within the upper oxycline of the eastern tropical South Pacific oxygen minimum zone, Limnology and Oceanography, 54, 132–144, 2009.

Fay, P. : Oxygen relations of nitrogen fixation in cyanobacteria., Microbiological reviews, 56, 340–373, 1992.

Fernandez, C., Farías, L., and Ulloa, O. : Nitrogen fixation in denitrified marine waters, PloS one, 6, e20 539, 2011.

Fernandez, C., González, M. L., Muñoz, C., Molina, V., and Farias, L. : Temporal and spatial variability of biological nitrogen fixation off the upwelling system of central Chile (35–38.5 S), Journal of Geophysical Research : Oceans, 120, 3330–3349, 2015.

Fernández-Castro, B., Mouriño-Carballido, B., Marañón, E., Chouciño, P., Gago, J., Ramírez, T., Vidal, M., Bode, A., Blasco, D., Royer, S.-J., Estrada, M., and Simó, R. : Importance of salt fingering for new nitrogen supply in the oligotrophic ocean, Nature Communications, 6, 8002, https ://doi.org/10.1038/ncomms9002, 2015.

Field, C. B., Behrenfeld, M. J., Randerson, J. T., and Falkowski, P. : Primary production of the biosphere : integrating terrestrial and oceanic components, science, 281, 237–240, 1998.

Finzi-Hart, J. A., Pett-Ridge, J., Weber, P. K., Popa, R., Fallon, S. J., and Gunderson, T. : Fixation and fate of C and N in the cyanobacterium Trichodesmium using nanometer-scale secondary ion mass spectrometry, Proceedings of the National Academy of Sciences, 106, 6345–6350, 2009.

Flores, E. and Herrero, A. : Nitrogen assimilation and nitrogen control in cyanobacteria, 2005.

Fong, A. A., Karl, D. M., Lukas, R., Letelier, R. M., Zehr, J. P., and Church, M. J. : Nitrogen fixation in an anticyclonic eddy in the oligotrophic North Pacific Ocean, The ISME journal, 2, 663, 2008.

Foster, R. A., Sztejrenszus, S., and Kuypers, M. M. M. : Measuring carbon and N2 fixation in field populations of colonial and free living cyanobacteria using nanometer scale secondary ion mass spectrometry, Journal of Phycology, 49, 502–516, 2013.

Fu, F. X., Mulholland, M. R., N., G., Beck, A., Bernhardt, P., Warner, M., Sañudo-Wilhelmy, S., and Hutchins, D. A. : Interactions between changing pCO2, N2 fixation, and Fe limitation in the marine unicellular cyanobacterium Crocosphaera, Limnology and Oceanography, 53, https ://doi.org/doi:10.4319/lo.2008.53.6.2472, 2008.

Fumenia, A., Moutin, T., Bonnet, S., Benavides, M., Petrenko, A., Helias Nunige, S., and Maes, C. : Excess nitrogen as a marker of intense dinitrogen fixation in the Western Tropical South Pacific Ocean : impact on the thermocline waters of the South Pacific, Biogeosciences Discussions, 2018, 1–33, 2018.

Galloway, J. N., Dentener, F. J., Capone, D. G., Boyer, E. W., Howarth, R. W., Seitzinger, S. P., Asner, G. P., Cleveland, C. C., Green, P., Holland, E. A., et al. : Nitrogen cycles : past, present, and future, Biogeochemistry, 70, 153–226, 2004.

Garcia, N., Raimbault, P., Gouze, E., and Sandroni, V. : Nitrogen fixation and primary production in western Mediterranean, Comptes Rendus Biologies, 329, 742–750, https ://doi.org/10.1016/j.crvi.2006.06.006, 2006.

Garcia, N., Raimbault, P., and Sandroni, V. : Seasonal nitrogen fixation and primary production in the Southwest Pacific : nanoplankton diazotrophy and transfer of nitrogen to picoplankton organisms, Marine Ecology Progress Series, 343, 25–33, 2007.

Glibert, P. M. and Bronk, D. : Release of dissolved organic nitrogen by marine diazotrophic cyanobacteria, *Trichodesmium* spp., Applied and Environmental Microbiology, 60, 3996–4000, 1994.

Glibert, P. M. and O'Neil, J. M. : Dissolved organic nitrogen release and amino-acid oxidase activity by *Trichodesmium*, in : Marine cyanobacteria, edited by ORSTOM, pp. 265–271, Bulletin de l'Institut Océanographoque, L. Charpy and T. Larkum, Paris, 1999.

Gregg, W. W., Casey, N. W., and McClain, C. R. : Recent trends in global ocean chlorophyll, Geophysical Research Letters, 32, 2005.

Griffiths, M. S., Gallon, J. R., and Chaplin, A. E. : The diurnal pattern of dinitrogen fixation by cyanobacteria in situ, New phytologist, 107, 649–657, 1987.

Großkopf, T., Mohr, W., Baustian, T., Schunck, H., Gill, D., Kuypers, M., Lavik, G., Schmitz, R. A., Wallace, G. W. R., and LaRoche, J. : Doubling of marine dinitrogen-fixation rates based on direct measurements, Nature, 488, 361–363, https ://doi.org/doi:10.1038/nature11338, 2012.

Gruber, N. : The dynamics of the marine nitrogen cycle and its influence on atmospheric CO_2 variations, in : The ocean carbon cycle and climate, pp. 97–148, Springer, 2004.

Gruber, N. : The marine nitrogen cycle : overview and challenges, Nitrogen in the marine environment, 2, 1–50, 2008.

Gruber, N. : Elusive marine nitrogen fixation, Proceedings of the National Academy of Sciences, https ://doi.org/10.1073/pnas.1603646113, 2016.

Gruber, N. and Sarmiento, J. : Global patterns of marine nitrogen fixation and denitrification, Glob Biogeochem Cycles, 11, 235–266, 1997.

Guidi, L., Calil, P. H., Duhamel, S., Björkman, K. M., Doney, S. C., Jackson, G. A., Li, B., Church, M. J., Tozzi, S., Kolber, Z. S., et al. : Does eddy-eddy interaction control surface phytoplankton distribution and carbon export in the North Pacific Subtropical Gyre ?, Journal of Geophysical Research : Biogeosciences, 117, 2012.

Guieu, C., Bonnet, S., Petrenko, A., Menkes, C., Chavagnac, V., Desboeufs, K., Maes, C., and Moutin, T. : Iron from a submarine source impacts the productive layer of the Western Tropical South Pacific (WTSP), Scientific reports, 8, 9075, 2018.

Guo, C. and Tester, P. A. : Toxic effect of the bloom-forming *Trichodesmium* sp. (cyanophyta) to the copepod *Acartia tonsa*, Natural Toxins, 2, 222–227, https ://doi.org/10.1002/nt.2620020411, 1994.

Hamersley, M. R., Lavik, G., Woebken, D., Rattray, J. E., Lam, P., Hopmans, E. C., Damsté, J. S. S., Krüger, S., Graco, M., and Gutiérrez, D. : Anaerobic ammonium oxidation in the Peruvian oxygen minimum zone, Limnology and Oceanography, 52, 923–933, 2007.

Hansell, D. A. and Carlson, C. A. : Biogeochemistry of total organic carbon and nitrogen in the Sargasso Sea : control by convective overturn, Deep Sea Research Part II : Topical Studies in Oceanography, 48, 1649–1667, 2001.

Hawser, S. P. and Codd, G. A. : The toxicity of *Trichodesmium* blooms from Caribbean waters, in : Marine Pelagic Cyanobacteria : Trichodesmium and other Diazotrophs, edited by Carpenter, E. J., Capone, D. G., and Rueter, J. G., pp. 319–329, Springer Netherlands, Dordrecht, 1992.

Hawser, S. P., O'Neil, J. M., Roman, M. R., and Codd, G. A. : Toxicity of blooms of the cyanobacterium *Trichodesmium* to zooplankton, Journal of Applied Phycology, 4, 79–86, https ://doi.org/10.1007/BF00003963, 1992.

Hegerl, G. C., Zwiers, F. W., Braconnot, P., Gillett, N. P., Luo, Y., Marengo Orsini, J., Nicholls, N., Penner, J. E., and Stott, P. A. : Understanding and attributing climate change, 2007.

Hewson, I., Govil, S. R., Capone, D. G., Carpenter, E. J., and Fuhrman, J. A. : Evidence of *Trichodesmium* viral lysis and potential significance for biogeochemical cycling in the oligotrophic ocean, Aquatic Microbial Ecology, 36, 1–8, https ://doi.org/10.3354/ame036001, 2004.

Hunt, B. P. V., Bonnet, S., Berthelot, H., Conroy, B. J., Foster, R., and Pagano, M. : Contribution and pathways of diazotroph derived nitrogen to zooplankton during the VAHINE mesocosm experiment in the oligotrophic New Caledonia lagoon, Biogeosciences, pp. 3131–3145, https ://doi.org/doi:10.5194/bg-13-3131-2016, 2016.

Hutchins, D. A., Fu, F. X., Zhang, Y., Warner, M. E., Feng, Y., Portune, K., Bernhardt, P. W., and Mulholland, M. R. : CO_2 control of *Trichodesmium* N_2 fixation, photosynthesis, growth rates, and elemental ratios : Implications for past, present, and future ocean biogeochemistry, Limnology and Oceanography, 52, 1293–1304, 2007.

Jackson, A. L., Inger, R., Parnell, A. C., and Bearhop, S. : Comparing isotopic niche widths among and within communities : SIBER–Stable Isotope Bayesian Ellipses in R, Journal of Animal Ecology, 80, 595–602, 2011.

Jickells, T. D., Buitenhuis, E., Altieri, K., Baker, A. R., Capone, D., Duce, R. A., Dentener, F., Fennel, K., Kanakidou, M., and LaRoche, J. : A reevaluation of the magnitude and impacts of anthropogenic atmospheric nitrogen inputs on the ocean, Global Biogeochemical Cycles, 31, 289–305, 2017.

Jouandet, M.-P., Trull, T. W., Guidi, L., Picheral, M., Ebersbach, F., Stemmann, L., and Blain, S. : Optical imaging of mesopelagic particles indicates deep carbon flux beneath a natural iron-fertilized bloom in the Southern Ocean, Limnology and Oceanography, 56, 1130–1140, 2011.

Kadoya, T., Osada, Y., and Takimoto, G. : IsoWeb : a Bayesian isotope mixing model for diet analysis of the whole food web, PloS one, 7, e41 057, 2012.

Kanakidou, M., Duce, R. A., Prospero, J. M., Baker, A. R., Benitez-Nelson, C., Dentener, F. J., Hunter, K. A., Liss, P. S., Mahowald, N., Okin, G. S., et al. : Atmospheric fluxes of organic N and P to the global ocean, Global Biogeochemical Cycles, 26, 2012.

Karl, D., Letelier, R., Tupas, L., Dore, J., Christian, J., and Hebel, D. : The role of nitrogen fixation in biogeochemical cycling in the subtropical North Pacific Ocean, Nature, 388, 533, 1997.

Karl, D., Michaels, A., Bergman, B., Capone, D., Carpenter, E., Letelier, R., Lipschultz, F., Paerl, H., Sigman, D., and Stal, L. : Dinitrogen fixation in the world's oceans, in : The Nitrogen Cycle at Regional to Global Scales, pp. 47–98, Springer, 2002.

Karl, D. M., Letelier, R., Hebel, D. V., Bird, D. F., and Winn, C. D. : Trichodesmium blooms and new nitrogen in the North Pacific gyre, Springer, 1992.

Karl, D. M., Bates, N. R., Emerson, S., Harrison, P. J., Jeandel, C., Liu, K. K., Marty, J. C., Michaels, A., Miquel, J. C., Neuer, S., Nojiri, Y., and Wong, C. S. : Temporal Studies of Biogeochemical Processes Determined from Ocean Time-Series Observations During the JGOFS Era, in : Ocean Biogeochemistry : The Role of the Ocean Carbon Cycle in Global Change, edited by Fasham, pp. 239–267, Springer, New York, 2003.

Karl, D. M., Church, M. J., Dore, J. E., Letelier, R. M., and Mahaffey, C. : Predictable and efficient carbon sequestration in the North Pacific Ocean supported by symbiotic nitrogen fixation, Proceedings of the National Academy of Sciences, 109, 1842–1849, https ://doi.org/10.1073/pnas.1120312109, 2012.

Klawonn, I., Lavik, G., Böning, P., Marchant, H., Dekaezemacker, J., Mohr, W., and Ploug, H. : Simple approach for the preparation of 15-15N2-enriched water for nitrogen fixation assessments : evaluation, application and recommendations, Frontiers in microbiology, 6, 769, 2015.

Kleiner, D. : Bacterial ammonium transport, FEMS Microbiology Letters, 32, 87–100, 1985.

Knapp, A. N., Sigman, D. M., and Lipschultz, F. : N isotopic composition of dissolved organic nitrogen and nitrate at the Bermuda Atlantic Time-series Study site, Global Biogeochemical Cycles, 19, 1–15, https ://doi.org/doi:10.1029/2004GB002320, 2005.

Knapp, A. N., Casciotti, K. L., Berelson, W. M., Prokopenko, M. G., and Capone, D. G. : Low rates of nitrogen fixation in eastern tropical South Pacific surface waters, Proceedings of the National Academy of Sciences, 113, 4398–4403, 2016.

Knapp, A. N., McCabe, K. M., Grosso, O., Leblond, N., Moutin, T., and Bonnet, S. : Distribution and rates of nitrogen fixation in the western tropical South Pacific Ocean constrained by nitrogen isotope budgets, Biogeosciences, 15, 2619–2628, https ://doi.org/10.5194/bg-15-2619-2018, 2018.

Koch, B. P., Witt, M., Engbrodt, R., Dittmar, T., and Kattner, G. : Molecular formulae of marine and terrigenous dissolved organic matter detected by electrospray ionization

Fourier transform ion cyclotron resonance mass spectrometry, Geochimica et Cosmochimica Acta, 69, 3299–3308, 2005.

Konno, U., Tsunogai, U., Komatsu, D. D., Daita, S., Nakagawa, F., Tsuda, A., Matsui, T., Eum, Y. J., and Suzuki, K. : Determination of total N_2 fixation rates in the ocean taking into account both the particulate and filtrate fractions, Biogeosciences, 7, 2369–2377, https ://doi.org/10.5194/bg-7-2369-2010, 2010.

Kujawinski, E. B., Freitas, M. A., Zang, X., Hatcher, P. G., Green-Church, K. B., and Jones, R. B. : The application of electrospray ionization mass spectrometry (ESI MS) to the structural characterization of natural organic matter, Organic geochemistry, 33, 171–180, 2002.

Labatut, M., Lacan, F., Pradoux, C., Chmeleff, J., Radic, A., Murray, J. W., Poitrasson, F., Johansen, A. M., and Thil, F. : Iron sources and dissolved-particulate interactions in the seawater of the Western Equatorial Pacific, iron isotope perspectives, Global Biogeochemical Cycles, https ://doi.org/doi:10.1002/2014GB004928, 2014.

Landolfi, A., Kähler, P., Koeve, W., and Oschlies, A. : Global Marine N2 Fixation Estimates : from Observations to Models, Frontiers in Microbiology, 9, 2112, 2018.

Landrum, J. P., Altabet, M. A., and Montoya, J. P. : Basin-scale distributions of stable nitrogen isotopes in the subtropical North Atlantic Ocean : Contribution of diazotroph nitrogen to particulate organic matter and mesozooplankton, Deep Sea Research Part I, 58, 615–625, 2011.

Larsen, T., Taylor, D. L., Leigh, M. B., and O'Brien, D. M. : Stable isotope fingerprinting : a novel method for identifying plant, fungal, or bacterial origins of amino acids, Ecology, 90, 3526–3535, 2009.

Le Quéré, C., Andrew, R. M., Friedlingstein, P., Sitch, S., Pongratz, J., Manning, A. C., Korsbakken, J. I., Peters, G. P., Canadell, J. G., Jackson, R. B., et al. : Global carbon budget 2017, Earth System Science Data, 10, 405, 2018.

Lenes, J. M. and Heil, C. A. : A historical analysis of the potential nutrient supply from the N2 fixing marine cyanobacterium Trichodesmium spp. to Karenia brevis blooms in the eastern Gulf of Mexico, Journal of Plankton Research, 32, 1421–1431, 2010.

Lenes, J. M., Darrow, B. P., Catrall, C., Heil, C. A., Callahan, L., Vargo, G. A., Byrne, R. H., Prospero, J. M., Bates, D. E., Fanning, K. A., and Walsh, J. J. : Iron fertilization and the *Trichodesmium* response on the West Florida shelf, Limnology and Oceanography, 46, 1261–1277, 2001.

Letelier, R. M. and Karl, D. M. : Role of *Trichodesmium* spp. in the productivity of the subtropical north Pacific Ocean, Marine Ecology Progress Series, 133, 263–273, 1996.

Levitan, O., Rosenberg, G., Šetlík, I., Šetlíkova, E., Gtigel, J., Klepetar, J., Prášil, O., and Berman-Frank, I. : Elevated CO2 enhances nitrogen fixation and growth in the marine cyanobacterium Trichodesmium, Global Change Biology, 13, 1–8, 2007.

Loescher, C. R., Großkopf, T., Desai, F. D., Gill, D., Schunck, H., Croot, P. L., Schlosser, C., Neulinger, S. C., Pinnow, N., Lavik, G., et al. : Facets of diazotrophy in the oxygen minimum zone waters off Peru, The ISME journal, 8, 2180, 2014.

Loick-Wilde, N., Dutz, J., Miltner, A., Gehre, M., Montoya, J. P., and Voss, M. : Incorporation of nitrogen from N2 fixation into amino acids of zooplankton, Limnology and Oceanography, 57, 199–210, https ://doi.org/10.4319/lo.2012.57.1.0199, 2012.

Longhurst, A., Sathyendranath, S., Platt, T., and Caverhill, C. : An estimate of global primary production in the ocean from satellite radiometer data, J. Plankton Res., 17, 1245–1271, 1995.

Luo, Y., Doney, S., Anderson, L., Benavides, M., Berman-Frank, I., Bode, A., Bonnet, S., Boström, K. H., Böttjer, D., Capone, D., et al. : Database of Diazotrophs in Global Ocean : Abundance, Biomass, and Nitrogen Fixation Rates, Earth System Science Data, 4, 2012.

Luo, Y.-W., Lima, I. D., Karl, D. M., Deutsch, C. A., and Doney, S. C. : Data-based assessment of environmental controls on global marine nitrogen fixation, Biogeosciences, 11, 691–708, 2014.

Mahaffey, C., Williams, R. G., Wolff, G. A., Mahowald, N. M., Anderson, W., and Woodward, M. : Biogeochemical signatures of nitrogen fixation in the eastern North Atlantic, Geophysical Research Letters, 30, 33–36, https ://doi.org/10.1029/2002GL016542, 2003.

McClain, C. R., Signorini, S. R., and Christian, J. R. : Subtropical gyre variability observed by ocean-color satellites, Deep Sea Research Part II : Topical Studies in Oceanography, 51, 281–301, 2004.

Menzel, D. and Ryther, J. : Nutrients limiting the production of phytoplankton in the Sargasso Sea, with special reference to iron, Deep Sea Research (1953), 7, 276–281, 1961.

Messer, L. F., Mahaffey, C., M Robinson, C., Jeffries, T. C., Baker, K. G., Bibiloni Isaksson, J., Ostrowski, M., Doblin, M. A., Brown, M. V., and Seymour, J. R. : High levels of heterogeneity in diazotroph diversity and activity within a putative hotspot for marine nitrogen fixation, ISME J, https ://doi.org/10.1038/ismej.2015.205, 2015.

Mills, M. M., Ridame, C., Davey, M., La Roche, J., and Geider, J. G. : Iron and phosphorus co-limit nitrogen fixation in the eastern tropical North Atlantic, Nature, 429, 292–294, 2004.

Mohr, W., Großkopf, T., Wallace, D. W. R., and LaRoche, J. : Methodological underestimation of oceanic nitrogen fixation rates, PLoS ONE, 5, 1–7, https ://doi.org/10.1371/journal.pone.0012583, 2010.

Moisander, P. H., Beinart, R. A., Hewson, I., White, A. E., Johnson, K. S., Carlson, C. A., Montoya, J. P., and Zehr, J. P. : Unicellular cyanobacterial distributions broaden the oceanic N2 fixation domain, Science, 327, 1512–1514, 2010.

Moisander, P. H., Benavides, M., Bonnet, S., Berman-Frank, I., White, A. E., and Riemann, L. : Chasing after non-cyanobacterial nitrogen fixation in marine pelagic environments, Frontiers in microbiology, 8, 1736, 2017.

Mompeán, C., Bode, A., Benítez-Barrios, V. M., Domínguez-Yanes, J. F., Escánez, J., and Fraile-Nuez, E. : Spatial patterns of plankton biomass and stable isotopes reflect the influence of the nitrogen-fixer *Trichodesmium* along the subtropical North Atlantic, Journal of Plankton Research, 35, 513–525, https ://doi.org/10.1093/plankt/fbt011, 2013.

Montoya, J. P., Voss, M., Kahler, P., and Capone, D. G. : A simple, high-precision, high-sensitivity tracer assay for N_2 fixation, Applied and Environmental Microbiology, 62, 986–993, 1996.

Montoya, J. P., Carpenter, E. J., and Capone, D. G. : Nitrogen fixation and nitrogen isotope abundances in zooplankton of the oligotrophic North Atlantic Ocean, Limnology and Oceanography, 47, 1617–1628, 2002.

Montoya, J. P., Holl, C. M., Zehr, J. P., Hansen, A., Villareal, T. A., and Capone, D. G. : High rates of N2 fixation by unicellular diazotrophs in the oligotrophic Pacific Ocean, Nature, 430, 1027, 2004.

Moore, C., Mills, M., Arrigo, K., Berman-Frank, I., Bopp, L., Boyd, P., Galbraith, E., Geider, R., Guieu, C., Jaccard, S., et al. : Processes and patterns of oceanic nutrient limitation, Nature Geoscience, 6, 701, 2013.

Mouriño-Carballido, B., Graña Bode Antonio , Varela Manuel , Domínguez J. Francisco , Escànez José , de Armas Demetrio , Marañón EmilioRocío, G., R. F. A., Fernàndez, A., Bode, A., Varela, M., Domínguez, J. F., Escànez, J., Armas, D., and Marañón, E. : Importance of N2 fixation vs. nitrate eddy diffusion along a latitudinal transect in the Atlantic Ocean, Limnology and Oceanography, 56, 999–1007, 2011.

Moutin, T. and Prieur, L. : Influence of anticyclonic eddies on the Biogeochemistry from the Oligotrophic to the Ultraoligotrophic Mediterranean (BOUM cruise), Biogeosciences, 9, 3827–3855, https ://doi.org/10.5194/bg-9-3827-2012, 2012.

Moutin, T., Thingstad, T. F., Van Wambeke, F., Marie, D., Slawyk, G., Raimbault, P., and Claustre, H. : Does competition for nanomolar phosphate supply explain the predominance of the cyanobacterium Synechococcus ?, Limnology and Oceanography, 47, 1562–1567, 2002.

Moutin, T., Van Den Broeck, N., Beker, B., Dupouy, C., Rimmelin, P., and Le Bouteiller, A. : Phosphate availability controls Trichodesmium spp. biomass in the SW Pacific Ocean, Marine Ecology Progress Series, 297, 15–21, 2005.

Moutin, T., Karl, D. M., Duhamel, S., Rimmelin, P., Raimbault, P., Van Mooy, B. A. S., and Claustre, H. : Phosphate availability and the ultimate control of new nitrogen input by nitrogen fixation in the tropical Pacific Ocean, Biogeosciences, 5, 95–109, 2008.

Moutin, T., Wagener, T., Caffin, M., Fumenia, A., Gimenez, A., Baklouti, M., Bouruet-Aubertot, P., Pujo-Pay, M., Leblanc, K., Lefevre, D., Helias Nunige, S., Leblond, N., Grosso, O., and de Verneil, A. : Nutrient availability and the ultimate control of the biological carbon pump in the western tropical South Pacific Ocean, Biogeosciences, 15, 2961–2989, https ://doi.org/10.5194/bg-15-2961-2018, 2018.

Mulholland, M., Bronk, D. A., and Capone, D. G. : Dinitrogen fixation and release of ammonium and dissolved organic nitrogen by *Trichodesmium* IMS101, Aquatic Microbial Ecology, 37, 85–94, 2004a.

Mulholland, M. R. : The fate of nitrogen fixed by diazotrophs in the ocean, Biogeosciences, 4, 37–51, https ://doi.org/10.5194/bg-4-37-2007, 2007.

Mulholland, M. R. and Bernhardt, P. W. : The effect of growth rate, phosphorus concentration, and temperature on N_2 fixation, carbon fixation, and nitrogen release in continuous cultures of *Trichodesmium* IMS101, Limnology & Oceanography, 50, 839–849, 2005.

Mulholland, M. R. and Capone, D. G. : The nitrogen physiology of the marine N_2-fixing cyanobacteria *Trichodesmium* spp., Trends in Plant Science, 5, 148–153, 2000.

Mulholland, M. R., Heil, C. A., Bronk, D. A., O'Neil, J. M., and Bernhardt, P. W. : Does nitrogen regeneration from the N_2 fixing cyanobacteria, *Trichodesmium* spp. fuel Karenia brevis blooms in the Gulf of Mexico ?, Harmful Algae 2002, pp. 47–49, 2004b.

Mulholland, M. R., Bernhardt, P. W., Heil, C. A., Bronk, D. A., and O'Neil, J. M. : Nitrogen fixation and release of fixed nitrogen by Trichodesmium spp. in the Gulf of Mexico, Limnology and Oceanography, 51, 1762–1776, 2006.

Murnane, R., Sarmiento, J., and Le Quéré, C. : Spatial distribution of air-sea CO_2 fluxes and the interhemispheric transport of carbon by the oceans, Global Biogeochemical Cycles, 13, 287–305, 1999.

Nelson, D. M., Tréguer, P., Brzezinski, M. A., Leynaert, A., and Quéguiner, B. : Production and dissolution of biogenic silica in the ocean : revised global estimates, comparison with regional data and relationship to biogenic sedimentation, Global Biogeochemical Cycles, 9, 359–372, 1995.

Ohki, K. : A possible role of temperate phage in the regulation of *Trichodesmium*, Bull. Inst. Oceanogr. Monaco, 19, 235–256, 1999.

Ohki, K., Kamiya, M., Honda, D., Kumazawa, S., and Ho, K. K. : Morphological and phylgenetic studies on unicellular diazotrophic cynaobacteria isolated from the coastal waters around Singapore, Journal of phycology, 44, 142–151, 2008.

Ohlendieck, U., Stuhr, A., and Siegmund, H. : Nitrogen fixation by diazotrophic cyanobacteria in the Baltic Sea and transfer of the newly fixed nitrogen to picoplankton organisms, Journal of Marine Systems, 25, 213–219, 2000.

Olson, R. J., Popp, B. N., Graham, B. S., López-Ibarra, G. A., Galván-Magaña, F., Lennert-Cody, C. E., Bocanegra-Castillo, N., Wallsgrove, N. J., Gier, E., Alatorre-Ramírez, V., et al. : Food-web inferences of stable isotope spatial patterns in copepods and yellowfin tuna in the pelagic eastern Pacific Ocean, Progress in Oceanography, 86, 124–138, 2010.

O'Neil, J. and Roman, M. R. : Grazers and Associated Organisms of Trichodesmium, in : Marine Pelagic Cyanobacteria : Trichodesmium and other Diazotrophs, edited by Carpenter Capone, D.G., and Rueter, J.G., E. J., NATO ASI Series, Springer Netherlands, 1992.

O'Neil, J. M. : Grazer interactions with nitrogen-fixing marine Cyanobacteria : adaptation for N-acquisition ?, Bull. Inst. Oceanogr. Monaco, 19, 293–317, 1999.

O'Neil, J. M., Metzler, P., and Glibert, P. M. : Ingestion of 15N2-labelled Trichodesmium, and ammonium regeneration by the pelagic harpacticoid copepod Macrosetella gracilis, Marine Biology, 125, 89–96, 1996.

Parrish, C. C. : Lipids in marine ecosystems, ISRN Oceanography, 2013, 2013.

Polovina, J. J., Howell, E. A., and Abecassis, M. : Ocean's least productive waters are expanding, Geophysical Research Letters, 35, 2008.

Radic, A., Lacan, F., and Murray, J. W. : Iron isotopes in the seawater of the equatorial Pacific Ocean : New constraints for the oceanic iron cycle, Earth and Planetary Science Letters, 306, 1–10, 2011.

Raimbault, P. and Garcia, N. : Evidence for efficient regenerated production and dinitrogen fixation in nitrogen-deficient waters of the South Pacific Ocean : impact on new and export production estimates, Biogeosciences, 5, 323–338, 2008.

Raupach, M. R., Marland, G., Ciais, P., Le Quéré, C., Canadell, J. G., Klepper, G., and Field, C. B. : Global and regional drivers of accelerating CO_2 emissions, Proceedings of the National Academy of Sciences, 104, 10 288–10 293, 2007.

Rembauville, M., Salter, I., Leblond, N., Gueneugues, A., and Blain, S. : Export fluxes in a naturally iron-fertilized area of the Southern Ocean–Part 1 : Seasonal dynamics of particulate organic carbon export from a moored sediment trap, Biogeosciences, 12, 3153–3170, 2015.

Robidart, J. C., Church, M. J., Ryan, J. P., Ascani, F., Wilson, S. T., Bombar, D., Marin III, R., Richards, K. J., Karl, D. M., Scholin, C. A., et al. : Ecogenomic sensor reveals controls on N2-fixing microorganisms in the North Pacific Ocean, The ISME journal, 8, 1175, 2014.

Robison, B. H. : Deep pelagic biology, Journal of Experimental Marine Biology and Ecology, 300, 253–272, 2004.

Rodier, M. and Le Borgne, R. : Population dynamics and environmental conditions affecting Trichodesmium spp.(filamentous cyanobacteria) blooms in the south–west lagoon of New Caledonia, J Exp Mar Bio Ecol, 358, 20–32, 2008.

Rousselet, L., De Verneil, A., Doglioli, A. M., Petrenko, A. A., Duhamel, S., Maes, C., and Blanke, B. : Large-to submesoscale surface circulation and its implications on biogeochemical/biological horizontal distributions during the OUTPACE cruise (southwest Pacific), Biogeosciences, 15, 2411, 2018.

Sabine, C. L., Feely, R. A., Gruber, N., Key, R. M., Lee, K., Bullister, J. L., Wanninkhof, R., Wong, C., Wallace, D. W., Tilbrook, B., et al. : The oceanic sink for anthropogenic CO_2, science, 305, 367–371, 2004.

Sandh, G., Xu, L., and Bergman, B. : Diazocyte development in the marine diazotrophic cyanobacterium Trichodesmium, Microbiology, 158, 345–352, https ://doi.org/10.1099/mic.0.051268-0, 2012.

Sarmiento, J. L. and Gruber, N. : Ocean biogeochemical dynamics, Princeton University Press, 2004.

Savoye, N., Trull, T., Jacquet, S., Navez, J., and Dehairs, F. : 234Th-based export fluxes during a natural iron fertilization experiment in the Southern Ocean (KEOPS), Deep Sea Research Part II : Topical Studies in Oceanography, 55, 841–855, 2008.

Scharek, R., Latasa, M., Karl, D. M., and Bidigare, R. R. : Temporal variations in diatom abundance and downward vertical flux in the oligotrophic North Pacific gyre, Deep Sea Research Part I : Oceanographic Research Papers, 46, 1051–1075, 1999a.

Scharek, R., Tupas, L. M., and Karl, D. M. : Diatom fluxes to the deep sea in the oligotrophic North Pacific gyre at Station ALOHA, Marine Ecology Progress Series, 182, 55–67, https ://doi.org/10.3354/meps182055, 1999b.

Shiozaki, T., Kodama, T., and Furuya, K. : Large-scale impact of the island mass effect through nitrogen fixation in the western South Pacific Ocean, Geophysical Research Letters, 41, 2907–2913, 2014.

Short, S. M., Jenkins, B. D., and Zehr, J. P. : Spatial and temporal distribution of two diazotrophic bacteria in the Chesapeake Bay, Applied and environmental microbiology, 70, 2186–2192, 2004.

Sipler, R. E., Bronk, D. A., Seitzinger, S. P., Lauck, R. J., McGuinness, L. R., Kirkpatrick, G. J., Heil, C. A., Kerkhof, L. J., and Schofield, O. M. : Trichodesmium-derived dissolved organic matter is a source of nitrogen capable of supporting the growth of toxic red tide Karenia brevis, Marine Ecology Progress Series, 483, 31–45, 2013.

Slawyk, G. and Raimbault, P. : Simple procedure for simultaneous recovery of dissolved inorganic and organic nitrogen in 15N-tracer experiments and improving the isotopic mass balance, Marine Ecology Progress Series, 124, 289–299, https ://doi.org/10.3354/meps124289, 1995.

Sohm, J. A., Webb, E. A., and Capone, D. G. : Emerging patterns of marine nitrogen fixation, Nature Reviews Microbiology, 9, 499, 2011.

Sommer, F., Hansen, T., and Sommer, U. : Transfer of diazotrophic nitrogen to mesozooplankton in Kiel Fjord, Western Baltic Sea : a mesocosm study, Marine Ecology Progress Series, 324, 105–112, 2006.

Spungin, D., Pfreundt, U., Berthelot, H., Bonnet, S., AlRoumi, D., Natale, F., Hess, H. R., Bidle, K. D., and Berman-Frank, I. : Mechanisms of Trichodesmium bloom demise within the New Caledonia Lagoon during the VAHINE mesocosm experiment, Biogeosciences, 13, 4187–4203, https ://doi.org/,doi:10.5194/bg-13-4187-2016, 2016.

Stal, L. J., Albertano, P., Bergman, B., von Bröckel, K., Gallon, J. R., Hayes, P. K., Sivonen, K., and Walsby, A. E. : BASIC : Baltic Sea cyanobacteria. An investigation of the structure and dynamics of water blooms of cyanobacteria in the Baltic Sea—responses to a changing environment, Continental Shelf Research, 23, 1695–1714, 2003.

Steinberg, D. K. and Landry, M. R. : Zooplankton and the ocean carbon cycle, Annual Review of Marine Science, 9, 413–444, 2017.

Stenegren, M., Caputo, A., Berg, C., Bonnet, S., and Foster, R. A. : Distribution and drivers of symbiotic and free-living diazotrophic cyanobacteria in the western tropical South Pacific, Biogeosciences, 15, 1559–1578, https ://doi.org/10.5194/bg-15-1559-2018, 2018.

Stramma, L., Peterson, R. G., and Tomczak, M. : The south Pacific current, Journal of Physical Oceanography, 25, 77–91, 1995.

Subramaniam, A., Yager, P., Carpenter, E. J., Mahaffey, C., Björkman, K. M., Cooley, S., Kustka, A. B., Montoya, J. P., Sanudo-Wilhelmy, S., Shipe, R., and Capone, D. G. : Amazon River enhances diazotrophy and carbon sequestration in the tropical North Atlantic Ocean, Pnas, 105, 10 460–10 465, https ://doi.org/10.1073/pnas.0710279105, 2008.

Takahashi, T., Sutherland, S. C., Sweeney, C., Poisson, A., Metzl, N., Tilbrook, B., Bates, N., Wanninkhof, R., Feely, R. A., Sabine, C., et al. : Global sea-air CO_2 flux based on climatological surface ocean pCO_2, and seasonal biological and temperature effects, Deep Sea Research Part II : Topical Studies in Oceanography, 49, 1601–1622, 2002.

Tomczak, M. and Godfrey, J. S. : Regional oceanography : an introduction, Elsevier, 2013.

Tyrrell, T. : The relative influences of nitrogen and phosphorus on oceanic primary production, Nature, 400, 525, 1999.

Van Den Broeck, N., Moutin, T., Rodier, M., and Le Bouteiller, A. : Seasonal variations of phosphate availability in the SW Pacific Ocean near New Caledonia, Marine Ecology Progress Series, 268, 1–12, 2004.

Van Dommelen, A., Keijers, V., Vanderleyden, J., and de Zamaroczy, M. : (Methyl) ammonium transport in the nitrogen-fixing bacterium Azospirillum brasilense, Journal of bacteriology, 180, 2652–2659, 1998.

Van Wambeke, F., Gimenez, A., Duhamel, S., Dupouy, C., Lefevre, D., Pujo-Pay, M., and Moutin, T. : Dynamics and controls of heterotrophic prokaryotic production in the western tropical South Pacific Ocean : links with diazotrophic and photosynthetic activity, Biogeosciences, 15, 2669–2689, https ://doi.org/10.5194/bg-15-2669-2018, 2018.

Villareal, T. A. : Widespread occurrence of the Hemiaulus-cyanobacterial symbiosis in the southwest North Atlantic Ocean, Bulletin of Marine Science, 54, 1–7, 1994.

Voss, M., Bange, H. W., Dippner, J. W., Middelburg, J. J., Montoya, J. P., and Ward, B. : The marine nitrogen cycle : recent discoveries, uncertainties and the potential relevance of climate change, Phil. Trans. R. Soc. B, 368, 20130 121, 2013.

Walsby, A. E. : The gas vesicles and buoyancy of *Trichodesmium*. In Marine pelagic cyanobacteria : Trichodesmium and other diazotrophs, Springer Netherlands, pp. 141–161, 1992.

Wannicke, N., Korth, F., Liskow, I., and Voss, M. : Incorporation of diazotrophic fixed N_2 by mesozooplankton - Case studies in the southern Baltic Sea, Journal of Marine Systems, 117-118, 1–13, 2013.

Webb, D. J. : Evidence for shallow zonal jets in the South Equatorial Current region of the southwest Pacific, Journal of Physical Oceanography, 30, 706–720, 2000.

Westberry, T. K. and Siegel, D. A. : Spatial and temporal distribution of Trichodesmium blooms in the world's oceans, Global Biogeochemical Cycles, 20, 2006.

White, A. E., Spitz, Y. H., and Letelier, R. M. : Modeling carbohydrate ballasting by Trichodesmium spp., Marine Ecology Progress Series, 323, 35–45, 2006.

White, A. E., Foster, R. A., Benitez-Nelson, C. R., Masqué, P., Verdeny, E., Popp, B. N., Arthur, K. E., and Prahl, F. G. : Nitrogen fixation in the Gulf of California and the Eastern Tropical North Pacific, Progess in Oceanography, 109, 1–17, https ://doi.org/doi:10.1016/j.pocean.2012.09.002,2012, 2012.

Wilson, S. T., Böttjer, D., Church, M. J., and Karl, D. M. : Comparative assessment of nitrogen fixation methodologies conducted in the oligotrophic Noth Pacific Ocean, Applied and Environmental Microbiology, 78, 6516–6523, https ://doi.org/10.1128/aem.01146-12, 2012.

Zehr, J. and Turner, P. : 14 Nitrogen Fixation : Nitrogenase Genes and Gene Expression, Marine microbiology, 30, 271, 2001.

Zehr, J. P. : Nitrogen fixation by marine cyanobacteria, Trends in microbiology, 19, 162–173, 2011.

Zehr, J. P., Mellon, M. T., and Zani, S. : New nitrogen-fixing microorganisms detected in oligotrophic oceans by amplification of nitrogenase (nifH) genes, Applied and environmental microbiology, 64, 3444–3450, 1998.

Zehr, J. P., Bench, S. R., Carter, B. J., Hewson, I., Niazi, F., Shi, T., Tripp, H. J., and Affourtit, J. P. : Globally distributed uncultivated oceanic N2-fixing cyanobacteria lack oxygenic photosystem II, science, 322, 1110–1112, 2008.

Annexe A

Contribution aux publications scientifiques

Les articles présentés dans le chapitre 2 de cette thèse (Bonnet et al., 2017 ; Bonnet et al., 2018) ont été écrit par Sophie Bonnet avec la contribution des co-auteurs. Je suis associé à ces articles en tant que second auteur. L'article de Bonnet et al. (2017) présente une synthèse des taux de fixation de N_2 mesurés dans l'océan Pacifique tropical sud-ouest aux cours de 5 campagnes océanographiques, dont la campagne OUTPACE à laquelle j'ai participé. Dans le cadre de cette campagne, j'ai participé à l'échantillonnage, aux marquages isotopiques à bord, et j'ai réalisé l'analyse des échantillons par spectrométrie de masse (EA-IRMS) qui ont permis de mesurer les taux de fixation de N_2. J'ai contribué, comme chacun des co-auteurs à la rédaction de l'article. L'article de Bonnet et al. (2018) se concentre sur les données de la campagne OUTPACE, en reprenant les données de fixation de N_2 publiées dans le premier article. En plus d'avoir participé à l'échantillonnage et à l'analyse des échantillons de fixation de N_2, j'ai réalisé les comptages par microscopie (microscopie par épifluorescence), participé au tri des cellules par cytométrie en flux et réalisé l'analyse des échantillons par spectrométrie de masse des ions secondaires (nanoSIMS) qui ont permis de quantifier les taux de fixation de N_2 spécifique des diazotrophes. J'ai participé à l'analyse des données et à la rédaction de l'article.

Le chapitre 3 présente l'article de Caffin et al. (2018b) dont je suis premier auteur. J'ai écrit cet article avec la contribution des co-auteurs. J'ai participé à l'échantillonnage, et j'ai réalisé l'analyse des échantillons par EA-IRMS qui ont permis de mesurer les taux de fixation de N_2. J'ai contribué à l'analyse des données qui ont permis de quantifier les apports de nitrate dans la couche euphotique par diffusion verticale turbulente. J'ai analysé les données de dépôts atmosphériques (données acquises et échantillons analysés par Cécile Guieu, Laboratoire d'Océanographie de Villefrance-sur-Mer (LOV)), de fixation de N_2, d'apports de nitrate (données acquises par avec Pascale Bouruet-Aubertot, Laboratoire d'Océanographie et du Climat : Expérimentations et Approches Numériques (LOCEAN)), d'export de matière particulaire (données acquises par Nathalie Leblond, Cellule pièges de l'Institut National des Sciences de l'Univers (INSU)) et de biologie moléculaire au

sein des pièges (échantillons analysés par Rachel Foster, Stockholm University), qui ont permis d'établir les bilans d'azote publiés dans cet article. La quantification des apports de nitrate dans la couche euphotique par diffusion verticale turbulente présentée dans ce chapitre a été réalisée en collaboration avec Pascale Bouruet-Aubertot. Une étude des flux biogéochimiques par diffusion turbulente a été réalisée dans l'article de Bouruet-Aubertot et al. (2018) dans lequel je suis impliqué comme co-auteur pour avoir travaillé sur ces flux.

Le chapitre 4 présente l'article de Caffin et al. (2018a) dont je suis premier auteur. J'ai écrit cet article avec la contribution des co-auteurs. J'ai participé à l'échantillonnage, et aux expériences in-situ publiés dans cet article. J'ai analysé les échantillons permettant de quantifier le relargage de l'azote fixé dans le compartiment dissous (expérience de diffusion et analyses EA-IRMS), et j'ai réalisé l'analyse des échantillons par EA-IRMS qui ont permis de mesurer les taux de fixation de N_2. J'ai réalisé les comptages des cellules par microscopie et par cytométrie en flux, mesuré les cellules diazotrophes par microscopie, participé au tri des cellules par cytométrie en flux et réalisé l'analyse des échantillons par nanoSIMS, permettant de quantifier le transfert d'azote fixé vers les organismes planctoniques non-diazotrophes.

En complément, j'ai réalisé à bord l'échantillonnage pour la mesure de l'alcalinité et du carbone inorganique dissous publiées dans l'article de Wagener et al. (2018), j'ai réalisé l'échantillonnage pour la mesure de la salinité permettant la calibration de la CTD. Les données d'alcalinité et de carbone inorganique dissous en surface ont été utilisées dans l'article de synthèse de Moutin et al. (2018) auquel j'ai participé. Enfin, j'ai réalisé l'échantillonnage permettant de quantifier le rapport isotopique des nitrates et de l'azote organique dissous (Angela Knapp, Florida State University (FSU)). Lors de la campagne OUTPACE je me suis impliqué dans les manœuvres de déploiement et de récupération des pièges à particules et des lignes de production.

Enfin, j'ai participé à des expériences d'enrichissement en éléments nutritifs en conditions ultra-propres durant la campagne OUTPACE (données analysées dans le cadre de mon stage de Master 2). Dans le cadre de ces expériences, j'ai quantifié l'abondance des cellules planctoniques par cytométrie en flux et mesuré les concentrations en chlorophylle *a*. J'ai également participé dans le cadre d'une expérience 'haute-fréquence', à l'échantillonnage pour les paramètres suivant : abondance d'organismes phytoplanctoniques et de bactéries par cytométrie, concentrations en éléments nutritifs et abondance des organismes diazotrophes par microscopie. J'ai réalisé les comptages de diazotrophes par microscopie. L'ensemble de ces données sont en cours d'analyse et feront probablement l'objet de publications ultérieures.

Annexe B

Article supplémentaire n°1

Nutrient availability and the ultimate control of the biological carbon pump in the western tropical South Pacific Ocean

Thierry Moutin[1], Thibaut Wagener[1], Mathieu Caffin[1], Alain Fumenia[1], Audrey Gimenez[1], Melika Baklouti[1], Pascale Bouruet-Aubertot[2], Mireille Pujo-Pay[3], Karine Leblanc[1], Dominique Lefevre[1], Sandra Helias Nunige[1], Nathalie Leblond[4], Olivier Grosso[1], and Alain de Verneil[1 5]

[1]Aix Marseille Univ., CNRS, Université de Toulon, IRD, OSU Pythéas, Mediterranean Institute of Oceanography (MIO), UM 110, 13288, Marseille, France
[2]Sorbonne Universités – UPMC Univ. Paris 06 – LOCEAN, BP100, 4 place Jussieu, 75252 Paris CEDEX 05, France
[3]Laboratoire d'Océanographie Microbienne – UMR 7321, CNRS – Sorbonne Universités, UPMC Univ Paris 06, Observatoire Océanologique, 66650 Banyuls-sur-mer, France
[4]Observatoire Océanologique de Villefranche, Laboratoire d'Océanographie de Villefranche, UMR 7093, Villefranche-sur-mer, France
[5]The Center for Prototype Climate Modeling, New York University in Abu Dhabi, Abu Dhabi, UAE

Publié dans *Biogeoscience* en Mai 2018

Biogeosciences, 15, 2961–2989, 2018
https://doi.org/10.5194/bg-15-2961-2018

Biogeosciences Open Access EGU

Nutrient availability and the ultimate control of the biological carbon pump in the western tropical South Pacific Ocean

Thierry Moutin[1], Thibaut Wagener[1], Mathieu Caffin[1], Alain Fumenia[1], Audrey Gimenez[1], Melika Baklouti[1], Pascale Bouruet-Aubertot[2], Mireille Pujo-Pay[3], Karine Leblanc[1], Dominique Lefevre[1], Sandra Helias Nunige[1], Nathalie Leblond[4], Olivier Grosso[1], and Alain de Verneil[1,5]

[1]Aix Marseille Univ., CNRS, Université de Toulon, IRD, OSU Pythéas, Mediterranean Institute of Oceanography (MIO), UM 110, 13288, Marseille, France
[2]Sorbonne Universités – UPMC Univ. Paris 06 – LOCEAN, BP100, 4 place Jussieu, 75252 Paris CEDEX 05, France
[3]Laboratoire d'Océanographie Microbienne – UMR 7321, CNRS – Sorbonne Universités, UPMC Univ Paris 06, Observatoire Océanologique, 66650 Banyuls-sur-mer, France
[4]Observatoire Océanologique de Villefranche, Laboratoire d'Océanographie de Villefranche, UMR 7093, Villefranche-sur-mer, France
[5]The Center for Prototype Climate Modeling, New York University in Abu Dhabi, Abu Dhabi, UAE

Correspondence: Thierry Moutin (thierry.moutin@mio.osupytheas.fr)

Received: 29 December 2017 – Discussion started: 10 January 2018
Revised: 23 March 2018 – Accepted: 24 April 2018 – Published: 16 May 2018

Abstract. Surface waters (0–200 m) of the western tropical South Pacific (WTSP) were sampled along a longitudinal 4000 km transect (OUTPACE cruise, DOI: 10.17600/15000900) during the austral summer (stratified) period (18 February to 3 April 2015) between the Melanesian Archipelago (MA) and the western part of the SP gyre (WGY). Two distinct areas were considered for the MA, the western MA (WMA), and the eastern MA (EMA). The main carbon (C), nitrogen (N), and phosphorus (P) pools and fluxes provide a basis for the characterization of the expected trend from oligotrophy to ultra-oligotrophy, and the building of first-order budgets at the daily and seasonal timescales (using climatology). Sea surface chlorophyll *a* well reflected the expected oligotrophic gradient with higher values obtained at WMA, lower values at WGY, and intermediate values at EMA. As expected, the euphotic zone depth, the deep chlorophyll maximum, and nitracline depth deepen from west to east. Nevertheless, phosphaclines and nitraclines did not match. The decoupling between phosphacline and nitracline depths in the MA allows for excess P to be locally provided in the upper water by winter mixing. We found a significant biological "soft tissue" carbon pump in the MA sustained almost exclusively by dinitrogen (N_2) fixation and essentially controlled by phosphate availability in this iron-rich environment. The MA appears to be a net sink for atmospheric CO_2, while the WGY is in quasi-steady state. We suggest that the necessary excess P, allowing the success of nitrogen fixers and subsequent carbon production and export, is mainly brought to the upper surface by local deep winter convection at an annual timescale rather than by surface circulation. While the origin of the decoupling between phosphacline and nitracline remains uncertain, the direct link between local P upper water enrichment, N_2 fixation, and organic carbon production and export, offers a possible shorter timescale than previously thought between N input by N_2 fixation and carbon export. The low iron availability in the SP gyre and P availability in the MA during the stratified period may appear as the ultimate control of N input by N_2 fixation. Because of the huge volume of water to consider, and because the SP Ocean is the place of intense denitrification in the east (N sink) and N_2 fixation in the west (N source), precise seasonal C, N, P, and iron (Fe) budgets would be of prime interest to understand the efficiency, at the present time and in the future, of the oceanic biological carbon pump.

Published by Copernicus Publications on behalf of the European Geosciences Union.

1 Introduction

The oceanic biological carbon pump corresponds to the transfer of carbon from the upper surface to the ocean interior by biological processes, greatly influencing atmospheric CO_2 concentration and therefore the earth's climate. It is a highly ranked priority in current research in oceanography (Burd et al., 2016). Two biological pumps have been defined (Volk and Hoffert, 1985), the "soft tissue" and "carbonate" pumps associated with organic matter or calcium carbonate processes (e.g., production, export, remineralization or dissolution). The "soft tissue" pump (see Moutin et al., 2017a; their Fig. 1), considering both its intensity and shorter timescales, is by far the larger contributor to the dissolved inorganic carbon gradient between the upper surface and the deep sea. Following climate alteration, the biological "soft tissue" pump begins to deviate from its equilibrium condition, meaning that its influence on atmospheric CO_2 change may occur at timescales shorter than previously thought (Sarmiento and Gruber, 2006). Because the strength of the biological carbon pump depends on nutrient availability in the upper ocean, and more particularly on N availability (Falkowski et al., 1998; Tyrell, 1999; Moore et al., 2013), which is in the long term regulated by external input by N_2 fixation and internal denitrification (Grüber and Sarmiento, 1997; Codispoti et al., 2001; Deutsch et al., 2001, 2007; Brandes and Devol, 2002; Grüber, 2004; Mahaffey et al., 2005; Codispoti, 2007; Capone and Knapp, 2007; Moutin et al., 2008; Deutsch and Weber, 2012; Landolfi et al., 2013; Jickells et al., 2017), quantitative evaluation of the regulation, interdependence, and patterns of change of these two processes require attention at the present time. It has been suggested earlier that N_2 fixation may play a large part in changing atmospheric CO_2 inventories (McElroy, 1983), but at long timescales and taking into account major differences in Aeolian iron input (Falkowski, 1997; Broecker and Henderson, 1998). Because N_2 fixation may ultimately be controlled by iron availability, and because dust delivery to the ocean is climate sensitive, there may be inextricably linked feedback mechanisms that regulate N_2 fixation, atmospheric CO_2 concentrations, and dust deposition over relatively long periods (Michaels et al., 2001; Karl, 2014). Although fundamental, the timescales by which N sources and sinks are coupled in the ocean remain uncertain (Falkowski et al., 1998; Brandes and Devol, 2002; Straub et al., 2013). Excess P emerges as a master variable to link them in the modern ocean (Deutsch et al., 2007), as well as from a paleobiogeochemical point of view (Straub et al., 2013). It has been suggested that the recent (since the beginning of the industrial era) increase in production by N_2-fixing cyanobacteria may have provided a negative feedback response to rising atmospheric carbon dioxide concentrations (McMahon et al., 2015), although an inverse trend was also proposed (Kim et al., 2017). While the observed changes in N_2 fixation and biogeochemical cycling reflect either natural oceanic variability or climate change (Karl et al., 1997; Karl, 2014), the most probable changes for the near future in both N_2 fixation and denitrification processes following climate forcing are predicted to be a strengthening control of the carbon cycle by P availability (Moutin et al., 2008).

The western tropical South Pacific (WTSP) is a poorly studied area where large blooms of diazotrophs were previously observed by satellite (Dupouy et al., 2000, 2011), and which has been recently qualified as a hotspot of N_2 fixation (Bonnet et al., 2017). It is hypothesized that following the South Equatorial Current (SEC), the N-depleted and P-enriched waters from areas of denitrification located in the east Pacific reach waters with sufficient iron in the west to allow N_2 fixation to occur (Moutin et al., 2008; Bonnet et al., 2017). While horizontal advection of waters from the east through the SEC probably supports an active biological pump in the WTSP, local vertical convection may also play a central role.

In addition to the main objective of following the same water mass for several days (de Verneil et al., 2018) by a quasi-Lagrangian experiment (Moutin et al., 2017a) in order to propose daily budgets (Caffin et al., 2018; Knapp et al., 2018), or short term biological trends (Van Wambeke et al., 2018), here we propose to work at larger space and time scales, in complement to the work by Fumenia et al. (2018) showing that N_2 fixation in the WTSP may influence the whole South Pacific (SP) Ocean. While many recent works focus on small spatial scales influencing the biological carbon pump (Lévy et al., 2012; Stukel et al., 2017), we found it important to also show results from a larger-scale study in the OUTPACE (Oligotrophy to the UlTra-oligotrophy PACific Experiment) special issue (Moutin et al., 2017b), showing that they are complementary rather than mutually exclusive. Another interest of this study is that we are far from resolving seasonal variations in the main biogeochemical variables in the WTSP, still largely under-sampled compared to the North Pacific and Atlantic. Therefore, the aim of this study is to provide a large spatial (hundreds of kilometers) and temporal (annual) scale study of the main biogeochemical C, N, and P stocks and fluxes in the upper 200 m of the WTSP Ocean from measurements gathered during the stratified period, and to evaluate the main seasonal trends on the basis of estimations of previous winter conditions and climatological analysis.

2 Material and methods

2.1 General method and strategy

2.1.1 Station locations, chronology, CTD measurements, and sample collection

The OUTPACE cruise was carried out between 18 February and 3 April 2015 from Nouméa (New Caledonia) to Papeete (French Polynesia) in the WTSP (Fig. 1). We sampled water

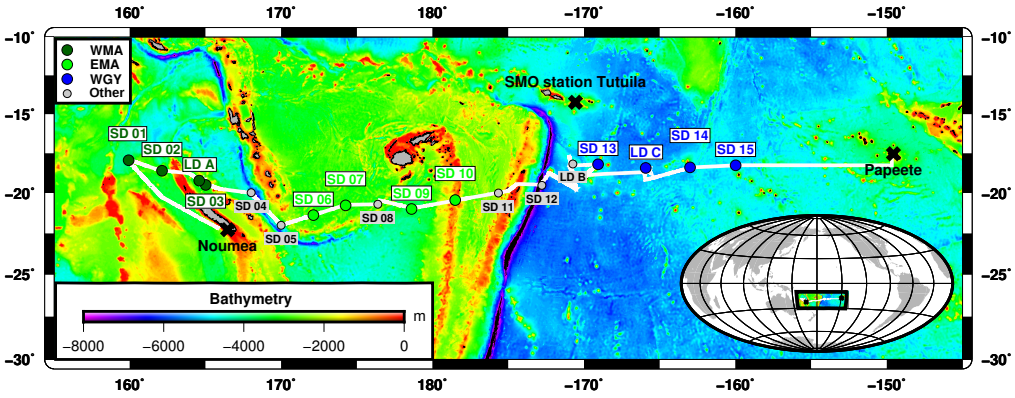

Figure 1. Transect of the OUTPACE cruise (18 February–3 April 2015) superimposed on a bathymetry map (GEBCO_2014 grid) of the western tropical South Pacific Ocean. The two types of stations, short duration and long duration, are indicated together with the stations chosen to represent three selected areas: the western Melanesian Archipelago (WMA in dark green), the eastern Melanesian Archipelago (EMA in light green), and the western SP gyre (WGY in blue). SMO station Tutuila (American Samoa; lat. 14.247° S, long. 170.564° W).

along a 4000 km transect from the oligotrophic water of the MA to the clearest ocean waters of the SP gyre (Moutin et al., 2017a) from a SBE 911+ CTD rosette. Euphotic zone depth (EZD) was immediately determined on board from the photosynthetically available radiation (PAR) at depth compared to the sea surface PAR(0^+), and used to determine the upper water sampling depths corresponding to 75, 54, 36, 19, 10, 3, 1 (EZD), 0.3, and 0.1 % of PAR(0^+). CTD sensors were calibrated and data processed post-cruise using Sea-Bird software in 1 m bins. Conservative temperature, absolute salinity, and potential density were computed using TEOS-10 (McDougall and Barker, 2011). Chlorophyll *a* (Chl *a*) in mg m^{-3} were measured with an Aqua Trak III fluorimeter (Chelsea Technologies Group Ltd.). All samples were collected from 24 12 L Niskin bottles equipped with silicone rubber closures and tubing for measurements (see Sect. 2.2, "Analytical chemical methods") for stock variables (dissolved oxygen; dissolved inorganic carbon, DIC; total alkalinity, TA; nutrients; Chl *a*; and particulate and dissolved organic C, N, and P) and fluxes (primary and bacterial production rates; N_2 fixation rates; and dissolved inorganic phosphate, DIP, turnover times, T_{DIP}; i.e., the ratio of DIP concentration to DIP uptake).

2.1.2 Group of stations

For our large-scale study, we considered three areas: the western MA (WMA), the eastern MA (EMA), and the western gyre (WGY) waters. Four 0–200 m CTD casts, mainly devoted to nutrient pool analyses, were considered for each area and correspond to the following stations: SD 1, SD 2, SD 3, and LD A for WMA; SD 6, SD 7, SD 9, and SD 10 for EMA; and SD 13, SD 14, SD 15, and LD C for WGY (Fig. 1, Tables 1 and 2). Therefore, the same number of CTD casts was used to characterize each area. The choice of the stations for each area was essentially geographical, but justified a posteriori by the results. SD 8 was discarded because no nutrient measurements were available. SD 11, SD 12, and LD B were also discarded because a bloom was sampled at LD B, meaning these measurements are outside the scope of this paper, which deals with large-scale spatial and temporal variations. The specificities of the transition area between the MA and WGY waters are presented in another paper of the OUTPACE special issue (de Verneil et al., 2018). WMA, EMA, and WGY will be presented in dark green, light green, and blue, respectively, in close relationship with the expected oligotrophic gradient.

2.1.3 Mixed layer depths

Mixed layer depth (MLD) was calculated using a threshold temperature of 0.2 °C deviation from the reference value at 10 m depth (de Boyer Montegut et al., 2004) from OUTPACE CTD profiles (Table 1). For climatological MLD data (Fig. 2a, d, g), values at each station were extracted from the global climatology at 2° resolution proposed by de Boyer Montegut et al. (2004) (downloaded from http://www.ifremer.fr/cerweb/deboyer/mld/Surface_Mixed_Layer_Depth.php, last access: 12 January 2017). The same criterion (threshold temperature deviation of 0.2 °C) was used.

2.1.4 Vertical eddy diffusivity measurement

The mean eddy vertical diffusivity K_z between 40 and 200 m was determined for each station from one to several casts undertaken using a using a vertical microstructure VMP-1000 profiler (Bouruet-Aubertot et al., 2018). Briefly, K_z is inferred from the dissipation rate of turbulent kinetic energy, ε, mixing efficiency, γ, and buoyancy frequency, N, according to the Osborn relationship: $K_z = (\gamma\varepsilon)/N^2$. Then ε is computed from the microstructure shear measurements (e.g., Xie

Table 1. General physical and biogeochemical characteristics of the stations investigated along the OUTPACE transect presented in columns: (1) short-duration (SD) or long-duration (LD) station; (2) station number; (3) CTD rosette number; (4) MLD: mixed layer depth (m); (5) EZD: euphotic zone depth (m); (6) K_z: mean 40–200 m vertical eddy diffusivity ($m^2\,d^{-1}$); (7) K_z error ($m^2\,d^{-1}$); (8) DCMD: deep Chl *a* maximum depth; (9) DCMC: deep Chl *a* maximum concentration; i.e., Chl *a* concentration at the DCMD ($mg\,m^{-3}$); (10 and 11) IChl *a*: integrated (0–70 m) and (0–200 m) Chl *a* concentration ($mg\,m^{-2}$); (12–24) D_x, eD_x, S_x, eS_x, N_x, and r_x^2: characteristics of nutriclines (depths in m where NO_3 or PO_4 reaches zero and slopes in $\mu mol\,m^{-4}$ with associated errors; N: number of samples for the linear relationship; r^2: correlation coefficient). QL: quantification limit; nd: no data; nc: not calculated (linear relationship not established); na: nutrient above QL at surface.

Station		CTD number	MLD (m)	EZD (m)	K_Z ($m^2\,s^{-1}$)	eK_Z ($m^2\,s^{-1}$)	Chl *a*				Nitracline						Phosphacline					
							DCMD (m)	DCMC ($mg\,m^{-3}$)	I 0–70 m ($mg\,m^{-2}$)	I 0–200 m ($mg\,m^{-2}$)	D_{NO_3} (m)	eD_{NO_3} (m)	S_{NO_3} ($\mu mol\,m^{-4}$)	eS_{NO_3} ($\mu mol\,m^{-4}$)	N	r^2	D_{PO_4} (m)	eD_{PO_4} (m)	S_{PO_4} ($\mu mol\,m^{-4}$)	eS_{PO_4} ($\mu mol\,m^{-4}$)	N	r^2
SD	1	out_c_006	12	70	9.37×10^{-6}	1.10×10^{-5}	88	0.40	5.0	18.9	73	8	53	9	3	0.97	25	18	2.8	0.6	5	0.89
SD	2	out_c_010	23	70	7.69×10^{-6}	7.28×10^{-6}	85	0.33	6.0	20.4	78	4	61	6	3	0.99	27	4	3.2	0.2	5	0.99
SD	3	out_c_019	14	70	5.04×10^{-6}	3.79×10^{-6}	69	0.28	9.4	20.0	87	8	61	8	4	0.97	17	5	2.7	0.3	4	0.98
LD	A	out_c_066	14	70	1.45×10^{-5}	1.83×10^{-4}	71	0.32	8.4	21.3	65	11	39	9	3	0.96	11	3	5.3	0.6	3	0.99
SD	4	out_c_070	12	70	7.15×10^{-6}	8.26×10^{-6}	62	0.49	9.2	19.8	54	15	24	3	5	0.96	22	18	2.0	0.5	3	0.95
SD	5	out_c_074	11	70	1.33×10^{-5}	1.33×10^{-5}	62	0.49	9.3	27.0	46	25	24	4	5	0.92	nc	nc	nc	nc	nc	nc
SD	6	out_c_078	13	79	7.49×10^{-6}	1.39×10^{-5}	119	0.29	5.4	22.3	118	6	56	11	3	0.96	40	10	1.9	0.2	5	0.97
SD	7	out_c_082	12	90	4.51×10^{-6}	2.79×10^{-6}	89	0.30	4.1	16.9	77	7	41	4	4	0.98	33	7	2.4	0.2	4	0.98
SD	8	out_c_086	12	90	5.95×10^{-6}	6.75×10^{-6}	114	0.28	3.3	17.5	nd	nd	nd	nd	nd	nd	nd	nd	nd	nd	nd	nd
SD	9	out_t_012	22	90	3.29×10^{-6}	2.36×10^{-6}	nd	nd	nd	nd	95	10	43	9	3	0.96	60	12	2.4	0.3	5	0.95
SD	10	out_c_094	13	90	4.90×10^{-6}	4.30×10^{-6}	103	0.28	4.2	18.1	112	1	64	1	3	1.00	nc	nc	nc	nc	nc	nc
SD	11	out_c_098	13	90	7.01×10^{-6}	8.37×10^{-6}	91	0.36	4.4	18.2	78	18	42	8	5	0.90	41	6	2.8	0.2	4	0.99
SD	12	out_c_102	16	85	5.25×10^{-6}	4.80×10^{-6}	94	0.33	5.1	18.8	84	2	57	2	3	1.00	na	na	na	na	na	na
LD	B	out_c_150	21	55	4.18×10^{-6}	6.66×10^{-6}	74	0.35	7.8	22.2	120	1	48	1	3	1.00	nc	nc	nc	nc	nc	nc
SD	13	out_c_152	27	nd	nd	nd	122	0.30	1.2	18.1	102	12	41	5	4	0.97	na	na	na	na	na	na
LD	C	out_c_198	34	120	4.25×10^{-6}	1.49×10^{-5}	129	0.29	1.9	19.6	117	4	51	3	5	0.99	na	na	na	na	na	na
SD	14	out_c_209	13	110	3.49×10^{-6}	4.11×10^{-6}	155	0.25	2.1	18.2	141	10	50	3	5	0.99	na	na	na	na	na	na
LD	15	out_c_212	19	116	3.06×10^{-6}	2.45×10^{-6}	131	0.26	2.7	20.3	105	12	45	7	4	0.96	na	na	na	na	na	na

Table 2. General physical and biogeochemical characteristics for the three selected areas presented in columns: (1) western Melanesian Archipelago (WMA), eastern Melanesian Archipelago (EMA), and western gyre (WGY) with the corresponding stations chosen; (2) mean or standard deviation (SD); (3) MLD: mixed layer depth (m); (4) EZD: euphotic zone depth (m); (5) K_z: mean 40–200 m vertical eddy diffusivity ($m^2\ d^{-1}$); (6) DCMD: deep Chl *a* maximum depth; (7) DCMC: deep Chl *a* maximum concentration = Chl *a* concentration at the DCMD ($mg\ m^{-3}$); (8 and 9) IChl *a*, integrated (0–70 m) and (0–200 m) Chl *a* concentration ($mg\ m^{-2}$); (10–13) D_x, S_x: characteristics of nutriclines (depths in m where NO_3 or PO_4 reaches zero and slopes in $\mu mol\ m^{-4}$). QL: quantification limit; na: nutrient above QL at surface.

					Chl *a*				Nitracline		Phosphacline	
		MLD (m)	EZD (m)	K_Z ($m^2\ d^{-1}$)	DCMD (m)	DCMC ($mg\ m^{-3}$)	I 0–70 m ($mg\ m^{-2}$)	I 0–200 m ($mg\ m^{-2}$)	D_{NO_3} (m)	S_{NO_3} ($\mu mol\ m^{-4}$)	D_{PO_4} (m)	S_{PO_4} ($\mu mol\ m^{-4}$)
WMA (SD 1,2,3 LD A)	Mean	16	70	0.79	78	0.33	7.2	20.2	76	53	20	3.5
	SD	5	0	0.34	10	0.05	2.1	1.0	10	10	7	1.2
EMA (SD 6,7,9,10)	Mean	15	87	0.44	104	0.29	4.6	19.1	100	51	44	2.2
	SD	5	6	0.15	15	0.01	0.7	2.8	18	11	14	0.3
WGY (SD 13,14,15 LD C)	Mean	23	115	0.31	134	0.28	2.0	19.0	116	47	na	na
	SD	9	5	0.05	14	0.03	0.6	1.1	18	5	na	na

et al., 2013) and the mixing efficiency is inferred from the Bouffard and Boegman parameterization as a function of turbulence intensity (Bouffard and Boegman, 2013).

2.1.5 Satellite data

Sea surface temperature (SST; Fig. 2b, e, h) and sea surface Chl *a* (SSChl *a*; Fig. 2c, f, i) from July 2014 to July 2015 were obtained using processed satellite data provided by the MODIS Aqua mission (downloaded from https://oceandata.sci.gsfc.nasa.gov/, last access: 3 January 2017). The mapped level 3 re-analysis has a 4 km spatial resolution produced at a monthly timescale. For each station, pixels within a rectangle with sides ±0.125° longitude and latitude away from the station position were averaged together to produce a single value.

2.1.6 Depth profiles of all discrete variables

All measurements are presented together with their estimated mean concentrations profile (thick line) in Figs. 3, 4, 5, and 6. In order to determine the mean concentrations, the profiles of the variable in question (concentration vs. depth) for all stations included in the group were interpolated between 5 and 200 m with a piecewise cubic hermite interpolating scheme (pchip function in the pracma R package). In case of missing values close to 200 m, the interpolation was stopped at the deepest (above 200 m) point available. The mean profile was estimated from the mean value of the interpolated profiles at every 1-meter depth horizon. For inorganic nutrient concentrations less than the quantification limit (QL; see Sect. 2.2), a zero was indicated to show that a measurement was taken.

2.1.7 Normalization

Concentrations normalized by salinity are used to study biological processes independent of variations related to evaporation or precipitation. At global scales, it is common to apply $S_P = 35$ (Millero, 2007). In order to estimate seasonal trends in our specific areas, we normalized to the mean absolute salinity measured at 70 m depth in each area, $S_A = 35.65 \pm 0.04$, 35.83 ± 0.04, and $35.91 \pm 0.02\ g\ kg^{-1}$ for the WMA, EMA, and WGY, respectively. This choice will be further justified hereafter. Important differences in the carbonate system require this normalization to be taken into account, which justifies its use for the other variables, even if changes are relatively small (e.g., for nutrients).

2.1.8 Inventories

Inventories were calculated from the depth profiles of the discrete variables of inorganic and organic C, N, and P dissolved and particulate pools (see Sect. 2.2), measured during the OUTPACE cruise (Table 3) between 0 and 70 m depth. The latter depth corresponded to the average deeper annual MLD obtained using climatology, as explained above and shown in Fig. 2a, d, g. The integrated fluxes were calculated considering the same depths.

2.1.9 Settling particulate matter mass and C, N, and P flux measurements

The settling of particles in the water column outside the upper layer was measured using two PPS5 sediment traps (1 m^2 surface collection, Technicap, France), deployed for 4 days at 150 and 330 m at LD A (MA) and LD C (WGY) stations (Fig. 1). The PPS5 traps are covered with baffled lids (sieve 1 cm^2) to reduce current shear at the mouth of the trap, but also to prevent large zooplankton and fish from entering the traps. Particle export was recovered in polyethylene flasks screwed on a rotary disk, which automatically changed the flask every 24 h to obtain daily material recovery. The flasks were previously filled with a 2 % (v/v) buffered solution of formaldehyde (final pH ≈ 8) prepared with in situ deep seawater. A sample of this water is kept to measure dissolved nutrients (phosphate and silicate). Immediately after trap retrieval, samples were stored at 4 °C in the dark until they were processed. Back in the laboratory, one part

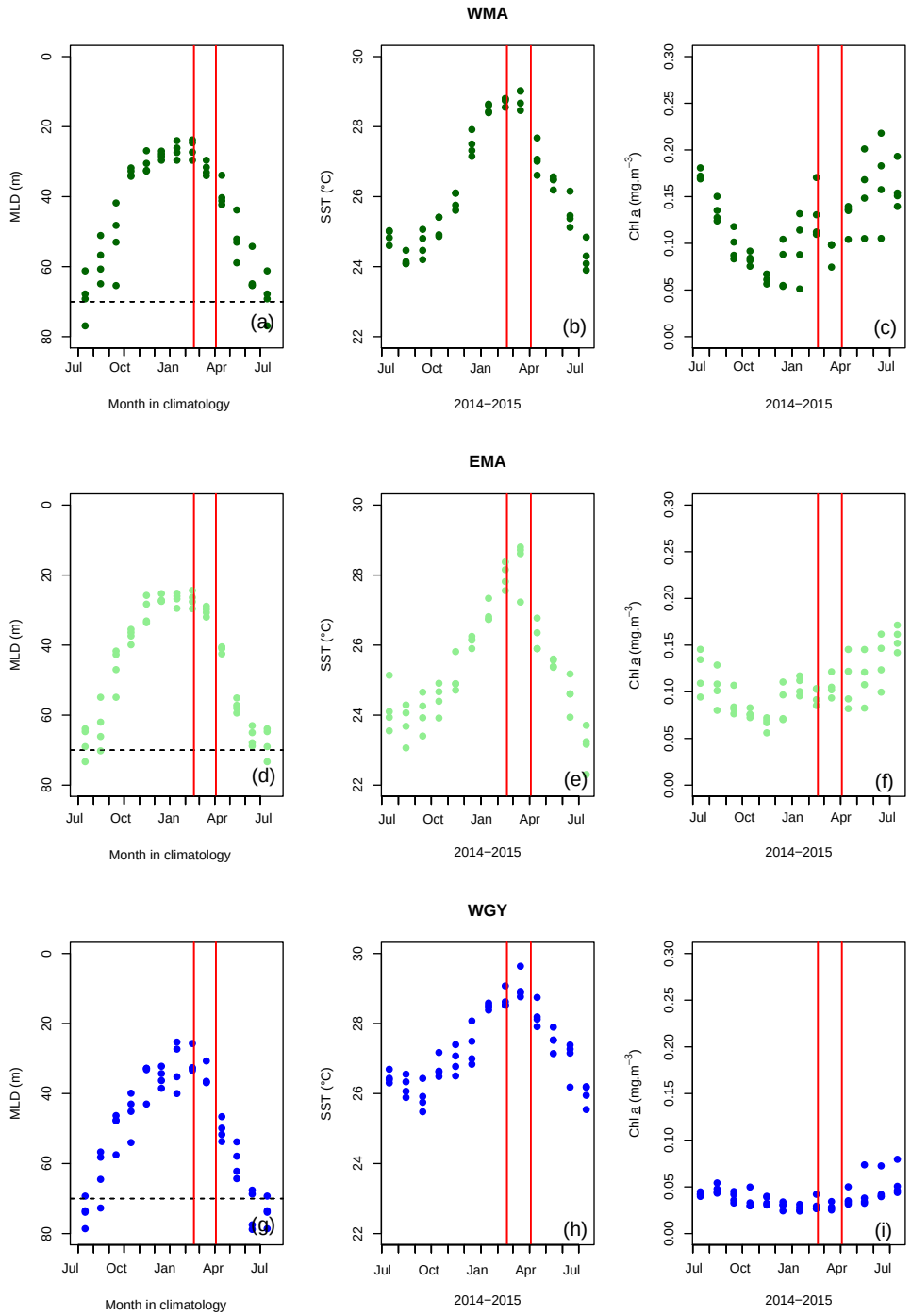

Figure 2. Monthly mean mixed layer depth (MLD) against month in climatology **(a, d, g)**, sea surface temperature (SST) **(b, e, h)**, and Chl *a* **(c, f, i)** against months from July 2014 to July 2015, respectively, for **(a, b, c)** the western Melanesian Archipelago (WMA), **(d, e, f)** the eastern Melanesian Archipelago (EMA) and **(g, h, i)** the western SP gyre (WGY). The horizontal dashed lines indicate the mixed layer depth of 70 m. The vertical red lines indicate the period of the OUTPACE cruise: 18 February to 3 April 2015.

of the sample's supernatant was kept and stored at 4 °C to measure dissolved nutrients (phosphate and silicate), and pH was checked on every trap sample. Swimmers (all organisms deemed to have actively entered the trap) were identified under a stereomicroscope and carefully removed with plastic fine-tipped forceps and placed in small vials with some of the reserved trap preservative. The main species removed were copepods, crustaceans (ostracods, euphausiids,

Table 3. Mean integrated 0–70 m C, N, and P pools (mol m^{-2}) during the OUTPACE cruise (austral summer period) for the three selected areas: western Melanesian Archipelago (WMA), eastern Melanesian Archipelago (EMA), and western gyre (WGY). Dissolved inorganic (DI), dissolved organic (DO), and particulate organic (PO) C, N, and P, respectively.

			DIC	DOC	POC	DIN	DON	PON	DIP	DOP	POP
Austral summer	WMA	Mean	141.2	5.07	0.21	0.000	0.392	0.035	0.0040	0.0112	0.0019
		SD	0.3	0.12	0.02	0.000	0.036	0.004	0.0020	0.0018	0.0002
	EMA	Mean	141.6	5.22	0.22	0.000	0.370	0.031	0.0011	0.0117	0.0018
		SD	0.6	0.07	0.02	0.001	0.017	0.002	0.0011	0.0010	0.0001
	WGY	Mean	141.9	5.35	0.09	0.000	0.378	0.015	0.0101	0.0136	0.0010
		SD	0.4	0.08	0.01	0.000	0.045	0.001	0.0012	0.0020	0.0001

amphipods), and pteropods. Microphotographs of each sample were taken. After the swimmers were removed, the whole sample was then rinsed 3 times with ultrapure (Milli-Q) water in order to remove salt and then freeze-dried. Mass particle fluxes were obtained by weighing the freeze-dried sample 5 times. The accuracy of the weighing (and thus of the flux) was 1 % over the whole data series. In this study, swimmers were rinsed and freeze-dried and their dry weight was also determined. Settling particulate matter and swimmers were analyzed separately on an elemental analyzer coupled to an isotope ratio mass spectrometer EA-IRMS (Integra2, Sercon Ltd.) to quantify total C and N. Total P was analyzed as described in Sect. 2.2. The total element measurements for the settling particulate matter were considered to represent the settling particulate organic C, N, and P. The results are presented in Sect. 2.2 (Table 4).

2.1.10 Ocean–atmosphere CO_2 fluxes

The Ocean–atmosphere CO_2 fluxes $\Phi_{CO_2} = -k_g \cdot (p^{atm}_{CO_2} p^{oc}_{CO_2})$ were calculated considering (1) a mean k_g of 0.031 ± 0.005 mol m^{-2} yr^{-1} µatm^{-1} (i.e., 85 µmol m^{-2} d^{-1} µatm^{-1}) for gas transfer velocity, estimated from the Liss and Melivat (1986) relationship and sea winds derived from satellite measurements (1999–2009). Data came from Boutin et al. (2009; downloaded from http://cersat.ifremer.fr/, last access: 3 March 2017 and extracted on a geographical grid; latitude −17 to −23° N, longitude +159 to +211° E; one grid was used because no significant differences were obtained in k_g for the three areas: WMA, EMA, and WGY), (2) a mean oceanic p_{CO_2} ($p^{oc}_{CO_2}$) determined for each area during the OUTPACE cruise, and (3) a mean atmospheric p_{CO_2} ($p^{atm}_{CO_2}$) estimated from the molar fraction of CO_2 (X_{CO_2}) in dry air measured at SMO station Tutuila (American Samoa; lat. 14.247° S, long. 170.564° W; north of LD B (Fig. 1); NOAA/ESRL – data downloaded from https://doi.org/10.7289/V51834DB, last access: 7 February 2017). A monthly averaged $X_{CO_2} = 398.4$ ppm for March 2015 was used, whereas X_{CO_2} varied from 396.0 to 398.4 ppm from July 2014 to July 2015 at Tutuila with an annual mean of 397.3 ppm. The X_{CO_2} data were converted to $p^{atm}_{CO_2}$ considering 100 % humidity and a total pressure of 1 atm (101 325 Pa), following Weiss and Price (1980), with surface seawater temperature and salinity of each area (Table 5). A total pressure of $101\,260 \pm 180$ Pa was determined considering NCEP-NCAR Reanalysis 1 on the OUTPACE area from July 2014 to July 2015, with no longitudinal trend, justifying the consideration of 1 atm as total pressure for the conversion (downloaded from https://www.esrl.noaa.gov/psd/data/gridded/data.ncep.reanalysis.html, last access: 19 December 2017).

2.1.11 Upper layer (0–70 m) daily C, N, and P budgets

Comparative daily C, N, and P budgets of the upper 70 m layer were established for each area (Table 6). Inputs from below associated with vertical turbulent diffusion were calculated using the mean vertical eddy diffusivity, and slopes of nutriclines (Table 2) and DIC gradients calculated between 70 and 200 m using linear regressions (data not shown). The ocean–atmosphere CO_2 fluxes were detailed in the previous paragraph. The input of N by N_2 fixation was calculated for each area (Table 6) using depth profile sampling and on-deck 24 h $^{15}N_2$ incubations (Sect. 2.2). The C, N, and P particulate and dissolved organic export were estimated. The method of obtaining particulate export by settling material (Table 4) was described above. Output of dissolved and particulate organic matter by turbulent diffusion was calculated from the mean vertical eddy diffusivity (Table 1) and from gradients estimated with linear regressions (data not shown) between the surface and 70 m depth of DOC-POC (Fig. 5d–g), DON-PON (Fig. 5e–h), and DOP-POP (Fig. 5f–i). When non-significant gradients were obtained, fluxes were nil.

2.1.12 Seasonal variations and upper layer (0–70 m) annual C, N, and P budgets

During OUTPACE, we sampled during the stratified period characterized by minimum MLDs close to 20–40 m (Fig. 2a, d, g), where the largest part of biological fluxes (Fig. 6) occurred. Because the only mechanism able to disrupt this strat-

ification at a large spatial scale is deep water mixing occurring during winter, and more specifically in July in this area (Fig. 2a, d, g), we postulated that conditions at 70 m depth (average depth of wintertime MLD) remained unchanged, or did not significantly change, throughout the year. Considering no large inter-annual differences in winter MLDs, we considered that the mean measurements at 70 m depth during OUTPACE well represented the homogeneous upper water column (0–70 m) variables and initial winter conditions (i.e., conditions in July 2014), allowing us to determine first-order winter to summer seasonal variations (Table 7) and 8-month C, N, and P budgets (Table 8). The dashed lines in Figs. 3, 4, and 5 indicate the upper surface expected values for all variables during the 2014 austral winter, and allow for an evaluation of the temporal variation toward the austral summer season (full lines) in each area.

2.1.13 Surface waters carbonate system climatology

The climatological gridded values proposed in Takahashi et al. (2014), hereafter referred as NDP-094 climatology, were used to validate our estimated values for the carbonate system in the upper surface previous winter conditions (July 2014). The dataset is based on interpolated $p^{OC}_{CO_2}$ and calculated TA data (based on regional linear potential alkalinity–salinity relationships) on a 4° latitude by 5° longitude monthly grid in the reference year 2005. The variable DIC (among others) is calculated from $p^{OC}_{CO_2}$ and TA. Data were downloaded from http://cdiac.ess-dive.lbl.gov/ftp/oceans/NDP_094/ (last access: 19 December 2017). Climatological July data centered on 20° S were extracted along the cruise transect and 2, 3, and 3 pixels were averaged for comparison in the WMA, EMA, and WGY areas, respectively (Table 5). In order to account for the $p^{atm}_{CO_2}$ increase at the earth's surface between 2005 and 2015, a constant offset of 1.5 µatm yr^{-1} was applied to $p^{atm}_{CO_2}$ and a corresponding constant offset of 1 µmol kg^{-1} yr^{-1} was also applied to DIC.

2.2 Analytical chemical methods

2.2.1 Oxygen and apparent oxygen utilization (AOU)

Oxygen concentration in the water column was measured with a Seabird SBE43 electrochemical sensor interfaced with the CTD unit. The raw signal was converted to an oxygen concentration with 13 calibration coefficients. The method is based on the Owens and Millard Jr. (1985) algorithm that has been slightly adapted by Seabird in the data treatment software using a hysteresis correction. A new set of calibration coefficients has been determined after the cruise to post-process the whole dataset. Only three coefficients (the oxygen signal slope, the voltage at zero oxygen signal, the pressure correction factor) among the 13 determined by the pre-cruise factory calibration of the sensor were adjusted with the following procedure: the oxygen concentrations measured

Table 4. Sediment trap data. Minimum, maximum, and mean values of particulate matter mass flux and swimmer contents, C, N, and P and Redfield ratio (RR) from particulate matter and swimmers (Zoo). * P calculated from the RR with adding the P measured in the supernatant. Last column: particulate matter mass flux and swimmer content ratio. MA: Melanesian Archipelago, WGY: western SP gyre.

		Particulate matter	Swimmer	POC	PON	POP	RR 106 : N : P proportion			Zoo-C	Zoo-N	Zoo-P	Zoo-P*	RR 106 : N : P proportion			*	Zoo/ Particulate
		mgDW d^{-1}	mgDW d^{-1}	µmol m^{-2} d^{-1}			C	N	P	µmol m^{-2} d^{-1}				C	N	P	P	mass flux ratio
MA ($N = 8$)	Min	14	69	241	22	0.6	106	9.8	0.3	2 994	492	4	22	106	12.4	0.0	0.2	0.7
	Max	122	403	3 084	395	68.9	106	15.4	2.9	11 742	1 653	26	55	106	20.2	0.6	1.1	26.0
	Mean	48	219	1 092	136	18.5	106	12.7	1.2	6 903	961	14	36	106	15.8	0.2	0.7	9.7
WGY ($N = 8$)	Min	7	24	138	20	0.4	106	11.2	0.2	609	75	2	5	106	13.1	0.2	0.5	1.4
	Max	28	148	385	59	2.1	106	20.4	0.8	4 552	1 067	16	28	106	25.2	0.5	0.9	7.1
	Mean	17	76	266	41	1.1	106	16.6	0.5	2 330	473	8	15	106	19.9	0.3	0.7	4.4

Table 5. Molar fraction of CO_2 (X_{CO_2}) in dry air measured at SMO station Tutuila (American Samoa; lat. 14.247° S, long. 170.564° W; see Fig. 1; source: NOAA/ESRL) and derived atmospheric p_{CO_2} ($p^{atm}_{CO_2}$). Mean values for the carbonate system, measured in the mixed layer depth (MLD) during the OUTPACE cruise (summer conditions), measured at 70 m depth (estimated winter conditions), and NDP-094 climatological data (Takahashi et al., 2014). Oceanic climatological p_{CO_2} ($p^{oc}_{CO_2}$) are given for different estimations of winter temperature (SST from NDP-094, mean T at 70 m depth from OUTPACE, SST from MODIS Aqua). CT: conservative temperature, S_P: practical salinity, nDIC: normalized dissolved inorganic carbon, nAlk: normalized alkalinity, SST: sea surface temperature; SSS: sea surface salinity. WMA: western Melanesian Archipelago, EMA: eastern Melanesian Archipelago, and WGY: western SP gyre sampled during the OUTPACE cruise.

SMO station TUTUILA	Monthly mean X_{CO_2} (Mar 2015)	ppm	398.4					
	Annual mean X_{CO_2} (Jul 2014–Jul 2015)		397.3 (SD = 0.8)					
			WMA		EMA		WGY	
		Unit	Mean	SD	Mean	SD	Mean	SD
	Monthly mean $p^{atm}_{CO_2}$ (March 2015)	µatm	383.0		382.7		382.5	
Mean values measured in the MLD (austral summer conditions, March 2015)	CT	°C	28.9	0.3	29.3	0.3	29.5	0.4
	S_P		35.0	0.1	35.1	0.2	35.1	0.1
	nDIC	µmol kg^{-1}	1974.6	9.5	1983.9	8.6	1993.6	3.2
	nAlk	µmol kg^{-1}	2333.7	1.9	2343.1	8.0	2347.7	6.1
	n$p^{oc}_{CO_2}$	µatm	366	11	376	8	390	6
Mean values at 70 m (estimated austral winter MLD conditions)	CT	°C	25.3	0.2	24.8	0.8	26.2	0.9
	S_P		35.5	0.0	35.7	0.0	35.7	0.0
	nDIC	µmol kg^{-1}	2007.5	3.0	2009.6	9.6	2008.9	3.7
	nAlk	µmol kg^{-1}	2332.4	5.0	2344.1	6.5	2350.8	2.7
	n$p^{oc}_{CO_2}$	µatm	372	10	355	15	364	8
Austral winter (July 2014) temperature at surface from MODIS Aqua	SST	°C	24.9	0.2	24.2	0.7	26.5	0.2
Mean climatological austral winter values at surface (from Takahashi et al., 2014)	SST	°C	23.9	0.0	24.4	0.1	25.1	0.1
	SSS		35.5	0.0	35.5	0.0	35.6	0.1
	DIC	µmol kg^{-1}	2006.4	0.7	2000.9	3.0	2004.7	9.9
	Alk	µmol kg^{-1}	2335.4	0.2	2333.6	1.7	2343.4	8.6
	$p^{oc}_{CO_2}$ at surface	µatm	344	1	345	4	349	7
Mean climatological austral winter $p^{oc}_{CO_2}$ at surface calculated with different temperatures	T from OUTPACE, mean CT at 70 m depth	µatm	366		353		368	
	SST from MODIS Aqua	µatm	361		344		371	

Table 6. The 0–70 m upper layer comparative C, N, and P daily budgets in the three selected areas (western Melanesian Archipelago, WMA; eastern Melanesian Archipelago, EMA; and western gyre, WGY) sampled during the OUTPACE cruise (µmol m^{-2} d^{-1}).

		WMA			EMA			WGY		
		C	N	P	C	N	P	C	N	P
INPUT	Dissolved inorganic turbulent diffusion	426	46	2.8	198	0	1.0	200	0	0.0
	Atmospheric CO_2 exchange or N_2 fixation	1675	642	negligible	825	452	negligible	0	41	negligible
OUTPUT	Particulate organic settling	−1092	−136	−18.5	−1092	−136	−18.5	−266	−41	−1.1
	Particulate organic turbulent diffusion	−29	−4	−0.2	−16	−1	−0.1	2	0	0.0
	Dissolved organic turbulent diffusion	−121	−8	−0.7	−58	−6	−0.3	−21	0	0.0
BUDGETS		859	540	−16.6	−143	309	−17.9	−85	0	−1.1

Table 7. Estimated temporal evolution of surface biogeochemical properties between austral winter (up) and summer (below) in µmol L^{-1} presented in columns: (1) Mean measurements at 70 m depth during OUTPACE were considered to represent the homogeneous upper water column (0–70 m) variables and initial winter conditions (i.e., conditions in July 2014). The summer conditions were those observed during the OUTPACE cruise (March 2015). Δ represents the summer minus winter condition differences. (2) Selected area: western Melanesian Archipelago (WMA), eastern Melanesian Archipelago (EMA), or western gyre (WGY). (3) Mean or standard deviation (SD), (4 to 15) dissolved inorganic (DI), dissolved organic (DO), particulate organic (PO), and total (T) C, N, and P, respectively. All variables were normalized to the mean absolute salinity measured at 70 m depth to discard evolution due to evaporation or precipitation.

			nDIC	nDOC	nPOC	nTC	nDIN	nDON	nPON	nTN	nDIP	nDOP	nPOP	nTP
Austral winter	WMA	Mean	2055.1	67.5	1.6	2124.2	0.00	5.06	0.38	5.44	0.142	0.125	0.022	0.289
		SD	3.0	4.4	0.5		0.00	0.38	0.06		0.030	0.024	0.005	
	EMA	Mean	2057.5	68.9	2.3	2128.7	0.03	4.93	0.34	5.30	0.059	0.140	0.021	0.220
		SD	10.2	2.0	0.4		0.04	0.27	0.05		0.046	0.028	0.004	
	WGY	Mean	2056.2	74.2	1.4	2131.8	0.01	5.52	0.24	5.77	0.142	0.182	0.015	0.339
		SD	4.3	2.3	0.2		0.01	0.74	0.01		0.020	0.037	0.001	
Austral summer	WMA	Mean	2018.1	77.6	4.3	2100.0	0.00	6.05	0.68	6.73	0.000	0.163	0.032	0.195
		SD	10.0	2.2	0.3		0.00	0.58	0.12		0.000	0.029	0.004	
	EMA	Mean	2027.5	78.2	4.5	2110.1	0.00	5.72	0.59	6.31	0.000	0.180	0.031	0.211
		SD	8.8	1.1	1.1		0.00	0.39	0.15		0.000	0.018	0.005	
	WGY	Mean	2037.6	79.2	1.2	2117.9	0.00	5.50	0.21	5.71	0.150	0.190	0.013	0.353
		SD	3.4	1.1	0.2		0.00	0.70	0.04		0.014	0.017	0.002	
Δ	WMA		−37.0	10.1	2.6	−24.2	0.00	1.00	0.29	1.29	−0.142	0.037	0.010	−0.095
	EMA		−30.0	9.3	2.2	−18.6	−0.03	0.79	0.25	1.01	−0.059	0.040	0.010	−0.009
	WGY		−18.7	5.0	−0.2	−13.9	−0.01	−0.02	−0.03	−0.06	0.008	0.008	−0.002	0.014

Table 8. Estimated temporal evolution of (0–70 m) biogeochemical inventories between austral winter and summer in mmol m^{-2} presented in columns: (1) Mean measurements at 70 m depth during OUTPACE were considered to represent the homogeneous upper water column (0–70 m) variables and initial winter conditions (i.e., conditions in July 2014). The summer conditions were those observed during the OUTPACE cruise (March 2015). Δ represents the summer minus winter conditions differences. (2) Selected area: western Melanesian Archipelago (WMA), eastern Melanesian Archipelago (EMA), or western gyre (WGY). (3) Mean or standard deviation (SD), (4 to 15) dissolved inorganic (DI), dissolved organic (DO), particulate organic (PO), and total (T) C, N, and P, respectively. All variables were normalized to the mean absolute salinity measured at 70 m depth to discard evolution due to evaporation or precipitation.

			nDIC	nDOC	nPOC	nTC	nDIN	nDON	nPON	nTN	nDIP	nDOP	nPOP	nTP
Δ (summer−winter)	WMA	Mean	−1563	391	102	−1070	0.0	40.8	8.5	49	−5.9	2.4	0.4	−3.1
		SD	209	307	33		0.0	35.6	4.1		2.1	1.8	0.4	
	EMA	Mean	−1355	445	55	−855	−1.7	28.0	7.5	34	−3.0	1.8	0.3	−0.9
		SD	713	139	26		3.1	19.0	3.7		3.2	2.0	0.3	
	WGY	Mean	−659	220	−8	−448	−0.3	−4.6	−1.5	−6	0.1	1.0	−0.1	1.1
		SD	298	162	14		0.9	51.5	1.3		1.4	2.6	0.1	

by Winkler were matched with the signal measured by the sensor at the closing of the Niskin bottles. The three values were fitted by minimizing the sum of the square of the difference between Winkler oxygen and oxygen derived from the sensor signal. Winkler oxygen concentration was measured following the Winkler method (Winkler, 1888), with potentiometric endpoint detection (Oudot et al., 1988) on discrete samples collected with Niskin bottles. For sampling, reagent preparation, and analysis, the recommendations from Langdon (2010) have been carefully followed. The thiosulfate solution was calibrated by titrating it against a potassium iodate certified standard solution of 0.0100N (WAKO). AOU was computed with oxygen concentration at saturation estimated following the algorithm proposed by Garcia and Gordon (1992), considering Benson and Krause values.

2.2.2 TA, DIC, and $p^{oc}_{CO_2}$

Samples for total alkalinity (TA) and dissolved inorganic carbon (DIC) were collected from Niskin bottles in one 500 mL glass flask (Schott Duran) and poisoned directly after collection with $HgCl_2$ (final concentration 20 mg L^{-1}). Samples were stored at 4 °C during transport and analyzed 5 months after the end of the cruise at the SNAPO-CO_2 (Service Na-

tional d'Analyse des paramètres Océaniques du CO_2, LOCEAN, Paris). TA and DIC were measured on the same sample based on one potentiometric titration in a closed cell (Edmond, 1970). A non-linear curve fitting approach was used to estimate TA and DIC (Dickson, 1981; DOE, 1994). Measurements were calibrated with reference materials (CRM) for oceanic CO_2 measurements purchased by the SNAPO-CO_2 from Prof. Andrew G. Dickson (Oceanic Carbon Dioxide Quality Control, USA). The reproducibility expressed as the standard deviation of the CRM analysis was 4.6 µmol kg^{-1} for TA and 4.7 µmol kg^{-1} for DIC. Moreover, the standard deviation on the analysis of 12 replicates collected at the same depth (25 m) at station LD C was 3.6 µmol kg^{-1} for TA and 3.7 µmol kg^{-1} for DIC. The estimation of $p^{oc}_{CO_2}$ was made with the SEACARB R package (Gattuso and Lavigne, 2009). The dissociation constants K_1 and K_2 (for carbonates in seawater) from Lueker et al. (2000) were used. When available, phosphate and silicate concentrations were used in the calculation.

2.2.3 Nutrient, dissolved and particulate C, N, and P pools

Total C, N, and P (TC, TN, TP) in seawater samples may be separated in three pools: the dissolved inorganic C, N, and P pools (DIC, DIN, DIP); the dissolved organic C, N, and P pools (DOC, DON, DOP); and the particulate organic C, N, and P pools (POC, PON, POP). No significant particulate inorganic pools are generally considered in open ocean waters.

Two samples for dissolved inorganic nutrient pool measurements were collected from Niskin bottles in 20 mL polyethylene bottles, and one sample was directly analyzed on board and the other poisoned with 50 µL $HgCl_2$ (20 g L^{-1}) and stored for analysis after the cruise in the laboratory. DIN $= [NO_3^-] + [NO_2^-] + [NH_4^+]$, sum of nitrate, nitrite, and ammonium, respectively. Because $[NO_2^-]$ and $[NH_4^+]$ were negligible compared to $[NO_3^-]$, DIN $= [NO_3^-]$. DIP $= [HPO_4^{2-}] + [PO_4^{3-}]$ which are orthophosphates and are also symbolized as PO_4. Nitrate, nitrite, and orthophosphate concentrations were determined on a segmented flow analyzer (AAIII HR Seal Analytical) according to Aminot and Kérouel (2007), with a QL of 0.05 µmol L^{-1}. Ammonium was measured by fluorometry (Holmes et al., 1999; Taylor et al., 2007) on a fluorimeter Jasco FP-2020 with a QL of 0.01 µmol L^{-1}.

The dissolved organic pools, DON and DOP, were measured using high-temperature (120 °C) persulfate wet-oxidation mineralization (Pujo-Pay and Raimbault, 1994). Samples were collected from Niskin bottles in 100 mL combusted glass bottles and immediately filtered through two pre-combusted (24 h, 450 °C) glass fiber filters (Whatman GF/F, 25 mm). Filtered samples were then collected in Teflon vials adjusted at 20 mL for wet oxidation. Nitrate and phosphate formed, corresponding to total dissolved pool (TDN and TDP), and were then determined as previously described for the dissolved inorganic pools. DON and DOP were obtained by the difference between TDN and DIN, and TDP and DIP, respectively. The precision and accuracy of the estimates decreased with increasing depth, as inorganic concentrations became the dominant component in the total dissolved nutrient pools. The limits of quantification were 0.5 and 0.05 µmol L^{-1} for DON and DOP, respectively. The same pre-filtration was used for dissolved organic carbon (DOC) measurements. Filtered samples were collected into glass pre-combusted ampoules that were sealed immediately after samples were acidified with orthophosphoric acid (H_3PO_4) and analyzed by high-temperature catalytic oxidation (HTCO; Sugimura and Suzuki, 1988; Cauwet, 1994, 1999) on a Shimadzu TOC-L analyzer. Typical analytical precision is ±0.1–0.5 (SD). Consensus reference materials (http://www.rsmas.miami.edu/groups/biogeochem/CRM.html, last access: 8 May 2018) were injected every 12 to 17 samples to insure stable operating conditions.

The particulate pools (PON, POP) were determined using the same wet oxidation method (Pujo-Pay and Raimbault, 1994). The 1.2 L samples were collected from Niskin bottles in polycarbonate bottles and directly filtered onto a pre-combusted (450 °C, 4 h) glass fiber filter (Whatman 47 mm GF/F). Filters were then placed in Teflon vials with 20 mL of ultrapure water (Milli-Q grade) and 2.5 mL of wet oxidation reagent for mineralization. Nitrate and orthophosphates produced were analyzed as described previously. QLs are 0.02 and 0.001 µmol L^{-1} for PON and POP, respectively. Particulate organic carbon (POC) was measured using a CHN analyzer and the improved analysis proposed by Sharp (1974).

2.2.4 Primary production rates and DIP turnover times

Vertical profiles of DIC uptake (V_{DIC}) and phosphate turnover time (T_{DIP}) were measured once at each station using a dual-labeling method (^{14}C and ^{33}P) considering a ^{33}P period $T_{1/2} = 25.55 \pm 0.05$ days (Duhamel et al., 2006). Each sample (150 mL polycarbonate bottle) was inoculated with 10 µCi of ^{14}C carbon (sodium bicarbonate, Perkin Elmer NEC086H005MC; 1 Ci $= 3.7 \times 10^{10}$ Bq) and 4 µCi of ^{33}P phosphate (H_3PO_4 in dilute hydrochloric acid, Perkin Elmer NEZ080001MC). The bottles were then placed in blue-screen on-deck incubators representing 75, 54, 36, 19, 10, 2.7, 1, 0.3, and 0.1 % incident PAR (PAR(0^+)), https://outpace.mio.univ-amu.fr/spip.php?article135, last access: 8 May 2018) and maintained at constant temperature using a continuous circulation of surface seawater. The same protocol was used for duplicate 150 mL samples, where 150 µL $HgCl_2$ (20 g L^{-1}) had been added as a control for non-biological uptake. After 3 to 24 h (the optimal incubation time was determined from a prior time-series experiment), incubations were stopped by the addition of 150 µL of non-radioactive KH_2PO_4 (10 mmol L^{-1}) and dark conditions. Filtrations of 50 mL triplicate subsamples were carried out on 25 mm polycarbonate filters (0.2 µm), placed

on DIP-saturated support GF/F filters, using a low-vacuum pressure (< 0.2 bar). Filters were not washed with filtered seawater at the end of the filtration, but pressure was briefly increased to 0.6 bar to remove non-cellular ^{33}P radioactivity from the filter. Filters were then placed in low-potassium 6 mL glass scintillation vials (Wheaton) with 500 µL of 0.5 M HCl for 12 h in order to drive off any unincorporated ^{14}C. Then, 6 mL of scintillation liquid (Ultima gold MV, Packard) was added and the radioactivity of the filters measured using a scintillation counter Packard Tri-Carb® 2100TR on board (first count). Initial radioactivity was also measured on 5 replicates for each profile. Samples were then stored until the second count in the laboratory after ^{33}P emission became unmeasurable (12 months). DIC uptake and DIP turnover time were then deduced from the following equations (details in Thingstad et al., 1993; Moutin et al., 2002): $T_{\mathrm{DIP}} = -\mathrm{Ti} / \ln(1 - (\mathrm{dpm}^{33}\mathrm{P} - \mathrm{dpm}_{b^{33}\mathrm{P}})/\mathrm{dpm}_{t^{33}\mathrm{P}})$, where T_{DIP} is DIP turnover time (in days), Ti is the incubation time, $\mathrm{dpm}^{33}\mathrm{P}$ is the disintegration per minute (dpm) attributable to the ^{33}P activity of the filtered sample, $\mathrm{dpm}_{b^{33}\mathrm{P}}$ is the dpm attributable to the blank, and $\mathrm{dpm}_{t^{33}\mathrm{P}}$ is the initial (total) activity of ^{33}P. $V_{\mathrm{DIC}} = [(\mathrm{dpm}^{14}\mathrm{C} - \mathrm{dpm}_{b^{14}\mathrm{C}})/\mathrm{dpm}_{t^{14}\mathrm{C}}] \cdot [\mathrm{DIC}]/\mathrm{Ti}$ where: V_{DIC} is the C uptake rate (nmol L^{-1} h^{-1}), $\mathrm{dpm}^{14}\mathrm{C}$ is the dpm attributable to the ^{14}C activity of the filtered sample, $\mathrm{dpm}_{b^{14}\mathrm{C}}$ is the dpm attributable to the blank, $\mathrm{dpm}_{t^{14}\mathrm{C}}$ is the initial (total) activity of ^{14}C added to the sample, [DIC] is the dissolved inorganic carbon concentration of the sample, and Ti is the incubation time. The daily surface photosynthetically available radiation (SPAR) data were used to estimate the daily primary production (PP) values from the PP rates obtained with short time incubation durations using a conversion model (Moutin et al., 1999).

2.2.5 N_2 fixation rates

N_2 fixation rates were measured using the $^{15}N_2$ tracer method (Montoya et al., 1996), adapted and precisely described in Bonnet et al. (2018). As for PP measurements, seawater was rapidly collected in triplicates from the Niskin bottles in 2.3 L polycarbonate bottles at six depths (75, 54, 19, 10, 1, and 0.1 % of PAR(0^+)). Then 2.5 mL of $^{15}N_2$ gas (99 atom% ^{15}N, Eurisotop) were injected in each bottle through the septum cap using a gas-tight syringe. All bottles were shaken 20 times to facilitate the $^{15}N_2$ dissolution and incubated for 24 h from dusk to dusk. To avoid any possible rate underestimation due to equilibration of the $^{15}N_2$ gas with surrounding seawater, final $^{\text{™}15}$N enrichment in the N_2 pool was quantified for each profile in triplicates at 5 m and at the deep Chl *a* maximum (DCM). After incubation, 12 mL of each 4.5 L bottle were subsampled in Exetainer vials, fixed with $HgCl_2$, and stored upside down at 4 °C in the dark and analyzed onshore within 6 months after the cruise, according to Kana et al. (1994), using a membrane inlet mass spectrometer. Incubation was stopped by gentle filtration of the samples onto pre-combusted (450 °C, 4 h) Whatman GF/F filters (25 mm diameter, 0.7 µm nominal porosity). Filters were stored in pre-combusted glass tubes at −20 °C during the cruise, then dried at 60 °C for 24 h before analysis onshore by an EA-IRMS on an Integra2 (Sercon Ltd.). The detection limit associated with the measurement was 0.14 nmol L^{-1} d^{-1}. The accuracy of the EA-IRMS system was systematically controlled using International Atomic Energy Agency (IAEA) reference materials, AIEA-N-1 and IAEA-310A. In addition, the natural δ^{15}N of particulate organic N needed for N_2 fixation rate calculations was measured in each profile at two depths (surface and DCM).

3 Results

3.1 General annual trends of MLD, SST, and SSChl *a* for the three selected areas

MLD against month in the climatology (Fig. 2a, d, g) varied annually from around 70 m depth in July during the austral winter to between 20 and 40 m during the austral summer for the three areas. The OUTPACE cruise from 18 February to 3 April 2015 (red lines) sampled during the stratified period was characterized by minimum MLD and maximum SST (Fig. 2b, e, h). SST varied from 24.2 ± 0.2 to 28.8 ± 0.3, 23.8 ± 0.5 to 28.3 ± 0.7, and 25.9 ± 0.4 to 29.0 ± 0.4 °C between July 2014 and July 2015 for WMA, EMA, and WGY, respectively. Mean March 2015 SST of 28.8 ± 0.3, 28.3 ± 0.7, and 29.1 ± 0.4 °C are close to the mean conservative temperature measurements measured in the MLD during the OUTPACE cruise of 28.9 ± 0.3, 29.3 ± 0.3, and 29.5 ± 0.4 °C for WMA, EMA, and WGY, respectively. The mean conservative temperature measurements at 70 m depth were 25.3 ± 0.3, 24.8 ± 0.9 °C, and 26.1 ± 0.9 °C for WMA, EMA, and WGY, respectively (Fig. 3a). These values are comparable with the SST measured during the deeper winter mixing in July 2014 of 24.9 ± 0.2, 24.2 ± 0.7, and 26.5 ± 0.2 for WMA, EMA, and WGY, respectively (Table 5). Our hypothesis to consider limited exchanges allowing properties to be conservative at 70 m depth seems reasonable for temperature. Expected seasonal upper surface temperature variations calculated from the differences between temperature at the surface and at 70 m depth were 3.6 ± 0.6, 4.5 ± 1.2, and 3.4 ± 1.3 °C for WMA, EMA, and WGY, respectively, agreed relatively well with SST variations observed between July 2014 and March 2015 of 3.9 ± 0.5, 4.2 ± 1.4, and 2.6 ± 0.6 °C (Fig. 2b, e, h). Following a similar reasoning, we established a relatively good comparison between Chl *a* measured at 70 m depth during OUTPACE of 0.217 ± 0.092, 0.091 ± 0.012, and 0.046 ± 0.010 mg m^{-3} for WMA, EMA, and WGY, respectively (Fig. 3f), and SSChl *a* obtained during the deeper mixing of 0.173 ± 0.005, 0.121 ± 0.023, and 0.042 ± 0.002 mg m^{-3} for WMA, EMA, and WGY, respec-

tively (Fig. 2c, f, i). SSChl *a* well reflected the expected oligotrophic gradient with higher values obtained at WMA, lower values at WGY, and intermediate values at EMA. The increase in SSChl *a* observed in July seems to be related to the deep mixing during winter. The comparison between measurements at 70 m depth and in the upper mixed layer during OUTPACE may be used as a first approach to characterize surface seasonal changes in physical and biogeochemical properties of upper surface waters (Sect. 4.3).

3.2 General hydrological and biogeochemical conditions allowing for characterization of oligotrophic states of the different upper water masses sampled during OUTPACE

The general hydrological and biogeochemical conditions during OUTPACE provide the means to characterize the oligotrophic states of the different water masses sampled (Table 1). The shallow austral summer MLD varied between 11 and 34 m with a mean of 16.7 m (SD = 6.4 m). The low variation is in agreement with the relatively similar weather conditions and SST along the zonal transect near 20° S (Moutin et al., 2017a). The EZD and the DCM depth (DCMD) deepen from west to east, from around 70 m to considerably deeper than 100 m, indicating the higher oligotrophy of the SP gyre water compared to the MA water with shallower nitracline depths. The DCM concentration decreases from west to east, but only slightly, from a maximum of 0.40 mg m^{-3} to a minimum of 0.25 mg m^{-3}. A better indicator of oligotrophic conditions is the depth of the nitracline (D_{NO_3}) which varied between 46 and 141 m, typical of oligotrophic to ultraoligotrophic areas of the world ocean (Moutin et al., 2012, their Fig. 9). A relative homogeneity of the slopes ($S_{NO_3} = 47.0 \pm 11.5$ µmol m^{-4}) was observed (Table 1). Phosphaclines and nitraclines did not match, as shown by the lower D_{PO_4} observed everywhere. No phosphaclines linked with upper water biological processes were determined in the SP gyre because phosphate concentrations above the QL were measured up to the surface. The S_{PO_4}, when measurable, was 2.8 ± 1.0 µmol m^{-4} (Table 1).

The same characteristics are presented for the three areas considered (WMA, EMA, and WGY) in Table 2 by their means and SD. The DCMD (about 10–20 m below the EZD in all areas) increased from 78 ± 10 m in the WMA to 134 ± 14 m in the WGY, with an intermediate value of 104 ± 15 m in EMA. D_{NO_3} follows the same pattern, with values of 76 ± 10, 100 ± 18, and 116 ± 18 m, respectively, showing a clear relationship between DCMD and D_{NO_3} (Table 2).

The three areas considered are characterized by similar trends of conservative temperature, absolute salinity, and potential density vs. depth between 0–200 m (Fig. 3a, b, c), i.e., a homogeneity in the mixed layer followed by a drastic change at the base of the mixed layer and a break in slopes around 70 m depth. Temperature increased from the deeper layer to the surface where higher temperature characterized the austral summer heating, while lower salinity above 70 m depth indicate significant fresh water input from rainfall. The deepening of the DCMD from WMA (dark green) to WGY (blue), with an intermediate value for EMA (light green), demonstrates the westward–eastward gradient of increased oligotrophy (Fig. 3f), also reflected by corresponding D_{NO_3} ($D_{NO_3} = D_{DIN}$, see Sect. 2.2) at similar depths (Fig. 5b). The 0–70 m integrated Chl *a* decreased considerably from west to east along the transect, from 7.2 ± 2.1 mg m^{-2} for WMA to 2.0 ± 0.6 mg m^{-2} for WGY, with an intermediate value of 4.6 ± 0.7 mg m^{-2} for EMA (Table 2). When integrated over the top 200 m, no difference between Chl *a* stocks were noticeable with a mean value for the whole dataset of 19.9 ± 2.4 mg m^{-2}.

AOU showed similar patterns in all areas, with a slight decrease from the surface to a minimum between 50 and 70 m, and an increase below 70 m (Fig. 3e). The values close to zero for the first depths indicated saturation or a light supersaturation following classical rapid exchanges with atmospheric oxygen. The AOU values below, and up to, 70 m at both WMA and EMA, and to 100 m depth at WGY, indicated oversaturation. Between 70 and 200 m, almost linear relationships between AOU and depth were observed for all areas.

3.3 C, N, and P pools

The dissolved inorganic (upper), dissolved organic (middle), and particulate organic (below) C, N and P (left to right) pools are represented in Fig. 5. For N and P graphs, a Redfield ratio (RR) of 16 : 1 was systematically applied between N and P axes, allowing for a more direct comparison. DIC in µmol kg^{-1} (Fig. 4a), nDIC (normalized DIC) in µmol kg^{-1} (Fig. 4c), and nDIC in µmol L^{-1} (Fig. 5a) showed linear increasing trends with depth in all areas between 70 and 200 m. The specific variations in nDIC close to the surface will be discussed later. Total alkalinity increased rapidly with depth between 0 and 70 m and was more or less constant down to 200 m (Fig. 4b). Normalized total alkalinity indicated no change in concentration with depth (Fig. 4d), showing that total alkalinity variations were related to fresh water input. Surface $p^{oc}_{CO_2}$ was everywhere close to or below the average atmospheric p_{CO_2} of 383 µatm (Table 5). Nitrate (DIN) was under the QL everywhere in the upper surface down to 70 m (Fig. 5b). Then the increase with depth (nitracline) was almost the same in each area (similar slopes, S_{NO_3}) but did not begin at the same depth (D_{NO_3}), as previously described. Phosphate (DIP) concentrations were considerably higher than nitrate concentrations (considering RR) everywhere except close to the surface at WMA and EMA, where they reached QL. High DIP concentrations around 0.2 µmol L^{-1} in the upper 70 m were observed at WGY (Fig. 5c). The depletion in DIP was higher in EMA than in WMA (Fig. 5c). DOC, DON, and DOP concentrations were higher close to

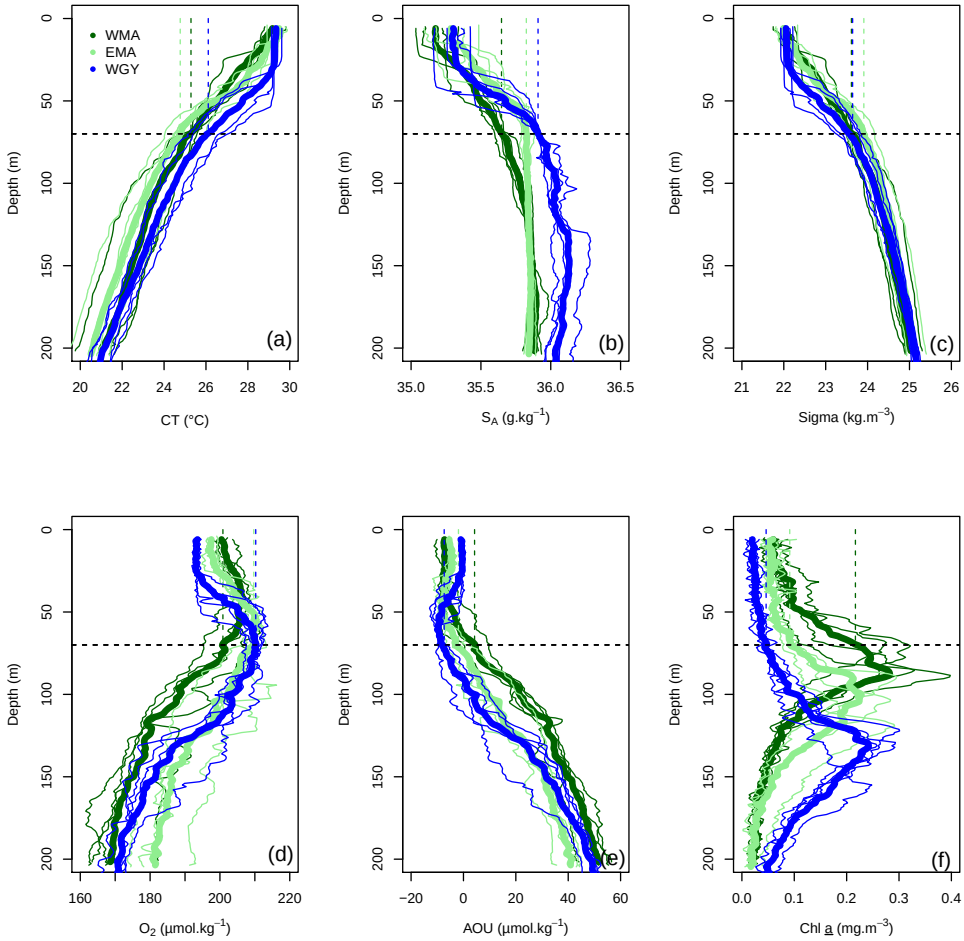

Figure 3. Vertical profiles of **(a)** conservative temperature (CT in °C), **(b)** absolute salinity (S_A in g kg^{-1}), **(c)** potential density (Sigma in kg m^{-3}), **(d)** dissolved oxygen (O_2 in µmol kg^{-1}), **(e)** apparent oxygen utilization (AOU in µmol kg^{-1}), and **(f)** Chl *a* (mg m^{-3}) versus depth (0–200 m) in the three distinct areas sampled during the OUTPACE cruise: the western Melanesian Archipelago (WMA in dark green), the eastern Melanesian Archipelago (EMA in light green), and the western SP gyre (WGY in blue). The horizontal dashed lines indicate the mixed layer depth of 70 m. The vertical dashed lines indicate the upper surface expected values for all variables during the 2014 austral winter.

the surface (Fig. 5d, e, f) and decreased almost linearly with depth down to 200 m with only slight differences between the different areas, particularly for the deeper depth measurements where ∼ 50, 4, and 0.07 µmol L^{-1} of DOC, DON, and DOP were measured, respectively. The concentration increases at the surface compared to the values at 200 m depth corresponded roughly to around 25, 1.5, and 0.1 µmol L^{-1} of DOC, DON, and DOP, respectively (in similar proportions to the RR for N and P, but more than 2-fold higher for C). The particulate organic C, N, and P pools showed similar patterns with depth between 70 and 200 m but diverged in the upper layer between the different areas (Fig. 5g, h, i). No significant changes were observed at WGY, while significant increases in concentration close to the surface were observed both in WMA and EMA. The increases in surface water concentrations compared to the value at 200 m depth corresponded roughly to changes around 5, 0.5, and 0.03 µmol L^{-1} of POC, PON, and POP, respectively (in relatively similar proportions to the RR for C, N, and P).

The 0–70 m depth inventories are presented in Table 3. Interestingly, there were very similar C stocks in the three areas, both for the dissolved inorganic and dissolved organic pools. The particulate organic C pool was twice lower in WGY than in the MA. Very similar observations were obtained for all N pools. Nevertheless, DIN stocks were negligible in all areas. DIP stocks were different, and higher in the gyre. The other P pools follow the same pattern as C and N pools, i.e., almost identical in the three areas concerning the dissolved organic pool and twice lower in the gyre for the particulate pool.

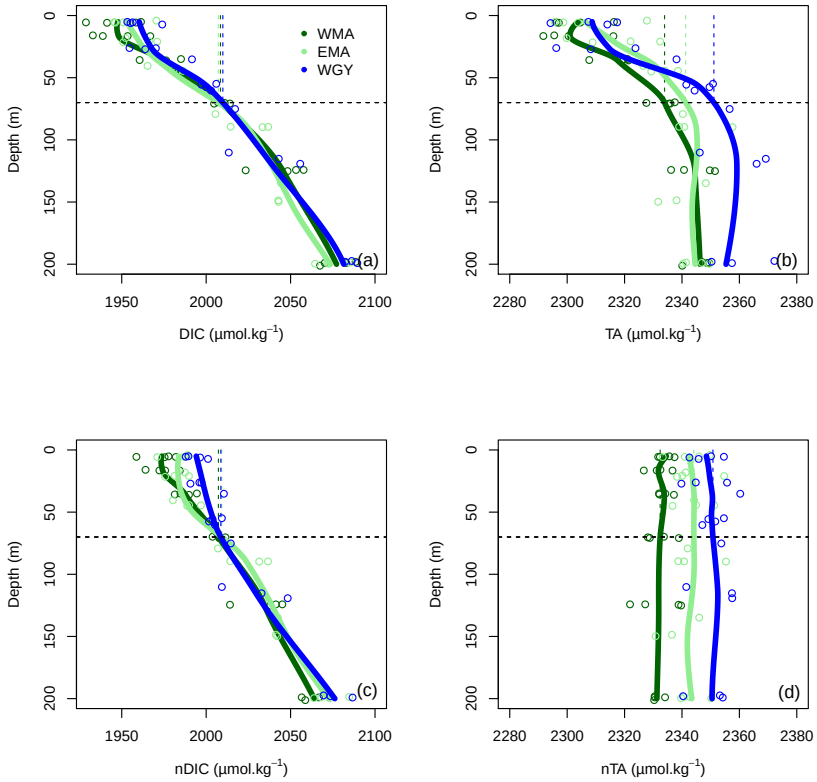

Figure 4. Vertical profiles of **(a)** dissolved inorganic carbon (DIC), **(b)** total alkalinity (TA), **(c)** normalized dissolved inorganic carbon (nDIC), and **(d)** normalized total alkalinity (nTA) against depth (m) for the three distinct areas sampled during the OUTPACE cruise: the western Melanesian Archipelago (WMA in dark green), the eastern Melanesian Archipelago (EMA in light green), and the western SP gyre (WGY in blue). The horizontal dashed lines indicate the mixed layer depth of 70 m. The vertical dashed lines indicate the upper surface expected values for all variables during the 2014 austral winter.

3.4 C, N, and P fluxes

Some major fluxes, PP and N_2 fixation rates, together with DIP turnover times, are shown Fig. 6. All rates are considerably higher for WMA and EMA than for WGY, where values indicated only slight differences with depth. Conversely, higher PP (Fig. 6a) and N_2 fixation (Fig. 6b) rates were measured close to the surface, and rapidly decreased with depth reaching negligible values below 50 m and beyond for WMA and EMA. T_{DIP} values of around 100 days for WGY contrast with lower values for WMA and EMA upper waters close to or even below 2 days (Fig. 6c).

Particulate matter mass flux and swimmer contents collected with sediment traps are presented in Table 4 with C, N, and P partitioning. Wide variability occurs between measurements as shown by the minimum and maximum values obtained. Nevertheless, a mean particulate matter mass flux of 48 mg d^{-1}, 3 times higher in the MA compared to WGY, was obtained, in good agreement with the higher PP rates and biomass in the MA compared to the gyre. Swimmer contents were also highly variable and represent, as a mean, 9.7 (min: 0.7, max: 26.0) times more mass (dry weight) per day than the settling particles in the MA, and 4.4 (min: 1.4, max: 7.1) times for WGY. The mean proportion of C, N, and P in the settling organic matter was 106 : 12.7 : 1.2 for MA and 106 : 16.6 : 0.5 for WGY are in relatively good agreement with the theoretical 106 : 16 : 1 RR. Note that this is also the case for C, N, and P proportions in swimmers both for MA (106 : 15.8 : 0.7) and WGY (106 : 19.9 : 0.7), particularly when P measured in the supernatant was added to the swimmers (see $*$ in Table 4). Otherwise, very low and improbable P contents were found in the swimmers (see the previous column in Table 4).

4 Discussion

4.1 A significant biological carbon pump in the WTSP fueled by N_2 fixation

We use the surface $p^{oc}_{CO_2}$ expected seasonal changes between austral winter and summer in order to draw a first picture of the role of the biological pump in the WTSP. Surface $p^{oc}_{CO_2}$ is determined by temperature and salinity changes, and by processes affecting the DIC and alkalinity concentrations, which

includes gas exchange, the biological pump, lateral and vertical advection, and mixing (Sarmiento and Grüber, 2006). We will consider that the horizontal spatial scale is large enough to avoid considering lateral advection. Numerical horizontal particle experiments integrating several months of satellite data using Ariane (Rousselet et al., 2018), together with the relative homogeneity of SST along the 4000 km water transect (Moutin et al., 2017a), provides support for this first assumption. Furthermore, we will consider that the influence of salinity changes on the "soft tissue" pump is negligible, as generally considered (Sarmiento and Grüber, 2006).

Upper surface temperature variations between the 2014 austral winter and the 2015 austral summer period were estimated to be 3.6 ± 0.6, 4.5 ± 1.2, and 3.4 ± 1.3 °C for WMA, EMA, and WGY, respectively. Estimated winter $p^{oc}_{CO_2}$ were 372, 355, and 364 µatm (Table 5). Following the Takahashi et al. (1993) calculation ($\Delta p^{oc}_{CO_2|Thermal} \approx p^{oc}_{CO_2} \cdot 0.0423 \cdot \Delta T$), considering a closed system with constant DIC and Alk, we estimate an increase in $p^{oc}_{CO_2}$ to be +57, +68, and +52 µatm following summer warming for WMA, EMA, and WGY, respectively. The seasonal warming should result in an ~ 60 µatm increase in $p^{oc}_{CO_2}$, which is not observed for any group of stations; indeed, the differences in $p^{oc}_{CO_2}$ were $366 - 372 = -6$, $376 - 355 = +21$, and $390 - 364 = +26$ µatm between winter and summer for WMA, EMA, and WGY, respectively (Table 5). The differences were obtained from normalized DIC and Alk measured during the OUTPACE cruise in the MLD and estimated from the expected normalized winter DIC and Alk. The lower than expected $p^{oc}_{CO_2}$ changes suggest that the seasonal variations of $p^{oc}_{CO_2}$ due to SST changes are counterbalanced by a seasonal reduction due to DIC and/or Alk changes. We can estimate this term by removing p_{CO_2} changes due to thermal variation from the observations ($\Delta p^{oc}_{CO_2|DIC,Alk} = \Delta p^{oc}_{CO_2|observed} - \Delta p^{oc}_{CO_2|thermal}$), resulting in −63, −47, and −26 µatm for WMA, EMA, and WGY, respectively. The negative signs imply a decrease in DIC or an increase in Alk between winter and summer. When normalized, we do not observe any difference in Alk with depth (Fig. 4d), suggesting that seasonal salinity changes due to high rainfall may explain the small change in Alk observed (Fig. 4b). Therefore, the carbonate pump does not seem to play a significant role in the WTSP, and consequently, we expect a major role of the "soft tissue" pump and thus DIC variations. Considering a Revelle factor γ_{DIC} of 9.5, we calculate DIC changes of −35.8, −28.0, and −15.0 µmol kg^{-1} ($\Delta DIC = DIC / p^{oc}_{CO_2} \gamma_{DIC} \cdot \Delta p^{oc}_{CO_2|DIC,Alk}$) necessary to explain the changes in $p^{oc}_{CO_2}$ observed. We did indeed observe a decrease in nDIC concentrations of 32.9, 25.7, and 15.3 µmol kg^{-1} (Table 5) for WMA, EMA, and WGY, respectively (37.0, 30.0, and 18.7 µmol L^{-1}; Table 7, Fig. 5a) between the estimated winter concentration and the mean value measured during the OUTPACE cruise. This may explain the negative sign and the order of magnitude of the DIC changes. This result based on estimated winter values is reinforced by the fact that winter DIC from NDP-094 climatology of 2006.4 ± 0.7, 2000.9 ± 3.0, and 2004.7 ± 9.9 µmol kg^{-1} are close to our estimates for winter conditions, 2007.5 ± 3.0, 2009.6 ± 9.6, and 2008.9 ± 3.7 µmol kg^{-1}, for WMA, EMA, and WGY, respectively (Table 5). TA also showed good agreement, 2335.4 ± 0.2, 2333.6 ± 1.7, and 2343.4 ± 8.6 µmol kg^{-1} from the NDP-094 climatology and 2332.4 ± 5.0, 2344.1 ± 6.5, and 2350.8 ± 2.7 µmol kg^{-1} with our estimates for winter conditions. The differences between climatological $p^{oc}_{CO_2}$ and our estimates for winter conditions are wider (Table 5) and can be related to differences in temperature (SST from NDP-094 climatology, SST from MODIS Aqua, and T from our estimates). If $p^{oc}_{CO_2}$ are calculated from DIC and Alk (NDP-094 climatology) with SST from MODIS Aqua (361, 344, and 371 µatm) or our estimated temperatures (366, 353, and 368 µatm), the values are close to our estimated winter upper surface $p^{oc}_{CO_2}$ (372, 355, and 364 µatm for WMA, EMA, and WGY, respectively) (Table 5). Upper surface estimated DIC seasonal changes may explain why counterintuitive low seasonal $p^{oc}_{CO_2}$ changes were obtained despite significant increases in temperature. Therefore, what controls the decrease in nDIC? Is it gas exchange at the air–sea interface, mixing, and/or the biological pump?

Gas exchange may be excluded because surface water $p^{oc}_{CO_2}$ ranged from 355 to 390 µatm while the $p^{atm}_{CO_2}$ is 383 µatm, with almost no seasonal variations (Table 5). Therefore, surface waters are close to saturation at WGY or under-saturated in the MA all year round and will uptake CO_2 from the atmosphere, and as a result DIC should then increase, which was not observed. Thus, our observations are more biological in origin, but there is an inconsistency. The significant decrease in nDIC (Fig. 5a and Table 7), indicating a significant biological soft tissue pump, coincided with no significant changes in nitrate concentration, which were ≤ 0.03 µmol L^{-1} in all areas (Fig. 5b, Table 7), indicating no or almost no nitrate input by deep winter mixing. Considering the low nitrogen input by upward nitrate turbulent diffusion (see later), we have to consider another nitrogen source, N_2 fixation (Fig. 6b), which is really high in the upper water of the WTSP, recently identified as a hotspot for N_2 fixation (Bonnet et al., 2017).

The estimated seasonal nDIC (ΔDIC) variations for the MA waters of 32.9 and 25.7 µmol kg^{-1} for WMA and EMA, respectively, can be compared to those measured in oceanic gyre time-series sites. They are higher than the $\Delta DIC \sim 15$ µmol kg^{-1} observed at the HOT station in the North Pacific subtropical gyre near Hawaii (Dore et al., 2003), and close to the $\Delta DIC \sim 30$ µmol kg^{-1} observed at BATS in the subtropical North Atlantic gyre near Bermuda (Bates et al., 2012), where ΔDIC is at least partially attributable to nitrate from below (Sarmiento and Grüber, 2006). Interestingly, the estimated amplitude of surface DIC

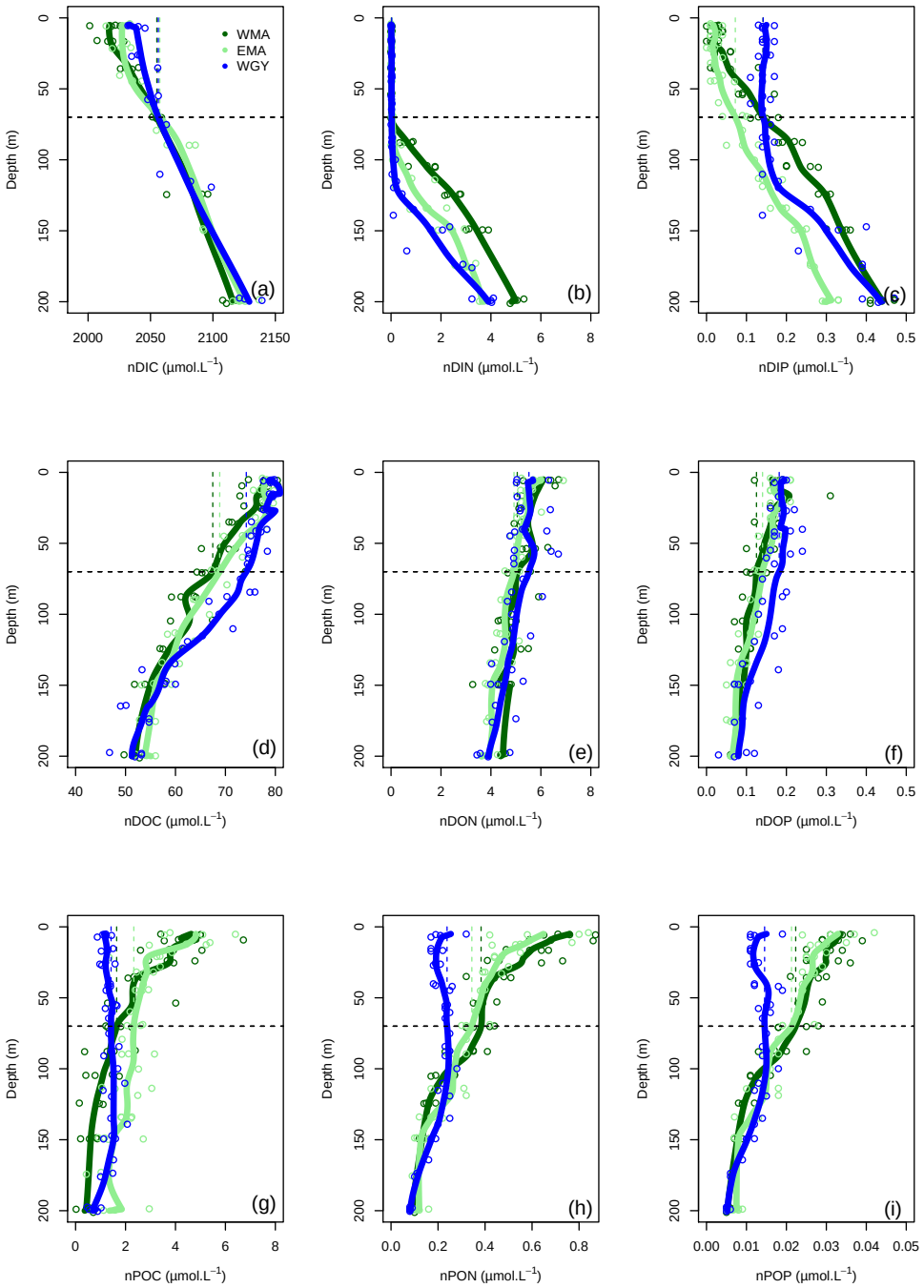

Figure 5. Vertical profiles of normalized (n) C, N, and P data against depth (m). Dissolved inorganic (DI), dissolved organic (DO) and particulate organic (PO) C **(a, d, g)**, N **(b, e, h)**, and P **(c, f, i)**, respectively, in µmol L^{-1}, for the three distinct areas sampled during the OUTPACE cruise: the western Melanesian Archipelago (WMA in dark green), the eastern Melanesian Archipelago (EMA in light green), and the western SP gyre (WGY in blue). The horizontal dashed lines indicate the mixed layer depth of 70 m. The vertical dashed lines indicate the upper surface expected values for all variables during the 2014 austral winter.

seasonal change for the MA is only twice lower than the around 50 µmol kg^{-1} DIC decrease measured between March and April in the North Atlantic (Merlivat et al., 2009), in an area known to experience a large bloom of phytoplankton. The biological "soft tissue" carbon pump, fueled almost exclusively by N_2 fixation (see Sect. 4.2), therefore plays a significant role in the WTSP.

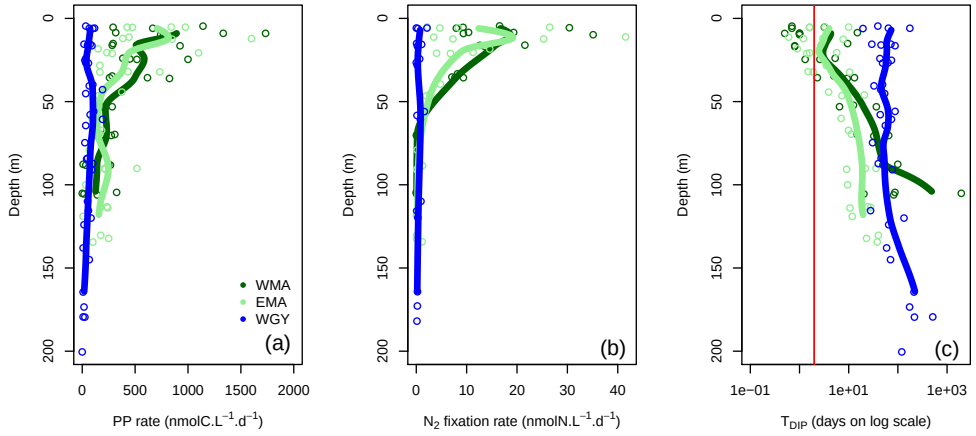

Figure 6. Vertical profiles of **(a)** primary production (PP rate in nmolC L^{-1} d^{-1}), **(b)** N_2 fixation rate (nmolN L^{-1} d^{-1}) and dissolved inorganic phosphate turnover times (T_{DIP} in days on log scale) against depth for the three distinct areas sampled during the OUTPACE cruise: the western Melanesian Archipelago (WMA in dark green), the eastern Melanesian Archipelago (EMA in light green), and the western SP gyre (WGY in blue). The vertical red line indicates the critical DIP turnover time of 2 days.

4.2 A net sink of atmospheric CO_2

Quantification of the major biogeochemical fluxes on a daily basis allows for certain conclusions to be drawn concerning the upper biogeochemical cycles of C, N, and P (Table 6). C-budgets of the 0–70 m upper layer showed that the MA area appears as a net sink of atmospheric CO_2 with a mean atmospheric carbon input in the ocean of 1250 µmol m^{-2} d^{-1}. Sediment trap POC export was one order of magnitude higher than POC or DOC export by turbulent diffusion, which represented only 7–12 % of the total organic export. Without considering any additional flux, the budget resulted in a surprising daily net accumulation of carbon of 859 µmol m^{-2} d^{-1} for WMA, and a quasi-equilibrium for EMA and WGY. Note that the accumulation at WMA resulting in an increase of only several nmol L^{-1} d^{-1}, is considerably below what we are able to measure at the present time, and longer timescales are thus needed to observe and study the changes (Sect. 4.3).

Averaged integrated PP (IPP) rates were 33.3 ± 12.1, 26.4 ± 16.2, and 6.5 ± 2.4 mmol m^{-2} d^{-1}, and export by settling and turbulent diffusion (Table 6, in µmol m^{-2} d^{-1}) represented only 1.2, 1.2, or 0.3 mmol m^{-2} d^{-1}, for WMA, EMA, and WGY, respectively. The organic matter exported daily compared to IPP represented 3.6, 4.5, and 4.6 %, respectively, in good agreement with previous measurements in oligotrophic areas (Moutin and Raimbault, 2002; Karl et al., 2012), with a high proportion relative to particles settling, 3.3, 4.1, and 4.1 %, rather than turbulent diffusion. Swimmer contents are really high in the sediment traps, considerably above fluxes by settling material (Table 4, last column) and diel vertical migrations of mesozooplankton-micronekton, already observed in the MA (Smeti et al., 2015) and might play a significant role in the transfer of carbon from the upper surface in deeper layers. These organisms spend half of the daytime at depth around 500 m where they loose carbon by respiration.

Except for the WMA area, there were no DIN gradients around 70 m depth and therefore no nitrate input from below by turbulent diffusion (Table 6). Nitrogen input by N_2 fixation was by far the largest input of new nitrogen (at least 83 %), and reached values among the highest measured anywhere in the open ocean (Caffin et al., 2018; Knapp et al., 2018). A net daily accumulation of nitrogen is estimated for MA and equilibrium for WGY. Zooplankton diel migrations may also play a significant role in daily N budgets through defecation, excretion, or mortality at depth (Caffin et al., 2018; Valdés et al., 2018). Averaged integrated N_2 fixation rates were 0.64 ± 0.21, 0.45 ± 0.27, and 0.04 ± 0.04 mmol N m^{-2} d^{-1} for WMA, EMA, and WGY, respectively. The very high N_2 fixation rates in the MA, compared to other areas in the world (Bonnet et al., 2017), may provide the new nitrogen required for new PP, creating the necessary decrease in $p^{oc}_{CO_2}$ to stimulate CO_2 invasion.

The daily P budgets of the 0–70 m upper layer showed losses greater than inputs, in complete contrast to daily C and N budgets showing accumulation in the WMA (Table 6). This observation indicates why this element, compared to carbon and nitrogen, may rapidly become a limiting factor for biological production and specifically of the input of nitrogen by N_2 fixation in the MA (Moutin et al., 2008). Nevertheless, the mean particulate P export seemed relatively high (Table 6) and should be considered with caution, considering the huge range of variation, from 0.6 to 68.9 µmol m^{-2} d^{-1}, for only eight measurements in the MA.

4.3 Estimated seasonal trends of the major biogeochemical stocks and fluxes

As already stated, the dashed lines in Figs. 3, 4, and 5 indicate the upper surface expected values for all variables during the 2014 austral winter, and allow evaluation of the temporal variation toward the 2015 austral summer season (full lines) in each area corresponding to the OUTPACE dataset. The hypothesis allowing this first-order estimation of seasonal variation was presented in Sect. 2.1, validated for SST and Chl *a* variations in Sect. 3.1, and shown to give good agreement with upper surface DIC expected seasonal changes (Sect. 4.2).

Conservative temperature (Fig. 3a) increased everywhere, but more for WMA and EMA than for WGY, while absolute salinity decreased everywhere. Potential density values were similar in each area at 70 m depth. Similar mean depths of convection were estimated for the three areas (min of 68 m at LD A and max of 73 m at LD C), and justified the mean value of 70 m taken into account for the whole OUTPACE area. The rapid exchange of oxygen between ocean and atmosphere pre-empted significant seasonal changes in the upper surface (Fig. 3d, e). The vertical homogeneous Chl *a* concentration expected in winter (Fig. 3f) was shown to be in good agreement with climatological SSChl *a* (Sect. 3.1). Part of the relatively high Chl *a* concentration estimated in July 2014, specifically in WMA, is probably linked to enhanced vertical winter mixing from the DCM.

The seasonal C, N, and P pool changes may be followed by concentration in Fig. 5 but are easier to discuss as 0–70 m water column inventories (Table 8). As previously indicated, DIC decreased in all areas but more so in the west than in the east (Fig. 5a), following the already described oligotrophic gradient clearly shown both in biomass (Fig. 3f) and in PP (Fig. 6a). The DIC decrease was partially compensated for by the increase in organic concentrations, with the increase in the dissolved concentrations (Fig. 5d) being larger than those of the particulates (Fig. 5g). No increase in the particulate carbon concentration was found for WGY. The decrease in TC (representing the sum of all pools) between winter and summer indicated that 68.1, 61.9, and 68.3 % of ΔDIC were lost from the upper layer, i.e., only 31.9, 38.1, and 31.7 % accumulated in the organic C pools for WMA, EMA, and WGY, respectively (Table 8). Therefore, organic matter accumulation may partly explain why the large input of atmospheric carbon did not result in DIC accumulation in the MA waters. It may partly explain why the total carbon pool decreased so much seasonally. Following the RR, DIN decreases of 236, 198, and 109 mmol m^{-2} might be expected from the DIC decreases. The DIN decreases were indeed around 0–2 mmol m^{-2}, which is in concordance with very poor DIN replenishment of the upper water column. Conversely, increases of the PON stocks of the same order of magnitude as the RR predicts from POC stocks for WMA and EMA were observed (C : N of 12.0 and 7.3, compared to the RR of $C:N = 106:16 = 6.6$), with a small PON decrease for WGY. The largest increases for the organic pools were for the dissolved phase in all areas (Table 8). DOC accumulation was 3.8 and 8.1 times higher than POC accumulation for WMA and EMA, respectively. Only DOC accumulated at WGY, but with a change twice lower in magnitude than in the MA waters (Table 8). A relatively stronger dissolved organic carbon production compared to particulate production may be observed in oligotrophic areas, depending largely on light and nutrient availabilities (Carlson, 2002). In oligotrophic areas characterized by a low export of particulate organic matter, relatively large dissolved organic matter production, and heterotrophic bacteria often limited by nutrients (Van Wambeke et al., 2002), DOC may accumulate (Copin-Montégut and Avril, 1993; Marañón et al., 2005; Pujo-Pay et al., 2011), which is indeed observed (Fig. 5d). Dissolved organic carbon accumulation reached 391, 445, and 220 mmol m^{-2} over 8 months (Table 8), which dispersed over 70 m gives a mean 8-month accumulation of 7.0, 7.1, and 3.0 µmol L^{-1} for the 0–70 m water column. These values, while lower, are of the same order of magnitude of DOC concentration changes observed in the upper mixed layers of 10.1, 9.3, and 5.0 µmol L^{-1} for WMA, EMA, and WGY, respectively (Fig. 5d, Table 7). Interestingly, the western SP was recently shown as a localized refractory dissolved organic carbon sink (Hansell and Carlson, 2013).

No significant DIN inventory changes were observed, while strong increases in the DON stocks and similar but relatively lower increases were observed for the PON stocks for WMA and EMA (Table 8; Fig. 5e, h). The TN evolution was a net increase in inventories between winter and summer of 49 and 34 mmol m^{-2} for WMA and EMA, respectively. No significant changes in the N pools were observed at WGY (Table 8, Fig. 5b, e, h). A decrease in DIP stocks was observed in the MA waters between the winter and summer, with no significant change for WGY (Table 8). Following the RR, DIP decreases of 14.7, 12.3, and 6.8 mmol m^{-2} might be expected from the DIC decreases. The DIP decreases were indeed less, 5.9 and 3.1 mmol m^{-2} for WMA and EMA, and no decrease was observed at WGY. The DIC decreases are probably only partially related to the DIP decreases in the MA. As for C and N, the highest organic P inventory increases were for the dissolved phase (Fig. 5f, Table 8). Nevertheless, the changes were close to the SD calculated for the mean concentrations and should be considered with caution. As an example, the 1.8 mmol m^{-2} increase in DOP concentrations for EMA (Table 8) corresponds to the difference between 11.6 ± 1.1 mmol m^{-2} during winter and 9.8 ± 2.0 mmol m^{-2} during summer. Note that the SD reported is the maximum SD calculated at each season (Table 8). Small or no decreases in the organic P pools were observed for WGY. Finally, it is clear that seasonal C losses were not compensated by organic carbon accumulation in the 0–70 m layer. Therefore, organic carbon production, which represents by far the largest flux in each area,

should be linked with an efficient export from the upper layer, not directly related to RR.

We shall now try to connect the seasonal variations in C, N, and P stocks with the estimated C, N, and P fluxes in order to determine first-order budgets and characterize the main seasonal trends in the WTSP. Our very simple model considers an instantaneous winter mixing followed by 8 months (240 days) of C, N, and P fluxes at the same rates as the mean rates measured during the OUTPACE cruise. All fluxes expressed in mmol m^{-2} and corresponding to the 8-month period defined (July 2014–March 2015) are summarized in Fig. 7. Accumulation rates are presented inside the boxes and input and output fluxes outside the boxes, with arrows for direction (+ for input, − for output). The X value corresponds to the flux necessary to reach equilibrium in each box. The main question is still how can we explain the large DIC losses in all areas? Even though we obtained (1) a significant DIC input by winter convection and turbulent diffusion, (2) low export of organic matter by settling or turbulent diffusion during the summer period, and (3) a $p^{oc}_{CO_2}$ lower than or equal to the $p^{atm}_{CO_2}$ meaning a DIC enrichment by atmospheric exchanges, and furthermore (4) no significant input of DIN from below in the 0–70 m upper layer.

The source of new N required to sustain new PP is clearly N_2 fixation (Fig. 7b, e, h). Converted to C using the RR of 6.6, new production may represent 12.8, 11.3, and 4.2 % of IPP of 7.94, 6.34, and 1.56 mol m^{-2} for the 8-month period in the WMA, EMA, and WGY, respectively. New production ≤ 5 % is typical of strong oligotrophic conditions (Moutin and Raimbault, 2002), while above 5 % is related to more productive areas or areas with high N_2 fixation rates (Karl et al., 2012). Taking into account the fact that the previous values are for 8 months only, we can estimate annual production rates of 145, 116, and 28 gC m^{-2} yr^{-1} for WMA, EMA, and WGY, respectively, close to the average rate of 170 gC m^{-2} yr^{-1} reported for the ALOHA station in the North Pacific central gyre (Karl et al., 1996), and to the 86–232 gC m^{-2} yr^{-1} range reported for the Mediterranean Sea at the DYFAMED site (Marty and Chiavérini, 2002), known as oligotrophic areas.

Having found the source of new N, several hypotheses may be considered in order to answer the question regarding DIC losses. A first hypothesis is an episodic or seasonal high export of matter considerably different from that measured during the end of the summer season (OUTPACE cruise). We cannot discard this hypothesis specifically because no seasonal data are available at the present time, and also because episodic yet large export fluxes have already been reported in other oligotrophic areas (Böttjer et al., 2017). Nevertheless, the relative constant Chl *a* concentration during the entire period considered in the upper water column (Fig. 2c, f, i), where most of the production is likely to occur (Fig. 6a), preferentially suggests relatively constant production and therefore export. Furthermore, the C, N, and P proportions of the X fluxes (Fig. 7) in all areas are completely different from RR, even in an opposite sense for P (Fig. 7c, f, i), suggesting that such C fluxes were not directly related to organic matter settling.

A second hypothesis might be in relation to diel vertical migrations of zooplankton-micronekton already described in the MA (Smeti et al., 2015), which may explain significant C losses with proportionally lower N losses and no P losses (Fig. 7). Indeed, mesozooplankton-micronekton feed at night in order to avoid predators and migrate to spend half of the time at around 500 m depth where they respire and lose carbon. Chl *a* varied only between 0.05 and 0.20 mg m^{-3} in the MA upper surface, suggesting a strong top-down control by zooplankton able to maintain pigment concentration in a quasi-steady state for many months (Banse, 2013). Zooplankton-micronekton diel vertical migrations, the latter being widespread in the ocean and forming a fundamental component of the biological pump generally overlooked in global models (Bianchi et al., 2013) and well known in the Pacific Ocean (Zhang and Dam, 1998; Al-Mutairi and Landry, 2001; Landry et al., 2011), might explain part of the unexplained ΔDIC observed in the upper surface waters. A third hypothesis might be an underestimation of the settling carbon through methodological issues, mainly concerning the performance of traps (Buesseler et al., 2007) or solubilization (Antia, 2005), which is impossible to take into account without specific measurements. There is in fact no reliable way to separate the swimmers contribution to different elements from that originating from the passive flux (Antia, 2005), and in particular, using formalin, we cannot measure the DOC in the trap supernatant.

Tropical storms, such as Cyclone Pam observed during the OUTPACE cruise (de Verneil et al., 2018), might have an influence on seasonal budgets. Law et al. (2011) reported the effect of such a cyclone in the north Tasman Sea. There was no nitrate entrainment but rather phosphate entrainment due to explicit differences in nitracline and phosphacline depths. This allowed nitrogen fixation to be enhanced in a process close to that we described in our study, albeit in response to physical forcing acting at a smaller spatial scale than winter mixing. During OUTPACE, the strong wind-forcing event Pam entered the southwest Pacific in early March, and a drop in SST and increase in Chl *a* followed in its wake. The storm did indeed have a fertilizing effect but at relatively short spatial (around Vanuatu islands) and time (around 2 weeks) scales, compared to the larger-scale processes highlighted in the present study.

Mesoscale structures have been previously shown to influence PP (Falkowski et al., 1991; Oschlies and Garçon, 1998; Moutin and Prieur, 2012; Levy et al., 2015). Nevertheless, the mesoscale vertical fluxes due to quasi-geostrophic forcing calculated from satellite data during OUTPACE were weak and acted on a layer displaced from the relevant nutrient reservoirs (de Verneil et al., 2018). The seasonal vertical nutrient input into the photic layer, mainly driven by deep

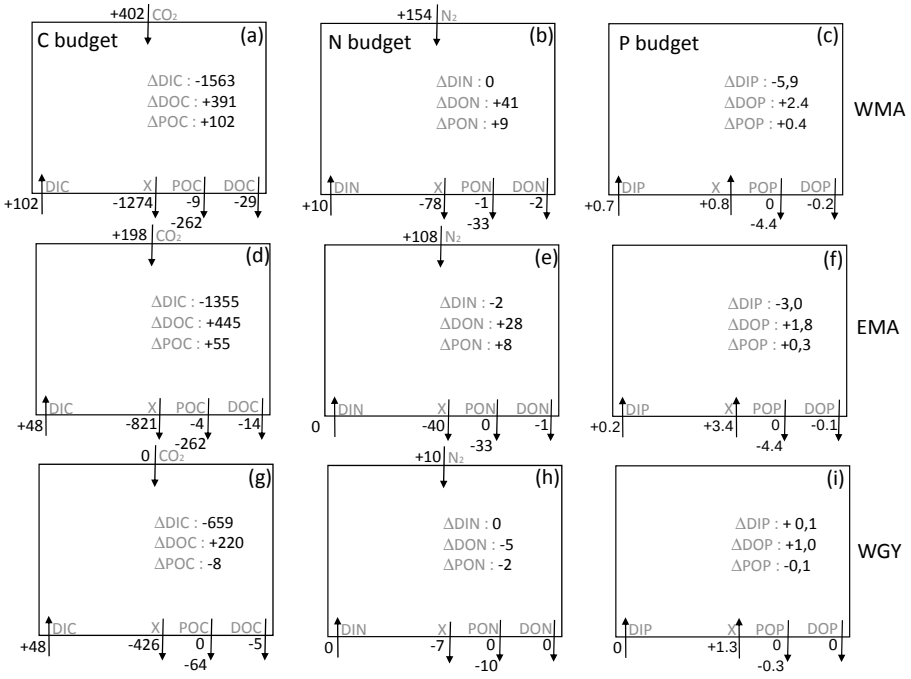

Figure 7. C, N, and P estimated budgets in the 0–70 m water column during the 8-month period between deep convection in July 2014 (austral winter) and strong stratification in March 2015 (austral summer) for the three distinct areas sampled during the OUTPACE cruise: the western Melanesian Archipelago (WMA, top), the eastern Melanesian Archipelago (EMA, middle), and the western SP gyre (WGY, bottom). C budgets **(a, d, g)**, N budgets **(b, e, h)**, and P budgets **(c, f, i)** are shown. Dissolved inorganic (DI), dissolved organic (DO), and particulate organic (PO) C, N, and P fluxes are considered, respectively. Atmospheric exchanges limited to CO_2 penetration and N_2 fixation are indicated. All fluxes are expressed in mmol m^{-2} (of elemental C, N, and P, respectively) with arrows indicating direction (input or output). The two numbers for the particulate fluxes correspond to fluxes by turbulent diffusion (above) and particle settling (below). Estimated accumulation rates for the same period are indicated inside the boxes.

vertical mixing, will be the main influence on annual biological production, whereas summertime mesoscale activity will primarily influence the horizontal spatial distribution of phytoplankton (Rousselet et al., 2018).

4.4 Iron and phosphate availabilities as key factors controlling the N input by N_2 fixation and the biological carbon pump in the WTSP

The western SP is known as an iron-rich area (Wells et al., 1999). Iron concentrations measured during the DIAPALIS cruises (http://www.obs-vlfr.fr/proof/vt/op/ec/diapazon/dia.htm, last access: 8 May 2018) near New Caledonia (Martine Rodier, unpublished data in Van den Broeck et al., 2004) were higher than concentrations reported in the subtropical North Pacific (Landing and Bruland, 1987), and indicated no clear seasonal variations. Average iron concentrations of 0.57 nmol L^{-1} were reported in the upper surface waters of the WTSP (Campbell et al., 2005), higher than the $\sim$0.1 nmol L^{-1} measured in the upper 350 m water column of the SP gyre (Blain et al., 2008) where fericline depths were located well below nitracline depths (Blain et al., 2008). The Equatorial Undercurrent, which originates near Papua New Guinea, close to New Caledonia, is known to be a source of iron in the SP Ocean (Wells et al., 1999; Ganachaud et al., 2017). Nevertheless, atmospheric deposition fluxes of iron are very low (Duce and Tindale, 1991; Wagener et al., 2008). During OUTPACE, the apparent contradiction between low atmospheric deposition of iron and high surface water iron concentration was resolved. The high iron average concentration within the photic layer in the MA (1.7 nmol L^{-1}) compared to WGY (0.3 nmol L^{-1}) was shown to be related to the influence of hydrothermal sources at shallower depths than commonly associated with volcanic activities (Guieu et al., 2018), confirming the importance of a hydrothermal contribution to the oceanic iron inventory (Tagliabue et al., 2010, 2017; Fitzsimmons et al., 2014). The averaged 0–70 m integrated concentrations were 0.57 ± 0.14, 1.18 ± 1.02, and 0.28 ± 0.03 nM for WMA, EMA, and WGY, respectively. Iron is a major component of the nitrogenase enzyme that catalyzes N_2 fixation (Raven, 1988). The high iron concentration likely alleviates the iron limitation of N_2 fixation in the WTSP, again considered as a hotspot of N_2 fixation (Bonnet et al., 2017).

Phosphate turnover time (T_{DIP}) represents the ratio between natural concentration and uptake by planktonic species (Thingstad et al., 1993) and is considered the most reliable measurement of phosphate availability in the upper ocean waters (Moutin et al., 2008). Phosphate availability in the MA, characterized by DIP $< 50\,nmol\,L^{-1}$ and T_{DIP} reaching below 2 days, is considerably lower than in the SP gyre, with DIP concentrations above $100\,nmol\,L^{-1}$ and T_{DIP} in the order of magnitude of months (Fig. 6c), as already reported (Moutin et al., 2008). Phosphate availability, as well as PP, were shown to follow the same seasonal patterns close to New Caledonia in the MA, suggesting that in this iron-rich area known to sustain high N_2 fixation rates, phosphate may appear as a key factor controlling carbon production (Van den Broeck et al., 2004). It was suggested that a seasonal pattern of phosphate availability with higher values (low DIP, high T_{DIP}) related to winter mixing and lower values (higher DIP, lower T_{DIP}) during the stratified period might control *Trichodesmium* spp. growth and decay in the SP near New Caledonia (Moutin et al., 2005). A T_{DIP} below 2 days was shown to be critical for *Trichodesmium* spp. growth (Moutin et al., 2005). T_{DIP} below or close to 2 days was measured in the MA upper waters during the OUTPACE cruise (Fig. 6c), and T_{DIP} as low as several hours was measured at LD B station and has been related to the strong biomass and specifically *Trichodesmium* spp. decline observed at this station (de Verneil et al., 2018). With T_{DIP} around or even below 2 days, the MA appears as a low P area during the stratified period, indicating a probable role of phosphate availability in the control of nitrogen input by the nitrogen fixers. The higher iron availability in the MA is probably the main factor allowing N_2 fixation to occur, and phosphate availability the main factor controlling the annual input of N by N_2 fixation. A T_{DIP} of 2 days corresponds to the lowest value reported at the ALOHA station in the North Pacific (NP; Table 2 in Moutin et al., 2008), where phosphate availability is considered to play a dominant role in the control of nitrogen fixers (Karl et al., 1997; Karl, 2014). T_{DIP} reached several hours, which is close to the phosphate availability of the Mediterranean Sea or the Sargasso Sea, known for a long time for their phosphate deficiency (Wu et al., 2000; Moutin et al., 2002). While phytoplankton and heterotrophic bacterioplankton may appear N-limited (Van Wambeke et al., 2018; Gimenez et al., 2018), the low availability of phosphate in the upper waters of the WTSP during the stratified period probably controls the biomass of nitrogen fixers and ultimately the input of nitrogen by this process. In a recent mesocosm experiment, high increases in N_2 fixation rates, PP rates, and carbon export were obtained after a DIP enrichment of WTSP waters (Berthelot et al., 2015). Nevertheless, several days were necessary to measure significant increases, indicating that regular short-term experiments to establish nutrient limitation as usually operated (Dekaezemacker et al., 2013; Moisander et al., 2012; Moore et al., 2013) may not be relevant in WTSP conditions (Gimenez et al., 2016).

The high DIP and low DIN (excess P or high P*) content of water was suggested as a preliminary condition allowing N_2 fixation to occur (Redfield, 1934; Capone and Knapp, 2007; Deutsch et al., 2007), and is a characteristic of surface waters of the SEC flowing from the east to the west in the SP, due to intense denitrification related to one of the main OMZ (oxygen minimum zone) areas in the east Pacific (Codispoti et al., 2001). The alleviation of iron limitation when waters originating from the east reach the WTSP was considered as the main factor explaining the hotspot of N_2 fixation observed in the OUTPACE area (Bonnet et al., 2017). The strong nitracline and phosphacline depth differences (Table 1), associated with winter mixing down to around 70 m, allows us to estimate a replenishment of DIP of the order of magnitude of ΔDIP ($5.9\,mmol\,m^{-2}$ for WMA and $3.0\,mmol\,m^{-2}$ for EMA; Fig. 7c, f), far above the vertical input by turbulent diffusion (around $0.7\,mmol\,m^{-2}$), together with no DIN replenishment. Alone, these DIP fluxes may support N_2 fixation of 94.4 and $48.0\,mmol\,m^{-2}$ during this period (following RR), of the order of magnitude of the fluxes of 154 and $108\,mmol\,m^{-2}$ calculated for WMA and EMA (Fig. 7b, e), respectively. While horizontal advection of high DIP and low DIN waters from the SP gyre toward the iron-rich WTSP was suggested to create the environmental conditions favorable for diazotroph growth (Moutin et al., 2008; Bonnet et al., 2017), here we suggest that local seasonal winter mixing may also play a significant role in providing excess P to the upper waters, and therefore in controlling nitrogen input by N_2 fixation and therefore the associated carbon cycle. Phosphate availability appears, in the iron-rich MA, as the ultimate control of the biological carbon pump. The simulations of the main C, N, and P fluxes at LD A and LD C, using a 1 vertical dimension model with similar physical forcing, strengthen the idea of strong seasonal variations being able to explain the control of N_2 fixation and carbon fluxes by the availability of phosphate in the MA and iron at WGY (Gimenez et al., 2018). Iron was hypothesized to prevent N_2 fixation at LD C and this allows us to obtain the high DIP concentration observed at LD C.

4.5 Toward reconciliation between simulations and observations?

During the past 10 years, global biogeochemical model simulations suggested relatively high N_2 fixation in the SP gyre and low fixation in the western part of the Pacific Ocean (Deutsch et al., 2007; Grüber, 2016), in contradiction with the little data then available. While the decrease in P* toward the center of the gyre observed during the BIOSOPE cruise (eastern tropical South Pacific, ETSP, toward the central gyre 10–30° S in latitude) corresponds to the trend observed by Deutsch et al. (2007), N_2 fixation in the simulation, with minimum values found on the edge and maximum values found in the center of the gyre, was contrary to our observations (Moutin et al., 2008). The high N_2 fixation expected in the

ETSP, because "downstream of OMZs, surface waters that initially carry a surplus of phosphorus (because of subsurface denitrification) lose this excess gradually through N_2 fixation" (Deutsch et al., 2007), was not confirmed by isotopic budgets (Knapp et al., 2016), suggesting an elusive marine N_2 fixation (Grüber, 2016). The discovery of a hotspot of N_2 fixation in the whole WTSP covered by the OUTPACE transect and other cruises in the Coral Sea (Bonnet et al., 2017) justifies considering a larger spatial coupling between denitrification and N_2 fixation than previously thought (Deutsch et al., 2007). Taking into account the role of iron to allow (or not) N_2 fixation to occur seems a necessary basis to reconcile simulations and observations (Dutkiewicz et al., 2012; Monteiro et al., 2011; Weber and Deutsch, 2014). These new modeling studies have identified the WTSP as a unique region with conditions seemingly favorable for significant N_2 fixation fluxes (Knapp et al., 2018). Interestingly, the opposite trends between expected N_2 fixation and P* observed during the BIOSOPE cruise and possibly attributed to non-Redfieldian processes (Moutin et al., 2008) may be rather due to horizontal advection and isopycnal mixing of water masses originating from the WTSP, and therefore marked by a strong signature of intense N_2 fixation (high N* corresponding to low P*; Fumenia et al., 2018), in an opposite sense than the better-known and more widely studied influence of water masses marked by a strong signature of intense denitrification originating from the OMZ (Yoshikawa et al., 2015). Furthermore, the deepening of isopycnals from the eastern to the western SP (Yoshikawa et al., 2015; Fumenia et al., 2018) suggests a deeper ($\sim$ 200 m) influence of excess P waters from the SEC in the MA, deeper than previously hypothesized (Moutin et al., 2008; Bonnet et al., 2017). Because the influence of isopycnal mixing is below the maximum mixing depth estimated in the WTSP ($\sim$ 70 m), the link between N sink in the east and N source in the west implies longer timescales than that associated only with surface circulation. The N budget of the SP Ocean is of prime interest to understand the efficiency, at the present time and in the future, of the oceanic biological carbon pump. Determining the budget requires a precise understanding of the general water mass circulation, which at the present time suffers from a lack of data, specifically during water mass formation (Fumenia et al., 2018).

5 Conclusion

We found a significant biological soft tissue carbon pump in the WTSP despite no winter replenishment of surface waters by DIN. N_2 fixation is the major process introducing the necessary N to sustain the biological soft tissue carbon pump allowing oceanic $p^{oc}_{CO_2} < p^{atm}_{CO_2}$ in the MA, and therefore significant atmospheric C input. Because of N_2 fixation, the WTSP is a significant atmospheric carbon sink.

The upper surface waters of the MA sampled during the stratified period were characterized by a DIP availability close to or below the level required for phosphate sufficiency, which contrasts with observations in the central Pacific gyre at the same latitude. We confirmed the geographical trend of a limitation of N_2 fixation in the SP, from a probable iron limitation in the east and central SP Ocean to a P limitation in the west. The limit was clearly shown to be associated with the lower depths of the MA, where sufficient iron was provided to upper surface waters to alleviate iron limitation of N_2 fixation, probably by hydrothermal sources at anomalously shallow depths. Extrapolating these data in order to obtain seasonal trends enables us to show that winter vertical mixing, although limited to 70 m depth, may bring sufficient excess P to allow most of the N_2 fixation to occur. In addition, more excess P may be locally provided in the upper surface (where N_2 fixation was shown to occur predominantly) by winter mixing than by horizontal transport from areas of excess P formation (OMZ). As previously hypothesized (Moutin et al., 2008), the low availability of phosphate in the iron-rich upper waters of the WTSP during the stratified period probably controls the biomass of nitrogen fixers and ultimately the input of nitrogen by this process, and the biological pump. As high nutrient concentrations in high nutrient low chlorophyll (HNLC) areas (Minas et al., 1986) may be considered as the result of an inefficient biological carbon pump (Sarmiento and Grüber, 2006), high phosphate concentrations (and high DIP turnover time) in the SP gyre (Moutin et al., 2008; this study) may be the result of inefficient or nonexistent N_2 fixation. Conversely, the low P availability (low concentration and DIP turnover time) in the upper surface of the WTSP is the result of intense N_2 fixation. Because iron concentrations are low in the gyre and high in the MA (even during the strongest stratified period), and because of the specific iron needs of diazotrophs, iron availability is the best candidate for preventing nitrogen fixation in the gyre and allowing nitrogen fixation in the MA. Therefore, iron availability and DIP availability may appear as the ultimate controls of biological production and export in the gyre and in the MA, respectively.

The SP Ocean deserves special attention because of its huge volume of water where the N budget is likely to be controlled by N lost in the east (denitrification) and N gain in the west (N_2 fixation). Furthermore, both diazotrophy and denitrification are expected to undergo drastic alterations due to climate change (McMahon et al., 2015; Lachkar et al., 2018). Our data suggest that one had better take into account the role of iron and phosphate in global biogeochemical models in order to better reconcile simulations and data, which seems to be the prerequisite to understand at the present time the relationship between N sources and sinks in the SP Ocean. Moreover, it will be of great interest to study future scenarios which consider iron coming from below (hydrothermal sources) in addition to that from above (atmospheric source) in the WTSP and in the whole SP Ocean. Changes in N_2

fixation following changes in dust (iron) supply have been suggested to play a central role in explaining past glacial or interglacial changes in CO_2 concentration and earth temperature. It was considered that N_2 fixation on a regional scale would change global nitrogen availability and the biological carbon pump on the timescale of ocean circulation. The direct link between N_2 fixation and carbon export proposed here for the WTSP, a hotspot of N_2 fixation, allows for a much closer coupling between N_2 fixation and the biological carbon pump, which may in turn require us to consider changes at shorter timescales such as that associated with climate change.

Data availability. All data and metadata are available at the French INSU/CNRS LEFE CYBER database (scientific coordinator: Hervé Claustre; data manager, webmaster: Catherine Schmechtig) at the following web address: http://www.obs-vlfr.fr/proof/php/outpace/outpace.php, INSU/CNRS LEFE CYBER (2017).

Competing interests. The authors declare that they have no conflict of interest.

Special issue statement. This article is part of the special issue "Interactions between planktonic organisms and biogeochemical cycles across trophic and N_2 fixation gradients in the western tropical South Pacific Ocean: a multidisciplinary approach (OUTPACE experiment)". It is not associated with a conference.

Acknowledgements. This is a contribution of the OUTPACE (Oligotrophy to the UlTra-oligotrophy PACific Experiment) project (https://outpace.mio.univ-amu.fr/, last access: 8 May 2018) funded by the French research national agency (ANR-14-CE01-0007-01), the LEFE-CYBER program (CNRS-INSU), the GOPS program (IRD), and the CNES (BC T23, ZBC 4500048836). The OUTPACE cruise (https://doi.org/10.17600/15000900) was managed by the MIO (OSU Institut Pytheas, AMU) from Marseille (France) and received funding from European FEDER fund under project 1166-39417. The authors thank Nicolas Metzl for constructive comments on the manuscript and the SNAPO-CO_2 (Service National d'Analyse des paramètres Océaniques du CO_2-LOCEAN – Paris). The authors also thank the crew of the R/V *L'Atalante* for outstanding shipboard operation. Gilles Rougier and Marc Picheral are warmly thanked for their efficient help in CTD rosette management and data processing, as is Catherine Schmechtig for the LEFE-CYBER database management. The satellite-derived data of sea surface temperature and Chl *a* concentration and current have been provided by CLS in the framework of the CNES funding; we warmly thank Marie Isabelle Pujol and Guillaume Taburet for their support in providing these data. Aurelia Lozingot is acknowledged for the administrative work.

We acknowledge NOAA, and in particular Rick Lumpkin, for providing the Surface Velocity Program drifter. The Argo data were collected and made freely available by the international Argo project and the national programs that contribute to it (http://www.argo.ucsd.edu, http://argo.jcommops.org, last access: 8 May 2018). Argo is a pilot program of the Global Ocean Observing System. Argo DOI (https://doi.org/10.17882/42182). All data and metadata are available at the following web address: http://www.obs-vlfr.fr/proof/php/outpace/outpace.php (last access: 8 May 2018).

Edited by: Emilio Marañón
Reviewed by: Fanny Monteiro and two anonymous referees

References

Al-Mutairi, H. and Landry, M. R.: Active export of carbon and nitrogen at station ALOHA by diel migrant zooplankton, Deep-Sea Res. Pt. II, 48, 2083–2103, https://doi.org/10.1016/S0967-0645(00)00174-0, 2001.

Aminot, A. and Kérouel, R.: Dosage automatique des nutriments dans les eaux marines : méthodes en flux continu, Ed. Ifremer, Méthodes d'analyse en milieu marin, 188 pp., 2007.

Antia, A. N.: Solubilization of particles in sediment traps: revising the stoichiometry of mixed layer export, Biogeosciences, 2, 189–204, https://doi.org/10.5194/bg-2-189-2005, 2005.

Banse, K.: Reflections about chance in my career, and on the top-down regulated world, Annu. Rev. Mar. Sci., 5, 2.1–2.19, 2013.

Bates, N. R., Best, M. H. P., Neely, K., Garley, R., Dickson, A. G., and Johnson, R. J.: Detecting anthropogenic carbon dioxide uptake and ocean acidification in the North Atlantic Ocean, Biogeosciences, 9, 2509–2522, https://doi.org/10.5194/bg-9-2509-2012, 2012.

Berthelot, H., Moutin, T., L'Helguen, S., Leblanc, K., Hélias, S., Grosso, O., Leblond, N., Charrière, B., and Bonnet, S.: Dinitrogen fixation and dissolved organic nitrogen fueled primary production and particulate export during the VAHINE mesocosm experiment (New Caledonia lagoon), Biogeosciences, 12, 4099–4112, https://doi.org/10.5194/bg-12-4099-2015, 2015.

Bianchi, D., Stock, C., Galbraith, E. D., and Sarmiento, J. L.: Diel vertical migration: Ecological controls and impacts on the biological pump in a one dimensional ocean model, Global Biogeochem. Cy., 27, 478–491, https://doi.org/10.1002/gbc.20031, 2013.

Blain, S., Bonnet, S., and Guieu, C.: Dissolved iron distribution in the tropical and sub tropical South Eastern Pacific, Biogeosciences, 5, 269–280, https://doi.org/10.5194/bg-5-269-2008, 2008.

Bonnet, S., Caffin, M., Berthelot, H., and Moutin, T.: Hot spot of N_2 fixation in the western tropical South Pacific pleads for a spatial decoupling between N_2 fixation and denitrification, P. Natl. Acad. Sci. USA, 114, E2800–E2801, https://doi.org/10.1073/pnas.1619514114, 2017.

Bonnet S., Caffin, M., Berthelot, H., Grosso, O., Guieu, C., and Foster, R.: Contribution of dissolved and particulate fractions to the Hot Spot of N_2 fixation in the Western Tropical South Pacific Ocean (OUTPACE cruise), Biogeosciences Discuss., in preparation, 2018.

Böttjer, D., Dore, J. E., Karl, D. M., Letelier, R. M., Mahaffey, C., Wilson, S. T., Zehr, J., and Church, M. J.: Temporal variability of nitrogen fixation and particulate nitrogen export at Station ALOHA, Limnol. Oceanogr., 62, 200–216, 2017.

Bouffard, D. and Boegman, L.: A diapycnal diffusivity model for stratified environmental flows, Dynam. Atmos. Oceans, 61, 14—34, 2013.

Bouruet-Aubertot, P., Cuypers, Y., Doglioli, A., Caffin, M., Yohia, C., de Verneil, A., Petrenko, A., Lefèvre, D., Le Goff, H., Rougier, G., Picheral, M., and Moutin, T.: Longitudinal contrast in Turbulence along a $\sim 19°$ S section in the Pacific and its consequences on biogeochemical fluxes, Biogeosciences Discuss., https://doi.org/10.5194/bg-2018-170, in review, 2018.

Boutin, J., Quilfen, Y., Merlivat, L., and Piolle, J. F.: Global average of air-sea CO_2 transfer velocity from QuikSCAT scatterometer wind speeds, J. Geophys. Res., 114, C04007, https://doi.org/10.1029/2007JC004168, 2009.

Buesseler, K. O., Antia, A. N., Chen, M., Fowler, S. W., Gardner, W. D., Gustafsson, O., Harada, K., Michaels, A. F., van der Loeff, M. R., Sarin, M., Steinberg, D. K., and Trull, T.: An assessment of the use of sediment traps for estimating upper ocean particle fluxes, J. Mar. Res., 65, 345–416, 2007.

Brandes, J. A. and Devol, A. H.: A global marine fixed nitrogen isotopic budget: Implications for Holocene nitrogen cycling, Global Biogeochem. Cy., 16, 67.61–67.14, https://doi.org/10.1029/2001GB001856, 2002.

Broecker, W. S. and Henderson, G. M.: The sequence of events surrounding Termination II and their implications for the cause of glacial-interglacial CO_2 changes, Paleoceanogr. Paleoclimatol, 13, 352–364, 1998.

Burd, A. B., Buchan, A., Church, M., Landry, M., McDonnell, A., Passow, U., Steinberg, D., and Benway, H.: Towards a transformative understanding of the biology of the ocean's biological pump: Priorities for future research, Report of the NSF Biology of the Biological Pump Workshop, 19–20 February (Hyatt Place New Orleans, New Orleans, LA) 6 pp., https://doi.org/10.1575/1912/8263, 2016.

Caffin, M., Moutin, T., Foster, R. A., Bouruet-Aubertot, P., Doglioli, A. M., Berthelot, H., Guieu, C., Grosso, O., Helias-Nunige, S., Leblond, N., Gimenez, A., Petrenko, A. A., de Verneil, A., and Bonnet, S.: N_2 fixation as a dominant new N source in the western tropical South Pacific Ocean (OUTPACE cruise), Biogeosciences, 15, 2565–2585, https://doi.org/10.5194/bg-15-2565-2018, 2018.

Campbell, L., Carpenter, E. J., Montoya, J. P., Kustka, A. B., and Capone, D. G.: Picoplankton community structure within and outside a Trichodesmium bloom in the southwestern Pacific Ocean, Vie Milieu, 55, 185–195, 2005.

Carlson, C. A.: Production and removal processes, in: Biogeochemistry of Marine Dissolved Organic Matter, edited by: Hansell, D. A. and Carlson, C. A., 91–151, Academic, San Diego, Calif., https://doi.org/10.1016/B978-012323841-2/50006-3, 2002.

Capone, D. G. and Knapp, A. N.: Oceanography – A marine nitrogen cycle fix?, Nature, 445, 159–160, 2007.

Cauwet, G.: HTCO method for dissolved organic carbon analysis in seawater: influence of catalyst on blank estimation, Mar. Chem., 47, 55–64, 1994.

Cauwet, G.: Determination of dissolved organic carbon (DOC) and nitrogen (DON) by high temperature combustion, in: Methods of seawater analysis, edited by: Grashoff, K., Kremling, K., and Ehrhard, M., 3rd Ed., Wiley-VCH, Weinheim, 407–420, 1999.

Codispoti, L. A.: An oceanic fixed nitrogen sink exceeding $400\,\mathrm{Tg\,N\,a^{-1}}$ vs the concept of homeostasis in the fixed-nitrogen inventory, Biogeosciences, 4, 233–253, https://doi.org/10.5194/bg-4-233-2007, 2007.

Codispoti, L. A., Brandes, J. A., Christensen, J. P., Devol, A. H., Naqvi, S. W. A., Paerl, H. W., and Yoshinari, T.: The oceanic fixed nitrogen and nitrous oxide budgets: Moving targets as we enter the anthropocene?, Sci. Mar., 65, 85–105, 2001.

Copin-Montégut, G. and Avril, B.: Vertical distribution and temporal variation of dissolved organic carbon in the North-Western Mediterranean Sea, Deep-Sea Res., 40, 1963–1972, 1993.

de Boyer Montégut, C., Madec, G., Fischer, A. S., Lazar, A., and Iudicone, D.: Mixed layer depth over the global ocean: an examination of profile data and a profile-based climatology, J. Geophys. Res., 109, C12003, https://doi.org/10.1029/2004JC002378, 2004.

Dekaezemacker, J., Bonnet, S., Grosso, O., Moutin, T., Bressac, M., and Capone, D. G.: Evidence of active dinitrogen fixation in surface waters of the eastern tropical South Pacific during El Nino and La Nina events and evaluation of its potential nutrient controls, Global Biogeochem. Cy., 27, 768–779, https://doi.org/10.1002/gbc.20063, 2013.

Deutsch, C. and Weber, T.: Nutrient Ratios as a Tracer and Driver of Ocean Biogeochemistry, Annu. Rev. Mar. Sci., 41, 4–113, 2012.

Deutsch, C., Gruber, N., Key, R., and Sarmiento, J. L.: Denitrification and N_2 fixation in the Pacific Ocean, Global Biogeochem. Cy., 15, https://doi.org/10.1029/2000GB001291, 2001.

Deutsch, C., Sarmiento J. L., Sigman D. M., Grüber N., and Dunne J. P.: Spatial coupling of nitrogen inputs and losses in the ocean, Nature, 445, 163–167, 2007.

de Verneil, A., Rousselet, L., Doglioli, A. M., Petrenko, A. A., Maes, C., Bouruet-Aubertot, P., and Moutin, T.: OUTPACE long duration stations: physical variability, context of biogeochemical sampling, and evaluation of sampling strategy, Biogeosciences, 15, 2125–2147, https://doi.org/10.5194/bg-15-2125-2018, 2018.

Dickson, A. G.: An exact definition of total alkalinity and a procedure for the estimation of alkalinity and total inorganic carbon from titration data, Deep-Sea Res., 28A, 609–623, 1981.

DOE: Handbook of methods for the analysis of the various parameters of the carbon dioxide system in sea water; version 2, edited by: Dickson, A. G. and Goyet, C., ORNL/CDIAC-74, 1994.

Dore, J. E., Lukas, R., Sadler, D. W., and Karl, D. M.: Climate-driven changes to the atmospheric CO_2 sink in the subtropical North Pacific Ocean, Nature, 424, 754-757, https://doi.org/10.1038/nature01885, 2003.

Duce, R. and Tindale, N.: Atmospheric transport of iron and its deposition in the ocean, Limnol. Oceanogr., 36, 1715–1726, 1991.

Duhamel, S., Zeman, F., and Moutin, T.: A dual-labeling method for the simultaneous measurement of dissolved inorganic carbon and phosphate uptake by marine planktonic species, Limnol. Oceanogr.-Meth., 4, 416–425, 2006.

Dupouy, C., Neveux, J., Subramaniam, A., Mulholland, M. R., Montoya, J. P., Campbell, L., Carpenter, E. J., and Capone, D. G.: Satellite captures Trichodesmium blooms in the southwestern tropical Pacific, EOS, 81, 13–16, 2000.

Dupouy, C., Benielli-Gary, D., Neveux, J., Dandonneau, Y., and Westberry, T. K.: An algorithm for detecting *Trichodesmium* surface blooms in the South Western Tropical Pacific, Biogeosciences, 8, 3631–3647, https://doi.org/10.5194/bg-8-3631-2011, 2011.

Edmond, J. M.: High precision determination of totration alkalinity and the total carbone dioxide contentof seawater by potentiometric titration, Deep Sea Res., 17, 737–750, 1970.

Dutkiewicz, S., Ward, B. A., Monteiro, F., and Follows, M. J.: Interconnection of nitrogen fixers and iron in the Pacific Ocean: Theory and numerical simulations, Global Biogeochem. Cy., 26, GB1012, https://doi.org/10.1029/2011GB004039, 2012.

Falkowski, P. G.: Evolution of the nitrogen cycle and its influence on the biological sequestration of CO_2 in the ocean, Nature, 387, 272–275, 1997.

Falkowski, P. G., Ziemann, D., Kolber, Z., and Bienfang, P. K.: Role of eddy pumping in enhancing primary production in the ocean, Nature, 352, p. 55, 1991.

Falkowski, P. G., Barber, R. T., and Smetacek, V.: Biogeochemical Controls and Feedbacks on Ocean Primary Production, Science, 281, 200–206, 1998.

Fitzsimmons, J. N., Boyle, E. A., and Jenkins, W. J.: Distal transport of dissolved hydrothermal iron in the deep South Pacific Ocean, P. Natl. Acad. Sci. USA, 25, 16654–16661, https://doi.org/10.1073/pnas.1418778111, 2014.

Fumenia, A., Moutin, T., Bonnet, S., Benavides, M., Petrenko, A., Helias Nunige, S., and Maes, C.: Excess nitrogen as a marker of intense dinitrogen fixation in the Western Tropical South Pacific Ocean: impact on the thermocline waters of the South Pacific, Biogeosciences Discuss., https://doi.org/10.5194/bg-2017-557, in review, 2018.

Ganachaud, A., Cravatte, S., Sprintall, J., Germineaud, C., Marion Alberty, M., Jeandel, C., Eldin, G., Metzl, N., Bonnet, S., Benavides, M., Heimburger, L.-E., Lefèvre, J., Michael, S., Resing, J., Quéroué, F., Sarthou, G., Rodier, Berthelot, H., Baurand, F., Grelet, J., Hasegawa, T., Kessler, W., Kilepak, M., Lacan, F., Privat, E., Send, U., Van Beek, P., Souhaut, S., and Sonke, J. E.: The Solomon Sea: its circulation, chemistry, geochemistry and biology explored during two oceanographic cruises, Elem. Sci. Anth., 5, 33, https://doi.org/10.1525/elementa.221, 2017.

Garcia, H. E. and Gordon, L. I.: Oxygen solubility in seawater: Better fitting equations, Limnol. Oceanogr., 37, 1307–1312, https://doi.org/10.4319/lo.1992.37.6.1307, 1992.

Gattuso, J.-P. and Lavigne, H.: Technical Note: Approaches and software tools to investigate the impact of ocean acidification, Biogeosciences, 6, 2121–2133, https://doi.org/10.5194/bg-6-2121-2009, 2009.

Gimenez, A., Baklouti, M., Bonnet, S., and Moutin, T.: Biogeochemical fluxes and fate of diazotroph-derived nitrogen in the food web after a phosphate enrichment: modeling of the VAHINE mesocosms experiment, Biogeosciences, 13, 5103–5120, https://doi.org/10.5194/bg-13-5103-2016, 2016.

Gimenez, A., Baklouti, M., and Moutin, T.: Diazotrophy as the main driver of planktonic production and biogeochemical C, N, P cycles in the Western Tropical South Pacific Ocean: results from a 1DV biogeochemical-physical coupled model, Biogeosciences Discuss., https://doi.org/10.5194/bg-2018-162, in review, 2018.

Grüber, N.: The dynamics of the marine nitrogen cycle and its influence on atmospheric CO_2, in: The ocean carbon cycle and climate, edited by: Follows, M. and Oguz, T., Kluwer Academic, Dordrecht, 2004.

Grüber, N.: Elusive marine nitrogen fixation, P. Natl. Acad. Sci. USA, 113, 4246–4248, 2016.

Grüber, N. and Sarmiento, J. L.: Global patterns of marine nitrogen fixation and denitrification, Global Biogeochem. Cy., 11, 235–266, 1997.

Guieu, C., Bonnet, S., Petrenko, A. A., Menkes, C., Chavagnac, V., Desboeufs, K., Maes, C., and Moutin, T.: Iron from a submarine source impacts the productive layer of the Western Tropical South Pacific (WTSP), Nature Sci. Rep., in revision, 2018.

Hansell, D. A. and Carlson, C. A.: Localized refractory dissolved organic carbon sinks in the deep ocean, Global Biogeochem. Cy., 27, 705–710, https://doi.org/10.1002/gbc.20067, 2013.

Holmes, R. M., Aminot, A., Kérouel, R., Hooker, B. A., and Peterson, B. J.: A simple and precise method for measuring ammonium in marine and freshwater ecosystems, Can. J. Fish. Aquat. Sci., 56, 1801–1808, 1999.

Jickells, T. D., Buitenhuis, E., Altieri, K., Baker, A. R., Capone, D. G., Duce, R. A., Dentener, F., Fennel, K., Kanakidou, M., LaRoche, J., Lee, K., Liss, P., Middelburg, J. J., Moore, J. K., Okin, G., Oschlies, A., Sarin, M., Seitzinger, S., Sharples, J., Singh, A., Suntharalingam, P., Uematsu, M., and Zamora, L. M.: A reevaluation of the magnitude and impacts of anthropogenic atmospheric nitrogen inputs on the ocean, Global Biogeochem. Cy., 31, 289–305, https://doi.org/10.1002/2016GB005586, 2017.

Kana, T. M., Darkangelo, C., Hunt, M. D., Oldham, J. B., Bennett, G. E., and Cornwell, J. C.: Membrane Inlet Mass Spectrometer for Rapid High-Precision Determination of N_2, O_2, and Ar in Environmental Water Samples, Anal. Chem., 66, 4166–4170, https://doi.org/10.1021/ac00095a009, 1994.

Karl, D. M.: Microbially mediated transformations of phosphorus in the sea: new views of an old cycle, Annu. Rev. Mar. Sci., 6, 279–337, 2014.

Karl, D. M., Christian, J. R., Dore, J. E., Hebel, D. V., Letelier, R. M., Tupas, L. M., and Winn, C. D.: Seasonal and interannual variability in primary production and particle flux at station ALOHA, Deep-Sea Res. Pt. II, 43, 539–568, 1996.

Karl, D. M., Letelier, R. M, Tupas, L. M., Dore, J. E., Christian, J. R., and Hebel, D. V.: The role of nitrogen fixation in biogeochemical cycling in the subtropical North Pacific Ocean, Nature, 388, 533–538, 1997.

Karl, D. M., Church, M. J., Dore, J. E., Letelier, R. M., and Mahaffey, C.: Predictable and efficient carbon sequestration in the North Pacific Ocean supported by symbiotic nitrogen fixation, P. Natl. Acad. Sci. USA, 109, 1842–1849, https://doi.org/10.1073/pnas.1120312109, 2012.

Kim, D., Jeong, D. J., Kim, T. W., Noh, J. H., Kim, H. J., Choi, D. H., Kim, E., and Jeon, D.: The reduction in the biomass of cyanobacterial N_2 fixer and the biological pump in the Northwestern Pacific Ocean, Nature Sci. Rep., 7, 41810, https://doi.org/10.1038/srep41810, 2017.

Knapp, A. N., Fawcett, S. E., Martínez-Garcia, A., Leblond, N., Moutin, T., and Bonnet, S.: Nitrogen isotopic evidence for a shift from nitrate- to diazotroph-fueled export production in the VAHINE mesocosm experiments, Biogeosciences, 13, 4645–4657, https://doi.org/10.5194/bg-13-4645-2016, 2016.

Knapp, A. N., McCabe, K. M., Grosso, O., Leblond, N., Moutin, T., and Bonnet, S.: Distribution and rates of nitrogen fixation in the western tropical South Pacific Ocean constrained by nitrogen isotope budgets, Biogeosciences, 15, 2619–2628, https://doi.org/10.5194/bg-15-2619-2018, 2018.

Lachkar, Z., Lévy, M., and Smith, S.: Intensification and deepening of the Arabian Sea oxygen minimum zone in response to increase in Indian monsoon wind intensity, Biogeosciences, 15, 159–186, https://doi.org/10.5194/bg-15-159-2018, 2018.

Landing, W. M. and Bruland, K. W.: The contrasting biogeochemistry of iron and manganese in the Pacific Ocean, Geochim. Cosmochim. Ac., 51, 29–43, 1987.

Landolfi, A., Dietze, H., Koeve, W., and Oschlies, A.: Overlooked runaway feedback in the marine nitrogen cycle: the vicious cycle, Biogeosciences, 10, 1351–1363, https://doi.org/10.5194/bg-10-1351-2013, 2013.

Landry, M. R., Selph, K. E., Taylor, A. G., Décima, M., Balch, W. M., and Bidigare, R. R.: Phytoplankton growth, grazing and production balances in the HNLC equatorial Pacific, Deep-Sea Res. Pt. II, 58, 524–535, 2011.

Langdon, C.: Determination of Dissolved Oxygen in Seawater by Winkler Titration Using the Amperometric Technique, in: The GO-SHIP Repeat Hydrography Manual: A Collection of Expert Reports and Guidelines, edited by: Hood, E. M., Sabine, C. L., and Sloyan, B. M., IOCCP Report Number 14, ICPO Publication Series Number 134, available at: http://www.go-ship.org/HydroMan.html (last access: 8 May 2018), 2010.

Law, C. S., Woodward, E. M. S., Ellwood, M. J., Marriner, A., Bury, S. J., and Safi, K. A.: Response of surface nutrient inventories and nitrogen fixation to a tropical cyclone in the southwest Pacific, Limnol. Oceanogr., 56, 1372–1385, 2011.

Lévy, M., Ferrari, R., Franks, P. J. S., Martin, A. P., and Rivière, P.: Bringing physics to life at the submesoscale, Geophys. Res. Lett., 39, L14602, https://doi.org/10.1029/2012GL052756, 2012.

Levy, M., Jahn, O., Dutkiewicz, S., Follows, M. J., and d'Ovidio, F.: The dynamical landscape of marine phytoplankton diversity, Royal. Soc. Interface, 12, 20150481, https://doi.org/10.1098/rsif.2015.0481, 2015.

Liss, P. S. and Merlivat, L.: Air-Sea Gas Exchange Rates: Introduction and Synthesis, in: The Role of Air-Sea Exchange in Geochemical Cycling, edited by: P., Buat-Ménard, NATO ASI Series (Series C: Mathematical and Physical Sciences), vol. 185, Springer, Dordrecht, https://doi.org/10.1007/978-94-009-4738-2_5, 1986.

Lueker, T. J., Dickson, A., and Keeling, C. D.: Ocean pCO_2 calculated from dissolved inorganic carbon, alkalinity, and equations for K1 and K2: validation based on laboratory measurements of CO_2 in gas and seawater at equilibrium, Mar. Chem., 70, 105–119, 2000.

Mahaffey, C., Michaels, A. F., and Capone, D. G.: The conundrum of marine N_2 fixation, Am. J. Sci., 305, 546–595, 2005.

Marañón, E., Cermeno, P., and Perez, V.: Continuity in the photosynthetic production of dissolved organic carbon from eutrophic to oligotrophic waters, Mar. Ecol.-Prog. Ser., 299, 7–17, 2005.

Marty, J. C. and Chiavérini, J.: Seasonal and interannual variations in phytoplankton production at DYFAMED time-series station, northwestern Mediterranean Sea, Deep-Sea Res. Pt. II, 49, 2017–2030, 2002.

McDougall, T. J. and Barker, P. M.: Getting started with TEOS-10 and the Gibbs Seawater (GSW) Oceanographic Toolbox, 28 pp., SCOR/IAPSO WG127, 2011.

McElroy, M. B.: Marine biological controls on atmospheric CO_2 and climate, Nature, 302, 328–329, 1983.

McMahon, K. W., McCarthy, M. D., Sherwood, O. A., Larsen, T., and Guilderson, T. P.: Millennial-scale plankton regime shifts in the subtropical North Pacific Ocean, Science, 350, 1530–1533, 2015.

Merlivat, L., Gonzalez Davila, M., Caniaux, G., Boutin, J., and Reverdin, G.: Mesoscale and diel to monthly variability of CO_2 and carbon fluxes at the ocean surface in the northeastern Atlantic, J. Geophys. Res., 114, C03010, https://doi.org/10.1029/2007JC004657, 2009.

Michaels, A. F., Karl, D. M., Capone, D. G.: Element stoichiometry, new production and nitrogen fixation, Oceanography, 14, 68–77, 2001.

Millero, F. J.: The marine inorganic carbon cycle, Chem. Rev., 107, 308–341, 2007.

Minas, H. J., Minas, M., and Packard, T. T.: Productivity in upwelling areas deduced from hydrographic and chemical fields, Limnol. Oceanogr., 31, 1182–1206, 1986.

Moisander, P. H., Zhang, R., Boyle, E. A., Hewson, I., Montoya, J. P., and Zehr, J. P.: Analogous nutrient limitations in unicellular diazotrophs and Prochlorococcus in the South Pacific Ocean, ISME J., 6, 733–744, 2012.

Monteiro, F. M., Dutkiewicz, S., and Follows, M. J.: Biogeographical controls on the marine nitrogen fixers, Global Biogeochem. Cy., 25, GB2003, https://doi.org/10.1029/2010GB003902, 2011.

Montoya, J. P., Voss, M., Kahler, P., and Capone, D. G.: A Simple, High-Precision, High-Sensitivity Tracer Assay for N_2 Fixation, Appl. Environ. Microb., 62, 986–993, 1996.

Moore, C. M., Mills, M. M. M., Arrigo, K. R., Berman-Frank, I., Bopp, L., Boyd, P. W., Galbraith, E. D., Geider, R. J., Guieu, C., Jaccard, S. L., Jickells, T. D., La Roche, J., Lenton, T. M., Mahowald, N. M., Maranon, E., Marinov, I., Moore, J. K., Nakatsuka, T., Oschlies, A., Saito, M. A., Thingstad, T. F., Tsuda, A., and Ulloa, O.: Processes and patterns of oceanic nutrient limitation, Nat. Geosci., 6, 701–710, 2013.

Moutin, T. and Raimbault, P.: Primary production, carbon export and nutrients availability in western and eastern Mediterranean Sea in early summer 1996 (MINOS cruise), J. Marine Syst., 33–34, 273–288, https://doi.org/10.1016/S0924-7963(02)00062-3, 2002.

Moutin, T., Raimbault, P., and Poggiale, J. C.: Production primaire dans les eaux de surface de la Méditerranée occidentale: Calcul de la production journalière, C. R. Acad. Sci. Paris, Sciences de la vie, 322, 651–659, 1999.

Moutin, T., Thingstad, T. F., Van Wambeke, F., Marie, D., Slawyk, G., Raimbault, P., and Claustre, H.: Does competition for nano-molar phosphate supply explain the predominance of the cyanobacterium Synechococcus?, Limnol. Oceanogr., 47, 1562–1567, 2002.

Moutin, T., Van Den Broeck, N., Beker, B., Dupouy, C., Rimmelin, P., and LeBouteiller, A.: Phosphate availability controls Trichodesmium spp. biomass in the SW Pacific ocean, Mar. Ecol.-Prog. Ser., 297, 15–21, 2005.

Moutin, T., Karl, D. M., Duhamel, S., Rimmelin, P., Raimbault, P., Van Mooy, B. A. S., and Claustre, H.: Phosphate availability and the ultimate control of new nitrogen input by nitrogen fixation in the tropical Pacific Ocean, Biogeosciences, 5, 95–109, https://doi.org/10.5194/bg-5-95-2008, 2008.

Moutin, T., Van Wambeke, F., and Prieur, L.: Introduction to the Biogeochemistry from the Oligotrophic to the Ultraoligotrophic

Mediterranean (BOUM) experiment, Biogeosciences, 9, 3817–3825, https://doi.org/10.5194/bg-9-3817-2012, 2012.

Moutin, T., Doglioli, A. M., de Verneil, A., and Bonnet, S.: Preface: The Oligotrophy to the UlTra-oligotrophy PACific Experiment (OUTPACE cruise, 18 February to 3 April 2015), Biogeosciences, 14, 3207–3220, https://doi.org/10.5194/bg-14-3207-2017, 2017a.

Moutin, T., Bonnet, S., Richards, K., Capone, D. G., Marañón, E., and Mémery, L. (Eds.): Interactions between planktonic organisms and biogeochemical cycles across trophic and N_2 fixation gradients in the western tropical South Pacific Ocean: a multidisciplinary approach (OUTPACE experiment), Biogeosciences, https://www.biogeosciences.net/special_issue894.html, 2017b.

NOAA ESRL Global Monitoring Division: Atmospheric Carbon Dioxide Dry Air Mole Fractions from quasi-continuous measurements at American Samoa, edited by: Thoning, K. W., Kitzis, D. R., and Crotwell, A., National Oceanic and Atmospheric Administration (NOAA), Earth System Research Laboratory (ESRL), Global Monitoring Division (GMD): Boulder, Colorado, USA, Version 2014-08 at: https://doi.org/10.7289/V51834DB, 2014.

Oschlies, A. and Garcon, V.: Eddy-induced enhancement of primary production in a model of the North Atlantic Ocean, Nature, 394, 266–269, 1998.

Oudot, C., Gerard, R., Morin, P., and Gningue, I.: Precise shipboard determination of dissolved-oxygen (Winkler Procedure) with a commercial system, Limnol. Oceanogr., 33, 146–150, 1988.

Owens, W. B. and Millard Jr., R. C.: A new algorithm for CTD oxygen calibration, J. Phys. Oceanogr., 15, 621–631, 1985.

Pujo-Pay, M. and Raimbault, P.: Improvement of the wet-oxidation procedure for simultaneous determination of particulate organic nitrogen and phosphorus collected on filters, Mar. Ecol.-Prog. Ser., 105, 203–207, 1994.

Pujo-Pay, M., Conan, P., Oriol, L., Cornet-Barthaux, V., Falco, C., Ghiglione, J.-F., Goyet, C., Moutin, T., and Prieur, L.: Integrated survey of elemental stoichiometry (C, N, P) from the western to eastern Mediterranean Sea, Biogeosciences, 8, 883–899, https://doi.org/10.5194/bg-8-883-2011, 2011.

Raven, J. A.: The iron and molybdenum use efficiencies of plant growth with different energy, carbon and nitrogen source, New Phytol., 109, 279–287, 1988.

Redfield, A. C.: On the proportions of organic derivatives in sea water and their relation to the composition of plankton, in: James Johnstone Memorial Volume, edited by: Daniel, R. J., University Press, 176–192, 1934.

Rousselet, L., de Verneil, A., Doglioli, A. M., Petrenko, A. A., Duhamel, S., Maes, C., and Blanke, B.: Large- to submesoscale surface circulation and its implications on biogeochemical/biological horizontal distributions during the OUTPACE cruise (southwest Pacific), Biogeosciences, 15, 2411–2431, https://doi.org/10.5194/bg-15-2411-2018, 2018.

Sarmiento, J. L. and Gruber, N.: Ocean Biogeochemical Dynamics, Princeton University Press, Princeton, 503 pp., 2006.

Sharp, J. H.: Improved analysis for "particulate" organic carbon and nitrogen from seawater, Limnol. Oceanogr., 19, 984–989, 1974.

Smeti, H., Pagano, M., Menkès, C., Lebourges Dhaussy, A., Hunt, B. P. V., Allain, V., Rodier, M., de Boissieu, F., Kestenare, E., and Sammari, C.: Spatial and temporal variability of zooplankton off New Caledonia (Southwestern Pacific) from acoustics and net measurements, J. Geophys. Res.-Oceans, 120, 2676–2700, 2015.

Straub, M., Sigman, D. M., Ren, H., Martínez-García, A., Meckler, A. N., Hain, M. P., and Haug, G. H.: Changes in North Atlantic nitrogen fixation controlled by ocean circulation, Nature, 501, 7466, https://doi.org/10.1038/nature12397, 2013.

Stukel, M. R., Aluwihare, L. I., Barbeau, K. A., Chekalyuk, A. M., Goericke, R., Miller, A. J., Ohman, M. D., Ruacho, A., Song, H., Stephens, B., and Landry, M. R.: Mesoscale ocean fronts enhance carbon export due to gravitational sinking and subduction, P. Natl. Acad. Sci. USA, 114, 1252–1257, https://doi.org/10.1073/pnas.1609435114, 2017.

Sugimura, Y. and Suzuki, Y.: A high-temperature catalytic oxidation method for the determination of non-volatile dissolved organic carbon in seawater by direct injection of a liquid sample, Mar. Chem., 24, 105–131, 1988.

Tagliabue, A., Bopp, L., Dutay, J. C., Bowie, A. R., Chever, F., Jean-Baptiste, P., Bucciarelli, E., Lannuzel, D., Remenyi, T., Sarthou, G., Aumont, O., Gehlen, M., and Jeandel, C.: Hydrothermal iron contribution to oceanic dissolved iron inventory, Nat. Geosci., 3, 252–256, https://doi.org/10.1038/ngeo818, 2010.

Tagliabue, A., Bowie, A. R., Boyd, P. W., Buck, K. N., Johnson, K. S., and Saito, M. A.: The integral role of iron in ocean biogeochemistry, Nature, 543, 51–59, https://doi.org/10.1038/nature21058, 2017.

Takahashi, T., Olafsson, J., Goddard, J., Chipman, D. W., and Sutherland, S. C.: Seasonal variation of CO_2 and nutrients in the high-latitude surface oceans: a comparative study, Global Biogeochem. Cy., 7, 843–878, 1993.

Takahashi, T., Sutherland, S. C., Chipman, D. W., Goddard, J. G., Cheng Ho, Newberger, T., Sweeney, C., and Munro, D. R.: Climatological Distributions of pH, pCO_2, Total CO_2, Alkalinity, and $CaCO_3$ Saturation in the Global Surface Ocean, and Temporal Changes at Selected Locations, Mar. Chem., https://doi.org/10.1016/j.jmarchem.2014.06.004, 2014.

Taylor, B. W., Keep, C. F., Hall, Jr., R. O., Koch, B. J., Tronstad, L. M., Flecker, A. S., and Ulseth, A. J.: Improving the fluorometric ammonium method: matrix effects, background fluorescence, and standard additions, J. N. Am. Benthol. Soc., 26, 167–177, 2007.

Thingstad, T. F., Skjoldal, E. F., and Bohne, R. A.: Phosphorus cycling and algal–bacterial competition in Sandsfjord, western Norway, Mar. Ecol.-Prog. Ser., 99, 239–259, 1993.

Tyrell, T.: The relative influences of nitrogen and phosphorus on oceanic primary production, Nature, 400, 525–531, 1999.

Valdés, V., Carlotti, F., Escribano, R., Donoso, K., Pagano, M., Molina, V., and Fernandez, C.: Nitrogen and phosphorus recycling mediated by copepods in Western Tropical South Pacific, Biogeosciences Discuss., https://doi.org/10.5194/bg-2017-563, in review, 2018.

Van Den Broeck, N., Moutin, T., Rodier, M., and Le Bouteiller, A.: Seasonal variations of phosphate availability in the SW Pacific Ocean near New Caledonia, Mar. Ecol.-Prog. Ser., 268, 1–12, 2004.

Van Wambeke, F., Christaki, U., Giannakourou, A., Moutin, T., and Souvemerzoglou, K.: Longitudinal and vertical trends of bacterial limitation by phosphorus and carbon in the Mediterranean Sea, Microbiol. Ecol., 43, 119–133, 2002.

Van Wambeke, F., Gimenez, A., Duhamel, S., Dupouy, C., Lefevre, D., Pujo-Pay, M., and Moutin, T.: Dynamics and controls of heterotrophic prokaryotic production in the western tropical South

Pacific Ocean: links with diazotrophic and photosynthetic activity, Biogeosciences, 15, 2669–2689, https://doi.org/10.5194/bg-15-2669-2018, 2018.

Volk, T. and Hoffert, M. I.: The carbon cycle and atmospheric CO_2: natural variations Archean to present, Chapman conference papers, 1984, edited by: Sundquist, E. T. and Broecker, W. S., American Geophysical Union, Geophysical Monograph 32, 99–110, 1985.

Wagener, T., Guieu, C., Losno, R., Bonnet, S., and Mahowald, N. M.: Revisiting atmospheric dust export to the Southern Hemisphere ocean: Biogeochemical implications, Global Biogeochem. Cy., 22, 1–13, https://doi.org/10.1029/2007GB002984, 2008.

Weber, T. and Deutsch, C.: Local versus basin-scale limitation of marine nitrogen fixation, P. Natl. Acad. Sci. USA, 111, 8741–8746, 2014.

Wells, M. L., Vallis, G. K., and Silver, E. A.: Tectonic processes in Papua New Guinea and past productivity in the eastern equatorial Pacific Ocean, Nature, 398, 601–604, 1999.

Weiss, R. F. and Price, B. A.: Nitrous oxide solubility in water and seawater, Mar. Chem., 8, 347–359, 1980.

Winkler, L. W.: Die Bestimmung des im Wasser gelosten Sauerstoffes, Ber. Dtsch. Chem. Ges., 21, 2843–2853, 1888.

Wu, J., Sunda, W., Boyle, E. A., and Karl, D. M.: Phosphate depletion in the western North Atlantic Ocean, Science, 289, 759–762, 2000.

Xie, X. H., Cuypers, Y., Bouruet-Aubertot, P., Ferron, B., Pichon, A., Lourenço, A., and Cortes, N.: Large-amplitude internal tides, solitary waves, and turbulence in the central Bay of Biscay, Geophys. Res. Lett., 40, 2748–2754, 2013.

Yoshikawa, C., Makabe, A., Shiozaki, T., Toyoda, S., Yoshida, O., Furuya, K., and Yoshida, N.: Nitrogen isotope ratios of nitrate and N^* anomalies in the subtropical South Pacific, Geochem. Geophy. Geosy., 16, 1439–1448, https://doi.org/10.1002/2014GC005678, 2015.

Zhang, X. and Dam, H. G.: Downward export of carbon by die1 migrant mesozooplankton in the central equatorial Pacific, Deep-Sea Res. Pt. II, 44, 2191–2202, 1998.

Annexe C

Article supplémentaire n°2

Longitudinal contrast in Turbulence along a ∼19S section in the Pacific and its consequences on biogeochemical fluxes

Pascale Bouruet-Aubertot[1], Yannis Cuypers[1], Andrea Doglioli[2], Mathieu Caffin[2], Christophe Yohia[2], Alain de Verneil[2], Anne Petrenko[2], Dominique Lefèvre[2], Hervé Le Goff[1], Gilles Rougier[2], Marc Picheral[3], and Thierry Moutin[2]

[1]Sorbonne Université – UPMC Univ. Paris 06 – LOCEAN, France
[2]Aix Marseille Univ, Université de Toulon, CNRS, IRD, MIO UM 110, 13288, Marseille, France
[3]LOV, Villefranche sur mer, France

En révision dans *Biogeosciences Discussion* depuis Avril 2018

Biogeosciences, 15, 7485–7504, 2018
https://doi.org/10.5194/bg-15-7485-2018

Biogeosciences Open Access EGU

Longitudinal contrast in turbulence along a ∼ 19° S section in the Pacific and its consequences for biogeochemical fluxes

Pascale Bouruet-Aubertot[1], Yannis Cuypers[1], Andrea Doglioli[2], Mathieu Caffin[2], Christophe Yohia[2], Alain de Verneil[2], Anne Petrenko[2], Dominique Lefèvre[2], Hervé Le Goff[1], Gilles Rougier[2], Marc Picheral[3], and Thierry Moutin[2]

[1]Sorbonne Université – UPMC Univ. Paris 06 – LOCEAN, Paris, France
[2]Aix Marseille Univ, Université de Toulon, CNRS, IRD, MIO UM 110, 13288, Marseille, France
[3]LOV, Villefranche-sur-Mer, France

Correspondence: P. Bouruet-Aubertot (pascale.bouruet-aubertot@upmc.fr)

Received: 13 April 2018 – Discussion started: 20 April 2018
Revised: 30 October 2018 – Accepted: 29 November 2018 – Published: 21 December 2018

Abstract. Microstructure measurements were performed along the OUTPACE longitudinal transect in the tropical Pacific (Moutin and Bonnet, 2015). Small-scale dynamics and turbulence in the first 800 m surface layer were characterized based on hydrographic and current measurements at fine vertical scale and turbulence measurements at centimeter scale using a vertical microstructure profiler. The possible impact of turbulence on biogeochemical budgets in the surface layer was also addressed in this region of increasing oligotrophy to the east. The dissipation rate of turbulent kinetic energy, ϵ, showed an interesting contrast along the longitudinal transect with stronger turbulence in the west, i.e., the Melanesian Archipelago, compared to the east, within the South Pacific Subtropical Gyre, with a variation of ϵ by a factor of 3 within [100–500 m]. The layer with enhanced turbulence decreased in vertical extent travelling eastward. This spatial pattern was correlated with the energy level of the internal wave field, higher in the west compared to the east. The difference in wave energy mostly resulted from enhanced wind power input into inertial motions in the west. Moreover, three long-duration stations were sampled along the cruise transect, each over three inertial periods. The analysis from the western long-duration station gave evidence of an energetic baroclinic near-inertial wave that was responsible for the enhanced ϵ, observed within a 50–250 m layer, with a value of 8×10^{-9} W kg^{-1}, about 8 times larger than at the eastern long-duration stations. Averaged nitrate turbulent diffusive fluxes in a 100 m layer below the top of the nitracline were about twice larger west of 170° W due to the higher vertical diffusion coefficient. In the photic layer, the depth-averaged nitrate turbulent diffusive flux strongly decreased eastward, with an averaged value of 11 µmolm^{-2}d^{-1} west of 170° W compared with the 3 µmolm^{-2}d^{-1} averaged value east of 170° W. Contrastingly, phosphate turbulent diffusive fluxes were significantly larger in the photic layer. This input may have an important role in sustaining the development of N_2-fixing organisms that were shown to be the main primary contributors to the biological pump in the area. The time–space intermittency of mixing events, intrinsic to turbulence, was underlined, but its consequences for micro-organisms would deserve a dedicated study.

1 Introduction

The subtropical South Pacific is one of the main oceanic deserts characterized by an increasing oligotrophy to the east and the centre of the gyre. A 43-day long cruise, the OUTPACE experiment, was performed in this region, along an ∼ 1919° S longitudinal transect, during the 2015 austral summer in order to characterize the biological pump and its coupling with dynamical processes (Moutin et al., 2017). In addition to the trophic gradient the OUTPACE transect is also characterized by a longitudinal contrast in dynamics between the "energetic" Melanesian Archipelago (MA) and the "quiet" South Pacific Subtropical Gyre (SPSG) (e.g., Rousselet et al., 2018). Hence the OUTPACE experiment provides a unique opportunity to focus on physical and

Published by Copernicus Publications on behalf of the European Geosciences Union.

biological interactions (e.g., Rousselet et al., 2018) that may prove crucial in understanding biological pump functioning (e.g., Guidi et al., 2012; Ascani et al., 2013). The influence of the mesoscale and submesoscale circulations on the spatial distribution and transport was detailed by Rousselet et al. (2018). In particular, they showed the strong impact of fronts on the spatial distribution of bacteria and phytoplankton. A detailed study of an anomalous surface bloom event by de Verneil et al. (2017) revealed instead the main impact of mesoscale advection. At smaller scales three-dimensional turbulence may have a strong impact on the biological pump through the input of nutrients into the photic layer and more generally in enhancing, in the stratified ocean, vertical transports through turbulent diffusion (e.g., Ledwell et al., 2008).

The level of turbulence is almost unknown in the OUTPACE area. To our knowledge, the only microstructure measurements were performed in the western part of the subtropical South Pacific during the Malaspina expedition (Fernández-Castro et al., 2014, 2015) as part of an extensive microstructure survey in the tropical and subtropical oceans. For the leg done in the OUTPACE region, the averaged ϵ below the mixed layer down to ~ 300 m depth was $\sim 10^{-8}\,\mathrm{W\,kg^{-1}}$, well above the typical background dissipation rate for open ocean. Indirect estimates of ϵ based on ARGO floats data fall in the same range as Fernández-Castro et al. (2014) as shown by Whalen et al. (2012). This study based on the global-scale ARGO floats dataset also revealed that the southern subtropical Pacific is one of the most undersampled areas. At the larger scale of the South Pacific Ocean, the equatorial zone is well known as a hotspot for turbulence where shear instability prevails as a result of the strongly sheared current system (e.g., Gregg et al., 1985; Sun et al., 1998; Richards et al., 2015; Smyth and Moum, 2013). At subtropical latitudes, where the background shear is lower, internal waves are expected to play a major role in the onset of turbulence in the stratified interior. Global maps of energy flux show enhanced semi-diurnal tide energy conversion in the western part of the subtropical South Pacific (Alford and Zhao, 2007a, Fig. 9b). The annual mean energy flux into inertial motions is enhanced at mid-latitudes in all ocean basins with also a south-east-oriented track in the Pacific from the Equator to 40° S and within $\sim 180°$ E–160° W longitude in the OUTPACE region (Alford and Zhao, 2007a, Fig.9a). The latter process is subject to seasonal variations, especially in subtropical regions where the generation of energetic baroclinic near-inertial waves is favoured during the cyclone season (e.g., Liu et al., 2008).

The contribution of the biological pump in the OUTPACE region to the main C, N, and P biogeochemical cycles was one of the main purposes of the OUTPACE project (Moutin et al., 2017). Moutin et al. (2018) built a first-order budget at daily scale of these main elements, while Caffin et al. (2018) focused on the role of N_2 fixation. N_2 fixation was evidenced as the dominant process involved in the N cycle in regions where *Trichodesmium* dominate. The input of nitrate through turbulent diffusion was found to make a negligible contribution in the photic layer as a result of a very deep nitracline. This raised the question of the available source of other nutrients in the photic layer that could sustain the development of N_2-fixing organisms, the main primary contributors to the biological pump in the area (Caffin et al., 2018).

The purpose of this paper is to characterize the spatial variability of turbulence along the OUTPACE transect with microstructure measurements performed at both 1-day short-duration stations and at long-duration stations lasting three inertial periods. The idea is also to provide insights into the main mechanisms responsible for the observed turbulence with a focus on long-duration stations that allow a characterization of the internal wave field. How this small-scale dynamics influences biogeochemical fluxes is another issue that is eventually addressed.

2 Data and methods

The OUTPACE cruise took place in early 2015 from 18 February to 3 April onboard French oceanographic research vessel *l'Atalante* (Moutin et al., 2017). A set of 15 short-duration stations (SD) over 24 h as well as 3 long-duration stations (LD) over three inertial periods (the inertial period being ~ 36 h) were performed along an almost zonal transect starting from west of New Caledonia and ending near Tahiti (Fig. 1).

2.1 CTD and LADCP

Conductivity–temperature–depth (CTD) measurements were performed on a rosette using a SeaBird SBE 9plus instrument. Data were averaged over 1 m bins to filter out spurious salinity peaks using Sea-Bird electronics software. Simultaneously, currents were measured from a 300 kHz RDI lowered broadband acoustic Doppler current profiler (LADCP). LADCP data were processed using the Visbeck inversion method (Visbeck, 2002) and provided vertical profiles of horizontal currents at 8 m resolution. These measurements were performed at all stations with a typical 3 h time interval between each deployment. In addition the ship was equipped with two SADCPs, RDI Ocean Surveyors with frequencies 150 and 38 kHz yielding processed currents averaged over 2 min time intervals and with vertical bins of 8 and 24 m respectively. Shear was computed using finite differences with current vertical profiles interpolated over a 1 m vertical grid with an estimated noise level of $5 \times 10^{-4}\,\mathrm{s^{-1}}$.

2.2 Microstructure measurements with VMP1000

Microstructure measurements were collected using a vertical microstructure profiler, "VMP1000" (Rockland Scientific). This tethered profiler was equipped with microstructure sensors, two shear sensors, and one temperature sensor, as well

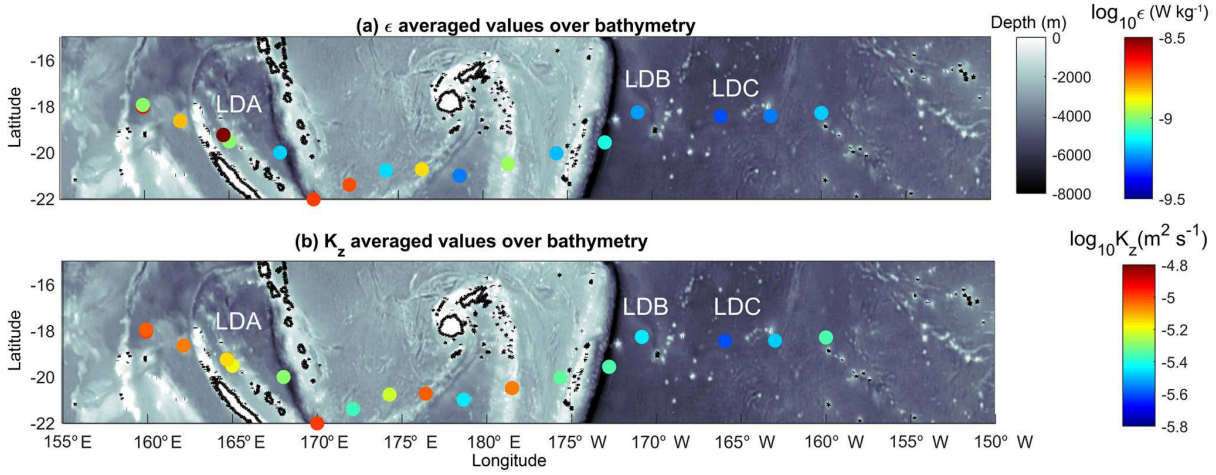

Figure 1. Dissipation rate of turbulent kinetic energy **(a)** and vertical diffusion coefficient **(b)** averaged below the mixed-layer depth (see Table 1 from Moutin et al., 2017), over 100–800 m (log scale); bathymetry is shown with grey color scale (ETOPO1, 1 arcmin, Amante and Eakins, 2009). Time-averaged values are displayed at long-duration stations LD-A, LD-B, and LD-C.

as with Sea-Bird temperature and conductivity sensors and a high-frequency fluorometer. A total number of 123 profiles were performed with repeated profiles at LD stations ($\sim$ 30 profiles over three inertial periods) and at least one profile at each SD station except at SD13 (see Table 1 for further details). The dissipation rate of turbulent kinetic energy (ϵ) was inferred from centimeter-scale shear measurements. The vertical wavenumber shear spectrum was computed within the inertial range, typically within meter to centimeter scales. The experimental spectrum was next compared to the empirical spectrum, the Nasmyth spectrum (Nasmyth, 1970), which allowed validation of the estimate of ϵ (e.g., for a detailed description, see Ferron et al., 2014). Shear measurements were processed using the routines developed by Rockland Scientific. Specific noise removal procedures were applied with the spikes in the shear data first removed and spectral coherence between the shear sensors and the accelerometers used to remove vibrational contamination. The first 20 m below the surface were not considered to avoid any contamination from the ship wake as well as the 20 m at the end of the profile because of the decreasing vertical velocity there. More generally ϵ values were excluded when the vertical velocity gradient of the VMP was larger than $2.5 \times 10^{-2}\,\mathrm{s}^{-1}$. The averaged ϵ from the two shear probes was taken provided that the ratio between the two estimates was smaller than 2; otherwise, the ϵ value with the smallest depth variation (compared to the neighbouring upper and lower ϵ values) was considered. ϵ was computed over a 1 m depth interval, and then a 8 m moving average was applied to this signal. The estimated noise level is $5 \times 10^{-11}\,\mathrm{W\,kg^{-1}}$ following Ferron et al. (2014).

Table 1. VMP profiles.

Station	Position	Depth (m)	Number of VMP profiles
SD1	[159°54.0′ E; 18°0.0′ S]	4068	2
SD2	[162°7.5′ E; 18°37.5′ S]	2567	1
SD3	[164°54′ E; 19°19.0′ S]	3252	1
LD-A	[164°41.28′ E; 19°12.78′ S]	3491	30
SD4	[168°0.0′ E; 20°0.0′ S]	4995	1
SD5	[170°0.0′ E; 22°0.0′ S]	4405	1
SD6	[172°8.0′ E; 21°22′ S]	2509	3
SD7	[174°16′ E; 20°44′ S]	2451	2
SD8	[176°24′ E; 20°06′ S]	2028	3
SD9	[178°39′ E; 20°57′ S]	3864	2
SD10	[178°31′ W; 20°28′ S]	819	1
SD11	[175°40′ W; 19°59′ S]	2234	1
SD12	[172°50′ W; 19°29′ S]	7717	1
LD-B	[170°51.5′ W; 18°14.4′ S]	4912	35
SD13	[169°4.37′ W; 18°12.04′ S]	4598	0
LD-C	[165°45.4′ W; 18°40.8′ S]	5277	37
SD14	[163°0.0′ W; 18°25′ S]	3640	1
SD15	[160°0.0′ W; 18°16′ S]	3916	1

2.3 Diffusivity estimates

The diapycnal diffusivity, K_z, is commonly inferred from the kinetic energy dissipation rate using the Osborn (1980) relationship:

$$K_z = \Gamma \epsilon N^{-2}, \quad (1)$$

where Γ is a mixing efficiency defined as the ratio between the buoyancy flux and the dissipation rate, $\Gamma = -\frac{g}{\rho_0}\frac{\overline{\rho' w'}}{\epsilon}$, with w' and ρ' the vertical velocity and density fluctuations,

and N the buoyancy frequency, inferred from the sorted density profile in order to avoid spurious negative values associated with overturns, $N = \sqrt{-\frac{g}{\rho_0}\frac{\mathrm{d}\rho_{\mathrm{sorted}}}{\mathrm{d}z}}$, with an 8 m moving average then applied to this signal. Γ was generally set to 0.2 until the recent findings of Shih et al. (2005) and Bouffard and Boegman (2013). These authors found a decrease in Γ for increasing turbulence intensity, I, defined as

$$I = \epsilon/(\nu N^2), \tag{2}$$

where ν is the molecular viscosity, $\nu = 1.2 \times 10^{-6}\,\mathrm{m^2\,s^{-1}}$. In terms of timescales, I is the ratio of the square of the Kolmogorov timescale, namely the dissipation timescale of eddies at the Kolmogorov scale ($\sqrt{\nu/\epsilon}$), and the buoyancy timescale ($1/N$). Shih et al. (2005) showed in a numerical study that the Osborn relationship overestimated K_z when $I > 100$ and proposed a new parameterization of K_z for this regime. A few years later Bouffard and Boegman (2013) proposed a refined parameterization of K_z including in situ microstructure measurements in lakes as well. They defined different regimes with the following formulations for K_z:

- $K_z = 10^{-7}\,\mathrm{m^2\,s^{-1}}$ within the diffusive sub-regime, $I < 1.7$;
- $K_z = \frac{0.1}{7^{1/4}}\nu I^{3/2}$ within the buoyancy-controlled sub-regime, I within [1.7; 8.5];
- $K_z = 0.2\nu I$, i.e., the Osborn relationship within the intermediate regime, I within [8.5, 400]; and
- $K_z = 4\nu I^{1/2}$ within the energetic regime, $I > 400$.

Note that for the OUTPACE dataset where most I values are smaller than 100, the K_z values inferred from the Bouffard and Boegman parameterization that is applied here do not differ significantly from those inferred from the Osborn relationship.

2.4 Internal forcing: estimates of internal tide generating force and wind power input into inertial motions

The internal tide generation is inferred from the depth integrated generating force following the linear approximation (e.g., Baines, 1982) that reads as

$$\|\boldsymbol{F}\| = \int \frac{N^2}{\omega}\frac{z|\boldsymbol{Q}\cdot\nabla\boldsymbol{h}|}{h^2}\mathrm{d}z,$$

where N is inferred from the World Ocean Atlas monthly climatology, ω is the tidal frequency, $\boldsymbol{Q}$ is the barotropic tidal flux, and h is the bottom depth. The barotropic tidal flux is inferred from the $1/30° \times 1/30°$ global inverse tidal model TPXO (Egbert and Erofeeva, 2002) for two main constituents, the diurnal K1 and the semi-diurnal M2.

The generation of baroclinic near-inertial waves occurs through inertial pumping at the base of the mixed layer (e.g., Gill, 1984; Price, 1984). Insight into possible generation of baroclinic near-inertial waves is estimated from the wind work on inertial oscillations following Alford (2003):

$$F_{\mathrm{f}} = \rho\frac{\tau_{\mathrm{f}}^2}{rH}, \tag{3}$$

where τ_{f}^2 is the square of the wind stress at the inertial frequency, r is the damping of near-inertial motions in the mixed layer as a result of baroclinic near-inertial wave radiation expressed as a function of the inertial frequency $r = 0.15f$, and H is the mixed-layer depth. The wind stress was inferred from numerical simulations over the time period of the cruise (Skamarock et al., 2005) and the mixed-layer depth from the seasonal climatology.

2.5 Biogeochemical turbulent diffusive fluxes

The vertical components of nitrate and phosphate turbulent diffusive fluxes were computed at all stations, using the diapycnal diffusivity, K_z, inferred from microstructure measurements:

$$F_{\mathrm{NO_3,PO_4}} = -K_z\partial_z c_{\mathrm{NO_3,PO_4}}, \tag{4}$$

where c_{NO3} and $c_{\mathrm{PO_4}}$ are the nitrate and phosphate concentrations. Measurements were performed daily at 12 depths in the first 200 m using standard colorimetric procedures (see Caffin et al., 2018, for further details). The quantification limits were $50\,\mu\mathrm{mol\,m^{-3}}$. At LD stations where six profiles were obtained, the quantification limit for the mean concentration dropped to $20\,\mu\mathrm{mol\,m^{-3}}$ (i.e., $50/\sqrt{6}$). Concentration values below the threshold for quantification were set to NaN. Vertical concentration profiles were interpolated over a 1 m vertical grid and a 10 m moving average was next applied. The top of the nitracline was defined as the depth where nitrate concentration is zero based on an extrapolation from the last detectable concentration ($> 50\,\mu\mathrm{mol\,m^{-3}}$) assuming a constant vertical gradient above this depth (see Moutin et al., 2018). It is only at long-duration stations that the top of the nitracline was defined in isopycnal coordinates: this allows us to get rid of a varying depth of the nitracline because of vertical displacements of isopycnals induced by internal waves (see Caffin et al., 2018). The minimum turbulent diffusive flux was estimated from the threshold concentration with the molecular K_z value ($K_z \sim 10^{-7}\,\mathrm{m^2\,s^{-1}}$): $0.4\,\mu\mathrm{mol\,m^{-2}\,d^{-1}}$ at SD stations and $0.17\,\mu\mathrm{mol\,m^{-2}\,d^{-1}}$ at LD stations where the mean concentration profile was taken to compute the flux. A reference profile was also defined in order to compare the nitrate diffusive flux variations along the OUTPACE within a 100 m layer below the top of the nitracline. To do so vertical profiles of concentration were first shifted vertically so that the reference depth matched with the top of the nitracline and the mean vertical $c_{\mathrm{NO_3}}$ profile within the nitracline was inferred from this set of re-scaled concentration profiles. K_z profiles were also rescaled onto this vertical grid and a

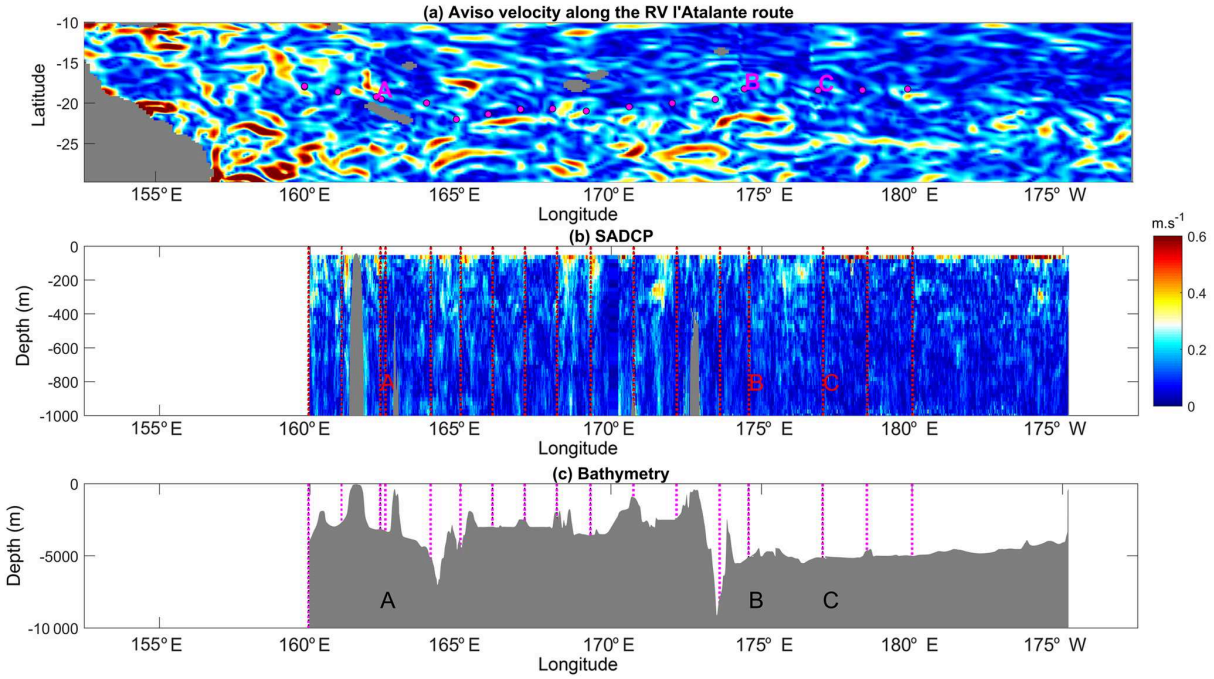

Figure 2. Surface geostrophic currents inferred from AVISO altimetric data **(a)**; longitude–depth section of the 38 kHz SADCP velocity modulus **(b)**; bathymetry along the RV *l'Atalante* route **(c)**; VMP stations are displayed with magenta circles in **(a)** and with vertical dashed red lines in **(b)** and magenta lines in **(c)**.

Table 2. Statistics in the western and eastern parts: percentage of $Ri < 1$ and mean values and standard deviations of ϵ and K_z within a 100–500 m surface layer.

	$Ri < 1$ (%)	$\langle\epsilon\rangle$ (W kg^{-1})	$\delta(\epsilon)$ (W kg^{-1})	$\langle K_z\rangle$ (m^2 s^{-1})	$\delta(K_z)$ (m^2 s^{-1})
West of 170° W	3.0	2.3×10^{-9}	6.0×10^{-9}	6.0×10^{-6}	7.1×10^{-5}
East of 170° W	0.05	7.0×10^{-10}	5.8×10^{-10}	2.8×10^{-6}	4.5×10^{-6}

mean K_z profile inferred. The relative contributions of the variations in K_z and that of $\partial_z c_{NO_3}$ with respect to the total variations of the flux were also inferred.

3 Spatial pattern of turbulence

3.1 Overview

An overview of the spatial pattern of turbulence is given with depth-averaged values of ϵ and K_z below 100 m depth at each station (Fig. 1). Depth-averaged dissipation rates, $\langle\epsilon\rangle$, vary within an order of magnitude within $[10^{-9.5}; 10^{-8.5}]$ W kg^{-1}. The highest values are observed west of 170° W, in the shallower part, while the lowest values are observed east of 170° W, in the deeper part. The same contrast is retrieved on $\langle K_z\rangle$ with values ranging within $[10^{-5.8}; 10^{-4.8}]$ m^2 s^{-1}. The western part of our study area which shows the highest turbulence level is also the region where the most intense velocities are observed, as illustrated with altimetry-derived currents produced by AVISO along the RV *l'Atalante* cruise path (Fig. 2a). The vertical section of the total velocity modulus inferred from the SADCP data shows that this contrast is also observed at depth with slightly larger velocities in the western part of our study area (Fig. 2b). There the bathymetry ranges typically from 4000 m up to a few hundred meters locally with significant topographic slopes, which is consistent with the higher velocity signal; by comparison, in the east the bathymetry is almost flat, with ∼ 5000 m depth. More insights into turbulence are given with vertical sections of ϵ and K_z in Fig. 3a and b. The range of ϵ values covers 3 orders of magnitude, $\sim [10^{-10}, 10^{-7}]$ W kg^{-1} below the mixed layer (magenta curve in Fig. 3a) down to 500 m depth. ϵ presents a typical patchy pattern with spots of intense turbulence with values up to $\sim 10^{-8}$ W kg^{-1} down to 500 m. These events are localized over a 10 m vertical scale except at LD-A around 165° E longitude where a 200 m layer of enhanced ϵ is ob-

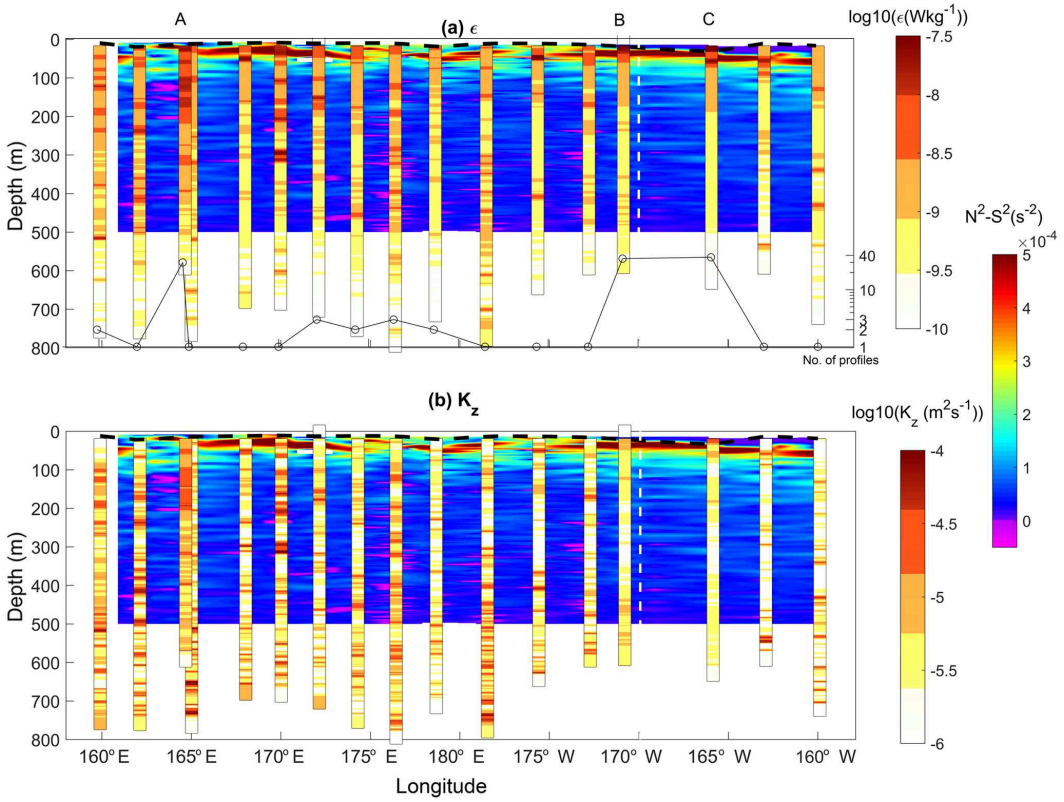

Figure 3. Log values of the dissipation rate of turbulent kinetic energy ($\mathrm{W\,kg^{-1}}$) **(a)** and vertical diffusion coefficient ($\mathrm{m^2\,s^{-1}}$) **(b)** with $N^2 - S^2$ in background color scale. The number of profiles at each station is displayed with black circles and profiles have been time-averaged at each station for better visualization. The mixed-layer depth is plotted (black dashed curve) as well as the limit between the two regions (dashed white line).

served. Most of these events are observed in the west, west of 170° W, and the few vertically localized large ϵ observed east of 170° W are no deeper than 200 m depth (Fig. 3a). Statistics of ϵ within a 100–500 m depth interval are given for each region in Table 2. The contrast between the mean 100–500 m depth-averaged ϵ in each of the two regions is a factor of 3 (Table 2). The contrast is larger for the standard deviation, a factor of 10, which points to the larger intermittency of turbulent events west of 170° W. The K_z pattern presents a similar contrast between the western and eastern parts with mean 100–500 m depth-averaged K_z between the two regions differing by a factor of 2 (Table 2). More importantly, the standard deviation of K_z is by far larger west of 170° W, by a factor of 15 (Table 2).

3.2 Shear instability

To gain further insights into the origin of this contrast in turbulence, the possible occurrence of shear instability is addressed with buoyancy frequency, N, shear, S, and $N^2 - S^2$ sections displayed in Fig. 4. The stratification is strong in the first 100 m, with a pycnocline that is generally well marked except westward of 165° E and around 172° W longitudes and a less stratified surface layer above 50 m east of 170° W. The shear is significantly higher west of 170° W, with high values over the 500 m depth layer of the measurements in the west except for a 165–170° E region (Fig. 4a and b). The likeliness of shear instability was estimated from $N^2 - S^2$, displayed in Fig. 4c. The upper 100 m surface layer is the most stable, with the highest $N^2 - S^2$ values as a result of both strong stratification and low shear. Shear instability is more likely to occur west of 170° W below the 100 m surface layer of strong stratification and where the shear is large: the percentage of data points that verifies the criterion for shear instability is 10 times larger west of 170° W than east of 170° W (Table 2). The fact that most of the subcritical Ri, $N^2 - S^2 < 0$, are observed west of 170° W is consistent with the enhanced dissipation observed there (Fig. 3 and 4c).

3.3 Tidal and atmospheric forcings for the internal wave field

The possible impact of internal waves was estimated indirectly through the two main energy sources of these waves, namely tidal forcing and wind power input (Figs. 5 and 6).

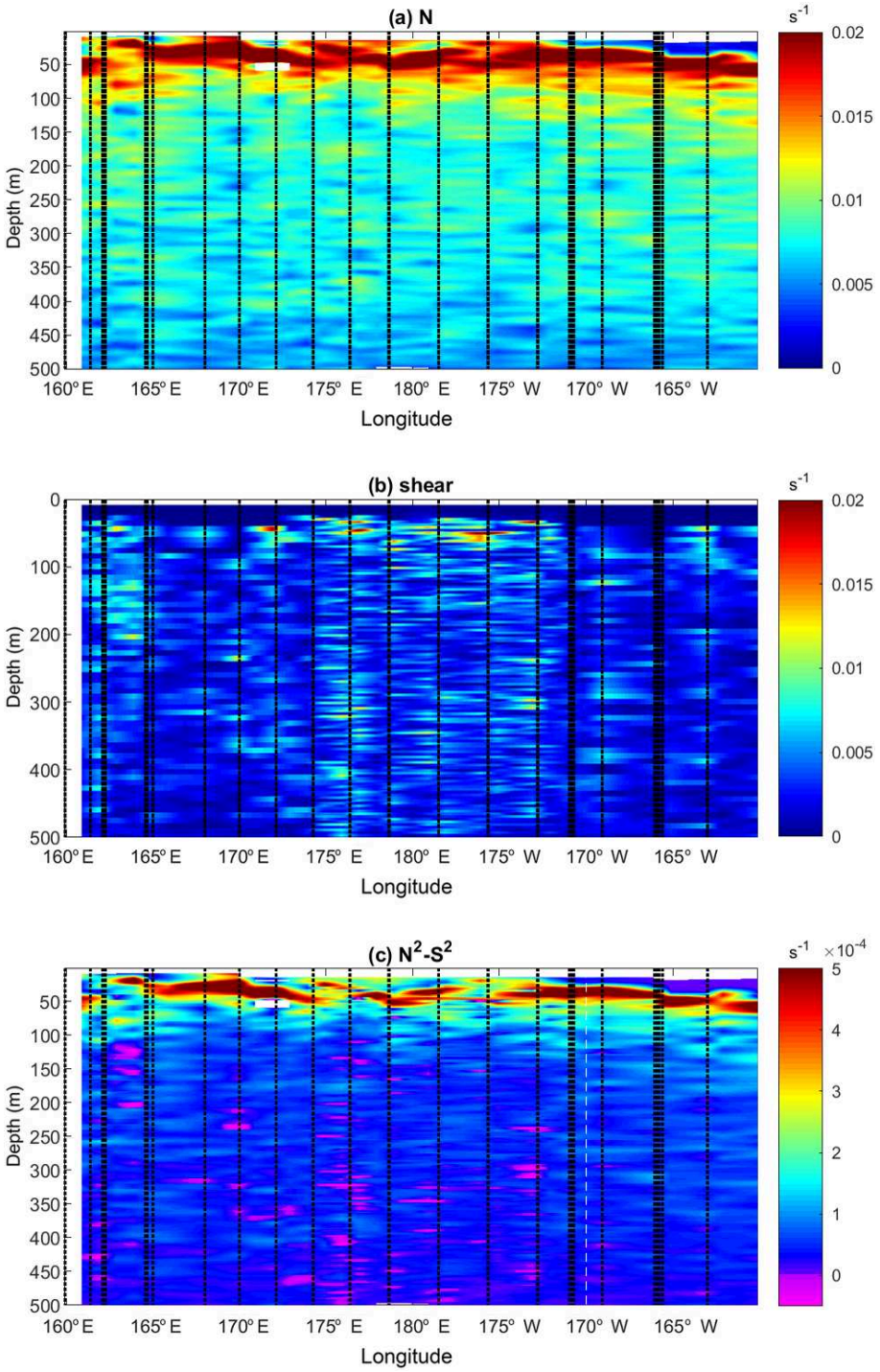

Figure 4. Buoyancy frequency, N **(a)**, shear, S **(b)**, and $N^2 - S^2$ **(c)** as a function of longitude and depth. The locations of the CTD and LADCP profiles are displayed with black dashed lines. S is inferred from LADCP data and N was vertically averaged over 8 m length vertical intervals for consistency with the 8 m bin of the LADCP data.

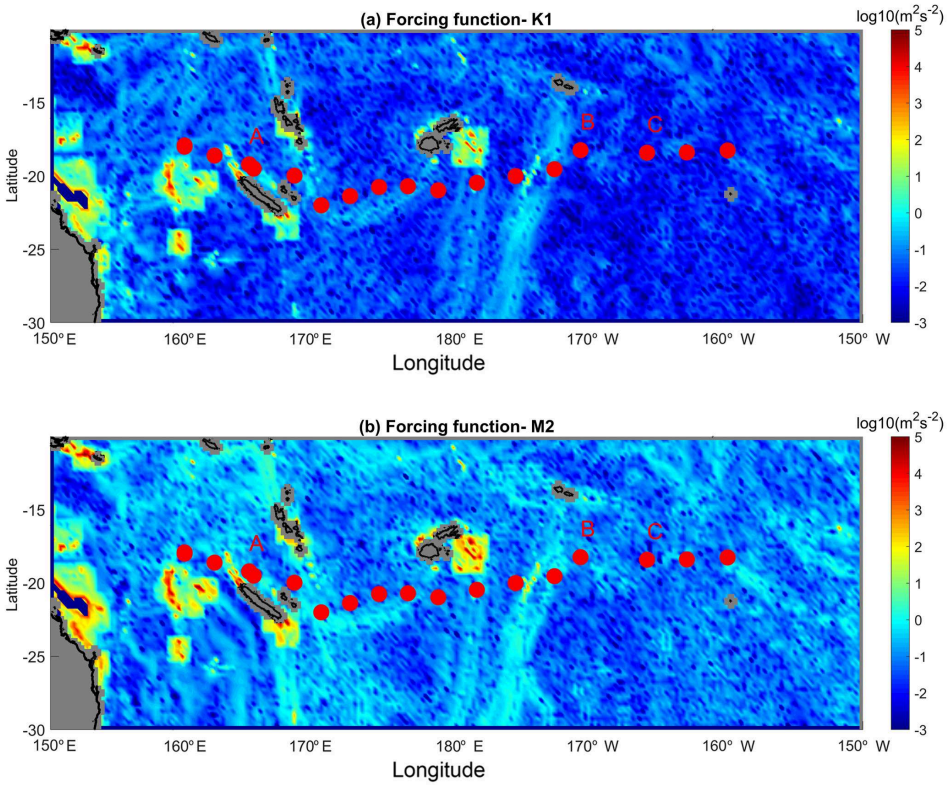

Figure 5. **(a)** Depth-integrated generation force for the K1 tidal constituent (log10($m^2\ s^{-2}$)); **(b)** same as in **(a)** but for the M2 tidal constituent. The stations are shown with a red circle and the LD stations are indicated.

The depth-integrated tidal generation force is displayed in Fig. 5 for the K_1 and M_2 constituents. There is a strong similarity between the two constituents with a generation that is favoured in the western part which is shallower and with stronger topographic gradients than the eastern part of our study area. The westernmost region is characterized by numerous spots of generation with a depth-integrated generation force of $10^3\ m^2\ s^{-2}$, while eastward of 170° E longitude there is only one main generation site around 180° E longitude (Fig. 5a). This spatial distribution of the internal tide forcing might suggest a similar contrast in the internal-tide-induced dissipation since the high modes responsible for turbulence are expected to dissipate within a few tens of kilometers of the generation site (e.g., St Laurent et al., 2002).

Maps of wind power input on inertial motions, also referred to as inertial flux, were computed using the spectral method described by Alford (2003). The wind stress data were inferred from WRF numerical simulations (Klemp et al., 2007; Skamarock et al., 2005) and the seasonal climatology was used for the mixed-layer depth. The power input into inertial motions gives insights into the generation of baroclinic near-inertial waves (niw) at the base of the mixed layer through inertial pumping (e.g., Gill, 1984). The maps reveal a strong longitudinal contrast in inertial flux until mid-March (Fig. 6a–e). The strongest wind power input was observed in the western part of our study area. This is consistent with the climatology of storms and cyclones in the area that are typically formed in the south-western tropical Pacific (e.g., Diamond et al., 2013). At the beginning of the cruise the largest power input was localized south-west of the cruise stations (Fig. 6a). Later a major event was observed (Fig. 6d) during the passage of a tropical cyclone over the area while RV *l'Atalante* was sampling to the east. Eventually by the end of the cruise the inertial flux was small over the OUTPACE region, with one spot of weak inertial flux observed in the east (Fig. 6f–g). These maps suggest that energetic niw are likely to be generated in the western part of our study area prior to the cruise and until mid-March (Fig. 6a–b). The first event of large inertial flux prior to the cruise may be particularly insightful since it is likely to lead to the generation of equatorward propagation niw within the OUTPACE sampling area, a scenario which is consistent with large ϵ values there (Fig. 1).

4 Possible impact of internal waves: focus on long-duration stations

Three long-duration stations were sampled each over three inertial periods, LD-A in the western part of the transect and LD-B and LD-C in the eastern part of the transect (see Ta-

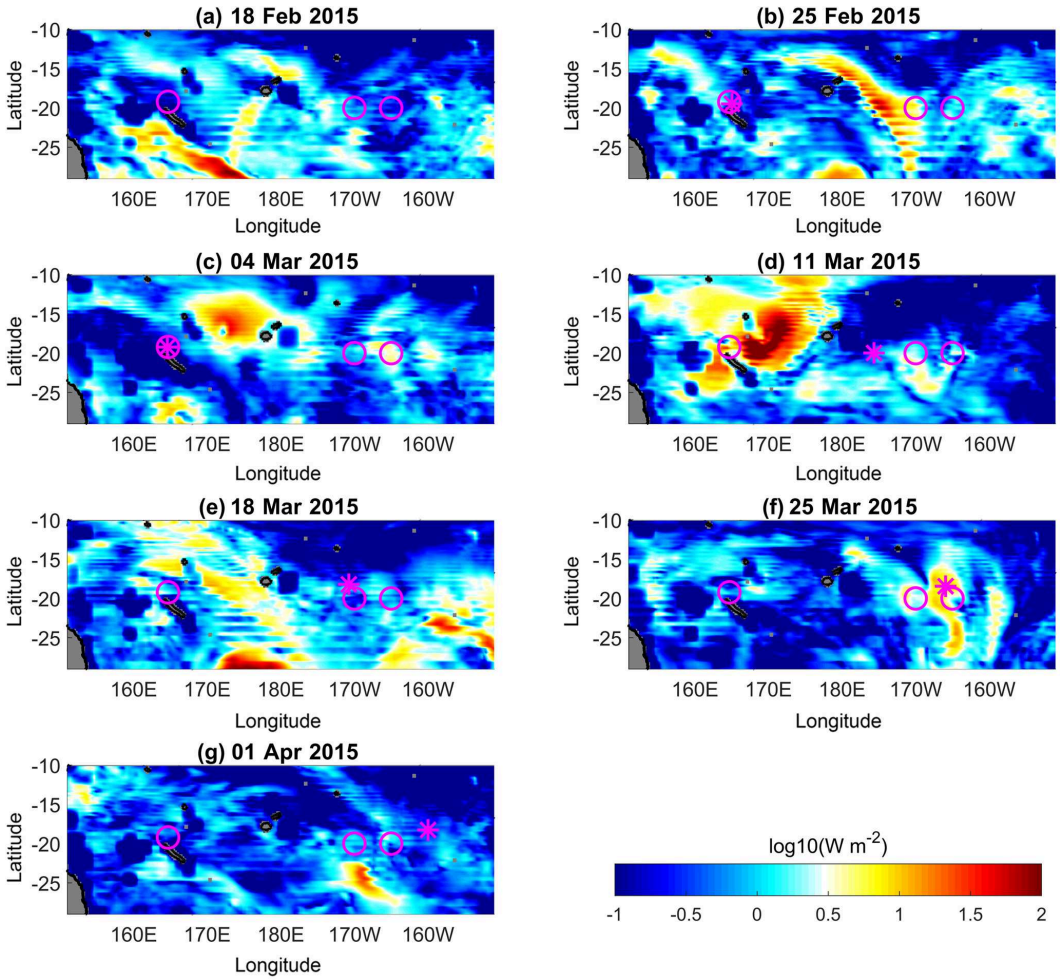

Figure 6. Maps of inertial energy flux (log10(W m^{-2})) every 7 days during the cruise. Long-duration stations are shown with magenta circles, and LD-A was held during **(b)** and **(c)**, LD-B during **(e)**, and LD-C during **(f)**. The ship position is displayed with a magenta star.

ble 1 and Fig. 1). Turbulence at LD-A is by far the largest down to 500 m depth, with contrasted mean ϵ and K_z between LD-A on the one hand and LD-B and LD-C on the other hand (Fig. 7a and b) by factors of 7 and 5 for the averaged, within [100 m, 500 m], ϵ and K_z respectively (Table 3). Possible occurrence of shear instability is examined by comparing mean profiles of shear square, S^2, and N^2 (Fig. 7c). While the mean stratification is fairly close, at the three stations the shear square is larger at LD-A compared to LD-B and LD-C within a factor of 10 within [50 m, 250 m] (Fig. 7c). Furthermore, within [100 m, 200 m] S^2 is larger than N^2 at LD-A, pointing to possible shear instability. This depth range coincides with local ϵ maxima, thus reinforcing the shear instability hypothesis.

We next focused on the characterization of the internal wave field that may reinforce the vertical shear and contribute to the onset of turbulence. Current magnitude at LD-A is the largest (Fig. 8a and b), of the order of 0.4 m s^{-1}. Detailed insights from the 150 kHz SADCP reveal a wavy pattern with two frequencies clearly identified (Fig. 8a): strong upward-propagating bands close to the inertial period, of about 1.5 days, and the semi-diurnal period, which manifests itself through semi-diurnal heaving of upward-propagation niw bands. The former is observed over the first 200 m only, while the latter is observed down to $\sim$ 800 m depth (Fig. 8a and b). The weaker currents at LD-B and LD-C are comparable with a maximum amplitude of 0.2 m s^{-1} (Fig. 8c–f). Periodic motions are also evidenced with inertial oscillations in the first few meters (Fig. 8c) and a combination of near-inertial and tidal periods at depth. Noticeably, an upward phase propagation of niw can be inferred at LD-B from the 38 kHz SADCP data (Fig. 8d). At LD-C the semi-diurnal tidal signal dominates (Fig. 8f). The dominance of niw at LD-A is consistent with the highest wind power input inertial motions at LD-A (Fig. 6a) compared to LD-B and LD-C (Fig. 6e). Instead the contrast observed between the semi-diurnal depth-integrated generating force at LD-A compared to that at LD-B and LD-C (Fig. 5b) is not evidenced on the

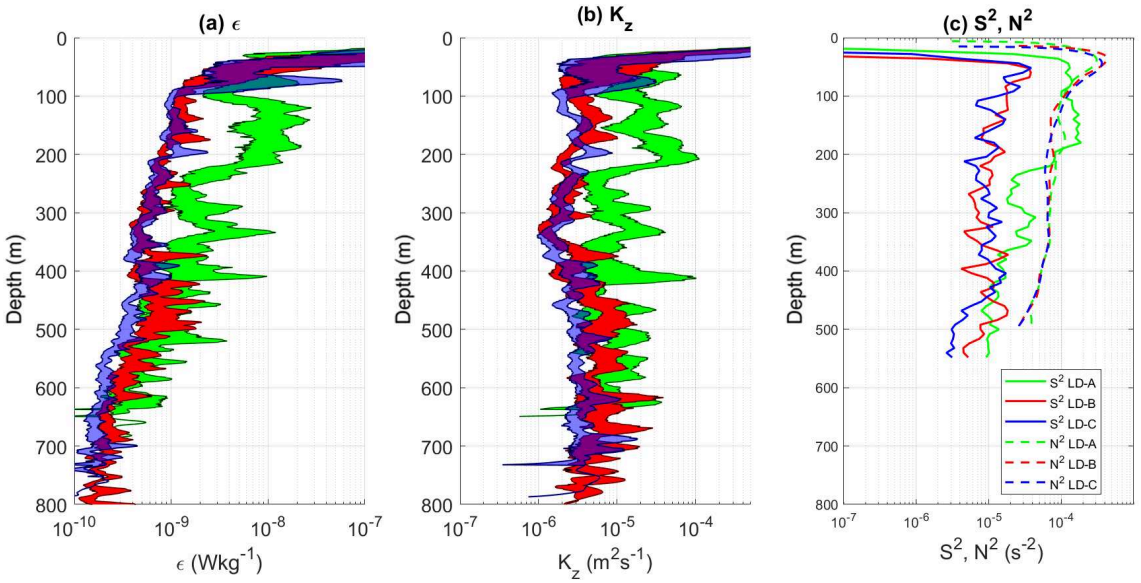

Figure 7. Mean profiles at long-duration stations: ϵ in **(a)**, K_z in **(b)**, and S^2 and N^2 in **(c)**. K_z was computed using N from the VMP measurements, while the profiles in **(c)** were inferred from the rosette-mounted CTD and LADCP instruments. The 95 % confidence interval for ϵ and K_z is displayed with a shading surface in **(a)** and **(b)**.

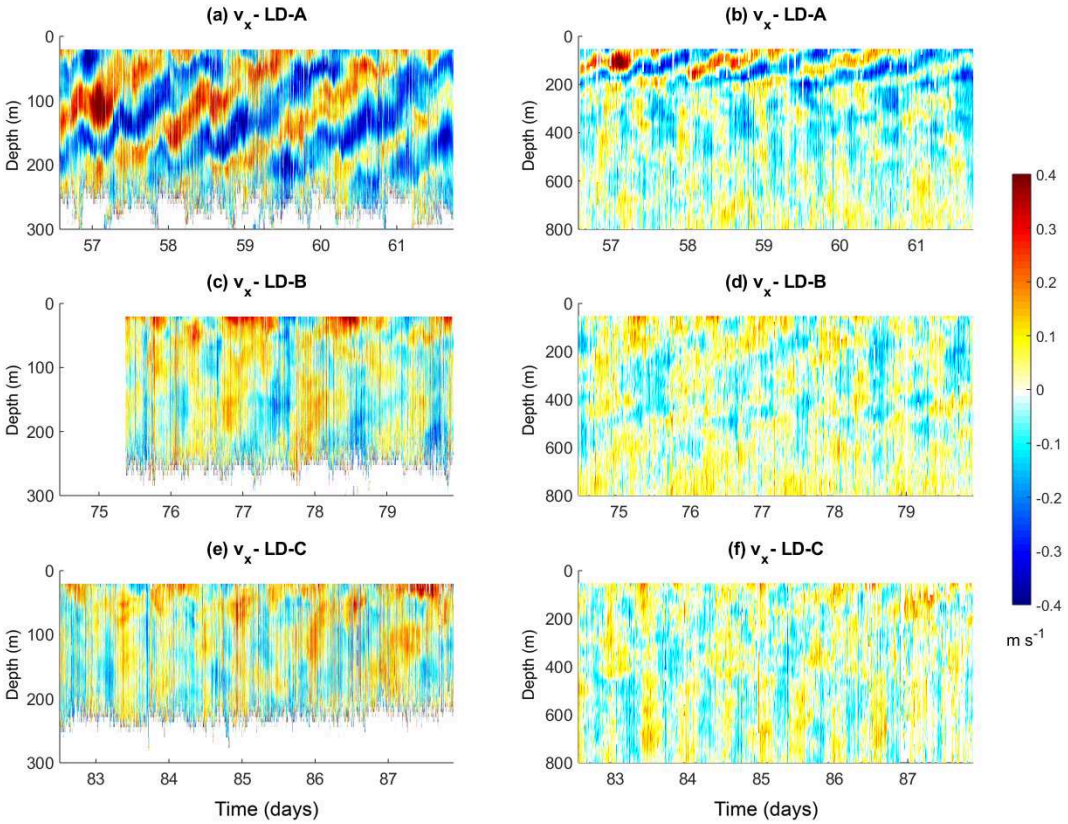

Figure 8. Zonal velocity ($\mathrm{m\,s^{-1}}$) as a function of time and depth at the long-duration stations; each row from 1 to 3 corresponds to LD-A, LD-B, and LD-C respectively. In the first column ship ADCP data from the 150 kHz instrument down to 300 m are displayed and in the second column those from the 38 kHz instrument down to 800 m. Note that in **(b)** the 150 kHz SADCP functioned only a few hours after the beginning of the station sampling.

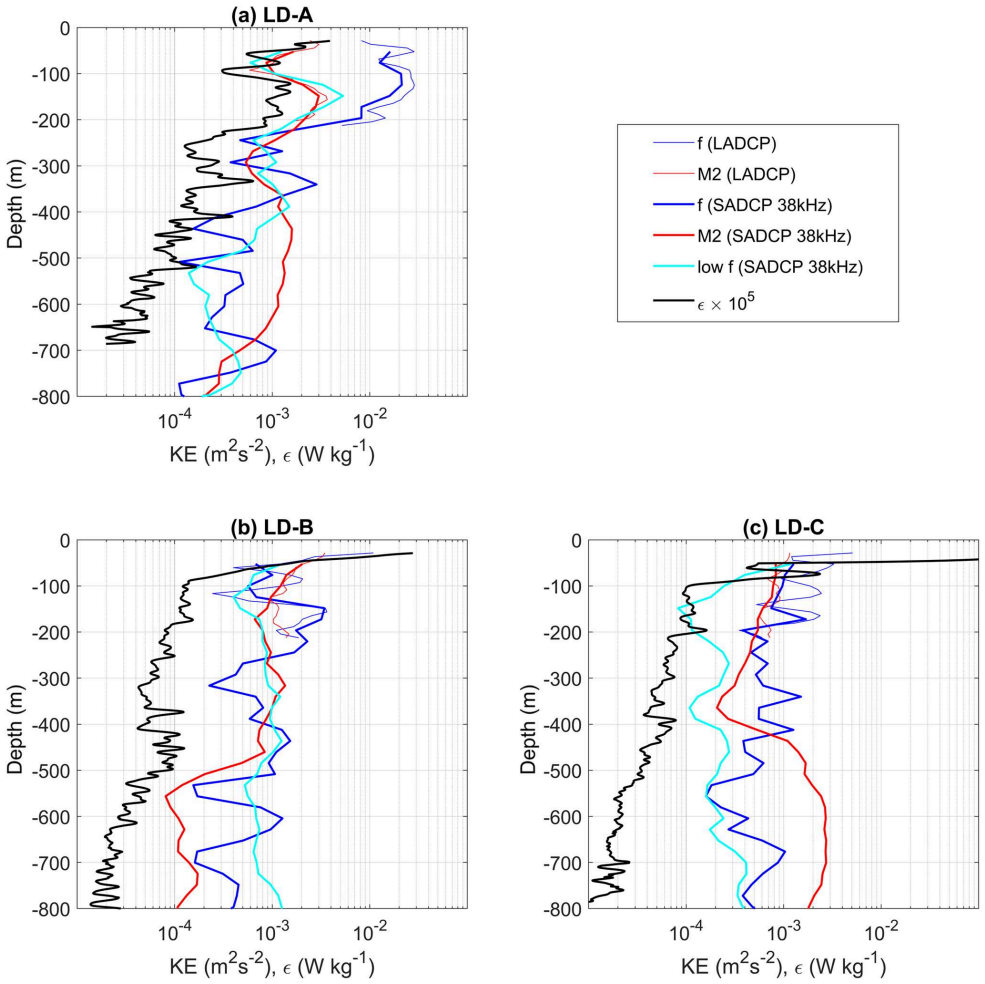

Figure 9. Time-mean profiles of the kinetic energy of the subinertial flow, the inertial and semi-diurnal frequencies, and ϵ at LD-A **(a)**, LD-B **(b)**, and LD-C **(c)**. The kinetic energy was derived from the 38 kHz SADCP data but also from the 150 kHz SADCP data for the inertial and semi-diurnal kinetic energies (thin blue and red curves).

semi-diurnal currents (Fig. 8). This is well evidenced below $\sim$ 300 m depth where the semi-diurnal tidal signal dominates at all stations (Fig. 8b, d, and f). This difference might result from localized generation areas of small scales that are not predicted by the estimate performed with low-resolution fields (tidal model and bathymetry) or from low modes with long-range propagation.

Figure 9 summarizes the main characteristics of the three long-duration stations, with vertical profiles of time-averaged ϵ and kinetic energy for the sub-inertial flow, the inertial frequency band, and the semi-diurnal tidal constituent, M2. Kinetic energies were inferred from the frequency spectra computed over three inertial periods. Depth-averaged values of ϵ, K_z as well as kinetic energy and shear within the different frequency bands are also given in Table 3. The average was computed over two depth intervals: the first one is 100–500 m, consistent with that chosen in Table 2, while the second one is 50–250 m, corresponding to the depth interval of maximum niw energy at LD-A. The enhanced ϵ at LD-A is coincident with an energetic niw (Fig. 9a). The contrast with LD-B and LD-C is striking within the depth interval 50–250 m with an averaged ϵ within 50–250 m about 8 times larger than at LD-B and a near-inertial kinetic energy that differs by almost an order of magnitude (Table 3). The significant decrease in ϵ, coincident with a sharp shutdown of the near-inertial baroclinic signal around 250 m, shows the main effect of niw on dissipation. This transition is associated with a strong variation in the subinertial flow that suggests a wave mean flow interaction (e.g., critical level; Soares et al., 2015). LD-B and LD-C present strong similarities in ϵ and niw and M2 kinetic energies with 100–500 m depth-averaged values that are close (Table 3). The local maxima in near-inertial kinetic energy may evidence niw beams around 150, 450, and 650 m at LD-B and 200, 350, 400, and 650 m at LD-C (Fig. 9b and c). The semi-diurnal kinetic energy presents an interesting contrast between LD-B and LD-C: while it is

Table 3. Statistics at the long-duration stations: percentage of $N^2 - S^2 < 0$ (i.e., $Ri < 1$), median values of ϵ, K_z, mean value of kinetic energy for the sub-inertial frequencies, inertial frequency and semi-diurnal M2 tidal constituent, and the same for shear variance. The average is performed over a 100–500 m surface layer (first three lines) as well as over a 50–250 m layer to highlight the impact of the niw at LD-A.

	$Ri < 1$ (%)	$\langle\epsilon\rangle$ (W kg^{-1})	$\langle K_z\rangle$ (m^2 s^{-1})	KE$_{\mathrm{If}}$ (m^2 s^{-2})	KE$_{\mathrm{f}}$ (m^2 s^{-2})	KE$_{\mathrm{M2}}$ (m^2 s^{-2})	S^2_{If} (s^{-2})	S^2_{f} (s^{-2})	S^2_{M2} (s^{-2})
LD-A	18 %	4.4×10^{-9}	1.1×10^{-5}	2.5×10^{-3}	4.6×10^{-3}	1.4×10^{-3}	1.0×10^{-6}	8.2×10^{-6}	3.3×10^{-7}
LD-B	0.86 %	8.3×10^{-10}	3.4×10^{-6}	1.6×10^{-3}	1.2×10^{-3}	8.3×10^{-4}	1.5×10^{-7}	1.5×10^{-6}	1.0×10^{-7}
LD-C	0.25 %	6.9×10^{-10}	2.7×10^{-6}	3.4×10^{-4}	7.5×10^{-4}	7.5×10^{-4}	9.4×10^{-8}	7.8×10^{-7}	8.4×10^{-8}
LD-A	38.6 %	8.26×10^{-9}	1.0×10^{-5}	3.7×10^{-3}	1.1×10^{-2}	1.7×10^{-3}	2.1×10^{-6}	2.0×10^{-5}	7.6×10^{-7}
LD-B	0.11 %	1.7×10^{-9}	3.7×10^{-6}	1.2×10^{-3}	1.6×10^{-3}	1.1×10^{-3}	2.0×10^{-7}	1.4×10^{-6}	1.4×10^{-7}
LD-C	0.10 %	2.7×10^{-9}	3.6×10^{-6}	5.5×10^{-4}	8.8×10^{-4}	6.2×10^{-4}	2.6×10^{-7}	1.2×10^{-6}	1.1×10^{-7}

Table 4. Statistics in the western and eastern parts: mean values of the NO_3 and PO_4 turbulent diffusive fluxes in the photic layer. The standard deviation is given within the brackets.

Flux (μmol m^{-2} d^{-1})	West of 170° W	East of 170° W	LD-A	LD-B	LD-C
Nitrate flux	11.38 [19.94]	3.15 [1.32]	8.41 [12.40]	–	–
Phosphate flux	2.66 [35.63]	4.01 [13.70]	2.13 [2.42]	2.16 [5.05]	0.31 [0.39]

larger at LD-B in the first 500 m and smaller below, the opposite is observed at LD-C with maximum semi-diurnal energy below 500 m depth, also suggesting a beam structure. The subinertial flow is weakest at LD-C (Fig. 9c) by a factor of 2 compared to LD-B and by a factor of 8 compared to LD-A for the 100–500 m depth-averaged value of the kinetic energy. Moreover, the depth-averaged low-frequency shear is below the noise level at LD-B and LD-C (Table 3), both features suggesting a weak influence on internal wave propagation. The subinertial flow is by far the largest at LD-A down to $\sim$ 250 m (Fig. 9a). The contrast in turbulence between the three stations is mostly confined in the upper few hundred meters as a result of an energetic niw and its interaction with the strongly sheared subinertial flow (Table 3). Deeper, variations in ϵ and kinetic energies are much weaker and of the same order of magnitude at the three stations (Fig. 9).

5 Impact of turbulence on biogeochemical fluxes: spatial pattern and intermittency

5.1 Overview of the OUTPACE section

The distribution of chlorophyll concentrations along the OUTPACE transect is typical of a transition from an oligotrophic area in the MA toward an ultra-oligotrophic area in the SPSG (e.g., Moutin et al., 2017) with a deepening of the deep chlorophyll maximum, DCM, from $\sim$ 60 to $\sim$ 160 m and an increase in the euphotic zone depth (Fig. 10a). There is one noticeable exception to this trend with a near-surface chlorophyll concentration maximum at $\sim$ 35 m depth, at LD-B. de Verneil et al. (2017), who focused on the characterization of this anomalous phytoplankton bloom event, explained its occurrence by the main impact of mesoscale advection and an island effect. The deepening of the DCM results from that of the nitracline and from the NO_3 depletion in the first 200 m, an evolution consistent with the increasing oligotrophy to the east (Fig. 10a and c). Moreover, east of 172° W the nitracline is most often deeper than the base of the euphotic layer, which reinforces the oligotrophy. The turbulent diffusive nitrate flux displays the same longitudinal trend (Fig. 10c) with a depth-averaged value in the photic layer that differs by almost a factor of 4 west of 170° W and east of 170° W (Table 4). The standard deviation is also by far larger in the west, by a factor of 15. Whether these flux variations are driven by K_z variations or c_z variations was examined within a 100 m depth interval below the nitracline all along the section. These large variations of the turbulent diffusive nitrate flux at small scales (Fig. 10c) mostly result from K_z variations with a weaker contribution of variations in the vertical gradient of nitrate concentration with a typical ratio of 3 between the two (Table 5). The latter contribution tends to weaken slightly the eastward decrease in the flux due to decreasing K_z. The variation of the nitrate diffusive flux was also examined at LD stations only in order to focus on the impact of the temporal intermittency of turbulent events at each LD station where a large number of VMP profiles were collected. The flux variation resulting from K_z variations, $-\Delta K_z c_z$, and those resulting from c_z variations, $-K_z \Delta c_z$, were compared to the averaged flux over the three LD stations. The $-\Delta K_z c_z$ always dominates and is by far the largest at LD-A, with a relative value of 105 % compared

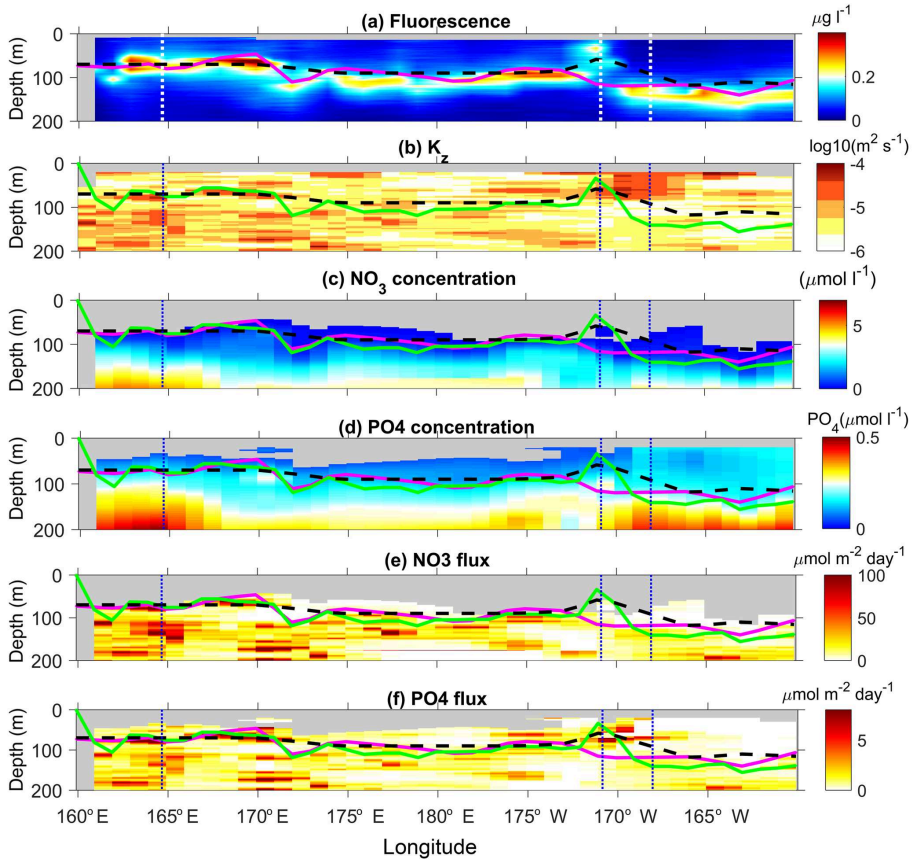

Figure 10. Longitude–depth sections of chlorophyll concentration **(a)**, K_z **(b)**, nitrate concentration **(c)**, phosphate concentration **(d)**, nitrate turbulent diffusive flux **(e)**, and phosphate turbulent diffusive flux **(f)**. The top of the nitracline is shown with a magenta line, the depth of maximum chlorophyll concentration with a green line, and the euphotic zone depth with a dashed black line. The locations of the LD stations are shown with a vertical dashed line. The scales of the color bar of the nitrate and phosphate concentration and turbulent diffusive flux are set to allow a direct comparison of concentrations and fluxes against nutrient requirements for phytoplankton (Redfield proportion: $N : P = 16 : 1$).

Table 5. Relative contributions to the flux variations of K_z and c_z depth-averaged over a 100 m vertical layer defined from the top of the nitracline, west of 170° W and east of 170° W and at long-duration stations. The mean value and standard deviation are also given.

	$-\Delta K_z c_z$ (μmol m^{-2} d^{-1})	$-K_z \Delta c_z$ (μmol m^{-2} d^{-1})	$\langle -K_z c_z \rangle$ (μmol m^{-2} d^{-1})	$\delta(-K_z c_z)$ (μmol m^{-2} d^{-1})
West of 170° W	+18 %	−6 %	19.5	20.8
East of 170° W	−56 %	+14 %	12.6	11
LD-A	+105 %	−16 %	44.77	91.77
LD-B	−50 %	+1 %	14.17	18.26
LD-C	−55 %	+8 %	13.1	15.68

with the −50 % and −55 % relative values at LD-B and LD-C (Table 5). This shows the major impact of the turbulence intermittency induced by the niw event at LD-A.

Phosphate turbulent diffusive flux is on average smaller than the nitrate turbulent diffusive flux, but its relative impact may be rescaled by a factor of 16 : 1 corresponding to the Redfield N : P ratio. Hence, for visual comparison between the two fluxes, the scale for the phosphate turbulent diffusive fluxes differs from that of the nitrate turbulent diffusive flux within the Redfield ratio in Fig. 10 and subsequently. The phosphate turbulent diffusive flux displays a similar longitudinal gradient in the first 200 m but presents an opposite trend in the photic layer, with a depth-averaged value higher by a factor of 1.5 east of 170° W (Table 5). The concentration of phosphate is not as strongly limiting as that of nitrate in the photic layer with significant turbulent diffusive flux, in a few

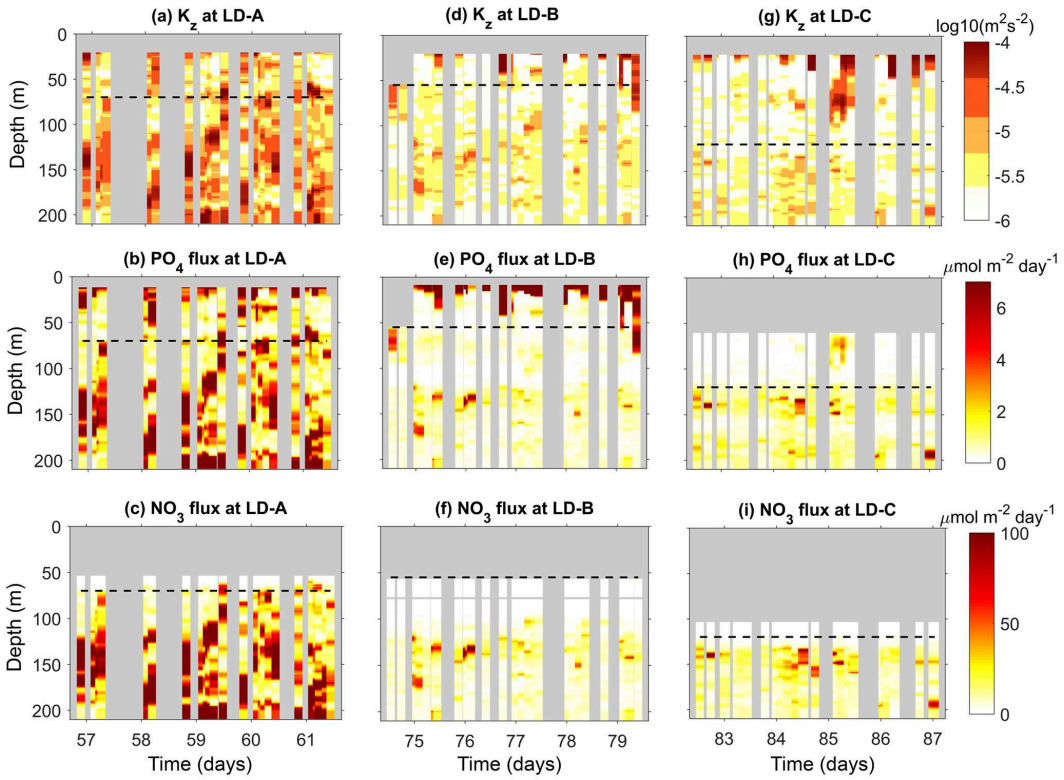

Figure 11. Time–depth sections of K_z **(a, d, g)**, phosphate turbulent diffusive flux **(b, e, h)**, and nitrate turbulent diffusive flux **(c, f, i)**. The scales of the color bar of the nitrate and phosphate diffusive flux are set to match with the typical Redfield ratio in the area ($N : P = 16 : 1$). The mean euphotic zone depth is displayed with a black dashed line. The top of the nitracline is defined by the isopycnal ρ_{NO_3} and falls at depths of ~ 83.5 m at LD-A, ~ 111.2 m at LD-B, and ~ 134.6 m at LD-C.

spots, especially around 170 and 190 longitudes (Fig. 10d). Consistently the same trend is obtained for the phosphate concentration in the photic layer, with an eastward increase in the photic layer as opposed to the nitrate concentration that tends to zero at the eastern stations (Fig. 10c and d). The absolute value of the photic layer depth-averaged value of the flux, east of 170° W, is 4.01 µmol m^{-2} d^{-1}. Considering a N : P Redfield ratio of 16, the phosphate turbulent diffusive flux is significant compared to the 3.15 µmol m^{-2} d^{-1} value for the nitrate turbulent diffusive flux (Fig. 10e and f, Table 4). This striking difference in phosphate and nitrate turbulent diffusive fluxes within the photic layer may play an important role in the development of micro-organisms as discussed later.

5.2 Focus on LD stations

Turbulent diffusive fluxes of nitrate and phosphate were further analysed at long-duration stations (Fig. 11). The time–depth evolution of K_z underlines the very large values encountered at the most turbulent station, LD-A, in contrast with values at LD-B and LD-C that show the occurrence of a few spots of intense mixing in a more quiescent background with $K_z \sim 3 \times 10^{-6}$ m^2 s^{-1} (Fig. 11a, d, and g). The largest nitrate turbulent diffusive fluxes occur at LD-A (Fig. 11b), while the smallest values are observed at LD-B and LD-C (Fig. 11f and i). The averaged values in the photic layer show that it is only at LD-A that there is a small input of nitrate through diffusion with an average flux of 8.41 µmol m^{-2} d^{-1} (Table 4).

In contrast, phosphate turbulent diffusive fluxes are significant well above the euphotic zone depth at all LD stations (Fig. 11b, e, and h), which may have an impact on primary production, whereas the nitrate input by turbulent diffusion is negligible (explanation below). Depth-averaged values in the photic layer are even comparatively larger than that of the nitrate turbulent diffusive fluxes at LD-A if one applies the $P/N = 1/16$ Redfield ratio (Table 4). Various spots of large phosphate turbulent diffusive fluxes are also evidenced in the first ~ 20–80 m that can be correlated with events of intense turbulence (Fig. 11b, e, and d). At LD-C the only event of significant phosphate turbulent diffusive flux results from a strong turbulent event (Fig. 11h).

5.2.1 Nitrate input at the top of the nitracline

The input of nitrate through turbulent diffusion was first examined at the top of the nitracline, within a ~ 4 m thick-

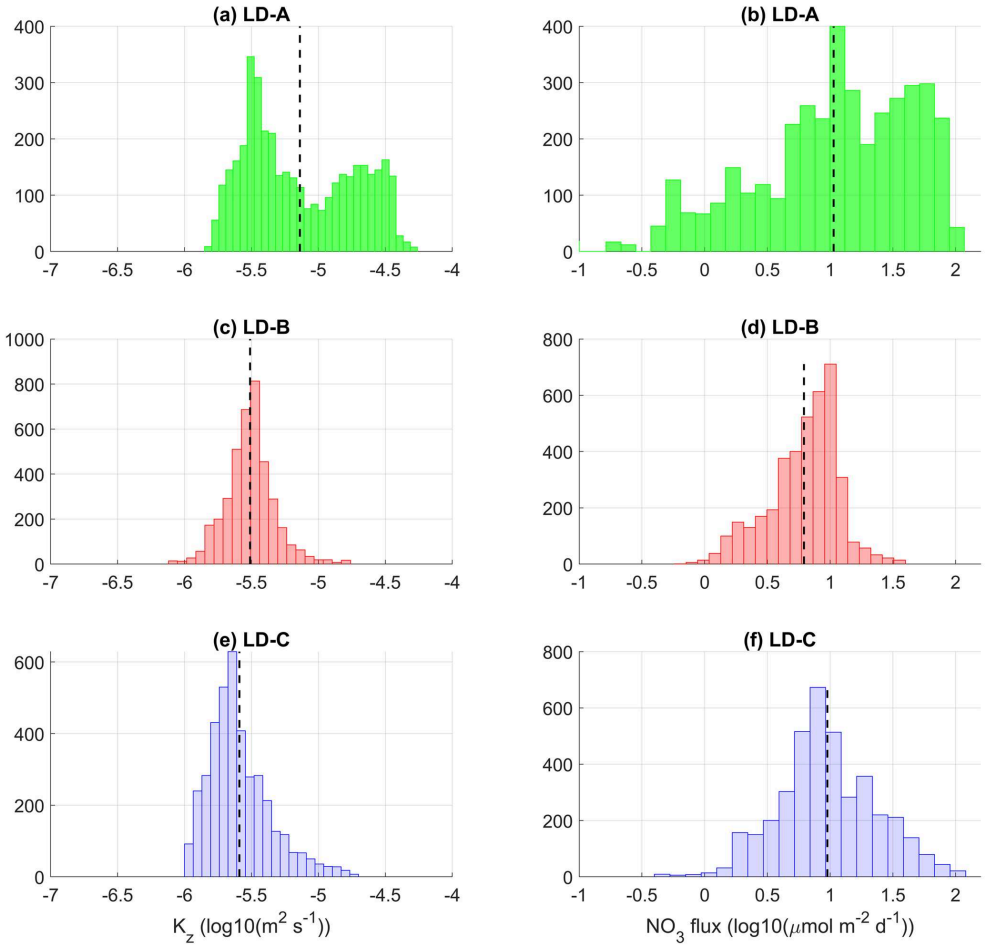

Figure 12. Histograms of K_z **(a, c, e)** and nitrate turbulent diffusive flux **(b, d, f)** at long-duration stations LD-A, LD-B, and LD-C around the top of the nitracline. The top of the nitracline is defined by the isopycnal, ρ_{NO_3}, with density values taken from Caffin et al. (2018), Table 4. A density interval of the upper bound equal to $\rho_{NO_3} + 3 \times 10^{-2}$ kg m^{-3}, of a typical vertical extension equal to 3–4 m, was chosen for the statistics. The mean value is shown in each subpanel with a dashed line.

ness layer, with histograms of the nitrate turbulent diffusive flux (Fig. 12). There is a strong contrast between LD-A and the eastern stations in the shape of the histograms: an atypical shape of the histogram is obtained at LD-A with a large standard deviation, while the distribution of the nitrate turbulent diffusive flux is fairly similar at LD-B and LD-C with one main peak (Fig. 12d and f). The atypical shape obtained at LD-A results from the large intermittency of K_z as illustrated in Fig. 12a. The distribution of K_z values covers 2 orders of magnitude and presents a bimodal distribution. The moderate K_z values are associated with the "background state", while the large values are associated with intense turbulent events related to the near-inertial baroclinic wave (e.g., Fig. 8a). The mean value of the nitrate turbulent diffusive flux within a ~ 4 m layer starting from the top of the nitracline is smaller at LD-B compared to LD-A and LD-C: 24.1 and 18.9 µmol m^{-2} d^{-1} at LD-A and LD-C compared with the mean value of 6.0 µmol m^{-2} d^{-1} at LD-B. This contrast may appear surprising, with a comparable mean value at LD-A and LD-C, but this results from the occurrence of a few turbulent events at LD-C where the nitracline is deepest. Nevertheless, the main point regarding the impact of the turbulent input of nitrate at the top of the nitracline on new primary production is whether or not the top of the nitracline falls within the photic layer. This point is addressed in the following with histograms in the photic layer.

5.2.2 New primary production sustained by phosphate turbulent diffusive fluxes at the western stations?

Figure 13 summarizes the contrast between long-duration stations in the photic layer with histograms of K_z, phosphate, and nitrate turbulent diffusive fluxes. The euphotic zone depth (EZD) was immediately determined on board from the photosynthetically available radiation (PAR) at depth compared to the sea surface PAR(0+), and used to determine the upper water sampling depths corresponding to 75, 54,

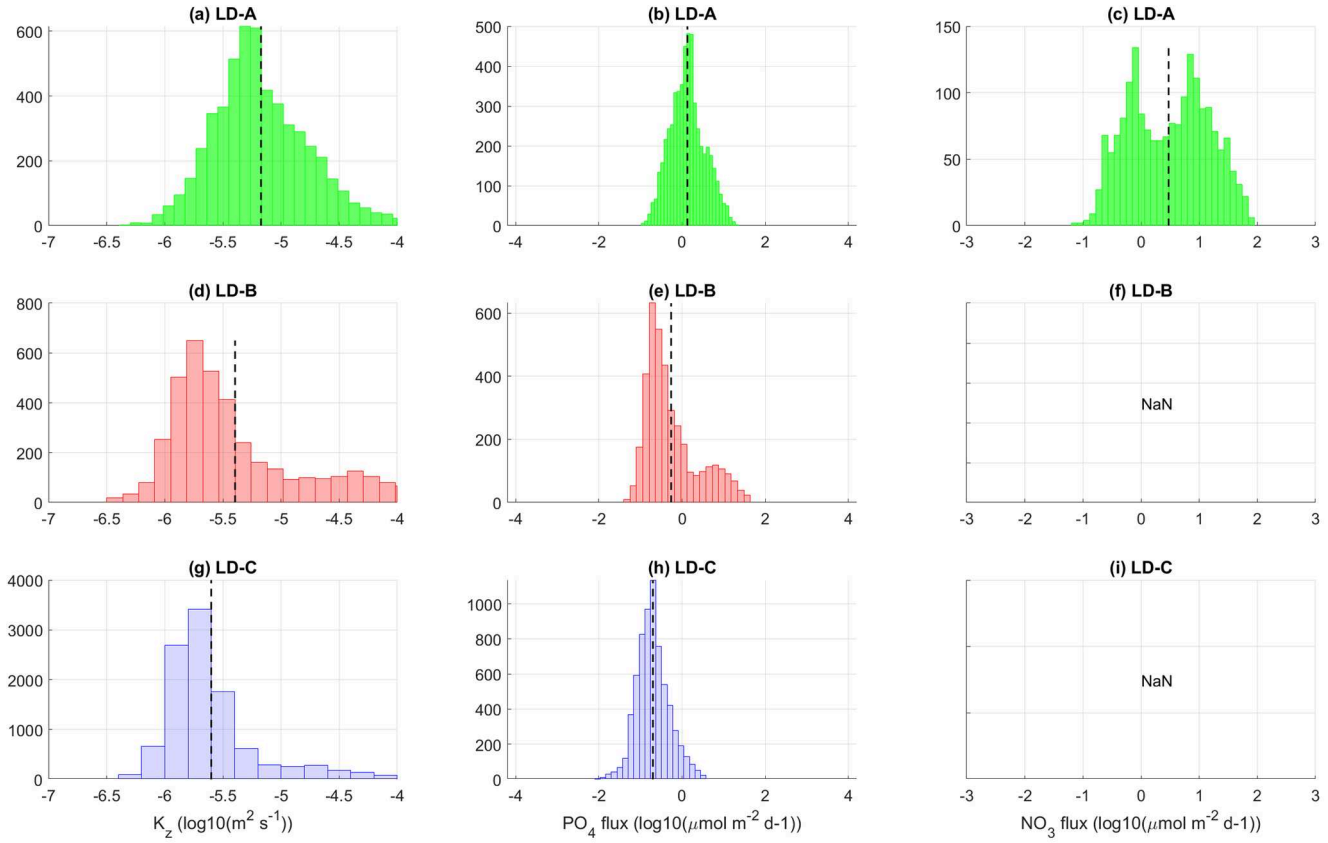

Figure 13. Histograms of K_z **(a, d, g)**, phosphate **(b, e, h)**, and nitrate **(c, f, i)** turbulent diffusive fluxes at long-duration stations LD-A, LD-B, and LD-C within the photic layer (down to 70, 55, and 120 m respectively). At LD-B and LD-C the nitrate turbulent diffusive flux is below the noise level within the considered depth interval **(f, i)**. The mean value is displayed with a dashed black line.

36, 19, 10, 3, 1 (EZD), 0.3, and 0.1 % of PAR(0+) (e.g., Herbland and Voituriez, 1977; Moutin and Prieur, 2012). The euphotic zone depth varies within [55–120 m] with a mean value of 70 m at LD-A, 55 m at LD-B, and 120 m at LD-C. As in the previous figures the scales for the nitrate and phosphate turbulent diffusive fluxes match with the Redfield ratio for visual comparison of the relative impact of each of these fluxes on micro-organisms. Significant nitrate turbulent diffusive flux is observed at LD-A as opposed to LD-B and LD-C as a result of shallower nitracline that falls within the photic layer at LD-A (Fig. 13c, f, and i). At LD-B and LD-C where the nitracline is below the euphotic zone depth the nitrate turbulent diffusive flux is zero (Fig. 13f and i). The station average of the phosphate turbulent diffusive flux is of the same order of magnitude at LD-A and LD-B and smaller by a factor of 10 at LD-C (Fig. 13b, e, and h; Table 4). These significant values of the phosphate turbulent diffusive flux observed at LD-A and LD-B suggest an impact on micro-organisms (Fig. 13e). Indeed, the presence of nitrogen fixers (micro-organisms able to use the atmospheric N_2; Dupouy et al., 2000) and high rates of N input by N_2 fixation were already noticed in the western tropical South Pacific (Moutin et al., 2008) and confirmed in the whole area (Bonnet et al., 2008). In contrast the smallest values observed at LD-C (Fig. 13h) are consistent with low nitrogen fixation rates measured there (Bonnet et al., 2017) or in the whole South Pacific gyre (Moutin et al., 2008), probably because of iron depletion (Bonnet et al., 2017; Moutin et al., 2008; Blain et al., 2007; Guieu et al., 2018). The lack of iron for N_2 fixers may explain their lower presence in the gyre and consequently the relatively higher phosphate concentrations measured there in the upper layer. Phosphate is not depleted by the N_2 fixers even with relatively low turbulent diffusive fluxes of phosphate from below.

Figure 14 summarizes the main features of the turbulent diffusive fluxes with time-averaged vertical profiles. The double x axis for the nitrate and phosphate turbulent diffusive fluxes is scaled within a Redfield ratio so that the fluxes are superimposed if they follow the Redfield proportion. At depth, NO_3 and PO_4 fluxes follow the Redfield proportion. Closer to the surface, NO_3 flux decreased: at LD-A there is a small input of nitrate in the photic layer, while at the eastern stations the nitrate flux vanishes above the base of the euphotic zone and reached zero before PO_4 fluxes. These

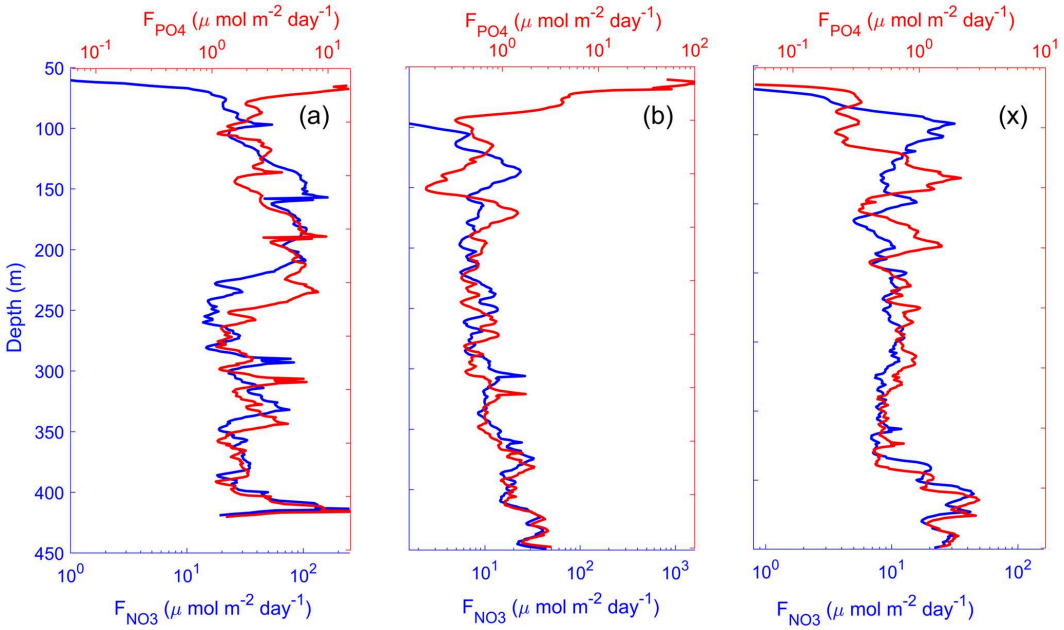

Figure 14. Time average of vertical profiles of nitrate and phosphate turbulent diffusive fluxes at long-duration stations LD-A **(a)**, LD-B **(b)**, and LD-C **(c)**. The scales of the nitrate and phosphate diffusive flux are set to match with the typical Redfield ratio ($N : P = 16 : 1$).

significant phosphate fluxes at shallower depths may potentially be fuelling nitrogen fixation, significant PO_4 sources through turbulent diffusion that are likely to provide the required conditions for the growth of N_2 fixers in the Melanesian Archipelago. Because phosphate availability likely sustains N_2 fixation and therefore N input by N_2 fixation in the WTSP, new primary production (Dugdale and Goering, 1967) might be sustained by new P (or new N including N_2 fixation) in the photic zone.

5.2.3 Turbulent diffusion and the oligotrophic to ultra-oligotrophic conditions encountered during the OUTPACE cruise

The decrease in nitrate turbulent diffusive flux eastward was found to be consistent with the increasing oligotrophy and the deepening of the nitracline (e.g., Moutin et al., 2018; Caffin et al., 2018). As a result the nitrate input into the photic layer through turbulent diffusion was found to provide only a subordinate contribution to the N budget with a 1 %–8 % contribution to the new N (Caffin et al., 2018). In the Melanesian Archipelago, the input of nitrate into the photic layer represents a small contribution during the stratified period (Caffin et al., 2018) as well as on an annual timescale, with a 46 µmol m^{-2} d^{-1} input by turbulent diffusion compared with a 642 µmol m^{-2} d^{-1} input of N by N_2 fixation (Table 6; Moutin et al., 2018).

In a 100 m layer starting from the top of the nitracline, the mean nitrate turbulent diffusive flux varies by a factor of 3 between the western LD station LD-A with a flux of ~ 45 µmol m^{-2} d^{-1} and the eastern LD-B and LD-C stations. The mean value obtained at LD-A is smaller than the average value obtained in the oligotrophic eastern Atlantic, ~ 140 µmol m^{-2} d^{-1}, by Lewis et al. (1986), suggesting an increased oligotrophy in the Pacific. It is typically 1 order of magnitude smaller than the values inferred further south, $\sim 30°$ S, by Stevens and Sutton (2012), where both larger Kz and nitrate vertical gradient are responsible for a larger nitrate turbulent diffusive flux. The comparison with Lewis et al. (1986) in the Atlantic Ocean also highlights the ultra-oligotrophy of the Pacific Ocean in the gyre compared to their counterpart in the Atlantic Ocean with diffusive fluxes at least 1 order of magnitude smaller as shown at LD-B and LD-C. The low and deep nitrate turbulent diffusive fluxes may not explain the higher primary production and N_2 fixation rates observed in the upper 0–40 m (Moutin et al., 2018, their Fig. 6a and b).

The input of phosphate in the photic layer was also addressed as a possible source for sustaining the development of N_2-fixing organisms. Phosphate turbulent diffusive fluxes mean values were significant in the photic layer with the exception of the easternmost station. In all cases, a few events of large fluxes driven by localized intense turbulent events were identified. The large variations in the turbulent diffusive fluxes resulting from the occurrence of strong turbulent events were thus underlined with a focus on long-duration stations (see also Caffin et al., 2018). This raised the question of the estimate of the turbulent input of nitrate in the photic layer when establishing C, N, and P budgets as well as the

impact of turbulence intermittency on micro-organisms (e.g., Liccardo et al., 2013).

6 Conclusions

Variations within a factor of 10 of the depth-integrated ϵ were observed along the OUTPACE transect. The largest ϵ observed in the west compare well with the few measurements performed by Fernández-Castro et al. (2014, 2015) in the area during the Malaspina expedition. The range of values is comparable with 80 % of ϵ values within $[6 \times 10^{-10}; 10^{-8}]\,\mathrm{W\,kg^{-1}}$ in the first 300 m below the mixed layer for the Malaspina expedition and 82 % for the OUTPACE ϵ within [30 m, 300 m] west of 180° longitude. Shear instability was evidenced as one main process responsible for turbulence, which is a well-known mechanism in the strongly sheared Pacific equatorial currents (e.g., Richards et al., 2015; Smyth and Moum, 2013). Richards et al. (2012) also mentioned the modulation of the turbulence level over a 3-year period with different ENSO states in the western equatorial Pacific, with a maximum shear during La Niña events compared to El Niño events. How this turbulence cycle is relevant to the OUTPACE region would be an interesting point to address with possible higher turbulence level provided that the OUTPACE cruise took place during an El Niño event. Shear instability was found to be more likely to occur in the western part of our study area, with most critical Ri encountered there. This basic analysis thus explained the contrast in dissipation observed along the transect. Whether the onset of shear instability may be driven by the low-frequency flow or the internal wave field could not be inferred from the short-duration stations, but insights into the impact of internal waves were given with estimates of the two main forcings for internal waves and the analysis of LD stations. The main forcings of internal waves were found to vary significantly along the 19° S longitudinal transect, thus pointing out the possible impact of internal waves on the contrast in energy dissipation. The most striking factor was related to the atmospheric forcing, with the occurrence of cyclones in the west leading to an energetic baroclinic near-inertial wave field. This internal wave component was characterized at the western long-duration station, LD-A, as well as its impact on energy dissipation. These scenarios are typically encountered in tropical regions where baroclinic near-inertial waves are known to contribute to energy dissipation in the upper ocean (e.g., Cuypers et al., 2013; Soares and Richards, 2013). The process of dissipation is often constrained by the mean subinertial flow with ray focusing or critical levels depending on the spatial structure of the flow (e.g., Whitt and Thomas, 2013; Soares et al., 2015). These mechanisms were not addressed here, but will be the focus of a future study using observations at the LD-A site. The context of the OUTPACE cruise with significant niw generated by a cyclone is very specific, of general interest for the studied region, where these meteorological phenomena are frequent at the end of the summer. It hides the more continuous influence of internal tides as a turbulence driver. Our measurements show only a slightly larger semi-diurnal kinetic energy in the west at LD-A compared to LD-B and LD-C, but suggest a larger contrast in shear variance.

The impact of turbulence on biogeochemical fluxes and trophic gradients was estimated based on nitrate and phosphate turbulent diffusive fluxes. The nitrate input into the photic layer through turbulent diffusion was found to provide only a subordinate contribution to the N budget as a result of the eastward decrease in nitrate turbulent diffusive fluxes and the deepening of the nitracline. New production is mainly supported by N_2 fixation and is located in the western tropical South Pacific. The higher phosphate turbulent fluxes compared to nitrate fluxes provide an excess P relative to Redfield stoichiometry and a potential ecological niche for N_2 fixing organisms in the west. In addition to the lower iron availability in the east preventing N_2 fixation from occurring, the high iron availability in the west allows this process and the excess P provided to the photic zone to sustain a higher new primary production, explaining the western–eastern oligotrophy gradient.

Data availability. All data and metadata are available at the French INSU/CNRS LEFE CYBER database (scientific coordinator: Hervé Claustre; data manager and webmaster: Catherine Schmechtig) at the following web address: http://www.obs-vlfr.fr/proof/php/outpace/outpace.php (last access: 21 December 2018, INSU/CNRS LEFE CYBER, 2017).

Competing interests. The authors declare that they have no conflict of interest.

Special issue statement. This article is part of the special issue "Interactions between planktonic organisms and biogeochemical cycles across trophic and N_2 fixation gradients in the western tropical South Pacific Ocean: a multidisciplinary approach (OUTPACE experiment)". It is not associated with a conference.

Acknowledgements. This is a contribution of the OUTPACE (Oligotrophy from UlTra-Oligotrophy PAcific Experiment) project (https://outpace.mio.univ-amu.fr, last access: 12 December 2018) funded by the French research national agency (ANR-14-CE01-0007-01), the LEFE-CyBER programme (CNRS-INSU), the GOPS programme (IRD), and the CNES (BC T23, ZBC 45000048836). We warmly acknowledge the assistance of the crew of the French research vessel *l'Atalante* during the deployment of the VMP. We thank Olivier Desprez for his technical support and help during the cruise. The microstructure profiler was funded through the ANR OUTPACE project.

Edited by: Laurent Mémery
Reviewed by: Bieito Fernández-Castro and one anonymous referee

References

Alford, M. H.: Improved global maps and 54-year history of wind-work on ocean inertial motions, Geophys. Res. Lett., 30, 1424, https://doi.org/10.1029/2002GL016614, 2003.

Alford, M. H. and Zhao, Z.: Global patterns of low-mode internal-wave propagation – Part I: Energy and Energy Flux, J. Phys. Oceanog., 37, 1829–1848, 2007.

Alford, M. H. and Zhao, Z.: Global patterns of low-mode internal-wave propagation – Part II: Group velocity, J. Phys. Oceanogr., 37, 1849–1858, 2007.

Amante, C. and Eakins, B. W.: ETOPO1 1 Arc-Minute Global Relief Model: Procedures, Data Sources and Analysis, NOAA Technical Memorandum NESDIS NGDC-24, National Geophysical Data Center, NOAA, https://doi.org/10.7289/V5C8276M, 2009.

Ascani, F., Richards, K. J., Firing, E., Grant, S., Johnson, K. S., Jia, Y., Lukas, R., and Karl, D. M.: Physical and biological controls of nitrate concentrations in the upper subtropical North Pacific Ocean, Deep-Sea Res. Pt. II, 93, 119–134, 2013.

Baines, P.: On internal tide generation models, Deep-Sea Res. Pt I, 29, 307–338, 1982.

Blain, S., Quéguiner, B., Armand, L., et al.: Effect of natural iron fertilization on carbon sequestration in the Southern Ocean, Nature, 446, 1070, https://doi.org/10.1038/nature05700, 2007

Bonnet, S., Caffin, M., Berthelot, H., and Moutin, T.: Hot spot of N_2 fixation in the western tropical south pacific pleads for a spatial decoupling between N_2 fixation and denitrification, P. Natl. Acad. Sci. USA, 114, E2800–E2801, 2017.

Bonnet, S., Guieu, C., Bruyant, F., Prášil, O., Van Wambeke, F., Raimbault, P., Moutin, T., Grob, C., Gorbunov, M. Y., Zehr, J. P., Masquelier, S. M., Garczarek, L., and Claustre, H.: Nutrient limitation of primary productivity in the Southeast Pacific (BIOSOPE cruise), Biogeosciences, 5, 215-225, https://doi.org/10.5194/bg-5-215-2008, 2008.

Bouffard, D. and Boegman, L.: A diapycnal diffusivity model for stratified environmental flows, Dynam. Atmos. Oceans, 61, 14–34, 2013.

Caffin, M., Moutin, T., Foster, R. A., Bouruet-Aubertot, P., Doglioli, A. M., Berthelot, H., Guieu, C., Grosso, O., Helias-Nunige, S., Leblond, N., Gimenez, A., Petrenko, A. A., de Verneil, A., and Bonnet, S.: N_2 fixation as a dominant new N source in the western tropical South Pacific Ocean (OUTPACE cruise), Biogeosciences, 15, 2565–2585, https://doi.org/10.5194/bg-15-2565-2018, 2018.

Cuypers, Y., Le Vaillant, X., Bouruet-Aubertot, P., Vialard, J., and Mcphaden, M. J.: Tropical storm-induced near-inertial internal waves during the cirene experiment: Energy fluxes and impact on vertical mixing, J. Geophys. Res.-Oceans, 118, 358–380, 2013.

de Verneil, A., Rousselet, L., Doglioli, A. M., Petrenko, A. A., and Moutin, T.: The fate of a southwest Pacific bloom: gauging the impact of submesoscale vs. mesoscale circulation on biological gradients in the subtropics, Biogeosciences, 14, 3471–3486, https://doi.org/10.5194/bg-14-3471-2017, 2017.

Diamond, H. J., Lorrey, A. M., and Renwick, J. A.: A southwest Pacific tropical cyclone climatology and linkages to the El Niño–Southern Oscillation, J. Climate, 26, 3–25, 2013.

Dugdale, R. and Goering, J.: Uptake of new and regenerated forms of nitrogen in primary productivity, Limnol. Oceanogr., 12, 196–206, 1967.

Dupouy, C., Neveux, J., Subramaniam, A., Mulholland, M. R., Montoya, J. P., Campbell, L., Carpenter, E. J., and Capone, D. G.: Satellite Captures Trichodesmium Blooms in the southwestern Tropical Pacific, EOS, 81, 13–16, 2000.

Egbert, G. D. and Erofeeva, S. Y.: Efficient inverse modeling of barotropic ocean tides, J. Atmos. Ocean. Tech., 19, 183–204, 2002.

Fernández-Castro, B., Mouriño-Carballido, B., Benítez-Barrios, V., Chouciño, P., Fraile-Nuez, E., Graña, R., Piedeleu, M., and Rodríguez-Santana, A.: Microstructure turbulence and diffusivity parameterization in the tropical and subtropical Atlantic, Pacific and Indian Oceans during the Malaspina 2010 expedition, Deep-Sea Res. Pt I, 94, 15–30, 2014.

Fernández-Castro, B., Mouriño-Carballido, B., Marañón, E., Chouciño, P., Gago, J., Ramírez, T., Vidal, M., Bode, A., Blasco, D., Royer, S.-J., Estrada, M., and Simó, R.: Importance of salt fingering for new nitrogen supply in the oligotrophic ocean, Nat. Commun., 6, 8002, https://doi.org/10.1038/ncomms9002, 2015.

Ferron, B., Kokoszka, F., Mercier, H., and Lherminier, P.: Dissipation rate estimates from microstructure and finescale internal wave observations along the A25 Greenland-Portugal OVIDE line, J. Atmos. Ocean. Tech., 31, 2530–2543, 2014.

Gill, A.: On the behavior of internal waves in the wakes of storms, J. Phys. Oceanogr., 14, 1129–1151, 1984.

Gregg, M., Peters, H., Wesson, J., Oakey, N., and Shay, T.: Intensive measurements of turbulence and shear in the equatorial undercurrent, Nature, 318, 140-144, 1985.

Guidi, L., Calil, P. H. R., Duhamel, S., Björkman, K. M., Doney, S. C., Jackson, G. A., Li, B., Church, M. J., Tozzi, S., Kolber, Z. S., Richards, K. J., Fong, A. A., Letelier, R. M., Gorsky, G., Stemman, L., and Karl, D. M.: Does eddy-eddy interaction control surface phytoplankton distribution and carbon export in the north pacific subtropical gyre?, J. Geophys. Res.-Biogeo., 117, G02024, https://doi.org/10.1029/2012JG001984, 2012.

Guieu, C., Bonnet, S., Petrenko, A., Menkes, C., Chavagnac, V., Desboeufs, K., Maes, C., and Moutin, T.: Iron from a submarine source impacts the productive layer of the Western Tropical South Pacific (WTSP), Sci. Rep., 8, 9075, https://doi.org/10.1038/s41598-018-27407-z, 2018.

Herbland, A. and Voituriez, B.: Production primaire, nitrate et nitrite dans l'Atlantique tropical: 1. Distribution du nitrate et production primaire, Cah. ORSTOM. Série Océanographie, 15, 47–55, 1977.

INSU/CNRS LEFE CYBER: OUTPACE, Oligotrophy to UlTra-oligotrophy PACific Experiment, Data and Metadata, available at: http://www.obs-vlfr.fr/proof/php/outpace/outpace.php (last access: 21 December 2018), 2017.

Klemp, J. B., Skamarock, W. C., and Dudhia, J.: Conservative split-explicit time integration methods for the compressible nonhydrostatic equations, Mon. Weather Rev., 135, 2897–2913, 2007.

Ledwell, J. R., McGillicuddy Jr., D. J., and Anderson, L. A.: Nutrient flux into an intense deep chlorophyll layer in a mode-water eddy, Deep-Sea Res. Pt. II, 55, 1139–1160, 2008.

Lewis, M. R., Hebert, D., Harrison, W. G., Platt, T., and Oakey, N. S.: Vertical nitrate flux in the oligotrophic ocean, Science, 234, 870–873, 1986.

Liccardo, A., Fierro, A., Iudicone, D., Bouruet-Aubertot, P., and Dubroca, L.: Response of the deep chlorophyll maximum to fluctuations in vertical mixing intensity, Prog. Oceanogr., 109, 33–46, 2013.

Liu, L. L., Wang, W., and Huang, R. X.: The mechanical energy input to the ocean induced by tropical cyclones, J. Phys. Oceanogr., 38, 1253–1266, 2008.

Moutin, T. and Bonnet, S.: Outpace cruise, rv l'atalante, French Oceanographic Cruises, https://doi.org/10.17600/15000900, 2015.

Moutin, T. and Prieur, L.: Influence of anticyclonic eddies on the Biogeochemistry from the Oligotrophic to the Ultraoligotrophic Mediterranean (BOUM cruise), Biogeosciences, 9, 3827–3855, https://doi.org/10.5194/bg-9-3827-2012, 2012.

Moutin, T., Doglioli, A. M., de Verneil, A., and Bonnet, S.: Preface: The Oligotrophy to the UlTra-oligotrophy PACific Experiment (OUTPACE cruise, 18 February to 3 April 2015), Biogeosciences, 14, 3207–3220, https://doi.org/10.5194/bg-14-3207-2017, 2017.

Moutin, T., Karl, D. M., Duhamel, S., Rimmelin, P., Raimbault, P., Van Mooy, B. A. S., and Claustre, H.: Phosphate availability and the ultimate control of new nitrogen input by nitrogen fixation in the tropical Pacific Ocean, Biogeosciences, 5, 9500109, https://doi.org/10.5194/bg-5-95-2008, 2008.

Moutin, T., Wagener, T., Caffin, M., Fumenia, A., Gimenez, A., Baklouti, M., Bouruet-Aubertot, P., Pujo-Pay, M., Leblanc, K., Lefevre, D., Helias Nunige, S., Leblond, N., Grosso, O., and de Verneil, A.: Nutrient availability and the ultimate control of the biological carbon pump in the western tropical South Pacific Ocean, Biogeosciences, 15, 2961–2989, https://doi.org/10.5194/bg-15-2961-2018, 2018.

Nasmyth, P. W.: Oceanic turbulence, University of British Columbia, 1970.

Osborn, T.: Estimates of the local rate of vertical diffusion from dissipation measurements, J. Phys. Oceanogr., 10, 83–89, 1980.

Price, J. F.: Internal wave wake of a moving storm. Part I. Scales, energy budget and observations, J. Phys. Oceanogr., 13, 949–965, 1984.

Richards, K., Kashino, Y., Natarov, A., and Firing, E.: Mixing in the western equatorial Pacific and its modulation by ENSO, Geophys. Res. Lett., 39, L02604, https://doi.org/10.1029/2011GL050439, 2012.

Richards, K. J., Natarov, A., Firing, E., Kashino, Y., Soares, S. M., Ishizu, M., Carter, G. S., Lee, J. H., and Chang, K. I.: Shear-generated turbulence in the equatorial Pacific produced by small vertical scale flow features, J. Geophys. Res.-Oceans, 120, 3777–3791, 2015.

Rousselet, L., de Verneil, A., Doglioli, A. M., Petrenko, A. A., Duhamel, S., Maes, C., and Blanke, B.: Large- to submesoscale surface circulation and its implications on biogeochemical/biological horizontal distributions during the OUTPACE cruise (southwest Pacific), Biogeosciences, 15, 2411–2431, https://doi.org/10.5194/bg-15-2411-2018, 2018.

Shih, L. H., Koseff, J. R., Ivey, G. N., and Ferziger, J. H.: Parameterization of turbulent fluxes and scales using homogeneous sheared stably stratified turbulence simulations, J. Fluid Mech., 525, 193–214, 2005.

Skamarock, W. C., William, C., Klemp, J. B., Dudhia, J., Gill, D. O., Barker, D. M., Wang, W., and Powers, J. G.: A description of the advanced research WRF version 2, National Center For Atmospheric Research, Tech. Note, 2005

Smyth, W. D. and Moum, J. N.: Marginal instability and deep cycle turbulence in the eastern equatorial Pacific Ocean, Geophys. Res. Lett., 40, 6181–6185, https://doi.org/10.1002/2013GL058403, 2013.

Soares, S. and Richards, K.: Radiation of inertial kinetic energy as near-inertial waves forced by tropical Pacific Easterly waves, Geophys. Res. Lett., 40, 1760–1765, 2013.

Soares, S. M., Richards, K. J., and Natarov, A.: Near inertial waves in the tropical Indian Ocean: Energy fluxes and dissipation, American Geophysical Union, Ocean Sciences Mtg., Honolulu HI, 2014.

Soares, S. M., Richards, K. J., and Natarov, A.: Near inertial waves in the tropical Indian Ocean: Energy fluxes and dissipation during CINDY, J. Geophys. Res., 121, 3297–3324, https://doi.org/10.1002/2015JC011600, 2015.

St Laurent, L., Simmons, H., and Jayne, S.: Estimating tidally driven mixing in the deep ocean, Geophys. Res. Lett., 29, 2106–2109, 2002.

Stevens, C. L. and Sutton, P. J.: Internal waves downstream of Norfolk Ridge, western Pacific, Limnol. Oceanogr., 57, 897–911, 2012.

Sun, C., Smyth, W. D., and Moum, J. N.: Dynamic instability of stratified shear flow in the upper equatorial Pacific, J. Geophys. Res.-Oceans, 103, 10323–10337, 1998.

Visbeck, M.: Deep velocity profiling using Lowered Acoustic Doppler Current Profilers: Bottom track and inverse solutions, J. Atmos. Ocean. Tech., 19, 794–807, 2002.

Whalen, C., Talley, L., and MacKinnon, J.: Spatial and temporal variability of global ocean mixing inferred from argo profiles, Geophys. Res. Lett., 39, L18612, https://doi.org/10.1029/2012GL053196, 2012.

Whitt, D. B. and Thomas, L. N.: Near-inertial waves in strongly baroclinic currents, J. Phys. Oceanogr., 43, 706–725, 2013.

Annexe D

Article supplémentaire n°3

Carbonate system distribution, anthropogenic carbon and acidification in the western tropical South Pacific (OUTPACE 2015 transect)

Thibaut Wagener[1], Nicolas Metzl[2], Mathieu Caffin[1], Jonathan Fin[2], Sandra Helias Nunige[1], Dominique Lefevre[1], Claire Lo Monaco[2], Gilles Rougier[1], and Thierry Moutin[1]

[1]Aix Marseille Univ., CNRS, Université de Toulon, IRD, OSU Pythéas, Mediterranean Institute of Oceanography (MIO), UM 110, 13288, Marseille, France
[2]Sorbonne Université, CNRS, IRD, MNHN, Laboratoire d'océanographie et du climat : expérimentation et approches numériques (LOCEAN), Case 100, 4 place Jussieu, 75252 Paris CEDEX 05, France

Publié dans *Biogeoscience* en Aout 2018

Biogeosciences, 15, 5221–5236, 2018
https://doi.org/10.5194/bg-15-5221-2018

Biogeosciences Open Access EGU

Carbonate system distribution, anthropogenic carbon and acidification in the western tropical South Pacific (OUTPACE 2015 transect)

Thibaut Wagener[1], Nicolas Metzl[2], Mathieu Caffin[1], Jonathan Fin[2], Sandra Helias Nunige[1], Dominique Lefevre[1], Claire Lo Monaco[2], Gilles Rougier[1], and Thierry Moutin[1]

[1]Aix Marseille Univ, CNRS, IRD, Université de Toulon, MIO UM 110, 13288, Marseille, France
[2]Sorbonne Université, CNRS, IRD, MNHN, Laboratoire d'océanographie et du climat: expérimentation et approches numériques (LOCEAN), Case 100, 4 place Jussieu, 75252 Paris CEDEX 05, France

Correspondence: Thibaut Wagener (thibaut.wagener@univ-amu.fr)

Received: 9 April 2018 – Discussion started: 17 April 2018
Revised: 24 July 2018 – Accepted: 27 July 2018 – Published: 29 August 2018

Abstract. The western tropical South Pacific was sampled along a longitudinal 4000 km transect (OUTPACE cruise, 18 February, 3 April 2015) for the measurement of carbonate parameters (total alkalinity and total inorganic carbon) between the Melanesian Archipelago (MA) and the western part of the South Pacific gyre (WGY). This paper reports this new dataset and derived properties: pH on the total scale (pH_T) and the $CaCO_3$ saturation state with respect to aragonite (Ω_{ara}). We also estimate anthropogenic carbon (C_{ANT}) distribution in the water column using the TrOCA method (Tracer combining Oxygen, inorganic Carbon and total Alkalinity). Along the OUTPACE transect a deeper penetration of C_{ANT} in the intermediate waters was observed in the MA, whereas highest C_{ANT} concentrations were detected in the subsurface waters of the WGY. By combining our OUTPACE dataset with data available in GLODAPv2 (1974–2009), temporal changes in oceanic inorganic carbon were evaluated. An increase of 1.3 to 1.6 µmol kg^{-1} a^{-1} for total inorganic carbon in the upper thermocline waters is estimated, whereas C_{ANT} increases by 1.1 to 1.2 µmol kg^{-1} a^{-1}. In the MA intermediate waters (27 kg m^{-3} $< \sigma_\theta <$ 27.2 kg m^{-3}) an increase of 0.4 µmol kg^{-1} a^{-1} C_{ANT} is detected. Our results suggest a clear progression of ocean acidification in the western tropical South Pacific with a decrease in the oceanic pH_T of up to -0.0027 a^{-1} and a shoaling of the saturation depth for aragonite of up to 200 m since the pre-industrial period.

1 Introduction

Human activities inject about 10 petagrams of carbon per year into the atmosphere, which might have major consequences on climate. It is recognized that the ocean plays a key role in the control of atmospheric CO_2 through uptake by the so-called "oceanic carbon pump". Through this "pump", the ocean sequesters ca. 25 % of the CO_2 injected annually into the atmosphere by human activities (Le Quéré et al., 2018). A consequence of the ocean carbon uptake is a decrease in the oceanic pH (Feely et al., 2004), which is described as ocean acidification (the so-called "other" CO_2 problem). Effects of ocean acidification have been observed in marine organisms and could affect the marine ecosystems (Riebesell et al., 2000). Improving our understanding of the oceanic CO_2 uptake relies primarily on observations of the marine carbonate cycle. Studies on the oceanic carbonate cycle have been mostly conducted in the framework of international programs. The World Ocean Circulation Experiment (WOCE) and the Joint Global Flux Study (JGOFS) in the 1990s coordinated oceanographic cruises along large sections in the ocean to collect samples through the water column and to perform accurate measurements of carbonate parameters and ancillary parameters (temperature, salinity, dissolved oxygen, nutrients, etc.). Since 2000, efforts have been made to revisit oceanic sections according to the WOCE strategy in order to assess oceanic changes at the scale of a decade. These programs have generated important databases

Published by Copernicus Publications on behalf of the European Geosciences Union.

for oceanic carbonate chemistry (e.g., GLODAPv2, Olsen et al., 2016; Key et al., 2015).

In order to better assess the role of the ocean for the global carbon cycle, the concept of oceanic anthropogenic carbon (C_{ANT}) has been introduced and refers to the fraction of dissolved inorganic carbon (C_T) in the ocean that originates from carbon injected into the atmosphere by human activities since the industrial revolution. As C_{ANT} is not a directly measurable quantity, it can only be estimated through assumptions that are subject to intense scientific debate (Sabine and Tanhua, 2010). In particular, it has been recently recognized that ocean circulation changes drive significant variability in carbon uptake (DeVries et al., 2017). Detecting, separating and attributing decadal changes in the carbonate system (C_T and total alkalinity, A_T), C_{ANT} and pH in the ocean at global or regional scales remains challenging.

Within this context, the Pacific Ocean is a particularly challenging area to study due to its size (ca. one-third of the Earth's and one half of the oceanic surface). Even if, due to its remoteness from land, it remains largely underexplored by oceanographic vessels compared to other oceanic areas, the Pacific Ocean has been covered by cruises along long sections (the "P sections" from the WOCE program). Most of these sections have been revisited during the last years (e.g., Sabine et al., 2008; Kouketsu et al., 2013). In a recent study based on repeated sections in the Pacific (P16 at 150° W), Carter et al. (2017) observed a significant increase in C_{ANT} in the top 500 m around 10–30° S and a local carbon storage maximum around 20° S in recent years (between 2005 and 2014). In this context, the OUTPACE data presented in this study, associated with historical observations (since the pioneer 1974 GEOSECS, Geochemical Ocean Sections Program) offer a new view to evaluate variability and decadal changes in C_T, C_{ANT} and pH_T in the tropical Pacific, here focusing on the western tropical South Pacific (WTSP).

The aim of this paper is to report a new dataset of oceanic inorganic carbon (based on measurements of C_T and A_T) acquired in the WTSP during the OUTPACE (Oligotrophic to UltTra oligotrophic PACific Experiment) cruise performed in 2015 (Moutin et al., 2017). The main focus of the OUTPACE cruise was to study the complex interactions between planktonic organisms and the cycle of biogenic elements on different scales, motivated by the fact that the WTSP has been identified as a hot spot of N_2 fixation (Bonnet et al., 2017). The data presented here have been partially used in another paper of this special issue (Moutin et al., 2018) in order to study the biological carbon pump in the upper (surface to 200 m) water column. In this paper we will explore the carbonate data between the surface and 2000 m depth. The OUTPACE transect (Fig. 1) is close to existing WOCE and GO-SHIP (Global Ocean Ship-based Hydrographic Investigations Program) lines in the South Pacific: it is parallel to the zonal P21 line (18° S visited in 1994 and 2009) and the P06 line (32° S visited in 1992, 2003 and 2010), it is crossed by the meridional P14 line (180° E visited in 1994 and 2007) and P15 line (170° W visited in 2001, 2009 and 2016), and it is situated at the eastern side of the P16 line (150° W visited in 1992, 2005 and 2014). However, the OUTPACE transect does not correspond to any earlier occupation of the "WOCE lines" in the South Pacific and no tracers of water mass age were measured during the cruise, which limits the possibilities of a robust analysis of C_{ANT} accumulation in the area. Moreover, the horizontal and vertical resolution of the OUTPACE dataset is low. In consequence, the OUTPACE dataset cannot be used to look at decadal changes in C_{ANT} content in the South Pacific (e.g., Carter et al., 2017; Kouketsu et al., 2013). Here, C_{ANT} estimates based on the TrOCA (Tracer combining Oxygen, inorganic Carbon and total Alkalinity) method will be used as as a tool to investigate changes in C_T. Moreover, comparing our data with the high-quality data (internally consistent through a secondary quality control; Olsen et al., 2016) available in the Global Ocean Data analysis Project version 2 (GLODAPv2 database) will allow us to evaluate C_T, A_T, C_{ANT} (from TrOCA) and pH_T trends in subsurface waters and at depth.

The paper is organized as follows: after describing the methods used to acquire the dataset and the way the auxiliary data have been used in Sect. 2, we briefly present the hydrographic context of the cruise in Sect. 3. We then present in Sect. 4, the carbonate dataset acquired during the cruise. In Sect. 5, estimated C_{ANT} values in the water column are presented, the validity of these estimates based on the TrOCA method is discussed and geographical patterns are evoked. In Sect. 6, the temporal changes in oceanic inorganic carbon in the WTSP combining data available in GLODAPv2 and our OUTPACE dataset are presented and discussed. Finally, in Sect. 7, some features in relation to ocean acidification are inferred from our dataset.

2 Material and methods

2.1 Cruise and sampling strategy

The OUTPACE cruise took place between 18 February and 3 April 2015 from Nouméa (New Caledonia) to Papeete (French Polynesia), in the WTSP on board the French research vessel *L'Atalante* (Fig. 1). A total of 18 stations were sampled, mostly in the top 2000 m of the water column along a $\sim$ 4000 km transect from Melanesia to the South Pacific gyre (Moutin et al., 2017). A conductivity–temperature–depth (CTD) rosette was deployed to acquire data with CTD and associated sensors along vertical profiles and to collect discrete seawater samples from twenty-four 12 L Niskin bottles for chemical analysis. Due to technical failures on the main CTD rosette, for two of the casts considered in this study, a trace metal clean CTD rosette (TM-R) equipped with 24 teflon-lined GO-FLO bottles devoted to trace metal analyses was used. The configurations of both CTD rosettes are detailed elsewhere (Moutin et al., 2017).

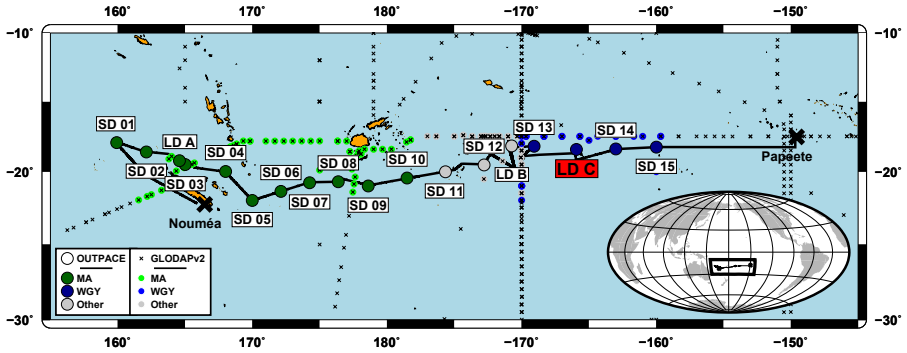

Figure 1. Map of the OUTPACE cruise transect. Melanesian Archipelago (MA) stations are indicated by large dark green large dots and the western gyre (WGY) stations by large dark blue dots. Stations outside of these two areas are in gray. The station in red corresponds to the station where the deep cast and intercomparison cast were made. Stations from the GLODAPv2 database are indicated with small crosses: small green dots correspond to GLODAPv2 stations considered for comparison in the MA area; small blue dots correspond to GLODAPv2 stations considered for comparison in the WGY area and small gray dots are the other GLODAPv2 stations considered for comparison.

For carbonate parameters, seawater was sampled from 37 casts over the 18 stations. At each station, on a regular basis, samples were collected at 12 depths between the surface and 2000 m on two distinct casts: six samples on a 0–200 m cast and six samples on a 0–2000 m cast. At station SD 13, only one cast was sampled down to 500 m depth. In addition, at station LD C, samples were collected at 24 depths on a deep cast (down to 5000 m) and 12 samples were collected at the same depth (25 m) on a "repeatability" cast. Details on the casts performed for this study are summarized in Table 1.

2.2 Chemical measurements on discrete samples

All samples were collected within less than 1 h after arrival of the CTD rosette on deck.

2.2.1 Total alkalinity and dissolved inorganic carbon

Samples for A_T and C_T were collected in one 500 mL borosilicate glass flask (Schott Duran®) and poisoned with $HgCl_2$ immediately after collection (final concentration 20 mg L^{-1}). Samples were stored at 4 °C during transport and were analyzed (within 10 days of each other) 5 months after the end of the cruise at the SNAPO-CO_2 (Service National d'Analyse des paramètres Océaniques du CO_2 – LOCEAN – Paris). A_T and C_T were measured on the same sample based on a potentiometric titration in a closed cell (Edmond, 1970). A nonlinear curve fitting approach was used to estimate A_T and C_T from the recorded titration data (Dickson, 1981; Dickson and Goyet, 1994). Measurements were calibrated with certified reference material (CRM) provided by Andrew Dickson, University of Southern California (batch 139 – C_T: 2023.23 ± 0.70 µmol kg^{-1} and A_T: 2250.82 ± 0.60 µmol kg^{-1}; see Dickson, 2010). The reproducibility, expressed as the standard deviation of the CRM analysis ($n = 15$), was 4.6 µmol kg^{-1} for A_T and 4.7 µmol kg^{-1} for C_T. Based on replicate measurements at station LD C (cast out_c_194; see Table 1), the reproducibility, expressed as the standard deviation of the analysis of the replicates collected at the same depth (ca. 25 m, $n = 12$) from different Niskin bottles, was 3.6 µmol kg^{-1} for A_T (average value : 2324.7 µmol kg^{-1}) and 3.7 µmol kg^{-1} for C_T (average value : 1969.7 µmol kg^{-1}).

2.2.2 Oxygen concentration

Dissolved oxygen concentration [O_2] was measured following the Winkler method (Winkler, 1888) with potentiometric endpoint detection (Oudot et al., 1988). For sampling, reagent preparation and analysis, the recommendations from Langdon (2010) were carefully followed. The thiosulfate solution was calibrated by titrating it against a potassium iodate certified standard solution of 0.0100 N (CSK standard solution – WAKO™). The reproducibility, expressed as the standard deviation of replicates samples was 0.8 µmol kg^{-1} ($n = 15$; average value : 195.4 µmol kg^{-1}).

2.3 Vertical profiles of hydrological and biogeochemical parameters

2.3.1 CTD measurements

CTD measurements were ensured by a Seabird™ 911+ underwater unit, which interfaced an internal pressure sensor, two redundant external temperature probes (SBE3plus) and two redundant external conductivity cells (SBE4C). The sensors were calibrated pre- and post-cruise by the manufacturer. No significant drift between the redundant sensors was observed. For vertical profiles, full-resolution data (24 Hz) were reduced to 1 dbar binned vertical profiles on the downcast with a suite of processing modules using the Seabird™ dedicated software (SbeDataProcessing). For values at the closure of the Niskin bottles, values collected at 24 Hz were averaged 3 s before and 5 s after closure of the bottle. In

Table 1. General description of the casts sampled for carbonate chemistry parameters during the OUTPACE cruise.

Cast	Station	Longitude (° E)	Latitude (° N)	Time (UTC)	Max. pres. (dbar)	Type[a]	Rosette[b]
out_c_006	SD 1	159.9255	−17.9418	2015/02/22 03:08:00	202	SHAW	CLA
out_t_002		159.9425	−17.9088	2015/02/22 07:43:00	2000	INT	TMC
out_c_010	SD 2	162.1248	−18.6078	2015/02/23 00:11:00	199	SHAW	CLA
out_c_016		162.1112	−18.5845	2015/02/23 08:16:00	1998	INT	CLA
out_c_019	SD 3	165.0093	−19.4955	2015/02/24 05:58:00	200	SHAW	CLA
out_c_020		165.0082	−19.4907	2015/02/24 08:14:00	1999	INT	CLA
out_c_066	LD A	164.5877	−19.2242	2015/03/02 14:39:00	200	SHAW	CLA
out_c_067		164.5787	−19.2233	2015/03/02 16:10:00	2002	INT	CLA
out_c_070	SD 4	168.0118	−19.9832	2015/03/04 10:55:00	201	SHAW	CLA
out_c_071		168.0157	−19.98	2015/03/04 12:43:00	1999	INT	CLA
out_c_074	SD 5	169.9943	−22.0002	2015/03/05 08:48:00	201	SHAW	CLA
out_c_075		169.9965	−21.9997	2015/03/05 10:27:00	1999	INT	CLA
out_c_078	SD 6	172.1198	−21.3732	2015/03/06 07:27:00	200	SHAW	CLA
out_c_079		172.1193	−21.3758	2015/03/06 09:08:00	1999	INT	CLA
out_c_082	SD 7	174.25	−20.7697	2015/03/07 05:09:00	201	SHAW	CLA
out_c_083		174.2512	−20.7677	2015/03/07 06:37:00	2000	INT	CLA
out_c_086	SD 8	176.3778	−20.7027	2015/03/08 02:31:00	201	SHAW	CLA
out_c_087		176.364	−20.6945	2015/03/08 04:19:00	1997	INT	CLA
out_c_091	SD 9	178.6087	−20.9963	2015/03/09 04:57:00	2002	INT	CLA
out_t_012		178.6062	−20.9892	2015/03/09 06:46:00	201	SHAW	TMC
out_c_094	SD 10	−178.5105	−20.4417	2015/03/10 04:10:00	200	SHAW	CLA
out_c_095		−178.5105	−20.44	2015/03/10 05:48:00	762	INT	CLA
out_c_098	SD 11	−175.6542	−20.0028	2015/03/11 00:53:00	207	SHAW	CLA
out_c_099		−175.6475	−20.0057	2015/03/11 02:46:00	2000	INT	CLA
out_c_102	SD 12	−172.7885	−19.5237	2015/03/12 00:38:00	200	SHAW	CLA
out_c_103		−172.7813	−19.5368	2015/03/12 02:26:00	2001	INT	CLA
out_c_150	LD B	−170.7433	−18.179	2015/03/20 12:38:00	204	SHAW	CLA
out_c_151		−170.7385	−18.1745	2015/03/20 14:16:00	1997	INT	CLA
out_c_152	SD 13	−169.0728	−18.2007	2015/03/21 10:27:00	501	INT	CLA
out_c_163		−165.9315	−18.4282	2015/03/24 12:23:00	5027	DEEP	CLA
out_c_194	LD C	−165.8647	−18.4952	2015/03/28 02:01:00	25	REPRO	CLA
out_c_198		−165.7915	−18.4912	2015/03/28 12:42:00	298	SHAW	CLA
out_c_199		−165.7792	−18.4842	2015/03/28 14:32:00	2001	INT	CLA
out_c_209	SD 14	−163.001	−18.395	2015/03/30 05:19:00	300	SHAW	CLA
out_c_210		−162.9992	−18.3952	2015/03/30 07:03:00	2000	INT	CLA
out_c_212	SD 15	−159.9913	−18.265	2015/03/31 04:01:00	300	SHAW	CLA
out_c_213		−159.9913	−18.2618	2015/03/31 05:41:00	2002	INT	CLA

[a] SHAW stands for casts up to 200 dbar, INT stands for casts up to 2000 dbar, DEEP stands for the deep cast and REPRO stands for the cast with reproducibility measurements. [b] A CTD was rosette used for the cast. CLA is the normal CTD rosette, and TMC is the trace metal clean rosette (see Sect. 2.1).

this study, for temperature and conductivity the signal of the first sensors has been used systematically. For the two TM-R casts, no significant difference with the main CTD rosette on temperature and conductivity was observed.

2.3.2 Oxygen measurements

$[O_2]$ was also measured with a SBE43 electrochemical sensor interfaced with the CTD unit. The raw voltage was converted to oxygen concentration with 13 calibration coefficients based on the Seabird™ methodology derived from Owens and Millard (1985). Three of these coefficients (the oxygen signal slope, the voltage at zero oxygen signal, the pressure correction factor) were adjusted with the concentrations estimated with the Winkler method on samples collected at the closure of the bottles. One unique set of calibration coefficients has been applied to all oxygen profiles from the cruise because no significant drift of the sensor was observed during the time of the cruise. For the two TM-R casts, values have been corrected with a drift and offset based on the comparison of 15 pairs of casts (main CTD rosette/TM-R) collected close in time (less than 2 h) and space (less than 1 nautical mile) over the entire OUTPACE transect.

2.4 Derived parameters

Practical salinity (S_P) was derived from conductivity, temperature and pressure with the EPS-78 algorithm. Absolute

salinity (S_A), potential temperature (θ), conservative temperature (Θ) and potential density (σ_θ) were derived from S_P, temperature, pressure and the geographic position with the TEOS-10 algorithms (Valladares et al., 2011). These five derived parameters were calculated within the processing with Seabird™ dedicated software.

Seawater pH on the total scale (pH_T) and the $CaCO_3$ saturation state with respect to aragonite (Ω_{ara}) were derived from A_T and C_T with the "Seacarb" R package (Gattuso and Lavigne, 2009). $CaCO_3$ saturation state with respect to calcite was not considered because seawater up to 2000 dbar was supersaturated with respect to calcite ($\Omega_{cal} > 1$). Following the recommendations from Dickson et al. (2007), the constants for carbonic acid K_1 and K_2 from Lueker et al. (2000), the constant for hydrogen fluoride K_F from Pérez and Fraga (1987), and the constant for hydrogen sulfate K_S from Dickson (1990) were used. Orthophosphate and silicate concentration were considered in the calculation. Methods for nutrient measurement are presented in detail in Fumenia et al. (2018). When nutrient data were not available (station SD 8), silicate and orthophosphate were estimated from the nutrient profile measured on cast out_c_163 (interpolated values). Apparent oxygen utilization (AOU) was computed from the difference between oxygen solubility (at $p = 0$ dbar, and S_P) estimated with the "Benson and Krause coefficients" in Garcia and Gordon (1992) and in situ $[O_2]$.

For the estimation of C_{ANT}, the TrOCA method was used. The TrOCA approach was first proposed in Touratier and Goyet (2004a, b) with improvements in Touratier et al. (2007). In brief, the TrOCA parameter is defined as a combination of A_T, C_T and $[O_2]$ that accounts for biologically induced relative changes among these parameters (with constant stoichiometric ratios). TrOCA is thus a quasi-conservative tracer derived from C_T in the ocean. Within a defined water mass, changes in TrOCA over time are independent of biology and can be attributed to the penetration of C_{ANT}. In consequence C_{ANT} can be calculated in a parcel of water from the difference between current and pre-industrial TrOCA (TrOCA°) divided by a stoichiometric coefficient. The simplicity of the TrOCA method relies on the fact that a simple formulation for TROCA° has been proposed based on potential temperature and alkalinity and thus an estimation of C_{ANT} can be done by a simple calculation using C_T, A_T, $[O_2]$ and θ. In this study, the formulation proposed in Eq. (11) in Touratier et al. (2007) is used to calculate C_{ANT} and is recalled here in Eq. (1).

$$C_{ANT} = \left([O_2] + 1.279 \left(C_T - \frac{A_T}{2} \right) - \exp\left(7.511 - 1.087 \times 10^{-2}\, \theta - \frac{7.81 \times 10^{-5}}{A_T^2} \right) \right) \Big/ 1.279 \quad (1)$$

This formulation is based on an adjustment of the TrOCA coefficients using $\Delta^{14}C$ and CFC-11 from the GLODAPv1 database (Key et al., 2004). Touratier et al. (2007) estimated the overall uncertainty of the C_{ANT} with TrOCA method to be ca. 6 µmol kg^{-1} based on the random propagation of the uncertainties in the variables (C_T, A_T, $[O_2]$ and θ) and coefficients used in Eq. (1). The limitations and validity of the TrOCA method will be discussed in detail in Sect. 5.

2.5 Data from available databases

For comparison with existing values of carbonate chemistry in the area of the OUTPACE cruise, relevant data were extracted from GLODAPv2 database (NDP-93 – Olsen et al., 2016; Key et al., 2015). The specific data file for the Pacific Ocean was used (downloaded from https://www.nodc.noaa.gov/ocads/oceans/GLODAPv2/, last access: 14 December 2017). For comparison with OUTPACE data, GLODAPv2 data were selected between 22 and 17° S and between 159° E and 159° W (going westwards). For specific comparisons in the MA and the South Pacific western gyre waters (WGY) a zonal subset of the extracted data was used: 159° E and 178° W for MA and 170 to 159° W for WGY (see Fig. 1).

3 Hydrological context along the OUTPACE transect

The hydrological context encountered during the OUTPACE transect is presented with a $\Theta - S_A$ diagram between 0 and 2000 dbar in Fig. 2. A detailed description of the water masses encountered during the OUTPACE cruise can be found in Fumenia et al. (2018). Briefly, from the surface to 2000 dbar, the following features are distinguished: the surface waters ($\sigma_\theta < 23.5$ kg m^{-3}) were characterized by temperatures over 25 °C with increasing temperature and salinity towards the east and AOU close to zero. Under the surface water, the upper thermocline waters (UTW) presented a maximum in salinity, reaching values higher than 36 g kg^{-1} in the eastern part of the cruise. In the lower thermocline waters, S_A decreased with depth with a more pronounced decrease in the eastern part than in the western part, whereas AOU is higher in the eastern part than in the western part of the studied area. These differences in lower thermocline waters have been described for South Pacific Central Waters (SPCW) with more saline western (WSPCW) and less saline eastern (ESPCW) waters (Tomczak and Godfrey, 2003). Below the thermocline, intermediate waters are made up of Subantarctic Mode Waters (SAMW) and Antarctic Intermediate Waters (AAIWs). AAIWs have a salinity minimum close to the $\sigma_\theta = 27$ kg m^{-3} isopycnal. Hartin et al. (2011) defines SAMW as having σ_θ values between 26.80 and 27.06 kg m^{-3}, corresponding to a minimum in potential vorticity, and AAIW as having σ_θ values between 27.06 and 27.40 kg m^{-3}. The separation of both waters is not trivial in the subtropical area.

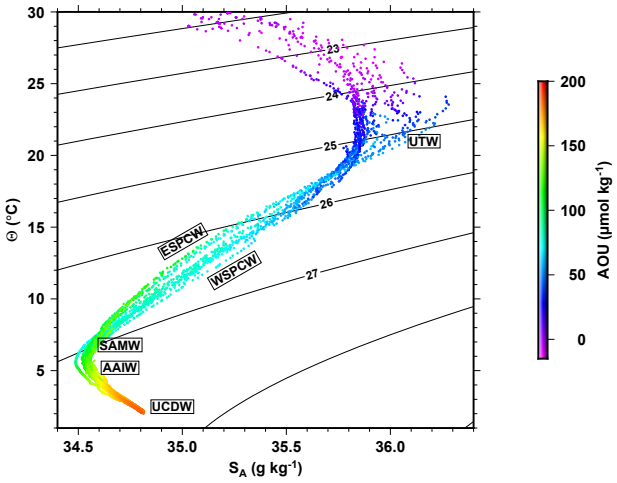

Figure 2. $\Theta - S_A$ diagram with colors indicating the AOU. Black contour lines represent the isopycnal horizons based on potential density referenced to a pressure of 0 dbar (σ_θ).

SAMW is generally associated with lower AOU than AAIW. Finally, deep waters made up of Upper Circumpolar Deep Waters (UCDW) correspond to an increase in salinity and AOU for depth corresponding to $\sigma_\theta > 27.4\,\mathrm{kg\,m^{-3}}$.

In this study, discussion will sometimes make a distinction between two subregions along the OUTPACE transect: MA and WGY (see Sect. 2.5 for definition). This distinction is mainly based on geographic and oceanographic arguments. Indeed, these two subregions are geographically separated by the Tonga volcanic arc. WGY is characterized by higher surface temperature and a higher salinity in the upper thermocline waters than MA. The difference between these subregions is evidenced by the difference in oligotrophy (Moutin et al., 2018). Due to specific conditions in the transition area between the MA and WGY (de Verneil et al., 2017), SD 11, SD 12 and LD B were discarded from both groups in this study following the arguments in Moutin et al. (2018).

4 Carbonate chemistry along the OUTPACE transect

A_T and C_T measured along the OUTPACE transect are presented in Fig. 3a and b. All vertical profiles for A_T, A_T normalized to $S_A = 35\,\mathrm{g\,kg^{-1}}$ ($A_{T\,n35}$) and C_T are presented in Fig. 3e, f and g. A_T ranged between 2300 and 2400 µmol kg^{-1}. Below the surface, a pronounced maximum in A_T was observed associated with the saltier upper thermocline waters. When normalized to $S_A = 35\,\mathrm{g\,kg^{-1}}$, $A_{T\,n35}$ values are remarkably constant in the upper 500 dbar with values between 2270 and 2310 µmol kg^{-1}. Below 500 dbar, A_T increases with depth up to ca. 2400 µmol kg^{-1} indicating that alkalinity changes are mostly due to salinity changes in the upper water column, whereas the increase in the deep waters is mainly due to carbonate biomineral remineralization. C_T values are close to 1950 µmol kg^{-1} in the surface and increase with depth up to 2300 µmol kg^{-1} at 2000 dbar. The C_T gradient in the upper water column has been described in Moutin et al. (2018). Below 2000 dbar, C_T is relatively invariant with slightly lower values in the bottom waters (below 4000 dbar) due to the presence of very old deep waters originating from the North Pacific relative to the northward moving bottom waters that have not accumulated as much carbon (Murata et al., 2007). A_T and C_T values in deep waters measured during OUTPACE are in good agreement with the data of the GLODAPv2 database (Fig. 3e, f and g). No systematic adjustment of the OUTPACE dataset with the GLODAPv2 dataset was performed because only very few data are available in the deep ocean where crossover comparison can be performed for cruises carried out in different decades. Nevertheless, for the only "deep" cast performed during OUTPACE (out_c_163 at station LD C), we performed a simple crossover analysis with the station 189 (located at 107 km kilometers from OUTPACE station LD C) of the Japanese "P21 revisited" cruise in 2009. We compared interpolated profiles on density surfaces values ($27.75\,\mathrm{kg\,m^{-3}} < \sigma_\theta < 27.83\,\mathrm{kg\,m^{-1}}$ corresponding to pressure levels of ca. 3000 to 5500 dbar). The estimated offsets are -2.0 ± 4.2 µmol kg^{-1} for A_T and -2.0 ± 4.4 µmol kg^{-1} for C_T suggesting measurement biases are likely no larger. This simple quality control procedure seems to indicate that no systematic adjustment is needed.

Derived parameters from the A_T and C_T measurements are presented in Fig. 3c for pH_T values (estimated at in situ temperature and pressure). pH_T decreases from values close to 8.06 in surface to values close to 7.84 at 2000 m. Surface values of pH_T are typical of subtropical warm waters and are in a similar range as the austral summer values estimated by Takahashi et al. (2014) in this area (8.06–8.08). Figure 3d represents the vertical distribution of computed values of Ω_{ara} along the OUTPACE transect. Seawater is supersaturated with respect to aragonite ($\Omega_{ara} > 1$) at the surface with Ω_{ara} values of ca. 4.0 again in good agreement with the austral summer values of 4–4.4 estimated by Takahashi et al. (2014) in this area. Values of Ω_{ara} decrease with depth, and seawater becomes undersaturated with respect to aragonite ($\Omega_{ara} < 1$) at an horizon situated below 1000 dbar in the west and above 1000 dbar in the eastern part of the cruise, with a general shoaling of the Ω_{ara} values from west to east, in good agreement with a previous study by Murata et al. (2015) in this area.

5 Anthropogenic carbon estimation along the OUTPACE transect

The TrOCA method is a way to quantify C_{ANT} in the ocean based on C_T, A_T, [O_2] and θ. This method has been used and compared to other methods in different oceanic areas (e.g., Lo Monaco et al., 2005; Álvarez et al., 2009;

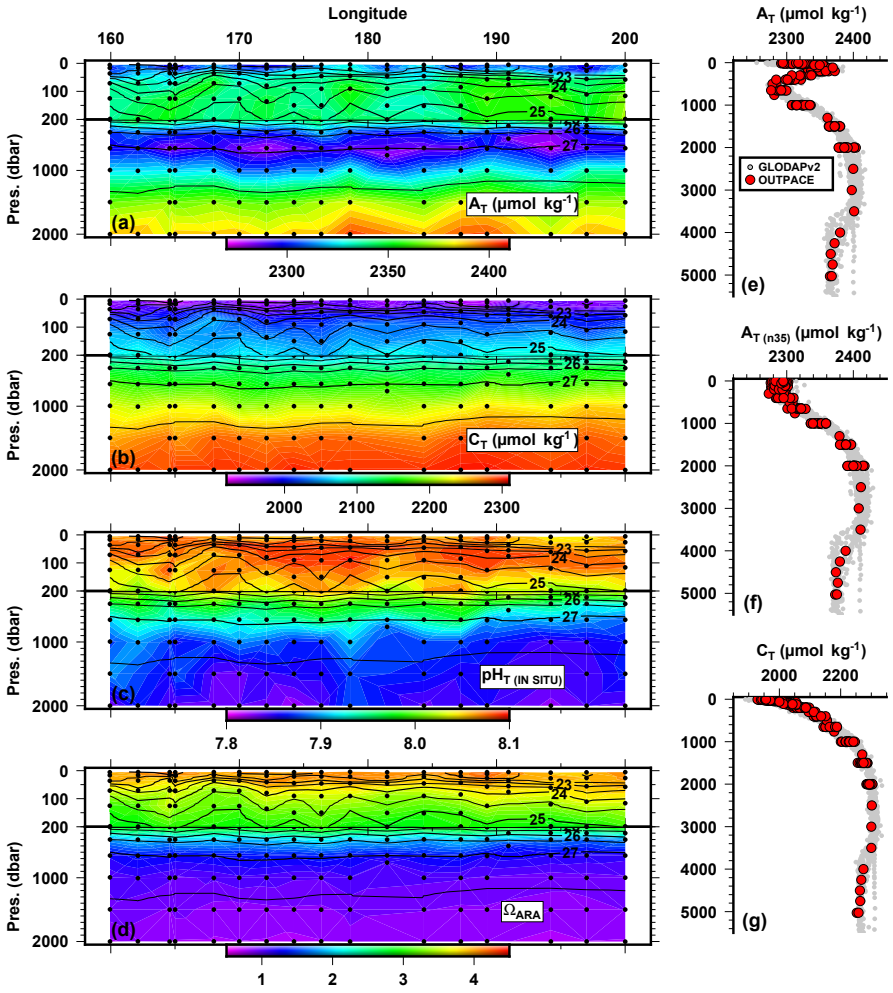

Figure 3. Longitudinal variations in **(a)** A_T, **(b)** C_T, **(c)** pH_T and **(d)** Ω_{ara} along the OUTPACE transect between the surface and 2000 dbar depth. Black contour lines represent the isopycnal horizons based on potential density referenced to a pressure of 0 dbar. Vertical profiles of **(e)** A_T, **(f)** $A_{T\,n35}$ and **(g)** C_T of the entire OUTPACE dataset (red dots) superimposed on the GLODAPv2 data corresponding to the OUTPACE area (gray dots).

Vázquez-Rodríguez et al., 2009). Based on specific C_{ANT} inventories in the water column, the TrOCA method reasonably agreed with the other methods (including the transient tracer-based method). However, Yool et al. (2010) "tested" the TrOCA method within an ocean general circulation model and argued that the use of globally uniform parameterization for the estimation of the pre-industrial TrOCA is a source of significant overestimation but also that even with regionally "tuned" parameters a global positive bias in the method exists. As no tracers of water mass age were measured during the OUTPACE cruise, the main motivation for using the TrOCA method was to make C_{ANT} estimations based on a simple calculation from parameters acquired within the cruise as done in other cruises conducted in tropical South Pacific waters (e.g., Azouzi et al., 2009; Ganachaud et al., 2017). Even if C_{ANT} estimates from TrOCA are biased, the application of a simple back-calculation method that accounts for biologically induced relative changes in C_T is used here to identify some spatial features in the distribution of the carbonate system along the OUTPACE transect. Here, an error in the TrOCA C_{ANT} estimates of 67 % will be considered based on the standard deviation for the TrOCA variant optimized with world ocean data and normalized such that standard deviation in the simulated C_{ANT} in the ocean general circulation model is exactly 1 (see Table 2 in Yool et al., 2010).

As mentioned by Touratier et al. (2007), C_{ANT} estimates cannot be considered within the mixed layer because the underlying hypotheses used in the formulation of TrOCA may not be verified due to biological activity and gas transfers across the air–sea interface. To avoid this issue, C_{ANT} estimates are generally used below the "permanent" mixed layer depth (e.g., Álvarez et al., 2009; Carter et al., 2017). For the OUTPACE area, Moutin et al. (2018) show that the mixed

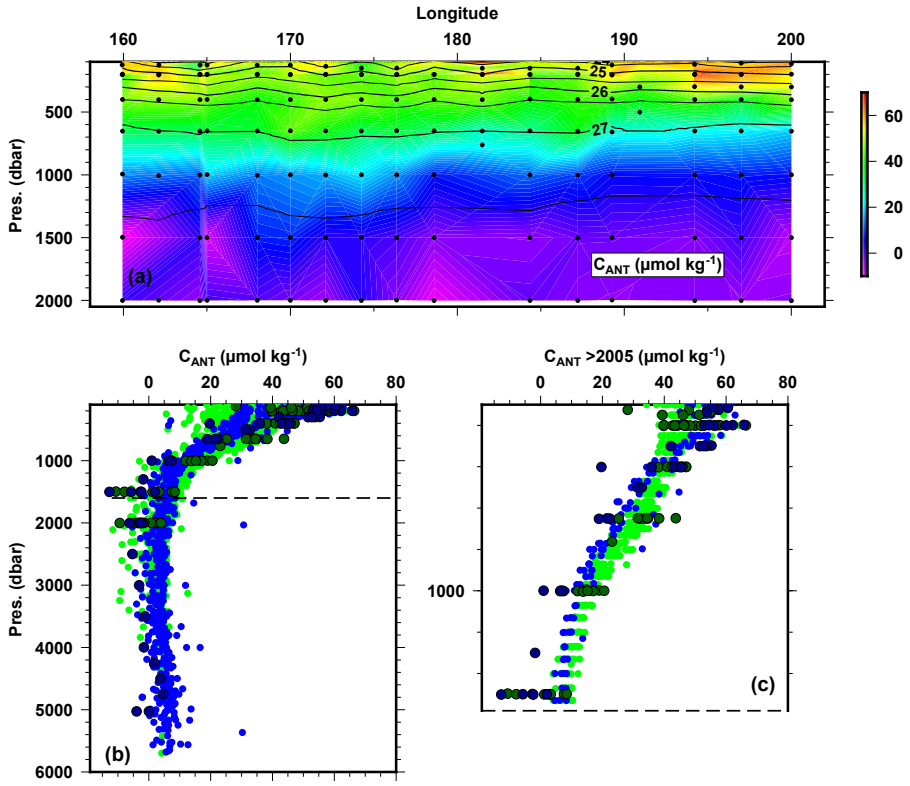

Figure 4. Longitudinal variations in C_{ANT} (estimated with the TrOCA method) along the OUTPACE transect between 100 and 2000 dbar depth **(a)**. Black contour lines represents the isopycnal horizons based on potential density referenced to a pressure of 0 dbar. Vertical profiles of C_{ANT} for the entire OUTPACE dataset superimposed on the values estimated from the GLODAPv2 data **(b)** and vertical profiles of C_{ANT} between 100 and 1500 dbar superimposed on the values estimated from the recent (after 2005) GLODAPv2 data **(c)**. The color code for the dots is the same as for Fig. 1.

layer depth does not exceed 70 m in the area. Even if the depths of the deep chlorophyll maximum were encountered below 100 dbar along the transect, we will consider C_{ANT} values up to 100 dbar. It can be mentioned that the C_{ANT} values of 50–60 µmol kg^{-1} in the top of the water column (100 dbar) are in reasonable agreement with a rough estimate of thermodynamically consistent C_T changes: by assuming that CO_2 in surface seawater is in equilibrium with the atmosphere, we estimated that with a partial pressure of CO_2 (pCO_2) of 280 µatm in the pre-industrial period, a pCO_2 of 380 µatm during OUTPACE (Moutin et al., 2018) and a constant A_T over time of 2300 µmol kg^{-1}, C_T change in surface waters between the pre-industrial period and 2015 is ca. 65 µmol kg^{-1} for a temperature of surface waters between 25 and 28 °C. For OUTPACE, C_{ANT} estimates below 1000 dbar were not significantly different from 0 µmol kg^{-1}, with a standard deviation of 6.3 µmol kg^{-1}.

C_{ANT} distribution along the OUTPACE transect is presented in Fig. 4a, and all vertical profiles for C_{ANT} are presented in Fig. 4b with a more detailed view of the first 1500 dbar of the water column in Fig. 4c. Figure 4b and c distinguish values from the MA and the WGY area. The C_{ANT} vertical profiles suggest a penetration of anthropogenic carbon up to 1000 dbar. As mentioned before, estimated values of C_{ANT} reach values of 60 ± 40 µmol kg^{-1} at a depth of 100 dbar; C_{ANT} then regularly decreases to values close to $10–20 \pm 13$ µmol kg^{-1} at a depth of 1000 dbar and reaches values close to 0 µmol kg^{-1} below 1500 dbar. The zonal C_{ANT} section along the OUTPACE transect (Fig. 4a) presents two features: (1) a deeper penetration of C_{ANT} in the western part of the transect with values of C_{ANT} reaching 40 ± 25 µmol kg^{-1} around the isopycnal layer of 27 kg m^{-3} (ca. 700 dbar) with a coherent behavior with the distribution of AOU and (2) a larger accumulation of C_{ANT} in the eastern part of the transect centered around the isopycnal layer of 25 kg m^{-3} (ca. 200 dbar).

Several studies have identified deeper C_{ANT} penetration in the western South Pacific than in the eastern South Pacific at tropical and subtropical latitudes. The primary reason for this longitudinal difference might be associated with deeper convection in the western part and upwelling in the eastern part. AAIW has been described as the lower limit of the penetration of C_{ANT} in the ocean interior of the South Pacific (Sabine et al., 2004). Moreover, a recent study by

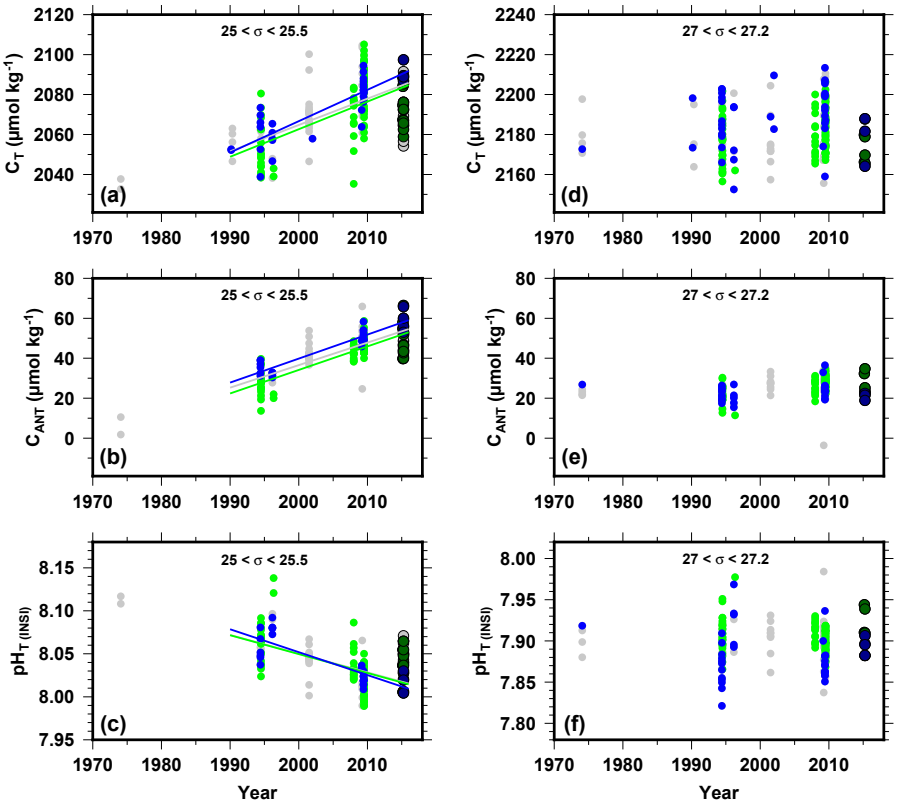

Figure 5. Temporal evolution in the OUTPACE area of C_T **(a, d)**, C_{ANT} **(b, e)** and pH_{Tinsi} **(c, f)** based on GLODAPv2 and OUTPACE data along two isopycnal layers: 25–25.5 kg m^{-3} **(a, b, c)** and 27–27.2 kg m^{-3} **(d, e, f)**. The color code for the dots is the same as for Fig. 1.

DeVries et al. (2017) shows that ocean circulation variability is the primary driver for changes in oceanic CO_2 uptake at decadal scales. Based on C_T changes between the two repeated visits of the longitudinal P21 line (18° S close to the OUTPACE transect) in 1994 and 2009, Kouketsu et al. (2013) show a faster increase in C_{ANT} in the western part than in the eastern part of the section. They also postulate that C_{ANT} may have been transported by deep circulation associated with the AAIW. In the subtropical Pacific along the P06 line (longitudinal section at ca. 32° S), Murata et al. (2007) also identified an increase in C_{ANT} in the SAMW and AAIW. Waters et al. (2011) attribute the deeper penetration of C_{ANT} in the western part of the section to the local formation of subtropical mode water in the area based on the extended multiple linear regression (eMLR) method along the P06 line (and taking into account a third visit).

In the eastern part of the OUTPACE cruise, the detected accumulation of C_{ANT} in the upper thermocline waters may be related to recent observations of a significant accumulation of C_{ANT} at latitudes around 20° S on the P16 meridional transect along 150° W by Carter et al. (2017). This change in C_{ANT} accumulation is attributed to changes in the degree of the water mass ventilation due to variability in a southern Pacific subtropical cell. Along the P16 line, Carter et al. (2017) observed high values of C_{ANT} (up to 60 µmol kg^{-1}) for the upper water column at the latitude of the OUTPACE area in good agreement with our estimates in WGY in the upper water column. Finally, it should also be mentioned that, due to the presence of one of the main oxygen minimum zone (OMZ) area, denitrification occurs in the eastern South Pacific and can be traced by the N^* parameter (Gruber and Sarmiento, 1997). Denitrification, by transforming organic carbon to inorganic carbon without the consumption of oxygen, could induce an overestimation of C_{ANT} by the TrOCA method (and other back-calculation methods) due to a biological release of C_T that is not taken into account in the formulation of the quasi-conservative TrOCA tracer. Horizontal advection by the south equatorial current of the strong negative N^* signal originating from the eastern Pacific towards the western Pacific has been described previously (Yoshikawa et al., 2015). Fumenia et al. (2018) have estimated N^* along the OUTPACE transect and show slightly negative N^* values in the upper thermocline waters at the eastern side of the OUTPACE transect where the highest C_{ANT} values are estimated. However, Murata et al. (2015) showed that, based on a direct relation between C_T and N^*, the influence of denitrification should be negligible on C_{ANT} estimations in this area. Therefore, the N^* correction has not

Table 2. Estimated trends on A_T, $[O_2]$, C_T , C_{ANT} and pH_T changes in two different layers of the water column defined by isopycnal layers between 1980 and 2015 based on GLODAPv2 with (column WITH) and without (column WITHOUT) OUTPACE data added. Estimated trends are obtained from slope values of a linear regression between the studied parameters and time.

	$25\,kg\,m^{-3} < \sigma_\theta < 25.5\,kg\,m^{-3}$		$27\,kg\,m^{-3} < \sigma_\theta < 27.2\,kg\,m^{-3}$	
	WITH	WITHOUT	WITH	WITHOUT
Trend on A_T in $\mu mol\,kg^{-1}\,a^{-1}$				
OUTPACE	-0.20 ± 0.07 ($n = 167$)*	-0.30 ± 0.07 ($n = 142$)*	-0.12 ± 0.07 ($n = 180$)	-0.01 ± 0.06 ($n = 174$)
MA	-0.30 ± 0.09 ($n = 85$)*	-0.47 ± 0.10 ($n = 70$)*	-0.16 ± 0.09 ($n = 99$)	-0.10 ± 0.09 ($n = 92$)
WGY	-0.20 ± 0.14 ($n = 28$)	-0.20 ± 0.19 ($n = 22$)	-0.20 ± 0.14 ($n = 35$)	-0.01 ± 0.13 ($n = 31$)
Trend on $[O_2]$ in $\mu mol\,kg^{-1}\,a^{-1}$				
OUTPACE	-0.31 ± 0.10 ($n = 167$)*	-0.61 ± 0.09 ($n = 143$)*	0.05 ± 0.11 ($n = 183$)	0.07 ± 0.10 ($n = 178$)
MA	-0.35 ± 0.16 ($n = 84$)*	-0.78 ± 0.17 ($n = 70$)*	0.06 ± 0.11 ($n = 99$)	0.04 ± 0.11 ($n = 93$)
WGY	-0.38 ± 0.11 ($n = 27$)*	-0.35 ± 0.14 ($n = 23$)*	-0.11 ± 0.30 ($n = 38$)	-0.22 ± 0.29 ($n = 34$)
Trend on C_T in $\mu mol\,kg^{-1}\,a^{-1}$				
OUTPACE	1.32 ± 0.13 ($n = 174$)*	1.63 ± 0.13 ($n = 149$)*	0.23 ± 0.13 ($n = 189$)	0.27 ± 0.11 ($n = 183$)*
MA	1.38 ± 0.21 ($n = 85$)*	1.87 ± 0.21 ($n = 70$)*	0.31 ± 0.16 ($n = 100$)	0.44 ± 0.17 ($n = 93$)*
WGY	1.57 ± 0.18 ($n = 31$)*	1.57 ± 0.23 ($n = 25$)*	0.23 ± 0.29 ($n = 40$)	0.23 ± 0.29 ($n = 36$)
Trend on C_{ANT} in $\mu mol\,kg^{-1}\,a^{-1}$				
OUTPACE	1.12 ± 0.07 ($n = 166$)*	1.25 ± 0.06 ($n = 142$)*	0.32 ± 0.05 ($n = 179$)*	0.25 ± 0.04 ($n = 174$)*
MA	1.18 ± 0.08 ($n = 84$)*	1.31 ± 0.08 ($n = 70$)*	0.40 ± 0.06 ($n = 98$)*	0.40 ± 0.06 ($n = 92$)*
WGY	1.20 ± 0.09 ($n = 28$)*	1.18 ± 0.10 ($n = 22$)*	0.13 ± 0.09 ($n = 35$)	0.11 ± 0.08 ($n = 31$)
Trend on pH_{TINSI} in a^{-1}				
OUTPACE	-0.0022 ± 0.0003 ($n = 167$)*	-0.0031 ± 0.0002 ($n = 142$)*	-0.0001 ± 0.0003 ($n = 181$)	-0.0002 ± 0.0002 ($n = 175$)
MA	-0.0022 ± 0.0004 ($n = 85$)*	-0.0033 ± 0.0004 ($n = 70$)*	-0.0004 ± 0.0003 ($n = 100$)	-0.0007 ± 0.0003 ($n = 93$)*
WGY	-0.0027 ± 0.0004 ($n = 28$)*	-0.0030 ± 0.0004 ($n = 22$)*	-0.00008 ± 0.0006 ($n = 35$)	-0.0007 ± 0.0006 ($n = 31$)

* Trend significant (p level < 0.05).

been introduced in the C_{ANT} estimates and the effect of denitrification was not quantified here.

6 Temporal changes in carbonate chemistry in the OUTPACE area

Based on the available GLODAPv2 data, temporal changes in the OUTPACE area have been assessed (Fig. 5 and Table 2). The variation in oceanic parameters with time is estimated on two isopycnal layers: a layer with $25\,kg\,m^{-3} < \sigma_\theta < 25.5\,kg\,m^{-3}$ (hereafter named $\sigma_{\theta\,25}$) and a layer with $27\,kg\,m^{-3} < \sigma_\theta < 27.2\,kg\,m^{-3}$ (hereafter named $\sigma_{\theta 27}$). These two layers correspond to the features in C_{ANT} discussed in the previous section. $\sigma_{\theta 25}$ can be considered characteristic of the upper thermocline waters (core of the salinity maximum, Fig. 2), whereas $\sigma_{\theta 27}$ can be considered characteristic of intermediate waters of southern origin (core of the salinity minimum). All the values associated with these two layers are spread between 145 and 301 dbar for $\sigma_{\theta 25}$ and between 571 and 896 dbar for $\sigma_{\theta 27}$. It must be mentioned that the study of temporal changes is based on a large sampling grid, which covers the entire OUTPACE transect (see Sect. 2.5 and Fig. 1). This could add a spatial variability that may interfere in the estimation of temporal changes.

Temporal variations in C_T and C_{ANT} between 1970 and 2015 are presented in Fig. 5. As mentioned earlier, even if C_{ANT} estimates from TrOCA are biased, a previous study by Pérez et al. (2010) suggests that the TrOCA method gives similar values to other methods for estimating C_{ANT} accumulation rates. A linear fit was applied to the observed temporal variations for A_T, $[O_2]$, C_T and C_{ANT} to check for significant trends on data collected between 1980 and 2015. The results of the performed regression analyses are presented in Table 2. Trends are evaluated with and without the data of the OUTPACE cruise in order to estimate the influence of this new dataset on the observed trends. Trends are evaluated for the entire OUTPACE area and for the MA and the WGY area. Even if presented in Fig. 5, data collected before 1980 from the GLODAPv2 database are disregarded in the estimation of the temporal trends. Indeed, for the OUTPACE area, data prior to 1980 originate from one single GEOSEC cruise in 1974, with only one measured point for $\sigma_{\theta 27}$ at WGY and no points at $\sigma_{\theta 25}$ for WGY and MA.

Table 3. Estimated depth of the $\Omega_{ara} = 1$ horizon along the OUTPACE cruise (see text for details). No values are available for stations where data up to 2000 dbar were not available (SD2 and SD13). No values were estimated for stations with $C_{ANT} < -6\,\mu mol\,kg^{-1}$.

Station	Longitude (° E)	Latitude (° N)	Depth of the $\Omega_{ara} = 1$ horizon (in m)		
			OUTPACE	Pre-ind.	Difference*
SD 1	159.9425	−17.9088	1225	NA	NA
SD 2	162.1248	−18.6078	NA	NA	NA
SD 3	165.0082	−19.4907	928	NA	NA
LD A	164.5787	−19.2233	1032	1185	153
SD 4	168.0157	−19.98	1029	1193	164
SD 5	169.9965	−21.9997	1126	1256	130
SD 6	172.1193	−21.3758	1097	1233	136
SD 7	174.2512	−20.7677	1015	1235	220
SD 8	176.364	−20.6945	1010	1171	161
SD 9	178.6087	−20.9963	1214	NA	NA
SD 11	−175.6475	−20.0057	1055	1172	117
SD 12	−172.7813	−19.5368	1013	1112	99
LD B	−170.7385	−18.1745	948	1046	98
SD13	−169.0728	−18.2007	NA	NA	NA
LD C	−165.7792	−18.4842	854	941	87
SD 14	−162.9992	−18.3952	889	1006	117
SD 15	−159.9913	−18.2618	917	1043	126

* Difference (in m) between the depth of the $\Omega_{ara} = 1$ horizon at the pre-industrial period and the OUTPACE cruise. NA – not available.

At $\sigma_{\theta 25}$, a significant decrease in A_T of $-0.20 \pm 0.07\,\mu mol\,kg^{-1}\,a^{-1}$ is observed over the entire OUTPACE area. A decrease of $-0.30 \pm 0.09\,\mu mol\,kg^{-1}\,a^{-1}$ is also observed in the MA area, whereas no significant trend is observed for the WGY area. However, when A_T is normalized to salinity, no significant trends are observed in $A_{T\,n35}$ suggesting that the observed trend in A_T can be attributed to salinity changes rather than changes in calcification. Significant negative trends are observed for $[O_2]$ over the entire area ($-0.31 \pm 0.10\,\mu mol\,kg^{-1}\,a^{-1}$), in MA ($-0.35 \pm 0.16\,\mu mol\,kg^{-1}\,a^{-1}$) and in WGY ($-0.38 \pm 0.11\,\mu mol\,kg^{-1}\,a^{-1}$). The decrease in $[O_2]$ which corresponds to a positive trend in AOU suggested an increase in the remineralization of organic matter at $\sigma_{\theta 25}$. Significant increasing trends were observed for C_T over the entire area ($+1.32 \pm 0.13\,\mu mol\,kg^{-1}\,a^{-1}$), in MA ($+1.38 \pm 0.21\,\mu mol\,kg^{-1}\,a^{-1}$) and in WGY ($+1.57 \pm 0.13\,\mu mol\,kg^{-1}\,a^{-1}$). For C_{ANT}, the trends were slightly slower ($+1.12 \pm 0.07$ to $+1.2 \pm 0.09\,\mu mol\,kg^{-1}\,a^{-1}$) and not significantly different between MA and WGY. Taking into account the OUTPACE dataset does not change the overall significance of the observed trends and only minor changes (mostly within the error of the estimates) are observed. If we assume a C_T increase of 0.5 to $1\,\mu mol\,kg^{-1}\,a^{-1}$ (depending on the buffer factors considered) associated with the recent rise in atmospheric CO_2 (see for example Murata et al., 2007), the C_T increase in the OUTPACE area is faster than thermodynamics would govern, whereas the C_{ANT} is closer to this thermodynamic value. The higher increase in C_T could be related to an increase in remineralization processes as deduced from $[O_2]$ trends, with an overall consistency between the rate of C_T increase and the rate of decrease in $[O_2]$. However, the important increase in C_{ANT} observed between 2005 and 2015 between 10 and 30° S on the P16 line (at the eastern side of the OUTPACE transect) by Carter et al. (2017) is not supported by significant differences in the trends of C_{ANT} observed between MA and WGY in this study.

At $\sigma_{\theta 27}$, the only significant trend observed is an increase in C_{ANT} of ca. $0.40 \pm 0.06\,\mu mol\,kg^{-1}\,a^{-1}$ in the MA area. When the OUTPACE dataset is not considered, a similar trend is observed for C_T in the MA area. This trend is compatible with the observed increase in C_{ANT} by Kouketsu et al. (2013) along the P21 line close to the isopycnal layer $27\,kg\,m^{-3}$. As this increase is not observed in WGY and if we assume that the $\sigma_{\theta 27}$ is filed with AAIWs, this suggest that the accumulation of C_{ANT} in AAIW is faster west of the 170° W line than to the east, but no clear explanation for this trend can be given.

7 Towards an enhanced "ocean acidification" in the WTSP?

Temporal variations in pH_T between 1970 and 2015 are presented in Fig. 5c and f with rates of pH_T decrease of $-0.0022 \pm 0.0004\,a^{-1}$ for MA and $-0.0027 \pm 0.0004\,a^{-1}$ for WGY at $\sigma_{\theta 25}$ (Table 2) between 1980 and 2015. Based on the C_{ANT} rates estimated in the previous section (1.1 to $1.2\,\mu mol\,kg^{-1}\,a^{-1}$) and based on a constant value of A_T of

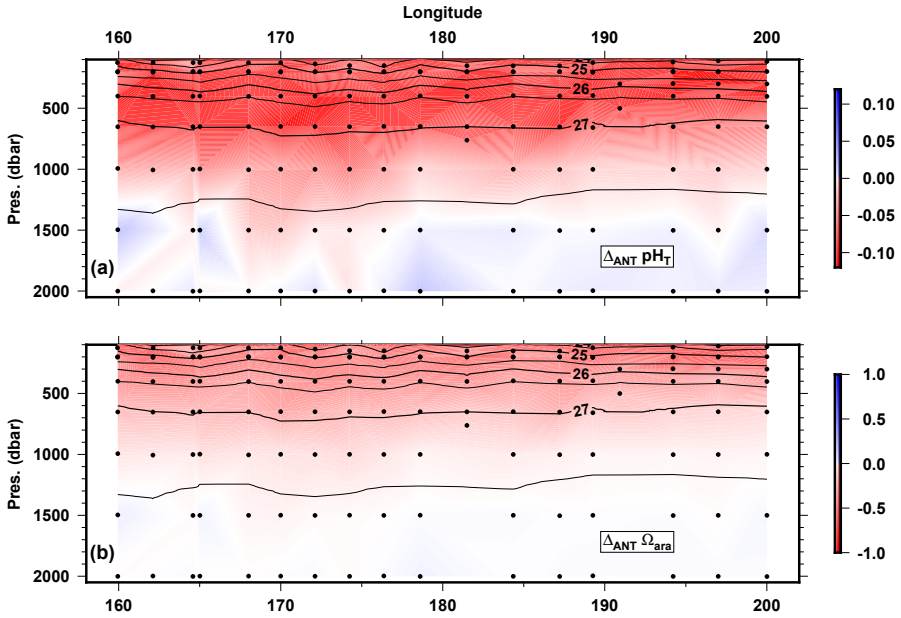

Figure 6. Longitudinal variations in **(a)** pH_T changes and **(b)** Ω_{ara} changes between the pre-industrial period and the present time along the OUTPACE transect between 100 and 2000 dbar depth (see text for details). Black contour lines represent the isopycnal horizons based on potential density referenced to a pressure of 0 dbar.

2285 µmol kg^{-1} (mean value of $A_{T\,n35}$ on $\sigma_{\theta 25}$) and a constant temperature of 20 °C (mean value of temperature on $\sigma_{\theta 25}$), we can estimate a pH_T decrease rate of -0.0023 to -0.0025 a^{-1}. This indicates that rates of oceanic pH_T decrease (ocean acidification) can mostly be explained by the increase in C_{ANT}. These rates of acidification are higher than the values reported by Waters et al. (2011) in the western South Pacific along the P06 Line (south of OUTPACE area at 32° S) between two visits in 1992 and 2008. They are also higher than the surface rates of pH_T decrease of -0.0016 ± 0.0001 a^{-1} recorded at the HOT station in the tropical North Pacific and of -0.0017 ± 0.0001 and -0.0018 ± 0.0001 a^{-1} in the tropical North Atlantic at BATS and ESTOC stations, respectively (Bates et al., 2014). However, differences in buffer factors between the surface and subsurface can partially explain these differences. Nevertheless, our results in the subsurface ($\sigma_{\theta 25}$) based on GLODAPv2 and OUTPACE data (C_T and A_T) are similar to pH_T trends derived from fCO_2 surface observations (e.g., Lauvset et al., 2015). In the southern subtropical and equatorial Pacific regions, using SOCAT version2, Lauvset et al. (2015) evaluate contrasting fCO_2 and pH_T trends, ranging between +1.1 and +3.5 µatm a^{-1} for fCO_2 and between -0.001 and -0.0023 a^{-1} for pH_T. If we revisit these estimates, using surface fCO_2 observations available in the OUTPACE region (18–22° S/170–200° E) in SOCAT version 6 (Bakker et al., 2016; http://www.socat.info, last access: 10 August 2018) and assuming a constant alkalinity (2300 µmol kg^{-1}, average of surface data), we can calculate pH_T and C_T from fCO_2 and temperature data. The resulting long-term trends for the period 1980–2016 for fCO_2, C_T and pH_T are, respectively, $+1.27 \pm 0.01$ µatm a^{-1}, $+1.03 \pm 0.01$ µmol kg^{-1} a^{-1} and -0.0013 ± 0.0001 a^{-1}. Interestingly, for the period 2000–2016 the trends are $+2.53 \pm 0.02$ µatm a^{-1}, $+2.02 \pm 0.02$ µmol kg^{-1} a^{-1} and -0.0025 ± 0.0003 a^{-1}, suggesting an acceleration of the signals in recent years. These results, based on fCO_2 observations in surface waters, confirm the trends we detected for C_T and pH_T in subsurface layers ($\sigma_{\theta 25}$).

In Fig. 6, estimates of the so-called "anthropogenic pH_T change" ($\Delta_{ANT}pH_T$) and "anthropogenic Ω_{ara} change" ($\Delta_{ANT}\Omega_{ara}$), which correspond to the difference in pH_T and Ω_{ara} between the time of the OUTPACE cruise (modern time) and the pre-industrial period, are presented. The pH_T and Ω_{ara} correspond to the values presented in Fig. 3, whereas the pre-industrial values corresponds to pH_T and Ω_{ara} estimated with C_T minus C_{ANT}. All other parameters (temperature, salinity, alkalinity and nutrients) are assumed to remain constant over time. The main features for the distribution of $\Delta_{ANT}pH_T$ and $\Delta_{ANT}\Omega_{ara}$ logically reflect the distribution of the estimated C_{ANT} in this study because C_{ANT} is the only driving force in these estimations. The estimated pH_T decrease reaches values slightly higher than 0.1 and the estimated Ω_{ara} decrease reaches values of 0.75 since the pre-industrial period for areas with the highest C_{ANT} accumulation. When considering an error in C_{ANT} of 6 µmol kg^{-1}, we can assume that we are able to distinguish changes of 0.0012 for pH_T and 0.06 for Ω_{ara}. Decreases in pH_T and Ω_{ara} are

thus detectable below 1000 dbar in the MA waters and above 1000 dbar in WGY waters.

A decrease in pH_T of 0.1 units since the pre-industrial period is a generally accepted value for oceanic waters affected by C_{ANT} penetration (e.g., Royal Society , Great Britain). Several studies have assessed the rate of ocean acidification based on successive visits to different oceanic areas. For the South Pacific Ocean, Carter et al. (2017) reports decreases in oceanic pH_T since the pre-industrial period of -0.09 and -0.11 pH_T units for the latitude band from 10 to 20° S and from 20 to 30° S, respectively, along the P16 line (150° W) situated on the eastern side of the OUTPACE area. These are in good agreement with our estimates in this area.

Based on an interpolation of the estimated Ω_{ara} during OUTPACE and the pre-industrial Ω_{ara}, we calculated the depth of the horizon where $\Omega_{ara} = 1$ for the different stations of the OUTPACE transect (Table 3) in 2015 and the pre-industrial period based on the $\Delta_{ANT}\Omega_{ara}$ estimates. We observed an upward migration of the aragonite saturation horizon of up to 220 m in the MA area along the OUTPACE transect (Table 3). This upward migration of the $\Omega_{ara} = 1$ horizon is higher than the migration of 30 to 100 m observed between the 1990s and the pre-industrial period in early studies (Feely et al., 2004) in the Pacific based on the WOCE dataset illustrating the continuous acidification of the WTSP.

8 Conclusions

Based on A_T and C_T data and related properties collected during the OUTPACE cruise, we estimated different parameters of the carbonate system along a longitudinal section of nearly 4000 km and up to 2000 dbar in WTSP. Even if the vertical and horizontal resolution is low compared to the WOCE lines and precludes a rigorous comparison with this high-quality dataset, we estimated that the measured carbonate chemistry parameters are in good agreement with previous data collected in this area. Based on the estimation of C_{ANT} from the TrOCA method, we find C_{ANT} penetration in the WTSP and impacts on pH_T and saturation state of calcium carbonate since the pre-industrial period that are in good agreement with previous observations in this area. As mentioned above, C_{ANT} values from TrOCA estimates are not reliable in surface layer. However, based on GLODAPv2 and the SOCAT database, our estimation of C_{ANT} in the subsurface seems to be in good agreement with expected changes in surface waters. The enhanced impact of ocean acidification in the subtropical South Pacific suggested by our study highlights the necessity of sustained research efforts in this largely underexplored part of the world ocean. The presented dataset collected along the OUTPACE transect could complement existing sections visited nearly every decade in the South Pacific Ocean and in particular the P21 line, which was last visited in 2009.

Data availability. OUTPACE cruise data are available at the French INSU/CNRS LEFE CYBER database (scientific coordinator: Hervé Claustre; data manager and webmaster: Catherine Schmechtig) at the following web address: http://www.obs-vlfr.fr/proof/php/outpace/outpace.php (last access: 10 August 2018). GLODAPv2 data are available at the following web address: https://www.glodap.info/ (last access: 10 August 2018). SOCAT version 6 data are available at the following web address: https://www.socat.info/ (last access: 10 August 2018).

Competing interests. The authors declare that they have no conflict of interest.

Special issue statement. This article is part of the special issue "Interactions between planktonic organisms and biogeochemical cycles across trophic and N_2 fixation gradients in the western tropical South Pacific Ocean: a multidisciplinary approach (OUTPACE experiment)". It is not associated with a conference.

Acknowledgements. This is a contribution of the OUTPACE (Oligotrophy from Ultra-oligoTrophy PACific Experiment) project (https://outpace.mio.univ-amu.fr/, last access: 10 August 2018) funded by the French national research agency (ANR-14-CE01-0007-01), the LEFE-CyBER program (CNRS-INSU), the GOPS program (IRD) and the CNES (BC T23, ZBC 4500048836). The OUTPACE cruise (https://doi.org/10.17600/15000900) was managed by the MIO (OSU Institut Pytheas, AMU) from Marseille (France), which has received funding from the European FEDER Fund under project 1166-39417. The SNAPO-CO_2 service at LOCEAN is supported by CNRS-INSU and OSU Ecce-Terra. The Surface Ocean CO_2 Atlas (SOCAT) is an international effort, endorsed by the International Ocean Carbon Coordination Project (IOCCP), the Surface Ocean Lower Atmosphere Study (SOLAS) and the Integrated Marine Biosphere Research (IMBeR) program, to deliver a uniformly quality-controlled surface ocean CO_2 database. The many researchers and funding agencies responsible for the collection of data and quality control are thanked for their contributions to SOCAT. The authors thank the crew of the R/V *L'Atalante* for outstanding shipboard operation. Catherine Schmechtig is warmly thanked for the LEFE CYBER database management. Aurelia Lozingot is acknowledged for the administrative work. Pierre Marrec is thanked for his insightful comments on the present work. The two anonymous referees are thanked for helping improve a previous version of this paper. The authors acknowledge the assistance of the editorial staff of *Biogeosciences*.

Edited by: Emilio Marañón
Reviewed by: two anonymous referees

References

Álvarez, M., Lo Monaco, C., Tanhua, T., Yool, A., Oschlies, A., Bullister, J. L., Goyet, C., Metzl, N., Touratier, F., McDonagh, E., and Bryden, H. L.: Estimating the storage of anthro-

pogenic carbon in the subtropical Indian Ocean: a comparison of five different approaches, Biogeosciences, 6, 681–703, https://doi.org/10.5194/bg-6-681-2009, 2009.

Azouzi, L., Goyet, C., Gonçalves Ito, R., and Touratier, F.: Corrigendum to "Anthropogenic carbon distribution in the eastern South Pacific Ocean" published in Biogeosciences, 6, 149–156, 2009, Biogeosciences, 6, 361–361, https://doi.org/10.5194/bg-6-361-2009, 2009.

Bakker, D. C. E., Pfeil, B., Landa, C. S., Metzl, N., O'Brien, K. M., Olsen, A., Smith, K., Cosca, C., Harasawa, S., Jones, S. D., Nakaoka, S.-I., Nojiri, Y., Schuster, U., Steinhoff, T., Sweeney, C., Takahashi, T., Tilbrook, B., Wada, C., Wanninkhof, R., Alin, S. R., Balestrini, C. F., Barbero, L., Bates, N. R., Bianchi, A. A., Bonou, F., Boutin, J., Bozec, Y., Burger, E. F., Cai, W.-J., Castle, R. D., Chen, L., Chierici, M., Currie, K., Evans, W., Featherstone, C., Feely, R. A., Fransson, A., Goyet, C., Greenwood, N., Gregor, L., Hankin, S., Hardman-Mountford, N. J., Harlay, J., Hauck, J., Hoppema, M., Humphreys, M. P., Hunt, C. W., Huss, B., Ibánhez, J. S. P., Johannessen, T., Keeling, R., Kitidis, V., Körtzinger, A., Kozyr, A., Krasakopoulou, E., Kuwata, A., Landschützer, P., Lauvset, S. K., Lefèvre, N., Lo Monaco, C., Manke, A., Mathis, J. T., Merlivat, L., Millero, F. J., Monteiro, P. M. S., Munro, D. R., Murata, A., Newberger, T., Omar, A. M., Ono, T., Paterson, K., Pearce, D., Pierrot, D., Robbins, L. L., Saito, S., Salisbury, J., Schlitzer, R., Schneider, B., Schweitzer, R., Sieger, R., Skjelvan, I., Sullivan, K. F., Sutherland, S. C., Sutton, A. J., Tadokoro, K., Telszewski, M., Tuma, M., van Heuven, S. M. A. C., Vandemark, D., Ward, B., Watson, A. J., and Xu, S.: A multidecade record of high-quality fCO_2 data in version 3 of the Surface Ocean CO_2 Atlas (SOCAT), Earth Syst. Sci. Data, 8, 383–413, https://doi.org/10.5194/essd-8-383-2016, 2016.

Bates, N., Astor, Y., Church, M., Currie, K., Dore, J., González-Dávila, M., Lorenzoni, L., Muller-Karger, F., Olafsson, J., and Santa-Casiano, M.: A Time-Series View of Changing Ocean Chemistry Due to Ocean Uptake of Anthropogenic CO_2 and Ocean Acidification, Oceanography, 27, 126–141, https://doi.org/10.5670/oceanog.2014.16, 2014.

Bonnet, S., Caffin, M., Berthelot, H., and Moutin, T.: Hot spot of N_2 fixation in the western tropical South Pacific pleads for a spatial decoupling between N_2 fixation and denitrification, P. Natl. Acad. Sci. USA, 114, E2800–E2801, https://doi.org/10.1073/pnas.1619514114, 2017.

Carter, B. R., Feely, R. A., Mecking, S., Cross, J. N., Macdonald, A. M., Siedlecki, S. A., Talley, L. D., Sabine, C. L., Millero, F. J., Swift, J. H., Dickson, A. G., and Rodgers, K. B.: Two decades of Pacific anthropogenic carbon storage and ocean acidification along Global Ocean Ship-based Hydrographic Investigations Program sections P16 and P02: Decadal Pacific C_{anth} Changes by EMLR, Global Biogeochem. Cy., 31, 306–327, https://doi.org/10.1002/2016GB005485, 2017.

de Verneil, A., Rousselet, L., Doglioli, A. M., Petrenko, A. A., and Moutin, T.: The fate of a southwest Pacific bloom: gauging the impact of submesoscale vs. mesoscale circulation on biological gradients in the subtropics, Biogeosciences, 14, 3471–3486, https://doi.org/10.5194/bg-14-3471-2017, 2017.

DeVries, T., Holzer, M., and Primeau, F.: Recent increase in oceanic carbon uptake driven by weaker upper-ocean overturning, Nature, 542, 215–218, https://doi.org/10.1038/nature21068, 2017.

Dickson, A.: An exact definition of total alkalinity and a procedure for the estimation of alkalinity and total inorganic carbon from titration data, Deep-Sea Res. Pt. A, 28, 609–623, https://doi.org/10.1016/0198-0149(81)90121-7, 1981.

Dickson, A.: Standards for Ocean Measurements, Oceanography, 23, 34–47, https://doi.org/10.5670/oceanog.2010.22, 2010.

Dickson, A. and Goyet, C. (Eds.): Handbook of methods for the analysis of the various parameters of the carbon dioxide system in sea water, version 2, no. 74 in ORNL/CDIAC-74, US Departement of Energy, 1994.

Dickson, A. G.: Standard potential of the reaction: $AgCl(s) + 12H_2(g)=Ag(s) + HCl(aq)$, and and the standard acidity constant of the ion HSO_4^- in synthetic sea water from 273.15 to 318.15 K, J. Chem. Thermodyn., 22, 113–127, https://doi.org/10.1016/0021-9614(90)90074-Z, 1990.

Dickson, A. G., Sabine, C. L., Christian, J. R., Bargeron, C. P., and North Pacific Marine Science Organization (Eds.): Guide to best practices for ocean CO_2 measurements, no. 3 in PICES special publication, North Pacific Marine Science Organization, Sidney, BC, 2007.

Edmond, J. M.: High precision determination of titration alkalinity and total carbon dioxide content of sea water by potentiometric titration, Deep-Sea Research and Oceanographic Abstracts, 17, 737–750, https://doi.org/10.1016/0011-7471(70)90038-0, 1970.

Feely, R. A., Sabine, C. L., Lee, K., Berelson, W., Kleypas, J., Fabry, V. J., and Millero, F. J: Impact of Anthropogenic CO_2 on the $CaCO_3$ System in the Oceans, Science, 305, 362–366, https://doi.org/10.1126/science.1097329, 2004.

Fumenia, A., Moutin, T., Bonnet, S., Benavides, M., Petrenko, A., Helias Nunige, S., and Maes, C.: Excess nitrogen as a marker of intense dinitrogen fixation in the Western Tropical South Pacific Ocean: impact on the thermocline waters of the South Pacific, Biogeosciences Discuss., https://doi.org/10.5194/bg-2017-557, in review, 2018.

Ganachaud, A., Cravatte, S., Sprintall, J., Germineaud, C., Alberty, M., Jeandel, C., Eldin, G., Metzl, N., Bonnet, S., Benavides, M., Heimburger, L.-E., Lefèvre, J., Michael, S., Resing, J., Quéroué, F., Sarthou, G., Rodier, M., Berthelot, H., Baurand, F., Grelet, J., Hasegawa, T., Kessler, W., Kilepak, M., Lacan, F., Privat, E., Send, U., Van Beek, P., Souhaut, M., and Sonke, J. E.: The Solomon Sea: its circulation, chemistry, geochemistry and biology explored during two oceanographic cruises, Elem. Sci. Anth., 5, 33, https://doi.org/10.1525/elementa.221, 2017.

Garcia, H. E. and Gordon, L. I.: Oxygen solubility in seawater: Better fitting equations, Limnol. Oceanogr., 37, 1307–1312, https://doi.org/10.4319/lo.1992.37.6.1307, 1992.

Gattuso, J.-P. and Lavigne, H.: Technical Note: Approaches and software tools to investigate the impact of ocean acidification, Biogeosciences, 6, 2121–2133, https://doi.org/10.5194/bg-6-2121-2009, 2009.

Gruber, N. and Sarmiento, J. L.: Global patterns of marine nitrogen fixation and denitrification, Global Biogeochem. Cy., 11, 235–266, https://doi.org/10.1029/97GB00077, 1997.

Hartin, C. A., Fine, R. A., Sloyan, B. M., Talley, L. D., Chereskin, T. K., and Happell, J.: Formation rates of Subantarctic mode water and Antarctic intermediate water within the South Pacific, Deep-Sea Res. Pt. I, 58, 524–534, https://doi.org/10.1016/j.dsr.2011.02.010, 2011.

Key, R. M., Kozyr, A., Sabine, C. L., Lee, K., Wanninkhof, R., Bullister, J. L., Feely, R. A., Millero, F. J., Mordy, C., and Peng, T.-H.: A global ocean carbon climatology: Results from Global Data Analysis Project (GLODAP): GLOBAL OCEAN CARBON CLIMATOLOGY, Global Biogeochem. Cy., 18, GB4031, https://doi.org/10.1029/2004GB002247, 2004.

Key, R., Olsen, A., Van Heuven, S., Lauvset, S., Velo, A., Lin, X., Schirnick, C., Kozyr, A., Tanhua, T., Hoppema, M., Jutterstrom, S., Steinfeldt, R., Jeansson, E., Ishi, M., Perez, F., and Suzuki, T.: Global Ocean Data Analysis Project, Version 2 (GLODAPv2), ORNL/CDIAC-162, ND-P093, dataset, https://doi.org/10.3334/CDIAC/OTG.NDP093_GLODAPv2, 2015.

Kouketsu, S., Murata, A., and Doi, T.: Decadal changes in dissolved inorganic carbon in the Pacific Ocean: DIC changes in the pacific, Global Biogeochem. Cy., 27, 65–76, https://doi.org/10.1029/2012GB004413, 2013.

Langdon, C.: Determination of Dissolved Oxygen in Seawater by Winkler Titration Using the Amperometric Technique, no. 14 in IOCCP Report, ICPO Publication, available at: http://www.go-ship.org/HydroMan.html (last access: 10 August 2018), 2010.

Lauvset, S. K., Gruber, N., Landschützer, P., Olsen, A., and Tjiputra, J.: Trends and drivers in global surface ocean pH over the past 3 decades, Biogeosciences, 12, 1285–1298, https://doi.org/10.5194/bg-12-1285-2015, 2015.

Le Quéré, C., Andrew, R. M., Friedlingstein, P., Sitch, S., Pongratz, J., Manning, A. C., Korsbakken, J. I., Peters, G. P., Canadell, J. G., Jackson, R. B., Boden, T. A., Tans, P. P., Andrews, O. D., Arora, V. K., Bakker, D. C. E., Barbero, L., Becker, M., Betts, R. A., Bopp, L., Chevallier, F., Chini, L. P., Ciais, P., Cosca, C. E., Cross, J., Currie, K., Gasser, T., Harris, I., Hauck, J., Haverd, V., Houghton, R. A., Hunt, C. W., Hurtt, G., Ilyina, T., Jain, A. K., Kato, E., Kautz, M., Keeling, R. F., Klein Goldewijk, K., Körtzinger, A., Landschützer, P., Lefèvre, N., Lenton, A., Lienert, S., Lima, I., Lombardozzi, D., Metzl, N., Millero, F., Monteiro, P. M. S., Munro, D. R., Nabel, J. E. M. S., Nakaoka, S.-I., Nojiri, Y., Padin, X. A., Peregon, A., Pfeil, B., Pierrot, D., Poulter, B., Rehder, G., Reimer, J., Rödenbeck, C., Schwinger, J., Séférian, R., Skjelvan, I., Stocker, B. D., Tian, H., Tilbrook, B., Tubiello, F. N., van der Laan-Luijkx, I. T., van der Werf, G. R., van Heuven, S., Viovy, N., Vuichard, N., Walker, A. P., Watson, A. J., Wiltshire, A. J., Zaehle, S., and Zhu, D.: Global Carbon Budget 2017, Earth Syst. Sci. Data, 10, 405–448, https://doi.org/10.5194/essd-10-405-2018, 2018.

Lo Monaco, C., Goyet, C., Metzl, N., Poisson, A., and Touratier, F.: Distribution and inventory of anthropogenic CO_2 in the Southern Ocean: Comparison of three data-based methods, J. Geophys. Res., 110, C09S02, https://doi.org/10.1029/2004JC002571, 2005.

Lueker, T. J., Dickson, A. G., and Keeling, C. D.: Ocean pCO_2 calculated from dissolved inorganic carbon, alkalinity, and equations for K_1 and K_2: validation based on laboratory measurements of CO_2 in gas and seawater at equilibrium, Mar. Chem., 70, 105–119, https://doi.org/10.1016/S0304-4203(00)00022-0, 2000.

Moutin, T., Doglioli, A. M., de Verneil, A., and Bonnet, S.: Preface: The Oligotrophy to the UlTra-oligotrophy PACific Experiment (OUTPACE cruise, 18 February to 3 April 2015), Biogeosciences, 14, 3207–3220, https://doi.org/10.5194/bg-14-3207-2017, 2017.

Moutin, T., Wagener, T., Caffin, M., Fumenia, A., Gimenez, A., Baklouti, M., Bouruet-Aubertot, P., Pujo-Pay, M., Leblanc, K., Lefevre, D., Helias Nunige, S., Leblond, N., Grosso, O., and de Verneil, A.: Nutrient availability and the ultimate control of the biological carbon pump in the western tropical South Pacific Ocean, Biogeosciences, 15, 2961–2989, https://doi.org/10.5194/bg-15-2961-2018, 2018.

Murata, A., Kumamoto, Y., Watanabe, S., and Fukasawa, M.: Decadal increases of anthropogenic CO_2 in the South Pacific subtropical ocean along 32° S, J. Geophys. Res., 112, C05033, https://doi.org/10.1029/2005JC003405, 2007.

Murata, A., Hayashi, K., Kumamoto, Y., and Sasaki, K.-I.: Detecting the progression of ocean acidification from the saturation state of $CaCO_3$ in the subtropical South Pacific, Global Biogeochem. Cy., 29, 463–475, https://doi.org/10.1002/2014GB004908, 2015.

Olsen, A., Key, R. M., van Heuven, S., Lauvset, S. K., Velo, A., Lin, X., Schirnick, C., Kozyr, A., Tanhua, T., Hoppema, M., Jutterström, S., Steinfeldt, R., Jeansson, E., Ishii, M., Pérez, F. F., and Suzuki, T.: The Global Ocean Data Analysis Project version 2 (GLODAPv2) – an internally consistent data product for the world ocean, Earth Syst. Sci. Data, 8, 297–323, https://doi.org/10.5194/essd-8-297-2016, 2016.

Oudot, C., Gerard, R., Morin, P., and Gningue, I.: Precise shipboard determination of dissolved oxygen (Winkler procedure) for productivity studies with a commercial system1, Limnol. Oceanogr., 33, 146–150, https://doi.org/10.4319/lo.1988.33.1.0146, 1988.

Owens, W. B. and Millard, R. C.: A New Algorithm for CTD Oxygen Calibration, J. Phys. Oceanogr., 15, 621–631, https://doi.org/10.1175/1520-0485(1985)015<0621:ANAFCO>2.0.CO;2, 1985.

Pérez, F. F. and Fraga, F.: A precise and rapid analytical procedure for alkalinity determination, Mar. Chem., 21, 169–182, https://doi.org/10.1016/0304-4203(87)90037-5, 1987.

Pérez, F. F., Vázquez-Rodríguez, M., Mercier, H., Velo, A., Lherminier, P., and Ríos, A. F.: Trends of anthropogenic CO_2 storage in North Atlantic water masses, Biogeosciences, 7, 1789–1807, https://doi.org/10.5194/bg-7-1789-2010, 2010.

Riebesell, U., Zondervan, I., Rost, B., Tortell, P. D., Zeebe, R. E., and Morel, F. M. M.: Reduced calcification of marine plankton in response to increased atmospheric CO_2, Nature, 407, 364–367, https://doi.org/10.1038/35030078, 2000.

Royal Society (Great Britain): Ocean acidification due to increasing atmospheric carbon dioxide, Royal Society, London, oCLC: 60805277, available at: https://royalsociety.org/topics-policy/publications/2005/ocean-acidification/ (last access: 10 August 2018), 2005.

Sabine, C. L. and Tanhua, T.: Estimation of Anthropogenic CO_2 Inventories in the Ocean, Annu. Rev. Mar. Sci., 2, 175–198, https://doi.org/10.1146/annurev-marine-120308-080947, 2010.

Sabine, C. L., Feely, R. A., Gruber, N., Key, R. M., Lee, K., Bullister, J. L., Wanninkhof, R., Wong, C. S., Wallace, D. W. R., Tilbrook, B., Millero, F. J., Peng, T.-H., Kozyr, A., Ono, T., and Rios, A. F.: The Oceanic Sink for Anthropogenic CO_2, Science, 305, 367–371, https://doi.org/10.1126/science.1097403, 2004.

Sabine, C. L., Feely, R. A., Millero, F. J., Dickson, A. G., Langdon, C., Mecking, S., and Greeley, D.: Decadal

changes in Pacific carbon, J. Geophys. Res., 113, C07021, https://doi.org/10.1029/2007JC004577, 2008.

Takahashi, T., Sutherland, S., Chipman, D., Goddard, J., Ho, C., Newberger, T., Sweeney, C., and Munro, D.: Climatological distributions of pH, pCO_2, total CO_2, alkalinity, and $CaCO_3$ saturation in the global surface ocean, and temporal changes at selected locations, Mar. Chem., 164, 95–125, https://doi.org/10.1016/j.marchem.2014.06.004, 2014.

Tomczak, M. and Godfrey, J. S.: Regional oceanography: an introduction, 2nd Edn., Daya Publ. House, Delhi, 2003.

Touratier, F. and Goyet, C.: Applying the new TrOCA approach to assess the distribution of anthropogenic CO_2 in the Atlantic Ocean, J. Marine Syst., 46, 181–197, https://doi.org/10.1016/j.jmarsys.2003.11.020, 2004a.

Touratier, F. and Goyet, C.: Definition, properties, and Atlantic Ocean distribution of the new tracer TrOCA, J. Marine Syst., 46, 169–179, https://doi.org/10.1016/j.jmarsys.2003.11.016, 2004b.

Touratier, F., Azouzi, L., and Goyet, C.: CFC-11, $\Delta^{14}C$ and ^{3}H tracers as a means to assess anthropogenic CO_2 concentrations in the ocean, Tellus B, 59, 318–325, https://doi.org/10.1111/j.1600-0889.2006.00247.x, 2007.

Valladares, J., Fennel, W., and Morozov, E.: Replacement of EOS – 80 with the International Thermodynamic Equation of Seawater – 2010 (TEOS–10), Deep-Sea Res. Pt. I, 58, p. 978, https://doi.org/10.1016/j.dsr.2011.07.005, 2011.

Vázquez-Rodríguez, M., Touratier, F., Lo Monaco, C., Waugh, D. W., Padin, X. A., Bellerby, R. G. J., Goyet, C., Metzl, N., Ríos, A. F., and Pérez, F. F.: Anthropogenic carbon distributions in the Atlantic Ocean: data-based estimates from the Arctic to the Antarctic, Biogeosciences, 6, 439–451, https://doi.org/10.5194/bg-6-439-2009, 2009.

Waters, J. F., Millero, F. J., and Sabine, C. L.: Changes in South Pacific anthropogenic carbon, Global Biogeochem. Cy., 25, GB4011, https://doi.org/10.1029/2010GB003988, 2011.

Winkler, L. W.: Die Bestimmung des im Wasser gelösten Sauerstoffes, Ber. Dtsch. Chem. Ges., 21, 2843–2854, https://doi.org/10.1002/cber.188802102122, 1888.

Yool, A., Oschlies, A., Nurser, A. J. G., and Gruber, N.: A model-based assessment of the TrOCA approach for estimating anthropogenic carbon in the ocean, Biogeosciences, 7, 723–751, https://doi.org/10.5194/bg-7-723-2010, 2010.

Yoshikawa, C., Makabe, A., Shiozaki, T., Toyoda, S., Yoshida, O., Furuya, K., and Yoshida, N.: Nitrogen isotope ratios of nitrate and N^* anomalies in the subtropical South Pacific, Geochem. Geophy. Geosy., 16, 1439–1448, https://doi.org/10.1002/2014GC005678, 2015.